Instructions to Authors

Scopes

Study areas include cell biology, genomics, microbiology, immunology, molecular biology, biochemistry, embryology, immunogenetics, cell and tissue culture, molecular ecology, genetic engineering and biological engineering, bioremediation and biodegradation, bioinformatics, biotechnology regulations, gene therapy, organismal biology, microbial and environmental biotechnology, marine sciences. The JJBS welcomes the submission of manuscript that meets the general criteria of significance and academic excellence. All articles published in JJBS are peer-reviewed. Papers will be published approximately one to two months after acceptance.

Type of Papers

The journal publishes high-quality original scientific papers, short communications, correspondence and case studies. Review articles are usually by invitation only. However, Review articles of current interest and high standard will be considered.

Submission of Manuscript

Manuscript, or the essence of their content, must be previously unpublished and should not be under simultaneous consideration by another journal. The authors should also declare if any similar work has been submitted to or published by another journal. They should also declare that it has not been submitted/ published elsewhere in the same form, in English or in any other language, without the written consent of the Publisher. The authors should also declare that the paper is the original work of the author(s) and not copied (in whole or in part) from any other work. All papers will be automatically checked for duplicate publication and plagiarism. If detected, appropriate action will be taken in accordance with International Ethical Guideline. By virtue of the submitted manuscript, the corresponding author acknowledges that all the co-authors have seen and approved the final version of the manuscript. The corresponding author should provide all co-authors with information regarding the manuscript, and obtain their approval before submitting any revisions. Electronic submission of manuscripts is strongly recommended, provided that the text, tables and figures are included in a single Microsoft Word file. Submit manuscript as e-mail attachment to the Editorial Office at: JJBS@hu.edu.jo. After submission, a manuscript number will be communicated to the corresponding author within 48 hours.

Peer-review Process

It is requested to submit, with the manuscript, the names, addresses and e-mail addresses of at least 4 potential reviewers. It is the sole right of the editor to decide whether or not the suggested reviewers to be used. The reviewers' comments will be sent to authors within 6-8 weeks after submission. Manuscripts and figures for review will not be returned to authors whether the editorial decision is to accept, revise, or reject. All Case Reports and Short Communication must include at least one table and/ or one figure.

Preparation of Manuscript

The manuscript should be written in English with simple lay out. The text should be prepared in single column format. Bold face, italics, subscripts, superscripts etc. can be used. Pages should be numbered consecutively, beginning with the title page and continuing through the last page of typewritten material.

The text can be divided into numbered sections with brief headings. Starting from introduction with section 1. Subsections should be numbered (for example 2.1 (then 2.1.1, 2.1.2, 2.2, etc.), up to three levels. Manuscripts in general should be organized in the following manner:

Title Page

The title page should contain a brief title, correct first name, middle initial and family name of each author and name and address of the department(s) and institution(s) from where the research was carried out for each author. The title should be without any abbreviations and it should enlighten the contents of the paper. All affiliations should be provided with a lower-case superscript number just after the author's name and in front of the appropriate address.

The name of the corresponding author should be indicated along with telephone and fax numbers (with country and area code) along with full postal address and e-mail address.

Abstract

The abstract should be concise and informative. It should not exceed **350 words** in length for full manuscript and Review article and **150 words** in case of Case Report and/ or Short Communication. It should briefly describe the purpose of the work, techniques and methods used, major findings with important data and conclusions. No references should be cited in this part. Generally non-standard abbreviations should not be used, if necessary they should be clearly defined in the abstract, at first use.

Keywords

Immediately after the abstract, **about 4-8 keywords** should be given. Use of abbreviations should be avoided, only standard abbreviations, well known in the established area may be used, if appropriate. These keywords will be used for indexing.

Abbreviations

Non-standard abbreviations should be listed and full form of each abbreviation should be given in parentheses at first use in the text.

Introduction

Provide a factual background, clearly defined problem, proposed solution, a brief literature survey and the scope and justification of the work done.

Materials and Methods

Give adequate information to allow the experiment to be reproduced. Already published methods should be mentioned with references. Significant modifications of published methods and new methods should be described in detail. Capitalize trade names and include the manufacturer's name and address. Subheading should be used.

Results

Results should be clearly described in a concise manner. Results for different parameters should be described under subheadings or in separate paragraph. Results should be explained, but largely without referring to the literature. Table or figure numbers should be mentioned in parentheses for better understanding.

Discussion

The discussion should not repeat the results, but provide detailed interpretation of data. This should interpret the significance of the findings of the work. Citations should be given in support of the findings. The results and discussion part can also be described as separate, if appropriate. The Results and Discussion sections can include subheadings, and when appropriate, both sections can be combined

Conclusions

This should briefly state the major findings of the study.

Acknowledgment

A brief acknowledgment section may be given after the conclusion section just before the references. The acknowledgment of people who provided assistance in manuscript preparation, funding for research, etc. should be listed in this section.

Tables and Figures

Tables and figures should be presented as per their appearance in the text. It is suggested that the discussion about the tables and figures should appear in the text before the appearance of the respective tables and figures. No tables or figures should be given without discussion or reference inside the text.

Tables should be explanatory enough to be understandable without any text reference. Double spacing should be maintained throughout the table, including table headings and footnotes. Table headings should be placed above the table. Footnotes should be placed below the table with superscript lowercase letters. Each table should be on a separate page, numbered consecutively in Arabic numerals.

Each figure should have a caption. The caption should be concise and typed separately, not on the figure area. Figures should be self-explanatory. Information presented in the figure should not be repeated in the table. All symbols and abbreviations used in the illustrations should be defined clearly. Figure legends should be given below the figures.

References

References should be listed alphabetically at the end of the manuscript. Every reference referred in the text must be also present in the reference list and vice versa. In the text, a reference identified by means of an author's name should be followed by the year of publication in parentheses (e.g.(Brown,2009)). For two authors, both authors' names followed by the year of publication (e.g.(Nelson and Brown, 2007)). When there are more than two authors, only the first author's name followed by "*et al.*" and the year of publication (e. g. (Abu-Elteen *et al.*, 2010)). When two or more works of an author has been published during the same year, the reference should be identified by the letters "a", "b", "c", etc., placed after the year of publication. This should be followed both in the text and reference list. e.g., Hilly, (2002a, 2002b); Hilly, and Nelson, (2004). Articles in preparation or submitted for publication, unpublished observations, personal communications, etc. should not be included in the reference list but should only be mentioned in the article text (e.g., Shtyawy,A., University of Jordan, personal communication). Journal titles should be abbreviated according to the system adopted in Biological Abstract and Index Medicus, if not included in Biological Abstract or Index Medicus journal title should be given in full. The author is responsible for the sccuracy and completeness of the references and for their correct textual citation. Failure to do so may result in the paper being withdraw from the evaluation process. Example of correct reference form is given as follows:-

Reference to a journal publication:

Bloch BK. 2002. Econazole nitrate in the treatment of *Candida vaginitis*. *S Afr Med J.* , **58**:314-323.

Ogunseitan OA and Ndoye IL. 2006. Protein method for investigating mercuric reductase gene expression in aquatic environments. *Appl Environ Microbiol.*, **64**: 695-702.

Hilly MO, Adams MN and Nelson SC. 2009. Potential fly-ash utilization in agriculture. *Progress in Natural Sci.*, **19**: 1173-1186.

Reference to a book:
Brown WY and White SR.1985. **The Elements of Style**, third ed. MacMillan, New York.

Reference to a chapter in an edited book:
Mettam GR and Adams LB. 2010. How to prepare an electronic version of your article. In: Jones BS and Smith RZ (Eds.), **Introduction to the Electronic Age**. Kluwer Academic Publishers, Netherlands, pp. 281–304.

Conferences and Meetings:
Embabi NS. 1990. Environmental aspects of distribution of mangrove in the United Arab Emirates. Proceedings of the First ASWAS Conference. University of the United Arab Emirates. Al-Ain, United Arab Emirates.

Theses and Dissertations:
El-Labadi SN. 2002. Intestinal digenetic trematodes of some marine fishes from the Gulf of Aqaba. MSc dissertation, The Hashemite University, Zarqa, Jordan.

Nomenclature and Units
Internationally accepted rules and the international system of units (SI) should be used. If other units are mentioned, please give their equivalent in SI.

For biological nomenclature, the conventions of the *International Code of Botanical Nomenclature, the International Code of Nomenclature of Bacteria,* and the *International Code of Zoological Nomenclature* should be followed. Scientific names of all biological creatures (crops, plants, insects, birds, mammals, etc.) should be mentioned in parentheses at first use of their English term.

Chemical nomenclature, as laid down in the *International Union of Pure and Applied Chemistry* and the official recommendations of the *IUPAC-IUB Combined Commission on Biochemical Nomenclature* should be followed. All biocides and other organic compounds must be identified by their Geneva names when first used in the text. Active ingredients of all formulations should be likewise identified.

Math formulae

All equations referred to in the text should be numbered serially at the right-hand side in parentheses. Meaning of all symbols should be given immediately after the equation at first use. Instead of root signs fractional powers should be used. Subscripts and superscripts should be presented clearly. Variables should be presented in italics. Greek letters and non-Roman symbols should be described in the margin at their first use.

To avoid any misunderstanding zero (0) and the letter O, and one (1) and the letter l should be clearly differentiated. For simple fractions use of the solidus (/) instead of a horizontal line is recommended. Levels of statistical significance such as: $^{*}P$ <0.05, $^{**}P$ <0.01 and $^{***}P$ <0.001 do not require any further explanation.

Copyright

Submission of a manuscript clearly indicates that: the study has not been published before or is not under consideration for publication elsewhere (except as an abstract or as part of a published lecture or academic thesis); its publication is permitted by all authors and after accepted for publication it will not be submitted for publication anywhere else, in English or in any other language, without the written approval of the copyright-holder. The journal may consider manuscripts that are translations of articles originally published in another language. In this case, the consent of the journal in which the article was originally published must be obtained and the fact that the article has already been published must be made clear on submission and stated in the abstract. It is compulsory for the authors to ensure that no material submitted as part of a manuscript infringes existing copyrights, or the rights of a third party.

Ethical Consent

All manuscripts reporting the results of experimental investigation involving human subjects should include a statement confirming that each subject or subject's guardian obtains an informed consent, after the approval of the experimental protocol by a local human ethics committee or IRB. When reporting experiments on animals, authors should indicate whether the institutional and national guide for the care and use of laboratory animals was followed.

Plagiarism

The JJBS hold no responsibility for plagiarism. If a published paper is found later to be extensively plagiarized and is found to be a duplicate or redundant publication, a note of retraction will be published, and copies of the correspondence will be sent to the authors' head of institute.

Galley Proofs

The Editorial Office will send proofs of the manuscript to the corresponding author as an e-mail attachment for final proof reading and it will be the responsibility of the corresponding author to return the galley proof materials appropriately corrected within the stipulated time. Authors will be asked to check any typographical or minor clerical errors in the manuscript at this stage. No other major alteration in the manuscript is allowed. After publication authors can freely access the full text of the article as well as can download and print the PDF file.

Publication Charges

There are no page charges for publication in Jordan Journal of Biological Sciences, except for color illustrations,

Reprints

Ten (10) reprints are provided to corresponding author free of charge within two weeks after the printed journal date. For orders of more reprints, a reprint order form and prices will be sent with article proofs, which should be returned directly to the Editor for processing.

Disclaimer

Articles, communication, or editorials published by JJBS represent the sole opinions of the authors. The publisher shoulders no responsibility or liability what so ever for the use or misuse of the information published by JJBS.

Indexing

JJBS is indexed and abstracted by:

DOAJ (Directory of Open Access Journals)	CABI
Google Scholar	EBSCO
Journal Seek	CAS (Chemical Abstract Service)
HINARI	ETH- Citations
Index Copernicus	Open J-Gat
NDL Japanese Periodicals Index	SCImago
SCIRUS	Clarivate Analytics (Zoological Abstract)
OAJSE	Scopus
ISC (Islamic World Science Citation Center)	AGORA (United Nation's FAO database)
Directory of Research Journal Indexing (DRJI)	SHERPA/RoMEO (UK)
Ulrich's	

The Hashemite University
Deanship of Scientific Research
TRANSFER OF COPYRIGHT AGREEMENT

Journal publishers and authors share a common interest in the protection of copyright: authors principally because they want their creative works to be protected from plagiarism and other unlawful uses, publishers because they need to protect their work and investment in the production, marketing and distribution of the published version of the article. In order to do so effectively, publishers request a formal written transfer of copyright from the author(s) for each article published. Publishers and authors are also concerned that the integrity of the official record of publication of an article (once refereed and published) be maintained, and in order to protect that reference value and validation process, we ask that authors recognize that distribution (including through the Internet/WWW or other on-line means) of the authoritative version of the article as published is best administered by the Publisher.

To avoid any delay in the publication of your article, please read the terms of this agreement, sign in the space provided and return the complete form to us at the address below as quickly as possible.

Article entitled:--

Corresponding author: ---

To be published in the journal: Jordan Journal of Biological Sciences (JJBS)

I hereby assign to the Hashemite University the copyright in the manuscript identified above and any supplemental tables, illustrations or other information submitted therewith (the "article") in all forms and media (whether now known or hereafter developed), throughout the world, in all languages, for the full term of copyright and all extensions and renewals thereof, effective when and if the article is accepted for publication. This transfer includes the right to adapt the presentation of the article for use in conjunction with computer systems and programs, including reproduction or publication in machine-readable form and incorporation in electronic retrieval systems.

Authors retain or are hereby granted (without the need to obtain further permission) rights to use the article for traditional scholarship communications, for teaching, and for distribution within their institution.

☐ I am the sole author of the manuscript

☐ I am signing on behalf of all co-authors of the manuscript

☐ The article is a 'work made for hire' and I am signing as an authorized representative of the employing company/institution

Please mark one or more of the above boxes (as appropriate) and then sign and date the document in black ink.

Signed:_____ Name printed: _____
Title and Company (if employer representative) : _____
Date: _____

Data Protection: By submitting this form you are consenting that the personal information provided herein may be used by the Hashemite University and its affiliated institutions worldwide to contact you concerning the publishing of your article.

Please return the completed and signed original of this form by mail or fax, or a scanned copy of the signed original by e-mail, retaining a copy for your files, to:

Hashemite University
Jordan Journal of Biological Sciences
Zarqa 13115 Jordan
Fax: +962 5 3903338
Email: jjbs@hu.edu.jo

Editorial Preface

Jordan Journal of Biological Sciences (JJBS) is a refereed, quarterly international journal financed by the Scientific Research and Innovation Support Fund, Ministry of Higher Education and Scientific Research in cooperation with the Hashemite University, Jordan. JJBS celebrated its 12th commencement this past January, 2020. JJBS was founded in 2008 to create a peer-reviewed journal that publishes high-quality research articles, reviews and short communications on novel and innovative aspects of a wide variety of biological sciences such as cell biology, developmental biology, structural biology, microbiology, entomology, molecular biology, biochemistry, medical biotechnology, biodiversity, ecology, marine biology, plant and animal biology, plant and animal physiology, genomics and bioinformatics.

We have watched the growth and success of JJBS over the years. JJBS has published 14 volumes, 60 issues and 800 articles. JJBS has been indexed by SCOPUS, CABI's Full-Text Repository, EBSCO, Clarivate Analytics- Zoological Record and recently has been included in the UGC India approved journals. JJBS Cite Score has improved from 0.7 in 2019 to 1.4 in 2021 (Last updated on 6 March, 2022) and with Scimago Institution Ranking (SJR) 0.22 (Q3) in 2021.

A group of highly valuable scholars have agreed to serve on the editorial board and this places JJBS in a position of most authoritative on biological sciences. I am honored to have six eminent associate editors from various countries. I am also delighted with our group of international advisory board members coming from 15 countries worldwide for their continuous support of JJBS. With our editorial board's cumulative experience in various fields of biological sciences, this journal brings a substantial representation of biological sciences in different disciplines. Without the service and dedication of our editorial; associate editorial and international advisory board members, JJBS would have never existed.

In the coming year, we hope that JJBS will be indexed in Clarivate Analytics and MEDLINE (the U.S. National Library of Medicine database) and others. As you read throughout this volume of JJBS, I would like to remind you that the success of our journal depends on the number of quality articles submitted for review. Accordingly, I would like to request your participation and colleagues by submitting quality manuscripts for review. One of the great benefits we can provide to our prospective authors, regardless of acceptance of their manuscripts or not, is the feedback of our review process. JJBS provides authors with high quality, helpful reviews to improve their manuscripts.

Finally, JJBS would not have succeeded without the collaboration of authors and referees. Their work is greatly appreciated. Furthermore, my thanks are also extended to The Hashemite University and the Scientific Research and Innovation Support Fund, Ministry of Higher Education and Scientific Research for their continuous financial and administrative support to JJBS.

Professor Wedyan ,Mohammed A.
March, 2024

CONTENTS

Original Articles

A novel *AUTS2* Variant in a Patient with Global Developmental Delay and Intellectual Disability

Mohammad A. Shboul[1,*], Reem F. Darweesh[1], Mohammad El-Khateeb[2], Rajaa Fathallah[2]

[1] *Department of Medical Laboratory Sciences, Faculty of Medical Sciences, Jordan University of Science and Technology, P.O. Box 3030, Irbid 22110, Jordan;* [2] *National Center for Diabetes, Endocrinology and Genetics, Jordan*

Abstract

AUTS2 haploinsufficiency causes a neurodevelopmental disorder known as AUTS2, which is characterized by global developmental delay, intellectual disability, autistic features, congenital brain anomalies, and other malformations. In this study, we report a case of AUST2 syndrome and describe the clinical manifestations and genetic etiology as well as provide a review of the literature. A 5-year-old girl presented with neurodevelopmental manifestations, skeletal features and dysmorphic features. Whole exome sequencing was carried out for the proband. A novel, heterozygous variant (c.1606C>T) in *AUTS2* gene was identified. Sanger sequencing confirmed the presence of this variant in the affected girl; however, it was not detected in all family members. The identified variant is predicted to cause premature termination of the corresponding AUTS2 protein (p.Gln536*), which will likely lack the C-terminal domain of the protein. This study revealed a novel *de novo* loss-of-function variant in the *AUTS2* gene and further expanded the phenotypic and genetic spectra of the AUTS2 syndrome. Moreover, this result might be helpful in genetic counseling for families with clinical phenotypes related to this syndrome. Further functional experiments are required to validate the impact of the identified variant.

Keywords: AUTS2, variant, Neurodevelopmental disorders, intellectual disability

1. Introduction

Neurodevelopmental disorders (NDD) are a heterogeneous group of disorders that affect the development and functions of the brain (Parenti *et al.*, 2020). NDD features, but is not limited to, developmental delay (DD), autism spectrum disorder (ASD), intellectual disability (ID), epilepsy, and other features (Pang *et al.*, 2021). Among these, NDD is the AUTS2 syndrome.

AUTS2 syndrome (OMIM #615834) is a combination of intellectual disability and developmental delay (reported in 80~100% of patients) in addition to autism (reported in 40% of patients) (Sultana *et al.*, 2002; Beunders *et al.*, 2013; Jolley *et al.*, 2013; Amarillo *et al.*, 2014; Liu *et al.*, 2015; Pang *et al.*, 2021). Nevertheless, other manifestations have also been reported such as low birth weight, short stature, craniofacial features microcephaly, epilepsy, and feeding difficulties, in addition to other variable neurological, brain, and skeletal abnormalities (Kalscheuer *et al.*, 2007; Beunders *et al.*, 2013, 2016; Jolley *et al.*, 2013).

AUTS2 syndrome is an autosomal dominant disorder resulting from disruption in *AUTS2* gene (OMIM 607270). By 2023, more than 60 AUTS2 patients have been reported, most of them carrying exonic deletions (Beunders *et al.*, 2013, 2015, 2016; Jolley *et al.*, 2013; Liu *et al.*, 2015; Fan *et al.*, 2016; Martinez-Granero *et al.*, 2021; Sanchez-Jimeno *et al.*, 2021), five patients with exonic or intragenic duplications (Ben-David *et al.*, 2011; Nagamani *et al.*, 2013; Martinez-Granero *et al.*, 2021), and three patients with balanced translocation that disrupt the *AUTS2* gene (Kalscheuer *et al.*, 2007), while a small number of sequencing variants such as missense, nonsense, and indels have been less frequently reported in the literature (Beunders *et al.*, 2015, 2016; Aldinger *et al.*, 2019; Saeki *et al.*, 2019; Stojanovic *et al.*, 2020; Zech *et al.*, 2020; Ziats *et al.*, 2020; Gieldon *et al.*, 2021; Martinez-Delgado *et al.*, 2021; Palumbo *et al.*, 2021; Sanchez-Jimeno *et al.*, 2021; Anikiej-Wiczenbach *et al.*, 2022; Fair *et al.*, 2023).

Activator of transcription and developmental regulator gene (AUTS2) previously named autism susceptibility candidate 2 was first reported as a candidate for autism in a monozygotic twin with ASD, epilepsy, and developmental delay because it was disrupted by a breakpoint of the t(7;20) (q11.2; p11.2) translocation in these patients (Sultana *et al.*, 2002).

The *AUTS2* gene is mapped to the long arm of chromosome 7 (7q11.22), spanning approximately 1.2 Mb of genomic DNA and comprising 19 coding exons that code for a 1,259 amino acid protein. These 19 exons are divided into 2 parts: Exons (1-6) at the 5' end have large introns, whereas exons (7-19) at the 3' end are separated by short introns. AUTS2 encodes the full-length (long) (1259 aa) isoform and two C-terminal (short) isoforms (produced by alternative transcription start sites in exons 8, and 9) that are differentially expressed during development

---

* Corresponding author. e-mail: maalshboul@just.edu.jo.

(Beunders *et al.*, 2013; Hori *et al.*, 2014). In humans, *AUTS2* mRNA is expressed in different tissues and cells with the highest expression reported in the brain, kidney, and skeletal muscle (Biel *et al.*, 2022; Lepagnol-Bestel *et al.*, 2022).

The molecular function of AUTS2 is not fully understood; however, its neurodevelopmental functions have been well-studied in various model systems. Loss-of-function experiments in *zebrafish* and mouse models have displayed neurological developmental phenotypes and highlighted a crucial role for AUTS2 in RNA metabolism, activation of transcription, central nervous system cytoskeleton regulation, and neuronal differentiation and migration (Oksenberg *et al.*, 2013; Yamashiro *et al.*, 2020; Hori *et al.*, 2020; Monderer-Rothkoff *et al.*, 2021; Biel *et al.*, 2022).

In this study, we evaluated a patient with AUST2 syndrome who carries a *de novo* heterozygous nonsense variant in *AUTS2*, which was novel and classified as likely pathogenic according to the guidelines of the American College of Medical Genetics (ACMG) (Richards *et al.*, 2015). We also presented detailed clinical and genetic descriptions of AUTS2. To the best of our knowledge, this is the first AUTS2 case in our region with an *AUTS2* variant.

2. Materials and Methods

2.1. Samples and DNA extraction

This study was approved by the institutional review board /ethical committee of National Center for Diabetes, Endocrinology and Genetics (Protocol number IRB-1/2022). A signed informed consent was obtained from the family. The family pedigree is illustrated in Figure 1A. Genomic DNA (gDNA) was extracted from venous blood samples collected from the proband (II.2), parents (I.1 and I.2), and her healthy sisters (II.1 and II.3) following manufacturer's instructions (BioRobot EZ1; Qiagen, Solna, Sweden). The purity and concentration of DNA were evaluated using a spectrophotometer (Nanodrop 2000 C; Thermo Fisher Scientific, Waltham, MA, USA) and 1% agarose gel electrophoreses.

2.2. Whole exome sequencing (WES) and variant detection

Agilent's SureSelect Human All Exon V6 kit was used for exome capture following the manufacturer's protocol. The generated library was sequenced on an Illumina platform. Around 25,000 genes were sequenced, and ~97.75% of these genes were covered at least >10x. GRCh37/hg19 genome assembly was used for reads alignment. All pathogenic variants reported in ClinVar, in HGMD, and all variants with minor allele frequency (MAF) <1% in the gnomAD database were considered. We focused on nonsense and nonsynonymous, splice site variants (+/-10 intronic bases) as well as insertions and deletions (indels). Several *in-silico* prediction tools such as SIFT (https://sift.bii.a-star.edu.sg/), Polyphen2 (http://genetics.bwh.harvard.edu/pph2/), Mutation Taster (http://www.mutationtaster.org/),CADD (https://cadd.gs.washington.edu/), DANN

(https://cbcl.ics.uci.edu/public_data/DANN/), PhyloP (http://compgen.cshl.edu/phast/),FATHMM (http://fathmm.biocompute.org.uk/index.html), and others were also used to predict the functional impact of identified variants. The classification of variants was based on ACMG guidelines. Partial AUTS2 amino acids sequences alignment was obtained from http://www.ncbi.nlm.nih.gov/protein/ website.

2.3. Confirmation of the identified variant

Sanger sequencing was carried out to validate the variant in *AUST2* (c.1606C>T). Genomic DNA samples were amplified using specific primers for Exon 9 (Forword-5'ggcagtccgatgtcctttc'3 and Rreverse-5'tccccattcgatctctggtg'3. The PCR condition was as follows: initial denaturation for 3 min at 95 °C, followed by 30 cycles of denaturation for 15 sec at 95 °C, annealing for 60 sec at 55 °C, extension for 60 sec at 72 °C and final extension for 5 min at 72°C. PCR products were then purified and bi-directionally sequenced on a genetic analyzer (3500x; Applied Biosystems, Thermo Fisher Scientific) using BigDye Terminator Cycle Sequencing Kit v3.1 following the manufacturer protocol.

3. Results

3.1. Clinical Description

The 5-year-old female patient (II.1) is the second child of a non-consanguineous Syrian family (Figure 1). Family history was unremarkable for ID/NDD or congenital anomalies.

The affected girl was born at full term by vaginal delivery without complications. Her birth weight was (2700 g; 5th-10th percentile), height (50 cm; 25th-50th percentile), and occipitofrontal head circumference (35 cm; 50th-75th percentile). In the first year, she complained of feeding problems and poor weight gain with mild developmental delay. At the age of 2 years, she started walking with a tendency to walk on her toes. Speech, social and motor development remained delayed. At the age of 3 years, she showed generalized hypotonia with high muscle tone, frequent seizures (3-5 times per day lasting for 1 min), and stereotypic movements. Brain MRI and electroencephalogram were normal.

Her latest examination was done at the age of 5 years. Her weight was (13,700 g; between the 10th and 15th percentiles), height (102 cm; between the 25th and 50th percentiles), and occipitofrontal head circumference (46 cm; between 0.1 and 1st percentile). She displayed minor facial anomalies including an open mouth, anteverted nares, highly arched eyebrows, upward slanting palpebral fissures, ptosis, hypertelorism, strabismus, and squint (Figure 1B). She had stereotypic actions with hyperactive behavior patterns, sensitivity to sounds, and sleeping difficulty. She had frequent salivation, ataxia, and involuntary movement as well as tip-toe walking. Her social and motor development remain delayed, IQ was not formally tested, but her intellectual disability can be described as severe. Scoliosis was also prominent.
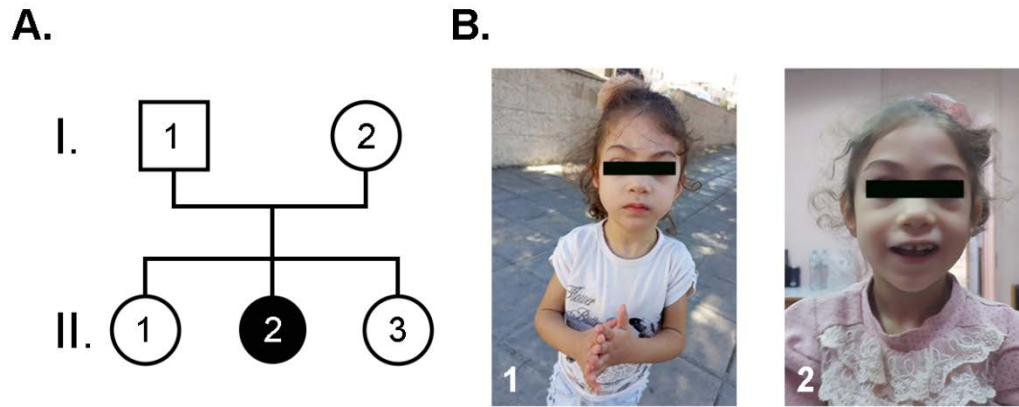
Figure 1. Family pedigree and patient characteristics. A. Pedigree of the family: Circle and square denote female and male, respectively. The filled circle represents the proband and unfilled symbols represent unaffected individuals, respectively. B. Clinical features of the affected patient (II.2) (Photos at the age of 3 (picture 1) and 5 years (picture 2)) showing dysmorphic features such as high-arched eyebrows, broad nasal bridge, and microcephaly.

3.2. Genetic findings

In this patient, around 25,000 genes have been sequenced, and ~97.75% of these genes are covered at least >10x. Out of 164,177 variants, 26,760 variants were detected across protein-coding exons (23,232 variants), and splice sites (3,528 variants). After filtration, we narrowed down the list of variants to 4 heterozygous variants. According to the clinical pictures and the pedigree, which indicates a dominant mode of inheritance, the nonsense variant in *AUTS2* gene c.1606C>T (p.Gln536*) was on the top of these variants and fits with diseases phenotype.

Segregation analysis revealed the absence of this variant in both parents and healthy siblings, implying a *de novo AUTS2* variant in the proband (Figure 2A). This variant lies in a conserved C-terminal domain of AUTS2 protein (Figure 2B). The identified variant is predicted to cause premature termination of the corresponding protein (p.Gln536*). This truncated protein will likely lack the C-terminal domain resulting in loss-of-function. The AUTS2 (p.Gln536*) variant was predicted as 'Disease Causing' as well as deleterious by various prediction tools (Table 1). The identified variant was absent from Genome Aggregation Database (gnomAD (https://gnomad.broadinstitute.org/),ClinVar (https://www.ncbi.nlm.nih.gov/clinvar/, and HGMD (https://www.hgmd.cf.ac.uk/ac/index.php) databases. The identified variant was classified as likely pathogenic according to ACMG guidelines.
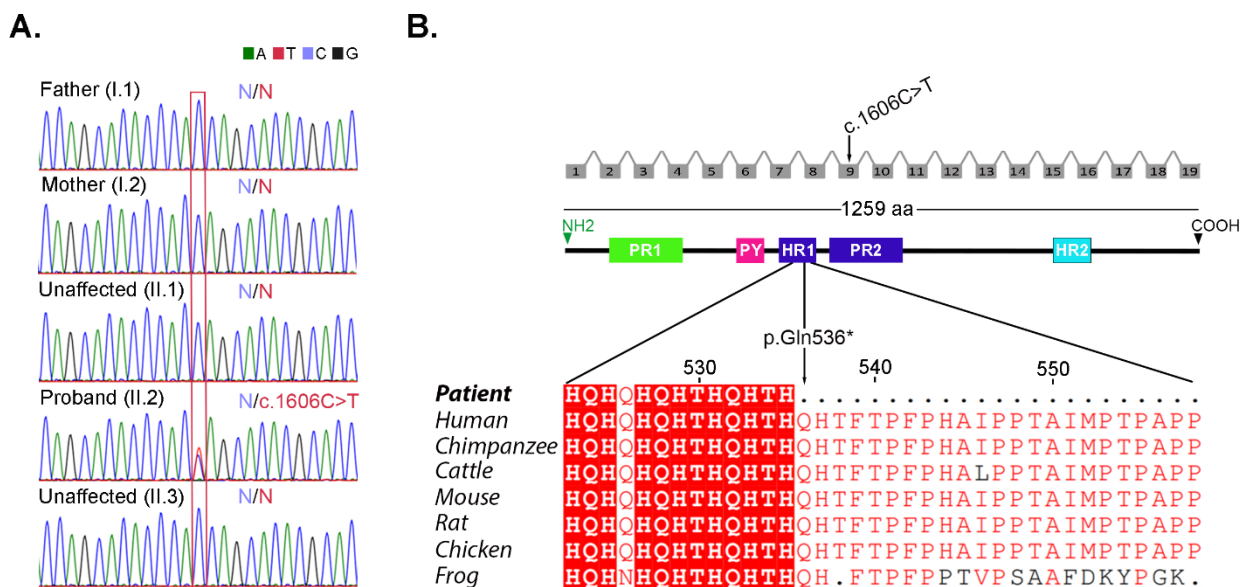
Figure 2. Segregation analysis and partial AUTS2 alignment. A. Sanger sequencing validated the *AUTS2* (c.1606C>T) variant in the affected girl and healthy parents and sisters (N: wild-type allele). B. Schematic illustrating the position of the variant in exon 9 and in the HR1 domain (PR: proline-rich domain; PY: PY domain; HR: histidine-rich domains). C. Partial amnio acid sequence alignment of AUTS2 illustrates the C-terminus region that is missing from the p.Gln536 amino acid residue in the patient, the position of the truncated variant is located in the HR1 domain (Arrow). The sequence of amino acids was obtained from http://www.ncbi.nlm.nih.gov/protein/ website: *Homo sapiens* (Human; NP_056385.1), *Pan troglodytes* (Chimpanzee; XP_009441212.2), *Bos taurus* (Cattle; XP_024841016.1), Mus musculus (Mouse; NP_001350409.1), Rattus norvegicus (Rat; UniProt# F1M388), *Gallus gallus* (Chicken; XP_015151429.1), and *Xenopus tropicalis* (Frog; XP_031752079.1). Alignment was carried out using http://multalin.toulouse.inra.fr/multalin/.

Table 1. Characteristics of the identified *AUTS2* variant.

Chromosome	chr7	
Start	70231237	
End	70231237	
Gene	*AUTS2* (NM_015570)	
Coding	Exon 9	
Variant	7:70231237 C>T c.1606C>T p.Q536*	
Read depth	140	
In-silico tool	Score	Interpretation
LRT	0.412	Deleterious
Mutation Taster	1	Disease causing
CADD	42	Deleterious
DANN	0.998	Deleterious
FATHMM	0.936	Deleterious
PredictSNP2	0.658	Deleterious
FunSeq2	4	Deleterious
BayesDel	0.625	Deleterious
GERP++	5.77	Highly conserved residue
phyloP	7.495	Highly conserved residue

4. Discussion

Pathogenic variants disrupting the *AUTS2* gene have been identified in more than 60 cases with AUTS2 syndrome, an autosomal dominant disorder characterized by developmental delay (DD), intellectual (ID) and mental dysfunction, and various neurodevelopmental manifestations (Sanchez-Jimeno *et al.*, 2021).

In the current study, we described a Syrian family with one affected 5-year-old female who harbors a heterozygous *de novo* nonsense variant (c.1606C>T; p.Gln536*), as it was absent in her parents and the two healthy siblings. According to ACMG guidelines, this variant is classified as a likely pathogenic (Richards *et al.*, 2015) and is predicted to cause a premature termination at (p.Gln536) of the AUTS2 protein. The resultant protein will likely lack the C-terminal domain, suggesting a loss-of-function effect of this variant. Moreover, the altered mRNA transcript could be subjected to nonsense-mediated mRNA decay (NMD) (Maquat, 2004).

The p.Gln536 is located within the histidine-rich region (HX) that contains alternating Histidine-Glutamine (HQ) and Histidine-Threonine (HT) residues (aa 525-542), a highly conserved region in the C-terminal domain, which has a crucial role in neuronal differentiation (Liu *et al.*, 2021).

Most AUTS2 patients carry *de novo* intragenic deletions, whereas missense, nonsense variants, and indels have been reported in a small number of cases (Sanchez-Jimeno *et al.*, 2021; Fair *et al.*, 2023). In the ClinVar database, around 129 AUTS2 variants have been classified as likely pathogenic or pathogenic (accessed on 10 March 2023), of which only 19 are single nucleotide nonsense variants lying upstream or downstream of the identified variant; however, no clinical descriptions were provided. Only two nonsense pathogenic variants have been reported in the literature so far, one of these variants (c.976C>T; p.Gln326*) was reported twice in patients with DD, ID and ASD (Fitzgerald *et al.*, 2015; Kosmicki *et al.*, 2017). The second variant (c.317C>T; p.Gln107*), however, shares some clinical features of our patient (Beunders *et al.*, 2016). The patient in the current study displays typical clinical manifestations of AUTS2 including intellectual developmental disability, microcephaly, substantial motor and language delay, hyperactive behavior, and mild dysmorphic facial features similar to the previously reported case. Additional features such as recurrent seizures, strabismus, scoliosis, frequent salivation, and tight heel cords were only observed in our patient.

In 2013, *Beunders* et al. suggested the AUTS2 syndrome severity score (ASSS) that measures the phenotype's severity and specificity and is categorized into four grades: 0-7, 8-12, 13-18, and 19-31 (Beunders *et al.*, 2013). The ASSS score focuses on around 32 clinical features reported in more than 10% of AUTS2 cases that affect growth parameters, feeding problems, dysmorphic features, skeletal disorders, neurodevelopmental features, as well as congenital anomalies (Hori *et al.*, 2022). The genotype-phenotype correlation (as measured by ASSS means) and the variant site in the *AUTS2* gene have been well established. The ASSS in our case was 14, which is considered high. This value is mostly associated with neurodevelopmental and growth defects. In comparison to previous cases, the median ASSS was 8.5 and 15 for mutations lie in the 5' end (exons 1-8) and 3' end (exons 9-19), respectively.

Our patient carries a truncated mutation in the C-terminal region of AUTS2 protein, which causes severe phenotypes, such as feeding difficulty. Other features were also observed such as squint, ataxia, and frequent salivation, in addition to other manifestations that are rarely seen in AUTS2 patients such as seizures, eczema, and sleeping difficulties. Previous studies have shown that the 3' end of AUTS2 comprises significant functional domains and cases harboring pathogenic variants affecting the C-terminal region of the AUTS2, particularly the HX repeat are significantly associated with more severe manifestations such as microcephaly, feeding difficulty, intellectual disability, and mental retardation (Beunders *et al.*, 2013; Saeki *et al.*, 2019; Martinez-Delgado *et al.*, 2021; Brunet *et al.*, 2021; Fair *et al.*, 2023).

5. Conclusions

In conclusion, this study reports a novel *de novo* loss-of-function variant in a patient with typical features of AUTS2 syndrome. Since this is the third nonsense variant that will be reported in the literature, our findings will expand the mutation spectrum in *AUTS2* gene and its clinical manifestations. However, additional functional experiments are needed to confirm the impact of the identified variant. These results will be helpful in genetic counseling as well as future prenatal testing and preimplantation genetic diagnosis for families with clinical phenotypes related to AUTS2.

References

Aldinger KA, Timms AE, Thomson Z, *et al.* (2019). Redefining the Etiologic Landscape of Cerebellar Malformations. *Am J Hum Genet* **105**:606–615.

Amarillo IE, Li WL, Li X, Vilain E, Kantarci S (2014). De novo single exon deletion of AUTS2 in a patient with speech and language disorder: A review of disrupted AUTS2 and further evidence for its role in neurodevelopmental disorders. *Am J Med Genet A* **164**:958–65.

Anikiej-Wiczenbach P, Mański A, Milska-Musa K, *et al.* (2022). Highly diverse phenotypes of mucopolysaccharidosis type IIIB sibling patients: effects of an additional mutation in the AUTS2 gene. *J Appl Genet* **63**:535–542.

Ben-David E, Granot-Hershkovitz E, Monderer-Rothkoff G, *et al.* (2011). Identification of a functional rare variant in autism using genome-wide screen for monoallelic expression. *Hum Mol Genet* **20**:3632–41.

Beunders G, van de Kamp J, Vasudevan P, *et al.* (2016). A detailed clinical analysis of 13 patients with AUTS2 syndrome further delineates the phenotypic spectrum and underscores the behavioural phenotype. *J Med Genet* **53**:523–32.

Beunders G, De Munnik SA, Van Der Aa N, *et al.* (2015). Two male adults with pathogenic AUTS2 variants, including a two-base pair deletion, further delineate the AUTS2 syndrome. *European Journal of Human Genetics* **23**:803–7.

Beunders G, Voorhoeve E, Golzio C, *et al.* (2013). Exonic deletions in AUTS2 cause a syndromic form of intellectual disability and suggest a critical role for the C terminus. *Am J Hum Genet* **92**:210–20.

Biel A, Castanza AS, Rutherford R, *et al.* (2022). AUTS2 Syndrome: Molecular Mechanisms and Model Systems. *Front Mol Neurosci* **15**:858582.

Brunet T, Jech R, Brugger M, *et al.* (2021). De novo variants in neurodevelopmental disorders—experiences from a tertiary care center. *Clin Genet* **100**:14–28.

Fair SR, Schwind W, Julian DL, *et al.* (2023). Cerebral organoids containing an AUTS2 missense variant model microcephaly. *Brain* **146**:387–404.

Fan Y, Qiu W, Wang L, Gu X, Yu Y (2016). Exonic deletions of AUTS2 in Chinese patients with developmental delay and intellectual disability. *Am J Med Genet A* **170A**:515–522.

Fitzgerald TW, Gerety SS, Jones WD, *et al.* (2015). Large-scale discovery of novel genetic causes of developmental disorders. *Nature* **519**:223–228.

Gieldon L, Jauch A, Obeid K, *et al.* (2021). Germ cell mosaicism for AUTS2 exon 6 deletion. *Am J Med Genet A* **185**:1261–1265.

Hori K, Nagai T, Shan W, *et al.* (2014). Cytoskeletal regulation by AUTS2 in neuronal migration and neuritogenesis. *Cell Rep* **9**:2166–2179.

Hori K, Shimaoka K, Hoshino M (2022). Auts2 gene: Keys to understanding the pathogenesis of neurodevelopmental disorders. *Cells* **11**:11.

Hori K, Yamashiro K, Nagai T, *et al.* (2020). AUTS2 Regulation of Synapses for Proper Synaptic Inputs and Social Communication. *iScience* **23**:101183.

Jolley A, Corbett M, McGregor L, *et al.* (2013). De novo intragenic deletion of the autism susceptibility candidate 2 (AUTS2) gene in a patient with developmental delay: A case report and literature review. *Am J Med Genet A* **161**:1508–12.

Kalscheuer VM, FitzPatrick D, Tommerup N, *et al.* (2007). Mutations in autism susceptibility candidate 2 (AUTS2) in patients with mental retardation. *Hum Genet* **121**:501–9.

Kosmicki JA, Samocha KE, Howrigan DP, *et al.* (2017). Refining the role of de novo protein-truncating variants in neurodevelopmental disorders by using population reference samples. *Nat Genet* **49**:504–510.

Lepagnol-Bestel A-M, Loe-Mie Y, Bensaid M, Simonneau M (2022). AUTS2 expression within mammalian lineage: a predictor of neural networks involved in Autism Spectrum Disorders. *bioRxiv* 2022.12.12.520025.

Liu S, Aldinger KA, Cheng CV, *et al.* (2021). NRF1 Association with AUTS2-Polycomb Mediates Specific Gene Activation in the Brain. *Mol Cell* **81**:4663–4676.

Liu Y, Zhao D, Dong R, *et al.* (2015). De novo exon 1 deletion of AUTS2 gene in a patient with autism spectrum disorder and developmental delay: A case report and a brief literature review. *Am J Med Genet A* **167**:1381–5.

Maquat LE (2004). Nonsense-mediated mRNA decay: Splicing, translation and mRNP dynamics. *Nat Rev Mol Cell Biol* **5**:89–99.

Martinez-Delgado B, Lopez-Martin E, Lara-Herguedas J, *et al.* (2021). De novo small deletion affecting transcription start site of short isoform of AUTS2 gene in a patient with syndromic neurodevelopmental defects. *Am J Med Genet A* **185**:877–883.

Martinez-Granero F, Blanco-Kelly F, Sanchez-Jimeno C, *et al.* (2021). Comparison of the diagnostic yield of aCGH and genome-wide sequencing across different neurodevelopmental disorders. *NPJ Genom Med* **6**:25.

Monderer-Rothkoff G, Tal N, Risman M, *et al.* (2021). AUTS2 isoforms control neuronal differentiation. *Mol Psychiatry* **26**:666–681.

Nagamani SCS, Erez A, Ben-Zeev B, *et al.* (2013). Detection of copy-number variation in AUTS2 gene by targeted exonic array CGH in patients with developmental delay and autistic spectrum disorders. *European Journal of Human Genetics* **21**:343–6.

Oksenberg N, Stevison L, Wall JD, Ahituv N (2013). Function and regulation of AUTS2, a gene implicated in autism and human evolution. *PLoS Genet* **9**:e1003221.

Palumbo P, Di Muro E, Accadia M, *et al.* (2021). Whole exome sequencing reveals a novel AUTS2 in-frame deletion in a boy with global developmental delay, absent speech, dysmorphic features, and cerebral anomalies. *Genes (Basel)* **12**:229.

Pang W, Yi X, Li L, Liu L, Xiang W, Xiao L (2021). Untangle the Multi-Facet Functions of Auts2 as an Entry Point to Understand Neurodevelopmental Disorders. *Front Psychiatry* **12**:580433.

Parenti I, Rabaneda LG, Schoen H, Novarino G (2020). Neurodevelopmental Disorders: From Genetics to Functional Pathways. *Trends Neurosci* **43**.

Richards S, Aziz N, Bale S, *et al.* (2015). Standards and guidelines for the interpretation of sequence variants: A joint consensus recommendation of the American College of Medical Genetics and Genomics and the Association for Molecular Pathology. *Genetics in Medicine* **17**:405–424.

Saeki S, Enokizono T, Imagawa K, *et al.* (2019). A case of autism spectrum disorder with cleft lip and palate carrying a mutation in exon 8 of AUTS2. *Clin Case Rep* **7**:2059–2063.

Sanchez-Jimeno C, Blanco-Kelly F, López-Grondona F, *et al.* (2021). Attention deficit hyperactivity and autism spectrum disorders as the core symptoms of auts2 syndrome: Description of five new patients and update of the frequency of manifestations and genotype-phenotype correlation. *Genes (Basel)* **12**:1360.

Stojanovic JR, Miletic A, Peterlin B, *et al.* (2020). Diagnostic and Clinical Utility of Clinical Exome Sequencing in Children With Moderate and Severe Global Developmental Delay / Intellectual Disability. *J Child Neurol* **35**:116–131.

Sultana R, Yu CE, Yu J, *et al.* (2002). Identification of a novel gene on chromosome 7q11.2 interrupted by a translocation breakpoint in a pair of autistic twins. *Genomics* **80**:129–134.

Yamashiro K, Hori K, Lai ESK, *et al.* (2020). AUTS2 Governs Cerebellar Development, Purkinje Cell Maturation, Motor Function and Social Communication. *iScience* **23**:101820.

Zech M, Jech R, Boesch S, *et al.* (2020). Monogenic variants in dystonia: an exome-wide sequencing study. *Lancet Neurol* **19**:30312–4.

Ziats MN, Ahmad A, Bernat JA, *et al.* (2020). Genotype–phenotype analysis of 523 patients by genetics evaluation and clinical exome sequencing. *Pediatr Res* **87**:735–739.

JJBS

Jordan Journal of Biological Sciences

Examining the Diversity and Abundance of Zooplankton across Different Gateways in the South-western Estuary of Bangladesh

Bhaskar Chandra Majumdar[1,*] , Md. Ariful Haque[2], Ilias Ebne Kabir[3], Md. Foysul Hossain[4], Md. Nur Amin Mukul[5], Aslam Hossain Sheikh[6], Md. Neamul Hasan Shovon[7] and A.S.M. Sadequr Rahman Bhuyain[8]

[1] *Department of Oceanography, Khulna Agricultural University, Khulna- 9100, Bangladesh;* [2] *Department of Oceanography, University of Dhaka, Dhaka- 1000, Bangladesh;* [3] *ECOFISH-II Activity, WorldFish Bangladesh & South Asia, Dhaka, Bangladesh;* [4] *Department of Aquatic Environment and Resource Management, Sher-e-Bangla Agricultural University, Dhaka- 1207, Bangladesh;* [5] *Department of Aquaculture, Bangabandhu Sheikh Mujibur Rahman Agricultural University, Gazipur- 1706, Bangladesh;* [6] *Department of Fisheries, Ministry of Fisheries and Livestock, Bangladesh;* [7] *Integrated Agricultural Unit, Palli Karma-Sahayak Foundation, Dhaka- 1207, Bangladesh;* [8] *Department of Fisheries Technology and Quality Control, Sylhet Agricultural University, Sylhet- 3100, Bangladesh.*

Abstract

The Pasur-Sibsa and Baleshwari River Estuary (PSBE) is the longest estuary located in the southwest part of Bangladesh on the Ganges-Brahmaputra delta which flows into the Bay of Bengal. The study was conducted to investigate the diversity and abundance of the zooplankton from three gateways (S1 station: Pasur river gateway; S2 station: Sibsa river gateway and S3 station: Baleshwari river gateway) in the PSBE from July 2022 to December 2022. Water samples were collected from these gateways using plankton net (55 µm mesh size) and preserved for analyzing in the laboratory. A total of 34 species of zooplankton belonging to 9 orders and 17 families were documented. The dominant orders were Calanoida and Dendrobranchiata, covering 59.52% and 18.20%, respectively. *Acartia bilobata* was the dominant species, while *Sagitta* sp. was the inferior species throughout the gateways. The Pasur river estuary gateway showed the highest percentage of abundance, accounting for 36.39% of the total individuals. The study calculated the Shannon-Wiener Diversity Index, Simpson's Dominance Index, Simpson's Index of Diversity, Margalef's Richness Index, and Evenness ranged from 1.33 to 1.43, 0.24 to 0.30, 0.70-0.76, 1.11 to 1.21, and 0.74-0.80, respectively. The results showed that the zooplankton composition was rich in the S1 station, which serves as a good indicator of marine productivity like zooplankton. The density of zooplankton in a body of water is indicative of the fish stocking rate.

Keywords: Estuary, Zooplankton diversity, Diversity index, Abundance.

1. Introduction

Zooplankton is an assortment of different microscopic or non-microscopic, unseen aquatic organisms that rely on water flowing for movement (Islam, 1999). They migrate hundreds of meters regularly during the day and night despite having very weak swimming abilities. They are known as living machines because they prefer to feed at night on the water's surface, effectively grazing phytoplankton. They frequently serve as a crucial bridge connecting the microbial part and the bigger grazers (Laval-Peuto *et al*., 1986; Pierce and Turner, 1994). All aquatic ecosystems' food chains and food webs are built on zooplankton. Heinbokel (1978) and Fenchel (1987) suggest that zooplankton serve as indicators in aquatic ecosystems due to their wide distribution, small size, rapid metabolism, and diverse species range (Gajbhiye, 2002; Al-Najjar and El-Sherbiny, 2008).

Zooplankton the minute organisms that float around on the ocean's surface and feed either on one another or the microscopic plants that make up phytoplankton.

Zooplankton plays crucial roles in food webs because they control phytoplankton populations by eating them (Wetzel, 2001). The presence of some planktonic groups can also be used to anticipate and determine the health of enclosed, open, and marine water bodies (Ismail and Adnan, 2016; Parmar *et al*., 2016). Therefore, variations in zooplankton density have an impact on phytoplankton dynamics (Carpenter *et al*., 1987). They also have a significant impact on the recycling of nutrients and energy in their particular ecosystems. Fish production depends on the qualitative and quantitative criteria of plankton and its relationship to environmental conditions. The species most suited for culture in different habitats depends on water quality (Dhawan, 2002). The primary factors of fish growth rates and development are the physicochemical characteristics of a water body (Jhingran, 1991). The main productivity of a water body, which serves as the foundation of the aquatic food chains, can be used to quickly determine the water body's overall productivity (Ahmed *et al*., 2004). The primary producers, which are phytoplankton and zooplankton, and the secondary producers make up the plankton community (Battish,

* Corresponding author. E-mail: bhaskar.bsmrau@gmail.com

1992; Ali, 2010). Zooplankton is the most preferable food for fish in the estuarine water body. According to a survey report by the UN's Food and Agriculture Organization (1985), zooplankton is relatively abundant in Bangladesh's tidal zones. Few studies have been done on the abundance of zooplankton and its ecology in the coastal and estuarine environment of Bangladesh. A study on zooplankton of the Bangladeshi coast's southeastern region, Islam and Aziz (1975) discovered a total of 18 genera and 18 species. In their observation of the macro-zooplankton in the Bay of Bengal's continental shelf, Bhuiyan *et al*. (1982) noted the presence and distribution of 18 calanoid copepods. In the coastal estuarine water in the southeast of Bangladesh, Ali *et al*. (1985) observed a periodic change in zooplankton diversity.

At the mouth of the Bay of Bengal, Bangladesh is situated. Bangladesh is a riverine country with numerous rivers, canals, floodplains, ponds, beels, haors, reservoirs, artificial lakes, and a long coastline with estuaries (Majumdar *et al*., 2020; Paul *et al*., 2021; Hemal *et al*., 2017). In Bangladeshi diets, fish alone provides over 63% of animal protein and many of the important vitamins and minerals (Majumdar *et al*., 2016; Majumdar and Rashid, 2017; Shovon *et al*., 2017). One of the top nations in the world for fish production is a country named Bangladesh (Sheikh *et al*., 2018). About 260 freshwater species and 474 marine water fish species are available in Bangladesh (Rahman, 1989; Majumdar, 2017). Both type species are highly preferred zooplankton as food in their diet. In addition to having a large nutrient yield, the near-shore upwelling zone serves as an estuary and is a significant primary producer of phytoplankton and associated zooplankton zones (Al-Nasrawi and Hughes, 2012). As a continuation of the Rupsa river, the Pasur river is significant water body in the Sundarbans region. The Bhairab or Rupsa river flows further south from Khulna, changes its name to Pasur river near Chalna, and then empties into the Bay of Bengal to the right of the islands of Trikona and Dubla. Sibsa river which is densely populated, and located in the region of Khulna in the south part of the country, with 222 inhabitants per square kilometer. The eastern and western borders of Bagerhat District and Barguna District, respectively, are shared by the Baleshwari River. The Haringhata River, which empties into the Bay of Bengal, is where the Baleshwari River empties into Pasur-Sibsa and Baleshwari river estuary (PSBE) are very important wetlands for Bangladesh. This estuary has been polluted day by day due to climate change like global warming; deforestation; industry, agriculture, and livestock farming; rubbish and faecal water dumping; maritime traffic and fuel spillages etc. For these reasons, the biodiversity of fish species is declined for inadequate zooplanktons which serve as food for the fish species. But data and research about primary and secondary production in this area are very inadequate. Therefore, this study aimed to identify the composition of zooplankton and its abundance in the Pasur-Sibsa and Baleshwari river estuary in Bangladesh.

2. Materials and Methods

2.1. Study area

The goal of the current inquiry was to learn about the zooplankton population status in Pasur-Sibsa and Baleshwari River Estuary (PSBE) of Bangladesh. The study region was separated into three sampling stations: Pasur river gateway (S1), Sibsa river gateway (S2), and Baleshwari river gateway (S3) the estuary to gather the data on species populations. Locations ranged from 21°41' to 21°48' North latitude to 89°30' to 89°41' East longitude in the Khulna district (Figure 1).
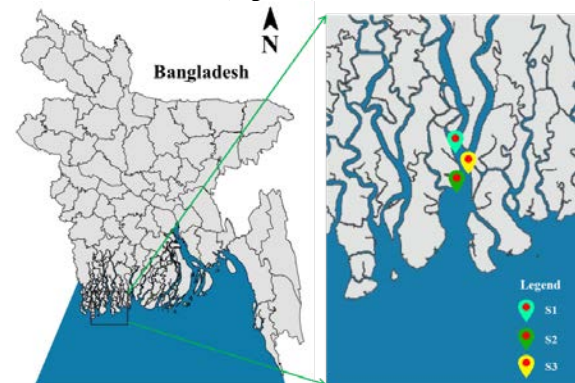
Figure 1: Map depicting the study zone of the Pasur-Sibsa and Baleshwari river estuary, indicating three sampling stations, S1 (Pasur river gateway; 21°47.209'N & 89°30.199'E), S2 (Sibsa river gateway; 21°41.316'N & 89°31.412'E) and S3 (Baleshwari river gateway; 21°48.46'N & 89°41.312'E).

Data were gathered from selected stations between the times of July 2022 to December 2022, which was the high tidal period. This area was expected highly productive because it receives a huge amount of nutrients from upstream.

2.2. Zooplankton sampling and analysis

A net with a cod end to keep the organisms and a mesh size of 55 µm was used to catch zooplankton, which was then dragged horizontally. The net was tilted at each station three times for 45 minutes each as the boat moved (around 20 km/hr) slowly. A sample was taken from the subsurface layer of the water column, specifically between 2 and 5 meters deep. The volume of flow water displaced through the plankton net was used to compute the abundance of organisms, which was then expressed as the number of individuals per cubic meter (Khan *et al*. 2015). The samples were kept in 5% formalin (45% formaldehyde) and labeled in 250 ml dark, sterile plastic bottles as soon as they were collected. Then the samples were taken to the laboratory of the Department of Oceanography under the Faculty of Fisheries and Ocean Sciences, Khulna Agricultural University (KAU) for quantitative and qualitative analysis. A phase contrast light microscope (Model No. XSZ21-05DN) with bright field and phase contrast illumination at magnifications of 16×40 and 16×10 was used to identify the zooplankton species according to the taxonomic references (Idris, 1983; Pennak, 1978; Shiel, 1995) in the laboratory of the Department of Oceanography. Zooplankton quantitative analysis was carried out in a Sedgewick-Rafter counting chamber (S-R cell). Each sample's 1 mL sub-sample was transferred to a Sedgewick-Rafter counter for analysis, and

cells within 10 randomly selected squares of the cells were counted. Using Stirling's (1985) predicted zooplankton density, the cell counts were utilized to calculate the cell density using the formula. The following formula was used to determine the zooplankton abundance; the total number of zooplankton specimens equals the sum of the specimen counts divided by the volume of filtered water and total counts divided by the volume of filtered water equals the total number of specimens of a specific zooplankton taxon.

The Shannon-Wiener Diversity Index (H) of diversity, which was determined by the significant species, was an insensitive indicator of the direction of the S:N (Proportion of entire pattern represented by means of species and complete amount of all individuals of species) connection. Indicator of Shannon-Wiener Diversity Index, $H = -\Sigma [(Pi) \ln (Pi)]$; in which $Pi = (S)/N$, S stands for the entire pattern as represented by species and N is the total number of individuals in the species (Shannon and Wiener, 1963).

For Evenness (E), the following equation was used to estimate, which was a percentage of the total abundance of the many species that make up a region's richness (Pielou, 1966): $E = e^H/S$.

The Simpson's Dominance Index (D) was frequently used to assess the biodiversity of living spaces, which takes into account the quantity of species, just as the plenitude of every species and Simpson's Index of Diversity (1-D) was a proportion of diversity, taking into account the quantity of species present, and the overall abundance of every species, and was calculated using the following equation:

$D = \sum ni(ni-1)/N(N-1)$ and $[1-D] = [1-\sum ni(ni-1)/N(N-1)]$

Where, *ni* was the total number of members of a certain species and *N* was the total number of individuals across all species.

By using the following formula, Margalef's Richness Index (d) was used to calculate the species richness (Margalef, 1968): $d = (S-1)/\ln(N)$, where S was the number of species and N was the sample size.

2.3. Statistical Analysis

One-way ANOVA was used to statistically analyze the zooplankton parameter data using Statgraphics Version 7's statistical package, while Microsoft Excel 2010 was used to plot graphs for results dissemination. The population data was then presented in text, tabular, and Shannon-Wiener Diversity Index (H), Evenness (E), Simpson's Dominance Index (D), Simpson's Index of Diversity (1-D), and Margalef's Richness Index (d) were presented in graphical format for easier comprehension.

3. Results

The order, families and scientific name of zooplankton that are regularly found in the Pasur-Sibsa and Baleshwari river estuary of Bangladesh were presented in Table 1. The current investigation on zooplankton composition in the Pasur-Sibsa and Baleshwari river estuary estimated about 34 species belonging to 09 orders and 17 families. In Table 1, among the identified families, only 01 family belongs to Aphragmophora, 05 to Calanoida, 01 to Cyclopoida, 01 to Cydippida, 03 to Dendrobranchiata, 02 to Harpacticoida, 01 to Lobata, 01 to Onychopoda and 02 to Poecilostomatoida. In our study, the highest number of species was found under the order Calanoida and the lowest under the order Aphragmophora, Cyclopoida, Cydippida, Lobata and Onychopoda. *Acartia bilobata* was the dominant species throughout the investigated area, donated 1644 individuals/m³ covering 16.10% and *Sagitta* sp. was the inferior species, donated 35 individuals/m³ covering 0.34% (Table 1).

About 34 species were found in the investigated area which was divided into three stations following S1, S2, and S3 station. According to their availability state, the percentage of abundance was given that 36.39% of total individuals were found in large at S1 as well as 29.11% in small quantities at S3 in the Pasur-Sibsa and Baleshwari river estuary (Figure 2).

Table 1. List of identified main species of zooplankton together with their numbers and percentage at the Pusur-Sibsa and Baleshwari river estuary.

Order	Family	Species	Total	Percent (%) within group	Overall (%)
Aphragmophora	Sagittidae	*Sagitta* sp.	35	100	0.34
Calanoida	Calanidae	*Calanus finmarchicus*	173	2.85	1.69
	Metridinidae	*Metridia lucens*	220	3.62	2.15
	Calanidae	*Calanus pacificus*	244	4.02	2.39
	Acartiidae	*Acartia bilobata*	1644	27.06	16.10
	Diaptomidae	*Leptodiaptomus minutus*	836	13.76	8.19
	Diaptomidae	*Skistodiaptomus mississippiensis*	312	5.13	3.06
	Acartiidae	*Acartia negligens*	313	5.15	3.07
	Acartiidae	*Acartia bifilosa*	384	6.32	3.76
	Acartiidae	*Acartia clause*	258	4.25	2.53
	Acartiidae	*Acartia tranteri*	328	5.40	3.21
	Acartiidae	*Acartia hudsonica*	318	5.23	3.11
	Pontellidae	*Calanopia* sp.	143	2.35	1.40
	Calanidae	*Calanus* sp.	364	5.99	3.57
	Diaptomidae	*Leptodiaptomus sicilis*	201	3.31	1.97
	Metridinidae	*Metridia pacifica*	338	5.56	3.31
Cyclopoida	Oithonidae	*Oithona* sp.	247	100	2.42
Cydippida	Pleurobrachiidae	*Pleurobrachia* sp.	150	100	1.47
Dendrobranchiata	Sergestidae	*Acetes erythraeus*	314	16.90	3.08
	Sergestidae	*Acetes indicus*	115	6.19	1.13
	Sergestidae	*Acetes japonicus*	209	11.25	2.05
	Luciferidae	*Lucifer* sp.	112	6.03	1.10
	Penaeidae	*Metapenaeus brevicornis*	202	10.87	1.98
	Penaeidae	*Metapenaeus monoceros*	209	11.25	2.05
	Penaeidae	*Penaeus indicus*	164	8.83	1.61
	Penaeidae	*Penaeus merguiensis*	199	10.71	1.95
	Penaeidae	*Penaeus monodon*	58	3.12	0.57
	Sergestidae	*Sergestes similis*	276	14.85	2.70
Harpacticoida	Euterpinidae	*Euterpina acutifrons*	399	75.28	3.91
	Ectinosomatidae	*Microsetella* sp.	131	24.72	1.28
Lobata	Bolinopsidae	*Bolinopsis vitrea*	161	100	1.58
Onychopoda	Podonidae	*Evadue* sp.	239	100	2.34
Poecilostomatoida	Ergasilidae	*Ergasilus* sp.	671	73.49	6.57
	Oncaeidae	*Oncaea* sp.	242	26.51	2.37

During the investigation period, around 15 species of the Calanoida orders were seen i.e. *Calanus finmarchicus*, *Metridia lucens*, *Calanus pacificus*, *Acartia bilobata*, *Leptodiaptomus minutu*, *Skistodiaptomus mississippiensis*, *Acartia negligens*, *Acartia bifilosa*, *Acartia clause*, *Acartia tranteri*, *Acartia hudsonica*, *Calanopia* sp., *Calanus* sp., *Leptodiaptomussicilis*, and *Metridia pacifica* etc. Out of these 15 different species, *Acartia bilobata* was more prevalent than the others. The present study found about 34 species from the three sampling stations in the study area, demonstrating the abundance of zooplankton fauna that exists in the Pasur-Sibsa Baleshwari river estuary. Table 2 showed that the dominance of identified species among the three sampling stations in accordance with species. At station S1 (Pasur river gateway) most dominant species were *Acartia bilobata*, *Leptodiaptomus minutus*, *Skistodiaptomus mississippiensis*, *Acartia bifilosa*, *Acartia*

clause, *Calanus pacificus*, *Leptodiaptomus sicilis*, *Metridia pacifica*, and *Microsetella* sp. showed in Figure 3.
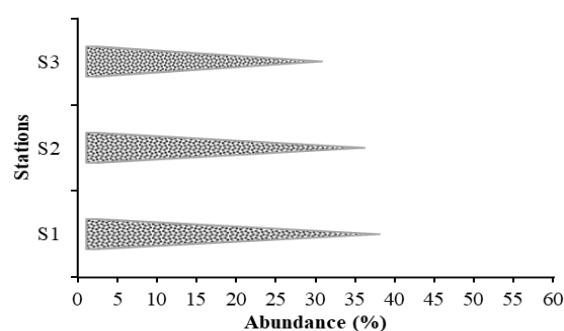
Figure 2: Abundance status of zooplankton population found in the Pusur-Sibsa and Baleshwari river estuary.

Table2: Dominance list of identified zooplankton species at Pusur-Sibsa and Baleshwari river estuary on the basis of sampling stations.

Order	Family	Species	Study area (Stations)		
			S1	S2	S3
Aphragmophora	Sagittidae	*Sagitta* sp.			✓
Calanoida	Calanidae	*Calanus finmarchicus*		✓	
	Metridinidae	*Metridia lucens*			✓
	Calanidae	*Calanus pacificus*	✓		
	Acartiidae	*Acartia bilobata*	✓		
	Diaptomidae	*Leptodiaptomus minutus*	✓		
	Diaptomidae	*Skistodiaptomus mississippiensis*	✓		
	Acartiidae	*Acartia negligens*		✓	
	Acartiidae	*Acartia bifilosa*	✓		
	Acartiidae	*Acartia clause*	✓		
	Acartiidae	*Acartia tranteri*		✓	
	Acartiidae	*Acartia hudsonica*		✓	
	Pontellidae	*Calanopia* sp.		✓	
	Calanidae	*Calanus* sp.			✓
	Diaptomidae	*Leptodiaptomus sicilis*	✓		
	Metridinidae	*Metridia pacifica*	✓		
Cyclopoida	Oithonidae	*Oithona* sp.		✓	
Cydippida	Pleurobrachiidae	*Pleurobrachia* sp.	✓		
Dendrobranchiata	Sergestidae	*Acetes erythraeus*	✓		
	Sergestidae	*Acetes indicus*		✓	
	Sergestidae	*Acetes japonicus*			✓
	Luciferidae	*Lucifer* sp.	✓		
	Penaeidae	*Metapenaeus brevicornis*		✓	
	Penaeidae	*Metapenaeus monoceros*	✓		
	Penaeidae	*Penaeus indicus*			✓
	Penaeidae	*Penaeus merguiensis*	✓		
	Penaeidae	*Penaeus monodon*		✓	
	Sergestidae	*Sergestes similis*		✓	
Harpacticoida	Euterpinidae	*Euterpina acutifrons*			✓
	Ectinosomatidae	*Microsetella* sp.			✓
Lobata	Bolinopsidae	*Bolinopsis vitrea*	✓		
Onychopoda	Podonidae	*Evadue* sp.			✓
Poecilostomatoida	Ergasilidae	*Ergasilus* sp.			✓
	Oncaeidae	*Oncaea* sp.			✓

In Figure 4, *Acartia bilobata*, *Calanus finmarchicus*, *Acartia negligens*, *Acartia tranteri*, *Euterpina acutifrons*, and *Acartia hudsonica* were the dominant species, found at Sibsa river gateway (S2). Similarly, *Acartia bilobata*, *Ergasilus* sp., *Metridia lucens*, *Acartia bifilosa*, *Euterpina acutifrons*, and *Microsetella* sp. were found at Baleshwari river gateway (S3) which was showed dominance among the others (Figure 5). Figure 6 illustrates the percentage of zooplankton in different orders. In particular, Dendrobranchiata (18.20%) showed considerable dominance among the orders, but Calanoida (59.52%) being the most dominant order.
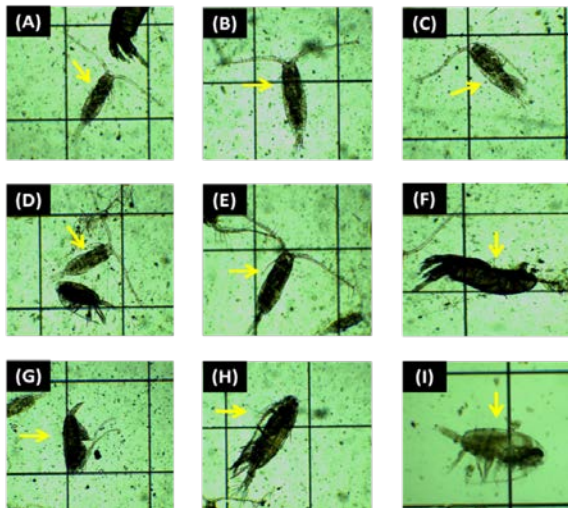
Figure 3. Photographic view of dominant major species of zooplankton (A) *Acartia bilobata*, (B) *Leptodiaptomus minutus*, (C) *Skistodiaptomus mississippiensis*, (D) *Acartia bifilosa*, (E) *Acartia clause*, (F) *Calanus pacificus*, (G) *Leptodiaptomus sicilis*, (H) *Metridia pacifica* and (I) *Microsetella* sp. found at Pasur river gateway (S1).
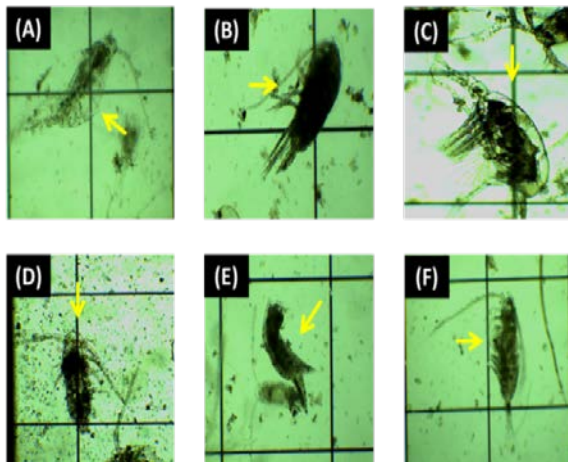
Figure 4. Photographic view of dominant major species of zooplankton (A) *Acartia bilobata*, (B) *Calanus finmarchicus*, (C) *Acartia negligens*, (D) *Acartia tranteri*, (E) *Euterpina acutifrons* and (F) *Acartia hudsonica* found at Sibsa river gateway (S2).
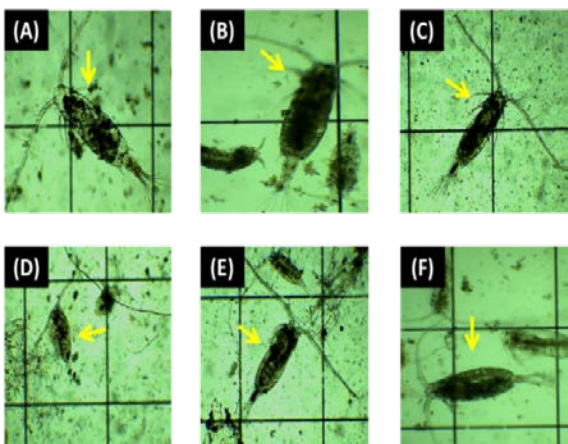
Figure 5. Photographic view of dominant major species of zooplankton (A) *Acartia bilobata*, (B) *Ergasilus* sp., (C) *Metridia lucens*, (D) *Acartia bifilosa*, (E) *Euterpina acutifrons* and (F) *Microsetella* sp. found at Baleshwari river gateway (S3).

On the contrary, Poecilostomatoida, Harpacticoida, Cyclopoida, Onychopoda, Lobata, Cydippida and Aphragmophora showed the least dominance established 8.94%, 5.19%, 2.42%, 2.34%, 1.58%, 1.47% and 0.34% contribution to the community, respectively (Figure 6). Additionally, throughout the study period, the family Acartiidae of the order Calanoida demonstrated dominance over the zooplankton fauna network of the research area (Figure 6). The families that contributed the fewest species to the network were the Sagittidae, Oithonidae, Pleurobrachiidae, Bolinopsidae, and Podonidae families throughout the study period.

Figure 7 showed the station-wise values for the Simpson's Index of Diversity (1-D), Margalef's Richness Index (d), Shannon-Wiener Diversity Index (H), Simpson's Dominance Index (D), and Evenness (E). Among these sampling stations, the S1 station had the greatest Shannon-Wiener Diversity Index value (1.43) designating the zooplankton-rich area, while the S2 station had few prosperities of zooplankton with the lowest value (1.33). Simpson's Dominance Index (D) was calculated to have the highest value in the S2 station (0.30), followed by S3 station (0.28) and S1 station (0.24), respectively. The highest Simpson's Index of Diversity value (0.76) found in S1 station, and the S2 station showed the lowest value (0.70). The greatest value for Margalef's Richness Index was 1.21 at the S1 station, while the lowest value was 1.11 at the S3 station. The S1 station recorded the maximum Evenness value was 0.80 and the minimum Evenness value was 0.74 at the S3 station (Figure 7). In contrast, the S1 station expressed a rich zooplankton profile because of its high value at Simpson's Index of Diversity, Margalef's Richness Index, and Evenness. Margalef's Richness Index ranged from 1.11 to 1.21 in the current study. This value serves as a marker to distinguish between sampling stations while also indicating a species-based variance (Vyas *et al*., 2012). The highest Margalef Richness Index value, however, represents the most population in the study area. Consequently, the sampling S1 station has a Margalef's Richness Index higher than other study stations, indicating the presence of noticeably more individuals (Figure 7).
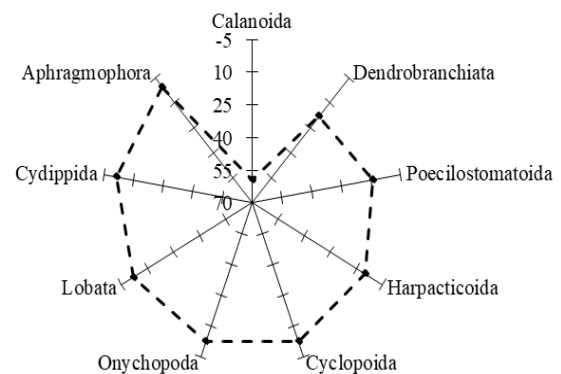
Figure 6: Zooplankton percentage based on the order in the Pusur-Sibsa and Baleshwari river estuary.
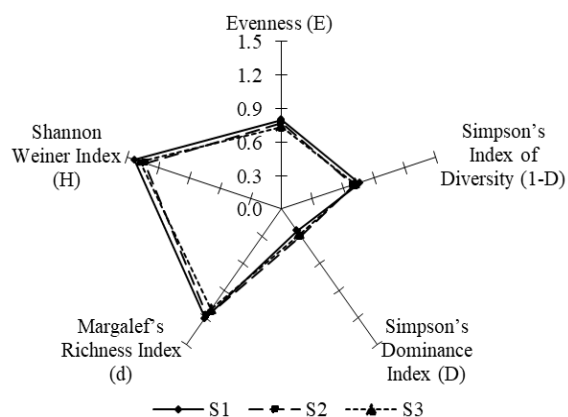
Figure 7: Distinct species diversity index of sampling stations of Pusur-Sibsa and Baleshwari river estuary.

4. Discussion

Researchers had identified 33 salt marsh estuary species (Abu-Hena *et al*., 2016) and 88 mangrove demersal zooplankton species (Melo *et al*., 2010). Around 48 species of zooplankton were discovered by Matias-Peralta and Yusoff (2015) in the Merambong Seagrass Meadow while 129 species were discovered in the Tinggi and Sibu Islands, all in Malaysia (Metillo *et al*., 2019).

According to Deepika *et al*. (2019), the density of zooplankton found in Indian seagrass meadows (89,300 to 935,300 individuals/m^3) was much higher than that found in the current study. Compared to the current study, Melo *et al*. (2010) discovered significantly lower zooplankton abundance (4,759 to 7,113 individuals/m^3) in the south-western Atlantic, and Azmi *et al*. (2016) found zooplankton abundance (3,030±855.6 individuals/m^3) at Merambong Shoal Seagrass Area, which is also lower than densities recorded in the present study. Zooplankton density measurements from certain river estuaries in the Sarawak Region of Malaysia ranged from 447 to 27,812 individuals/m^3 (Aiman *et al*., 2020). Overall, past findings supported the current results (Bhavan *et al*., 2015; Dhanasekaran *et al*., 2017; Manickam, 2015; Manickam *et al*., 2012; Manickam *et al*., 2014; Manickam *et al*., 2015). Within the orders, the highest number of species was *Acartia bilobata* (27.06%) and the lowest was *Calanopia* sp. (2.35%) in the order of Calanoida. Similarly, the highest and the lowest amount species were *Acetes erythraeus* (16.90%), *Euterpina acutifrons* (75.28%), *Ergasilus* sp. (73.49%) and *Penaeus monodon* (3.12%), *Microsetella* sp. (24.72%), *Oncaea* sp. (26.51%) in the order of Dendrobranchiata, Harpacticoida, and Poecilostomatoida, respectively. On the other hand, *Sagitta* sp., *Oithona* sp., *Pleurobrachia* sp., *Bolinopsisvitrea*, and *Evadue* sp. were the only species found under the order of Aphragmophora, Cyclopoida, Cydippida, Lobata, and Onychopoda, respectively. The richness of nutrients, accessibility of rich phytoplankton, and ocean circulation may have contributed to the diverse species and groups of zooplankton that were discovered. The results, however, are consistent with the research from Aiman *et al*. (2020), Azmi *et al*. (2016), Deepika *et al*. (2019), Melo *et al*. (2010), Matias-Peralta and Yusoff (2015).

Abdul *et al*. (2016) conducted a study in an estuary and found a relative abundance that was higher than any zooplankton species. According to Melo *et al*. (2010), copepods always had a higher relative abundance than any other zooplankton group. According to Tonapi (1980), the distribution of different species was influenced by physico-chemical factors such as water's conductivity, pH, chloride, and free CO_2 level as well as temperature.

Calanoida was found to be prominent in all groups in the current study among all orders of zooplanktons due to its distribution and similarity to results previously noted by several studies, including Abdullahi *et al*. (2007), Adeyemi *et al*. (2009), APHA (1989), Benarjee *et al*. (2008), Balamurugan *et al*. (1999). Similar findings have also been made by Boxshall and Evstigneeva (1994), Davies *et al*. (2009), Devika *et al*. (2006), Gayathri *et al*. (2014), Goswami and Mankodi (2012), Jalilzadeh *et al*. (2007), MVSSS (2000), Raghunathan and Kumar (2002).

The bulk of the copepod species from the genera *Paracalanus*, *Oithona*, and *Acartia* are found in abundance on near shore and in estuaries in Malaysian seas (Chew and Chong, 2011). The identified groups Appendicularia (2.46%), Chaetognatha (2.45%), Cladocera (2.31%), Copepoda (26.05%), Ctenophora (5.86%), Crustacean zooplankton (21.64%), Ichthyoplankton (17.77%) and Meroplankton (21.45%) were found at Sitakunda coast of Chittagong, Bangladesh (Khan *et al*. 2015). In the coastal seas of Malaysia, the copepod species *P. crassirostris*, *P. parvus* and *Bestiolina similis* were established dominating species (Johan *et al*., 2013; Matias-Peralta and Yusoff, 2015; Rezai *et al*., 2004). According to reports, *Oithona simplex* predominates in inshore and shallow seas, is suited to low salinity water, and is common in mangrove estuaries (Johan *et al*., 2013). The major dominant species were characterized by visual inspection using a light microscope according to the basis of stations (Figures 3, 4 & 5). The distribution patterns and species composition of plankton are significantly influenced by the physico-chemical characteristics and nutrient content of lake water (Horne and Goldman, 1994; Mahar *et al*., 2000; Omoregie, 2017).

Rajashekhar *et al*. (2010) further supported our findings by confirming a higher number of zooplankton genera and discovered 24 species, of which 10 species are Rotifera, 6 species are Cladocera, 5 species are Copepoda, and 3 species are Ostracoda. Their study's results on a group level are consistent with ours. However, Hossain *et al*. (2006), Rahman and Hussain (2008), Roy *et al*. (2010), Das *et al*. (2011) had all found fewer zooplankton genera than the current study. However, earlier works had also observed similar outcomes (Bhavan *et al*., 2015; Dede and Deshmukh, 2015; Dhanasekaran *et al*., 2017; Ezhili *et al*., 2013; Manickam *et al*., 2012, Manickam *et al*., 2014, Manickam *et al*., 2015; Patel *et al*., 2013; Thirupathaiah *et al*., 2011; Watkar and Barbate, 2013).

A lower Simpson's Dominance Index value indicates a higher zooplankton population (Majumdar *et al*., 2020). The plankton diversity index, according to Magurran (1988), refers to the quantification of variety in a sample or community as a single number. Due to the fact that all fish species will produce an equally plentiful population, which will consider the diversity. In order to compare the estimated values in three specifically chosen locations of the Pasur-Sibsa and Baleshwari river estuary, multiple

diversity index assessments were carried out for the analysis of zooplankton diversity. But the Shannon-Wiener Diversity Index (H) varied from 1.33 to 1.43 at various sites in the area under investigation (Figure 7). The average value of species diversity in the current study served to show the health of the chosen ecosystem. Higher Shannon-Wiener Diversity Index (H) values and zooplankton populations were noted by Das (1996) and Manickam *et al.* (2012) during their research period. Lower zooplankton species diversity in the area denotes significant pollution, which is harmful to the aquatic ecology (Manickam *et al.*, 2015; Ismail and ELawad, 2015). In stressed and contaminated ecosystems, there appears to be less variety of zooplankton species (Bass and Harrel, 1981). The most often used biodiversity measure for assessing species variety is Margalef's Richness Index (d).

The Evenness (E) value, which ranged from 1 to 0, counts the number of members of a species. When compared to other periods, the tidal period had very high species equitability (Evenness), which suggests that the diversity of the plankton was declining (Adesalu and Nwankwo, 2008). Studies by Abu-Hena *et al.* (2016), Aiman *et al.* (2020), Deepika *et al.* (2019), Ismail and Zaidin (2015) were found to have similar findings to the present study. Additionally, Simpson's Dominance Index (D), a measure of diversity, takes both the total number of species present and the relative abundance of each species into account. Generally, the Simpson's Dominance Index (D) value spans from 0 to 1, and the greater the range of values, the less biodiversity is often represented. As a result, while considering the Simpson's Dominance Index (D) value into account, it was discovered that the S1 location was the most enriched with species variety and the S2 site was the least enriched. The Simpson's Index of Diversity (1-D), on the other hand, is dependent upon the Simpson's Dominance Index (D), where S1 and S2 were found to have the highest and lowest Simpson's Index of Diversity (1-D), respectively. Thus, the S1 area has a wide variety of species. The temporal fluctuation in dominant status among the three sampling locations may be the cause of this slight discrepancy. Finally, this investigation demonstrated the variety and abundance of zooplankton in various regions of the Pasur-Sibsa and Baleshwari river estuaries. Based on different biodiversity index outcomes, we can declare that sampling station S1 (Pasur river gateway) is comparatively rich in zooplankton biodiversity.

5. Conclusion

Zooplankton diversity strongly impacts estuary health, serving as a key indicator of marine productivity and environmental well-being. About 34 species from the diversity of zooplankton's nine orders and seventeen families were counted in the current study. This study established that sampling station S1 (Pasur river gateway) was rich in zooplankton profile. The biodiversity is currently in threat owing to global warming; deforestation; industry, agriculture and livestock farming; rubbish and waste water dumping; maritime traffic, fuel spillages and others human activity. Maintaining updated knowledge of the aquatic species diversity like fish biodiversity is necessary for the conservation of biodiversity. Future research can be done to improve fish production and protect the diversity of zooplankton in the Pasur-Sibsa and Baleshwari river estuary in Khulna, Bangladesh. Based on the estuary's current condition, this study may be useful for the growth of fisheries production in the future.

Conflict of interests

The authors declare no conflicting interests.

References

Abdul WO, Adekoya EO, Ademolu, KO, Omoniyi, IT, Odulate DO, Akindokun TE and Olajide AE. 2016. The effects of environmental parameters on zooplankton assemblages in tropical coastal estuary, South-west, Nigeria. *Egypt J Aquat Res.*, **42(3)**: 281-287. https://doi.org/10.1016/j.ejar.2016.05.005

Abdullahi HA, Azionu BC and Ajayi O. 2007. Check list of zooplankton in culture tanks, at NIFFR Green House, New Bussa. Proceedings of the 22nd Annual Conference of Fisheries Society of Nigeria (FISON), 290 pp.

Abu-Hena MK, Idris MH, Johan I, Nesarul NH, Aysha A and Islam MS. 2016. Seasonal distribution of zooplankton composition and abundance in a sub-tropical mangrove and salt marsh estuary. *Malaysian J Sci.*, **35(2)**: 275-289. https://mjs.um.edu.my/article/view/6349

Adesalu TA and Nwankwo DI. 2008. Effect of water quality indices on phytoplankton of a sluggish tidal creek in Lagos, Nigeria. *Pak J Biol Sci.*, **11(6)**: 836-844.

Adeyemi SO, Adikwu IA, Akombu PM and Iyela JT. 2009. Survey of zooplanktons and macro-invertebrates of Gbedikere Lake, Bassa Local Government Area, Kogi State Nigeria. *Int J Trop Agric Food Sys.*, **3(4)**: 274-278.

Ahmed KKU, Hasan KR, Ahamed SU, Ahmed T andMustafa G. 2004. Ecology of Shakla beel (Brahmanbaria), Bangladesh. Bangladesh Fisheries Research Institute, Riverine station, Chandpur 3602, Bangladesh. *Bangladesh J Fish.*, **9**: 101-110.

Aiman WM, Yusoff FM, Arshad A, Kamal AHM, Ismail J, Idris MH, Karim NU and Al-Asif AB. 2020. Distribution of zooplankton community in Toli shad (*Tenualosa toli*) habitats, Sarawak, Malaysia. *Biodiversitas*, **21(9)**. https://doi.org/10.13057/biodiv/d210913

Ali A, Sukanta S and Mahmood N. 1985. Seasonal abundance of plankton in Moheskhali channel, Bay of Bengal. In Proceeding of SAARC Seminar on Protection of Environment from Degradation, 128-140 pp.

Ali LA. 2010. Seasonal variation in physico-chemical properties and zooplankton biomass in greater Zab River, Iraq. *Jordan J. Biol. Sci.*, **3(3)**: 115-120.

Al-Najjar TH and El-Sherbiny MM. 2008. Spatial and seasonal variations in biomass and size structure of zooplankton in coastal waters of the Gulf of Aqaba. *Jordan J. Biol. Sci.*, **1(2)**: 55-59.

Al-Nasrawi HG and Hughes AR. 2012. Fungal diversity associated with salt marsh plants *Spartina alterniflora* and *Juncus roemerianus* in Florida. *Jordan J. Biol. Sci.*, **5(4)**: 247-254.

APHA. 1989. Standard methods for the examination water and waste water. American public health Association, 19th Edition Washington, USA.

Azmi AA, Yoshida T, Toda T, Ross OBH and Cob ZC. 2016. Comparison of zooplankton abundance and community in seagrass and non-seagrass areas of Merambong shoal. In AIP Conference Proceedings (vol. 1784, no. 1, p. 060002). AIP Publishing LLC. https://doi.org/10.1063/1.4966840

Balamurugan S, Mohideen BG and Subramanian P. 1999. Biodiversity of zooplankton in Cauveri river at Tirucherapalli, Tamilnadu. *J Aquat Biol.*, **14(1)**: 21-25.

Bass D and Harrel RC. 1981. Water quality of a southeast Texas stream. *Hydrobiologia*, **76(1)**: 69-79.

Battish SK. 1992. Freshwater zooplankton of India Oxford & IBH Publishing Co. Pvt. Ltd., New Delhi, India.

Benarjee G, Srikanth K, Ramu G, Ramulu KN and Ravinder B. 2008. The climatic influence on zooplanktonic population in historical lake of Kakatiya Dynasty. In Proc. of 8th Indian Fisheries Forum, 22-26 pp.

Bhavan PS, Selvi A, Manickam N, Srinivasan V, Santhanam P and Vijayan P. 2015. Diversity of zooplankton in a perennial Lake at Sulur, Coimbatore, India. *Int J Extensive Res.*, **5**: 31-44.

Bhuiyan AL, Mohi SA, Khair SA and Das NG. 1982. Macro-zooplanktons of the continental shelf of the Bay of Bengal. *Chittagong Uni. Stud.*, **6**: 51-59.

Boxshall GA and Evstigneeva TD. 1994. The evolution of species flocks of copepods in Lake Baikal: a preliminary analysis. *Ergeb Limnol.*, **44**: 235-246.

Carpenter SR, Kitchell JF, Hodgson JR, Cochran PA, Elser JJ, Elser MM, Lodge DM, Kretchmer D, He X and Ende C. 1987. Regulation of lake primary productivity by food web structure. *Ecology*, **68(6)**: 1863-1876.

Chew LL and Chong VC. 2011. Copepod community structure and abundance in a tropical mangrove estuary, with comparisons to coastal waters. *Hydrobiologia*, **666(1)**: 127-143. https://doi.org/10.1007/s10750-010-0092-3

Das DR, Haque MR, Choudury BBP, Haque MA and Alam MN. 2011. Study on monthly variations of plankton in relation to the physico-chemical condition of rice-fish fields in boro season. *Int J Sustain Crop Prod.*, **6(1)**: 43-49.

Das MC. 1996. Fundamentals of ecology. New Delhi, India: Tata McGraw-Hill Publishing.

Davies OA, Abowei JFN and Otene BB. 2009. Seasonal abundance and distribution of plankton of Minichinda stream, Niger Delta, Nigeria. *Am J Sci Res.*, **2(2)**: 20-30.

Dede AN and Deshmukh AL. 2015. Study on zooplankton composition and seasonal variation in Bhima river near Ramwadi village, Solapur District (Maharashtra), India. *Int J Curr Microbiol Appl Sci.*, **4(3)**: 297-306.

Deepika S, Srinivasan A, Padmavathy P and Jawahar P. 2019. Diversity of zooplankton in seagrass ecosystem of Mandapam coast in Gulf of Mannar. *Int J Curr Microbiol Appl Sci.*, **8(7)**: 2034-2042.

Devika R, Rajendran A and Selvapathy P. 2006. Variation studies on the physico-chemical and biological characteristics at different depths in model waste stabilsation tank. *Pollut Res.*, **25(4)**: 771.

Dhanasekaran M, Bhavan PS, Manickam N and Kalpana R. 2017. Physico-chemical characteristics and zooplankton diversity in a perennial lake at Dharmapuri (Tamil Nadu, India). *J Entomol Zool Stud.*, **5(1)**: 285-292.

Dhawan CJ. 2002. Marine Botany. 2nd edition. John Wiley and Sons Inc., New York, USA.

Ezhili N, Manikandan R and Ilangovan R. 2013. Diversity and seasonal variation of zooplankton in Ukkadam lake, Coimbatore, Tamil Nadu, India. *Int J Curr Res.*, **5(8)**: 2091-2094.

Fenchel T. 1987. Ecology of protozoa- The biology on free-living phagotrophic protists Science Tech Publishers. Madison, Wisconsin.

Food and Agriculture Organization of the United Nations (FAO). 1985. Report on tidal area study (Fisheries Resources Survey System. FAO/UNDP-BGD/79/015). Dhaka, Bangladesh: FAO, 32 pp.

Gajbhiye SN. 2002. Zooplankton- Study methods, importance and significant observations. In: Quardros G, (Ed.) The National Seminar on Creeks, Estuaries and Mangroves - Pollution and Conservation, 28- 30th November, 2002, Thane, 21-27 pp.

Gayathri S, Latha N and Ramachandra MM. 2014. Studies on population dynamics and seasonal abundance of zooplankton community in Doddavoderahalli lake, Bangalore. *Int J Emerg Trends Eng Dev.*, **1(4)**: 50-55.

Goswami AP and Mankodi PC. 2012. Study on zooplankton of fresh water reservoir Nyari–II Rajkot district, Gujarat, India. *ISCA J. Bio. Sci.*, **1(1)**: 30-34.

Heinbokel JF. 1978. Studies on the functional role of tintinnids in the Southern California Bight. I. Grazing and growth rates in laboratory cultures. *Mar Biol.*, **47(2)**: 177-189.

Hemal S, Uddin MS, Uddin MS, Majumdar BC, Rasul MG and Alam MT. 2017. Present status and problems of fish seed marketing in Sylhet district, Bangladesh. *Res Agri Liv Fish.*, **4(1)**: 45-54. http://dx.doi.org/10.3329/ralf.v4i1.32405

Horne AJ and Goldman CR. 1994. Limnology. McGraw-Hill Science, Engineering & Mathematics. New York, 576 pp.

Hossain MY, Begum M, Ahmed ZF, Hoque MA, Karim MA and Wahab MA. 2006. A study on the effects of iso-phosphorus fertilizers on plankton production in fish ponds. *S Pac Stu.*, **26(2)**: 101-110.

Idris BAG. 1983. Freshwater zooplankton of Malaysia (Crustacea: Cladocera). Malaysia: Universiti Pertanian Malaysia, Serdang, Selangor, 10-151 pp.

Islam A. 1999. Pholito Matshyo Bijnan. Bangla Academy Dhaka, 1000. 5-10 pp.

Islam AKMN and Aziz A. 1975. A preliminary study on zooplankton of the North-Eastern Bay of Bengal, Bangladesh. *Bangladesh J Zool.*, **3(2)**: 125-138.

Ismail AH and Adnan AAM. 2016. Zooplankton composition and abundance as indicators of eutrophication in two small man-made lakes. *Trop Life Sci Res.*, **27(1)**: 31-38. https://doi.org/10.21315/tlsr2016.27.3.5

Ismail AH and Zaidin SA. 2015. A comparative study of zooplankton diversity and abundance from three different types of water body. In 2nd International Conference on Agriculture, Environment and Biological Sciences (ICAEBS'15), Bali, Indonesia, 16-17thAugust, 2015, 37-41 pp.

Ismail IM and ELawad AA. 2015. Phytosociological analysis and species diversity of herbaceous layer in Rashad and Alabassia localities, South Kordofan State, Sudan. *Jordan J. Biol. Sci.*, **8(2)**: 151-157.

Jalilzadeh AK, Yamakanamardi SM and Altaff K. 2007. Abundance of zooplankton in three contrasting lakes of Mysore city, Karnataka state, India. In Proceedings of Taal, 2007: The 12th World Lake Conference, 464-469 pp.

Jhingran VG. 1991. Fish and Fisheries of India. 3rd Edition, Hindustan Pub. Co., New Delhi, 727 pp.

Johan I, Hena MA, Idris MH and Arshad A. 2013. Taxonomic composition and abundance of zooplankton Copepoda in the coastal waters of Bintulu, Sarawak, Malaysia. *J Fish Aquat Sci*., **8(3)**: 472-479. https://doi.org/10.3923/jfas.2013.472.479

Khan MSK, Uddin SA and Haque MA. 2015. Abundance and composition of zooplankton at Sitakunda coast in Chittagong, Bangladesh. *Res Agri Liv Fish*., **2(1)**: 151-160.

Laval-Peuto M, Heinbokel JF, Anderson OR, Rassoulzadegan F and Sherr BF. 1986. Role of micro-and nanozooplankton in marine food webs. *Int J Trop Insect Sci*., **7(3)**: 387-395.

Magurran AE. 1988. Ecological diversity and its measurement. Princeton University Press.

Mahar MA, Baloch WA and Jafri SIH. 2000. Diversity and seasonal occurrence of planktonic rotifers in Manchar Lake, Sindh, Pakistan. *Pak J Fish*., **1(1)**: 25–32.

Majumdar BC and Rashid I. 2017. Microbiological properties of dry salted Hilsa, *Tenualosa ilisha* (Hamilton, 1822) fish of Bangladesh. *J Fish. Life Sci*., **2(2)**: 4-9.

Majumdar BC, Paul SI, Hasan M, Kabir T, Islam M and Kabir IE. 2020. Fish biodiversity assemblages and fishing gears used at Chinadi Beel in Narsingdi District of Bangladesh. *Int J Agric Environ Biotechnol*., **13(4)**: 403-413. https://doi.org/10.30954/0974-1712.04.2020.4

Majumdar BC, Shaha DC, Rasul MG and Khan M. 2016. Fish production in floodplain of Bangladesh: A Review. *Int J Natural Sci*., **6(2)**: 89–95.

Majumdar BC. 2017. Comparison of the changes in nutritional quality of three important small indigenous fish species in Bangladesh at room temperature (27-31 ˚C): A review. *J Ani Res Nutr*., **2(2)**: 15.

Manickam N, Bhavan PS, Santhanam P, Chitrarasu P and Ali AJ. 2012. Zooplankton diversity in a perennial freshwater lake. Diversity and Physiological Processes, Goa University, Goa, India, 25-37 pp.

Manickam N, Bhavan PS, Santhanam P, Muralisankar T, Srinivasan V, Radhakrishnan S, Vijayadevan K, Chitrarasu P and Ali AJ. 2014. Seasonal variations of zooplankton diversity in a perennial reservoir at Thoppaiyar, Dharmapuri District, South India. *Austin J Aquac Mar Bio*., **1(1)**: 1-7.

Manickam N, Bhavan PS, Santhanam P, Muralisankar T, Srinivasan V, Vijayadevan K and Bhuvaneswari R. 2015. Biodiversity of freshwater zooplankton and physico-chemical parameters of Barur Lake, Krishnagiri District, Tamil Nadu, India. *Malaya J Biosci*., **2(1)**: 1-12.

Manickam N. 2015. Biodiversity of plankton in two perennial lakes of Coimbatore, India and suitability of wild mixed zooplankton as live feed for rearing of the giant freshwater prawn *Macrobrachium rosenbergii* early post larvae, PhD Thesis, Bharathiar University, Tamil Nadu, India, 1-145 pp.

Margalef R. 1968. Perspectives in Ecological Theory. Chicago, IL.: University of Chicago Press, 111 pp.

Matias-Peralta HM and Yusoff F. 2015. Status of planktonic copepod diversity in the Merambong seagrass meadow, Johor, Peninsular Malaysia. *Int J Ecosyst*., **5(2)**: 39-43. https://doi.org/10.5923/j.ije.20150502.01

Melo PA, Silva TA, Neumann-Leitão S, Schwamborn R, Gusmão LM and Porto-Neto F. (2010). Demersal zooplankton communities from tropical habitats in the southwestern Atlantic. *Mar Biol Res*., **6(6)**: 530-541. https://doi.org/10.1080/17451000903426557

Metillo EB, Nishikawa J, Ross OB, Yoshida T, Yusoff, FM, Kuppan P, Ohtsuka S, Sekiguchi H, Toda T and Nishida S. 2019. Diel patterns of zooplankton community structure in nearshore waters of different substrates off Tinggi and Sibu Islands,

Malaysia, with special reference to copepods. *Aquat Ecosyst Health Manag*., **22(1)**: 86-102.

MVSSS D. 2000. Taxonomic notes on the Rotifers from India (from 889-2000). IAAB, Hyderabad (AP) India.

Omoregie IP. 2017. Heavy Metals, Nutrients, Total Hydrocarbons and Zooplankton Community Structure of Osse River, Edo State, Nigeria. *Jordan J. Biol. Sci*., **10(2)**: 109-116.

Parmar TK, Rawtani D and Agrawal YK. 2016. Bioindicators: The natural indicator of environmental pollution. *Front Life Sci*., **9(2)**: 110-118. https://doi.org/10.1080/21553769.2016.1162753

Patel V, Shukla SN and Patel VK. 2013. Studies on the diversity of zooplankton and their seasonal variation in Govindgarh Lake at Rewa, Madhya Pradesh, India. *Indian J Appl Res*., **3(11)**: 544-546.

Paul SI, Majumdar BC, Hasan M, Sarker AK, Baidya A and Hakim M. 2021. Fish biodiversity, threat status and conservation significance of the Jamuna River, Bangladesh. *Croat J Fish*., **79(4)**: 173-186. http://dx.doi.org/10.2478/cjf-2021-0019

Pennak RW. 1978. Freshwater invertebrates of the United States. New York: John Wiley & Sons, Inc., 1-803 pp.

Pielou EC. 1966. Species-diversity and pattern-diversity in the study of ecological succession. *J Theor Biol*., **10(2)**: 370-383.

Pierce RW and Turner JT. 1994. Plankton studies in Buzzards Bay, Massachusetts, USA. IV. Tintinnids, 1987 to 1988. *Mar Ecol Prog Ser*.. **112(3)**: 235-240.

Raghunathan MB and Kumar SR. 2002. Cladocera (Crustacea) of Tamil Nadu: Checklist and bibliography. *Zoos' Print J*., **17**: 959-960.

Rahman AA. 1989. Freshwater fishes of Bangladesh. Zoological Society of Bangladesh. University of Dhaka, Bangladesh, 234 pp.

Rahman S and Hussain MA. 2008. A study on the abundance of zooplankton of a culture and a non-culture pond of the Rajshahi University campus. *Univ J Zool Rajshahi Univ*., **27**: 35-41.

Rajashekhar M, Vijaykumar K and Paerveen Z. 2010. Seasonal variations of zooplankton community in freshwater reservoir Gulbarga District, Karnataka, South India. *Int J Syst Biol*., **2(1)**: 6-11.

Rezai H, Yusoff FM, Arshad A, Kawamura A, Nishida S and Ross OBH. 2004. Spatial and temporal distribution of copepods in the Straits of Malacca. *Zool Stud*., **43(2)**: 486-497.

Roy U, Shaha BK, Mazhabuddin KH, Haque MF and Sarower MG. 2010. Study on the diversity and seasonal variation of zooplankton in a brood pond, Bangladesh. *Marine Res Aqua*., **1(1)**: 30-37.

Shannon CE and Wiener W. 1963. The Mathematical Theory of Communications, Urbana, IL: University of Illinois Press, 125 pp.

Sheikh AH, Mondal AR, Majumdar BC, Rayhan A and Hossen MN. 2018. Spawning and mortality of eggs and larvae produced by different brood sizes of Walking Catfish (*Clarias batrachus* L.). *J Appl Adv Res*., **3(3)**: 78-83. http://dx.doi.org/10.21839/jaar.2018.v3i3.174

Shiel RJ. 1995. A guide to identification of Rotifers, Cladocerans and Copepods from Australian inland waters. Albury: Co-operative Research Centre for Freshwater Ecology, Murray-Darling Freshwater Research Centre, 1-142 pp.

Shovon MNH, Majumdar BC and Rahman Z. 2017. Heavy metals (lead, cadmium and nickel) concentration in different organs of three commonly consumed fishes in Bangladesh. *Fish Aquac J*., **8(3)**: 207. http://dx.doi.org/10.4172/2150-3508.1000207

Stirling HP. 1985. Chemical and biological methods of water analysis for aquaculturists. Institute of Aquaculture, University of Stirling, Scotland, 119 pp.

Thirupathaiah M, Samatha C and Sammaiah C. 2011. Diversity of zooplankton in freshwater Lake of Kamalapur, Karimnagar District (A.P.), India. *The Ecoscan*, **5(1&2)**: 85-87.

Tonapi GT. 1980. Fresh water animals of India. An Ecological Approach. Oxford and IBH Publishing Co., New Delhi, Bombay, Calcutta, 341 pp.

Vyas V, Dinesh D and Vivek P. 2012. Fish biodiversity of Betwa River in Madhya Pradesh, India with special reference to a sacred ghat. *Int J Biodivers Conserv.*, **4(2)**: 71-77.

Watkar AM and Barbate MP. 2013. Studies on zooplankton diversity of River Kolar, Saoner, Dist- Nagpur, Maharashtra. *J Life Sci Technol.*, **1(1)**: 26-28.

Wetzel RG. 2001. Limnology: lake and river ecosystems. 3rd Edn., Gulf professional publishing. Academic Press, San Diego, 1006 pp.

Overexpression of 3-hydroxy-3-methylglutaryl coenzyme-A reductase-1 *(HMGR1)* enhanced andrographolide accumulation in *Andrographis paniculata* (Burm.F.)

Erly Marwani[1,*], Juane Plantika Menra , Amanda Nadhira , Tati Kristianti[2], Karlina Febrianti , Fenny Martha Dwivany

[1]School of Life Sciences and Technology, Institut Teknologi Bandung, Bandung 40132, Indonesia;[2] Institut Pendidikan Indonesia, Garut West Java, Indonesia

Abstract

3-hydroxy-3-methylglutaryl coenzyme-A reductase (*HMGR*) enzyme plays an important role in the biosynthesis of diterpene lactones such as andrographolide, a specialized metabolite that is widely used as a therapeutic agent. This study aimed to enhance the content of andrographolide through the overexpression of 3-hydroxy-3-methylglutaryl coenzyme-A reductase-1 (*HMGR1*) in *A. paniculata*. *HMGR1* was constructed into the pBI121 expression vector controlled by the cauliflower mosaic virus (CaMV 35S) promoter. The pBI121-*HMGR1* construct was transformed to *A. paniculata* through Agrobacterium-mediated transformation followed by plant regeneration to obtain transgenic plants. Polymerase chain reaction (PCR) analysis was conducted to validate the transgenic plants, quantitative reverse transcription PCR (RT-qPCR) was used for the *HMGR1* expression analysis, and high-performance liquid chromatography was employed to quantify the andrographolide content of the transgenic plants. PCR analysis on the transgenic plantlets indicated the presence of a 2,262 bp fragment that corresponded to *HMGR1*, thus confirming the integration of *HMGR1* into the *A. paniculata* genome. The RT-qPCR results showed a 52.5-fold greater *HMGR1* expression in the transgenic plant under the CaMV 35S promoter compared to the normal plant. As the expression level of *HMGR1* increased, the amount of andrographolide was enhanced by up to 2.6 times in the transgenic plant compared to the control plant. This study demonstrates that the overexpression of *HMGR1* driven by CaMV 35S can enhance the production of andrographolide in *A. paniculata*.

Keywords: Andrographolide, overexpression, transgenic, HMGR, CaMV 35S .

1. Introduction

Andrographis paniculata has long been recognized as a traditional medicinal plant in various tropical and subtropical countries, including Thailand, Indonesia, Malaysia, Sri Lanka, and India (Akbar, 2011; Benoy *et al.,* 2012; Kabir *et al*., 2014). Extract from the plant has shown a broad spectrum of pharmacological activities, i.e. immunostimulatory (Kumar *et al*., 2004), antiviral/anti-HIV (Churiyahi *et al*., 2015), antibacterial (Jarukamjorn and Nemoto, 2008), anticancer (Harjotaruno *et al*., 2008), antidiabetic, antimalarial, hepatoprotective (Jarukamjorn and Nemoto, 2008), and anti-inflammatory (Chandrasekaran *et al.,* 2012) activities. Currently, the dried extract of *A. paniculata* in capsule or dried leaf form is available commercially and is used as an immunostimulant.

Based on the identification of its chemical constituents, *A. paniculata* contains various bioactive compounds in the form of diterpenoids, flavonoids, and polyphenols (Chao and Lin, 2010). Among the diterpenoid group in *A. paniculata*, andrographolide has previously been identified as the main bioactive compound (Rao *et al.,* 2004).

Andrographolide is a bitter crystalline compound, colorless, with various biological activities, namely anti-HIV, as shown by its inhibition of the HIV-induced cell cycle dysregulation (Calabrese *et al.* 2000), antiviral, as demonstrated by its viricidal activity against the herpes simplex virus (Wiart *et al.,* 2005), as well as antipyretic, immunostimulant, analgesic, anticancer (Suebsana *et al.,* 2009), and anti-inflammatory activities (Levita *et al.,* 2010). Recently, *A. paniculata* extract and andrographolide compounds have been reported to potentially show anti-SARS-CoV-2 activity (Shi *et al*., 2020), Additionally, based on the results of in silico studies, it has been hypothesized that andrographolide may show anti-SARS-CoV-2 activity (Lakshmi *et al.*, 2021; Enmozhi *et al*., 2020; Laksmiani *et al*., 2020). However, andrographolide has only been detected in the leaves of *A. paniculata* at a concentration of 2.2% (Royani *et al.,* 2014). As the market need for andrographolide grows, so does the need to develop a technique for improving the andrographolide levels in *A. paniculata*. Metabolic engineering is one of the promising techniques used to enhance secondary metabolite accumulation.

Metabolic engineering to increase secondary metabolites can be performed in different ways. These

---

* Corresponding author. e-mail: erly@itb.ac.id.

include the overexpression of certain genes to regulate metabolic pathways (Alvarez and Marconi, 2011). Similarly, Lu *et al.* (2016) stated that overexpressing genes in the terpenoid biosynthetic pathway in homologous and ectopic plants provided a reliable method for increasing terpenoids. In addition, overexpression of the *PGSQS1* gene in the ginsenosides biosynthesis pathway may enhance the expression of β-amyrin synthase (β-AS) and cycloartenol synthase (CAS), resulting in increases in phytosterols and ginsenosides of up to 2.0 and 1.6 times, respectively, in root cultures of transgenic ginseng (Shim *et al.,* 2010). Moreover, Han *et al.* (2013) reported an increase in oleanane-type ginsenoside in *P. ginseng* plants following overexpression of the *CYP716A52V2* gene. Similar results have shown that overexpression of the 3-hydroxy-3-methylglutaryl coenzyme-A reductase (*HMGR*) gene produced a 1.5- to 2-fold rise in the ginsenosides content of adventitious ginseng root cultures resulting from genetic transformation (Kim *et al.,* 2014).

Recently, overexpression of the *HMGR* gene in transgenic roots and stems of *Ligularia fischeri* has been shown to increase the shionone content by up to 16.67% and 12.25%, respectively, when compared to controls (Juan Du *et al.,* 2020). When seeking to overexpress a gene to enhance enzyme activity, the proper promoters should be selected. The cauliflower mosaic virus (CaMV 35S) promoter is frequently used as a standard promoter for transgene expression in plants (Somssich, 2019; Amack and Antunes, 2020). It is known as a strong, constitutive promoter and is frequently used in expression in transgenic plants (Somssich, 2019).

Song *et al.* (2012) reported how the use of the CaMV 35S promoter for overexpression of the endogenous *HMGR* gene enhanced the accumulation of β-sesquiphellandrene by 1.25–1.60 fold. Similarly, Dong *et al.* (2013) reported that overexpression of one of the isoprenoid pathway enzymes, i.e. *HMGR*, in *Parthenium argentatum* increased carbon flux to the isoprenoid pathway; for example, for the synthesis of plant growth substances. Moreover, Putter *et al.* (2017) indicated that overexpression of the three main enzymes in the mevalonate cascade, which include *HMGR*, in *Taraxacum brevicorniculatum* can increase enzyme activity and result in an increase in high squalene concentrations in dandelion roots. Another report indicated that 3-hydroxy-3-methylglutaryl-CoA reductase-1 (*HMGR1*) showed a correlation with andrographolide biosynthesis in *A. paniculata* (Jha *et al.*, 2011).

Our interest in this study was to employ metabolic engineering in a bid to enhance the amount of andrographolide through overexpression of the *HMGR1* gene involved in the mevalonate pathway, a biosynthetic pathway that produces various secondary metabolites including diterpenoids such as andrographolide. To date, however, no overexpression of the *HMGR1* gene driven by CaMV 35S in *A. paniculata* to enhance the accumulation of andrographolide has been reported. Therefore, the present research aimed to overexpress the *HMGR1* gene in *A. paniculata* under the control of a strong promoter, namely CaMV 35S. This was expected to lead to an increase in the accumulation of andrographolide. This paper reports the construction of the *HMGR1* gene into pBI121 plasmid, the transformation of *A. tumefaciens* with this recombinant plasmid, the development of an *A.*

paniculata transgenic line using *Agrobacterium* transformation method, plant regeneration, gene expression, and andrographolide analysis of the *A. paniculata* transgenic plant.

2. Materials and Methods

2.1. Plant Material

A. paniculata seeds and mature plants were obtained from the Research Institute for Medicinal Plants and Spices (Balitro), Bogor, West Java. The plant material used for the isolation of RNA comprised three-month-old leaves from the *A. paniculata* plant after Sharma *et al.* (2013) reported that the leaves of *A. paniculata* contain higher levels of andrographolide (2–3%) compared to other parts of the plant. Meanwhile, the explants used for genetic transformation were cotyledons of three-week-old *A. paniculata* seedlings.

2.2. Bacterial Strain and Plasmid

pGEM-T Easy from Promega was employed as the cloning vector to amplify the *HMGR1* gene. *Escherichia coli* strain DH5α was used in the cloning of pGEM-T Easy-*HMGR1*, while pBI121 was used as the binary vector for construction. *Agrobacterium tumefaciens* strain GV3101 was used for plant transformation, which was provided by Dr. Sony Suhandono from the Molecular Genetics laboratory, School of Life Sciences and Technology, Institut Teknologi Bandung.

2.3. Medium and Reagents

The medium for plant regeneration was prepared according to the protocol from Marwani *et al.* (2013). GoTaq® Green Master Mix was the reagent used for Polymerase Chain Reaction (PCR), which was obtained from Promega™. Agarose (Top Vision Agarose), and 1 Kb ladder were used for gel electrophoresis and were obtained from Fermentas™. The purification kit for gel electrophoresis was obtained from Geneaid™. The primers were sourced from Macrogen Inc.

2.4. Amplification of HMGR1 cDNA

The *HMGR1* cDNA was first isolated from *A. paniculata* leaf by Menra (2013). The *HMGR1* cDNA was amplified using touchdown PCR (Applied Biosystems 2720 thermal cycler) with specific primers for *HMGR1*, forward primer 5'AGA ATG GCC GCC CTC CG3' and reverse primer 5'ATC GAC TCT CTC TGT CTC CAA TCT CAA GT3', to give a DNA length of around 1,800 bp. The PCR reaction comprised 25 µl GoTaq® Green Master Mix, 2.5 µl *HMGR1* forward primer, 2.5 µl *HMGR1* reverse primer, 1 µl cDNA template, and 19 µl nuclease-free water. The process began with initial denaturation for 3 minutes at 95°C followed by 10 cycles of amplification. Annealing and extension were performed at 50–60°C for 30 seconds and 72°C for 2.5 minutes, respectively. The PCR products were subjected to electrophoresis, followed by visualization using ethidium bromide staining, and observed under UV light irradiation for later documentation. The *HMGR1* fragment was then purified using a gel purification kit from Geneaid in line with the procedure provided by the kit manufacturer. Next, the fragments from the purification results were ligated into the pGEM-T Easy vector from Promega. The ligated

pGEM-T-Easy-*HMGR1* was subsequently used to transform competent *E. coli* DH5α cells using heat shock transformation following the method used by Chang *et al.* (2017). The transformants were spread onto LB agar containing ampicillin (100 mg/l), IPTG (0.1 M), and X-gal (100 mg/l), and subsequently incubated at 37°C for 16 hours to select the recombinant clones. White colonies indicated the presence of pGEM-T-Easy with the *HMGR1* gene inserted.

A single colony of transformants was selected and suspended in a 5 ml LB medium containing 100 ppm of ampicillin and stored in the shaker at 37°C, 200 rpm overnight. The plasmids were isolated according to the alkaline lysis method employed by Amara (2018), with modification. The isolated plasmid of *HMGR1* gene-pGEM-T-Easy was sequenced at Macrogen Inc. (Seoul Korea) to test for the presence of the *HMGR1* gene using primers T7 and SP6. The sequencing results were then analyzed by bioinformatics using BLAST software at the NCBI website (http://ncbi.nlm.nih.gov/blast).

2.5. Construction of pBI121-HMGR1 Plasmid Vector

pBI121 was used as the backbone in constructing the expression vector carrying the *HMGR1* gene. The *HMGR1* gene would be expressed under the CaMV35S promoter. The multiple cloning sites at the pBI121 plasmid contained *Xba*I, *Bam*HI, *Sma*I, *Xma*I, and *Bsr*GI restriction sites between the CaMV 35S promoter and *GUS* gene. Of the five restriction enzyme recognition sites, *Xba*I and *Bsr*GI do not cleave the *HMGR1* gene. Therefore, a pair of primers was designed with *Xba*I (5-TCT AGA AGA ATG GCC GCC CTC CGC CGC CGA) and *Bsr*GI (TGT ACA AAT CGA CTC TCT CTG TCT CTC AAT) recognition sequences added to the forward and reverse primers, respectively. These were then used to amplify the *HMGR1* gene in the recombinant pGEM-T Easy. Next, the amplicon was ligated into the pBI121 fragment digested with *Xba*I and *Bsr*GI, with a volume ratio of 3:1 using T4 DNA ligase. The ligation reaction comprised 3 µl DNA insert, 1 µl DNA backbone, 1 µl *Xba*I enzyme, 1 µl T4 DNA ligase, 1 µl T4 DNA Ligase buffer, and 13 µl deionized water. The reaction was performed at 4°C for 16–18 hours. Ligation produced a recombinant pBI121-*HMGR1* construct with a length of 15,004 bp (Figure 1).
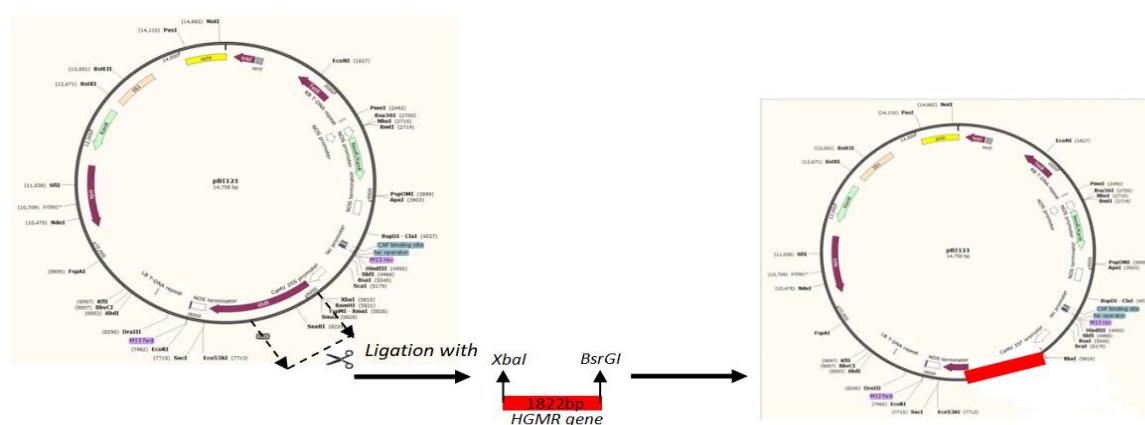
Figure 1. Diagram of the construction of *HMGR1* in binary vector pBI121

Applying the heat shock transformation method of Chang et al. (2017), the pBI121-*HMGR1* construct was transformed into competent cells of E. coli DH5α. Afterward, the E. coli DH5α containing the pBI121-*HMGR1* construct was cultured in LB medium supplemented with 50 mg/l kanamycin at 37°C. The plasmid was subsequently isolated using the alkaline lysis method according to Amara's (2018) standard protocol with modification. To confirm the success of the plasmid ligation, the isolated pBI121-HMGR1 fragment was digested with *Xba*I and *Bsr*GI restriction enzymes and observed by 1% agarose gel electrophoresis. The restriction digest resulted in two fragments with sizes of 1,822 bp and 13,182 bp. The final step was sequencing the *HMGR1* gene in pBI121-*HMGR1* recombinant plasmid at Macrogen Inc., Seoul, Korea. Bioinformatics analysis was performed on the sequencing results using the BLAST nucleotide program from NCBI (www.ncbi.nlm.nih.gov).

2.6. Transformation of A. tumefaciens GV3101 with Recombinant Plasmid pBI121-HMGR1

Agrobacterium tumefaciens strain GV3101 was transformed with the constructed pBI121-*HMGR1* plasmid using heat shock based on the procedure of Chang *et al.* (2017) with a slight adjustment. A total of 2–5 µl pBI121-*HMGR1* plasmid was placed in 50 µl competent *A. tumefaciens* cells in microtubes. Afterward, the tubes were inverted repeatedly and then incubated in ice for 10 minutes or immersed in liquid nitrogen for 5 minutes. Next, the microtubes were incubated in a water bath at 37°C for 25 minutes and 1 ml of liquid YEP (10 g/l yeast extract, 10 g/l peptone, 5 g/l NaCl, 15% bacto agar, pH 7) medium consisting of 50 mg/l kanamycin and 50 mg/l rifampicin was added and grown at 25°C, 200 rpm in the dark for 3 hours and then centrifuged at 14,000 rpm for 1 minute. The supernatant was removed, and the pellet was suspended and plated on a solid YEP medium consisting of 50 mg/l rifampicin and 50 mg/l kanamycin and stored in an incubator at 25°C for 2 days. A selected colony was suspended in 25 µl deionized water, and 3 µl of the

suspension was applied to the PCR assay to test for the presence of the *HMGR1* gene.

The PCR mixture comprised 5 µl GoTaq® Green Master Mix, 1 µl forward primer, 1 µl reverse primer, 1 µl DNA template, and deionized water to a total volume of 10 µl. PCR was performed using specific primers for the *HMGR1* gene (forward 5'-TCT AGA AGA ATG GCC GCC CTC CGC CGC CGA-3' and reverse 5'-TGT ACA AAT CGA CTC TCT CTG TCT CTC AAT-3'), giving an expected DNA length of around 1,822 bp. Amplification was set as follows: initial denaturation at 95°C for 3.5 minutes followed by 30 cycles of denaturation at 95°C for 30 seconds, annealing at 60°C for 30 seconds, elongation at 72°C for 2 minutes, and final elongation at 72°C for 7 minutes. The PCR product was analyzed on 1% agarose gel electrophoresis (Top vision agarose) and 1 Kb DNA Ladder #331 (Fermentas). A DNA band of 1,822 bp indicated the presence of the *HMGR1* gene.

2.7. Transformation and Regeneration of Andrographis paniculata

2.7.1. Preparation of A. tumefaciens

A colony of *A. tumefaciens* GV 3101 containing recombinant plasmid pBI121-*HMGR1* was suspended in 25 ml yeast extract peptone medium enriched by 50 mg/l kanamycin and 25 mg/l rifampicin and incubated overnight at 28°C, 200 rpm in the dark. The *Agrobacterium* cells were collected after centrifugation at 4000 rpm for 20 minutes. The pellet of *Agrobacterium* cells was re-suspended in liquid half-strength Murashige and Skoog (MS) medium to reach a concentration of 10^6 cells/ml or $OD_{600nm} = 0.8$. Finally, 100 µM acetosyringone and Silwet L-77 with a ratio of 1:3 was added into the *A. tumefaciens* suspension.

2.7.2. Agrobacterium-mediated Genetic Transformation, Co-cultivation, and Regeneration

For the purpose of plant transformation, the *A. tumefaciens* GV3101 harboring pBI121-*HMGR1* was used to infect *A. paniculata* by agroinfiltration. First, the cotyledons of *A. paniculata* were immersed for 60 minutes in the *A. tumefaciens* suspension. Subsequently the cotyledons were drained on sterile filter paper and co-cultivated for 3 days on agar-solidified (0.8% w/v) MS medium enriched with 2 mg/l 6-benzylaminopurine (BAP), 1 mg/l indole-3-acetic acid (IAA), 1% Silwet L-77, 100 µM acetosyringone, and 50 mg/l kanamycin at 28°C in the dark. The tissue was then rinsed using sterilized distilled water 3 times for 5 minutes and immersed for 15 minutes in cefotaxime 400 mg/l or augmentin 300 mg/l to eliminate bacteria. The cotyledons were then transferred to an MS medium containing 2 mg/l BAP, 1 mg/l IAA, 250 mg/l augmentin, and 350 mg/l cefotaxime for 6 days according to the method of Konagaya *et al.* (2020). The surviving tissues were transferred to a selection medium (solid MS medium consisting of 2 mg/l BAP, 1 mg/l IAA, kanamycin 20 mg/l) at 25°C for 2 weeks under a 36-watt Tungsten lamp (TL) with a light intensity of 1000 lux and 12-hour photoperiod. To induce shoot formation, the transformed cotyledon tissues were moved to a shoot regeneration medium (solid MS medium consisting of 2 mg/l BAP, 1 mg/l IAA with the addition of 20 mg/l kanamycin) and incubated at 25°C for 2 to 3 weeks under a 12-hour photoperiod. To induce root formation, the regenerated shoots were implanted on a solid MS medium with the addition of 1 mg/l indole butyric acid (IBA) and incubated at 25°C for 3 to 4 weeks until the primary plantlets were formed.

Transformed plantlets (transgenic progeny) that measured 7–10 cm in length and were vigorous were carefully removed from the culture bottle, cleaned under running tap water to remove adhered agar, and subsequently planted in a plastic pot containing a mixture of sterilized husks and sandy soil with a 1:1 ratio and maintained in a greenhouse at 27°C under a 12-hour photoperiod. To prevent excessive evaporation, the plastic pots were covered with transparent plastic for the first month, which was subsequently removed when the plants showed more vigor. The transgenic plants were cultivated in the pots for 3 months, after which the leaves, stem, and roots were harvested to determine the andrographolide concentration.

2.8. PCR of Transgenic Plant

PCR was performed to test the integration of the *HMGR1* gene into the *transformed A. paniculata* genomic DNA following the method of Han *et al.* (2017) with a slight modification. The genomic DNA of three biological replicates (marked as TA1, TA2, and TA3) of the T0 generation transformed plantlets were isolated using the Plant Genomic DNA Kit from Tiagen. Up to 1 µl of the isolated DNA was mixed with 5 µl GoTaq® Green Master Mix, 1 µl forward primer, 1 µl reverse primer, and 1 µl deionized water. PCR analysis was performed using specific primers of pBI121 (forward 5'-TTC GTC AAC ATG GTG GAG CA and *HMGR1* reverse 5'-TGT ACA AAT CGA CTC TCT CTG TCT CTC AAT-3'), resulting in a DNA length of around 2,262 bp. The PCR cycle was programmed as follows: initial denaturation at 95°C for 3 minutes, followed by 25 cycles of 95°C for 30 seconds, 60°C for 30 seconds, 72°C for 2 minutes, and finally, elongation at 72°C for 7 minutes. The PCR product was applied to 1% agarose gel electrophoresis and observed under a UV transilluminator.

2.9. RNA Isolation and Quantitative Real-Time Expression Analysis of HMGR1 Gene in Transformed A. paniculata

Using the TRIzol (Thermo Fisher Scientific, United States) procedure, transformed *A. paniculata* RNA was isolated from three transformed plant tissues, labeled TA1, TA2, and TA3, as well as from the control plant tissue. Trizol was used in this work because, compared to other techniques, it has a better reputation for isolating RNA from plant tissues (Mohammed *et al.*, 2019). The quality of the RNA was assessed based on concentration and electrophoretic bands. RNA with an $A_{260}/A_{280} \geq 1.8$ was selected due to its high purity, as stated by Sukumaran (2011). The total RNA was converted into cDNA using a Sensi FAST cDNA Synthesis Kit from Bioline. The cDNA reaction (20 µl total volume) consisted of 8 µl total RNA (100 ng), 4 µl TransAmp Buffer, 1 µl Reverse Transcriptase, and 7 µl nuclease-free water. The following program was established in a thermal cycler: 25°C for 10 min (primer annealing); 42°C for 15 min (reverse transcription); 85°C for 5 min (inactivation), and 4°C hold (or chill on ice). In the RT-qPCR assays, each reaction (20 µl total volume) consisted of 2 µl diluted cDNA, 10 µL qPCR Promega master mix, 1 µl each forward and reverse

primers, and 6 μl RNAse-free water. To ensure reliability and validity, three technical replicates were performed per sample. The RT-q PCR cycle was programmed as follows: 95°C for 5 min, followed by 40 cycles of 95°C for 10 s, and 56°C for 30 s. The specific primers were determined using Primer 3 software (Table 1). The relative expression levels of the genes were normalized against the actin housekeeping gene and were later expressed as a function of the non-transgenic (control) plant values, whose *HMGR1* transcript levels were defined as one (1) in line with the method of Livak and Schmittgen (2001). The relative gene expression levels were determined using the $2^{-\Delta\Delta Ct}$ method (Livak and Schmittgen, 2001), where $\Delta Ct=$ Ct target -Ct reference and $\Delta\Delta Ct= \Delta Ct$ transgenic plant - ΔCt control (non-transgenic plant). An average of three biological replicates (three transformed tissues) were used to calculate the expression levels.

Table 1. List of primers for relative expression analysis

Primers	Sequences	Product size
Actin-F	5'GAGGTGCTCTTTCAGCCATC'3	250bp
Actin-R	5'TTGATCTTCATGGTGCTTGG'3	
HMGR-F	5'GCATCGGTTTTGTCCAGTCT'3	250bp
HMGR-R	5'GAAGAGGCGATTTTGCAGTC'3	

2.10. Determination of Andrographolide Content

Analysis of the andrographolide content in transgenic and non-transgenic *A. paniculata* was conducted using high-performance liquid chromatography (HPLC) Shimadzu CR-and A Plus according to the method of Majee *et al.* (2011) with modification. Leaf, stem, and root samples from the transformed and non-transformed (control) A. *paniculata* were harvested from the age of 3 months. Triplicate samples of leaf, stem, and root were used for the HPLC analysis of andrographolide. The samples were freeze-dried for 24 hours followed by extraction with methanol (sample: methanol ratio of 1:10) for 48 hours. The crude extracts were filtered using a polytetrafluoroethylene (PTFE) membrane, after which the solvent was evaporated using a vacuum evaporator. The dried extracts were dissolved in 1 ml HPLC grade methanol. The extracts were then loaded into an HPLC system equipped with a UV detector, Bondapak C_{18} column (Ø 4.6 mm x 250 mm), using methanol: H_2O (6:4) as the mobile phase at a flow rate of 1 ml/min, and monitored at λ 254 nm. The reference solution was the

andrographolide compound purchased from Sigma-Aldrich. To produce the calibration curve for andrographolide, a standard andrographolide solution was prepared in a separate flask using an appropriate dilution of 0.5 mg/ml stock solution with the same volume of solvent (HPLC grade methanol) to final concentrations of 0.25, 0.125, 0.0625, and 0.0312 mg/ml. Each standard solution was injected into HPLC, and each peak area value was plotted to the corresponding concentration to obtain the linear calibration curve. A linear equation was obtained from the linear curve, and the concentration of the injected samples was determined.

2.11. Statistical analysis

Statistical analysis was conducted to assess the significance of the difference in the data variation for the andrographolide concentrations and the number of shoot regenerations in the normal and transformed tissues. The analysis was performed using SPSS Statistics software version 29, employing a one-way ANOVA (analysis of variance) test. A p-value of less than 0.05 was considered to indicate statistical significance. The ANOVA test was followed by a post-hoc Tukey test to observe the variations in andrographolide concentration between the transformed and normal tissues. The andrographolide concentration data were presented as the mean ± SD (standard deviation) of triplicate biological samples.

3. Results

3.1. Construction of pBI121-HMGR1 Plasmid Vector

The cDNA fragment (around 1,800 bp) isolated from *A. paniculata* was verified as *HMGR1* by DNA sequencing (GenBank accession nos. AY429658.1). The insertion of the *Xba*I and *Bsr*G1 restriction enzyme site to the *HMGR1* fragment produced a fragment measuring between 1,500 bp and 2,000 bp in length (Figure 2A), which corresponded to the expected *Xba*I-*HMGR1*- *Bsr*G1gene (1,822 bp). The digestion of pBI121 with *Xba*I and *Bsr*GI restriction enzymes at specific nucleotide sequences eliminated the *GUS* gene and produced the pBI121 backbone with a length of 13,182 bp (Figure 2B), whereas digesting the pGEM-TEasy *HMGR1* with the same restriction enzymes produced a DNA fragment between 1,500 bp and 2,000 bp in length, which corresponded to the *HMGR1* gene (Figure 2C).
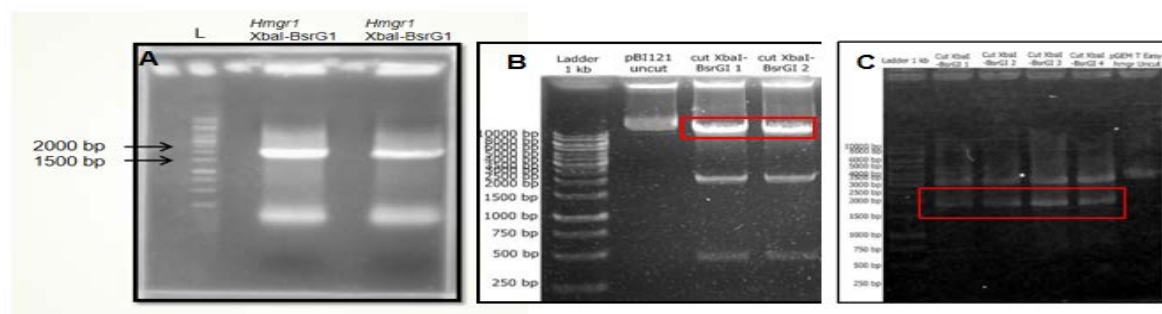
Figure 2. (A) *HMGR1* gene fragment containing *Xba*I and *Bsr*G1 restriction sites with a length of 1,500 bp–2,000 bp, corresponding to the size of *HMGR1* (1,822 bp). (B) Gel electrophoresis of pBI121 digested with *Xba*I and *Bsr*GI restriction enzymes, which produced the pBI121 backbone with a length of 13,182 bp, indicated by the red box. (C) Gel electrophoresis of pGEM-T Easy-*HMGR1* digested with *Xba*I and *Bsr*GI restriction enzymes, which produced a fragment with a length of 1,500 bp–2,000 bp, corresponding to the size of *HMGR1* (1,822 bp), indicated by the red box.

In general, restriction enzymes digest DNA at specific nucleotide sequences by hydrolyzing phosphodiester bonds on both DNA strands, producing a phosphate group at the 5' end and an OH group at the 3' end of the DNA strands (Allison, 2007), resulting in either cohesive or blunt ends (Koerniati and Widhianata, 2012). After purification by agarose gel electrophoresis, the pBI121 backbone and *HMGR1* insert were ligated using T4 DNA ligase, which produced a recombinant plasmid named

pBI121-*HMGR1* with a length of 15,004 bp (Figure 3A). To test for the presence of *HMGR1* insert in the pBI121 plasmid, the recombinant pBI121-*HMGR1* plasmid was digested with restriction enzymes *Xba*I and *Bsr*GI. This produced two fragments, a 13,182 bp fragment corresponding to the pBI121 backbone and a fragment with a length between 1500 and 2000 bp (1,822 bp), which correspond to the *HMGR1* insert (Figure 3B).

Figure 3. (A) The pBI121-*HMGR1* recombinant with a length of 15,004 bp. (B) Gel electrophoresis of pBI121-*HMGR1* plasmid digested with *Xba*I and *Bsr*GI restriction enzymes resulting in two bands.

As previously mentioned, the pBI121 backbone and HMGR1 insert were successfully ligated using T4 DNA ligase; this produced the recombinant plasmid pBI121-*HMGR1* with a length of 15,004 bp. To confirm this finding, the pBI121-*HMGR1* recombinant plasmid using *HMGR1* forward and reverse primers was sequenced and

analyzed using the BLAST program at NCBI followed by alignment using BioEdit Sequence Alignment Editor version 7.2.5. High homology was exhibited between the pBI121-*HMGR1* sequence and *HMGR1 A. paniculata* from the NCBI database. The results indicated 99% identity and an expectation (E) value of 0.0 (Figure 4).

Figure 4. BLAST analysis of pGEM-T Easy *HMGR1*

3.2. Transformation of A. tumefaciens with pBI121-HMGR1 Plasmid

The successful transformation of *A. tumefaciens* with recombinant plasmid pB121-*HMGR1* was demonstrated by the ability of *A. tumefaciens* colonies to grow on the selection medium, i.e. medium with the addition of 50 mg/l kanamycin (Figure 5A). The non-transformed *A. tumefaciens*, in contrast, was unable to grow on that medium. This was caused by the kanamycin antibiotic's method of action, which prevents translation by disrupting ribosome functionality (Allison, 2007).

Moreover, a single band between 1,500 bp and 2,000 bp in length was detected via PCR amplification of *A. tumefaciens* cultured on a YEP medium containing kanamycin using a pair of specialized HMGR1 primers (Figure 5B). This result aligned with the *HMGR1* DNA fragment length of around 1,822 bp. This result demonstrated that the *A. tumefaciens* colony was successfully transformed and thus contained the pBI121-*HMGR1* construct.
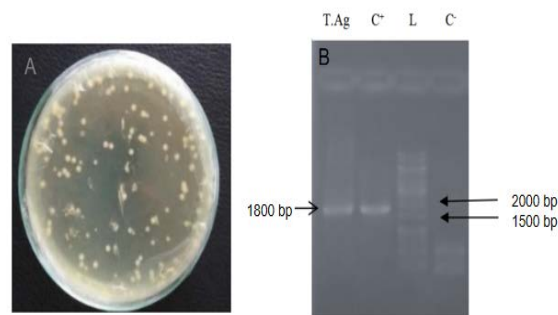
Figure 5. (A) Colonies of *A. tumefaciens* harboring recombinant plasmid pB121-*HMGR1* on YEP solid medium consisting of 50 mg/l kanamycin and 50 mg/l rifampicin. (B) Electropherogram of *A. tumefaciens* colony PCR product using a pair of *HMGR1* primers (T. Ag: the colony of *A. tumefaciens*, C+: recombinant pBI121-*HMGR1*, L: Ladder 1 Kb, C-: negative control).

3.3. Transformation and Plant Regeneration

After transformation, some of the transformed cotyledonary tissues survived on the selection medium , MS medium consisting of 2 mg/l BAP, 1 mg/l IAA, and 20 mg/l kanamycin, (Figure 6A). However, the untransformed tissues did not grow on that medium and eventually died (Figure 6B). In the MS medium comprising 2 mg/l BAP and 1 mg/l IAA without kanamycin (control medium), the cotyledonary tissues grew well (Figure 6C). On days 28–30 following initiation, multiple new shoots (1–3 transgenic shoots for each explant) appeared directly from the transformed tissue when they were cultivated in the shoot regeneration medium, i.e. MS medium consisting of

2 mg/l BAP and 1 mg/l IAA, with the addition of 20 mg/l kanamycin (Figure 6D). Multiple shoots (7–9 shoots for each explant) only appeared from the non-transformed cotyledonary tissues when these tissues were cultivated in a medium with no kanamycin added (Figure 6E). In this medium, the non-transformed cotyledonary tissues produced multiple shoots more rapidly, i.e. 14–16 days after initiation. Thus, among the cotyledon explants, an average of 1.3 shoots per explant regenerated from the transformed tissue on the media with the addition of kanamycin. Meanwhile, an average of 8.0 shoots per explant regenerated from the non-transformed tissue on the control medium. The number of regenerated shoots from normal tissue was significantly higher (P<0.05) compared to the transformed tissue.

Roots were successfully formed in the transformed shoots (Figure 6F) on MS medium supplemented with 1 mg/l IBA and 20 mg/l kanamycin. Root formation also occurred in the non-transformed shoots on the same medium with no addition of kanamycin (Figure 6G). In this report, plant regeneration from transformed tissues was induced by direct organogenesis through direct shoot formation from the cotyledon explants followed by root formation to produce transgenic plantlets. Three of the transgenic plantlets were then transferred to a mixture of husk and soil (1:1) for acclimatization and maintained for further growth. The plantlets grew well in the plastic pots, and thus the three transgenic plantlets (TA1, TA2, and TA3) were further analyzed by PCR. Within 12 weeks of observation, the normal plants had grown higher than the transgenic plants. The non-transgenic (normal) plants reached 25 cm in height whereas the transgenic plants reached only 18 cm in height. However, no morphological differences were found between the transgenic and non-transgenic plants (Figure 6H).
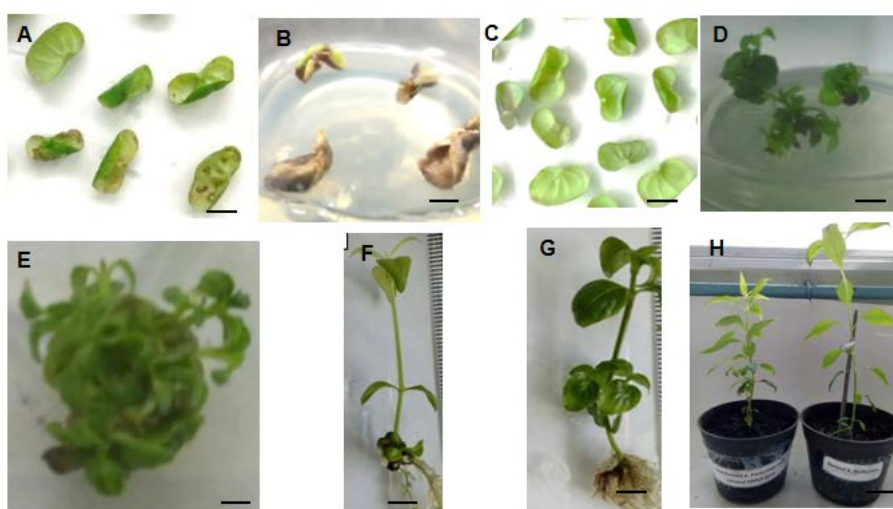
Figure 6. *In vitro* regeneration and acclimatization of plantlets from transformed cotyledon tissues of *A. paniculata* mediated by *A. tumefaciens* harboring recombinant plasmid pBI121-*HMGR1*. (A) Transformed cotyledonary tissues and (B) Non-transformed cotyledonary tissues on medium with the addition of kanamycin, (C) Cotyledonary tissues on medium without kanamycin, (D) Shoot regeneration of transformed tissue on medium with the addition of kanamycin, (E) Shoot regeneration of non-transformed tissue on medium without kanamycin, (F) Root induction of transformed shoot, (G) Root induction of non-transformed shoot, (H) The acclimatization of transformed (left) and non-transformed (right) plantlets on soil media in plastic pots (bar = 1cm).

3.4. PCR Detection of Transgenic Plant

The results of the PCR analysis of genomic DNA using specific primers of pBI121 forward and *HMGR1* reverse in three transformed plantlets marked TA1, TA2, and TA3 from generation 0 (T0) *A. paniculata* revealed the presence of the *HMGR1* gene, as indicated by the production of a DNA fragment of around 2,262 bp in length (Figure 7A). This corresponded to the length of the *HMGR1* gene in the pBI12-*HMGR1* plasmid (positive control PCR), at 2,262 bp, whereas the negative control contained no *HMGR1* band. The use of pBI121 forward and *HMGR1* reverse was intended to avoid false positives because the *HMGR1* gene was isolated from *A. paniculata* tissue; therefore, if the integration assays of the *HMGR1* gene used the specific *HMGR1* gene, then the non-transformant plants would also produce DNA bands of the *HMGR1* gene. In brief, these results demonstrated the successful transformation of *A. paniculata* with pBI12-*HMGR1* by agroinfiltration. As such, the integration of pBI121-*HMGR1* into the genome of regenerated transgenic plants (T0) was confirmed. However, to prove the stability of a genetic transformation, it is necessary to confirm the presence of inserts in the first, second, and up to third offspring (Chaudhury et al., 2019). Due to resource constraints, we were unable in this present study to verify the stable integration of pBI121-HMGR1 on subsequent offspring, either T1, T2, or T3.
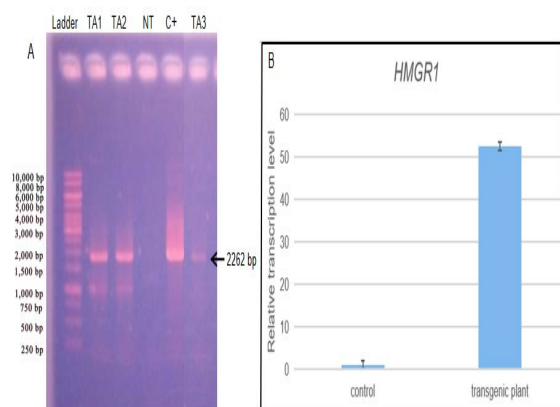
Figure 7. (A) PCR product detection of *HMGR1* gene from transgenic *A. paniculata.;*1Kb: ladder, non-transformant (NT), Positive control (control (+)): specific primers of pBI121 forward and *HMGR1* reverse, transformant repetition 1 (TA1), transformant repetition 2 (TA2), transformant repetition 3 (TA3); (B) Relative transcription level of *HMGR1* gene in control (non-transgenic) and transgenic plant; each transcript level was normalized with respect to the transcript level of the actin gene. Error bars represent the ± SD (standard deviation) of three biological replicates.

3.5. Expression of *HMGR1* Gene

The results showed that the relative transcript level of the *HMGR1* gene in the transgenic plant was significantly higher compared to the non-transgenic plant, specifically 52.5-fold higher (Figure 7B). This indicated that the expression of the *HMGR1* gene under the CaMV 35S promoter was up-regulated. Up-regulation of the *HMGR1* gene was expected to enhance the activity of the HMGR enzyme.

3.6. Up-regulation of HMGR1 Gene Increased the Andrographolide Content

Separate ANOVA tests in this study revealed significantly higher andrographolide levels in transgenic leaf tissue compared to normal leaf tissue, specifically 34.1 mg/g and 11.0 mg/g, respectively. Similarly, the average andrographolide levels in the transformed stems were significantly greater (P<0.05) than in normal stems, measuring 6.2 mg/g compared to 2.1 mg/g. Consequently, the transformed plants had a markedly elevated total andrographolide content (P<0.05) compared to the normal plants, namely 45.3 mg/g versus 17.6 mg/g. Notably, the andrographolide level in the transformed roots (5.0 mg/g) showed no significant difference from that in the normal roots (4.5 mg/g).

However, a post-hoc Tukey test applied across all tissues indicated no significant differences in the andrographolide levels between the transformed stem tissues, transformed roots, normal leaves, normal stems, and normal roots. Only the transformed leaves showed a noteworthy difference when compared to the transformed stems, transformed roots, normal leaves, normal stems, and normal roots (Table 2).

Table 2. Concentration of andrographolide in leaf, stem, root, and whole plant of the control and transgenic *A. paniculata*

Sample	Average andrographolide concentration* ± SD (mg/g)		Increment (fold)
	control plant	transgenic plant	
leaf	11.0^a±4.1	34.1^b±5.5	3.1
stem	2.1^a±0.3	6.2^a±2.5	2.9
root	4.5^a±0.3	5.0^a±3.3	1.1
Total (whole plant)	17.6^x±1.6	45.3^y±3.8	2.6

*The concentration of andrographolide in leaf, stem, and root was obtained from control plants and transgenic plants. The data represent an average of three biological replications ± SD (standard deviation). The different superscript letters against the andrographolide concentration numbers for the control and transgenic tissues indicate a significant difference (P < 0.05).

4. Discussion

4.1. Construction of pBI121-HMGR1 Plasmid Vector

The pBI121 backbone and *HMGR1* insert were successfully ligated using T4 DNA ligase, producing a recombinant plasmid named pBI121-*HMGR1* with a length of 15,004 bp. By using *HMGR1* forward and reverse primers, the recombinant plasmid was sequenced and analyzed using the BLAST program at NCBI followed by alignment using BioEdit Sequence Alignment Editor version 7.2.5. This demonstrated a high homology between the pBI121-*HMGR1* sequence and *HMGR1 A. paniculata* from the NCBI database, which indicated 99% identity and an expectation (E) value of 0.0. The E value was equal to zero in the BLAST results, indicating a high level of confidence in the analysis results and the presence of a homological relationship between the query sequences and NCBI database sequences (Xiong, 2006). Another study showed that the HMGR gene was successfully constructed into the pBS plasmid, resulting in a pBS-HMGR recombinant that was used as a plant expression vector in *Ligularia fischeri* (Du, *et al.,* 2020).

4.2. Transformation and Plant Regeneration

The transformed cotyledonary tissues of *A. paniculata* survived on the selection medium, i.e. medium containing the antibiotic kanamycin (20 mg/l), whereas non-transformed tissues on the same medium did not develop and eventually died. These results indicate that the surviving tissues were successfully transformed by DNA containing the kanamycin resistance gene that was present in the pBI121-*HMGR1* construct, while the non-transformed tissue was sensitive to kanamycin as these normal tissues did not possess the resistance gene. The integration of the kanamycin resistance gene into the *A. paniculata* genome meant that other genes located in the T-DNA region of the pBI121-*HMGR1* construct, including the *HMGR1* gene and the CaMV35S promoter, also integrated into the *A. paniculata* genome. These results confirmed that the *HMGR1* gene had been inserted into *A. paniculata* tissue. This result is similar to that previously reported in the transformation of *Trachyspermum ammi* mediated by *A. tumefaciens*. The researchers in that study used kanamycin as the antibiotic for tissue selection and

PCR analysis to test for the gene of interest (Nomani and Tohidfar, 2021).

Multiple shoots from the transformed tissue appeared on days 28–30 after initiation in the shoot regeneration medium (MS medium consisting of 2 mg/l BAP and 1mg/l IAA) with the addition of 20 mg/l kanamycin (Figure 6D), while the non-transformed tissue generated multiple shoots faster in a shoot regeneration medium with no added kanamycin, i.e., within 14–16 days after initiation (Figure 6E). It seemed that the addition of kanamycin in the selection medium may have resulted in stress to the transformed tissues, extending the shoot formation time compared to that of the non-transformed tissue. These findings are similar to those reported by Vidal et al. (2010).

The average number of regenerated shoots from transformed tissue in the medium with kanamycin added was significantly lower ($P < 0.05$) than the number regenerated from non-transformed tissue in the medium with no added kanamycin, i.e. 1.3 compared to 8.0. These results demonstrate that the addition of kanamycin to the medium reduced the number of shoot regenerations. Similar results were reported in the regeneration of transgenic Citrus aurantifolia on a medium containing kanamycin as a selective agent, resulting in a low regeneration rate, i.e., 1.3 shoots per explant (Molphe-Balch and Alejo, 1998). Similarly, the number of regenerated shoots from transformed tissue of Vitis vinifera cv. Thompson in a medium with the addition of kanamycin was much lower than the number of regenerated shoots from non-transformed tissue in a medium with no added kanamycin, i.e. 4.7 compared to 28 (Sabbadini, et al., 2019). These findings demonstrate that sensitivity to the presence of antibiotic-selective agents in a medium strongly influences the number of shoot regenerations. In this context, antibiotics used as selecting agents can lead to necrosis and tissue browning due to the production of reactive oxygen species, which can impact regeneration capacity (Zhou, et al., 2014).

In this study, the regeneration of transformed plant tissues was enabled by direct organogenesis through direct shoot formation from the cotyledon explants followed by root formation to produce transgenic plantlets. Root formation in the transformed and non-transformed shoots (Figure 6F and 6G) was successfully achieved on MS medium with the addition of IBA (1.0 mg/l). These results were in line with Tangapo et al. (2012) and Barpete et al. (2014) for the promotion of adventitious roots in transgenic shoots whereby an auxin such as IBA was required. Similarly, rooting in Artemisia sp. microshoots was successfully achieved in MS medium with the addition of 0.5 mg/l IBA (Shibli, et al., 2018). The application of IBA growth hormone effectively induced root formation, since IBA has been widely used in various plants to promote root formation.

4.3. Expression of HMGR1 Gene

The relative expression of the HMGR1 gene under the CaMV 35S promoter in transgenic A. paniculata was 52.5-fold higher compared to in the non-transgenic plant. This is similar to previously reported results that specific promoters can induce structural gene expression (Fu et al., 2018). In addition, the promoter CaMV 35S is a strong constitutive promoter used in transgenic expression in plants (Somssich, 2019).

Up-regulating the HMGR1 gene was expected to enhance the activity of the HMGR enzyme. As reported, the HMGR activity showed a positive correlation with andrographolide biosynthesis in A. paniculata (Jha et al., 2011); as such, the increase in HMGR enzyme activity would enhance andrographolide content. Moreover, Jha et al. (2011) reported that the application of GA3 and Jasmonic acid enhanced andrographolide by 0.31 fold and 0.56 fold, respectively.

4.4. Up-regulation of HMGR1 Gene Increased the Andrographolide Content

Using a separate ANOVA test, significant differences were observed between the transformed leaf and normal leaf tissues, the transformed stem and normal stem tissues, and the transformed plant and normal plant tissues. Meanwhile, the ANOVA test revealed no significant difference between the transformed and the normal root tissue. However, when advanced tests were conducted to examine differences between groups of samples simultaneously, namely through Tukey's post-hoc test, different results emerged. These revealed no significant differences between the levels of andrographolide in the transformed stem tissues, transformed roots, normal leaves, normal stems, and normal roots. Only the transformed leaves exhibited a notable difference when compared to the transformed stems, transformed roots, normal leaves, normal stems, and normal roots.

It was obvious that the results of this ANOVA test revealed only the presence of differences in the levels of andrographolide in the samples in the normal leaf, normal stem, normal root, transformed leaf, transformed stem, and transformed root tissue, while Tukey's post-hoc test identified the actual groups that differed significantly. This study revealed that the levels of andrographolide in transgenic leaf tissue differed significantly from those in normal leaves, normal stems, normal roots, transformed stems, and transformed roots.

Furthermore, the study demonstrated that andrographolide levels in the transgenic leaves, stems, and roots increased by 3.1, 2.9, and 1.1 times, respectively. Consequently, the average total andrographolide content in the entire transgenic plant was 2.6 times higher than in the normal plant (Table 2). The increased andrographolide levels were primarily driven by a significant increase in the level within the leaf tissue as opposed to in the stem and root tissues. This finding aligns with Royani et al. (2014), whose study reported higher andrographolide content in the leaves of A. paniculata compared to the stem or root.

The increase in andrographolide levels in the transgenic plant was most likely related to overexpression of the HMGR1 gene, which has been reported to be 52.5 times higher than in the controls. This aligned with a previous finding that andrographolide biosynthesis was enhanced by 0.31- to 0.6-fold as the expression level of HMGR genes increased (Jha et al., 2011). Another study reported that the production of β-sesquiphellandrene increased by 1.25–1.60 fold when the endogenous HMGR gene in the eukaryotic mevalonate pathway was overexpressed (Song et al., 2012).

Nevertheless, in this study, it appears that the increase in andrographolide concentration was not as high as the increase in *HMGR1* gene expression. This probably reflected how the working position of *HMGR* was at an early stage in the andrographolide biosynthesis pathway via the mevalonate pathway, while andrographolide synthesis occurs further downstream of the pathway, with several steps still required before reaching the andrographolide synthesis stage (Figure 8). In andrographolide biosynthesis via the mevalonate cascade, several intermediate compounds are involved, including mevalonate, FPP (farnesyl diphosphate), and GGPP (Geranyl-geranyl diphosphate), as described by Jha *et al.* (2011). These intermediate compounds are used as the precursors of many compounds; for example, FPP is used as a precursor for the synthesis of sesquiterpenes and triterpenes, GGPP is used not only for the synthesis of andrographolide (diterpene lactone) but also for the biosynthesis of other diterpenes such as ent-kaurene and Gibberellins and for the synthesis of polyterpenes (Taiz and Zeiger, 2002). Consequently, the substrate for the synthesis of andrographolide was reduced. This potentially explains why the increase in andrographolide content was not as high as the increase in *HMGR1* gene expression in *A. paniculata*.
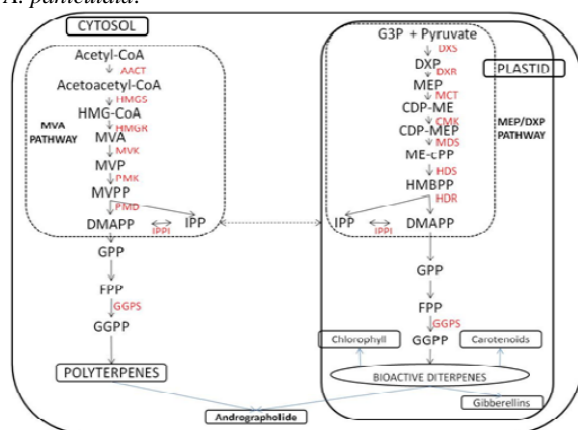
Figure 8. Biosynthetic pathway of andrographolide (Jha *et al.*, 2011)

5. Conclusions

Andrographis paniculata tissue was successfully transformed by recombinant plasmid pBI121-*HMGR1* using the *Agrobacterium tumefaciens* GV3101-mediated transformation procedure. The overexpression of *HMGR1* under the CaMV 35S promoter in the whole plant enhanced the andrographolide content by up to 2.6 times compared to the control plant. This demonstrates that the amount of andrographolide was associated with the expression level of the *HMGR1* gene in the andrographolide biosynthetic pathway. This study is the first to report that overexpression of the *HMGR1* gene under the CaMV 35S promoter in the *A. paniculata* medicinal plant can enhance the principal active constituent andrographolide. This finding is, therefore, beneficial for biotechnological research in medicinal plants.

References

Akbar S. 2011. *Andrographis paniculata:* A review of pharmacological activities and clinical effects. Altern Med Rev., **6(1)**:66–77. https://www.researchgate.net/publication/50865161_Andrographis_paniculata_A_Review_of_Pharmacological_Activities_and_Clinical_Effects

Allison LA. 2007. **Fundamental Molecular Biology** 1st edition. Blackwell Publishing, Oxford. https://molbiomadeeasy.files.wordpress.com/2013/09/fundamental_molecular_biology.pdf

Alvarez MA, Marconi PL. 2011. Genetic transformation for metabolic engineering of tropane Alkaloids in **Genetic Transformation** E-book. https://doi.org/10.5772/34216

Amack SC, Antunes MS. 2020. CaMV35S promoter–A plant biology and biotechnology workhorse in the era of synthetic biology. Curr. Plant Biol., **24**: 100179. https://doi.org/10.1016/j.cpb.2020.100179

Amara AA. 2018. Fast plasmid slot lysis and gram-negative bacteria ghost preparation protocol. Austin J. proteom bioinfo & genom., **5(1)**:1025. https://www.researchgate.net/publication/328841226

Barpete S, Khawar KM, Özcan S. 2014. Differential competence for in vitro adventitious rooting of grass pea (*Lathyrus sativus* L.). PCTOC., **119(1)**:39–50. https://doi.org/10.1007/s11240-014-0512-6

Benoy GK, Animesh DK, Aninda M, Priyanka DK, Sandip H. 2012. An overview on *Andrographis paniculata* (Burm.F.) Nees. Int J Res in Ayurveda and Pharm., **3(6):**752–760. https://doi.org/10.7897/2277-4343.03610

Calabrese C, Berman SH, Babish JG. 2000. A phase I trial of andrographolide in HIV positive patients and normal volunteers. Phytotherapy Res., **14(5)**:333–338. https://doi.org/10.1002/1099-1573(200008)14:5<333::aid-ptr584>3.0.co;2-d.

Chandrasekaran C, Murali B, Deepak M, Agarwal A. 2012. In vitro comparative evaluation of non-leaves and leaves extracts of *Andrographis paniculata* on modulation of inflammatory mediators. Anti-Inflam & Anti-Allerg Agents in med Chem., **11(2):**191-197. https://doi.org/10.2174/187152312803305731.

Chang AY, Chau VWY, Landas JA, Pang Y. 2017. Preparation of calcium competent *Escherichia coli* and heat-shock transformation. JEMI-methods., **1**: 22-25. https://ujemi.microbiology.ubc.ca/sites/default/files/Chang%20et%20al%20JEMI-methods%20Vol%201%20pg%2022-25.pdf

Chao WW, Lin BF. 2010. Isolation and identification of bioactive compounds in *Andrographis paniculata* (Chuanxinlian). Chin Med., **5(17)**: 1-15. https://doi.org/10.1186/1749-8546-5-17

Chaudhury A, Dalal AD, Sheoran NT. 2019. Isolation, cloning and expression of CCA1 gene in transgenic progeny plants of Japonica rice exhibiting altered morphological traits. PLOS ONE., **14(8)**. https://doi.org/10.1371/journal.pone.0220140.

Churiyahi, Pongtulurani OB, Rofaani E, Tawardi. 2015. Antiviral and Immunostimulant Activities of *Andrographis paniculata*. HAYATI J Biosci., **22(2)**: 67-72. https://doi.org/10.4308/hjb.22.2.67

Dong N, Ponciano G, McMahan CM, Coffelt TA, Johnson L, Creelman R, Whalen MC, Cornish K. 2013. Overexpression of 3-hydroxy-3-methylglutaryl coenzyme A reductase in *Parthenium argentatum.* Ind Crops Prod., **46**:15-24. https://doi.org/10.1016/j.indcrop.2012.12.044

Du J, Wenzhong Hu W, Yang D, Meng F, , Li Y, 2020. Cloning and functional analysis of HMGR gene in *Ligularia fischeri.* IOP Conf. Ser.: Earth Environ. Sci., 615:012112. https://doi.org/10.1088/1755-1315/615/1/012112

Enmozhi SK, Raja K, Sebastine I, Joseph J. 2020. Andrographolide as a potential inhibitor of SARS-CoV-2 main protease: An in silico approach. J Biomol Struct Dyn., **39(9)**:3092-3098. https://doi.org/10.1080/07391102.2020.1760136.

Fu R, Martin C, Zhang Y. 2018. Next-Generation Plant Metabolic Engineering Inspired by an Ancient Chinese Irrigation System. Mol. Plant **11(1)**: 47–57. https://doi.org/10.1016/j.molp.2017.09.002

Han JY, Kim MJ, Ban YW, Hwang HS, Choi YE. 2013. The involvement of b-Amyrin 28-oxidase (CYP716A52v2) in oleanane-type ginsenoside biosynthesis in Panax ginseng. Plant Cell Physiol., **54(12)**: 2034–2046. https://doi.org/10.1093/pcp/pct141

Han L, Li J, Guo J, Ma Y, Guo X. 2017. Expression vector construction and genetic transformation of *Paeonia lactiflora* gibberellin 20-oxidase gene. Am. J. Plant Sci., **8(7)**: 1525-1533. https://doi.org/10.4236/ajps.2017.87105

Harjotaruno S, Widyawaruyantil A, Zaini NC. 2008. Apoptosis inducing effect of andrographolide on TD-47 human breast cancer cell line. AJTCAM., **4(3)**:345–351. https://doi.org/10.4314/ajtcam.v4i3.31228

Jarukamjorn K, Nemoto N. 2008. Pharmacological aspects of *Andrographis paniculata* on health and its major diterpenoid constituent andrographolide. J. Health Sci., **54(4)**:370–381. https://doi.org/10.1248/jhs.54.370

Jha Z, Sharam SH, Sharma DK. 2011. Differential expression of 3-hydroxy-3-methylglutaryl-coenzyme A reductase of *Andrographis paniculata* in andrographolide accumulation. J. Chem. Pharm. Res., **3(3)**:499-504. https://www.jocpr.com/articles/differential-expression-of-3hydroxy3methylglutarylcoenzyme-a-reductase-of-andrographis-paniculata-in-andrographolide-acc.pdf

Kabir MH, Hasan N, Rahman MM. 2014. A survey of medicinal plants used by the Deb barma clan of the Tripura tribe of Moulvibazar district, Bangladesh. J. Ethnobiol. Ethnomed., **10(19)**:1-28. https://doi.org/10.1186/1746-4269-10-19.

Kim YJ, Lee OR, Oh JY, Jang MG, Yang DC. 2014. Functional analysis of 3-hydroxy-3-methylglutaryl coenzyme-a reductase encoding genes in triterpene saponin producing ginseng. Plant Physiol., **165(1)**:373–387. https://doi.org/10.1104/pp.113.222596

Koerniati S, Widhianata H. 2012. Construction and transformation of HVA1 gene expression vector into Indoensian elite rice varietis. J. AgroBiogen., **8(2)**:54-6. https://doi.org/10.21082/jbio.v8n2.2012.p54-61

Konagaya KI, Nanasato Y, Taniguchi T. 2020. A protocol for Agrobacterium-mediated transformation of Japanese cedar, Sugi (*Cryptomeria japonica* D. Don) using embryogenic tissue explants. Plant Biotech., **37(2)**:147–156. https://doi.org/10.5511/plantbiotechnology.20.0131a

Kumar RA, Sridevi K, Vijaya KN, Nanduri S, Rajagopal S. 2004. Anticancer and immunostimulatory compounds from *Andrographis paniculata*. J. Ethnopharmacol., **92(2-3)**:291–295. https://doi.org/ 10.1016/j.jep.2004.03.004.

Laksmiani NPL, Larasanty LPF, Santika AAGJ, Prayoga PAA, Dewi AAIK, Dewi NPAK. 2020. Active Compounds Activity from the Medicinal Plants Against SARS-CoV-2 using in Silico Assay. Biomed. Pharmacol. J., **13(2)**:73–881. https://dx.doi.org/10.13005/bpj/1953

Lakshmi SA, Shafreen RMB, Priya A, Shunmugiah KP. 2021. Ethnomedicines of Indian origin for combating COVID-19 infection by hampering the viral replication: using structure-based drug discovery approach. J. Biomol. Struct. Dyn., **39(13)**:4594-4609. https://doi.org/ 10.1080/07391102.2020.1778537.

Levita J, Nawawi A, Mutholib A, Ibrahim S. 2010. Andrographolide: a review of its anti-inflammatory activity via inhibition of NF-kappaβ activation from computational chemistry aspects. Int J. Pharmacol., **6(5)**:569–76. https://doi.org/10.3923/ijp.2010.569.576

Livak KJ, Schmittgen TD. 2001. Analysis of relative gene expression data using real time quantitative PCR and the 2-ΔΔCT method. Methods., **5(4)**:402–408. https://doi.org/10.1006/meth.2001.1262

Lu X, Tang K, Li P. 2016. Plant metabolic engineering strategies for the production of pharmaceutical terpenoids. Front. Plant Sci., **7**:1647. https://doi.org/10.3389/fpls.2016.01647

Majee C, Gupta BK, Mazumder R, Chakraborthy GS. 2011. HPLC method Development and Characterization of Bio-Active Molecule Isolated from *Andrographis paniculata.* Int. J. Pharmtech Res., **3(3)**: 1586-1592.

Marwani E, Tangapo A, Dwivany FM. 2013. Agrobacterium-mediated stable transformation of medicinal plant *Andrographis paniculata* callus expressing ß-glucuronidase (GUS) gene. IJB., **18 (2)**: 92-100. https://doi.org/10.22146/ijbiotech.7873.

Menra JP. 2013. Isolation and construction of 3-hydroxy-3-methylglutaryl-coenzyme A reductase 1 gene (*HMGR1*) from *Andrographis paniculata* (Burm.f.) Wallich. ex Nees . [Unpublished master's thesis]. Institut Teknologi Bandung.

Mohammed S, Samad AA, Rahmat Z. 2019. Isolation, Cloning, and Sequence Analysis of the Full-Length RFT1 Gene from Malaysian Upland Rice (*Oryza sativa*, subsp. Indica, Cultivar Wai). JJBS., **12(3)**: 259-265**.** https://jjbs.hu.edu.jo/files/vol12/n3/Paper%20number%202.pdf

Molphe-Balch EP, Ochoa-Alejo N. 1988. Regeneration of transgenic plants of Mexican lime from *Agrobacterium rhizogenes*-transformed tissues. Plant Cell Rep., **17**: 591–596. doi: 10.1007/s002990050448

Nomani M, Tohidfar M. 2021. Plant regeneration and transformation of *Trachyspermum ammi* using *Agrobacterium tumefaciens* and zygotic embryos. JGEB., **19(1)**: 1-10. https://doi.org/10.1186/s43141-021-00173-8

Putter KM, Deenan NV, Unland K, Prufer D, Gronover CS. 2017. Isoprenoid biosynthesis in dandelion latex is enhanced by the overexpression of three key enzymes involved in the mevalonate pathway. BMC Plant Biol., **17(88)**:1-13. https://doi.org/10.1186/s12870-017-1036-0

Rao KY, Vimalamma G, Rao CV, Tzeng YM. 2004. Flavonoids and andrographolides from *Andrographis paniculata*. Phytochem., **65(16)**:2317-2321. https://doi.org/10.1016/j.phytochem.2004.05.008

Royani JI, Hardianto D, Wahyuni S. 2014. Analisis kandungan andrographolide pada tanaman sambiloto (*Andrographis paniculata*) dari 12 lokasi di Pulau Jawa. JBBI., **1(1)**:15-20.

https://doi.org/10.29122/jbbi.v1i1.547

Sabbadini S, Capriotti L, Molesini B, Pandolfini T, Navacchi O, Limera C, Ricci A, Mezzetti B. 2019. Comparison of regeneration capacity and *Agrobacterium*-mediated cell

transformation efficiency of different cultivars and rootstocks of Vitis spp. via organogenesis. Sci Rep., **9**: 582. doi: 10.1038/s41598-018-37335-7

Sharma SN, Jha Z, Sinha RK. 2013. Establishment of in vitro adventitious root cultures and analysis of andrographolide in *Androgrphis paniculata*, Nat Prod Cummon., **8(8)**:1045-7. : https://www.researchgate.net/publication/256196934

Shibli RA, Sharaf SA, Kasrawi MA, Al-Qudah T. 2018. In Vitro Multiplication of the White Wormwood, Artemisia. JJBS., **11(3)**: 265-271. https://jjbs.hu.edu.jo/files/v11n3/Paper%20Number%205.pdf

Shi TH, Huang YL, Chen CC, Pi WC, Hsu YL, Lo LC, Chen WY, Fu SL, Lin CH. 2020. Andrographolide and its fluorescent derivative inhibit the main proteases 2019-nCoV and SARS-CoV through covalent linkage. BBRC., **533(3)**:467-473. https://doi.org/10.1016/j.bbrc.2020.08.086

Shim JS, Lee OR, Kim YJ, Lee JH, Kim JH, Jung DY. 2010. Overexpression of PgSQS1 increases ginsenoside production and negatively affects ginseng growth rate in Panax ginseng. JGR., **34(2)**:98-103. https://doi.org/10.5142/jgr.2010.34.2.098

Somssich, M. 2019. A short history of the CaMV 35S promoter. PeerJ Prepr., **7**: e27096v3. https://doi.org/10.7287/peerj.preprints.27096v3

Song AAL, Abdullah JO, Abdullah MP, Shafee N, Othman R, Tan EF, Noor NM, Raha AR. 2012. Overexpressing 3-Hydroxy-3-Methylglutaryl coenzyme A reductase (HMGR) in the Lactococcal mevalonate pathway for heterologous plant sesquiterpene production. PLos One., **7**: e52444. https://doi.org/10.1371/journal.pone.0052444

Suebsana S, Pongnaratorn P, Sattayasai J, Arkaravichien T, Tiamkao S, Aromdee C.2009. Analgesic, antipyretic, anti-inflammatory, and toxic effect of andrographolide derivates in experimental animal. Arch Pharm Res., **32(9)**:1191-1200. https://doi.org/10.1007/s12272-009-1902-x.

Sukumaran S. 2011. Concentration determination of nucleic acids and proteins using the micro-volume bio-spec nano spectrophotometer. JoVE., **48**: 1-5. https://doi.org/10.3791/2699.

Tangapo AM, Marwani E, Dwivany FM. 2012. Transformasi dan ekspresi transien gen pelapor gus pada *Androgrphis paniculata* (Burm.F.) Wallich Ex Ness or transformation and expression of reporter gene Gus on *Androgrphis paniculata* (Burm.F.) Wallich Ex Ness. JBL., **2(1)**: 1-10. https://doi.org/10.35799/jbl.2.1.2012.375

Taiz L and Zeiger E. 2002. **Plant Physiology**, 5th Edition. Sinauer Associates Inc., Sunderland. https://www.academia.edu/27225799/Plant_Physiology_Taiz_and _Zeiger_

Vidal N, Mallon R, Valladares S, Meijomin AM. 2010. Regeneration of transgenic plants by Agrobacterium-mediated transformation of somatic embryos of juvenile and mature *Quercus robur* Abbreviations AS Acetosyringone BA Benzyladenine Kan Kanamycin MS Murashige and Skoog NAA a-Naphthaleneacetic acid X-Gluc 5-Bromo-4-chloro-3-indolyl-b-D-glucuronide. Plant Cell Rep., **29(12)**: 1411-1422. https://doi.org/10.1007/s00299-010-0931-8

Wiart C, Kumar K, Yusop MY, Hamimah H, Fauzi ZM, Sulaiman M. 2005. Antiviral properties of Ent-labdene diterpenes of *Androgrphis paniculata* Nees, inhibitors of herpes simplex virus type 1. Phytother Res., **19(12)**:1069-1070. https://doi.org/10.1002/ptr.1765

Xiong J. 2006. **Essential Bioinformatics**. Cambridge: Cambridge University Press. https://books.google.co.id/books?id=92K1QgAACAAJ&hl=id

Zhou Q, Dai L, Cheng S, He J. 2014. A circulatory system useful both for long-term somatic embryogenesis and genetic transformation in *Vitis vinifera* L. cv. Thompson Seedless. PCTOC., **118(1)**:157–168. doi: 10.1007/s11240-014-0471-y.

The Role of Artocarpin In Inhibiting Wnt/B-Catenin Signalling Pathway Through Its Binding to Tcf-4/B-Catenin Complex in H460-Derived Lung Cancer Stem Cells.

Nik Nurul Najihah Nik Mat Daud[1], Noor Azlina Abu Bakar[2,*], Abdi Wira Septama[3], Badrul Hisham Yahaya[4], Norashikin Zakaria[4], Noor Zafirah Ismail[5], and Hasni Arsad[5]

[1] Department of Biomedical Science,Faculty of Applied Science, Lincoln University College Main Campus,No.2, Jalan Stadium, SS7/15, Kelana Jaya, 47301, Petaling Jaya, Selangor; [2] Faculty of Medicine, Universiti Sultan Zainal Abidin, Jalan Sultan Mahmud 20400, Kuala Terengganu, Terengganu,Malaysia; [3] Research Center for Pharmaceutical Ingredients and Traditional Medicine, National Research and Innovation Agency (BRIN), Cibinong Science Center (CSC), Bogor, West Java 16911, Indonesia; [4] Regenerative Medicine Cluster, Advanced Medical and Dental Institute (AMDI), Universiti Sains Malaysia, Bertam, 13200 Kepala Batas, Pulau Pinang, Malaysia; [5] Laboratory of Biocrystallography and Structural Bioinformatics, Advanced Medical and Dental Institute (AMDI), Universiti Sains Malaysia, Bertam, 13200 Kepala Batas, Pulau Pinang, Malaysia

Abstract

The presence of cancer stem cells (CSCs) in lung cancer could contribute to cancer development and unsuccessful treatment. β-Catenin protein has been found to play a crucial role in cell survival. As artocarpin has been postulated to exert important antitumor properties, this research was conducted to elucidate the effect of artocarpin in the suppression of CSCs through modulating the β-Catenin signalling pathway. Using isolated CSCs from lung adenocarcinoma cell lines (H460), the potential of artocarpin in suppressing CSC was assessed using MTT assay. The stemness gene expression was analysed using real-time quantitative polymerase chain reaction; meanwhile, the assessment of artocarpin binding affinity against the β-Catenin active site was performed using docking analysis and validated with RT-qPCR. A 62.5% of lung CD166$^+$CD44$^+$ CSCs cells and 37.5% of lung CD166$^-$CD44$^-$ non-CSCs cells were identified in the H460 cell line. The results revealed that artocarpin exerted the highest cytotoxic value against lung CD166$^+$CD44$^+$ CSCs with an IC$_{50}$ value of 5.07 µg/mL compared to CD166$^-$CD44$^-$ non-CSCs and H460 cells which were 8.67 µg/mL and 9.07 µg/mL, respectively. Additionally, the expression of stemness genes such as KLF4, SOX2, and NANOG was found to be significantly reduced ($P< 0.05$) in the treated lung CSCs with fold change (FC) values of 0.025, 0.104, 0.074, respectively in 10 µM artocarpin. The molecular docking analysis showed that artocarpin possessed the best-docked complexes with β-Catenin and WNT protein with high binding energy values (-7.04 kcal/mol and -14.91 kcal/mol), respectively compared to other WNT/β-Catenin inhibitors including isorhamnetin, fisetin, genistein, silibinin, catechin, luteolin, coumestrol and β-naphthoflavone. These findings support the inhibitory activity of artocarpin on lung CSCs with low WNT and β-Catenin gene expression levels and FC values (0.155, $P<0.01$ and 0.129, $P<0.05$) in 10 µM artocarpin compared to untreated cells, respectively. Therefore, based on this study, it is suggested that artocarpin has the potential to be developed as a therapeutic agent to inhibit stem cell regeneration in lung cancer via the WNT/β-Catenin signalling pathway through inhibition of TCF-4/β-Catenin complex formation.

Keywords: artocarpin, cancer stem cells, differentiation assay, molecular docking and stemness gene.

1. Introduction

Cancer recurrence or relapse is one of the major concerns in cancer therapy. It is estimated that around one-third of all cancer patients will experience a recurrence at some point after their initial treatment. The risk of recurrence varies depending on the type of cancer, the stage at diagnosis, and the type of treatment received. Nowadays, there are many major treatments for cancer management including surgery, cytotoxic chemotherapy, targeted therapy, radiation therapy, endocrine therapy, and immunotherapy. Despite the achievements made in treating cancers during the past decades, resistance to

---

classical chemotherapeutic agents and novel targeted drugs continues to be a challenge. With decades of research on cancer recurrent, it was found due to the presence of a small subsets of cells resides within the tumour, which can self-renew and maintain the tumorigenic characteristics. These cells are known as cancer stem cells (CSCs). CSCs are cancer cells that can self-renew and give rise to heterogeneous cancer cell lineages that comprise *an* entire tumour (Khatami *et al*., 2020; Almajali *et al*., 2021). According to Jahanafrooz *et al*. (2020), various studies have consistently found that the signalling pathway of CSCs is a critical factor and plays a crucial role in disease progression. Although the presence of CSCs has been studied in detail in many solid tumours (Huang *et al*., 2020), insufficient attention has been paid to lung cancer cells, especially H460 cell lines. In addition, it is still unclear if CSCs are present in all or only specific cancer cells. This is due to the resilience of CSC markers and the underestimation of tumorigenic cell frequencies detected by the current available techniques. Thus, the present study sought to isolate CSCs from H460 cells and investigate the effect of artocarpin in suppressing the proliferation of CSCs in H460 cells as a model cell line for non-small cell lung cancer cells (NSCLC), as well as to investigate the mechanism of action that triggers the suppression through the WNT/β-Catenin degradation pathway.

Several CSCs regulators have been determined, and the findings provide understanding of how CSCs drive tumour homeostasis. In many cancer types, aberrant gene expression is highly related to tumour development, progression, and treatment resistance (Huang *et al*., 2020). The process that governs the pluripotency maintenance and plasticity of CSCs involves the regulation of multiple transcription factors such as octamer-binding transcription factor 3/4 (OCT3/4), Sry-related HMG box 2 (SOX2), Kruppel-like factor 4 (KLF4), NANOG, and c-MYC (Van Schaijik *et al*., 2018). Although these transcription factors play essential roles in controlling the activity of specific genes in embryonic stem cells (ESCs), particularly those associated with stem cell pluripotency, cell differentiation, and cellular reprogramming, regulations of its expressions lead to cancerous growth (Pouremamali *et al*. (2022). While the precise source of CSCs remains a topic of ongoing research, multiple studies have put forth several hypotheses regarding their origin. These hypotheses include the fusion of a normal stem cell with a transformed cell, the horizontal transfer of an oncogene from an apoptotic cell to a normal stem cell resulting in its transformation into a CSC, and the potential for stem cells residing in a tissue for repair purposes to transform into CSCs in response to an inflammatory microenvironment, triggered by the release of cytokines during infection and inflammation (Nimmakayala *et al*., 2019).

In addition, other intracellular activities, such as the WNT/β-Catenin signalling pathway, also regulate CSC phenotypes (Yang *et al*., 2020). Fundamentally, this cascade is responsible for embryonic development. However, dysregulation of this signalling and its interaction with other critical regulatory components, such as the TCF4/β-Catenin complex, leads to self-renewal, tumorigenesis or malignancies, and metastasis of CSCs (Zhan *et al*., 2017). Marked overexpression of β-Catenin and TCF-4 protein was recorded in the CSCs population compared to non-CSCs, while its inhibition was reported to attenuate CSCs metastasis in various cancer types (Makena *et al*., 2020). TCF-4 is an E-protein (E-box) involved in various developmental aspects (Forrest *et al*., 2014). For example, the TCF-4 protein plays a role in the maturation of cells to carry out specific functions, including regulating a variety of neural genes involved in early development, differentiation, intrinsic excitability, synapses, and survival (Chen *et al*., 2021). According to Hwang *et al*. (2020), TCF-4's involvement in cell survival, and induction of anti-apoptosis mechanisms suggested that TCF-4 may be a molecular target for CSC regeneration.

Among many potentially natural-derived anticancer agents, artocarpin is on the list. This compound's anticancer activity against lung cancer cells has been studied extensively (Mat Daud *et al*., 2021); however, the mechanism of how this compound inhibits tumour progression and stemness characteristic of CSCs remains unexplored. The advancement of molecular docking technology can provide insight into the interaction of this compound with the specifically targeted component (β-Catenin and WNT protein) of the signalling pathway. What are the possible consequences of the binding energy between artocarpin with both proteins β-Catenin and WNT obtained to the level of the oncogene expression? This study sets out to address this research gap, contribute to the knowledge of isolating CSCs from the parental H460 cell lines, and explain the possible regulatory mechanisms exerted by this compound on isolated cells, thereby elucidating its anticancer mechanisms.

2. Materials and methods

2.1. Cell lines

The human lung adenocarcinoma (H460) cell line was purchased from the American Type Culture Collection (ATCC, Manassas, VA, USA). The cells were routinely cultured and incubated at 37°C with 5% CO_2. The cells were grown in 75 cm^2 tissue culture flasks and collected with 0.25% trypsin-EDTA once they reached 80% confluence.

2.2. Chemicals and reagents

All cancer cell lines were cultured in RPMI-1640 medium containing 10% foetal bovine serum (FBS) and 1% penicillin/streptomycin (Gibco, Life Technologies, Foster City, CA, USA). The DMSO was purchased from Sigma-Aldrich in Munich, Germany. The antibodies used includes CD44-FITC (Clone: L178; Isotype: Mouse IgG1, κ), CD166-PE (Clone: 3A4; Isotype: Mouse IgG1, κ) (BD Biosciences, San Jose, CA, USA), and EpCAM–FITC (Clone: 158206; Isotype: Mouse IgG2B; Isotype: Mouse IgG1, κ) (R&D System, Minneapolis, MN, USA).

2.3. Preparation of artocarpin compound

The pure compound of artocarpin was generously provided by Septama and Panichayupakaranant who isolated the sample as mentioned in Septama and Panichayupakaranant, 2015. In this study, artocarpin compound was prepared as a stock solution by dissolving 500 μg into 1 mL of absolute DMSO. Then, 1000 μL of artocarpin compound was mixed with 1 μL of absolute DMSO and 999 μL of culture media to produce 2000 μL of test solution for each tube containing 0.1% DMSO. Prior to cell treatment, five concentrations (31.25, 15.63,

7.81, 3.91, 1.95 µg/mL) for each compound were prepared for cytotoxicity test meanwhile two concentrations of artocarpin (10µM and 100µM) were prepared for CSCs characterization assays and gene expression. The prepared concentrations were determined based on dose-response curves obtained from MTT assay in a preliminary study for artocarpin on the H460 cell line. For conducting the experiments, stock solutions of artocarpin were prepared by dissolving 500 µg of the compound in 1 mL DMSO and stored at -20°C. The final DMSO concentration in each well was kept between 0.1% and 0.11% for the treatment of cells throughout the experiments.

2.4. Isolation of CSCs phenotype

CSCs were isolated based on their specific surface markers using corresponding specific antibodies (Satar *et al.* (2018). In detail, the confluent (80%) lung cancer cells were detached using trypsin and washed with 2% FBS mixed with phosphate buffer solution (PBS). The antibodies which include CD44-FITC (Clone: L178; Isotype: Mouse IgG1, κ), CD166-PE (Clone: 3A4; Isotype: Mouse IgG1, κ) (BD Biosciences, San Jose, CA, USA), and EpCAM–FITC (Clone: 158206; Isotype: Mouse IgG2B; Isotype: Mouse IgG1, κ) (R&D System, Minneapolis, MN, USA) were then used to label all of the cell suspensions. Following that, cells were mixed in 90 µL of 2% FBS PBS, to which 10 µL of each antibody was added, and incubated for 30 minutes in the dark. The unbound antibodies were then washed with PBS. Each cell pellet received 500 µL of 2% FBS PBS, and the mixture was filtered through a 40 µm cell filter to ensure the formation of a single-cell suspension. Using a fluorescence-activated cell sorter (FACS Aria III, BD Biosciences), cancer stem cell markers CD166, CD44, and EpCAM expressions were examined and sorted (Masciale *et al.*, 2019).

2.5. Co-Expression of CSCs Surface Markers in Lung Cancer Cells

Briefly, the H460 cells were detached by incubating with trypsin at 0.25% concentration (80% confluency) for 5 minutes, followed by washing with phosphate buffer solution (PBS) containing 2% of Foetal bovine serum (FBS). Then, the cells were labelled with only two antibody types: CD44-FITC and CD166-PE excluded EpCAM–FITC as they were not detected in the identification process. A 10 µL of each of the respective antibodies were added into cell suspension containing 90 µL of PBS and 2% of FBS. They were incubated for 30 minutes in the dark condition. The cell suspension was centrifuged to obtain the cells bound with antibody, while the remaining unbound antibody in the supernatant was discarded. Afterward, 500 µL of PBS containing 2% of FBS was added into each cell pellet and re-suspended before the filtration process using 40 µm cell filters to ensure that a single cell suspension was obtained.

2.6. The cytotoxic assay of artocarpin compound

A cultured H460, lung CSC and non-CSC in RPMI-1640 media with 10% v/v FBS, 1% v/v penicillin-streptomycin in 25 cm^2 T-flask (GIBCO, USA), humidified with 5% CO2 at 37°C were plated in a 96-well plate (5×10^3 cells/well) and incubated for 24 hours. Each well was then filled with the prepared artocarpin compound and a medium containing 0.1% DMSO.

Following 48 hours of incubation, 20 µL of MTT reagent (5 mg/mL) was added and incubated for another four hours. Following observation through a microplate reader (Spectra 340, Tecan Magellan PRO, Molecular Device, Sunnyvale, CA) at 570 nm, the aspirated medium was replaced with 150 µL of absolute DMSO. The number of viable cells was determined by measuring the absorbance value. The inhibitory percentage was obtained by dividing the absorbance of the sample by the absorbance of the control. The untreated cell served as a negative control meanwhile, cisplatin-treated cells served as a positive control.

2.7. CSCs transcription factors expression

To investigate the expression of CSCs transcription factors, two-step quantitative reverse transcription polymerase chain reaction (RT-qPCR) analyses were employed. Briefly, using a RNeasy Plus Mini Kit (Qiagen), the total amount of RNA was extracted from the isolated cells. cDNA was synthesized from 250 ng/µL of total RNA by using the GoScript Reverse Transcription System (Promega, Woods Hollow Road Madison, USA) focusing on random primer and oligo (dT)15 primer. Assays-on-Demand primer/probe sets, and TaqMan Universal PCR Master Mix (Applied Biosystems) were utilized for the RT-qPCR reactions. Assays included the stem cell-related genes SOX2, KLF4, NANOG, OCT 3/4, DACT3 (β-Catenin), and the reference gene; GAPDH genes (Applied Biosystems) were used. The RT-qPCR reaction was conducted using the ABI StepOnePlusTM PCR System (Applied Biosystems, Foster City, USA) with the following thermal cycling conditions: 10 minutes at 95°C (holding stage), followed by 40 cycles of denaturation for 15 seconds at 95°C and annealing and extension steps for 1 minute at 60°C using a StepOnePlusTM Real-Time PCR System Thermal Cycling Block (Applied Biosystems). The comparative CT (ΔΔCT) method was utilized for quantification. In this study, untreated cells served as the control sample, while the GAPDH gene served as the endogenous control (Zakaria *et al.,* 2015).

2.8. Data extraction

The β-Catenin protein 3D structural file (PDB ID: 1JDH) was extracted from the protein data bank (PDB) (www.rcsb.org/pdb), while artocarpin structures molecules were analysed and depicted using ChemDraw Ultra V6.0. PyMOL viewer 1.5.4 was used for the interactive visualization and analysis of protein-ligand. ADME-T properties of artocarpin were predicted in-silico using the organic chemistry portal at http://www.organic-chemistry.org/prog. Molecular docking was conducted using AutoDock v4.24 on Windows 10 platform (64-bit) with Lenovo 120S-11IAP machine (Intel® Celeron® CPU N3350 @ 1.10 GHz, 4 GB memory) (Hassan *et al.,* 2021).

2.9. Inhibition analysis by docking

Docking analysis was done using AutoDock v4.24 by comparing the docking results with other known inhibitors of WNT/β-Catenin pathway (isorhamnetin, fisetin, genistein, silibinin, catechin, luteolin, coumestrol, and β-naphthoflavone) exhibited -6.50 to -5.22 kcal/mol (Iftikhar and Rashid, 2014), whereby polar hydrogen atoms have been added to the β-Catenin receptor protein. Rotatable ligand torsions permit flexible ligand docking, including

arbitrary flexible orientations and torsions for ligands. A $40 \times 40 \times 40$ Å3 grid with 0.375 between each point was constructed around the protein receptor to ensure all residues were accessible in any zone for ligand binding. The number of docking runs has been set at 100, with a population of 150 starting out, 2.5×10^6 energy assessments, a total of 27,000 iterations, a mutation rate of 0.02, and a crossover rate of 0.80. AutoDock performed cluster analysis on initially docked conformations with a root mean square tolerance of 1.0 Å to obtain final docking data (Hassan *et al.*, 2021; Abd Wahab and Ibrahim, 2022).

2.10. β-Catenin and WNT knockdown analysis

In mammalian cells, a scalable approach for detecting changes in gene expression following RNA was developed (Fleige *et al.*, 2006). This technique describes how to transfect cells, collect total RNA, synthesize cDNA, run qPCR reactions with multiplexed TaqMan dual hydrolysis probes and interpret qPCR findings using relative quantification (Muraro *et al.*, 2012). The relative knockdown of a set of β-Catenin and WNT genes against a target can be measured using this method. The protocol for doing RT-qPCR was outlined in the previous section on CSC transcription factors expression.

2.11. Statistical analysis

All data were expressed as the mean ± Standard Error Mean (SEM) of three independent experiments. MTT assay was statistically analysed using Graph Pad Prism® v6.01. Meanwhile, the expression of selected genes was analysed using an ABI StepOnePlus™ v2.3 Real-Time PCR machine (Applied Biosystems, Foster City, CA, USA). The RT-qPCR reaction was prepared using a Taqman® gene expression assay (Applied Biosystems). The comparison between artocarpin treatment group with the untreated group was performed using an unpaired t-test. *P* values of <0.05 were considered statistically significant for each test's n=3 sample size.

3. Results

3.1. Expression of cancer stem cell (CSCs) markers

Since the small population subtype of CSCs in lung cancer cell lines ranged across cell lines, specific markers, including CD166, CD44, and EpCAM, as CSCs markers in human lung cancer cell lines are required for the identification and isolation processes. In the identification process, the H460 cell exhibited 52.6% of CD166 expression and 13.8% of CD44 expression; meanwhile, 0% of EpCAM expression was observed. In this study, both surface markers of CD166 and CD44 excluding EpCAM, have been expressed with varying levels of expression in all H460 cell lines (Figure 1A). As depicted in Figure 1B, two markers' (CD166 and CD44) co-expression was examined in which 62.5% of the H460 cells were CD166$^+$CD44$^+$ mwanwhile CD166$^-$CD44$^-$ with the percentage of expression as 37.5% cells were identified as a non-CSC population.
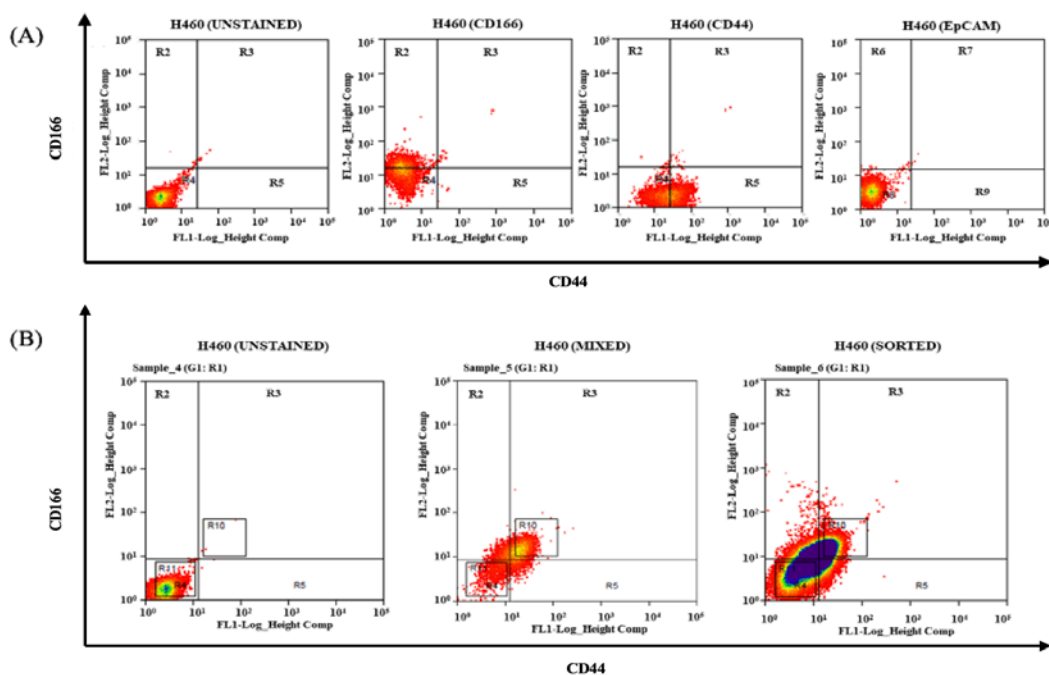
Figure 1. Flow cytometry analysis. (A) Identification of CD166, CD44, and EpCAM cells in H460 cancer cell line and (B) identification of co-expression of CD166/CD44 in H460 cancer cell lines. The cells were stained with anti-CD166 PE and anti-CD44 FITC.

3.2. Artocarpin cytotoxic assay on cancer cells line

The cytotoxic effect of artocarpin on cancer cells and cancer stem cells was demonstrated by the reduction in the number of living cells observed in the MTT assay. Artocarpin demonstrated an inhibitory impact on all cancer cell lines, as shown in Table 1. A significant difference was seen in each concentration (P<0.05) compared to control drug cisplatin. According to the result, a significant cytotoxic effect of artocarpin was observed against lung CSCs CD166$^+$CD44$^+$ followed by lung CSCs CD166$^-$CD44$^-$ (non-CSC) and H460 with IC$_{50}$ values of 5.07±0.12, 8.67±0.10, and 9.07±0.24 µg/mL, respectively.

Table 1. Inhibitory concentration (IC$_{50}$) of artocarpin and cisplatin against parental H460 and lung CSCs

Cells Types	Artocarpin	Cisplatin
	IC$_{50}$ (µg/mL) ± SEM	IC$_{50}$ (µg/mL) ± SEM
Lung CSC CD166$^+$/CD44$^+$	5.07 ± 0.12*	9.16 ± 0.05
Lung Non-CSC CD166$^-$/CD44$^-$	8.67 ± 0.10*	10.29 ± 0.05
H460	9.07 ± 0.24*	14.16 ± 0.19

Each data in the column represents the mean ± Standard Error Mean (SEM) with n=3. Unpaired t-test was used and the asterisk (*) indicates the significant difference of the compounds compared to cisplatin in each cell with P < 0.05.

3.3. Attenuation of stemness genes expression upon artocarpin treatment

All cell lines demonstrated detectable levels of the stem cell-related genes expression (Figure 2) except OCT 3/4. The KLF4, SOX2, and NANOG genes observed to be down-regulated with fold change (FC) values of 0.383 (P<0.001), 0.550 (P<0.001), and 0.338 (P<0.001), respectively in 10 µM of artocarpin treatment compared to their expression in the untreated cells. Further down-regulation was shown when using a higher dose of artocarpin (100 µM) with FC values of 0.055 (P<0.0001), 0.006 (P<0.0001), 0.040 (P<0.001) respectively.
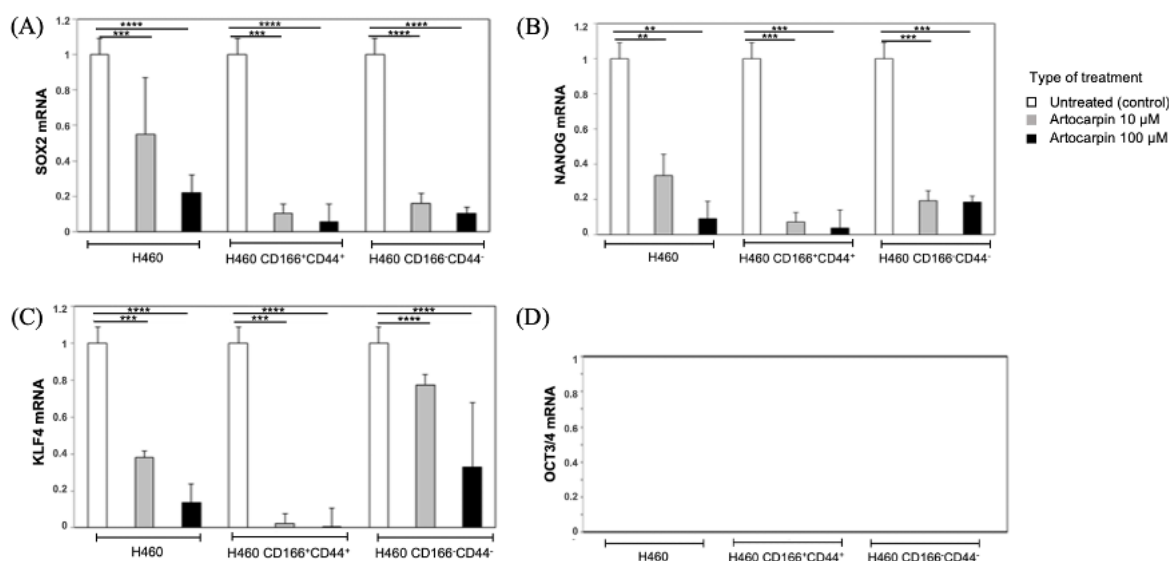
Figure 2. Analyses of the expression of stem cell-related genes in various H460 cell lines. Detectable levels of gene expression (A) SOX2, (B) NANOG and (C) KLF4 were found in all putative CSCs except (D) OCT 3/4. All detectable mRNA levels in cell lines are expressed as fold change. The negative control was a PCR reaction without a template. Data from three independent cell passages is given as mean ± Standard Error Mean (n=3). One Way ANOVA was used to compare between respective control group. * P <0.05, **P <0.01, *** P <0.001, **** P <0.0001.

3.4. Docking analysis with β-Catenin

The interaction specificities of the artocarpin with β-Catenin were thoroughly examined during the docking study. According to the results obtained, artocarpin formed the best-docked complexes (-7.04 kcal/mol) when compared to the binding energies displayed by known inhibitors such as isorhamnetin, fisetin, genistein, and silibinin (-5.68 to -4.98 kcal/mol), followed by other inhibitors such as catechin, luteolin, coumestrol, and β-naphthoflavone (-6.50 to -5.22 kcal/mol) (Iftikhar and Rashid, 2014). Throughout the test, artocarpin was found to inhibit the binding of β-Catenin. Hydrophobic and hydrogen bonding interactions of docked molecules were compared using the LigPlot program. In any case, Lys345, Val346, and Asn387 residues of β-Catenin were discovered to interact with hydrogen binding. Artocarpin interacted with β-Catenin to form H-bonds in the TCF-interactive region involving residues Glu24, Gln27, Glu29, and Gly25 at distances 2.76893 Å, 2.86867 Å, 2.64498 Å,

and 3.74859 Å, respectively. Trp383 formed pi-pi interactions with artocarpin at 4.34458 Å, 4.27395 Å, 5.03811 Å, and 5.02537 Å, respectively. Arg386 formed pi-cation interaction with artocarpin at 3.94659 Å. Meanwhile, artocarpin formed pi-cation interaction with Trp383 at 4.43971 Å, 4.87218 Å, 3.94334 Å, 4.94015 Å, 4.98735 Å, and 4.54912 Å, respectively. Arg386 formed pi-donor H-bond with artocarpin at 3.94659 Å, and Lys345 formed pi-donor H-bond with β-Catenin at 4.0286 Å, respectively.

β-Catenin residues Trp383 and Cys419 were found to be involved with hydrophobic interactions (Figure 3). The interaction of artocarpin with β-Catenin and TCF-4 involved a H-bond acceptor, a H-bond donor, and an aromatic ring. The inhibitory effect of artocarpin that targeting β-Catenin in the Wnt signaling pathway correlates with known inhibitors as they tend to occupy the same binding cavity (Figure 4).
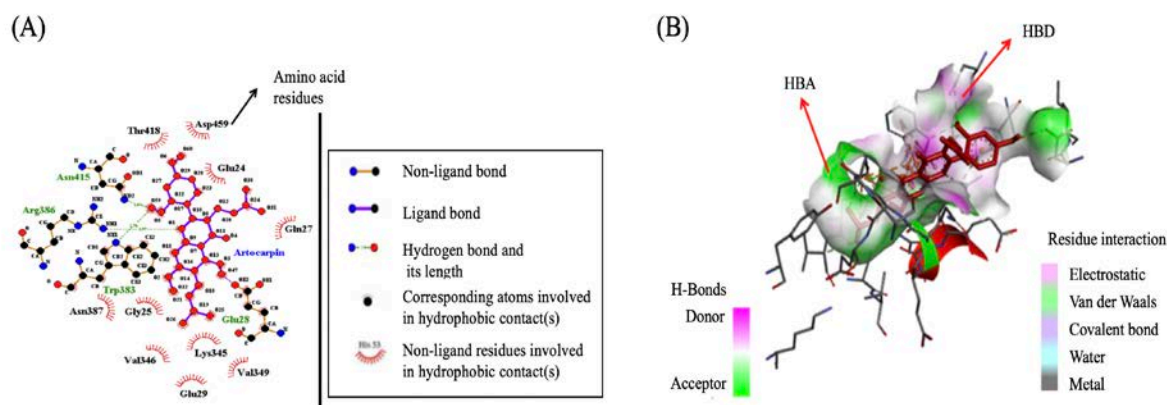
Figure 3. (A) The interacting residues of β-Catenin with the potential inhibitor artocarpin using LigPlot+ (B) Analysis of ligand with β-Catenin active site residue interactions using Discovery Studio Visualizer 4.1 Client.
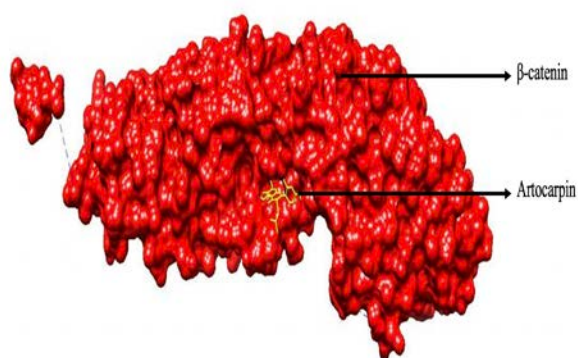
Figure 4. Multiple Ligand Simultaneous Docking (MLSD) Analysis and Molecular Interaction of Artocarpin (shown in yellow) at the Binding Site of β-Catenin. The β-Catenin/Artocarpin complex structure were generated in PyMOL version 2.1.1 (https://pymol.org)

3.5. Docking analysis with WNT

The interaction between artocarpin with WNT protein resulted in the highest binding energy values (-14.91 kcal/mol) compared to other WNT/β-Catenin inhibitors. This result supports the inhibitory activity of artocarpin on lung CSCs with low WNT and β-Catenin gene expression levels. In contrast to the results obtained in this study, Ser120: OG residue of WNT1 was the only one that interacted with hydrogen binding at a distance of 3.76146 Å compared to β-Catenin. Nevertheless, artocarpin and WNT1 formed a hydrophobic interaction that involved many residues, including Pro130, Cys77, Cys122, Pro132, and Leu144, at distance 4.15022 Å (C4); 3.45597 Å; 4.54061 Å, 5.21859 Å for Pro130, 5.11105 Å (C60) for Cys77, 4.05568 Å (C60) and 3.70246 Å (C5) for Cys122, 3.5248 Å (C30) and 3.45622 Å (C31) for Pro132, 4.06423 Å (C26) and 4.71292 Å (C25) for Leu144, respectively. Artocarpin was also interacted with itself to form hydrophobic interaction at a distance 3.40135 Å (C59) and 3.15232 Å (C31). Meanwhile, WNT1 residue (Thr143: CG2) interacted with artocarpin to form hydrophobic interaction at a distance of 3.75129 Å. Other types of interaction were between Cys122: SG residue of WNT1 with artocarpin at a distance of 5.86659 Å and 3.42835 Å (Figure 5).

Ser120: OG formed pi-donor with artocarpin, whereby H-Donor of Ser120: OG interacted with pi-orbitals of artocarpin through this molecular inhibition study. Thr143: CG2 and artocarpin itself (C59 and C31) formed pi-sigma with artocarpin, whereby C-H of Thr143: CG2 and two residues of artocarpin have the interaction with pi-orbitals of artocarpin. WNT1 residue (Cys 122: SG) formed two pi-sulfur interactions with artocarpin, whereby a sulfur group of two residues of Cys122: SG have the interaction with pi-orbitals of artocarpin. Three types of artocarpin residues formed pi-alkyl interaction with Pro130, whereby pi-orbitals of artocarpin have the interaction with the alkyl group of Pro130. Artocarpin residues formed alkyl have the interaction with Pro130 at C4, Cys77 at C60, Cys122 at C60 and C5, Pro132 at C30 and C31, Leu144 at C26 and C25 (Figure 5). The models or figures were evaluated using the PyMOL program (Figure 6).
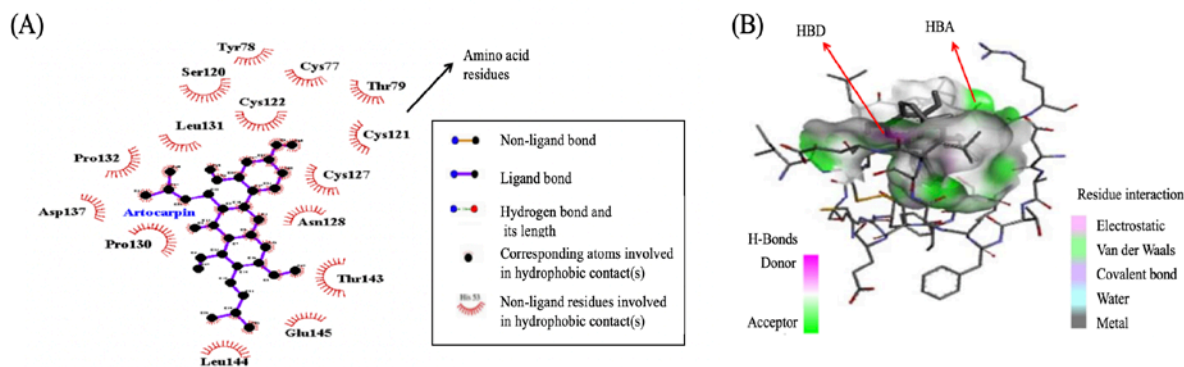
Figure 5. (A) The interacting residues of WNT with the potential inhibitor artocarpin using LigPlot+ (B) Analysis of ligand with WNT active site residue interactions using Discovery Studio Visualizer 4.1 Client.
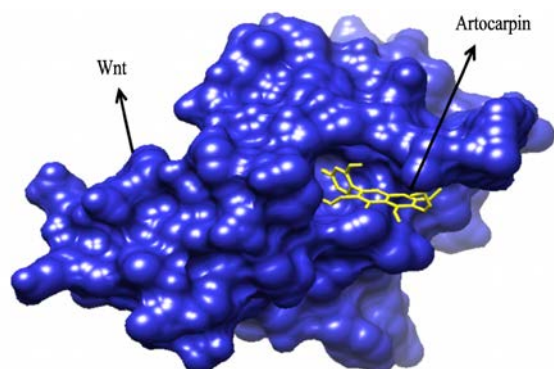
Figure 6. Multiple Ligand Simultaneous Docking (MLSD) Analysis and Molecular Interaction of Artocarpin (shown in yellow) at the Binding Site of WNT. The WNT-Artocarpin complex structure were generated in PyMOL version 2.1.1 (https://pymol.org)

3.6. β-Catenin and WNT expression knockdown

As depicted in Figure 7, artocarpin treatment significantly reduced the expression of both targeted genes; β-Catenin (DACT3) and WNT in all examined cell lines as compared to their respective untreated cell lines. In the artocarpin treated (10 µM and 100 µM) H460 cell lines, the expression of β-Catenin gene was significantly down-regulated with FC value of 0.400, (P<0.01) and 0.1920, (P<0.001) respective to the untreated cells. Similar pattern of inhibition was observed in artocarpin treated lung CSCs CD166$^+$CD44$^+$ cells (FC values of 0.400, (P<0.001) and 0.192, (P<0.001) and non-CSCs CD166$^-$CD44 cells (FC value of 0.419, (P<0.01) and 0.339, (P<0.001) respectively for 10 µM and 100 µM artocarpin concentration (Figure 7). Compared to the other two types of cell lines, prominent inhibition was observed in lung CSCs CD166$^+$CD44$^+$ cells.

In the expression of WNT gene, similar result was observed in which artocarpin treatment at the dose of 10 µM and 100 µM significantly inhibited its expression in all three examined cell lines compared to their respective untreated groups. The fold change expression for 10 µM and 100 µM artocarpin-treated H460 cells were 0.449 (P <0.01) and 0.387 (P <0.001), meanwhile in lung CSCs CD166$^+$CD44$^+$, the result were 0.155 (P<0.05) and 0.078 (P <0.001) and in non-CSCs CD166$^-$CD44$^-$, the value were 0.275 (P <0.01) and 0.251(P <0.001), respectively. Based on the readings, artocarpin exerted obvious inhibition in lung CSCs CD166$^+$CD44$^+$ compared to the other cell lines similar to β-Catenin (DACT3) gene expression.
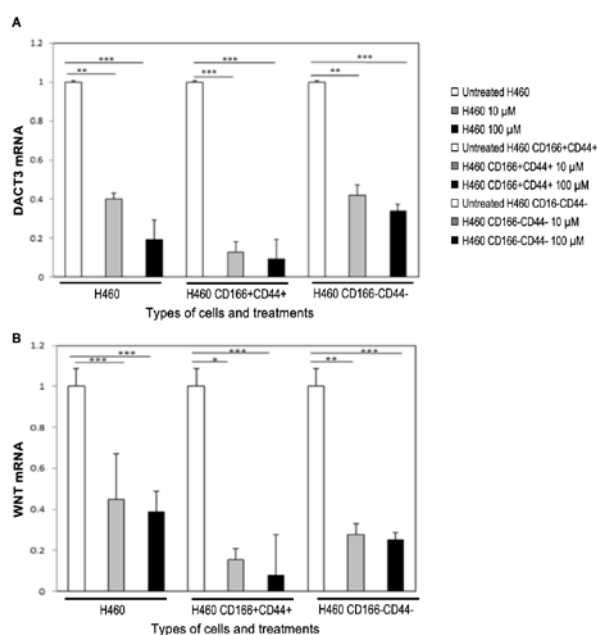
Figure 7. Analysis of targeted genes expression in different cell lines; A) β-catenin (DACT3) and B) WNT. The negative control was the PCR reaction without template. The β-catenin (DACT3) and WNT mRNA levels in cell lines were expressed as mean ± Standard Error Mean (n=3) of fold change from three independent cell passages. Significant *P* value was calculated using the ANOVA test by comparing the treatment groups with the respective untreated group. * P <0.05, **P <0.01, *** P <0.001.

4. Discussion

CSCs, by nature, are the subpopulation of tumour cells responsible for tumour initiation and relapse. Research revealed several regulatory pathways involved in maintaining their self-renewal and differentiation capabilities. Knowing that they own specific biomarkers, targeting this subpopulation and their regulatory signalling has become a promising cancer therapeutic strategy.

Up to the present, neither the scientific data on the isolation of CD166$^+$CD44$^+$ CSCs from H460 cell lines nor the effect of artocarpin on these isolated cells has been reported. As a result, this research adds to the pool of data available. In line with the aim of specific targeting, isolation of the CSCs according to their biomarkers in conventional cancer cell lines is one of the fundamental research steps. Several techniques were documented. According to a previous report, several CSC markers were

identified in the lung, such as CD166, CD133, CD44, CD24, ABCG2, ALDH1A1, and EpCAM (Phiboonchaiyanan *et al.,* 2016; Muraro *et al.,* 2012). Therefore, this study was conducted to determine the specific surface biomarkers expressed in isolated CSCs from the H460 lineage using the FACS technique. The results of the flow cytometry analysis in this study supported the hypothesis that the CSCs comprise a heterogeneous population by demonstrating the presence of several phenotypes (CD166$^+$CD44$^+$, CD166$^-$CD44$^-$). This finding was aligned with those reported previously in which CD44 and CD166 were detected in parental H460 cancer cell lines (Eun *et al.,* 2017). In this study, the obtained double-positive cells (CD166$^+$CD44$^+$) were regarded as lung CSCs, meanwhile double-negative cells (CD166$^-$CD44$^-$) were regarded as non-CSCs. The detection of CD166 and CD44 in this H460 cell line showed that their expressions were the most prominent compared to other CSCs markers. Even though elevated levels of EpCAM expression in many types of cancer demonstrated tumour advancement and malignancy, its levels of expression can be up or downregulated in a certain condition (Mohtar et al., 2020). EpCAM exert potential biphasic influence on the regulation of Epithelial-Mesenchymal Transition (EMT). This multifaceted phenomenon suggests that EpCAM can either augment or mitigate the EMT process in which EpCAM expression is downregulated when cancer cells are in the midst of an EMT event. Within breast and lung cancer cells, there is observable evidence of a transient diminishment in EpCAM expression concurrent with the cells' engagement in EMT during the metastatic progression (Hyun et al., 2016). As has been shown by the result obtained in this study, it is stipulated that the absent of the EpCAM expression in this CSCs population is due to the origin of the cells which is from the pleural effusion which indicates the metastatic characteristic and represent the loss of adhesive properties as it is shed from the primary origin. It is also reported that EpCAM expression is often reduced in certain types of NSCLC (Gastl *et al.*, 2000).

Two markers' co-expression was examined to establish a more robust phenotype for the potential CSC population. The previous investigation with a single marker expression revealed that CD166 and CD44 were dominant markers in H460 cell lines, so we investigated CD166 co-expression with CD44 for further sorting in H460 cell lines. The H460 cell line was chosen to be investigated further in this study because the cells express easily detectable p53 mRNA at levels compared to other cells. Figure 1B shows that 62.5% of the H460 cells were CD166$^+$CD44$^+$ in this isolation process. The H460 cell line's CD166$^+$CD44$^+$ cells have been sorted and designated as the population of lung CSCs. To confirm the stemness characteristics of the lung CSCs, the CD166$^-$CD44$^-$ was also isolated where these cells were identified as a non-CSC population with the percentage of expression as 37.5% cells.

As the antiproliferative activity of a compound towards cellular growth is suggestive of its anticancer properties, a toxicity study of artocarpin on parental H460 cell line was performed, and the result positively reflected our hypothesis. In determining the capability of artocarpin in targeting the isolated subpopulation of CSCs in the H460 cell line, the MTT assay was carried out. The reduction in the number of living cells of H460 CSCs observed upon artocarpin treatment indicates that artocarpin acts as an effective H460 CSCs cytotoxic compound, incidating that this compound inhibits lung CSCs. A strong cytotoxic activity against this subpopulation proposed the specific supression of this compound on the CSCs, thus postulating the possible targeted inhibition of artocarpin to cancer progression. This data further supports the previous evidence that artocarpin has anticancer effects due to its chemical structure, which includes C-3 prenylated flavones that contribute to the compound's cytotoxic effects thus suggesting it as a potential anticancer agent (Satar et al., 2018).

In the context of pluripotency, certain transcription factors play a pivotal role in maintaining tumour heterogeneity. To further evaluate the anti-cancer mechanism exerted by artocarpin towards the CSCs, the study on the pluripotency-associated markers such as NANOG, SOX2, KLF4 and OCT3/4 was conducted in all H460 cell lineages. The result revealed that artocarpin attenuated the expression of examined genes except OCT3/4. NANOG is correlatively expressed in many CSCs, especially in CD133$^+$ and CD44$^+$ cancer cells. The involvement of NANOG in embryonic development and cellular reprogramming validates their significant contribution to disease prognosis (Mahalaxmi *et al.,* 2019).

Further evidence supports that dysregulation of SOX2 induces resistance toward cell death and chemotherapy as this gene initiates the cell cycle (Hüser *et al.,* 2018). Along with the role of SOX2, NANOG, and c-MYC in generating an induced pluripotent cell, KLF4 helps reprogram the somatic cell into its pluripotent state and maintenance. In addition, KLF4 was found to be associated with Epithelial-Mesenchymal Transition (EMT) that implicated cancer metastasis (Zhou *et al.,* 2022). The OCT3/4, also known as POU5F1, is a transcription factor essential for developing pluripotent stem cells. It is expressed in embryonic stem cells, germ cells, and some cancer cells (Torres-Padilla & Chambers, 2014). The unexpressed level of OCT3/4 in our studied lung CSC was supported by previous findings in which this gene was undetected in H460 cell lineage using variety of detection techniques, including as immunohistochemistry, Western blotting, and RT-PCR. Another possible explanation for this finding includes the state of the cell itself in which H460 cells are more differentiated than the embryonic stem and germ cells, and yet they undergo changes in gene expression profile. Besides, there was possible mutation or alteration in the gene's regulatory regions and complex machinery that led to its downregulation, expression, or silencing (Yang *et al.,* 2011). The lack of detection of the OCT 3/4 gene in this study is consistent with previous data on the presence or absence of OCT 3/4 genes in a variety of cell lines, including distal oesophageal adenocarcinoma (ESO51), cervical cancer cell line (HeLa), lung adenocarcinoma (H460), and colorectal adenocarcinoma (H716B) (Rijlaarsdam *et al.,* 2011). As this compound significantly attenuates the expression level of the dominant oncogene, it brings hope to a novel therapeutic target for CSC elimination.

As artocarpin can inhibit the activity of CSCs development (Nonpanya *et al.,* 2021); it is worthwhile to identify the mechanistic action of this potential anticancer agent. In order to investigate the effect of artocarpin against the WNT/β-Catenin pathway, the preliminary

investigation was done through the molecular docking process of both WNT and β-Catenin protein with artocarpin and validated with gene expression assay of WNT and β-Catenin mRNA levels of the treated isolated CSCs. These methods provided useful preliminary evidence to support the selection of a suitable target for treating lung CSCs via the WNT/β-Catenin pathway.

Up to current research, many flavonoids, a family of naturally occurring compounds, have been found to mediate their regulatory activity towards a variety of cellular targets using a WNT/β-Catenin pathway. WNT/β-Catenin inhibitors, including fisetin, apigenin, isorhamnetin, silibinin, genistein, catechin, luteolin, coumestrol, and β-napthoflavone are well-known to suppress WNT/β-Catenin complex activation (Sferrazza *et al.*, 2020). As artocarpin is a member of the flavonoid and capable of attenuating the CSC activities, the possible interaction of this compound with WNT and β-Catenin was further studied. The molecular docking of this compound against the WNT/β-Catenin complex was performed to screen the binding site details. Molecular docking is a computational method that is used to predict the interactions between two molecules. In the context of the WNT/β-Catenin signaling pathway, molecular docking can be used to predict the interactions between artocarpin with the WNT and β-Catenin proteins. Compared to the other flavonoids, artocarpin was shown to form a best-dock complex with both proteins.

In this study, artocarpin molecule binds to its respective targets (β-Catenin and WNT protein) with a high affinity. Docking studies of prenyl flavone artocarpin at the bioactive sites of β-Catenin and WNT indicated that 3D structural folding at the protein-ligand groove is a distinguishing feature for molecular recognition of targeted chemicals and predicting their biological function. Artocarpin interacted with TCF-4/β-Catenin through an H-bond acceptor, an H-bond donor, and an aromatic ring. This means that artocarpin is likely to bind to the complex binding site. A similar interaction trend in terms of binding energy and region on targeted WNT/β-Catenin complex makes artocarpin comparable to other known inhibitors. The findings also showed that hydrogen bonding and hydrophobic interactions maintained the ligands at the target site, influencing binding affinity and therapeutic efficacy. In this molecular docking study, it is postulated that artocarpin binds to the WNT and β-Catenin proteins, thus inhibiting the interaction of the protein with the other complex molecules.

Behind the expression of stemness, angiogenesis, and cell cycle regulator's gene in cancer homeostasis, transcription factors act as drivers in this signalling, which includes TCF/LEF (Moon *et al.*, 2008), FOX (Ito & van den Heuvel, 2011) and SOX family (Zhang & Wang, 2014). In lung CSCs, the WNT/β-Catenin pathway is often dysregulated, thus leading to the overexpression of transcription factors such as TCF7L2 that promote CSC growth and survival (Zhang *et al.,* 2015). T-cell factor 4 (TCF-4), the family of TCF/LEF, is the master player of the canonical WNT signalling pathway. In response to the activation of the pathway by binding of the WNT ligand to its receptor, accumulated β-Catenin will interact with TCF-4, forming β-Catenin/TCF-4 complex. The binding of this complex molecule had switched the role of TCF-4 from repressor to the activator of gene expression. The DNA-binding domain on this molecule allows the complex to bind to the specific DNA target, known as WNT response elements (WREs), and subsequently undergoes gene transcription (Wang *et al.*, 2018).

Regarding the knowledge of this signalling, inhibition of any component in the signalling, especially the β-Catenin and TCF-4, may inhibit progressive cell proliferation and thus inhibit the proliferation of cancer cells (Lu *et al*., 2014). Previous structural and biochemical studies showed that the central portion of the TCF/β-Catenin binding domain is required for TCF to be anchored to β-Catenin via two conserved lysines in β-Catenin (Anthony *et al.* 2020). Liu and his team stated that TCF proteins act as a transcriptional enhancer by binding with an enzyme known as histone methyltransferase (HMT) (Liu *et al*., 2015). As the core of TCF-4 binding residues in the β-Catenin active site pocket was pre-loaded with an inhibitor, transcription of the target genes would be prevented. The interaction of artocarpin with TCF-4/β-Catenin complex with crystal structure showed that this compound occupied a similar inhibitory mechanism. From molecular docking analysis, it is stipulated that artocarpin attenuates the stemness gene expression by intercepting the interaction of β-Catenin to this molecule, thus preventing the TCF-4/β-Catenin complex formation and subsequent gene expression.

This result further supports the previous findings on the anticancer activity of this compound on various cancer cell lines, including human leukaemia HL-60 (CCL-240) cells, colorectal adenocarcinoma HT-29 (HTB38) cells, breast adenocarcinoma cancer MCF-7 (HTB-22) cell, and non-small lung cancer H460 (HTB-177) cell lines (Daud *et al.,* 2019; Mat Daud *et al*., 2021). Furthermore, in H460, artocarpin displayed antiproliferation, antidifferentiation, antimigration, and anti-invasion capabilities (Daud *et al.,* 2020). Though molecular docking analysis is useful in predicting the interaction between molecules and identifying potential therapeutic agents, confirmatory analysis is a must. The expression of DACT3, a member of the DACT (Drp/Frodo) gene family WNT/β-Catenin genes upon treatment with this compound, was further evaluated to determine the reliability of the docking simulation. The ability of artocarpin to reduce the DACT3 gene expression determines the direct inhibition of this compound on this signalling pathway. Reduction in nuclear β-Catenin prevents the direct formation of the TCF-4/β-Catenin complex, thus down-regulating the subsequent mechanism (He *et al*., 2014). Unlike other WNT signalling inhibitors, which suppressed DNA methylation, DACT3 repression was linked to bivalent histone modification. Both histone methylation and deacetylation strongly inhibit Dishevelled (Dvl)-mediated WNT/β-Catenin signalling, resulting in cancer cell death (Trejo-Solis *et al*., 2021). The result clarifies the specific mechanism artocarpin exerts in suppressing the growth and stemness characteristic of lung CSCs. All these shreds of evidence and the current findings supported the involvement of intracellular signalling cascade by artocarpin to ameliorate several detrimental occasions in the onset of cancer relapses. Participation of this compound by binding to the respective proteins down to the modulation of oncogene expression makes artocarpin on par with the other anticancer candidates. Resolution of the WNT/β-Catenin degradation

pathway by artocarpin greatly enhanced the current understanding of the biological roles of artocarpin and the diverse functions of transcription factors as such WNT signalling intermediates or target genes in the normal and disease state.

These data provide valuable insights of artocarpin and its anticancer activity. However, it is important to acknowledge the limitations inherent in this research. Despite the most expressed and studied surface marker detected in H460 cell lines, another possible marker could be evaluated, such as ALDH1, which is believed to be expressed at a low level in certain cancer stem cells as being recently published (Wei *et al.,* 2022). As ALDH1 is responsible for producing an enzyme that is crucial for cellular processes, and its overexpression was observed in certain types of cancer, it is worthwhile to investigate the presence of this molecule in H460 cell lines and thus evaluate the interaction of artocarpin on this molecule in the future study.

These overall findings provide a conceptual framework for the protective effect of artocarpin on these cell lines against metastasis and cancer resistance. These molecular mechanisms may be harnessed to develop drugs that help prevent and treat the impairment of abnormal cell division. The study has shed light on developing an envisaged therapeutic strategy using the active compounds from plant-based natural products against cancer resistance in lung cancer. Overall, it is believed that a better understanding of the mechanisms underlying the anticancer properties of artocarpin and its attributive roles would facilitate the development of promising lung cancer therapeutics using herbal medicine.

5. Conclusion

As CSCs are at the core of cancer treatment failure, targeting this subpopulation has been shown to be a promising treatment strategy. This study established the possibility of isolating the CSCs from the lung's H460 cell line and proved the artocarpin capability to inhibit the stemness characteristic of this subpopulation. With the aid of molecular docking, screening this compound's binding activity towards the specific component of the cancer signalling pathway helps understand its anticancer activities. However, further research is required into the suggested inhibitor, particularly its binding and inhibitory potential *in vivo*. This data has yet to generate a pharmacophore model with common pharmacophoric features. It can be used to screen more compounds, which will aid in discovering novel inhibitors of β-Catenin and, hence, the WNT signalling activation pathway in lung cancer.

Acknowledgements

References

Abd Wahab NZ and Ibrahim N. 2022. Styrylpyrone Derivative (SPD) Extracted from Goniothalamus umbrosus Binds to Dengue Virus Serotype-2 Envelope Protein and Inhibits Early Stage of Virus Replication. *Molecules*, **27(14)**:4566.

Almajali B, Al-Jamal H, Taib W, Ismail I, Johan MF, Doolaanea AA and Ibrahim WN. 2021. Thymoquinone, as a Novel Therapeutic Candidate of Cancers. *Pharmaceuticals,* **14(4)**:369.

Anthony CC, Robbins DJ, Ahmed Y and Lee E. 2020. Nuclear regulation of Wnt/β-catenin signaling: It'sa complex situation. *Genes,* **11(8)**:886.

Chen HY, Bohlen JF and Maher BJ. 2021. Molecular and Cellular Function of Transcription Factor 4 in Pitt-Hopkins Syndrome. *Dev Neurosci.* **43(3-4)**:159-167.

Daud NN, Septama AW, Simbak N, Rahmi EP. 2020. The phytochemical and pharmacological properties of artocarpin from Artocarpus heterophyllus. 2020. *Asian Pac J Trop Med.,***1;13(1)**:1-7.

Daud NN, Septama AW, Simbak N, Bakar NH, Rahmi EP 2019. Synergistic Effect of Flavonoids from Artocarpus heterophyllus Heartwoods on Anticancer Activity of Cisplatin Against H460 and MCF-7 Cell Lines. 2019. *Nat. Prod. Sci.,* **1;25(4)**:311-6.

Eun K, Ham SW and Kim H. 2017. Cancer stem cell heterogeneity: origin and new perspectives on CSC targeting. *BMB Rep.,* **50(3)**:117.

Fleige S, Walf V, Huch S, Prgomet C, Sehm J and Pfaffl MW. 2006. Comparison of relative mRNA quantification models and the impact of RNA integrity in quantitative real-time RT-PCR. *Biotechnol Lett.*, **28**:1601-13.

Forrest MP, Hill MJ, Quantock AJ, Martin-Rendon E and Blake DJ. 2014. The emerging roles of TCF4 in disease and development. *Trends Mol Med.*, **20(6)**:322-331.

Gastl G, Gunsilius E, Beug H, v. Schweinitz D. 2000. Epithelial cell adhesion molecule expression in non-small cell lung cancer (NSCLC). *Lung Cancer*, **29(3)**: 215-221.

Hassan M, Baig AA, Attique SA, Abbas S, Khan F, Zahid S, Ain QU, Usman M, Simbak NB, Kamal MA and Yusof HA. 2021. Molecular docking of alpha-enolase to elucidate the promising candidates against Streptococcus pneumoniae infection. *Daru.*, **29**:73-84.

He QZ, Luo XZ, Wang K, Zhou Q, Ao H, Yang Y, Li SX, Li Y, Zhu HT and Duan T. 2014. Isolation and characterization of cancer stem cells from high-grade serous ovarian carcinomas. *Cell Physiol Biochem.*, **33(1)**:173-84.

Huang T, Song X, Xu D, Tiek D, Goenka A, Wu B, Sastry N, Hu B and Cheng SY. 2020. Stem cell programs in cancer initiation, progression, and therapy resistance. *Theranostics,* **10(19)**:8721-8743.

Hüser L, Novak D, Umansky V, Altevogt P and Utikal J. 2018. Targeting SOX2 in anticancer therapy. *Expert Opin Ther Targets.*, **22(12)**:983-91.

Hwang JS, Yoon CK, Hyon JY, Chung TY and Shin YJ. 2020. Transcription Factor 4 Regulates the Regeneration of Corneal Endothelial Cells. *Invest Ophthalmol Vis Sci.*, **61(4)**, 21.

Hyun, Kyung-A., Gi-Bang Koo, Hyunju Han, Joohyuk Sohn, Wonshik Choi, Seung-Il Kim, Hyo-Il Jung, and You-Sun Kim. 2016. Epithelial-to-mesenchymal transition leads to loss of EpCAM and different physical properties in circulating tumor cells from metastatic breast cancer. *Oncotarget.,* **7(17)**: 24677.

Iftikhar H and Rashid S. 2014. Molecular docking studies of flavonoids for their inhibition pattern against β-catenin and pharmacophore model generation from experimentally known flavonoids to fabricate more potent inhibitors for Wnt signaling pathway. *Pharmacogn Mag.*, **10(Suppl 2)**:S264.

Ito T and van den Heuvel MJ. 2011. FOX transcription factors in Wnt signaling. *Curr Opin Cell Biol.*, **23(5)**: 584-591.

Jahanafrooz Z, Mosafer J, Akbari M, Hashemzaei M, Mokhtarzadeh A and Baradaran B. 2020. Colon cancer therapy by focusing on colon cancer stem cells and their tumour microenvironment. *J Cell Physiol.*, **235(5)**:4153-4166.

Khatami, F., Aghaii, M. and Tehrani, F.D., 2020. Cancer stem cells. **Stem Cells in Urology**, pp.15-34.

Liu RL, Dong Y, Deng YZ, Wang WJ and Li WD. 2015. Tumor suppressor miR-145 reverses drug resistance by directly targeting DNA damage-related gene RAD18 in colorectal cancer. *Tumour Biol.*, **36 (7)**: 5011-5019.

Lu FI, Sun YH, Wei CY, Thisse C and Thisse B. 2014. Tissue-specific depression of TCF/LEF controls the activity of the Wnt/β-catenin pathway. *Nat Commun.*, **5(1)**:5368.

Mahalaxmi I, Devi SM, Kaavya J, Arul N, Balachandar V and Santhy KS. 2019. New insight into NANOG: A novel therapeutic target for ovarian cancer (OC). *Eur J Pharmacol.*, **852**:51-7.

Makena MR, Ranjan A, Thirumala V and Reddy AP. 2020. Cancer stem cells: Road to therapeutic resistance and strategies to overcome resistance. *Biochim Biophys Acta Mol Basis Dis.*, **1866(4)**:165339.

Masciale V, Grisendi G, Banchelli F, D'Amico R, Maiorana A, Sighinolfi P, Stefani A, Morandi U, Dominici M and Aramini B. 2019. Isolation and identification of cancer stem-like cells in adenocarcinoma and squamous cell carcinoma of the lung: a pilot study. *Front Oncol.*, **9**:1394.

Mat Daud NN, Abu Bakar NA, Septama AW. 2021. In Vitro Anti-proliferative Properties of Flavonoids Isolated from Artocarpus Heterophyllus on Cancer Cell Lines. *Nat Prod J.*, **1;11(5)**:755-61.

Mohtar MA, Syafruddin SE, Nasir SN, Low TY. 2020. Revisiting the roles of pro-metastatic EpCAM in cancer. *Biomolecules*. **7;10(2)**:255.

Muraro MG, Mele V, Däster S, Han J, Heberer M, Cesare Spagnoli G and Iezzi G. 2012. CD133$^+$, CD166$^+$ CD44$^+$, and CD24$^+$ CD44$^+$ phenotypes fail to reliably identify cell populations with cancer stem cell functional features in established human colorectal cancer cell lines. *Stem Cells Transl Med.*, **1(8)**:592-603.

Moon RT and Glass CK. 2008. TCF/LEF transcription factors: key regulators of Wnt signaling. *Genes Dev.*, **22(20)**: 2785-2810.

Nimmakayala RK, Batra SK, Ponnusamy MP. 2019. Unraveling the journey of cancer stem cells from origin to metastasis. *Biochim Biophys Acta Rev Cancer.*, **1871(1)**:50-63.

Nonpanya N, Sanookpan K, Sriratanasak N, Vinayanuwattikun C, Wichadakul D, Sritularak B and Chanvorachote P. 2021. Artocarpin Targets Focal Adhesion Kinase-Dependent Epithelial to Mesenchymal Transition and Suppresses Migratory-Associated Integrins in Lung Cancer Cells. *Pharmaceutics*, **13(4)**:554.

Phiboonchaiyanan PP, Kiratipaiboon C, Chanvorachote P. 2016. Ciprofloxacin mediates cancer stem cell phenotypes in lung cancer cells through caveolin-1-dependent mechanism. *Chem Biol Interact.*, **250**: 1–11.

Pouremamali F, Vahedian V, Hassani N, Mirzaei S, Pouremamali A., Kazemzadeh H and Maroufi NF. 2022. The role of SOX family in cancer stem cell maintenance: With a focus on SOX2. *Pathol Res Pract.*, **153783**.

Rijlaarsdam MA, Van Herk HA, Gillis AJ, Stoop H, Jenster G, Martens J, Van Leenders GJ, Dinjens W, Hoogland AM, Timmermans M and Looijenga LH. 2011. Specific detection of OCT3/4 isoform A/B/B1 expression in solid (germ cell) tumours and cell lines: confirmation of OCT3/4 specificity for germ cell tumours. *Br J Cancer.*, **105(6)**:854-63.

Satar NA, Fakiruddin KS, Lim MN, Mok PL, Zakaria N, Fakharuzi NA, Abd Rahman AZ, Zakaria Z, Yahaya BH and Baharuddin P. 2018. Novel triple-positive markers identified in human non-small cell lung cancer cell line with chemotherapy-resistant and putative cancer stem cell characteristics. *Oncol Rep.*, **40(2)**:669-81.

Septama AW and Panichayupakaranant P. 2015. Antibacterial assay-guided isolation of active compounds from Artocarpus heterophyllus heartwoods. *Pharm Biol.*, **53(11)**:1608-13.

Sferrazza G, Corti M, Brusotti G, Pierimarchi P, Temporini C, Serafino A and Calleri E. 2020. Nature-derived compounds modulating Wnt/β-catenin pathway: A preventive and therapeutic opportunity in neoplastic diseases. *Acta Pharm Sin B.*, **10(10)**:1814-34.

Torres-Padilla ME, Chambers I. 2014. Transcription factor heterogeneity in pluripotent stem cells: a stochastic advantage. *Development*, **141(11)**:2173-81.

Trejo-Solis C, Escamilla-Ramirez A, Jimenez-Farfan D, Castillo-Rodriguez RA, Flores-Najera A and Cruz-Salgado A. 2021. Crosstalk of the Wnt/β-catenin signaling pathway in the induction of apoptosis on cancer cells. *Pharmaceuticals*, **14(9)**:871.

Van Schaijik B, Davis PF, Wickremesekera AC, Tan ST and Itinteang T. 2018. Subcellular localisation of the stem cell markers OCT4, SOX2, NANOG, KLF4 and c-MYC in cancer: a review. *J Clin Pathol.*, **71(1)**: 88-91.

Wang J, Chen J and Chen J. 2018. The WNT signaling pathway in cancer. *Cancer Biol. Ther.*, **19(2)**: 217-228.

Wei Y, Li Y, Chen Y, Liu P, Huang S, Zhang Y, Sun Y, Wu Z, Hu M, Wu Q and Wu H. 2022. ALDH1: A potential therapeutic target for cancer stem cells in solid tumors. *Front Oncol.*, **12**:1026278.

Yang L, Shi P, Zhao G, Xu J, Peng W and Zhang J. 2020. Targeting cancer stem cell pathways for cancer therapy. *Signal Transduct Target Ther.*, **5**:8.

Zakaria N, Yusoff NM, Zakaria Z, Lim MN, Baharuddin PJ, Fakiruddin KS and Yahaya B. 2015. Human non-small cell lung cancer expresses putative cancer stem cell markers and exhibits the transcriptomic profile of multipotent cells. *BMC cancer*, **15(1)**:1-6.

Zhan T, Rindtorff N and Boutros M. 2017. Wnt signaling in cancer. *Oncogene*, **36**:1461–73.

Zhang X and Wang Y. 2014. SOX transcription factors in Wnt signaling. *J Cell Physiol.*, **229(10)**: 2287-2297.

Zhou H, Guan Q, Hou X, Liu L, Zhou L, Li W and Liu H. 2022. Epithelial-mesenchymal reprogramming by KLF4-regulated Rictor expression contributes to metastasis of non-small cell lung cancer cells. *Int J Biol Sci.*, **18(13)**:4869.

Copper Nanoparticles and Culture Media Elicit Biomass, Secondary Metabolites, and Antioxidant Activity in the Cell Suspension Culture of *Momordica charantia* L.

Nisreen A. Jdayea[1] and Shamil I. Neamah[2, *]

Anbar Education Directorate, Ministry of Education, Anbar 31001, Iraq; [2]Plant Tissue Culture Laboratory, Department of Combat Desertification, Center of Desert Studies, University of Anbar, Anbar 55431, Iraq. [2]Department of Horticulture and LandScape Gardening, College of Agriculture, University of Anbar, Anbar 55431, Iraq.

Abstract

Medicinal plants are characterized by their high content of secondary metabolites. They are known to possess pharmaceutical properties. Based on this, the present study describes the ability of laboratory-synthesized copper nanoparticles (Cu NPs) to influence the biomass properties, secondary metabolism, and biological activity of cell suspension culture (CSC) induced from the hypocotyl extirpated from sterilized seedlings of *Momordica charantia* L. CSC were grown in various cultures, including Linsmaier and Skoog (LS), Murashige and Skoog (MS), and Woody Plant Medium (WPM), supplemented with different concentrations of Cu NPs 0, 40, 80, 120, 160, and 200 µg ml^{-1} respectively. The highest biomass accumulation for calli cultures was induced from the hypocotyl. CSC obtained from two-month-old calli cultures were subjected to Cu NPs treatments in different cultures for 21 days, which increased the biomass of the CSC. The increasing concentrations of Cu NPs caused a decreasing trend in biomass and cell vitality and an increase in the accumulation of Cu, hydrogen peroxide (H_2O_2), and malondialdehyde (MDA). The lowest values appeared for CSC grown in a WPM at a concentration of 200 µg ml^{-1} Cu NPs. CSC grown in a WPM treated by 200 µg ml^{-1} Cu NPs provided the highest total flavonoids production (TFP) and the most increased activity of phenylalanine ammonia-lyase (PAL), polyphenol oxidase (PPO), 3-(4,5-dimethylthiazole-2-yl)-2,5-diphenyltetrazolium bromide (MTT), and diphenyl-picrylhydrazyl (DPPH). On the other hand, exogenous 200 µg ml^{-1} Cu NPs in MS medium improved total phenolic production (TPP). In conclusion, these results indicate the promising role of plant tissue culture technology in achieving sustainable biomass production and thus improving the production of secondary metabolites through the hypocotyl growth of *M. charantia* L. in specific cultures using Cu NPs as an effective elicitor.

Keywords: *Momordica charantia* L.; Cell Suspension Culture; Culture Media Elicitation; Phenolic compounds; Flavonoids compound.

1. Introduction

Momordica charantia L. is a medicinal plant that belongs to the cucurbit family. It has therapeutic properties because it contains many secondary metabolites, including phenols, alkaloids, saponins, triterpene glycosides, vicaine, momordin, charantin, triterpenes, momorcharin, and oleanolic acids (Grover and Yadav, 2004). In addition, it contains brevifolincarboxylic acid, margarolic acid, ascorbic acid, goyaglycoside G, 3-malonylmomordicin I, quercetin 3-O-glycoside, kuguacin H, and cucurbitacin E (Perumal *et al.,* 2021). Several previous reports on the biological activities of phenolic compounds and available secondary compounds have been previously reported as antioxidant, antimicrobial (Deshaware *et al.,* 2017), antidiabetic, anti-inflammatory, anticancer (Svobodova *et al.,* 2017), anti-ulcer, antibacterial, antiviral, antitumor, antifertility, antilipid, antimutagenic, immunomodulatory, anthelmintic, and hepatoprotective activities (Jia *et al.,* 2017).

Cell suspension culture (CSC) technology has provided alternative possibilities for enhancing in vitro production of secondary metabolites from natural plant sources (Sarkate *et al.*, 2017; Setiowati *et al.*, 2022). It contributes to the sustainable production of these compounds in a short period through the positive effects of different combinations of chemicals added to the culture medium. Moreover, CSC avoids the problems that the plant may be exposed to in the field like diseases, weeds, insects, and changes in climatic conditions. It also provides essential compounds in the pharmaceutical industry without being restricted by the growing season. CSC technology has succeeded in supplying the pharmaceutical industry with several secondary compounds, including vincristine, vinblastine, camptothecin, and Taxol (Wilson and Roberts, 2012). Added to this is the ability of CSC to produce compounds that are difficult to synthesize chemically (Kolewe *et al.,* 2008; Siahsar *et al.,* 2011; Chung *et al.*, 2018).

Nanomaterials are materials as small as 1–100 nm in size with unique physicochemical properties (Veisi *et al.,* 2018). These characteristics can qualify them to activate

---

* Corresponding author. e-mail: ds.dr.shamil@uoanbar.edu.iq.

many important biological processes of the plant cell, including eliciting the biological pathways responsible for synthesizing secondary metabolites (Sharafi *et al.,* 2013; Ghorbanpour and Hadian, 2015; Hatami *et al.*, 2016; Chung *et al.,* 2018; Bsoul *et al.*, 2023). Moreover, nanomaterials are believed to have a role in protecting the plant cell from the negative effect of oxidative stress (Thiruvengadam *et al.,* 2015).

Copper is a trace element important of plant growth. It has many positive effects in improving the physiological characteristics of plant cell growth. In addition, it plays a role in plant biochemistry by increasing the activity of several enzymes. It is a catalyst for the synthesis of many proteins. Moreover, it is a structural component of regulatory proteins and is involved in many important physiological processes, including the electron transport chain, hormone signalling, and cell wall metabolism (Parida and Das, 2005). Previous literature has concluded that copper oxide nanoparticles (CuO NPs) are vital in promoting plant tissue growth and reducing oxidative stress (Anwaar *et al.,* 2016).

This study investigated the potential effects of laboratory-synthesized Cu NPs on biomass accumulation and production of phenolic compounds and their impact on improving the biological activities of CSC grown in different cultures of *M. charantia* L.

2. Materials and Methods

2.1. Chemicals

Plant tissue culture media were purchased from Caisson labs company, USA. Sucrose and agar were purchased from Merck KGaA company. All other chemicals were purchased from Sigma Aldridge company Ltd.

2.2. Plant material

This experiment was carried out in plant tissue culture laboratory, Center of Desert Studies, University of Anbar (33° 24′ 11″ N, 43° 15′ 43″ E). *M. charantia* L. seeds were surface-sterilized with 70% ethanol for 30 sec. Then, they were sterilized using sodium hypochlorite (NaOCl) 1.0% for 5 min. After that, they were rinsed five times with sterile distilled water. Sterilized seeds were grown in flasks under aseptic conditions in B5 media (Gamborg *et al.,* 1968). Moreover, the components and media, including 30 g l^{-1} sucrose and 7.0 g l^{-1} agar, were added to the B5 media. The pH of the medium was adjusted to 5.6. The cultures were incubated in a growth chamber at 25 ±1°C under an illumination intensity of 1000 lux for 8/16 h light/dark, respectively.

2.3. Calli cultures induction

Media cultures were used to induce calli cultures such as LS (Linsmair and Skoog, 1965), MS (Murashige and Skoog, 1962), and WPM (Lloyd and McCown, 1980). They were supplemented with specific combinations of growth regulators naphthaleneacetic acid (NAA) at 0.1, 0.25, and 0.5 mg l^{-1} and benzyladenine (BA) at 0.25, 0.5, and 1.0 mg l^{-1}. The media components included 30 g l^{-1} sucrose and 7.0 g l^{-1} agar. pH was adjusted to 5.6. The hypocotyl of 1 cm sterile seedlings was excised to be cultured in the media. The best combination for obtaining biomass was determined based on the fresh weight (FW)

of calli cultures after growing for 28 days. Callus tissue was propagated based on the combination producing the highest biomass of explant.

2.4. Preparation of Cu NPs

The colloidal material of Cu NPs was prepared according to the method described (Fernandez-Ariasa *et al.,* 2020). It was based on the liquid phase laser ablation technique covering the metal material at room temperature. Copper foil with a purity of 99.99% was used. It was immersed in methyl alcohol up to 2 mm. The laser source was a picosecond infrared (IR) at 1064 nm with an energy of 0.03 mJ and a pulse duration of 800 ps. The flask was covered with foil to protect it from light.

2.5. Characterization of Cu NPs

The prepared Cu NPs were characterized using a UV-Vis spectrophotometer. The topographical properties were determined using a transmission electron microscope (Figure 1). The Cu content in the colloidal solution was estimated by atomic absorption.
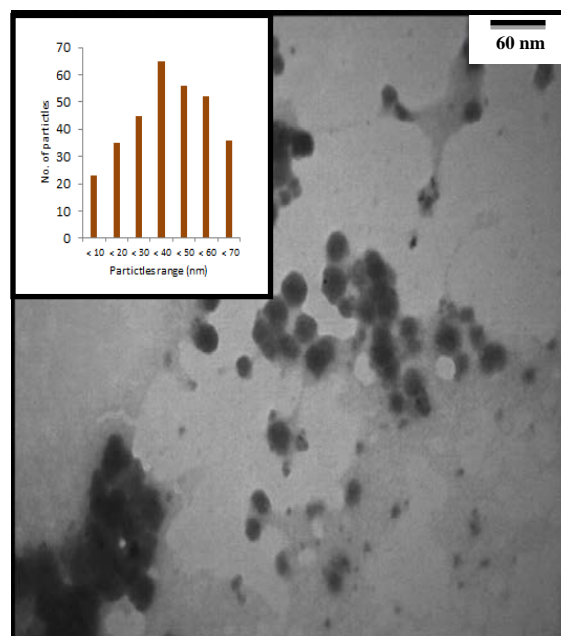
Figure 1. TEM image of Cu NPs with particle size distribution.

2.6. Establishment and treatment of CSC

Calli cultures grown in media containing the optimum combination were used to obtain biomass. The suspensions were obtained from two-month-old calli cultures. CSC were cultured from 5.0 g of FW calli cultures after filtering by a sieve with a 300 μm hole in a 250 ml Erlenmeyer flask containing 50 ml medium consisting of LS, MS, and WPM cultures with 30 g l^{-1} sucrose supplemented with 0, 40, 80, 120, 160, and 200 μg ml^{-1} Cu NPs. The cultures were grown in a shaking incubator at 120 rpm at 25°C and 24 h illumination. CSC were harvested at 28 days of age for the quantification of the following parameters.

2.6.1. Biomass accumulation, cell viability, and Cu content of CSC

CSC growing in the cultures of the different treatments were harvested to determine biomass accumulation through FW determination. Moreover, the validity was determined based on previously described reports (Sahraroo *et al.,* 2016).

CSC samples were dried in a hot air oven at $60^{\circ}C$ for weight stability. 250 mg of the dried sample was pre-dissolved in HCl and HNO_3 (1:3 v/v). The mixture was heated at $100^{\circ}C$ for 3 h on a hot plate stirrer. The filtrate was adjusted to 25 ml with deionized distilled water. The copper ion content of the samples was estimated by ICP-OES (Arteaga *et al.*, 2018).

2.6.2. Hydrogen peroxide (H_2O_2) and malondialdehyde (MDA) content

The H_2O_2 content was estimated using the spectrophotometric method described by Alexieva *et al.* (2001). Briefly, 500 mg of fresh samples of CSC was homogenized in 5.0 ml of 0.1% (w/v) trichloroacetic acid. Then, the centrifugation was carried out at 15000 rpm for 15 min. Then, 0.5 ml of the supernatant was supplemented into 0.5 ml potassium phosphate buffer (10 mM, pH 7.0) with 1.0 ml potassium iodide (1.0 M). The absorbance was recorded at 390 nm.

MDA content was determined in CSC by the method described by Heath and Packer (1968). Briefly, a mixture of 300 mg of a homogenized fresh sample of suspended cells was mixed in 1.5 mL of 1% (w/v) trichloroacetic acid. Then, centrifugation was performed at 10000 rpm at $4^{\circ}C$ for 5 min. 1.0 ml of the supernatant was supplemented with 4 ml of 0.5% thiobarbituric in 20% trichloroacetic acid (TCA). The reaction mixture was heated at $95^{\circ}C$ for 30 min. The absorbance of the supernatant was recorded at 532 and 600 nm by spectrophotometer (UV-Vis). The MDA value was determined from the absorbance difference using the 155 mM^{-1} cm^{-1} extinction coefficient.

2.6.3. Antioxidant enzymatic activity

Antioxidant enzymes were extracted according to the method described by Gapinska *et al.* (2008). Briefly, 500 mg of homogeneous fresh CSC was weighed. 5 ml of potassium phosphate buffer (pH = 7.0, 50 mM) was added, containing 1.0 mM of ethylenediamine tetraacetic acid (EDTA) and 1% polyvinylpyrrolidone (PVP). The sample was centrifuged at 10000 rpm for 15 min at $4^{\circ}C$. The activity of polyphenol oxidase (PPO) and lipoxygenase (LPO) enzymes was estimated using the supernatant.

PPO activity was quantified by the protocol of Soliva *et al.* (2000). Briefly, 100 µL of the enzyme extract was mixed with 1900 µl of 0.1 M potassium phosphate (pH, M 0.1=7.0) containing 0.1 M catechol as a substrate. The absorbance was recorded at 410 nm. Phenylalanine ammonia-lyase (PAL) activity was estimated based on cinnamic acid production by the protocol of D'Cunha *et al.* (1996). Briefly, 100 µL of enzyme extract was added to 1000 µl of buffer extract, 500 µl of L-phenylalanine (10 mM), and 400 µl of deionized water. The mixture was incubated at $37^{\circ}C$ for 1 h. Then, 500 µl of hydrochloric acid (6.0 M) was added. The absorbance was recorded at 290 nm.

2.6.4. Secondary metabolites

Phenolic compounds and flavonoids were extracted from homogenized samples of CSC according to the method described by Velioglu *et al.* (1998).

100 mg of powdered samples was dried in an oven at $50^{\circ}C$ for 48 h in 20 ml aqueous methanol (80%) and added to room temperature for 20 min. Samples were centrifuged at 15000 rpm for 20 min. A vacuum evaporator dried the supernatant. 1 ml of methanol was re-added. The

supernatant was carefully isolated and stored for quantification.

Total phenol production (TPP) was estimated using Folin-Ciocalteu (FC) and gallic acid. It is expressed by mg gallic acid/g dry weight (Ainsworth and Gillespie, 2007). Total flavonoid production (TFP) was estimated as rutin equivalents described in mg rutin g^{-1} DW (Miliauskas *et al.*, 2004).

2.6.5. Antioxidant activity

Antioxidant activity was evaluated by diphenyl-picrylhydrazyl (DPPH) and 3(4,5-dimethylthiazol-2-yl)-2,5-diphenyltetrazolium bromide (MTT). Free radical scavenging activity was estimated based on the DPPH assay. Briefly, 100 mg of homogenized CSC had 0.02 ml of ethanol. Then, it was centrifuged at 10000 rpm for 20 min. The supernatant was isolated and added to 2.0 ml of DPPH (0.1 mM) in 95% ethanol. The reaction mixture was mixed and incubated at $25^{\circ}C$ for 60 min. The absorbance was measured at 517 nm (Zhu *et al.*, 2006).

The MTT assay was determined according to the modified method described by Neamah (2016). Briefly, 2.0 ml of dimethyl sulfoxide (DMSO) was added to the supernatant of a 500 mg sample extracted by centrifugation at 10000 rpm for 20 min using 5.0 ml of methanol aqueous (80%). The sample was mixed by the vortex. It was dried by a vacuum evaporator. 10 µl of the reaction was added to the 190 µl MTT solution. Then, it was incubated at $37^{\circ}C$ for 24 h. DMSO solution was added. Then, 200 µl was isolated and placed in a 96-well CSC. The absorbance was recorded using a universal microplate reader at a wavelength of 570 nm.

2.7. Experimental design and statistical analysis

A factorial experiment was conducted using a completely randomized design. It included 18 treatments with three replicates in each treatment. Standard deviation values were calculated for all mean values. Data were statistically subjected to two-way ANOVA using the GenStat package version 12 significant values were determined using L.S.D at $p \leq 0.01$.

3. Results

3.1. Biomass accumulation of calli cultures

The best biomass accumulation was determined for *M. charantia* L. calli cultures grown in diverse cultures, including LS, MS, and WPM containing different NAA and BA treatments. The aim was to obtain the most appropriate chemical components of the medium through which calli cultures can be grown for CSC. Media cultures did not show a significant difference in biomass accumulation. In contrast, it increased significantly ($p \leq 0.01$) by treatment with NAA and BA at concentrations 0.25+1.0 mg l^{-1}, respectively. It recorded the highest significant biomass accumulation for media cultures, which amounted to 2.04, 2.24, and 2.14 g, respectively (Figure 2).
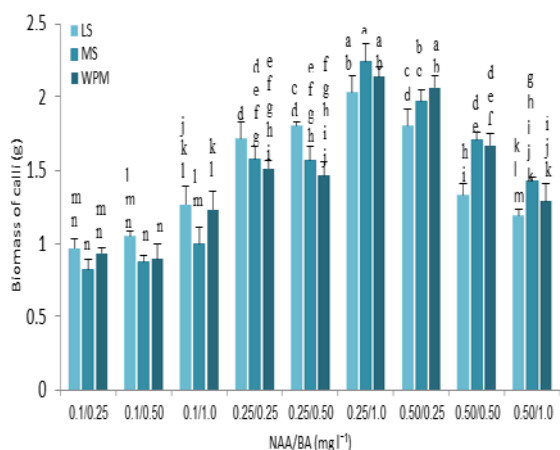
Figure 2. Assessment of biomass of calli cultures in *M. charantia* L. induced by different concentrations of NAA and BA. Vertical bars represent the mean ± standard deviation of three replicates. Different letter treatments indicate significant differences at $p \leq 0.01$ based on LSD test.

3.2. Biomass accumulation, cell viability, and Cu content of CSC

Some morphological parameters of CSC derived from calli cultures were evaluated (Figure 3). Treatment with Cu NPs significantly increased the biomass accumulation of CSC ($p \leq 0.01$). The highest biomass accumulation was 5.27 g for MS medium treated with 120 µg ml^{-1} of Cu NPs. In contrast, treatment with high concentrations caused a decrease in biomass to its lowest level at a concentration of 200 µg ml^{-1} for culture media (Figure 4A).

Cell vitality also increased significantly as a result of treatment with Cu NPs, as treatment with a concentration of 80 µg ml^{-1} increased the vitality of cells growing in LS medium by 93.92%, while treatment with a concentration of 200 µg ml^{-1} led to recording the lowest vitality of cells growing in WPM amounting to 66.11% (Figure 4B).

The accumulation of Cu increased significantly with high concentrations of Cu NPs, and the increase in treatment caused an increase in the accumulation of Cu. The highest accumulation occurred for CSC of WPM, which reached 0.129 mg g^{-1} DW in 200 µg ml^{-1}, while the accumulation was lower for lower concentrations of Cu NPs (Figure 4C)

Figure 3. The stages of study on the hypocotyl derived from *M. charantia* L. under in vitro conditions on WPM with 0.25 mg l^{-1} NAA+1.0 mg l^{-1} BA. The hypocotyl extirpated from sterilized seedlings (A). Callus induction start (B). Callus formation complete (C). CSC (D).
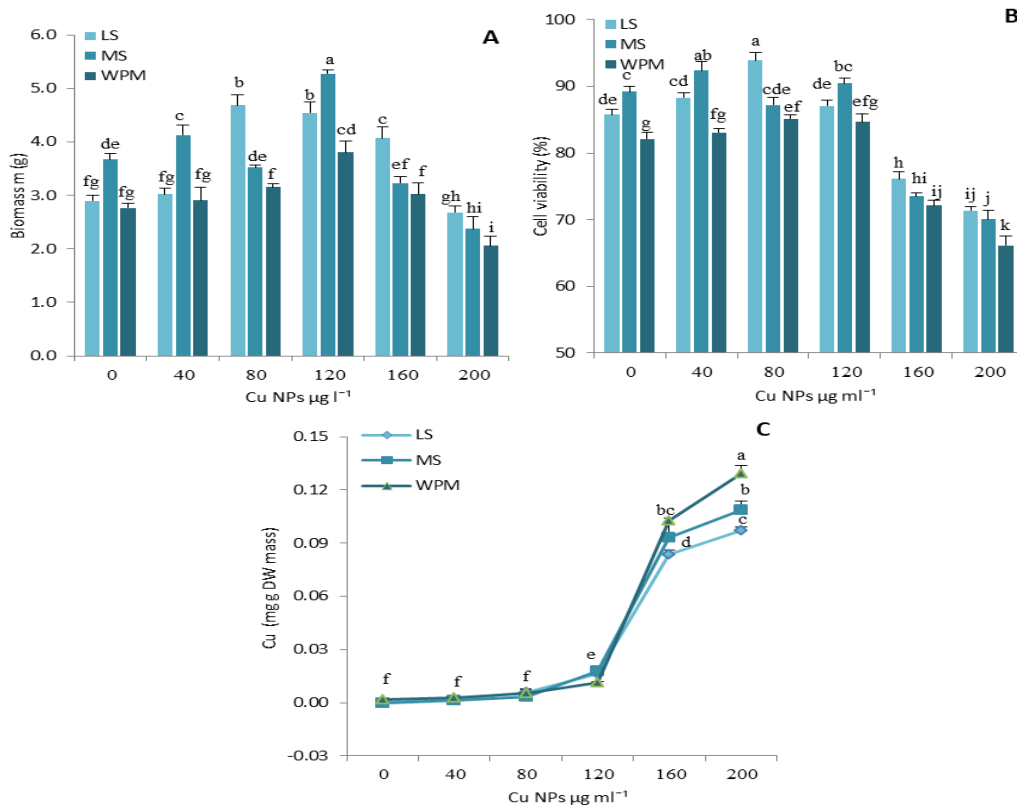
Figure 4. Assessment of mor-physiological parameters such as biomass accumulation (A), cell viability (B), and Cu content (C) of CSC in *M. charantia* L. elicited by different culture media and Cu NPs concentrations. Vertical bars represent the mean ± standard deviation of three replicates. Different letter treatments indicate significant differences at $p \leq 0.01$ based on L.S.D test.

3.3. H2O2 and MDA content of CSC

H_2O_2 and MDA are fundamental indicators to determine the effect of treatments on stimulating the vital pathways responsible for the synthesis of secondary metabolites in the plant cell (Guo *et al*., 2018; Sarmadi *et al*., 2018).

The treatments significantly ($p \leq 0.01$) affected the H_2O_2 content of CSC. The treatment with 200 µg ml^{-1} of Cu NPs recorded the highest content of H_2O_2 for CSC growing in WPM, equal to 361.67 µmol g^{-1} FW. The increase was 3.2-fold compared to the control (Figure 5A).

The results showed a significant change in MDA content. The highest level of suspensions treated with a high concentration of Cu NPs appeared when added to the WPM by 6.4 µmol g^{-1} FW. The control treatment of the MS medium recorded the lowest, equal to 0.67 µmol g^{-1} FW (Figure 5B).
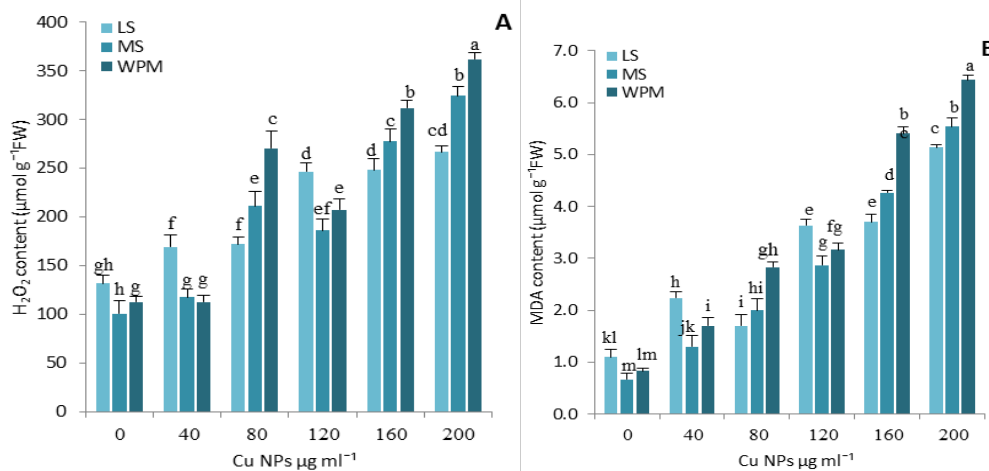
Figure 5. Assessment of oxidative stress parameters such as H_2O_2 (A) and MDA (B) of CSC in *M. charantia* L. elicited by different culture media and Cu NPs concentrations. Vertical bars represent the mean ± standard deviation of three replicates. Different letter treatments indicate significant differences at p ≤ 0.01 based on L.S.D test.

3.4. Antioxidant enzymatic activity of CSC

PAL and PPO are essential enzymes in protecting cellular components from the effects of oxidative stress. Thus, they have a major role in sustaining the production of secondary metabolites in the cell (Sarmadi et al., 2018). The different treatments caused a significant improvement ($p \le 0.01$) in the enzyme activity.

The results showed an upward trend in PAL activity due to the change of cultures and treatment with Cu NPs. The concentration was 200 μg ml^{-1} of Cu NPs with a mean WPM of 7.38 U mg^{-1} protein on all treatments. MS

medium untreated with Cu NPs showed the lowest enzyme activity of 1.10 U mg^{-1} protein (Figure 6A).

As for PPO enzyme activity, the results showed the importance of treatments in improving its activity, and the cultures medium enriched with Cu NPs recorded a significant increase in activity, which reached a concentration of 200 μg ml^{-1} with WPM 5.47 U mg^{-1} protein. However, it was not significantly different with an MS medium of the same concentration. In contrast, we found the lowest activity of PPO when the control treatments of cells were cultured in an MS medium (Figure 6B)
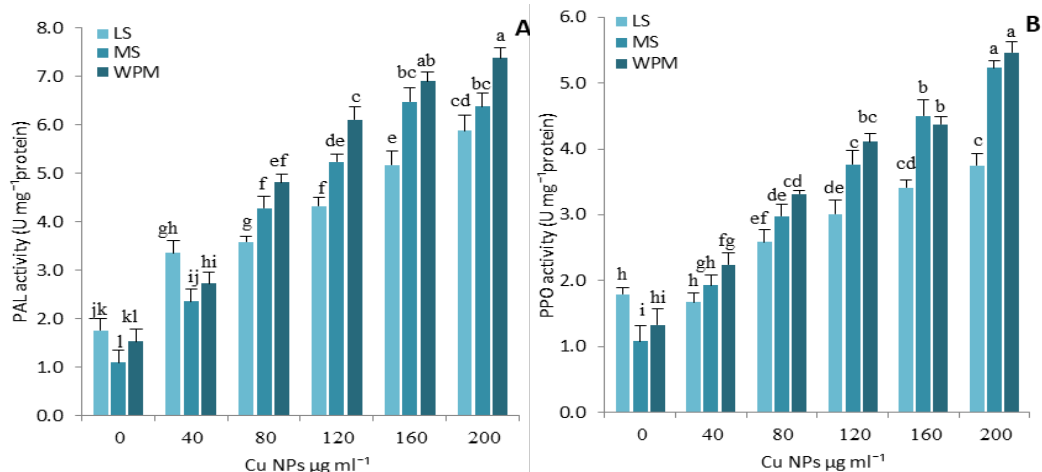
Figure 6. Assessment of antioxidant enzymatic activity parameters such as PPO (A) and LPO (B) of CSC in *M. charantia* L. elicited by different culture media and Cu NPs concentrations. Vertical bars represent the mean ± standard deviation of three replicates. Different letter treatments indicate significant differences at p ≤ 0.01 based on L.S.D test.

3.5. Secondary metabolites of CSC

Phenols and flavonoids are secondary metabolites available in *M. charantia* L., known for their therapeutic properties (Chung et al., 2018). The different treatments caused a significant improvement ($p \le 0.01$) in the production of CSC from secondary metabolites.

The TPP increased due to different media cultures and Cu NPs treatment concentrations. The treatment of CSC with MS+200 μg ml^{-1} recorded the highest yield of 8.23

mg g^{-1} DW, which did not differ significantly from the production of a WPM of the same concentration. The control group showed the lowest production for all cultures (Figure 7A).

The change of cultures and the concentration of Cu NPs significantly affected the TFP. The treatment of 200 μg ml^{-1} of Cu NPs with WPM recorded the highest yield with an increase of 4.4-fold over the control treatment of the same medium (Figure 7B).
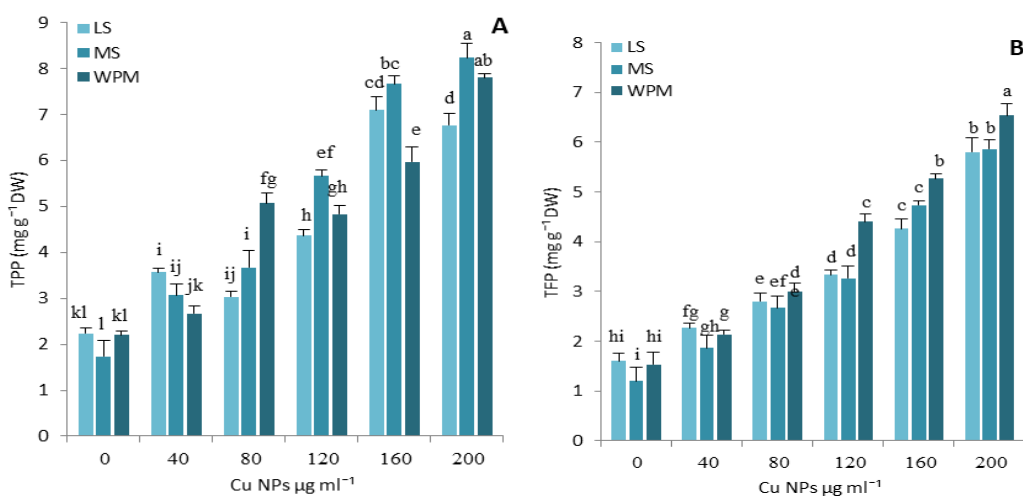
Figure 7. Assessment of secondary metabolites parameters such as TPP (A) and TFP (B) of CSC in *M. charantia* L. elicited by different culture media and Cu NPs concentrations. Vertical bars represent the mean ± standard deviation of three replicates. Different letter treatments indicate significant differences at p ≤ 0.01 based on L.S.D test.

3.6. Antioxidant activity of CSC

Antioxidant activities are the final result of evaluating the ability of different treatments to stimulate the production of secondary metabolites (Neamah and Almehemdi, 2017). MTT and DPPH assays are essential in evaluating antioxidant activity. The treatments significantly ($p \leq 0.01$) affected the antioxidant activities of CSC.

To assess antioxidant efficacy based on the MTT assay, the media under varying concentrations of Cu NPs differed significantly. CSC grown in the MS medium showed the highest activity under 160 μg ml^{-1} of Cu NPs, which was 0.89. The level of difference was not significant with the MTT radical scavenging activity of CSC grown in WPM and MS medium under 200 μg ml^{-1} concentration of Cu NPs (Figure 8A).

In the DPPH assay, WPM containing a high concentration of Cu NPs recorded the highest antioxidant activity with a significant increase of 9.0% and 13.67% over MS and LS cultures under the same concentration, respectively. In comparison, the control group showed the lowest mean values of antioxidant activity (Figure 8B).
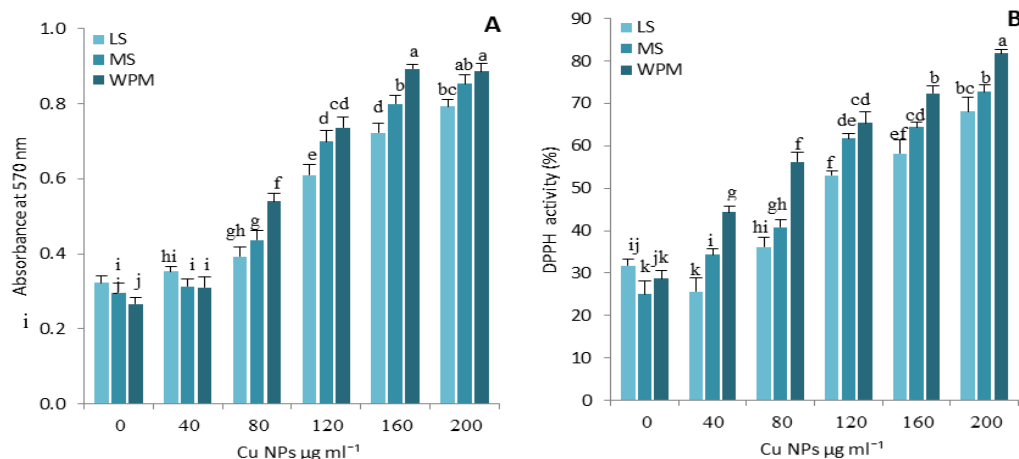
Figure 8. Assessment of antioxidant activity parameters such as MTT (A) and DPPH (B) of CSC in *M. charantia* L. elicited by different culture media and Cu NPs concentrations. Vertical bars represent the mean ± standard deviation of three replicates. Different letter treatments indicate significant differences at p ≤ 0.01 based on L.S.D test.

4. Discussion

There was a variance in the results of media cultures for the mor-physiological parameters. It may be due to the different components of the chemical cultures thus reflected on the characteristics of CSC. Copper nanoparticles may have the ability to penetrate cell walls and have high reactivity by increasing their surface area. Biomass accumulation and cell viability were enhanced by treatment with Cu NPs (Figures 4A and 4B). This may be due to the role of copper in synthesizing some essential enzymes in the vital activities of the plant. In contrast, over-treatment contributed to stress on the culture medium of CSC. This inhibited the growth of CSC biomass under high concentrations because of the toxicity generated by over-treatment. This led to copper accumulation in plant cells (Figure 4C). These results are similar to previous reports showing the role of treatment with CuO NPs in enhancing the induction of calli cultures in *Oryza sativa* L. (Anwaar *et al.,* 2016). The concentrations of Cu NPs enhanced the biomass of *Balanites aegyptiaca* L. (Ebad *et al.,* 2019). Hayat *et al*. (2021) reported that there was a significant difference in the biomass accumulation of *Artemisia absinthium* calli cultures treated with Cu NPs.

In general, the accumulation of metals in the plant cell is one of the leading causes of nutritional disorders (Neamah and Hamad, 2020). In our study, the oxidative stress indicators appeared due to the increased treatment of Cu NPs and the different media cultures. The accumulation of H_2O_2 increased (Figure 5A), contributing to cell membrane degradation in CSC. Hence, MDA content increased (Figure 5B).

On the other hand, the excessive increase in ROS and the rapid deterioration of cell membranes are controlled by defense systems. The plant cell has a defense mechanism that enables it to confront dangers resulting from various stresses, including metal stress. It is believed that H_2O_2 acts as a mediating signal that stimulates the synthesis of defense systems (Sanjari *et al.,* 2019).

PAL and PPO are two types of antioxidant enzymes (Figure 6). The PAL enzyme enhances the biosynthetic pathways responsible for synthesizing phenolic compounds (Asghari and Zahedipour, 2016; Manquián-Cerda *et al.,* 2016). In comparison, the PPO enzyme contributes to the oxidation of phenolic compounds under tensile conditions. Cu NPs played an essential role in membrane protection of vitals from damage, thus protecting the phenols stored in the cellular vacuoles from oxidative stress.

Phenolic compounds are classified as potent non-enzymatic antioxidants and an essential secondary metabolite (El Jabboury *et al*., 2022). They mitigate ROS's toxic effects and can chelate minerals (Mierziak *et al.,* 2014).

There was a positive effect of the Cu NPs treatment (Figure 7). The effect of CSC by stress may have led to the elicitation of phenolic compounds.

MTT and DPPH assays assess antioxidant activity (Neamah, 2016; Chung *et al.,* 2018) based on their ability to accept an electron or hydrogen (Sharma and Ramawat, 2014). The results showed that the antioxidant activity could be increased by treatment with Cu NPs, as well as the different chemical components of CSC media cultures (Figure 8). Increased TPP or TFP can lead to enhanced antioxidant activity (Figure 7). These results are similar to

the report by Choudhary *et al.* (2011) on *Raphanus sativus* under Cu stress. This is consistent with the announcement by Hayat *et al.* (2021) of *Artemisia absinthium* L. callus cultures treated with Cu NPs.

5. Conclusion

The effect of media cultures and Cu NPs treatments on the CSC of *M. charantia* L. was reported for the first time. MS medium was more consistent in improving biomass accumulation compared to LS or WPM. In general, the exogenous Cu NPs at lower concentrations improved biomass accumulation, whereas the increasing concentrations of Cu NPs caused an increase in the accumulation of H_2O_2 and MDA. Thus, this enhanced the activity of non-enzymatic defense systems that contributed to the inhibition of phenolic oxidation and the elicitation of secondary metabolites by Cu NPs. These results can be exploited in the commercial production of secondary metabolites.

Acknowledgements

References

Ainsworth EA and Gillespie KM. 2007. Estimation of total phenolic content and other oxidation substrates in plant tissues using Folin–Ciocalteu reagent. *Nat Protoc.*, **2:** 875–877.

Alexieva V, Sergiev I, Mapelli S and Karanov E. 2001. The effect of drought and ultraviolet radiation on growth and stress markers in pea and wheat. *Plant Cell Environ.*, **24:** 1337–1344.

Anwaar S, Maqbool Q, Jabeen N, Nazar M, Abbas F, Nawaz B, Hussain T and Hussain SZ. 2016. The effect of green synthesized CuO nanoparticles on callogenesis and regeneration of Oryza sativa L. *Front Plant Sci.*, volume **7**, Article 1330.

Arteaga, LOH, Tovias ML, Martínez RA, Jasso MEC, Montero IA and Ruiz F. 2018. Determination of silver concentration in tomato seeds (*Solanum lycopersicum* L.) exposed to silver nanoparticles using AAS-F and a validated method. *Acta Univ.*, **28(5):** 58-65.

Asghari M and Zahedipour P. 2016. 24-Epibrassinolide acts as a growth promoting and resistance-mediating factor in strawberry plants. *J Plant Growth Regul.*, **35:** 722–729.

Bsoul EY, Othman SA, Al-Ghzawi AA and Massadeh MI. 2023. Effect of silver nanoparticles on growth and physiological responses of spinach (*Spinacia oleracea* L.) under salt stress. *Jordan J Biol Sci.*, **16(1):** 1-6.

Choudhary SP, Bhardwaj R, Gupta BD, Dutt P, Gupta RK, Kanwar M and Biondi S. 2011. Enhancing effects of 24-epibrassinolide and putrescine on the antioxidant capacity and free radical scavenging activity of *Raphanus sativus* seedlings under Cu ion stress. *Acta Physiol Plant*, **33:** 1319–1333.

Chung I, Rekha K, Rajakumar G and Thiruvengadam M. 2018. Elicitation of silver nanoparticles enhanced the secondary metabolites and pharmacological activities in cell suspension cultures of bitter gourd. *3 Biotech.*, **8:** 412.

D'Cunha GB, Satyanarayan V and Nair PM. 1996. Purification of phenylalanine ammonia lyase from *Rhodotorula glutinis Phytochem.*, **42:** 17–20.

Deshaware S, Gupta S, Singhal RS and Variyar PS. 2017. Enhancing anti-diabetic potential of bitter gourd juice using pectinase: a response surface methodology approach. *LWT Food Sci Technol.*, **86:** 514–522

Ebad FA, Hussein EA, Aref MS and Abdul-Hakim AS. 2019. Effect of treatment with some nanoparticles on morphology, growth and some active secondary metabolites in callus culture of *Balanites aegyptiaca* L., Egypt *J Biotechnol.*, **58:** 107-122.

El Jabboury Z, Aazza S, Ousaaid D, Chater O, Squalli W, El Ghadraoui O, Benjelloun M and El Ghadraoui L. 2022. Optimisation of total phenolic compound extraction and antioxidant activity from dried inflorescence of *Ammi visnaga* using mixture design and triangular surfaces. *Jordan J Biol Sci.*, **15(4):** 679—687.

Fernández-Ariasa M, Boutinguiza M, del Vala J, Covarrubias C, Bastias F, Gomez L, Vargas MIM, Arias-Gonzalez F, Riveiro A and Pou J. 2020. Copper nanoparticles obtained by laser ablation in liquids as bactericidal agent for dental applications. *Appl Surf Sci.*, **507:** 145032.

Gamborg, OLC, Miller RA and Ojima K. 1968. Nutrient requirements of suspension cultures of soybean root cells. *Exp Cell Res.*, **50:** 151–158.

Gapinska M, Skłodowska M and Gabara B. 2008. Effect of short and long-term salinity on the activities of antioxidative enzymes and lipid peroxidation in tomato roots. *Acta Physiol Plant.*, **30:** 11–18.

Ghorbanpour H. 2015. Multi-walled carbon nanotubes stimulate callus induction, secondary metabolites biosynthesis and antioxidant capacity in medicinal plant *Satureja khuzestanica* grown in vitro. *Carbon*, **94:** 749–759

Grover JK and Yadav SP. 2004. Pharmacological actions and potential uses of *Momordica charantia*: a review. *J Ethnopharmacol,* **93:** 123–132

Guo Y, Yu H, Yang M, Kong D and Zhang Y. 2018. Effect of drought stress on lipid peroxidation, osmotic adjustment and antioxidant enzyme activity of leaves and roots of *Lycium ruthenicum* Murr. Seedling. *Russ J Plant Physiol.*, **65:** 244–250

Hatami M, Kariman K and Ghorbanpour M. 2016. Engineered nanomaterial-mediated changes in the metabolism of terrestrial plants. *Sci Total Environ.*, **571:** 275–291

Hayat K, Ali S., Ullah S, Fu Y and Hussain M. 2021. Green synthesized silver and copper nanoparticles induced changes in biomass parameters, secondary metabolites production, and antioxidant activity in callus cultures of *Artemisia absinthium* L. *Green Process Synth.*, **10:** 61–72

Heath RL and Packer L. 1968. Photoperoxidation in isolated chloroplasts: I. Kinetics and stoichiometry of fatty acid peroxidation. *Arch Biochem Biophys.*, **125:** 189–198.

Jia S, Shen M, Zhang F and Xie J, 2017. Recent Advances in *Momordica charantia*: functional components and biological activities. *Int J Mol Sci.,* **18:** 2555.

Kolewe ME, Gaurav V and Roberts SC. 2008. Pharmaceutically active natural product synthesis and supply via plant cell culture technology. *Mol Pharm.,* **5 (2):** 243–256.

Linsmair EM and Skoog F. 1965. Organic growth factor requirement of tobacco tissue culture. *Physiol Plant.*, **18:** 100–27.

Lloyd G. and McCown B. 1980. Commercially- feasible micropropagation of mountain laurel, Kalmia latifolia, by use of shoot-tip culture. *Combined Proceedings- International Plant Propagator's Society.*, **30**: 421–427.

Manquian-Cerda K, Escudey M, Zuniga G, Arancibia-Miranda N, Molina M and Cruces E. 2016. Effect of cadmium on phenolic compounds, antioxidant enzyme activity and oxidative stress in blueberry *Vaccinium corymbosum* L. plantlets grown in vitro. *Ecotoxicol Environ Safety*., **133:** 316–326.

Mierziak J, Kostyn K and Kulma A. 2014. Flavonoids as important molecules of plant interactions with the environment. *Molecules*, **19:** 16240–16265.

Miliauskas G, Venskutonis P and Van Beek T. 2004. Screening of radical scavenging activity of some medicinal and aromatic plant extracts. *Food Chem.*, **85:** 231–237.

Murashige T and Skoog F. 1962. A revised medium for rapid growth and bioassays with tobacco cultures. *Physiol Plant*., **15:** 473-497.

Neamah SI and Almehemdi AF. 2017. Extraction of natural compounds from callus inducted of common sage plant *Salvia officinalis* L. and their evalution of antioxidant activity. *Iraqi J Agric Sci*, **48 (6):** 1541-1548.

Neamah SI and Hamad AH. 2020. The effects of paclobutrazol on enhancing tolerance of *Plantago major* L. to cadmium stress in vitro. *Aust J Crop Sci.,* **14(12):** 2028-2035

Neamah SI. 2016. Antioxidant and Lipid Peroxidantion Inhibitory of Compounds in Common Buckwheat. *Iraqi J Agric Sci*, **47(5):** 8222-8231.

Parida AK and Das AB. 2005. Salt tolerance and salinity effects on plants: a review. *Ecotoxicol Environ Saf.,* **60:** 324–349.

Perumal V, Khatib A, Ahmed QU, Uzir BF, Abas F, Murugesu S, Saiman MZ, Primaharinastiti B and El-Seedi H. 2021. Antioxidants profile of *Momordica charantia* fruit extract analysed using LC-MS-QTOF-based metabolomics. *Food Chemistry: Molecular Sciences*, **2:** 100012

Sahraroo A, Mirjalili MH, Corchete P, Babalar M and Moghadam MRF. 2016. Establishment and characterization of a *Satureja khuzistanica* Jamzad (Lamiaceae)cell suspension culture: a new in vitro source of rosmarinic acid. *Cytotechnology*, **68:** 1415–1424.

Sanjari S, Keramat B, Nadernejad N and Mozafari H. 2019. Ameliorative effects of 24-epibrassinolide and thiamine on excess cadmium-induced oxidative stress in Canola (*Brassica napus* L.) plants. *J Plant Interact.,* **14 (1):** 359–368.

Sarkate A, Banerjee S, Iqbal Mir J, Roy P and Sircar D. 2017. Antioxidant and cytotoxic activity of bioactive phenolic metabolites isolated from the yeast-extract treated cell culture of apple. *Plant Cell Tiss Org Cult.*, **130(3):** 641–649

Sarmadi M, Karimia N, Palazónb J, Ghassempourc A and Mirjalili MH. 2018. The effects of salicylic acid and glucose on biochemical traits and taxane production in a *Taxus baccata* callus culture. *Plant Physiol Biochem.*, **132:** 271–280

Setiowati FK, Widoretno W, Prasetyawan S and Lukiati B. 2022. Enhanced production of organosulfur bioactive compounds in cell suspension culture of single garlic (*Allium sativum* L.) using precursor feeding. *Jordan J Biol Sci.*, **15(2):** 183-191.

Sharafi E, Nekoei SMK, Fotokian MH, Davoodi D, Mirzaei HH and Hasanloo T. 2013. Improvement of hypericin and hyperforin production using zinc and iron nano-oxides as elicitors in cell suspension culture of St John's wort (*Hypericum perforatum* L.). *J Med Plants Byprod.*, **2:** 177–184

Sharma V and Ramawat K. 2014. Salt stress enhanced antioxidant response in callus of three halophytes (*Salsola baryosma, Trianthema triquetra, Zygophyllum simplex*) of Thar Desert. *Biologia.*, **69:** 178–185.

Siahsar B, Rahimi M, Tavassoli A and Raissi AS. 2011. Application of biotechnology in production of medicinal plants. *Am Eurasian J Agric Environ Sci.*, **11(3):** 439–444

Soliva RC, Elez P, Sebastian M and Martín O. 2000. Evaluation of browning effect on avocado puree preserved by combined methods. *Innovat. Food Sci. Emerg. Technol.*, **1:** 261–268.

Svobodova B, Barros L, Calhelha RC, Heleno S, Alves MJ, Walcott S, Bittova M, Kubanb V and Ferreira ICFR. 2017. Bioactive properties and phenolic profile of *Momordica charantia* L. medicinal plant growing wild in Trinidad and Tobago. *Ind Crops Prod*, **95:** 365–373.

Thiruvengadam M, Gurunathan S and Chung IM. 2015. Physiological, metabolic, and transcriptional effects of biologically-synthesized silver nanoparticles in turnip (*Brassica rapa* ssp. rapa L.). *Protoplasma*, **252(4):** 1031–1046

Veisi H, Hemmati S and Safarimehr P. 2018. In situ immobilized palladium nanoparticles on surface of poly-methyldopa coated-magnetic nanoparticles (Fe3O4@PMDA/Pd): a magnetically recyclable nanocatalyst for cyanation of aryl halides with K_4 [Fe $(CN)_6$]. *J Catal.*, **365:** 204–212.

Velioglu Y, Mazza G, Gao L and Oomah B. 1998. Antioxidant activity and total phenolics in selected fruits, vegetables, and grain products. *J Agric Food Chem.*, **46:** 4113–4117.

Wilson SA and Roberts SC. 2012. Recent advances towards development and commercialization of plant cell culture processes for synthesis of biomolecules. *Plant Biotechnol J*., **10(3):** 249–268

The Morphological and Histological Developmental Study of the Gastrointestinal Tract of Peres Fish (*Osteochilus kappenii*) Larvae

Dedi Fazriansyah Putra[1,*], Fathia Salsabila[1], Irma Dewiyanti[2], Agung Setia Batubara[3], Muhammad Nasir[4]

[1]*Department of Aquaculture, Faculty of Marine and Fisheries Universitas Syiah Kuala Banda Aceh Indonesia 23111;* [2]*Department of Marine Science, Faculty of Marine and Fisheries Universitas Syiah Kuala Banda Aceh Indonesia 23111;* [3]*Department of Biology, Faculty of Mathematics and Natural Sciences Universitas Negeri Medan, Medan Indonesia 20221;* [4]*Department of Biology, Faculty of Mathematics and Natural Sciences Universitas Syiah Kuala Banda Aceh Indonesia 23111*

Abstract

Peres fish (*Osteochilus kappenii*) is a native freshwater fish in Central Aceh, Indonesia. This study aimed to determine the morphology and histology development of the digestive tract of Peres larvae. Understanding the developmental stages is essential to support the success of larval rearing during ontogeny. The parameters observed include the total length (TL) of larvae, daily growth rate, larval morphology, and histology of the digestive tract. Furthermore, the total length of the larvae was measured from 1 to 25 day after hatching (DAH). The larvae sampling was conducted at 1, 2, 3, 4, 8, 10, 15, 20, and 25 DAH. Morphological and histological observations were carried out microscopically, and data were analyzed descriptively. The results showed that the TL of larvae growth at the beginning (1 DAH) and termination (25 DAH) of the study was 4.58 ± 0.24 mm and 9.62 ± 0.79 mm, respectively. Based on the structural development of the body and food sources, the development of percussion larvae was divided into four phases, namely the yolk sac (0-4 DAH), pre-flexion (5-15 DAH), flexion (16-20 DAH), and post-flexion (21- 25 DAH). The yolk was completely absorbed 4 DAH, marking the end of the yolk sac phase, as the Peres fish larvae began to use external feed. At 25 DAH, the larval morphology was fully formed and pigmentation spread throughout the body. The digestive organs and glands are well-developed with differentiation of the midgut and hindgut, increased goblet cells in the intestine, and increased lipid vacuoles in the liver and zymogen in the pancreas to utilize feed optimally.

Keywords: Fish, development, endogenous, exogeneous.

1. Introduction

Peres fish (*Osteochilus kappenii*) is a native freshwater fish in Central Aceh that is spawned and cultivated. This fish is essential for nutritional needs, specifically protein for the people of Central Aceh, situated in the highlands at ± 1000 Meter Above Sea Level and relatively far from the sea (± 100 km to the coastal area of Bireuen Regency) (BPS Aceh Tengah, 2021). The marine fish supply is determined by distributors from coastal areas, although there has been a decline in quality due to poor handling and relatively long distances. Therefore, increasing the production of freshwater fish commodities is necessary, specifically *O. kappenii,* to meet the needs of the residents in Central Aceh District.

O. kappenii experiences several problems at the cultivation stage, specifically high larval mortality. This is due to the lack of information about the functional developmental stages of the larval digestive system, particularly the critical transition from the yolk sac to exogenous feeding during the rearing period. The larval stage is vital to the success of fish farming because it is prone to mortality, specifically during the transition period (Staaterman *et al*., 2012; McCasker *et al*., 2014). Furthermore, survival in the larval stage is influenced by food and environmental factors (Muchlisin *et al.*, 2003). The fish undergo morphological changes, and digestive system differentiation becomes more complex during the larval to juvenile stages. In general, each teleost has similar digestive system development, although there were variations in the differentiation period and the functional development during ontogeny (Trevino *et al.,* 2011).

There are several studies on the morphology and histology development of the digestive tract of fish larvae. Putra *et al.* (2012) studied the development of morphology and digestive tract of tomato clownfish (*Amphiprion frenatus*) in a controlled environment. Other studies include Croaker croceine fish, *Pseudosciaena crocea* (Mai *et al.,* 2005), humpback grouper, *Cromileptes altiveles* (Abol-Munafi *et al*., 2011), catfish, *Mystus nemurus* (El Hag *et al*., 2012), striped murrel, *Channa striata* (Paray *et al.,* 2015), ontogeny and morphological development of tilapia (*Oreochromis niloticus*) in Aceh Province, Indonesia (Ismarica *et al*., 2022), yellowtail tetra fish *Astyanax lacustris* (Characiformes: Characidae) (dos Santos *et al*., 2020), *Schizothorax waltoni Regan* and *Percocypris retrodorslis* (Xu *et al*., 2023), orchid

---

[*] Corresponding author. e-mail: dfputra@usk.ac.id.

dottyback fish, *Pseudochromis fridmani* (Chen *et al*., 2022), yellowfin tuna, *Thunnus albacares* larvae (Kwan *et al*., 2019), red sea bream, *Pagrus major* (Khoa *et al*., 2019), Black Amur bream, *Megalobrama terminalis* (Liu *et al*., 2020), *Culter alburnus* (Huang *et al*., 2021), Shi drum, *Umbrina cirrosa* (Karacaoğlan *et al.,* 2023), Yellowfin seabream, *Acanthopagrus latus*, Houttuyn 1782 (Morshedi *et al*., 2021), and Arctic fish, *Leptoclinus maculatus* (Pekkoeva *et al*., 2023).

Currently, there are no studies on the development of morphology and histology of the digestive tract of *O. kappenii* larvae. This study on the digestive system development is important to determine the activity of digestive enzymes (Babaei *et al*., 2011), the period of endogenous (occurs during the early developmental stages of fish, primarily in the embryonic and larval stages) and exogenous (begins when fish larvae have absorbed the nutrients from their yolk sac and need to start feeding on external sources for further growth) feeding (Faulk *et al*., 2007), the period of functional changes in the digestive organs (Infante and Cahu, 2001), the process of absorption of food nutrients (Lallès, 2020), and digestive capacity (Gawlicka *et al*., 1995). Therefore, this paper aims to investigate the morphology and histology development of the digestive tract to support the success of rearing *O. kappenii* larvae in the future.

2. Materials and Methods

2.1. O. kappenii peres larvae cultivation

The broodstock of male and female Peres fish was obtained from the Regional Technical Implementation Unit (UPTD) of the Lukup Badak Fish Seed Center (BBI), Pegasing District, Central Aceh, and Indonesia. Furthermore, brood spawning was conducted in a 70 x 45 x 45 cm aquarium, with a male-to-female brooders ratio of 2:1. A semi-artificial spawning technique was employed, and, on completion, the parent was separated from the eggs. The hatched larvae were transferred to a larval rearing tank with aeration until their yolk runs out. In the early phase, plankton was given 3 times a day after the yolk thinned, which was obtained from green water. Furthermore, the larvae were given thawed pellet powder 7 days after hatching.

2.2. Observation of digestive organs and histology

The larvae were sampled on 1, 2, 3, 4, 8, 10, 15, 20, and 25 for morphological and histological analysis. A total of 15 samples were collected from rearing container, and preserved in a sample bottle using a 10% neutral buffer formalin (NBF) solution. For morphological observations, 5 samples of the preserved larvae were randomly selected, then examined using a stereo microscope (Olympus SZX16) and photographs were taken. Meanwhile, 15 samples aged 1 to 7 DAH were used for histological analysis (Putra *et al*. 2012), as well as 5 random samples aged 8 to 25 DAH. The histological preparation process followed methods outlined by Drury and Wallington (1967) Kiernan (1990) and Abdullah-Al Mamun *et al*. (2022). This involved tissue fixation with 10% NBF fixative solution, tissue dehydration with graded alcohol, tissue clarification using xylene, infiltrating the tissue with

paraffin, immersing the preparations with paraffin wax, cutting the tissue using a microtome with a thickness of 5 μm, and staining with Haematoxylin and Eosin (H&E). The results were observed under a microscope (Olympus CX21) with digital photos integrated with a computer.

2.3. Data analysis

The total length of the larvae was measured from 1 to 25 DAH with a digital caliper (mm) with an accuracy of ± 0.2 mm. Five samples were collected daily to measure the total body length, then the average was calculated using standard deviation (SD). The length growth pattern of Peres fish larvae was analyzed using Excel software. Measurement of the daily growth rate (DGR) was calculated based on Hopkins (1992): $DGR = Lt\text{-}Lo/t$, where DGR represented the Daily Growth Rate (mm/day), Lt and Lo represented the average total length at the end and the start of the study (mm), respectively. The data obtained were analyzed descriptively.

3. Results

3.1. Growth of Peres Fish Larvae (O. kappenii)

Length growth pattern of the larvae showed an exponential pattern during rearing (Figure 1). The daily length growth rate from 1 - 25 DAH was 0.201 mm/day. Also, the average total length at 1 DAH was 4.58 ± 0.24 mm TL and reached 9.62 ± 0.79 mm TL at 25 DAH. The total length of the pre-flexion phase from 5–15 DAH was 4.96 ± 0.28 mm TL – 5.84 ± 0.32 mm TL. Growth was rapid at the 16-20 DAH flexion phase, ranging from 5.86 ± 0.53 mm TL – 8.34 ± 0.69 mm TL. The final stage was the post-flexion phase *at* 21-25 DAH, comprising 8.42 ± 0.60 mm TL – 9.62 ± 0.79 mm TL.
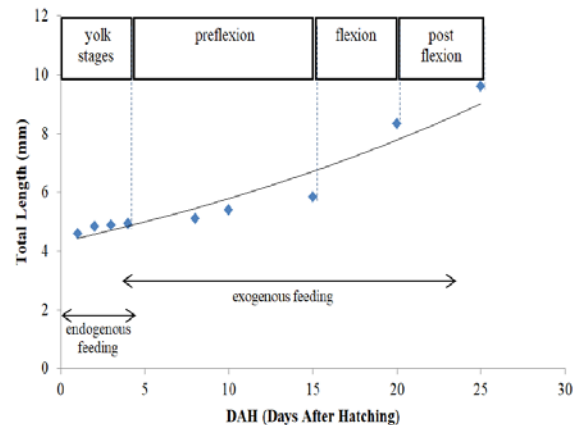
Figure 1. Length growth pattern of Peres (*O. kappenii*) larvae from 1 DAH to 25 DAH.

3.2. Morphology Development of Peres Larvae (O. kappenii)

The stages of morphological development of the Peres fish larvae are divided into 4 based on the structural development of the body and food sources, namely the yolk sac phase, pre-flexion, flexion, and post-flexion (Table 1). Morphological development in the pre-flexion phase occurs 11 days after passing through the yolk sac phase (4 DAH), while the flexion and post-flexion phases have equal durations of 5 days each.

Table 1. Stages of morphological development of Peres fish (*O. kappenii*) larvae

No.	Phase	Characteristics of Morphological Observation	DAH	Food Source
1.	Yolk sac	The mouth is still closed, the eyes are not pigmented, and the body is still transparent.	0-1	Endogenous feeding
		The mouth is starting to open, the eyes are getting pigmented, and the body is still transparent.	2-4	Endogenous-exogenous feeding
2.	Pre-flexion	The yolk has run out, the body still looks transparent, the fins are starting to form but are still simple, the eye organs are starting to enlarge, and the tail bones of the larvae are starting to bend.	5-15	Exogenous feeding
3.	flexion	The fins begin to develop and separate, pigmentation begins to appear on the head, abdomen, and fins.	16-20	Exogenous feeding
4.	Post-flexion	The dorsal fins, pelvic fins, pectoral fins, anal fins, and caudal fins are fully formed, and pigmentation has spread all over the body.	21-25	Exogenous feeding

The results of the morphological development analysis showed fin folds after hatching, located along the body including the dorsal, caudal, anal, and ventral fin folds (2a, b, c, d, e, f, g). However, underdeveloped fins hinder the larvae from swimming actively. The fins are completed at 15-20 DAH and the rays are perfectly formed, specifically on the dorsal and caudal fins (Figures 2 g-h). At 25 DAH, the fish resemble an adult morphologically due to the development of cranial structures including premaxilla, maxilla, dentary, preopercle, and opercle. In addition, the development of the fins is complete at 25 DAH, with the caudal fin structure having urostyle, hypural, parhypural, uroneural, and epural bones (Figure 2i).
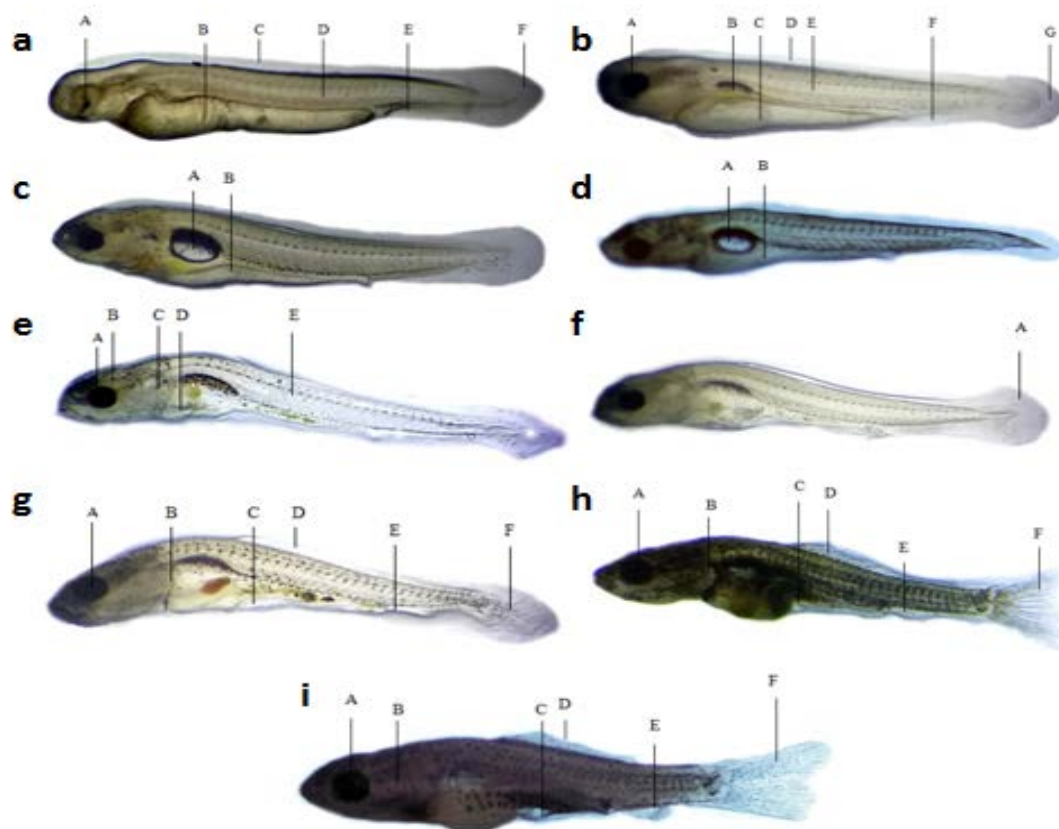
Figure 2. Morphological development of Peres fish (*O. kappenii*) larvae. **(a)** 1 DAH (4.58 ± 0.24 mm TL) A, eye; B, egg yolk (yolk sac); C, dorsal fin folds; D, notochord; E, anal fin folds; F, caudal fin fold; **(b)** 2 DAH (4.82 ± 0.30 mm TL) A, eye; B, swim bladder; C, egg yolk (yolk sac); D, dorsal fin folds; E, notochord; F, anal fin folds; G, caudal fin fold; **(c)** 3 DAH (4.88 ± 0.21 mm TL). A, swim bladder; B, egg yolk (yolk sac); **(d)** 4 DAH (4.94 ± 0.31 mm TL). A, swim bladder; B, egg yolk (yolk sac); **(e)** 8 DAH (5.1 ± 0.12 mm TL). A, eyes; B, head; C, pectoral fins; D, abdomen; E, notochord; **(f)** 10 DAH (5.4 ± 0.29 mm TL). A, caudal fin; **(g)** 15 DAH (5.84 ± 0.32 mm TL). A, eyes; B, pectoral fins; C, pelvic fins; D, dorsal fin; E, anal fin; F, inclined coccyx; **(h)** 20 DAH (8.34 ± 0.69 mm TL). A, eyes; B, pectoral fins; C, developed pelvic fins; D, developed dorsal fin; E, developing anal fin; F, developed caudal fin; **(i)** at 25 DAH (9.62 ± 0.79 mm TL). A, eyes; B, pectoral fins; C, pelvic fins; D, dorsal fin; E, anal fin; F, caudal fin.

3.3. Development of Digestive Tract Histology of Peres Larvae (O. kappenii)

A day after hatching, the digestive tract appeared as a small straight undifferentiated tube covered by a system of simple columnar epithelium, attached dorsally to the yolk. The yolk, acting as a food reserve, appears large and is surrounded by simple squamous epithelium (Figure 3), and the food source is endogenous feeding. Gastrointestinal tract differentiation occurs at 4 DAH during the transition phase to exogenous feeding where the esophagus, stomach, and intestines differentiate and the mouth, pharynx, and anus have completely opened (Figure 4a). The intestinal lumen volume (intestine) expands at 4 DAH as well as the opening of the mouth, indicating that they are prepared to receive food from outside.

The organs, digestive glands, liver (food secretion), and pancreas (enzyme secretion) start differentiating in 2-3 DAH, though they are unwell developed. At 4 DAH, the liver and pancreas are visibly growing, indicating that digestion is commencing. The exogenous feeding has been started at 4 DAH based on the development of digestive organs and glands.

Figure 4b showed that the intestine separated into 2 parts, the midgut and hindgut, at 15 DAH. The length increases with development and intestinal folds become more complex. Additionally, goblet cells are observed in the folds 15 DAH.
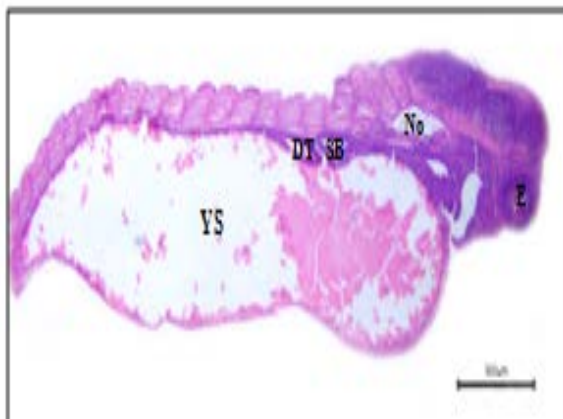
Figure 3. Cross sections of Peres fish (*O. kappenii*) larvae at 1 DAH (HE, x 4). YS, yolk sac; DT, digestive tract; SB, swim bladder; No, notochord; E, eye.

The intestinal volume increases at 20 DAH, accompanied by an increased villi length in the midgut and hindgut. In addition, the liver was enlarged, followed by a rapid increase in vacuolar lipid granules and hepatocytes (Figure 4c). The liver lobes were enlarged and elongated, with increased hepatocytes and lipid vacuoles, which were clearly visible. At 24 DAH, the midgut and hindgut were fully differentiated, with a complex villi complex, and increased goblet cells. In the liver, enlargement continues, and it appears to be filled with vacuolated lipid granules. The amount of zymogen in the pancreas increased greatly (Figure 4d). Figure 2f showed that the tail fin develops at 10 DAH. The caudal fin separates from the dorsal fin (Figure 2g) at the end of the pre-flexion phase.
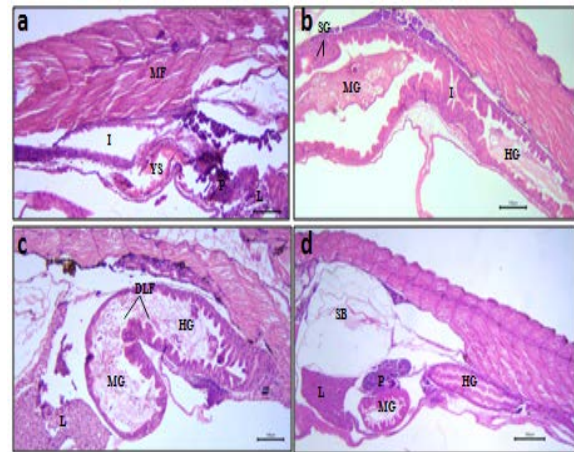
Figure 4. Cross-sectional micrograph of the digestive tract of Peres (*O. kappenii*) larvae. **(a)** 4 DAH (HE, x 10) YS, yolk sac; I, intestines; L, liver; MF, muscular fiber; P, pancreas; **(b)** 15 DAH (HE, x 10). MG, midgut; HG, hindgut; I, intestines; SG, goblet cells; **(c)** 20 DAH (HE, x 10). MG, midgut; HG, hindgut; L, liver; DLF, digested live feed; **(d)** 25 DAH (HE, x 4).

4. Discussion

The results showed that the average total length of the larvae in the early phase of the yolk sac was quite lower, ranging from 4.58 ± 0.24 mm – 4.94 ± 0.31 mm TL. This is because the larvae utilize the yolk for the ontogeny development of the body, specifically the cranial and appendicular structures (Woltering *et al*., 2018). According to Sari *et al.* (2015), the slow growth is due to the energy intake from endogenous feeding to perfect the immature organs, whereas excess energy is used for growth in length and weight at the end of the larval phase.

Figures 2a, b, c, and d illustrated that the yolk sac phase showed incomplete morphology. The larvae rely on endogenous feeding, obtaining nutrients from the egg yolk at 1-3 DAH. However, there is a transition from endogenous to exogenous feeding (food from outside) at the end of this phase (4-5 DAH). The food in the pre-flexion to post-flexion phases originates from exogenous feeding. At 4 DAH, the larvae have functioning eyes and mouth, enabling exogenous feeding activities. The yolk was still visible; hence, the larvae were not fully dependent on external feed. There are differences regarding the yolk expiration in other species, including Snakehead, *Channa striata* (Paray *et al.,* 2014), and Spotted murrel, *Channa punctatus* (Haniffa, 2003), where the yolk was completely absorbed in 3 DAH. In Caspian cutus, *Rutilus frisii cutum* (Jafari *et al.*, 2009), the yolk sac was completely absorbed 20 DAH and the mouth opens 3 DAH allowing external feeding.

The pre-flexion stage begins when the yolk is depleted (4-5 DAH) and continues until the development of larval urostyle bones in the caudal fin (15 DAH). This urostyle bone supports the epural, uroneural, hypural, parhypural, and fin bones (Senevirathne *et al*., 2020). The bending of the tailbone (notochord) and the maturation of the caudal fin of the tomato clownfish, *Amphiprion frenatus,* was found at 4 DAH indicating a transitional phase from pre-flexion to post-flexion (Putra *et al.,* 2012; Boglione *et al*., 2013). However, the development of the urostyel bone structure in the Rainbow kurumoi fish, *Melanotaenia*

parva, occurs at the age of 16-20 DAH (Kadarini *et al.,* 2013).

At 8 DAH, *O. kappenii* larvae showed more signs of development. Although they remained simple and their bodies retained its transparency, the larvae progressed into developing bigger eyes and pigmented cranium and abdomen (Figure 2e). Similar results on the Striped snakehead, *Channa striatus,* were reported by Marimuthu and Haniffa (2007).

The flexion stage started from 16-20 DAH, where pigmentation began to appear on the cranium, abdomen, and fins. Furthermore, the fins began to develop fully and the dorsal, caudal, anal, and ventral fins were separated to enable the larvae to swim at 20 DAH (Figure 2h). The post-flexion stage began at 21-25 DAH, showing the formation of the dorsal, ventral, pectoral, anal, and caudal fins to resemble adult fish and the pigmentation spread throughout the body (Figure 2i). After 25 DAH, no significant morphological development was observed. The changes that occurred involved an increase in body length and weight, indicating the end of this phase. Furthermore, the larvae enter the final stage, the juvenile phase. Previous studies on fish from the same family (Cyprinidae), such as *Chalcaburnus tarichi,* revealed that the larval period ended at 35 DAH (Unal *et al.*, 2001), while that of in *Schizothorax zarudnyi* Nikolskii, 1987 *(Actinopterigii: Cyprinidae)* ended at 21 DAH (Moghadam *et al.*, 2014).

The histological analysis showed that *O. kappenii* larvae at 1 DAH exhibited an undifferentiated, small straight tube-shaped digestive tract, located at the top and connected to the yolk (Figure 3). Furthermore, the digestive tract is lined by a network of simple columnar epithelium and the food sources are endogenous. This result was similar in the Hamun mahi, *Schizothorax zarudnyi* (Moghadam *et al.*, 2014); Malaysian river catfish, *Mystus nemurus* (El Hag *et al.*, 2012), Stripped murrel, *Channa striatus* (Paray *et al.,* 2015), and Large yellow croaker, *Pseudoscianea crocea* (Mai *et al.,* 2005).

Gastrointestinal tract differentiation of *O. kappenii* commenced at 4 DAH during the transition phase to exogenous feeding, where the esophagus, stomach, and intestine begin to differentiate and the mouth, pharynx, and anus have completely opened (Figure 4a). The volume of the intestinal lumen (intestine) increases at 4 DAH as well as the opening of the mouth, indicating the readiness to consume external food. Although the early phase (yolk sac) of the larval exhibit intestinal functionality, it is structurally and functionally less complex than the late larval phase (post-flexion) (El Hag *et al.,* 2012). In other species of the Cyprinidae family, namely *Chalcaburnus tarichi,* the digestive tract differentiate at 5 DAH and exogenous feeding begins at 6 DAH (Unal *et al.*, 2001), while *Schizothorax zarudnyi* at 3-8 DAH (Moghadam *et al.,* 2014).

The digestive gland organs of *O. kappenii,* such as the liver start differentiating at 2-3 DAH and are unwell developed (Figure 4). Andriyanto and Marzuqi (2012) reported similar results on *Cromileptes altivelis* fish, Mai *et al.* (2005) on *Pseudosciaena crocea* fish, and Paray *et al.* (2015) on *Channa striata* fish. The liver and pancreas grow and become clearly visible at 4 DAH, indicating the initiation of the food digestion process. Based on the development of digestive organs and glands, the larvae utilize external feed 4 DAH.

The histological results showed that the intestine was clearly separated into 2 parts, the midgut (middle intestine) and hindgut at 15 DAH (Fig. 4b). However, previous studies reported that they were separated at 2 DAH in *Amphiprion frenatus* (Putra *et al.*, 2012) and 6-7 DAH in *Cromileptes altiveles* fish (Abol-Munafi *et al.*, 2011; Andriyanto and Muzaki, 2013). The histological results also showed an increase in intestinal length and the complexity of intestinal folds as development progressed. Elongated and complex intestinal folds facilitate food absorption in the intestine (Andriyanto and Muzaki, 2013). At 15 DAH, the microvilli network in the intestine developed, expanding the surface to enable efficient absorption (Merrifield *et al.*, 2009; Firdus *et al.*, 2020a; Firdus *et al.*, 2020b). The intestinal volume increased at 20 DAH and the villi lengthened in the midgut and hindgut. Furthermore, the liver was enlarged at 20 DAH, accompanied by a rapid increase in vacuolar lipid granules and hepatocytes (Figure 4c).

The midgut and hindgut were differentiated and formed at 25 DAH. Furthermore, the villi were complex and the goblet cells increased. The liver became larger and was filled with vacuolated lipid granules, while the zymogen in the pancreas increased (Figure 4d). The pancreas developed around the intestines, corresponding to the complexity and quantity of digested food (Andriyanto and Muzaki, 2013). The development of digestive tract organs and glands at 25 DAH indicated the final larval phase. The well-developed functional digestion at this stage enables the larvae to utilize feed optimally.

5. Conclusions

The end of the yolk sac phase in Peres fish is characterized by the complete absorption of the yolk at 4 DAH, which marks the transition from the endogenous to the exogenous feeding phase. Furthermore, the development of digestive organs and glands showed that the larvae were able to feed externally at 4 DAH. At 25 DAH, the developed larvae resemble adult fish and the pigmentation spread throughout their bodies, signaling the final phase of the larvae. The development of the well-developed digestive tract and glands at 25 DAH allowed the larvae to efficiently utilize feed. Future studies on enzymatic activity within the digestive system is suggested to obtain more comprehensive information regarding to the larvae developmental of Peres fish.

Acknowledgments

Conflict of Interest

None.

References

Abdullah-Al Mamun M, Nasren S, Rathore SS and Mahbub AMM. 2022. Histopathological Analysis of Striped Catfish, *Pangasianodon hypophthalmus* (Sauvage, 1878) Spontaneously Infected with *Aeromonas hydrophila*. *Jordan J Biol Sci*., **15(1)**: 93-100.

Abol-Munafi AB, Andriyanto W, Ismi S, Nirmala AY, Mastuti I, Muzaki A and Effendy AWM. 2011. The ontogeny of the digestive tract and associated organs of humpback grouper (*Cromileptes altiveles*) larvae. *Asian Fish Sci*., **24**: 379-386.

Andriyanto W and Marzuqi M. 2012. Hubungan perkembangan morfologi dengan organ pencernaan kerapu bebek (*Cromileptes altivelis*) turunan ke-3 (f-3). *J Perikanan (J Fish. Sci)*., **14(1)**: 46-56. (in Indonesian).

Andriyanto W and Muzaki A. 2013. Diferensiasi organ pencernaan larva kerapu bebek turunan ke-3 (f-3) dan beberapa aktivitas enzim yang terkait. *J Ris Akuakultur*., **8(1)**: 51-63. (in Indonesian).

Babaei SS, Kenari AA, Nazari R and Gisbert E. 2011. Developmental changes of digestive enzymes in Persian sturgeon *(Acipenser persicus)* during larval ontogeny. *Aquac*., **318(1-2)**: 138-144.

Boglione C, Gisbert E, Gavaia P, Witten P, Moren M, Fontagné S, and Koumoundouros G. 2013. Skeletal anomalies in reared European fish larvae and juveniles. Part 2: main typologies, occurrences and causative factors. *Reviews in Aquac*., **5**: S121-S167.

BPS Aceh Tengah. 2021. Aceh Tengah dalam angka tahun 2021. Badan Pusat Statistik Kabupaten Aceh Tengah, Takengon. (in Indonesian).

Chen JY, Zeng C, and Cobcroft JM. 2022. Digestive system ontogeny and the effects of weaning time on larval survival, growth and pigmentation development of orchid dottyback *Pseudochromis fridmani*. *Aquac*., **549**, 737737.

Dos Santos JA, Soares CM, and Bialetzki A. 2020. Early ontogeny of yellowtail tetra fish *Astyanax lacustris* (Characiformes: Characidae). *Aquac Res*., **51(10)**: 4030-4042.

Drury RAB, and Wallington EA. 1967. **Carleton's histological tecnique, 4ᵗʰ Edition**. Oxford University Press, 432p.

El Hag GA, Kamaruddin MS, Saad CR, and Daud SK. 2012. Gut histology of Malaysian river catfish, *Mystus nemurus* (C & V) larvae. *Life Sci J*., **9(2)**: 342-347.

Faulk CK, Benninghoff AD, and Holt GJ. 2007. Ontogeny of the gastrointestinal tract and selected digestive enzymes in *cobia Rachycentron canadum* (L.). *J Fish Biol*., **70(2)**: 567-583.

Firdus F, Samadi S, Muhammadar AA, Sarong MA, Muchlisin ZA, Sari W, and Batubara AS. 2020a. Gut and intestinal biometrics of the giant trevally, *Charanx ignobilis*, fed an experimental diet with difference sources of activated charcoal. *F1000Research*., **9**: 444.

Firdus F, Samadi S, Muhammadar AA, Sarong MA, Muchlisin ZA, Sari W, Mellisa S, Satria S, Boihaqi B, and Batubara AS. 2020b. Supplementation of rice husk activated charcoal in feed and its effects on growth and histology of the stomach and intestines from giant trevally, *Charanx ignobilis*. *F1000Research*., **9**: 1274.

Gawlicka A, Teh SJ, Hung SSO, Hinton DE, and De La Noüe J. 1995. Histological and histochemical changes in the digestive tract of white sturgeon larvae during ontogeny. *Fish Physiol Biochem*., **14(5)**: 357-371.

Haniffa MA, Nagarajan M, Marimuthu K, and Jesu Arockia Raj A. 2003. Embryonic and larval development of spotted murrel, *Channa punctatus* (Bloch). *Indian J Fish*., **50(3)**: 355-362.

Hopkins KD. 1992. Reporting fish growth: a review of the basics 1. *J World Aquac Soc*., **23**: 173-179.

Huang YF, Song BL, Deng TH, Wang Q, Shen Q, and Liu LG. 2021. Ontogenetic development, allometric growth patterns, and daily increment validation of larvae and juvenile *Culter alburnus*. *Environ Biol Fishes*., **104**: 1593-1610.

Infante JZ, and Cahu CL. 2001. Ontogeny of the gastrointestinal tract of marine fish larvae. *Comp Biochem Physiol Part C: Toxicol Pharmacol*., **130(4)**: 477-487.

Ismarica I, Putra DF, and Khairina U. 2022. Ontogeny and morphological development of Tilapia (*Oreochromis niloticus*) larvae in Aceh Province, Indonesia. *E3S Web of Conferences*., **339**: 01007.

Jafari M, Kamarudin MS, Saad CR, Arshad A, Oryan S, and Bahmani M. 2009. Development of morphology in hatchery-reared *Rutilus frisii* kutum larvae. *Eur J Sci Res*., **38(2)**: 296-305.

Kadarini T, Zamroni M, dan Pambayuningrum EK. 2013. Perkembangan larva ikan rainbow kurumoi *(Melanotaenia parva)* dari hasil pemijahan. *J Ris Akuakultur*., **8(1)**: 77-86. (in Indonesian).

Karacaoğlan A, Fırat K, Hekimoğlu MA, Saka Ş, Suzer C, Midilli S, and Çoban D. 2023. Enzymatic, skeletal, and histological ontogeny of shi drum *(Umbrina cirrosa)* larvae under intensive culture conditions. *Fish Physiol Biochem*., 1-20.

Khoa TND, Waqalevu V, Honda A, Shiozaki K, and Kotani T. 2019. Early ontogenetic development, digestive enzymatic activity and gene expression in red sea bream *(Pagrus major)*. *Aquac*., **512**: 734283.

Kiernan JK. 1990. **Histological a1nd histochemical methods theory and practice, 2ⁿᵈ edition**. Pergamon Press plc., 433p.

Kwan GT, Wexler JB, Wegner NC, and Tresguerres M. 2019. *O*ntogenetic changes in cutaneous and branchial ionocytes and morphology in yellowfin tuna (*Thunnus albacares*) larvae. *J Comp Physiol B*., **189**: 81-95.

Lallès JP. 2020. Intestinal alkaline phosphatase in the gastrointestinal tract of fish: biology, ontogeny, and environmental and nutritional modulation. *Reviews in Aquac*., **12(2)**: 555-581.

Liu Y, Chen W, Li Y, Li J, and Li X. 2020. Growth and ontogenetic development of digestive functionality in black Amur bream (*Megalobrama terminalis*). *Aquac Res*., **51(9)**: 3593-3601.

Mai K, Yu H, Ma H, Duan Q, Gisbert E, Infante JLZ, and Cahu CL. 2005. A histological study on the development of the digestive system of *Pseudosciaena crocea* larvae and juveniles. *J Fish Biol*., **67(4)**: 1094-1106.

Marimuthu K, M, and Haniffa MA. 2007. Embryonic and larval development of the striped striped snakehead *Channa striatus*. *Taiwania*., **52(1)**: 84-92.

McCasker N, Humphries P, Meredith S, and Klomp N. 2014. Contrasting patterns of larval mortality in two sympatric riverine fish species: a test of the critical period hypothesis. *PloS one*., **9(10)**: e109317.

Merrifield DL, Dimitroglou A, Bradley G, Baker RTM, and Davies SJ. 2009. Soybean meal alters autochthonous microbial populations, microvilli morphology and compromises intestinal enterocyte integrity of rainbow trout, *Oncorhynchus mykiss* (Walbaum). *J fish dis*., **32(9)**: 755-766.

Moghadam MS, Abtahi B, Rezaei S, and Rahdari A. 2014. Early ontogenetic development of digestive system in *Schizothorax zarudnyi* Nikolskii, 1987 *(Actinopterigii: Cyprinidae)* larvae. *Ital J Zool*., **81(2)**: 194-203.

Morshedi V, Hamedi S, Pourkhazaei F, Mozanzadeh MT, Tamadoni R, Ebadi M, and Gisbert E. 2021. Larval rearing and ontogeny of digestive enzyme activities in yellowfin seabream (*Acanthopagrus latus*, Houttuyn 1782). Comp. *Biochem. Physiol Part A: Mol Integr Physiol*., **261**: 111044.

Muchlisin ZA, Damhoeri A, Fauziah R, Muhammadar, dan Musman M. 2003. Pengaruh beberapa jenis pakan alami terhadap pertumbuhan dan kelulushidupan larva ikan lele dumbo *(Clarias gariepinus)*. *J Biol*., **3(2)**: 105-113. (in Indonesian)

Paray BA, Haniffa MA, Kumar YA. 2014. Studies on embryonic and larval development of induced bred *Channa striatus*. *Ecol Environ Conserv*., **20(3)**: 929-941.

Paray BA, Haniffa MA, War MUD, Al-Sadoon MK, Park YH, and Rather IA. 2015. Histological changes in the digestive tract of striped murrel larvae during ontogeny. *Indian J Mar Sci*., **44(7)**: 984-992.

Pekkoeva SN. Kondakova EA, Falk-Petersen S, Berge J, and Murzina SA. 2023. Ontogenetic changes in the body structure of the Arctic fish *Leptoclinus maculatus*. *Sci. Rep*., **13(1)**: 3688.

Putra DF, Abol-Munafi AB, Muchlisin ZA, and Chen JC. 2012. Preliminary study on morphology and digestive tract development of tomato clownfish, *Amphiprion frenatus* under captive condition. *Aquac Aquar Conserv Legis Inter J Bioflux Society*., **5 (1)**: 29-35.

Sari RM, Yulisman, dan Muslim. 2015. Laju pertumbuhan kelangsungan hidup larva ikan betok *(Anabas testudineus)* pada berbagai periode pergantian jenis pakan. *J Akuakultur Rawa Indonesia*., **3(1)**: 70-81. (in Indonesian)

Senevirathne G, Baumgart S, Shubin N, Hanken J, and Shubin NH. 2020. Ontogeny of the anuran urostyle and the developmental context of evolutionary novelty. *P Natl A Sci*., **117(6)**: 3034-3044.

Staaterman E, Paris CB, and Helgers J. 2012. Orientation behavior in fish larvae: a missing piece to Hjort's critical period hypothesis. *J Theor Biol*., **304**: 188-196.

Trevino L, Gonzales CAA, Garcia NP, and Galan LA. 2011. A histological study of the organogenesis of the digestive system in bay snook *Petenia splendida* Gunther, 1862 from hatching to the juvenile stage. *J Appl Ichthyol*., **27(1)**: 73-82.

Unal G, Cetinkaya O, Kankaya E, and Elp M. 2001. Histological study of the organogenesis of the digestive system and swim bladder of the *Chalcalburnus tarichi* Pallas, 1811 (Cyprinidae). *Turk J Zool*., **25**: 217-228.

Woltering JM, Holzem M, Schneider RF, Nanos V, and Meyer A. 2018. The skeletal ontogeny of *Astatotilapia burtoni*–a direct-developing model system for the evolution and development of the teleost body plan. *BMC Develop Biol*., **18(1)**: 1-23.

Xu B, Li D, Wei K, Zhu X, Xu J, and Ma B. 2023. Allometric growth patterns and ontogenetic development during early larval stages of *Schizothorax waltoni* Regan and *Percocypris retrodorslis* in Southwest China. *Water*., **15(4):** 824.

JJBS

Jordan Journal of Biological Sciences

Infectious Parasites in Coral Reef Fish and Their Potential Use for Habitat Quality Assessment in Jordan's Gulf of Aqaba, Red Sea

Mohammad Al-Zibdah[1,*], Mohammad Wahsha[2], Raid Al-Jawasreh[2], Marouf Khalaf[1]

[1] School of Basic and Marine Science, The University of Jordan, Aqaba; [2] Marine Science Station, The University of Jordan, Aqaba, Jordan

Abstract

Incidents of parasitic infections of coastal (0-40m deep) fish species were investigated to assess ecosystem health and stability along Jordan's Gulf of Aqaba (GoA). The aim was to compare sites of probable anthropogenic impacts using the extent of infections and species richness indices. A total of 828 fish belonging to 60 species were collected and examined from 7 sites. Fish were brought to laboratory and examined for skin and gill lesions and/or parasites. Fish necropsy was undertaken to assess organ-specific parasitic infections. The infection prevalence (IV) of 8 disease agents pooled from all sites was *Psuedodactylogyrus sp.*, *Dactylogyrus sp.*, Copepod (*Gnathia sp.*), *Ergasilus sp.*, Maxillopoda, Nematodes (*Anisakis sp*), Isopods and Platy helminthes. The highest IV was reported in fish gills by Flukes (helminthes), and Isopods and monogeneans were recorded in 88% of the examined fish. However, the highest % of infection was the copepods, *Ergasilus sp.* and *Psuedodactylogyrus sp.*, while the lowest % was the helminthes (fish flukes). The gut parasites *pseudodactylogyrus sp.* and *dactelogyrus sp.* prevailed highest in fish collected at northern sits of GoA. These together with one nematode dominated sites of increasing urban activities. By comparing species richness indices of heteroxenous vs. monoxenous parasites in some fish, results suggest increased incidents of monoxenous parasite in fish collected at areas likely impacted by human activities along the coast.

Keywords: Anthropogenic, Coastal quality, Fish parasites, Gulf of Aqaba, Heteroxenous, Infection prevalence, Monoxenous, Red Sea

1. Introduction

The Gulf of Aqaba is fringed by a rich and well developed yet very diverse coral reef. Consequently, it supports a broad variety of bio-fauna. Existence of this highly diverse and complex ecosystem depends exclusively on the stability of the prevailing natural conditions represented here by the oligotrophic nature of this body (Rasheed et al. 2012; Badran and Foster 1998). The coastal ecosystem of the northern Gulf of Aqaba (Red Sea) has been under constant anthropogenic environmental impacts for the last 3 decades due to the profound effects of rapid growth and development at Jordan's major urban city of Aqaba. This process, along with global environmental changes, is attributed to a list of varieties of human borne causes (Wahsha et al. 2017). These include crowded maritime activity, airborne phosphate dust due to export, incidental sewage effluents together with coastal siltation and land runoff, large scale tourism as well as extensive scuba diving activity (Lacerda et al. 2018; Rasheed et al. 2012; Badran and Foster 1998; Abelson et al. 1999). In view of the fact that the Gulf was a nearly pristine body of water as recently as the mid 70's, the rate of habitat degradation in recent years could be considered quite alarming.

Fish populations are an integral part of the coastal ecosystem of GoA. Since extensive parts of the original shallow coastal habitats around this area have been modified, some to the extent of near destruction, it is hardly surprising that fish abundance and diversity have changed and are on a noticeable decline (Al-Ma'ayta 2015; Al-Zibdah and Odat 2007; Golani and Diamant 1999). Hence, detailed studies on the condition of reef fish communities in GoA are crucial for the management and conservation of regional coral reef ecosystems (Khalaf 2004; Khalaf and Kochzius 2002). Coastal localities that previously supported sizeable fish communities seem to have been largely abandoned by many species. Although there is a rarity of coral reef fish studies in the region, historic evidence suggests that mature individuals belonging to larger reef species (e.g., Serranidae, Labridae, Scaridae, Lethrinidae) are in continuous decline (Al-Zibdah 2013; Khalaf 2004).

In recent years, there have been reports of sharp increase in the global prevalence of diseases in the marine environment, a situation which has been linked with climate changes and numerous anthropogenic factors (Al-Hasawi 2019; Harvell et al. 1999; McVicar 1997). The fact that increased incidence of diseases and mortalities of fish populations often associated with pollution is not new (Lacerda et al. 2018; Overstreet 1997). However, the increase in sporadic mortality events associated with infective agents recently encountered in the marine environment at such a magnitude is definitely of concern.

The present study was carried out to investigate fish diseases and parasites along the coast of GoA during December 2017 to October 2018. Aim is to find out

---

potential infectious parasites in selected fish species collected from different coastal locations at depth range 0-40m. The phenomenon of declining fish populations from shallow coastal waters is evident along the entire coastline of Jordan's GoA (Al-Ma'ayta 2015; Al-Zibdah et al. 2018). GoA coastline most likely is one of the more extensively impacted shorelines probably due to occasional and sporadic spills, tourism, fishing and water-sports. Deterioration of environmental quality is known to affect the natural immunity of fish as well as stressful conditions are known to facilitate dispersal and transmission of infective stages of parasites and diseases (Al-Hasawi 2019; Diamant et al. 2010, 2001; Lafferty and Kuris 1999). In this study, we conducted a monitoring program for examining different fish species fished at various sites along the coast of GoA. Purpose is to understand the extent of stress-related infectious diseases occur in indigenous fish populations of GoA. Investigation was focused on parasitic infections in fish captured from 0-40m depth coastal areas. In addition, rabbit fish, *Siganus rivulatus*, was selected as an indicator fish for evaluating the ecosystem health and stability.

2. Materials and methods

During 10 months of sampling period, specimens belonging to 60 species were collected and identified from the seven sampling sites that represented different urban activities along the coast of GoA (Figure 1, Table 1).
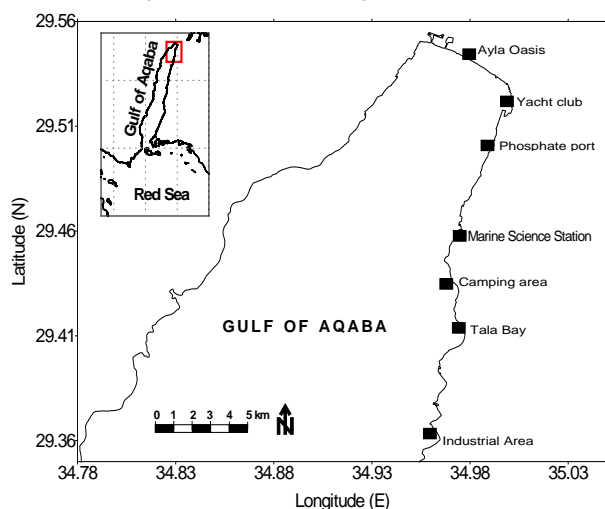
Figure 1. Sites selected for the collection of different fish species during a 10 months' period (Dec 2017-October 2018)

The sampling stations were chosen to represent a range of anthropogenic-impacted and reference habitats on various coastal locations along GoA. The following 7 sites were selected (clockwise): Ayla Oasis sea front, Yacht Club beach, Phosphate Loading Berth (PLB), Marine Science Station (MSS), Tourist Camp, Tala Bay and Jordan Fertilizer Industry (JFI) area.

Table 1. Description of sites selected for the fish sampling.

Name of site	Latitudes	Longitude	Description of existing activities
Ayla Oasis	29.539678°	34.979913°	Inlet outlet of artificial lagoons at north of Aqaba Gulf
Yacht club	29.529096°	34.997922°	Harbour of yachts at northern Gulf of Aqaba
Phosphate Loading Berth	29.498126°		Old Harbour to export crude phosphate
Marine science station (MSS)	29.458590°	34.975976°	Scientific marine environment studies
Tourist camp			Beach for public use (sea sports and camping)
Tala bay	29.405711°	34.975182°	Gated tourist resort
J. Fert. Indust. (JFI)			Fertilizers Industry

The sampling period was between December 2017 and October 2018. A total of 828 fish individuals belong to 60 species were collected and examined from all sites of GoA coastal areas. Fish were mostly obtained from fishermen operating baited mesh traps. Other fish were collected by MSS staff using a similar trap technique and gill nets. Baits used were selective in order to catch as many varieties as possible on a monthly basis. Fish samples were sorted to species level following Khalaf and Disi, 1997. Similarly, fish parasite taxonomy and identification was in accordance to various sources including Atlas of Fish Histology, 2009; world register of marine species WoRMS and FishBase. This is in addition to some publications on fish parasites that were utilized for the current study.

Fish samples were kept frozen until further examination for parasitological/pathological inspections. In laboratory, fish samples of the different species were thawed and examined to search for ecto and indo parasites. Specimens were initially examined externally for skin and gill lesions and/or parasites, followed by a complete necropsy in which the alimentary tract, and suspect organs were examined for lesions or the presence of parasitic infections. An incision was made from the dorsal spine to caudal fin to visually inspect and count the parasites, if present. The organs inspected were skin, internal tissue, gills, hepato pancreas, spleen, and gut. Any visible white pseudo cysts encountered in the tissue were counted (Codex guidelines for sensory evaluation of fish and shellfish in laboratories, CAC-GL 31-1999). In most cases, gills, liver, spleen, kidney and intestine were fixed in 4% buffered neutral formalin (BNF) for further processing of paraffin histology. Freshly prepared skin, gill, spleen, intestinal mucosa and digestive tract imprints were studied microscopically and in some cases, smears were air dried, fixed and stained with Giemsa or Z-N. Further, in the second part of work (unpublished) organs and suspected tissues were fixed with buffered neutral formalin to be processed with paraffin histology.

Moreover, the approach of Gelnar et al. (1997) and D'Amelio and Gerasi (1997) considering using an asymptotic curve to estimate species richness of a given population of parasites in a selective indicator fish species and here the rabbit fish (*Siganus sp.*) was taken into account. The fish were collected from three different sites

in 2021 and proved suitable fish as far as heteroxenous species are concerned since they accumulate but cannot proliferate on the host. Results on parasitological models were backed by data analyses employing species diversity and richness indices (Soberon and Llorente, 1993; Walther et al., 1995) using one way ANOVA statistics.

3. Results and discussion

All fish species examined during this study period were sorted by family and categorized according to the trophic level, namely C: carnivore, H: herbivore, O: omnivore, and P: planktivore (Table 2).

Fish samples were somewhat biased towards Aqaba's southern coast, with 828 specimen fish examined. Fish are obviously more abundant toward the south of Jordanian GoA shoreline. This is certainly true as these areas are dominated by coral reef (Al-Zibdah et al. 2008; Al-Horani et al. 2006; Khalaf 2004). Fish populations were found in all sites with coral reef along the coast of GoA (Al-Zibdah and Odat 2007; Khalaf 2004). However, the majority of fish species as well as the number of individuals examined were collected from sites located in southern GoA (Figures 2 and 3).
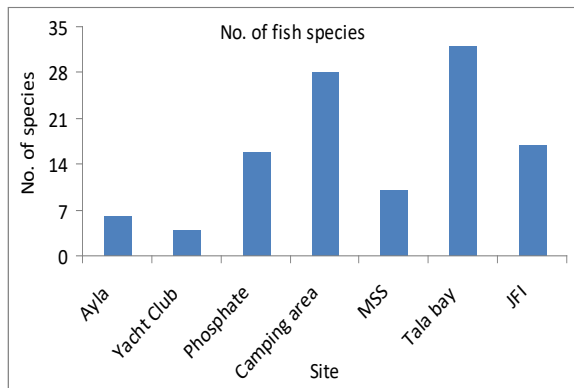
Figure 2. Number of fish species collected and examined from each sampling site (fish were found belong to 58 species and 21 families).
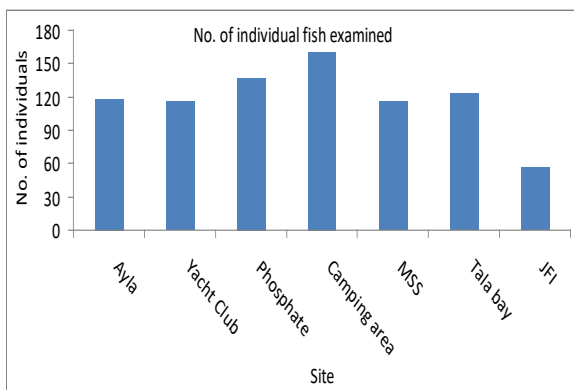
Figure 3. Number of individual fish inspected for pathological and parasitological infections from all sites along the coast of GoA

The infectious agents or parasites recovered from each species are given in the right-hand column in Table 2. Natural infections with Monogenea, Copepods, Isopoda, Nematode, and Helminthes were recorded, and some were identified to species level. For further histological

examinations, specimens were fixed and preserved whole for paraffin sections of tissue and/or parasites from the examined fish. The infection prevalence of 8 disease agents that were pooled from all sampling sites is shown in Figure 4. These disease agents were *Psuedodactylogyrus sp., Dactylogyrus sp.*, Copepod (*Gnathia sp.*), *Ergasilus sp.*, Maxillopoda, Nematodes (*Anisakis* sp.), Isopods and Helminthes (Jerônimo et al. 2022; Hoai 2020; Diamant et al. 2001). The highest prevalence of infection observed was with the gill racks, which were Flukes (helminthes), Isopods and monogeneans and were recorded in nearly 88% of the examined fish. However, the highest in infection % was for the two copepod species, *Ergasilus sp.* and *Psuedodactylogyrus sp.,* while the lowest % of infection was for the helminthes (fish flukes). The infection prevalence details according to each sampling site are also shown in Figure 5.
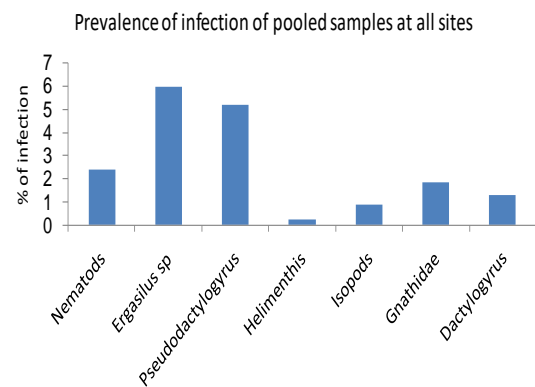
Figure 4. Prevalence of infection by different parasites of fish samples pooled from all sites
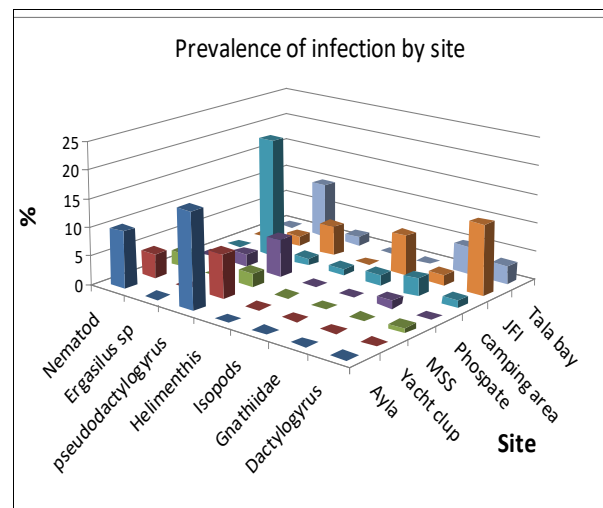
Figure 5. Prevalence of infectious parasites observed in examined fish species from the investigated sites along the coast of GoA

Table 2. Collected and examined fish species showing incidents of parasitic infections, fish trophic level and number of individual fishes in the present study.

Fish family	Species	Trophic level	No. fish examined	Parasitological findings
Acanthuridae	*Acanthurus nigrofuscus*	(H) Herbevore	7	
	Ctenochaetus striatus	H	12	*pseudodactylogyrus, Helminths*
	Zebrasoma xanthurum	H	14	*pseudodactylogyrus, Gnathiids*
Apogonidae	*Cheilodipterus macrodon*	(P) Plankitivore	1	
Baslistidae	*Balistapus undulates*	(C) Carnivore	7	
	Sufflamen albicaudatus	(O) Ominvore	3	
Bothidae	*Bothus pantherinus*	C	1	*Ganthiids*
Chaetodontidae	*Chaetodon Auriga*	O	1	*Ergasilus sp*
	Chaetodon austriacus	C	3	*Dactylogyrus*
	Chaetodon fasciatus	O	4	*Ergasilus sp*
	Chaetodon paucifasciatus	O	22	*Trichodina sp., Ergasilus sp*
	Heninochus diphreutes	P	76	*Ergasilus sp, Helminths, Isopodes*
Echeneidae	*Remora remora*	C	1	
Fistulariidae	*Fistularia petimba*	C	1	
Holocentridae	*Myripristis chryseres*	C	8	*Ergasilus sp, Ganthiids*
	Myripristis murdjan	C	42	*pseudodactylogyrus, Ergasilus sp, Dactylogyrus, Isopodes*
labridae	*Bodianus anthoides*	C	1	
	Cheilinus mentalis	C	4	
	Cheilinus abudjubbe	C	1	
	Cheilio inermis	C	1	
	Coris caudimacula	C	20	
Lethrinidae	*Lethrinus borbonicus*	C	5	*Isopods, Ergasilus sp*
	Lethrinus variegatus	C	37	*Monogenenean*
Monacanthidae	*Amanses scopas*	C	2	
	Cantherhines pardalis	O	11	
Mullidae	*Parupeneus forsskali*	C	2	
	Parupeneus rubescens	C	1	
	Pempherisvanicolensis	C	40	*Ganthiidae*
Ostraciidae	*Ostracioncubicus*	O	1	1
Pomacanthidae	*Apolemichthysxanthotis*	H	5	
	Genicanthuscaudovittatus	P	7	
	Abudefduf vaigiensis	P	2	
	Chromis pembae	P	5	
	Dascyllustrimaculatus	P	17	*Trichodina sp., pseudodactylogyrus*
	Pomacentrustrichourus	P	23	*Isopods*
	Amblyglyphidodonleucogaster	P	5	
Scaridae	*Calatomusviridescens*	H	7	
	Scarus fuscopurpureus	H	9	*Ganthiida, Dactylogyrussp, Isopods, pseudodactylogyrus, Ergasilus sp*
	Scarus ghobban	H	3	*Dactylogyrussp*
	Scarus niger	H	97	*pseudodactylogyrus, Ganthiids, Dactylogyrus, Isopods, monogenenean*
	Scarus sordidus	H	2	
	Scarus ferrugineus	H	10	*monogenenean, Ganthiids*
	Scarus genazonatus	H	1	
Scombridae	*Scomber japonicas*	C	1	
	Rastrelligerkanagurta	C	1	
Scorpionidae	*Dendrochirusbrachypterus*	C	1	
	Petrois miles	C	14	*Trichodina sp., pseudodactylogyrussp*
	Petrois radiate	C	5	
	Scorpaenopsis barbatus	C	1	
Serranidae	*Epinephelus fasciatus*	C	9	*Trichodina sp., monogenenean*
	Cephalopholishemistiktos	C	1	
	Variola louti	C	2	
Siganidae	*Siganus argenteus*	H	16	
	Siganusluridus	H	1	
	Siganusrivulatus	H	114	*Nematods, monogenenean*
Sparidae	*Acanthopagrus bifasciatus*	C	2	
	Diplodus noct	H	136	*Monogenenean*
Synodontidae	*Synodus variegatus*		2	

At some sites, the prevalence of certain infections was considerably higher than the mean. Moreover, the two parasites, *pseudodactylogyrus sp.* and *dactelogyrus sp.* were mostly noticed in different fish species that were caught at sites from north to south. This could explain the natural existence of these parasites in fish gills known to have multiple hosts. This might indicate abundance of several hosts in habitats that reveal forms of anthropogenic interventions along the coastline GoA (Hoai 2020; Ojwala et al. 2018). The prevalence of infection per site showed also dominance of the above two parasites and another

parasite, nematodes, with a high % prevalence. These parasites actually were detected at sites of increased urban activities which might suggest its diverse abundance in different fish species. Nevertheless, this study considers selective fish species as potential indicators for the quality of the different coastal habitats. The generated data have shown that the fish *S. rivulatus* (Diamant et al. 2001, 1999) could be a good example species to express the ecological status and quality of different habitats along the coast of GoA (Figure 6).
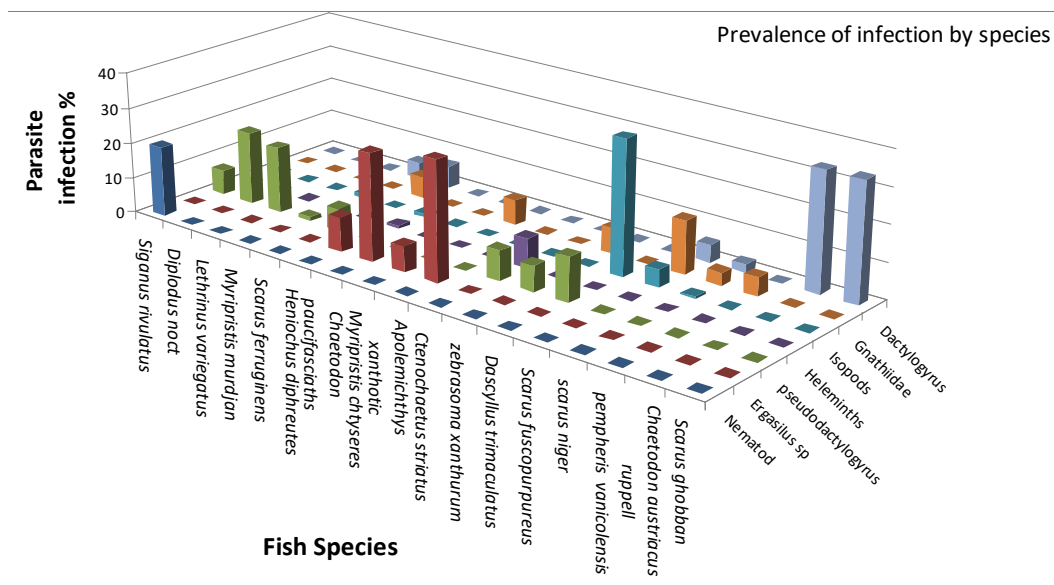
Figure 6. Prevalence of infection to each infectious agent by host species in the examined fish.

The GoA was a near-pristine area before 2-3 decades ago. However, there is now increasing evidence that coastal ecosystem in this area is experiencing environmental modifications (Ashmawy et al. 2018; Schumacher et al. 1995). Incidences of pollution from different sources were reported to result in forms of eutrophication most probably due to rapid urban development (Jerônimo et al. 2022; Silverman et al. 2004; Abelson et al. 1999). Such shifts from the pristine condition may lead to phytoplankton elevation above normal, which will result in an increase in zooplankton and/or benthic fauna of different taxa (copepods, polychaetes etc.), and these might represent potential hosts of fish parasites. In this study, we attempted to quantify some evidence on the above predictions. Indeed, the study showed some changes which were significant at certain points, shown here by the decline in the heteroxenous vs. monoxenous parasite species ratios. We noticed an increase in abundance of monoxenous parasites at certain sampling stations, while heteroxenous species remained plentiful, primarily at sites located away from those that showed sorts of anthropogenic impacts. This pattern was illustrated by a model that describes what is named "true"

species richness of the habitat based on the sample size of a particular parasite population (Dzikowski et al. 2003; Walther et al. 1995) in selected indicator species, and here is the *S. rivulatus*. This fish is abundant in several habitats along the coast and easily caught at nearly all sites. Our main objective by this study was to provide some evidence that, in an environment of susceptible impacts, heteroxenous parasites refrain to complete their life cycles due to the depletion of their intermediate hosts in natural environment compared to monoxenous parasites that can proliferate with single host (Paperna 1997; Dzikowski et al. 2003; Al-Hasawi 2019). This relationship is particularly relevant as far as heteroxenous species are concerned (Digeneans, Acanthocephalan and many species of nematodes) since they accumulate but cannot thrive on the host. Hence, the generated data and results of this study were analyzed by employing species diversity and richness indices specifically for parasitological models (Al-Hasawi 2019; Dzikowski et al. 2003; Soberon and Llorente 1993; Walther et al. 1995). Such analysis was helpful to demonstrate distinct values of heteroxenous (H) vs. monoxenous (M) parasites between the different study sites in the indicator fish species (Figure 7).
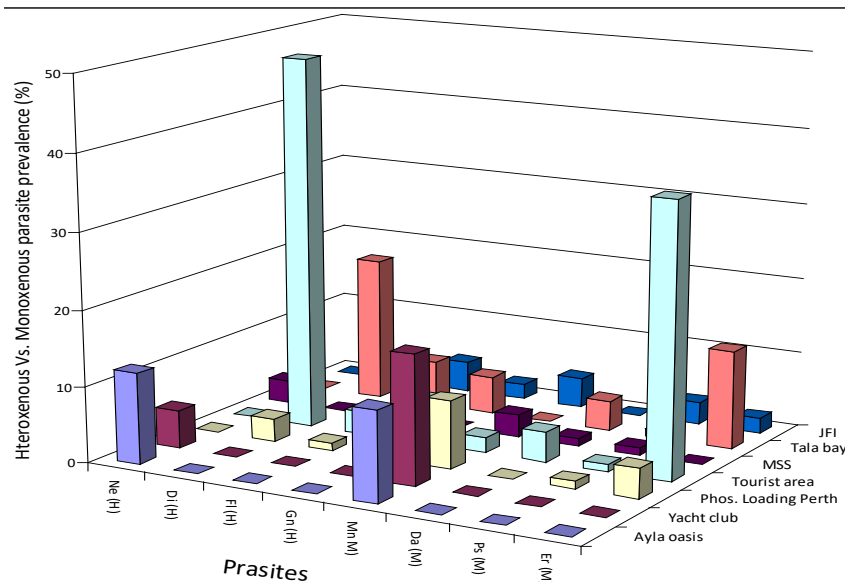
Figure 7. Cumulative number of encountered fish parasites in the different location and the prevalence (%) between heteroxenous vs. monoxenous. *Monogenean (Mo), Nematodes (Ne), Ergasillus sp. (Er), pseudodactylogyrus sp. (Ps), flukes (Fl), fish lice (Li), Gnathiids (Gn), dactylogyrus (Da), digenean sp.*

This study also used the cumulative species plot that extrapolates species abundance of a given habitat as a function of increasing sample size. The heteroxenous and monoxenous species were discretely considered for each site, and comparison of plots yielded comparable results when pooled samples were used. This method aided in approximating the abundance and diversity of parasite species within a particular habitat, allowing for the characterization of communities in potentially affected coastal marine ecosystems. However, findings suggest that there were variations in parasite abundance of the different sites along the coast. Despite the presence of various urban activities at these sites, the distribution of parasite communities did not show any clear pattern, except for what was observed at the Tourist camp site. A notable increase in visitor numbers was observed at this site, which might have anthropogenic implications, yet the ratio of heteroxenous to monoxenous parasites remains approximately 1:1.

Many case reports illustrate the negative effects of pollution on parasite communities, which are often reflected by a decline in species abundance and diversity, especially in those with multiple hosts during their life cycles (Lafferty and Kuris 2009; Dzikowski et al. 2003; MacKenzie et al. 1995). The current study was implemented to use such an approach as a practical tool for distinguishing between habitats subjected to differing degrees of adverse anthropogenic impact on Jordan's GoA coast.

As mentioned above, the higher ratio of heteroxenous vs. monoxenous parasites will explain greater stability in pristine habitats than in other sites that witness some forms of anthropogenic intrusions along the coast. Nevertheless, the results indicate that additional Red Sea and hence Gulf of Aqaba species are sensitive to several pathogens, and that an infection reservoir is now firmly established in the local feral fish communities. Consequently, any form of stress and/or pollution (e.g., ports and public beaches) may show increase prevalence of monoxenous parasites. Some host species were found to be particularly susceptible to

some parasite agents. For example, the lion fish (*Pterios miles*) could be a potential indicator for the quality of habitats. The fish was collected from three different sites (Hotels area and Al-Ghandor beach at the northern most portion of Jordan's Gulf of Aqaba and old power station located just to the south of the Phosphate port) in 2021. Indeed, this fish and also the damselfish *Dascyllus trimaculatus* often carried heavy loads of *Trichodina sp.* on their gills. These findings warrant some explanation. *Pterois miles* samples were sufficiently large to allow a fairly detailed population study, and over 63.7% of the individuals examined supported gill infections with *Trichodina sp.* Infact, *Trichodina* ciliates have been shown to be an excellent bioindicator for sewage eutrophication in freshwater habitats (Yeomans et al. 1997; Lacerda et al. 2018). Almost all lionfish individuals examined in this study were from the north beaches and PLB area, the two sites which might be liable to the impacts of eutrophication. *Trichodina sp.* infections were also found on the gills in some other coral reef fishes (i.e. *Chaetodon paucifasciatus, Dascyllus trimaculatus* and *Epinephelus fasciatus*). However, it has yet to be determined whether these infections were with the same species known from impacted sites. In any case, trichodinids are often considered as ecto-commensal and probably have limited significance as pathogens (Diamant et al. 2001).

As stated earlier, the composition of natural fish parasite communities reflects the stability and evolutionary stage reached by the ecosystem in which the fish live because heteroxenous parasites (with complex, multiple-host life cycles) can persist only in habitats that include all host species, both intermediate and definite hosts required for completion of the natural parasite life cycles (Shehata et al. 2018). In environmentally susceptible environments, communities will display a reduced biodiversity, and here we expect mainly monoxenous (single-host) parasites to persist. Here, we compared the ecological indices of the parasite assemblages at each of the three distinctive sites, and employed the relation Sh/Sm, which is the ratio of

heteroxenous vs. monoxenous parasites richness indices (Dzikowski et al. 2003; Walther et al. 1995).

A sufficient sample volume of the herbivore rabbit fish *S. rivulatus* was collected and employed because *S. rivulatus* was reported to support a rich parasite fauna of both heteroxenous and monoxenous species. Some of it is found to infect the gut helminthes (heteroxenous species) and gill monogeneans (monoxenous sp.) which are readily quantifiable. Table 3 shows a list of fish samples examined with some parasite species found in *S. rivulatus* that were utilized for the parasite richness and diversity analyses.

We employed 345 individual fish of *S. rivulatus* utilizing the approach of monoxenous-heteroxenous parasite analyses, some of which were collected during two interconnected seasons. The *S. rivulatus* parasite analysis was based on fish collected from three sites, namely Ayla Oasis, Yacht club and Marine Science Station (see Table 1).

Table 3. Number of rabbit fish (*S. rivulatus*) as indicator species, collected from two urban sites at north of GoA and in south (MSS) representing a marine conservatory.

Collection season	Ayla Oasis	Yacht club	MSS	Total
Summer-Fall	92	47	62	201
Winter-Spring	41	63	55	159
Total	133	95	117	345

In all fish of *S. rivulatus* samples, counts were conducted for parasitic metazoans (e.g. helminthes) belonging to heteroxenous (gut digeneans, nematodes and acanthocephalans) and monoxenous (gill monogeneans) as shown in Table 4.

Table 4. Major taxonomic groups of fish parasites reported in literature of both monoxenous (M) and heteroxenous (H) development at different target organs of the *S. rivulatus*.

Taxonomic group	Parasite Species	Development*	Target organ
Monogenea	*Pseudohaliotrematoides polymorphuseilaticus*	M	Gills
	Pseudohaliotrematoides polymorphussuezicus	M	Gills
	Pseudohaliotrematoides polymorphus indicus	M	Gills
	Pseudohaliotrematoides polymorphus "nagatyi"	M	Gills
	Pseudohaliotrema plectocirra	M	Gills
	Polylabris sigani	M	Gills
Digenean	*Hexangium sigani*	H	Gut
	Gyliauchen volubilis	H	Posterior gut
	Opisthogonoporoides hanumanthai	H	Gut
	Opisthogonoporoides spp.	H	Gut
Nematode	*Cucullanussigani*	H	Posterior gut
	Procamallanus elatensis	H	Anterior gut
Acanthocephalan	*Sclerocolum rubrimaris*	H	Anterior gut

*Diamant et. al. (1999)

Species richness and other diversity indices of *S. rivulatus* parasite assemblages during the present study period of host capture are shown in Table 5. Moreover, the parameters on species richness indices are presented in Figure 8.

Table 5. Diversity parameters employed on the *S. rivulatus* fish in this study.

	Ayla Oasis	Yacht club	MSS
N	92	47	62
Parasite species	13 *(7)*	15 *(8)*	17 *(5)*
Fish weight (g)	180.3±7.7[a]	87±7.9[c]	170.6±6.7[ab]
Fish length (cm)	22.7±0.3[a]	17.8±0.3[b]	20.5±0.3[b]
Condition factor (W/L^3)	14.8±0.4[b]	14.7±0.4[b]	17.1±0.3[a]
Diversity indices:			
S (heteroxenous)	6.3±1.25[b]	7.1±0.81[b]	12.1±3.09[a]
S (monoxenous)	7.3±2.21[b]	8.1±1.53[b]	5.1±1.51[b]
Sh/Sm	0.86	0.88	2.4

Numbers that bear different superscript letters are significantly different $P<0.05$ (one way ANOVA); numbers in brackets is for heteroxenous parasite species. S: species richness, $Y=a(1-e-bx)/b$ (Walter et al 1995).
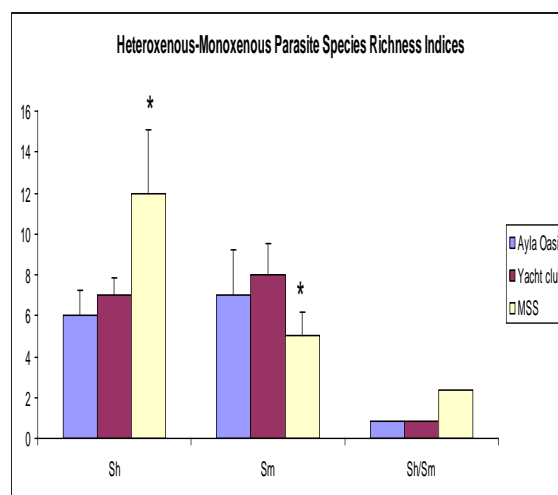
Figure 8. Species richness indices of the heteroxenous vs. monoxenous parasites as encountered in the indicator fish represented here by the *S. rivulatus*

Implementing the concept of Sh/Sm as a tool for evaluating the state of an ecosystem has been documented in several reports (D'Amelio and Gerasi 1997; Diamant et al. 1999, 2001). At some sites of increased urban activities along the coast, our results showed a noticeable increase in monoxenous species abundance associated with a decline in heteroxenous species, although still insignificant (Khan and Thulin 1991; Gelnar et al. 1997). In fact, the decline in heteroxenous species was found to be associated with habitats that witness some sorts of impacts along the coast. This was mainly noticed with the abundance of monogeneans being a monoxenous species. The impacts of pollution at the bottom sediment were reported also to develop monoxenous ciliate infections, mainly the trichodinids (Yeomans et al. 1997; Lacerda et al. 2018). The validation of such approaches as an indirect effect either physiological or immunosuppressive (Shehata et al. 2018) on the hosts under such conditions was a matter of

additional investigation, and the data are still under processing (Al-Zibdah et. al., unpublished data). Fish examined from Aqaba's urban areas (public beach and phosphate port, both environmentally perturbed sites) show an increased incidence of elevated levels of certain infections, suggesting that resident fish populations could have been affected by anthropogenic stress which might be linked to habitat degradation. Moreover, the *S. rivulatus*, and based on previous reports, is an ideal species for the application of biochemical and histo-chemical biomarker tests (Diamant 2001, 2010; Martens and Moens 1995). These parameters were also part of the current study, but results are still under evaluation. Our results demonstrate that *S. rivulatus* in addition to other territorial fishes caught at different sites were observed to carry parasite communities that differ in their composition (heteroxenous or monoxenous development), all of which could be used as a measure for the degree of habitat integrity and stability along the coastline of GoA..

Acknowledgements

References

Abelson A Steinman B Fine M and Kaganovsky M. 1999. Mass transport from pollution sources to remote coral reefs in Elat, Gulf of Aqaba, and Red Sea. *Mar Pollution Bull.,* **38**:25-29.

Al-Hasawi Z. 2019. Environmental Parasitology: intestinal helminthes parasites of the siganid fish *Siganus rivulatus* as bioindicators for trace metal pollution in the Red Sea. *Parasite,* **26**:12.

Al-Horani F. Al-Rousan S Al-Zibdah M and Khalaf M. 2006. The status of coral reefs on the Jordanian coast of the Gulf of Aqaba, Red Sea. *Zool Middle East*, **38**:99-110.

Al-Ma'ayta S. 2015. Fish stock assessment in Aqaba for the development of management plan of fishery. MSc. thesis, University of Jordan, Aqaba.

Al-Zibdah M Jawasrah R and Badran M. 2018. Socioeconomic and cultural ethics of fishermen community in Aqaba, Red Sea. Jor. J. of Social Science, 11(1):43-58

Al-Zibdah M. 2013. The Aqaba Marine Protected Area - integration of marine science and resource management in the Gulf of Aqaba - Red Sea. *Int. J. Marine Sci*., **3(44)**: 361-367.

Al-Zibdah M and Odat N. 2007. Fishery status, growth, reproduction biology and feeding habit of two Scombrid fish from the Gulf of Aqaba, Red Sea. *Lebanese Sci. J.*, **8(2)**: 3-20.

Al-Zibdah M Oqaily F Al-Najjar T and Manasrah R. 2008. Neighboring cage fish farming affecting water and seabed quality of the Jordanian northern Gulf of Aqaba, Red Sea. *Ocean Sci. J.*, **43(1)**: 9-16.

Ashmawy K Hiekal F Abo Akadda S and Laban M. 2018. The inter-relationship of water quality parameters and fish parasite occurrence. *Alex. J. Vet. Sci*., **59(1)**:97-108

Badran M and Foster P. 1998. Environmental quality of the Jordanian coastal waters of the Gulf of Aqaba, Red Sea. *Aquatic Ecosystem Health Management,* **1**:83-97.

Codex guidelines for sensory evaluation of fish and shellfish in laboratories. 1999. CAC GL #31-1999

D'Amelio S and Gerasi L. 1997. Evaluation of environmental deterioration by analyzing fish parasite biodiversity and community structure. In: Paperna I. (Ed):VII European Multicolloquium of Parasitology, Parma. *Fish parasites as indicators of environmental quality. Parassitologia* **39**:237–242.

Diamant A Goren M Yokes, M Galil B Klopman Y Huchon D Szitenberg A and Karhan S. 2010. *Dasyatispora levantinae gen*. et sp. nov., a new microsporidian parasite from the common stingray Dasyatis pastinaca in the eastern Mediterranean. *Dis Aqua., Org* **91**: 137–150.

Diamant A Banet A Ucko M Colorni A Knibb W Kvitt H. 2001. Mycobacteriosis in wild rabbit fish *Siganus rivulatus* associated with cage farming in the Gulf of Eilat, Red Sea. *Dis. Aquat. Organ.,* **39**:211-219.

Diamant A Banet A Paperna I Westernhagen H Broeg K Kruener G Koertin W and Zander S. 1999. The use of fish metabolic, pathological and parasitological indices in pollution monitoring. II. The Red Sea and Mediterranean. *Helgol Mar Res.,* **53**:195–208.

Dzikowski R Paperna I and Diamant A. 2003. Use of fish parasite species richness indices in analyzing anthropogenically impacted coastal marine ecosystems. *Helgol. Mar. Res.* **57**:220–227

Eddy FG T and Danguy A. 2009. Atlas of Fish Histology. Universite Libre de Bmxelles (U.L.B), Brussels, Belgium

Gelnar M Sebelova S Dusek L Koubkova B Jurajda P and Zahradkova S. 1997. Biodiversity of parasites in freshwater environment in relation to pollution. In: I. Paperna (Ed). *Fish parasites as indicators of environmental quality*. VII European Multicolloquium of Parasitology, Parma. *Parassitologia* **39**:189–199.

Gibson DI. 1996. *Trematoda*. In: L. Margolis and Z. Kabata (eds). Guide to the parasites of fishes of Canada. Part 1V. Can. Spec. Publ. Fish Aquat. Sci. **124**. 373 p.

Golani D and Diamant A. 1999. Fish colonization of an artificial reef in the Gulf of Eilat, northern Red Sea. *Environ Biol Fish,* **54**:275-282.

Harvell CD Kim K Burkholder JM Colwell RR Epstein PR Grimes DJ Hofmann EE Lipp EK Osterhaus AD Overstreet RM Porter JW Smith GW and Vasta GR. 1999. Emerging marine diseases - climate links and anthropogenic factors. *Science,* **285**(5433): 1505-1510.

Hoai TD 2020. Reproductive strategies of parasitic flatworms (*Platyhelminthes, Monogenea*): the impact on parasite management in aquaculture. *Aquac Int.,* **28(1)**: 421- 447

Jerônimo GT da Cruz MG de Aguiar Bertaglia E Furtado WE and Martins ML. 2022. Fish parasites can reflect environmental quality in fish farms. *Rev Aqua.,* **14**:1558–1571. doi:10.1111/raq.12662

Kabata Z. 1988. *Copepoda and Branchiura*, p. 3-127. In: L. Margolis and Z. Kabata (Eds) Guide to the parasites of fishes of Canada. Part II — Crustacea. Can. Spec. Publ. Fish. Aquat. Sci. **101**: 184 p.

Khalaf M. 2004. Fish fauna of the Jordanian coast, Gulf of Aqaba, Red Sea. *J. KAU. Mar. Sci* . **15:**23-50.

Khalaf M and Kochzius M. 2002. Community structure and biogeography of shore fishes in the Gulf of Aqaba, Red Sea. *Helgol Wissenschaftliche Meeresunters,* **55**:252-284.

Khan RA and Thulin J. 1991. Influence of pollution on parasites of aquatic animals. *AdvancesParasitology*, **30:** 201-238.

Lacerda ACF Roumbedakis K Bereta JGS Nuñer APO Petrucio MM and Martins ML. 2018. Fish parasites as indicators of organic pollution in southern Brazil. *J Helminthol.,* **92(3)**:322- 331. doi:10.1017/S0022 149X1 7000414

Lafferty KD and Kuris AM. 1999. How environmental stress affects the impacts of parasites. *Limnol Oceanogr.*, **44(3)**: 925–931.

Lafferty KD and Kuris AM. 2009. Parasites reduce food web robustness because they are sensitive to secondary extinction as illustrated by an invasive estuarine snail. *Phil Trans R Soc Lond B Biol Sci.*, **364:** 1659–1663.

MacKenzie K Williams HH Williams B McVicar AH and Siddall S. 1995. Parasites as indicators of water-quality and the potential use of helminth transmission in marine pollution studies. *Adv Parasitol.,* **35**:85–144.

Martens E and Moens J. 1995. The metazoan ecto- and endoparasites of the rabbit fish, *Siganus sutor* (Cuvier and Valenciennes, 1835) of the Kenyan coast. *Afr J Ecol.,* **33**:405–416.

McVicar AH 1997. The development of marine environmental monitoring using fish diseases. In: I. Paperna *(Ed). Fish parasites as indicators of environmental quality.* VII European Multicolloquium of Parasitology, Parma. *Parassitologia* **39**:177-181.

Ojwala RA Otachi EO and Kitaka NK. 2018. Effect of water quality on the parasite assemblages infecting Nile tilapia in selected fish farms in Nakuru County,Kenya. *Parasitol Res.,* **117(11)**:3459- 3471.

Overstreet RM. 1997. Parasitological data as monitors of environmental health. In: I. Paperna (Ed). *Fish parasites as indicators of environmental quality*. VII European Multicolloquium of Parasitology, Parma. *Parassitologia,* **39**:169–176.

Paperna I. 1997. Fish parasites as indicators of environmental quality.VII European Multicolloquium of Parasitology, Parma. Università di Roma, La Sapienza, 255 p.

Rafi F. 1988. *Isopoda*, p. 129-148. In: L. Margolis and Z. Kabata (Eds) Guide to the parasites of fishes of Canada. Part II — Crustacea. Can. Spec. Publ. Fish. Aquat. Sci. **101**: 184 p.

Rasheed M Al-Trabeen K and Badran M. 2012. Long-term water quality monitoring at an industrial site on the northern Gulf of Aqaba, Red Sea. *Mediterranean Marine Sci.*, **13**:250–258.

Schuhmacher H Krol DK and Reinicke GB. 1995. Long-term fluctuation of coral communities at Aqaba and on Sanguine Atoll (northern and central Red Sea) over more than a decade. *Beitr Palaeontol.,* **20**:89–97.

Shehata SM Mohammed RA Ghanem MH Abdelhadi YM and Radwan MK. 2018. Impact of the stresses environmental condition on the prevalence of parasite in freshwater aquaculture. *J Fish Sci.,* **12(2)**:1–8.

Silverman J Lazar B and Erez J. 2004. Monitoring the health of a coral reef using community metabolism. In: E. Rosenberg and Y. Loya (Eds). *Coral health and disease,* 367–376. Springer, New York

Soberon MJ and Llorente BJ. 1993. The use of species accumulation functions for the prediction of species richness. *Cons Biol.*, **7:**480–487.

Wahsha M Juhmani AS Buosi A and Sfriso A. 2017. Assess the environmental health status of macrophyte ecosystems using an oxidative stress biomarker. Case studies: The Gulf of Aqaba and the lagoon of Venice. *Energy Procedia.,* **125**: 19-26.

Walther BA Cotgreave P Price RD Gregory RD and Clayton DH. 1995. Sampling effort and parasite species richness. *Parasitol Today*, **11**:306–310.

Yeomans WE Chubb JC and Sweeting RA. 1997. Use of protozoan communities for pollution monitoring. In: I Paperna (Ed). *Fish parasites as indicators of environmental quality*.VII European Multicolloquium of Parasitology, Parma. *Parassitologia*, **39**:201–212.

Exploring the potential of *Ulva lactuca* from the Gulf of Aqaba for Micro-scale Biodiesel Production: Designing a Small-scale Photo-bioreactor

Walid Al-Zyoud[1,*], Salma Hamzeh[1], Dana Masri[1], Munib Saket[1], Jeanine Abdel Qader[1], Raghda Al-Qaraghuli[1] and Mohammad Wahsha[2]

[1] *School of Applied Medical Sciences, German Jordanian University, Amman 11180, Jordan;* [2] *Marine Science Station, The University of Jordan, Aqaba branch, Jordan*

Abstract

Algae are photosynthetic organisms which can be cultivated and produced in photo-bioreactors; therefore, choosing the design parameters and conditions are critical in order to achieve high efficiency and maximum productivity. Algae are of interest to biochemical industries because of their diverse species. This project seeks to build a photo-bioreactor tank to maximize *Ulva lactuca* non-seasonal survival to produce biodiesel from its biomass. The chosen design was because of the ease of monitoring, and the tank design effectively kept *Ulva lactuca* alive and fresh. Biodiesel was accomplished using an alkaline esterification for 50 g of dry mass of *Ulva lactuca* giving a relatively limited yield of approximate 13% of *Ulva lactuca* oil (4 ml) that was converted to (0.5 ml) biodiesel, compared with other oils such as soybean (42%), corn oil (60%) and cooked corn oil (40%). The yield of *Ulva lactuca* oil was statistically significantly lower than the other three types of oil (*p-value* = 0.0032). However, this project still aids in the economics of Jordan, as *Ulva lactuca* is grown locally in the Gulf of Aqaba. *Ulva lactuca* investment is worth considering because of its natural exposure, high yield, low cost, reduced algae contamination risk, and space requirements.

Keywords: Aqaba; Biodiesel; Bioreactor; Energy Sustainability; *Ulva lactuca*.

1. Introduction

A Photo-Bioreactor (PBR) is commonly used to culture phototrophic organisms (Richmond, 2004). Photo-Bioreactors are used to cultivate microalgae because of many characteristics such as sterility, efficiency, and convenience. These characteristics vary based on the type of photo-bioreactor if it laboratory or industrial scale reactors (Spier et al., 2011). The body of a PBR is described as a closed tank, which is subjected to automatic or manually controlled conditions (Singh & Sharma, 2012). Photo-bioreactors come in different sizes and shapes and can operate in batch, fed-batch, or continuous modes to convert raw material into products. Using PBRs for the cultivation of algae means fewer contaminants entering the system because of the closed system structure. Maintaining the levels of CO_2 and H_2O during the operation with minimum losses is also easier. Controlling the system is more accurate by using the features related to the PBR such as pH, light, and temperature meters (Spier et al., 2011). High productivity is important, but low operation and maintenance costs are crucial when choosing a photo-bioreactor. Therefore, choosing the design of the PBR depends on the species, location, costs, the final product, and profit. PBRs come in numerous designs, such as a stirred tank, a bubble column, an airlift, a membrane, a tube, a flat plate, a helix, and a pyramid. These designs reach a high surface-to-volume ratio, which improves the photosynthetic efficiency (Carvalho et al., 2006). Many limitations and problems are faced when processing in a photo-bioreactor; therefore, a study in 2013 included simple solutions for commonly occurring problems, such as biofouling which can be avoided by providing perfect mixing, and ensuring a light–dark cycle, while loss of algae density is prevented when the algae is continuously filtered and harvested (Borowitzka, 2013). All parameters should be controlled to prevent complications from happening during the operation; therefore, sensors for CO_2, pH, and temperature should be installed and monitored regularly. In addition, O_2 build up can be avoided if high mass-transfer capacity is provided. This work focuses on making biofuel from a type of green seaweed called *Ulva lactuca* (Guiry & Guiry, 2013). *Ulva lactuca* reproduces asexually through accidental fragmentation, where fragments become mature clones. This type of reproduction explains the rapid growth rate of the species. *Ulva lactuca* is ideal for biodiesel because of its rapid growth and high lipid content. The attraction to biodiesel is because of the high availability of the different biomasses needed to produce it, the non-toxicity of the fuel emissions as well as the biodegradability of the fuel. It has also been reported that the consumption of biodiesel resulted in a 78% reduction of CO_2 emission compared to

conventional diesel fuel, thus further increasing the fuel's demand (El Maghraby & Fakhry, 2015). Biodiesel is made from a mixture of different sources like vegetable oils, animal fats, and other living things such as algae and bacteria. The most commonly used oils to produce biodiesel are soybean, sunflower, palm and rapeseed. Waste vegetable oils and non-edible vegetable oils are cheaper than edible, fresh vegetable oil. This is because of the differences in their natural properties. In regards to animal fats, they are highly viscous and solid (Singh & Singh, 2010). Vegetable oils can be used as diesel fuels in traditional diesel engines, but depending on the kind and grade of oil, some drawbacks may arise. Vegetable oil in diesel engines has unique qualities in atomization and combustion compared to regular diesel. Poorly combined oil and air leads to incomplete combustion, causing smoke and lower volatility (Barnwal & Sharma, 2005). Biodiesel can be produced through the transesterification of a variety of oils. In transesterification, an ester is transformed into a different one by exchanging the alkoxy group. Transesterification is an equilibrium process; therefore, mixing the two components will cause a reaction. However, in order to accelerate the process, acid or base catalysts are usually utilized (Otera, 1993).

2. Methods

2.1. The design of bubble-tank photo-bioreactor

The *Ulva lactuca* species was kept alive in artificial seawater using a bubble-tank photo-bioreactor. The photo-bioreactor was built locally with the assistance of Ja'afar Aquatics, a company based in Amman, Jordan (Figure 1). The photo-bioreactor tank was built using Plexiglas® with specifications as shown in Table 1. The water, along with the added sea salt, was changed weekly because the bioreactor was treated as a fish aquarium which needs a water change every week. Ja'afar Aquatics experts recommended the weekly water change and adding a CO_2 pump to maintain the level of CO_2 for algae survival, which was one bubble per second. Sea salt was used to maintain alkalinity and the water's salinity. Another important parameter that was considered was the light intensity; a light-dark cycle was provided by using a light-emitting diode (LED) lamp operating at 8 hours of light and 16 hours of darkness to mimic nature.
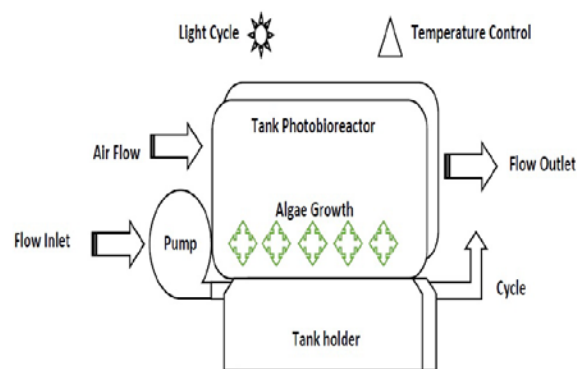
Figure 1. The designed tank photo-bioreactor.

Table 1. Dimensions of the designed photo-bioreactor tank.

Dimensions	
Length(cm)	60
Width(cm)	60
Height(cm)	55
Volume (L)	198
Water Level (cm³)	24
Water Volume(L)	86.4

2.2. Providing the algae species

Fresh and pure *Ulva lactuca* were verified and handpicked by the scientists of the Marine Science Station (MMS) from the beach near the Station in Aqaba, Jordan (GPS: 29.458344881113, 34.97665168083726) (Figure 2). The fresh algae (Figure 3) with seawater were transferred by car to Amman using water gallons and portable aeration pumps. The algae were later transferred into the photo-bioreactor tank along with the seawater (Figure 4).
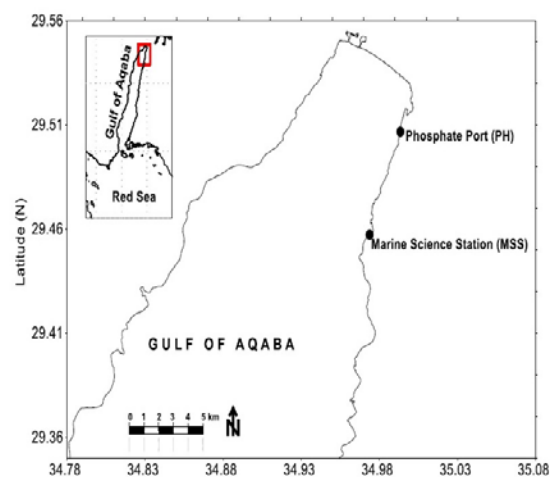
Figure 2. The map location of *Ulva lactuca* collection site on the beach of Aqaba (MSS).

Figure 3. *Ulva Lactuca* found near the beach of Aqaba.

Figure 4. The designed photo-bioreactor

2.3. Optimal conditions for Ulva lactuca

For optimal growth and survival of algae, the pH level should be between 6.5 and 7.5, and the temperature should be between 23°C and 27°C (Kusumaraga et al., 2021). A certain amount of CO_2 is needed for the algae to grow, and the recommended amount is between 500 and 1400 µatm (Bockmon et al., 2013). The photo-bioreactor was set to these parameters: pH 7.5, 1500 watts of light, 500 µatm of CO_2, temperature of 24.5 °C, and salinity around 30 ppt to get the best conditions. Algae were incubated for 7 weeks. Two sensors for CO_2 and pH were inserted in the water to make sure that the values of CO_2 and pH are properly controlled.

2.4. Oil extraction for biodiesel production

Oil extraction from the *Ulva lactuca* is necessary since the fundamental ingredient for the production of biodiesel is the oil. The oil extraction process was conducted through the use of a Soxhlet extractor (Luque de Castro & Priego-Capote, 2010). 50 g of the algae collected from the aquarium was placed into the thimble and fitted into the Soxhlet extractor. 200 ml of the solvent extractor *n*-hexane was added into the round bottom flask and placed onto the heating mantle (Suganya et al., 2013). Tubes were connected to the inlet and outlet of the condenser. The heat was adjusted so that the boiling point of the hexane is reached since leaching occurs at the boiling point of the solvent, which is 69°C. The oil could leach continuously from the algae for several days until complete extraction was achieved. Extraction was executed inside a fume hood to allow for proper ventilation and to prevent harmful fumes from escaping to the surroundings. Prior to the transesterification of the oil, oil purification was required to remove any impurities.

2.5. Purification using a rotary evaporator

The rotary evaporator, also known as the rotarvap, was used to separate the hexane from the extracted oil (Suganya & Renganathan, 2012). To separate the *n*-hexane from the extracted oil, the following steps were conducted: First, water was added to the water bath, whose temperature was set to 40°C. Then the vacuum pump was turned on with the pressure reaching around 370 mbar. Finally, the flask was lowered into the water bath with a rotation of 45 rpm. The hexane could evaporate for around 20 min to ensure full separation. The oil was collected, measured, and processed after removing it from the rotating flask. To purify the oil, a syringe filter with a 0.2 µm disc filter was used after removing the hexane solvent with rotarvap.

2.6. Transesterification of oils

Following the extraction and purification of the oil, the transesterification reaction was performed. A solution of potassium methoxide with KOH and methanol was prepared before commencing the procedure. The potassium methoxide solution was prepared through the following steps: 4 g of KOH was added to 50 ml of methanol and stirred a stir plate; 4 ml of extracted algae oil was placed into a 100 ml glass beaker and onto the hot plate, and a thermometer was used to ensure that the oil temperature remained around 55°C. 1.25 ml of the potassium methoxide solution was added to the heated algae oil. An additional three types of ready oils (soya bean oil, cooked corn oil, and corn oil) were transesterificated for comparison. The beaker covered with aluminum foil was placed onto the stir plate for 30 min. The mixture was removed from the stir plate and placed into a burette because of its very small volume and left for 24 hr to allow the layers to settle. The lower glycerol layer was slowly removed from the biodiesel top layer, and the biodiesel was collected and measured. The transesterification reaction is shown in Equation (1) (Mata et al., 2010):

Triglycerides + Methanol → Biodiesel + Glycerol   *Equation 1*
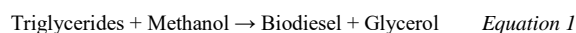
3. Results

3.1. Photo-bioreactor tank

The first aim of this project was achieved, as shown in Figure 1 and Table 1, from the first stage of building a photo-bioreactor, applying some modifications on the system to meet the requirements needed, until the last step of producing biodiesel. The photo bioreactor was constructed for simulating artificial seawater that was needed for the survival of algae. Many modifications were made to the system for an appropriate algae environment. Cultivating the algae was insignificant in terms of the growth of the biomass. However, the non-seasonal survival was achieved, and oil extraction could still be performed. From 2500 g inoculum, the algae retrieved for oil extraction was around 50 g in wet mass and included sludge and excess material from the tank that was too difficult to remove from the algae to avoid further damaging the organisms.

3.2. Oil extraction for biodiesel production

As previously mentioned, the oil extraction was conducted using the Soxhlet extractor. The oil was separated from hexane using the rotarvap after extraction. Considering the discolored and somewhat stable size of the algae used, even a tiny volume of extracted oil was considered a success (Table 2) since it was predicted beforehand that the algae would yield no oil. In addition, from the difference in volume of the hexane before and after extraction, about 50 ml of hexane is lost in each extraction cycle.

Table 2. Extraction and separation results

Material	Volume
Inoculum	2500 g
Wet mass utilized for oil extraction	50 g
Extracted Algal Oil	4 ml
Recycled hexane	150 ml
Algal biodiesel yield	13%

3.3. Transesterification of oils

Table 3 shows the results of the transesterification of the different oils used. From the results, it can be deduced that the larger the volume of oil used in the transesterification reaction, the better the biodiesel yield. Larger volumes were used because they were easier to manage during the experiment and the procedure was not suitable for small-scale production. Using a general formula in the Equation 2, the % *yield* can be calculated, where *Vf* is the final biodiesel volume and *Vi* is the initial oil volume. The statistical analysis was calculated by using *t*-distribution table.

% Yield = (Vf/Vi)* 100%   Equation 2

Table 3. Oil transesterification results

Oil Type	Oil Volume	Biodiesel Volume	Yield	*p-value*
Soya Bean oil	10 ml	4.2 ml	42%	
Cooked corn oil	5 ml	2 ml	40%	0.0032
Corn oil	5 ml	3 ml	60%	
Ulva lactuca algae oil	4 ml	0.5 ml	~13%*	

* *Ulva lactuca* algae oil was with the lowest yield compared with other oils.

4. Discussion

This study investigated the potential of *Ulva lactuca*, a readily available algae species in Jordan, as a sustainable feedstock for biodiesel production. We aimed to establish a non-seasonal survival system within a designed bubble-tank photo-bioreactor, while simultaneously highlighting the economic probability of biodiesel production, even with potentially low oil yields. Despite the careful design of the photo-bioreactor to mimic *Ulva lactuca's* natural habitat, successful cultivation proved challenging. This highlights the crucial role of in-depth understanding and consideration of the native environment for effective cultivation of any biomass resource. Despite the relatively low oil yield, *Ulva lactuca*-derived biodiesel could be a cost-effective fuel source compared to corn oil-based biodiesel because of that fact that corn production includes expensive activities linked with its agriculture. This paves the way for further optimization and scaling up of the process for large-scale biodiesel production in Jordan. Our findings align with prior research regarding *Ulva lactuca's* suitability for biodiesel production in Egypt (Abomohra et al., 2018). However, deeper investigation of the fatty acid methyl ester (FAME) profile and optimization of growth conditions are crucial for yield improvement. This study shows the potential of *Ulva lactuca* as a sustainable biodiesel source in Jordan. Future research should address challenges related to yield optimization, biomass availability, and energy balance, while exploring avenues for by-product valorization. These efforts will be key to maximizing the economic and environmental benefits of this renewable fuel resource. This might be the first of its kind study in Jordan; however, a larger scale study, similar to the one by (Bruhn et al., 2011) at Seden Beach (Odense Fjord) in Denmark is needed to determine the realistic economic feasibly of biodiesel production in Jordan and even in the countries that have beaches on the Red Sea such as Yemen, Egypt and Saudi Arabia. The above-mentioned study of Denmark suggested the adoption of bio-refinery concept and revealed that *Ulva lactuca* has a relatively high biomass production potential of 45 T (TS) ha^{-1} y^{-1} where (TS) is the total solid; however, the study does not address the scalability and feasibility of large-scale cultivation and harvesting of *Ulva lactuca* for bio-energy production.

5. Conclusion

This study well designed and implemented a non-seasonal bubble-tank photo-bioreactor, demonstrating its potential as a closed-system approach. This system offers the advantage of maintaining algal viability during storage, facilitating further research and potential commercialization. However, further optimization is crucial for large-scale biodiesel production. The study identified two key limitations; Low oil yield: *Ulva lactuca* exhibited a relatively low oil yield in this study. Future research should focus on optimizing cultivation parameters and exploring alternative extraction methods to enhance oil production. Small sample size: The limited sample size employed in this study restricts the generalizability of our findings. Future studies should utilize larger sample sizes to validate the observed trends and refine the economic feasibility analysis. Despite these limitations, this research provides a valuable foundation for future studies investigating *Ulva lactuca* as a sustainable biodiesel feedstock in Jordan. Further research addressing yield optimization, biomass scalability, and economic viability assessment will be crucial for maximizing the potential of this renewable fuel source.

References

Abomohra AE, El-Naggar AH, Baeshen AA. 2018. Potential of macroalgae for biodiesel production: Screening and evaluation studies. *J Biosci Bioeng.*, **125(2)**: 231-237. https://doi.org/10.1016/J.JBIOSC.2017.08.020

Barnwal BK, Sharma MP. 2005. Prospects of biodiesel production from vegetable oils in India. *Renew Sustain Energy Rev*., **9(4)**: 363-378. https://doi.org/10.1016/J.RSER.2004.05.007

Bockmon EE, Frieder CA, Navarro MO, White-Kershek LA, Dickson AG. 2013. Technical Note: Controlled experimental aquarium system for multi-stressor investigation of carbonate chemistry, oxygen saturation, and temperature. *Biogeosciences*., **10(9)**: 5967-5975. https://doi.org/10.5194/BG-10-5967-2013

Borowitzka MA. 2013. **Algae for Biofuels and Energy** Developments in Applied Phycology **5**. https://doi.org/10.1007/978-94-007-5479-9

Bruhn A, Dahl J, Nielsen HB, Nikolaisen L, Rasmussen MB, Markager S, Olesen B, Arias C, Jensen PD. 2011. Bioenergy potential of *Ulva lactuca*: Biomass yield, methane production and combustion. *Bioresour Technol.*, **102(3)**: 2595-2604. https://doi.org/10.1016/J.BIORTECH.2010.10.010

Carvalho AP, Meireles LA, Malcata FX. 2006. Microalgal reactors: A review of enclosed system designs and performances. *Biotechnol Prog*., **22(6)**: 1490-1506. https://doi.org/10.1021/bp060065r

El Maghraby DM, Fakhry EM. 2015. Lipid content and fatty acid composition of Mediterranean macro-algae as dynamic factors for biodiesel production. *Oceanologia*., **57(1)**: 86-92. https://doi.org/10.1016/J.OCEANO.2014.08.001

Kusumaraga BS, Syahrorini S, Hadidjaja D, Anshory I. 2021. Aquarium water quality monitoring based on Internet of Things. *Procedia Eng Life Sci*., **1(2)**. https://doi.org/10.21070/PELS.V1I2.966

Luque de Castro MD, Priego-Capote F. 2010. Soxhlet extraction: Past and present panacea. *J Chromatogr A*., **1217(16)**: 2383-2389. https://doi.org/10.1016/J.CHROMA.2009.11.027

Guiry MD, Guiry GM. 2013. AlgaeBase. World-Wide Electronic Publication. National University of Ireland, Galway. Retrieved July 1, 2023, from https://www.scirp.org/(S(351jmbntvnsjt1aadkposzje))/reference/ReferencesPapers.aspx?ReferenceID=1047746

Mata TM, Martins AA, Caetano NS. 2010. Microalgae for biodiesel production and other applications: A review. *Renew Sustain Energy Rev*., **14(1)**: 217-232. https://doi.org/10.1016/J.RSER.2009.07.020

Otera J. 1993. Transesterification. *Chem Rev*., **93(4)**: 1449-1470. https://doi.org/10.1021/CR00020A004/ASSET/CR00020A004.FP.PNG_V03

Richmond A. 2004. **Handbook of microalgal culture: biotechnology and applied phycology**/edited by Amos Richmond. *Orton.Catie.Ac.Cr.*, 472. https://doi.org/10.1002/9780470995280

Singh RN, Sharma S. 2012. Development of suitable photobioreactor for algae production - A review. *Renew Sustain Energy Rev*., **16(4)**: 2347-2353. https://doi.org/10.1016/j.rser.2012.01.026

Singh SP, Singh D. 2010. Biodiesel production through the use of different sources and characterization of oils and their esters as the substitute of diesel: A review. *Renew Sustain Energy Rev*., **14(1)**: 200-216. https://doi.org/10.1016/J.RSER.2009.07.017

Spier MR, Vandenberghe LPDS, Medeiros ABP, Soccol CR. 2011. Application of different types of bioreactors in bioprocesses. **Bioreactors: Design, Properties and Applications,** pp. 55-90.

Suganya T, Nagendra Gandhi N, Renganathan S. 2013. Production of algal biodiesel from marine macroalgae *Enteromorpha compressa* by two step process: optimization and kinetic study. *Bioresour Technol*., **128**: 392-400. https://doi.org/10.1016/J.BIORTECH.2012.10.068

Suganya T, Renganathan S. 2012. Optimization and kinetic studies on algal oil extraction from marine macroalgae *Ulva lactuca*. *Bioresour Technol*., **107**: 319-326. https://doi.org/10.1016/J.BIORTECH.2011.12.045

An Insight on Potential Role of Glucomannan, Mannan, and Flavonoids in Porang Tubers (*Amorphophallus muelleri* Blume) as Anti-Diabetic Through the Alpha-amylase Inhibition

Dwi Gusmalawati[1,*], Rodiyati Azrianingsih[2,3], Muhamad Agus Wibowo[4], Yuli Arif Tribudi[5], Diah Wulandari Rousdy[1], Didik Wahyudi[6], Ayu Tri Agustin[7], Nashi Widodo[2,3]

[1]Department of Biology, Faculty of Mathematics and Natural Sciences, Tanjungpura University, Indonesia; [2]Department of Biology, Faculty of Mathematics and Natural Sciences, Brawijaya University, Indonesia; [3]Porang Research Center (PRC) Brawijaya University, Indonesia; [4]Department of Chemistry, Faculty of Mathematics and Natural Sciences, Tanjungpura University, Indonesia; [5]Department of Animal Science, Faculty of Agriculture, Tanjungpura University, Indonesia; [6]Biology Department Universitas Islam Negeri Maulana Malik Ibrahim Malang, Indonesia; [7]Medical Laboratory Technology Study Program, dr. Soebandi University, Indonesia

Abstract

Exploring the natural product as a potential alpha-amylase inhibitor with no adverse side effects is still being concerned in developing diabetes mellitus drugs. This study aims to identify the phytochemical components of porang tuber extract. We also investigated bioactivity and predicted the biological function of the porang tubers bioactive in inhibiting human pancreatic alpha-amylase. The phytochemical components were analyzed by Liquid Chromatography Mass Spectrophotometry (LCMS). We investigated the biological activity of compounds as anti-diabetic agents by the PASS server. The 3D structure of the active compound that was showing anti-diabetic activity was prepared using PyRx software. Docking simulations were analyzed using Hex 8.0 software, while for visualization Discovery Studio Client 4.1 software was used. Our study found the presence of 67 phytochemical constituents in porang tuber extract. The five largest compounds with anti-diabetic activity are glucomannan, mannan, and flavonoids (quercetin, orientin, and hyperoside). PASS analysis showed that glucomannan and mannan had the most potential as anti-diabetic. It was determined by the Pa value of 0.77. The active sites of alpha-amylase (ASP197, GLU233, and ASP300 residues) were bound by glucomannan, mannan, orientin, and hyperoside, which plays an essential role in catalytic activity. Glucomannan showed the strongest interaction with the pancreatic alpha-amylase domain (lowest binding energy -394.1 kcal/mol). This result indicates that porang tubers are very potential as an alpha-amylase inhibitor. Further research is needed to validate this finding.

Keywords: anti-diabetic, alpha-amylase inhibitor, functional food, natural remedies.

1. Introduction

Currently, natural bioactive compounds from plants are studied since their therapeutic properties can be commercialized (Aldayel *et al*., 2020). Porang (*Amorphophallus muelleri* Blume) is an herbaceous plant-producing tuber with nutraceuticals that promise to treat health problems, such as hyperglycemia and hyperlipidemia (Chen *et al*., 2019; Harijati *et al*., 2012). Porang tubers are rich in macronutrients, including carbohydrates (80.16%), starch (54.23%), fiber (4.96%), protein (5.77%), fat (4.96%), and glucomannan (Wulan *et al*., 2019).

Glucomannan is the main carbohydrate component in porang tuber with 99,436.85 µg/g concentration shown by LCMS analysis (Gusmalawati *et al*., 2019). Besides glucomannan, other carbohydrate compounds such as mannan, trehalose, mannose, galactose, glucose, rhamnose, arabinose, and xylose were detected in

postharvest porang tubers (Gusmalawati *et al*., 2021). In addition, several secondary metabolite including flavonoids, alkaloids, saponins, coumarins, tannins, steroids, and quinones were also detected in porang tuber. Traditionally, *Amorphophallus* species tubers were beneficial to treat hemorrhoids, stomach pain, tumors, asthma, and rheumatism. Furthermore, the extract of *Amorphophallus* sp. tuber was also reported to have anti-diabetic, antioxidant, anti-cholesterol, and anti-bacterial properties (Firdouse and Alam, 2011; Shete *et al*., 2015; Van *et al*., 2020).

Foods rich in phytochemicals such as polysaccharides and polyphenols are suitable for medicinal and dietary supplements. Several plant polysaccharides have been confirmed to have secure anti-diabetic activity through various mechanisms. One potential mechanism is by inhibiting alpha-amylase activity (Chen *et al*., 2019). Diabetes mellitus is a chronic metabolic disease with high blood glucose levels due to insufficient insulin secretion or insulin tolerance, or a combination of both. Hyperglycemia

---

conditions can trigger health complications such as cardiovascular disease, ischemic heart disease, and other diabetes complications (Quek *et al*., 2020).

One of the therapeutic approaches to overcome metabolic disorders is drugs that inhibit the digestion and absorption of carbohydrates. Pancreatic alpha-amylase is the main enzyme that plays a role in breaking down starch into simple sugars (glucose, maltose, maltotriose, and dextrin) through hydrolytic activity. High intake of simple carbohydrates in the human body can lead to weight gain and escalated postprandial glycemia. Reduction of postprandial hyperglycemia can be achieved by inhibition of alpha-amylase (Quek *et al*., 2020; Xie *et al*., 2020). Acarbose is a synthetic drug to treat diabetes mellitus, which inhibits the enzyme alpha-amylase. However, the use of acarbose causes some side effects, such as gastrointestinal disorders (Alqahtani *et al*., 2019). Therefore, alpha-amylase inhibitors that did not generate adverse side effects from natural sources are needed.

This study aims to determine the phytochemical content of porang tubers by LCMS analysis. An in-silico study of biological function was carried out to predict the potential role of porang tuber bioactive compounds as inhibitors of human pancreatic alpha-amylase.

2. Materials And Methods

2.1. Extraction of Porang Tubers

The specimens used in this study were fresh porang tubers for the third growing period obtained from East Java. The mashed porang tubers were extracted using 95% methanol as solvent by the maceration. Briefly, maceration was carried out for 24 hours at room temperature. The homogenate was filtered with the Erlenmeyer vacuum. A rotary evaporator at a temperature of 40°C was used for generating concentrated filtrate. The concentrated extract was centrifuged for 20 minutes at 5000 rpm. The supernatant obtained was then stored at 4°C for further analysis (Gusmalawati *et al*., 2019; Babu & Radhamany, 2021).

2.2. LCMS Analysis of Methanol Extract of Porang Tubers

A Shim Pack FC-ODS column (2 mm x 150 mm, 3 m) with a column temperature of 35°C was used for liquid chromatography separation (Zhao *et al*., 2015). The eluent used was 95% methanol with 0.8 mL/minute flow rate and a maximum pump pressure of 15 kgf/cm^2. The wavelengths used are 254 nm and 190 nm with polarity (+) and AUX range (2AU/V). Furthermore, liquid chromatography runs for 80 minutes followed by mass spectrophotometry analysis with the following parameters: probe temperature= 250°C, CDL temperature= 250°C, nebulizer gas flow= 1.5 mL/minute, and block temperature= 400°C. The experiment was set up as follows: acquisition mode= scan +, interval= 0.5 sec, detector gain= 1.5 kV, start m/z= 50, stop m/z= 500, scan speed= 1000, probe voltage= +4 .5 kV, and CDL voltage= 25 V. Chromatograms were displayed using the LCMS PostRun program.

2.3. Ligand and Receptor Preparation

The 3D chemical structures of glucomannan (CID: 24892726), mannan (CID: 25147451), quercetin (CID: 5280343), orientin (CID: 5281675), and hyperoside (CID: 5281643) were obtained from NCBI PubChem database (https://www. ncbi.nlm.nih.gov/) in sdf format. RSCB PDB (https://www.rcsb.org/) was used as a database to derive the 3D structure of pancreatic alpha-amylase (PDB ID: 4W93). Ligands (glucomannan, mannan, quercetin, orientin, and hyperoside) were prepared using PyRx software. Receptor preparation (pancreatic α-amylase) was via eliminating water molecules or ligands bound to receptors using Discovery studio software. Then, the receptor was saved in .pdb format using open babel (Agustin *et al*., 2020).

2.4. Biological Activity Prediction

Bioactivity analysis was carried out to identify compounds from porang tubers that have the potential as anti-diabetic. This study employs a PASS server (http://www.pharmaexpert.ru/passonline/). PASS is a database containing compound activity data (Krieger *et al*., 2015).

2.5. Molecular Docking and Visualizations

Molecular docking between the receptor and the ligand was performed using Hex 8.0 software. Further, the docking was set in Shape+Electro+DARS mode. Then, docking results are saved with the .pdb extension. Analysis and visualization of binding interactions were established using the Discovery studio 2016 software (Agustin *et al*., 2022).

2.6. Molecular Dynamics Simulations

Our study used YASARA structural software for molecular dynamics simulation with a run time of 20,000 ps and autosaved every 25 ps. The following cell physiology conditions are performed when running the software: temperature 37°C, pH 7.4, salt content 0.9%, and pressure 1 atm. The simulation is conducted utilizing the macro program md_runfas. Furthermore, root-mean-square deviation (RMSD) protein backbone was performed using the md_analyze macro, and root-mean-square (RMSF) fluctuation analysis was performed using the md_analyzeres macro (Krieger *et al*., 2015).

3. Results

3.1. LCMS Analysis of Porang Tubers

Identification of phytochemical components of fresh porang tubers using LCMS analysis showed 67 compounds (Figure 1). Interestingly, our study found the main compounds identified included glucomannan (RT = 54,184), mannan (RT = 46,166), quercetin (RT = 11,427), orientin (RT = 22,172), and hyperoside (RT = 24,02) (Table 1). Glucomannan has the chemical formula $C_{30}H_{52}O_{26}$ defined by m/z 828; mannan with chemical formula $C_{24}H_{42}O_{21}$ has an m/z value of 66; the chemical formula for quercetin is $C_{15}H_{10}O_7$ with m/z 302. Orientin and hyperoside have the chemical formulas $C_{21}H_{20}O_{11}$ and $C_{21}H_{20}O_{12}$ with m/z 448 and 464, respectively.
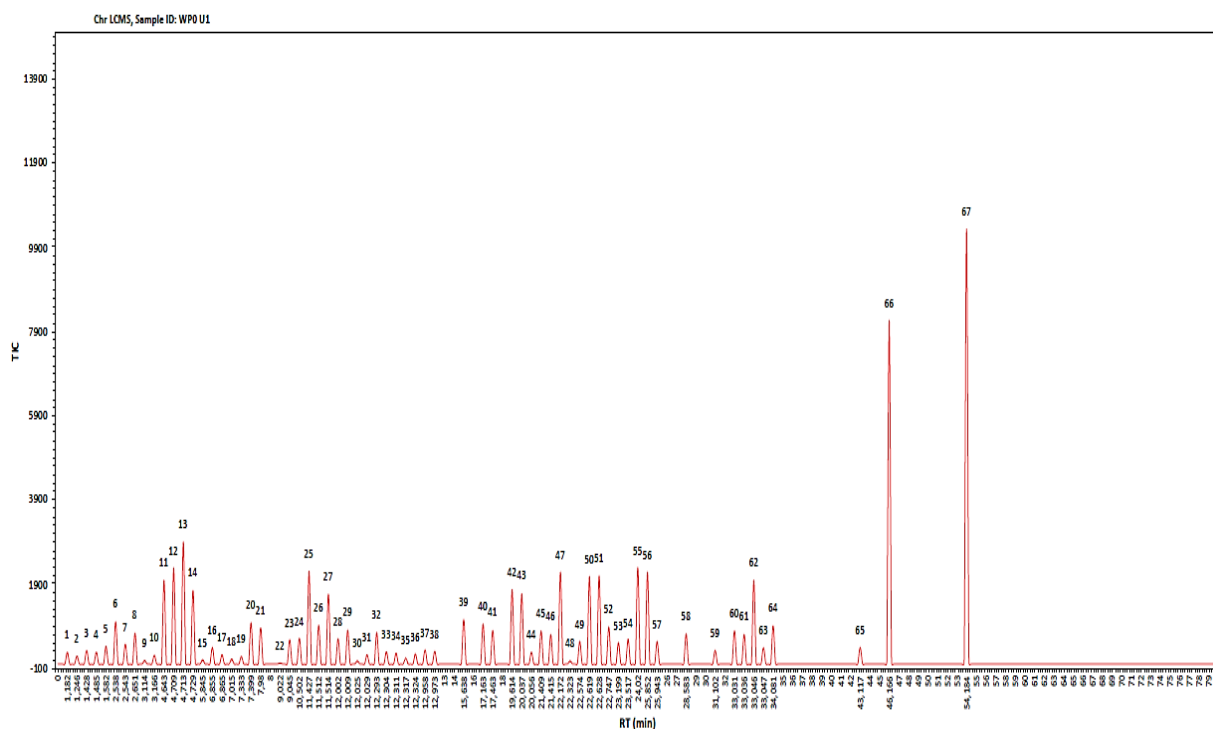
Figure 1. Chromatogram of porang tuber extract by LC-MS analysis. 25. Quercetin, 47. Orientin, 55. Hyperoside 66. Mannan, 67. Glucomannan.

Evaluation of biological activity based on PASS server showed that glucomannan, mannan, quercetin, orientin, and hyperoside from porang tubers were bioactive compounds that have the potential as anti-diabetic. It was indicated by the Pa value of >0.2 in quercetin; besides, glucomannan, mannan, and hyperoside have a Pa value (>0.6) (Table 1). The PASS server was a structural approach by comparing the inputted compounds with fixed compounds to have certain activities. The assessment is based on the Probability to be active (Pa) value of the bioactive compound. The current study showed that glucomannan and mannan occupied the highest Pa value of 0.77. It was indicated as the most potent active compound as anti-diabetic.

Table 1. Results of LC-MS analysis of methanol extract from porang tubers and predictions of their biological activity represent an anti-diabetic role.

Peak number	Compound	Chemical formula	RT (min)	m/z	Composition (%)	Pa value
67	Glucomanan	$C_{30}H_{52}O_{26}$	54,184	828	14,24644	0,777
66	Mannan	$C_{24}H_{42}O_{21}$	46,166	66	11,25441	0,777
25	Quercetin	$C_{15}H_{10}O_7$	11,427	302	3,03861	0,273
47	Orientin	$C_{21}H_{20}O_{11}$	22,172	448	3,01088	0,774
55	Hyperoside	$C_{21}H_{20}O_{12}$	24,02	464	3,15940	0,661

3.2. Molecular Docking Analysis of Pancreatic Alpha-amylase with Glucomannan, Mannan, Quercetin, Orientin, and Hyperoside

The receptor-ligand interactions were indicated by the binding site of the amino acid residue, chemical bond types, and the binding affinity (Table 2). The molecular mechanism of inhibition of pancreatic alpha-amylase through the interaction of bioactive compounds has been established. Five bioactive compounds of porang tuber can bind to the active site of pancreatic alpha-amylase in several residues.

Six amino acid residues of domain A of pancreatic alpha-amylase interact with glucomannan, including Gln63, Arg195, Trp59, His299, Asn53, and Asp197. Mannan compounds can bind amino acid residues Gln63, Thr163, Arg195, Glu233, Tyr62. The Asp 197 amino acid residue acts as a nucleophile in the alpha-amylase catalytic mechanism, whereas Glu 233 plays as an acid-base catalyst during the starch hydrolysis reaction. Asp 300 was crucial in optimizing substrate orientation at the S1 subsite through multiple hydrogen bonds. Our study showed that glucomannan and mannan could bind amino acid residues (Asp197 and Glu233), critical in catalytic activity through hydrogen interactions.

The interaction of quercetin with the binding site of the pancreatic alpha-amylase complex involves residues Thr264, Gly308, Ala260, Leu237, Lys257, and Lys261. Hydrogen and hydrophobic binding stabilized these interactions (Thr264, Gly308, Ala260, Leu237, Lys257, and Lys261) (Figure 2). Molecular docking results showed that eight amino acid residues in domains A and B of pancreatic alpha-amylase were able to bind to orientin, including Gln63, His299, Glu233, Asp197, Asp300, Leu165, His305, and Trp59 residues. This binding site is stabilized by hydrogen bonding, hydrophobic, and electrostatic interactions. The interaction of pancreatic alpha-amylase complex and hyperoside occurs in domain A. Acarbose is a commercial alpha-amylase inhibitor used to treat type 2 diabetes mellitus. In silico studies of acarbose-pancreatic α-amylase complexes show only one Trp59 residue bound to acarbose via hydrogen interactions.
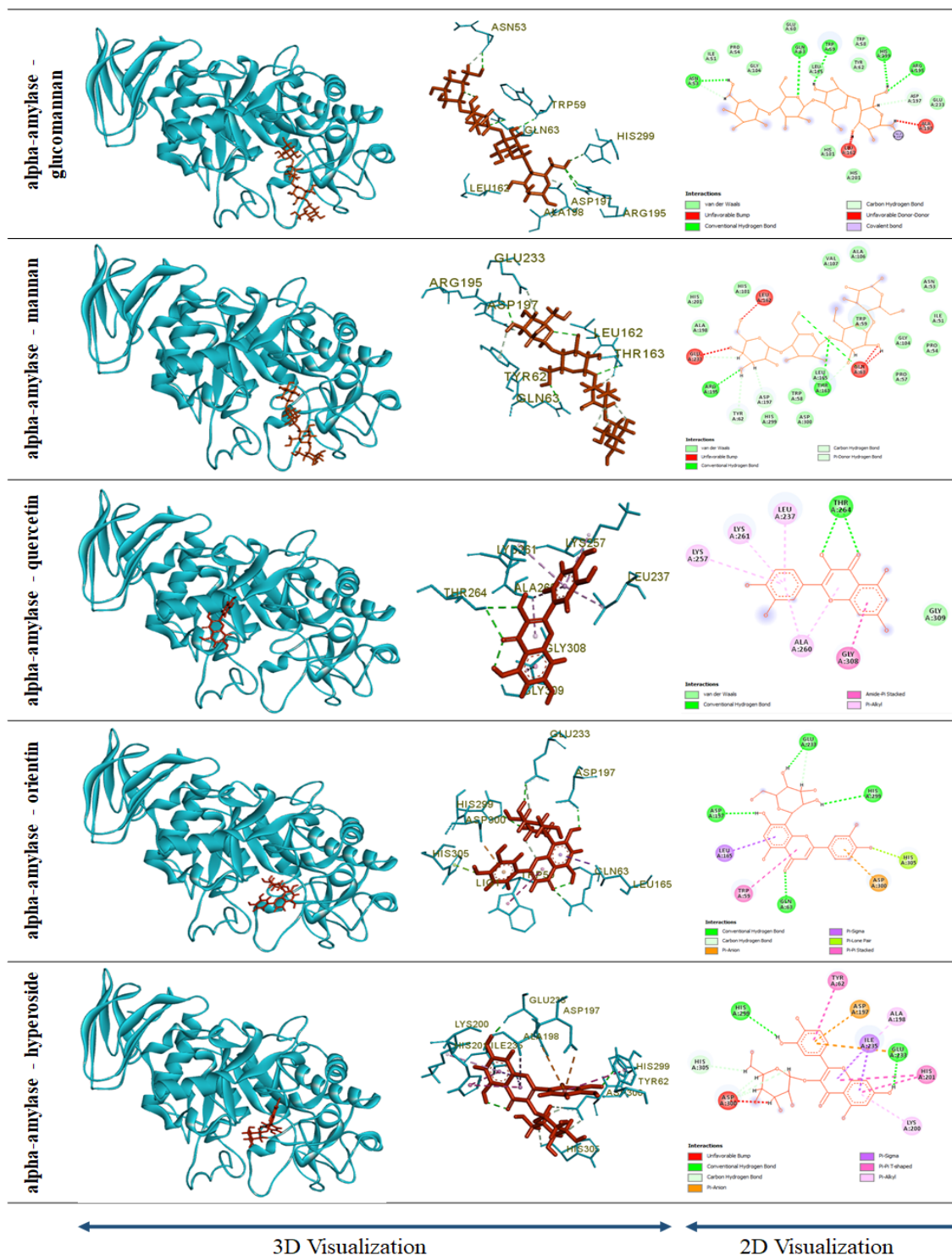
Figure 2. Interaction of pancreatic alpha-amylase with glucomannan, mannan, quercetin, orientin, and hyperoside.

Hyperoside can bind ten amino acid residues, including Glu233, His299, Asp300, His305, Asp197, Ile235, Tyr62, His201, Ala198, and Lys200 through hydrophobic interactions and hydrogen bonds. Interestingly, orientin and hyperoside could inhibit all three catalytic residues of pancreatic alpha-amylase (Glu233, Asp197, and Asp300). Thus, orientin and hyperoside from porang tubers were indicated to have a potential anti-diabetic role through inhibition of the active site of pancreatic alpha-amylase (Figure 2).

Glucomannan showed the maximum interaction with a binding energy of -394.1 kcal/mol lowest among five main compounds docked. The binding energy of mannan, quercetin, orientin, and hyperoside was -338.0 kcal/mol, -267.6 kcal/mol, -298.4 kcal/mol, and -304.2 kcal/mol, respectively (Table 2).

Table 2. Molecular docking results of the interaction between pancreatic alpha-amylase with glucomannan, mannan, quercetin, orientin, and hyperoside.

Compounds	Point interaction	Chemistry bond	Type	Binding energy (kcal/mol)
Glucomannan	A:GLN63:HE21 - :LIG1:O	Hydrogen Bond	Conventional Hydrogen Bond	
	A:ARG195:HH11 - :LIG1:O	Hydrogen Bond	Conventional Hydrogen Bond	
	A:ARG195:HH21 - :LIG1:O	Hydrogen Bond	Conventional Hydrogen Bond	
	:LIG1:H - A:TRP59:O	Hydrogen Bond	Conventional Hydrogen Bond	
	:LIG1:H - :LIG1:O	Hydrogen Bond	Conventional Hydrogen Bond	-394.1
	:LIG1:H - A:HIS299:NE2	Hydrogen Bond	Conventional Hydrogen Bond	
	:LIG1:H - A:ASN53:O	Hydrogen Bond	Conventional Hydrogen Bond	
	:LIG1:H - A:ASP197:OD1	Hydrogen Bond	Carbon Hydrogen Bond	
	:LIG1:H - A:ASN53:O	Hydrogen Bond	Carbon Hydrogen Bond	
Mannan	A:GLN63:HE21 - :LIG1:O	Hydrogen Bond	Conventional Hydrogen Bond	
	A:THR163:HG1 - :LIG1:O	Hydrogen Bond	Conventional Hydrogen Bond	
	A:ARG195:HH21 - :LIG1:O	Hydrogen Bond	Conventional Hydrogen Bond	
	:LIG1:H - :LIG1:O	Hydrogen Bond	Conventional Hydrogen Bond	
	:LIG1:H - A:THR163:O	Hydrogen Bond	Carbon Hydrogen Bond	
	:LIG1:H - :LIG1:O	Hydrogen Bond	Carbon Hydrogen Bond	-338.0
	:LIG1:H - A:ASP197:OD1	Hydrogen Bond	Carbon Hydrogen Bond	
	:LIG1:H - A:GLU233:OE2	Hydrogen Bond	Carbon Hydrogen Bond	
	:LIG1:H - :LIG1:O	Hydrogen Bond	Carbon Hydrogen Bond	
	:LIG1:H - :LIG1:O	Hydrogen Bond	Carbon Hydrogen Bond	
	:LIG1:H - A:TYR62	Hydrogen Bond	Pi-Donor Hydrogen Bond	
Quercetin	A:THR264:HG1 - :LIG1:O	Hydrogen Bond	Conventional Hydrogen Bond	
	A:THR264:HG1 - :LIG1:O	Hydrogen Bond	Conventional Hydrogen Bond	
	:LIG1:H - :LIG1:O	Hydrogen Bond	Conventional Hydrogen Bond	
	A:GLY308:C,O;GLY309:N - :LIG1	Hydrophobic	Amide-Pi Stacked	
	:LIG1 - A:ALA260	Hydrophobic	Pi-Alkyl	-267.6
	:LIG1 - A:LEU237	Hydrophobic	Pi-Alkyl	
	:LIG1 - A:LYS257	Hydrophobic	Pi-Alkyl	
	:LIG1 - A:ALA260	Hydrophobic	Pi-Alkyl	
	:LIG1 - A:LYS261	Hydrophobic	Pi-Alkyl	
Orientin	A:GLN63:HE21 - :LIG1:O	Hydrogen Bond	Conventional Hydrogen Bond	
	:LIG1:H - A:HIS299:NE2	Hydrogen Bond	Conventional Hydrogen Bond	
	:LIG1:H - A:GLU233:OE2	Hydrogen Bond	Conventional Hydrogen Bond	
	:LIG1:H - A:ASP197:OD2	Hydrogen Bond	Conventional Hydrogen Bond	
	:LIG1:H - :LIG1:O	Hydrogen Bond	Conventional Hydrogen Bond	
	:LIG1:H - :LIG1:O	Hydrogen Bond	Carbon Hydrogen Bond	-298.4
	:LIG1:H - A:GLU233:OE2	Hydrogen Bond	Carbon Hydrogen Bond	
	A:ASP300:OD1 - :LIG1	Electrostatic	Pi-Anion	
	A:LEU165:CD1 - :LIG1	Hydrophobic	Pi-Sigma	
	:LIG1:O - A:HIS305	Other	Pi-Lone Pair	
	A:TRP59 - :LIG1	Hydrophobic	Pi-Pi Stacked	

*Bold letter indicates donor residue

Analysis of the structural stability and fluctuation of pancreatic alpha-amylase residues bound to glucomannan, mannan, quercetin, and orientin was carried out. Molecular dynamics simulation results show the interaction of the pancreatic alpha-amylase protein with the four compounds (glucomannan, mannan, quercetin, and orientin) as stable as indicated by an RMSD value of less than 2.5 from beginning to end (Figure 3a). Ligand movement and ligand configuration from beginning to end showed RMSD values of about 2 – 10 and 0.5 – 2, respectively (Figure 3b-

c). Molecular dynamics analysis showed the RMSF value of less than three from the beginning to the end, which indicated the stable particle position (Figure 3d).
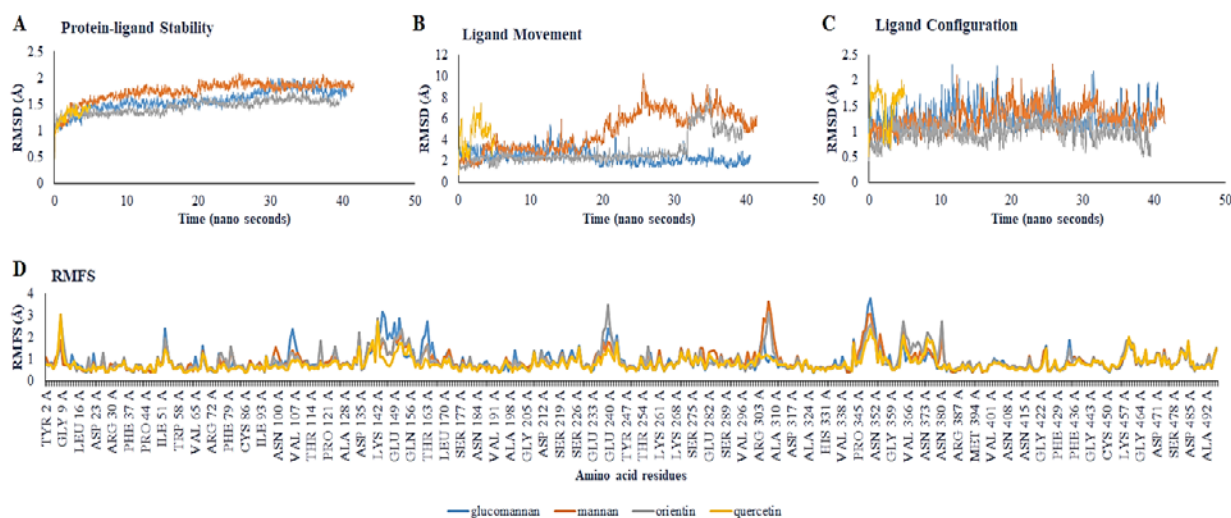
Figure 3. The molecular dynamics of the complex structure between pancreatic alpha-amylase with glucomannan, mannan, quercetin, and orientin interactions during simulation. A. The stability of protein-ligand complex can be seen from the RMSD value. B. Ligand movement. C. Ligand configuration. D. RMSF value represents the stability of amino acid residues.

4. Discussion

This study found the chemical components to be similar to the previous study, which reported 67 compounds contained in porang tuber extract, both from the second and third growing periods (Gusmalawati *et al*., 2019). Exploration of natural bioactive compounds within plant is critical to predicting the pharmacological activity of plants. Glucomannan and mannan are polysaccharides with nutraceutical roles, such as relieving constipation and reducing weight and cholesterol. In addition, quercetin, orientin, and hyperoside are flavonoids known to have antioxidant, anti-inflammatory, antiapoptotic, and anti-diabetic activities (Harijati *et al*., 2012; Shi *et al*., 2019). Previous studies reported that Moringa oleifera was effective as an anti-diabetic through the inhibition of TNF-α (tumor necrosis factor) and IFN-γ (interferon-gamma) in male BALB/c mice (Lestari *et al*., 2022). This effectiveness is likely due to bioactive phenolic compounds, flavonoids, tannins, terpenoids, and alkaloids, which have anti-diabetic activity. The assessment based on the Probability to be active (Pa) value of the bioactive compound. The Pa value reflects the ability of an active compound in particular biological processes. The higher the value of Pa means the more potential (Syamsul *et al*., 2019; Setiawan *et al*., 2018). The current study showed that glucomannan and mannan occupied the highest Pa value of 0.77. In conclusion, bioactive in porang tuber extract was indicated as the most potent active compound as anti-diabetic.

The result in this study ensures that the compounds contained in porang tuber extract have many health benefits as herbal medicine. The main compounds (glucomannan, mannan, quercetin, orientin, and hyperoside) identified in porang tubers were targeted for molecular docking to investigate their potential role as anti-diabetic. Three amino acid residues, Asp197, Glu233, and Asp300 of domain A, revealed in this study were identified as active sites of pancreatic alpha-amylase (Kikiowo *et al*., 2020). Here, the presence of hydrogen bonding plays a vital role in stabilizing the structure of biomolecules and catalyzing enzymes (Alqahtani *et al*., 2019; Kikiowo *et al*., 2020). The binding of glucomannan and mannan to Asp197 and Glu233 amino acid residues were critical in catalytic activity through hydrogen interactions. As a result, alpha-amylase activity can be inhibited and then slows down the digestion of carbohydrates, so glucose absorption into the bloodstream will be reduced (Quek *et al*., 2020).

A previous study correlated the compound structure with its activity. It showed that the interaction of flavonoids and pancreatic alpha-amylase inhibit the activation of one of the enzyme conformations by shifting the equilibrium to the most stable conformation. As a result, enzymatic activity will be decreased (Martinez-Gonzalez *et al*., 2019). The type of interaction in the binding of the ligand-receptor complex is affected by the binding energy. The lower binding energy indicated the docked compound is easier binding to the receptor-binding domain (RBD) (Matthew *et al*., 2021).

5. Conclusion

The present study is a novel discovery investigating phytochemical components, and in silico approach revealed the pancreatic alpha-amylase inhibitory of porang tubers grown in East Java, Indonesia. LCMS analysis showed 67 compounds, and it was dominated by glucomannan, mannan, and flavonoids. The main flavonoid components in porang tubers were represented by quercetin, orientin, and hyperoside. Our finding reveals that porang tuber extract can be employed as a natural medicine for diabetes mellitus by inhibiting the pancreatic alpha-amylase enzyme. Further study regarding the function of primary and secondary metabolite of porang as alpha-amylase inhibitor both in vitro and in vivo is required to confirm this result.

References

Agustin, A. T., Julianto, E., Julianus, J., & Riranto, J. (2022). Potential Role of Betel Leaf (*Piper betle* L.) Water Extract as Antibacterial *Escherichia coli* Through Inhibition of β-Ketoacyl-[Acyl Carrier Protein] Synthase I. *Tropical Journal of Natural Product Research*, **6(11)**: 1802–1808.

Agustin, A. T., Safitri, A., & Fatchiyah, F. (2020). An in-Silico Approach Reveals the Potential Function of Cyanidin-3-o-glucoside of Red Rice in Inhibiting the Advanced Glycation End Products (AGES)-Receptor (RAGE) Signaling Pathway. *Acta Informatica Medica*, **28(3)**: 170–179.

Aldayel, T. S., Grace, M. H., Lila, M. A., Yahya, M. A., Omar, U. M., & Alshammary, G. (2020). LC-MS Characterization of Bioactive Metabolites from Two Yemeni *Aloe* spp. with Antioxidant and Antidiabetic Properties. *Arabian Journal of Chemistry*, **13(4):** 5040–5049.

Alqahtani, A. S., Hidayathulla, S., Rehman, M. T., ElGamal, A. A., Al-Massarani, S., Razmovski-Naumovski, V., Alqahtani, M. S., El Dib, R. A., & AlAjmi, M. F. (2019). Alpha-Amylase and Alpha-Glucosidase Enzyme Inhibition and Antioxidant Potential of 3-Oxolupenal and Katononic Acid Isolated from *Nuxia oppositifolia*. *Biomolecules*, **10(1):** 61.

Babu, V. S., & Radhamany, P. M. (2021). Phytochemical Profiling and In Vitro α-amylase Inhibitory Activity of *Glycosmis pentaphylla* (Retz.) DC. *Jordan Journal of Biological Sciences*, **14(2)**: 199–203.

Chen, H., Nie, Q., Hu, J., Huang, X., Zhang, K., Pan, S., & Nie, S. (2019). Hypoglycemic and Hypolipidemic Effects of Glucomannan Extracted from Konjac on Type 2 Diabetic Rats. *Journal of Agricultural and Food Chemistry*, **67(18):** 5278–5288.

Firdouse, S., & Alam, P. (2011). Phytochemical Investigation of Extract of *Amorphophallus campanulatus* Tubers. *International Journal of Phytomedicine*.

Gusmalawati, D., Arumingtyas, E. L., Azrianingsih, R., & Mastuti, R. (2019). LC-MS Analysis of Carbohydrate Components in Porang Tubers (*Amorphophallus muelleri* Blume) from the Second and the Third Growth Period. *IOP Conference Series: Earth and Environmental Science*, **391**: 012022.

Gusmalawati, D., Arumingtyas, E. L., Mastuti, R., & Azrianingsih, R. (2021). Determination of Postharvest Quality of Porang (*Amorphophallus Muelleri* Blume) Tubers Based on the Dynamics of Weight Loss, Water Content and Carbohydrate Components for the Pharmaceutical Industry. *Farmacia*, **69(6)**: 1145–1152.

Harijati, N., Widyarti, S., & Azrianingsih, R. (2012). Effect of Dietary *Amorphophallus* sp From East Java on LDL-C Rats (*Rattus novergicus* Wistar Strain). *Journal of Tropical Life Science*, **1(2)**: 50–54.

Kikiowo, B., Ogunleye, J. A., Iwaloye, O., & Ijatuyi, T. T. (2020). Therapeutic Potential of *Chromolaena odorata* Phyto-constituents Against Human Pancreatic α-amylase. *Journal of Biomolecular Structure and Dynamics*.

Krieger, E., & Vriend, G. (2015). New Ways to Boost Molecular Dynamics Simulations. *Journal of Computational Chemistry*, **36(13)**: 996–1007.

Lestari, N. D., Rahmah, A. C., Adharini, W. I., Vivian, R., Dwi, Y., Widodo, N., J., Rahayu, S., & Rifa, M. (2022). Bioactivity of *Moringa oleifera* and Albumin Formulation in Controlling TNF-α and lFN-γ Production by NK Cells in Mice Model Type 1 Diabetes. *Jordan Journal of Biological Sciences*, **15(2):** 205–208.

Martinez-Gonzalez, A. I., Díaz-Sánchez, Á. G., de la Rosa, L. A., Bustos-Jaimes, I., & Alvarez-Parrilla, E. (2019). Inhibition of α-amylase by Flavonoids: Structure Activity Relationship (SAR). *Spectrochimica Acta Part A: Molecular and Biomolecular Spectroscopy*, **206**: 437–447.

Mathew, S. M., Benslimane, F., Althani, A. A., & Yassine, H. M. (2021). Identification of Potential Natural Inhibitors of the Receptor-binding Domain of the SARS-CoV-2 Spike Protein Using a Computational Docking Approach. *Qatar Medical Journal*, **2021(1)**.

Quek, A., Kassim, N. K., Ismail, A., Latif, M. A. M., Shaari, K., Tan, D. C., & Lim, P. C. (2020). Identification of Dipeptidyl Peptidase-4 and α-Amylase Inhibitors from *Melicope glabra* (Blume) T. G. Hartley (Rutaceae) Using Liquid Chromatography Tandem Mass Spectrometry, In Vitro and In Silico Methods. *Molecules (Basel, Switzerland)*.

Setiawan, L. T. K., Nugraha, J., Tamayanti, W. D., & Utomo, D. H. (2018). The Computational Study Reveals the Immunomodulatory and Antimicrobial Effects of *Vernonia amygdalina* Extract. *Asian Journal of Microbiology, Biotechnology and Environmental Sciences*, **20**: 83–87.

Shete, C. C., Wadkar, S. S., Gaikwad, N. B., Patil, K. S., & Ghosh, J. S. (2015). Phenolic Contents and Antioxidant Capacity of *Amorphophallus commutatus* and *Amorphophallus paeonifolius*. *International Food Research Journal*.

Shi, Y., Qiu, X., Dai, M., Zhang, X., & Jin, G. (2019). Hyperoside Attenuates Hepatic Ischemia-Reperfusion Injury by Suppressing Oxidative Stress and Inhibiting Apoptosis in Rats. *Transplantation Proceedings*.

Syamsul Hidayat, M. K., Kusworini, Rudijanto, A., & Sumitro, S. B. (2019). Potential of Biological Activities from Chemical Compounds of *Nigella sativa* as Anti-osteoporosis, an In-Silico Study. *Journal of Global Pharma Technology*, **11(4)**: 185–191.

Van, H.-T., Nguyen, H. H.-M., Huynh, N. T.-A., Le, V.-S., & Tran, G.-B. (2020). Chemical Composition and Antibacterial Activities of the Ethanol Extracts from the Leaves and Tubers of *Amorphophallus pusillus*. *Plant Science Today*, **7(2)**: 296–301.

Wulan, D.I., Setiawan, A. A., & Laksmitawati, D. (2021). Macronutrients Analysis of Porang Tubers (*Amorphophallus muelleri* Blume) Fermentation with *Lactobacillus Bulgaricus* Bacteria. *Advances in Health Sciences Research*.

Xie, L., Mo, J., Ni, J., Xu, Y., Su, H., Xie, J., & Chen, W. (2020). Structure-Based Design of Human Pancreatic Amylase Inhibitors from the Natural Anthocyanin Database for Type 2 Diabetes. *Food & Function*, **11(4)**: 2910–2923.

Zhao, Y., Yang, P., & Qian, S. (2015). Determination of 14 Aniline Derivatives in Water by Liquid Chromatography-Tandem Mass Spectrometry. *Chinese Journal of Chromatography*, **33(5)**: 508.

Investigation of Quorum Sensing, Biofilm Production, and Detection of Virulence-associated Genes Among Clinical Isolates of *Acinetobacter baumannii*

Sayran S. Qader[1] and Aryan R. Ganjo[1,2,*]

[1]*Department of Clinical Analysis, College of Pharmacy, Hawler Medical University, Erbil, Iraq;* [2] *Department of Medical Analysis, Faculty of Applied Science, Tishk International University, Erbil, Iraq.*

Abstract

Acinetobacter baumannii (A.baumannii) is an opportunistic microorganism able to survive in harsh environments and develop resistance to antibiotics often used in hospitals, which makes it one of the most common and pervasive causes of infections in healthcare facilities.The currentstudy was conducted to investigate the existence of*A.baumannii* and their antimicrobialresistantpattern, dispersion of Quorum Sensing(QS), and virulent related genes.In this investigation, the identification and susceptibility of 65non-repetitive *A. baumannii* isolates to antimicrobial drugs were evaluated. The QS encoding genes,and virulence-related genes were detected,and biofilm development was examined.In a total, 65 isolates of *A. baumannii*, 62 (95.38%) formed biofilm, with the vast majority being strong biofilm produces24(36.92%). The isolates showed a remarkable resistance to the antibiotics commonly used to treat *A. baumannii*as amikacin, which had a resistance rate of 100% among isolatesd.Results from virulence gene studies were as follows*csg*A (30.76%), *iut*A (24.61%), *cnf*I (16.92%), and *cva*C (6.15%). The two QS genes were *abal* (90.76%) and *abaR* (87.69%).Our findings confirm that the QS-related genes (*aba*I/*aba*R) were broadly dispersed across *A. baumannii* clinical isolates and were strongly associated with antibiotic resistance,and*csgA* was apredominant virulence gene followed by *itu*A.

Keywords*: Antibiotic resistance, Acinetobacter baumannii,Biofilm, Virulence-related gene, Quorum sensing*

1. Introduction

The opportunistic *Acinetobacter baumannii* causes a wide variety of clinical infections. Recently, it has come to light on a global scale, and it frequently leads to rise in antimicrobialineffectiveness and encoding of virulent-related genes(Zhang et al., 2022). Colicin V production (*cva*C), curli fibers (*csg*A), siderophores like aerobactin (*iut*A), and cytotoxic necrotizing factor (*cnf*I) are amongthe extremely important virulence-associated genes in*A. baumannii* isolates (Darvishi, 2016). Determination ofconcealed virulent-associated genes in clinical samples of *A. baumannii* has significant epidemiological repercussions that aid in controlling the spread of illnesses induced by this pathogen(Eraç et al., 2014, Eijkelkamp et al., 2014). *A. baumannii*capacity to acquire several virulence characteristics, particularly resistance determinants including efflux pumps, and iron acquirement pathways and motility, enables it to persist in hostile environments and promotes the occurrence of infections. This pathogen has been measured as a top member of nosocomial infections outstanding to its capacity to thrive in hospital conditions(Martinez et al., 2021).QS is a mechanism that bacteria use to accomplisha group of activities through sensing their population size, and constant production of small diffusible compounds known as autoinducers, such as N-acyl-homoserine lactones (AHLs) in some gram-negative pathogens(Gajdács and Spengler, 2019).The QS mechanism is widespread in bacteria and is associated with numerous biological mechanisms, such as locomotion, conjugation, biofilm development, synthesis of virulentfactors. The QS mechanism of *A. baumannii* consists of *aba*I/*aba*R, a two-component structure *aba*R gene encodes the receptor protein that adheres to AHLs and functions as a transcriptional regulator. The 3-hydroxy-C12-homoserine lactones tend to be the most common AHLs generated by the pathogen(Erdönmez et al., 2017).Main aims of this study include determining *Acinetobacter baumannii* from clinical samples and their antibiotic resistance profile, and detecting QS, virulence-associated genes.

2. Materials and Methods

2.1. Specimens collection

Between the 1st of October 2021 and the 30th of March 2022, 65 samples were collected from different sources, including sputum, wounds, and blood. Samples were collected from patients with impaired immunity at Erbil city, Kurdistan region-Iraq hospitals.

---

* Corresponding author. e-mail: aryan.ganjo@hmu.edu.krd.

2.2. Identification and antibiotic sensitivity testing

Identification of the isolates was accomplished using conventional microbiological techniques. The VITEK 2 GN card (BioMérieux, France) verified *A. baumannii* isolates. Antibacterial sensitivity testing on isolated bacteria was also accomplished using the compact automated system VITEK 2 to Pinracillin (PIP), Piperacillin/tazobactam (TZP), cefoperazone (CFP), ceftazidime (CAZ), Imipinim (IMP), Meropenem (MEM), Amikacin(AK), Gentamicin (GN),Netilmicin (NET), Tobramycin (TOB), Ciprofloxacin (CIP), Levofloxacin(LEV), Tagycycline (TGC), trimethoprim/sulfamethoxazole (SXT), colistin (CST).

2.3. A Carb NP protocol (CarbAcineto NP test)

CarbAcineto NP test was assessed asstated byDortet et al. (2014). *A.baumannii* clinical specimens were overnight cultivated in TSA. Two tubes were used (Tube A and B). One loop of the tested bacteria was resuspended by vortexing it for 15 seconds at maximum agitation in 100 μL of lysis buffer containing a 5.0 M NaCl solution. 100 μL of the phenol red-containing revealing solution was introduced to tube A; simultaneously, 100 μL of the same solution was introduced to tube B, including 6 mg/mL of imipenem. Both tubes were incubated at 37°C for two hour. Visual examination of the color shift in both tubes was recorded.

2.4. Motility characteristics

Swarming and twitching motility was evaluated using LB broth with 0.4% or 0.8% agar. Positive swarming motility was defined as a zone larger than 10mm surrounding the inoculation siteafter plates incubated at 37°C for 48 hours, For twitching motility, bacteria were dyed with a 0.2% crystal violet solution. Positive twitchers had zone diameters of 5mm or more. Each isolate was examined 3 times(Clemmer et al., 2011).

2.5. Biofilm detection by microtiter plate

Biofilm development capability was tested with crystal violet.After overnight incubation, bacteria were diluted to an optical density of 600 (OD_{600}) = 0.1. Then, 180 μL of Luria-Bertani (LB) broth and 20 μL of bacterial suspensions were put on 96-well polystyrene microtiter plates. The plates were incubated at 37°C for 24 hours and then washed three times with phosphate-buffered saline (PBS) and stained with 200 μL of 0.1% crystal violet (Oxoid, UK). Consequently, the plates were rinsed three times with PBS. The plates were dissolved in 200 μL of 95% ethanol by gently stirring at room temperature for 20 minutes. At 570nm, the absorbance was determined. Three standard deviations (SD) above the average OD of the negative control (LB broth only) were defined as the cut-off OD (ODc). The classification rules were as follows: OD≤ODC indicates non-biofilm producers (-); ODC<OD≤2×ODC indicates weak biofilm producers (+); 2×ODC<OD≤4×ODC shows moderate biofilm producers (++), and OD>4×ODC suggests strong biofilm producers (+++)(Li et al., 2021).

2.6. Genomic extraction fromA. baumannii isolates

Genomic DNA was isolated from a bacterial colony using a Fermentas Germany kit accordingtothe manufacturer's guidelines.Nanodrop was used to assess

DNA concentration by spectrophotometer at 260 nm, then stored at –20°C until use(Darvishi, 2016).

2.7. Molecular detection of QS and virulence-related genes

Employing standard polymerase chain reaction (PCR), the existence of the QS and virulence-associated gene in all isolates was determined. The experiment was conducted in a 25 μL reaction mixture including 12.5 μL of 2× master mix (AMPLIQON, Denmark), 1.0 μL of each primer (10 pmol), and 1.5 μL of genome template. The amount reached 25 μL using PCR water. The following was cyclingconditions: First 1 cycle at 95°C for 4 min; thirty cycles at 95°C for 50 sec, 58°C for 60 sec, and 72°C for 45 sec; one cycle at 72°C for 8 min (Al-Kadmy et al., 2018a). The program for QS genes was as follows: 30 cycles of denaturation at 94 °C for 1 min, annealing at 52 °C for 30 s, and extension at 72 °C for 1.5 min, with a final elongation step at 72 °C for 5 min.occurrence of the QS and virulence-related genes were identified by applying the primer sequences of*aba*I 435bp and*aba*R 310bp (Tang et al., 2020). *cnf*I 498bp, *csg*A 200bp, and *iut*A 300bp (Al-Kadmy et al., 2018b) as shown in (Table.1).

Table 1. Primer sequences and size of PCR products for QS and virulence-associated genes.

Target genes	Oligonucleotide primers Sequences (5'-3')	Product size (bp)
***aba*I**	Forward:AAAGTTACCGCTACAGGG	435bp
	Reverse: CACGATGGGCACGAAA	
***aba*R**	Forward:TCCTCGGGT CCCAATA	310 bp
	Reverse: TAAATCTACCGCATCAA	
***cnf*I**	Forward:AAGATGGAGTTCCCTATGCAGGAG	498 bp
	Reverse:CATTCAGAGTCTTGCCCTCATTATT	
***csg*A**	Forward:ACTCTGACTTGACTATTACC	200 bp
	Reverse: AGATGCAGTCTGGTCAAC	
***cva*C**	Forward:CACACACAAACGGGAGCTGTT	680 bp
	Reverse: CTTCCCGCAGCATAGTTCCAT	
***iut*A**	Forward:GGCTGGACATCATGGGAACTGG	bp
	Reverse: CGTCGGGAACGGGTAGAATCG	

2.8. Statistical analyses

GraphPad Prism 9.01 was used for all statistical analysis. Data were evaluated using the X^2 test,χ2 test, or Fisher's exact test and Kruskal – Wallis test. The p-value ≤ 0.05 was used to identify the differences as statistically significant.

3. Results

3.1. QS and virulence-associated gene distribution among A. baumannii isolates

In this invistigation, sixty-five (65) isolates of*A. baumannii* were diagnoseddepending on colonial morphology on cultural media and various biochemical characteristicsthen confirmed by VITEK 2 system. The gender distribution of the isolates was as follows: 24 (36.92 %) for females and 41 for males (63.07%). Out of the 65 isolates, 59 (90.76 %) had the *aba*I QS gene, while *aba*R found in 57 (87.69 %),andthe virulence genes were

distributed as follows: *csgA* = 20 (30.76%), *iutA* = 16 (24.61%), *cnfI* = 11 (16.92%), and *cvaC* = 4 (6.15%) (Table.2).

Table 2. Distribution of QS genes and virulence-related genes among *A. baumannii isolates.*

Gene type	Gene function	Prevalence	
		n.	%
*aba*I	Quorum sensing genes	59	90.76
*aba*R		57	87.69
*csg*A	Curli fiber adhesive virulence	20	30.76
*iut*A	Sidrophore like aerobactin	15	24.61
*cnf*I	Cytotoxic necrotizing factor	11	16.92
*cva*C	Colicin V production	4	6.15

3.2. Resistance to antimicrobial agents

All isolates demonstrated complete resistance to amikacin. Followed by ciprofloxacin 95.38%, each of pipracillin tazobactum, ceftazidime, imipenem, and levofloxacin exhibited 93.85%. Colistin had the most significant efficiency towards *A. baumannii*, as all the isolates were sensitive to colistin(figure.1).
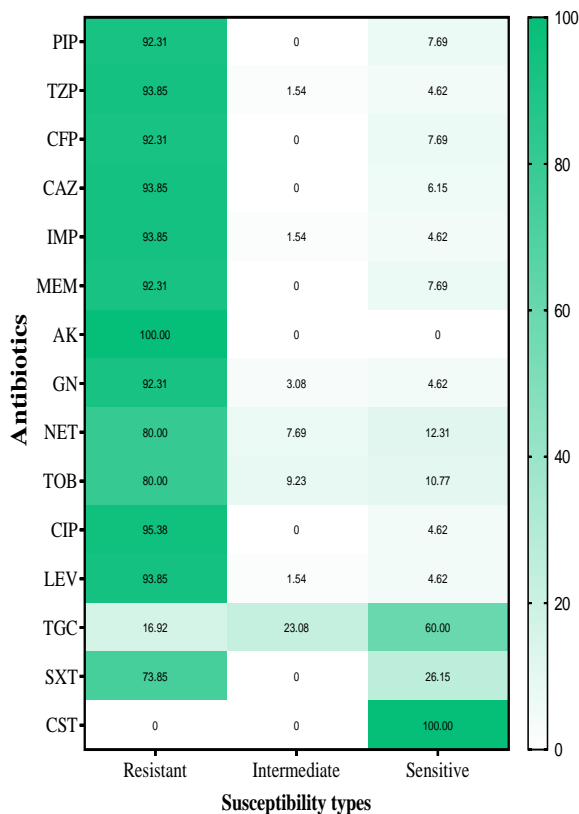
Figure 1. Antimicrobial resistance patterns in *A. baumannii*

3.3. CarbAcineto NP assay

The ability of carbapenemase production was assessed for 65 isolates using a CarbAcineto NP test. Forty (61.53 %) of the isolates tested showed positive results in the carbAcineto NP test. as shown in figure.2.
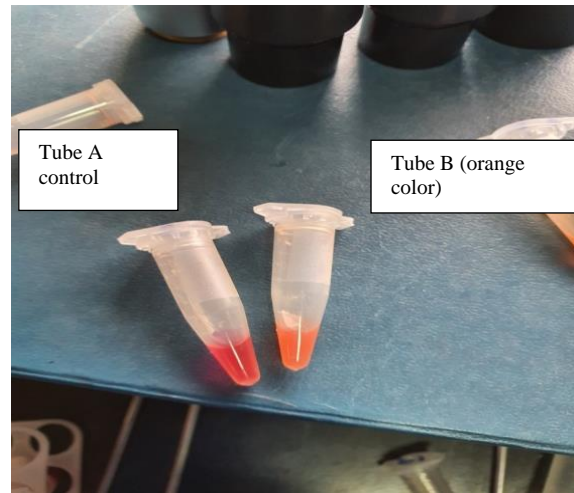
Figure 2. Craba NP test colour change in tube B to (orange colour) indicate positive result.

3.4. Motility characteristics and source of specimens

All of the isolated bacteria were tested for their motility. Surface-associated motility (swarming) was detected in 17 (26.15%), and twitching motility was observed in 26 (40%) of the *A. baumannii* isolates.As depicted in (*Figure. 3*), sputum isolates had superior twitching motility over wound and blood samples. 21/45 (46.6%) sputum isolates exhibited twitching movements. Similarly, the swarming motility among all isolates of *A. baumannii* recorded the highest frequency in sputum sources.Our findings revealed that the high prevalence of the swarming motility was in sputum 15/45 (33.33%), while the lowest incident of swarming motility was in the blood and wound specimens (*n* =1).
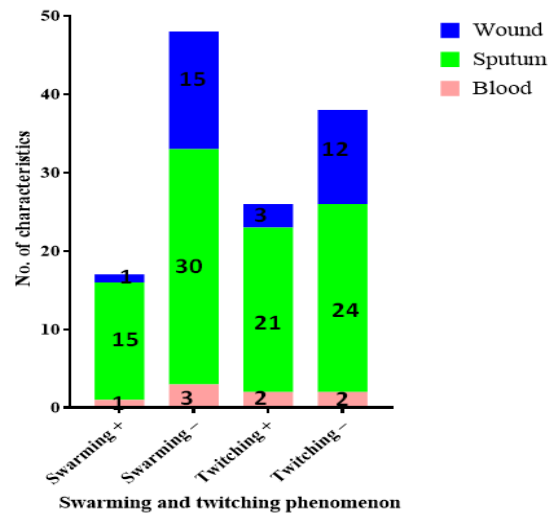
Figure 3. Prevalence of phenotypic swarming and twitching phenomenon among the source of specimens.

3.5. Biofilm formation, QS, and virulence-related

In terms of biofilm production, the results indicated that 62 (95.38%) isolates were able to form biofilms, of which 24 (36.92%) were strong biofilm producers, 18 (27.69%) and 20 (30.77%) were moderate and weak producers, respectively.

On the other hand, 3.6% of the isolates do not have the ability to develop biofilm. We diligently investigated the

association between biofilm development and genes associated with QS signaling molecules and virulence factors in *A. baumannii* isolates. A highly developed ability to form biofilms is demonstrated by isolates that possess the genes for QS signaling molecules (*abaI* and *abaR* genes), Additionally, a notable disparity was noted in comparison to the isolates lacking the QS-related genes (Figure. 4). Conversely, there was no significant correlationbetween the isolates that have the virulence-related genes to produce the biofilm and the isolates that do not bear the virulence-related gene.
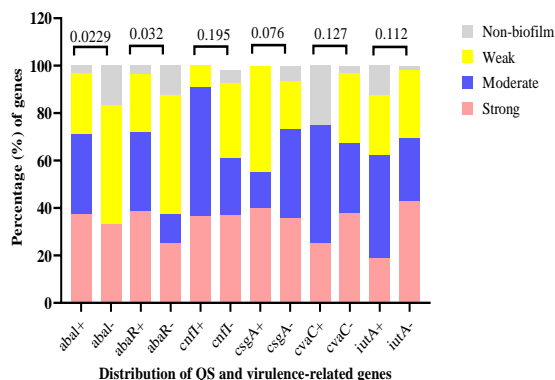
Figure4. Quorum sensing and virulence gene distribution across biofilm formation states

Table 3. Existence of virulence-associated genes with antibiotic-resistant among*A.baumannii*.

| | Antibiotics | | | | | | | | | | | | | |
Genes	PIP	TZP	CFP	CAZ	IMP	MEM	AK	CN	NET	TOB	CIP	LEV	TGC	SXT
QS gene														
*aba*I (59)	91.5	93.2	91.5	93.2	93.2	91.5	100.0	91.5	76.3	78.0	93.2	18.6	71.2	71.2
*aba*R (56)	92.9	94.6	92.9	94.6	94.6	92.9	100.0	92.9	78.6	78.6	96.4	94.6	17.9	73.2
Virulence-Related Genes														
*cnf*I (11)	46.7	53.3	46.7	53.3	53.3	46.7	73.3	46.7	26.7	26.7	53.3	53.3	6.7	46.7
*csg*A (20)	90.5	90.5	90.5	85.7	90.5	90.5	95.2	90.5	85.7	85.7	95.2	90.5	14.3	81.0
*cva*C (4)	33.3	50.0	33.3	50.0	33.3	33.3	66.7	33.3	16.7	16.7	33.3	50.0	0.0	33.3
*iut*A (16)	80.0	85.0	80.0	85.0	80.0	50.0	100.0	80.0	60.0	70.0	85.0	85.0	20.0	70.0

3.6. Association between virulence genes with antibiotic-resistant

Isolates that are resistant to antibiotics have higher number of QS and virulence genes compared to isolates that are susceptible. The prevalence of *cnf*I in isolates resistant to aminoglycosides (tobramycin and amikacin), imipenem, and meropenem was significantly higher than in comparable sensitive isolates. Among the great majority of antibiotic-resistant isolates, the proportion of csgA was much higher than susceptible isolates. The ratio of *cva*C across all antibiotic-resistant isolates was substantially greater than comparable susceptible isolates. The proportion of *iut*A in isolates resistant to ciprofloxacin, gentamicin, tobramycin, amikacin, imipenem, and meropenem was significantly greater than isolates susceptible to comparable antibiotics (Table.3).

3.7. Association of QS with antibiotic resistance

The frequency of antibiotic susceptibility pattern inisolates containing QS genes (*aba*I and *aba*R) is depicted in (Figure.5).54 of isolates expressing the *abaI* gene were resistant to antibiotics, while only 5 of isolates lacking the *abaI* gene were resistant to antimicrobials. Only 9 of the resistant isolates were found to be deficient in the *abaR* gene, while 51 of the isolates expressing the gene were antibiotic-resistant bacteria. Antibiotic resistance was found to be significantly associated with the presence of the *abaI* and *abaR* genes in the isolates (*p*-value = 0.002).

Figure 5. Association between antibiotic resistance and carrier position of QS genes.

4. Discussion

*Acinetobacter baumannii*is an opportunistic bacterium that can spread in healthcare facilities, potentially resulting in the emergence of nosocomial illnesses(Jahangiri et al., 2019, Nowak et al., 2014). Because of its adhesive properties, it poses a significant risk of colonization and transmission among hospitalized patients(Choi et al., 2010). This pathogen is able to withstand a wide range of modern antibiotics due to the acquisition of resistance determinants and the upregulation of intrinsic resistance pathways(Zeighami et al., 2019). Multidrug-resistance*A. baumannii*produces severe illness and significant mortality, particularly in immune-compromised individuals(Howard et al., 2012, Poirel et al., 2011).In the current study, several widely used antibiotics had no effect on the *A. baumannii* isolates.All were resistant to amikacin and sensitive to colistin, which is consistent with findings from other Iranian studies (Vahdani et al., 2011, Saffari et al., 2017). Even though all isolates were susceptible to colistin, colistin remains the most effective antimicrobial agent (Amin et al., 2019). In our study,90.76%and 87.69% of isolates were positive for each*abaI* and *abaR*respectively*;* we also found an association between antibiotic susceptibility and QS genes andrevealed that a greater number of resistance isolates carried both QS genes. This demonstrates that *aba*I and *aba*R genes were substantially linked with multidrug-resistant pathogens, signifying that isolates having QS genes were more likely to be drug-resistant, although the pathogenicity and virulence factors of *A. baumannii* are not completely known. In terms of the incidence of virulence genes, *csg*A 20(30.76%) was the predominant once, and *cva*C 4(6.15%) had the lowest frequency.No correlation was found between virulence genes and biofilm production, but antibiotic susceptibilityisolates carried a greater number of virulence genes than antibiotic insusceptible isolates.The results of this study are consistent with those of an Iraqi investigation showing a maximum frequency of 66.7% for *csgA* and a lowest frequency of *cvaC* (9.5 %), Al-Kadmy et al. (2018a).Comparatively, another study indicated that *cvaC* had lowest frequency only 10% and *csgA* was 55%among tested isolates, Momtaz et al. (2015). Nevertheless, the findings of the current study contrasted withthose of two other studies, Darvishi (2016)and Nazari et al. (2021), whosehighest frequency was *cnf*1(35.53%), and the lowest occurence was*csc*A (12.39%).*A. baumannii* ability to form biofilms isalso largely depend on virulence factors(Rosales-Reyes et al., 2017, Sanchez-Larrayoz et al., 2017). The potential of *A. baumannii* to inhabit and formbiofilm on different surfaces is a crucial element in chronic and persistent infections(Thummeepak et al., 2016). According to our findings, 62(95.38%) *A. baumannii* isolates generated biofilm. Other studies found that greater than 75% of *A. baumannii* isolates develop biofilms, which agrees with our results (Thummeepak et al., 2016, Sung, 2018, Al-Shamiri et al., 2021). Our isolates exhibit a twitching form of motility more than a swarming form, and the majority of both formsof movement were from sputum source, which disagrees with (Loraine et al., 2020, Skerniškytė et al., 2019) who found both forms of motility from other source like blood. According to our finding carbaNP test was able to detect 61.53% of carbapenem producer.Similar findings were detected by other the studies(Khuntayaporn et al., 2021, Nguyen and Joshi, 2021). The use of carbapenems is the very last resort in the fight against illness induced by gram-negative multi-drug resistant pathogens; nonetheless, carbapenem insusceptiblity is becoming more prevalent in *A. baumannii*. Consequently, crucial and precise diagnosis of carbapenemase-producing *A.baumannii* is essential for the treatment effectiveness of these illness.

5. Conclusion

The propensity of *Acinetobacter baumannii* to form biofilms and its resistance to several drugs have made it challenging for healthcare providers to manage and reduce the spread of this pathogen. The vast majority of isolates displayed their ability to form biofilms and carbapenemase production. However, isolates showed a high frequency of the QS genes (*abaI/abaR*), and virulence genes *CsgA* and *ItuA* were more abundant than the others.

6. Ethical considerations

This research was sanctioned by the research ethics committee of Hawler Medical University (Reference number: HMU.PH.EC-20212508-206).

7. Authors' contributions

QS made significant contributions to specimen collection and analysis. GA designed and supervised the research, and contributed substantially to analysis and interpretation of data. QS drafted the manuscript with assistance from GA, and GA revised it for critically important intellectual content.

8. Conflicts of interest

The authors have nothing to declare.

References

AL-Kadmy I, AliA, Salman I,and Khazaal, S. 2018. Molecular characterization of *Acinetobacter baumannii* isolated from Iraqi hospital environment. *New microbes and new infect,***21,** 51-57.

AL-Shamiri M M, Zhang S, Mi P, Liu Y, Xun M, YangE, AI L, Han L,and Chen Y. 2021. Phenotypic and genotypic characteristics of *Acinetobacter baumannii* enrolled in the relationship among antibiotic resistance, biofilm formation and motility. *Microb pathog,***155,** 104922.

Amin M, Navidifar T, ShooshtariF S, Rashno M, SavariM, JahangirmehrF,and Arshadi,M. 2019. Association between biofilm formation, structure, and the expression levels of genes related to biofilm formation and biofilm-specific resistance of *Acinetobacter baumannii* strains isolated from burn infection in Ahvaz, Iran. *Infect Drug Resist,***12,** 3867.

Choi WS, Kim S H, Jeon E G, Son M H, Yoon Y K, Kim J-Y, Kim M J, Sohn J W, Kim M J and Park D W. 2010. Nosocomial outbreak of carbapenem-resistant *Acinetobacter baumannii* in intensive care units and successful outbreak control program. *J Korean medsci,* **25,** 999-1004.

ClemmerKM, Bonomo RA and RatherP N. 2011. Genetic analysis of surface motility in *Acinetobacter baumannii*. *Microbiol,***157,** 2534.

DarvishiM. 2016. Virulence factors profile and antimicrobial resistance of *Acinetobacter baumannii* strains isolated from various infections recovered from immunosuppressive patients. *Biomed Pharmacol J,***9,** 1057-1062.

Dortet L, Poirel L, ErreraC and NordmannP. 2014. CarbAcineto NP test for rapid detection of carbapenemase-producing *Acinetobacter* spp. *J clinic microbiol,***52,** 2359-2364.

Eijkelkamp BA, Stroeher U H, Hassan K A, Paulsen I T. and Brown M H. 2014. Comparative analysis of surface-exposed virulence factors of *Acinetobacter baumannii. BMC genomics,***15,** 1-12.

Eraç B, Yılmaz F, Hoşgör limoncu M, Oztürk Iand Aydemir, S. 2014. Investigation of the virulence factors of multidrug-resistant *Acinetobacter baumannii* isolates. *Mikrobiyol Bul,***48,** 70-81.

Erdönmez D, Rad Y. and Aksöz N. 2017. Quorum sensing molecules production by nosocomial and soil isolates *Acinetobacter baumannii. Archmicrobiol,***199,** 1325-1334.

GajdácsM. and SpenglerG. 2019. The role of drug repurposing in the development of novel antimicrobial drugs: Non-antibiotic pharmacological agents as quorum sensing-inhibitors. *Antibiot J,***8,** 270.

Howard A, O'donoghue M, Feeney A. andSleator R D. 2012. *Acinetobacter baumannii*: an emerging opportunistic pathogen. *Virulence,* **3,** 243-250.

Jahangiri S, Malekzadegan Y, Motamedifar M. and Hadi N. 2019. Virulence genes profile and biofilm formation ability of *Acinetobacter baumannii* strains isolated from inpatients of a tertiary care hospital in southwest of Iran. *Gene Rep,***17,** 100481.

KhuntayapornP, ThirapanmetheeK, KanathumP, Chitsombat K and Chomnawang M T. 2021. Comparative study of phenotypic-based detection assays for carbapenemase-producing *Acinetobacter baumannii* with a proposed algorithm in resource-limited settings. *Plose one,***16,** e0259686.

KIM S W, Choi C H, Moon D C, Jin J S, Lee J H, Shin J-H, Kim J M, Lee Y C, Seol S Y and Cho D T. 2009. Serum resistance of *Acinetobacter baumannii* through the binding of factor H to outer membrane proteins. *FEMS microbiol lett,***301,** 224-231.

Li Z, Ding Z, Liu Y, Jin X, Xie J, Li T, Zeng Z, Wang Z and Liu J. 2021. Phenotypic and genotypic characteristics of biofilm formation in clinical isolates of *Acinetobacter baumannii. Infect drug resist,***14,** 2613.

Loraine J, HeinzE, Soontarach R, BlackwellG A, StablerR A, Voravuthikunchai S P, Srimanote P, Kiratisin P, Thomson NR and Taylor P W. 2020. Genomic and phenotypic analyses of *Acinetobacter baumannii* isolates from three tertiary care hospitals in Thailand. *Front microbiol,***11,** 548.

Martinez J, Razo-gutierrezC, Le C, Courville R, Pimentel C, Liu C, Fung S E, Tuttobene M R, Phan K. and Vila A J. 2021. Cerebrospinal fluid (CSF) augments metabolism and virulence expression factors in *Acinetobacter baumannii. Sci rep,***11,** 1-13.

MomtazH, Seifati S M and Tavakol M. 2015. Determining the prevalence and detection of the most prevalent virulence genes in *Acinetobacter baumannii* isolated from hospital infections. *Int J Med Lab,***2,** 87-97.

NazariM, YouzbashiZ, Khaledi M, Fathi J and Afkhami H. 2021. Detection of carbapenem resistance and virulence genes among *Acinetobacter baumannii* isolated from hospital environments in center of Iran. *J Curr Biomed Rep,* **2,** 14.

Nguyen M. and Joshi S. 2021. Carbapenem resistance in *Acinetobacter baumannii*, and their importance in hospital-acquired infections: a scientific review. *J App Microb,***131,** 2715-2738.

Nowak P, PaluchowskaP and Budak A. 2014. Co-occurrence of carbapenem and aminoglycoside resistance genes among multidrug-resistant clinical isolates of *Acinetobacter baumannii*from Cracow, Poland. *Med sci monitor basic res,***20,** 9.

POIREL, L., BONNIN, R. A. & NORDMANN, P. 2011. Genetic basis of antibiotic resistance in pathogenic *Acinetobacter* species. *IUBMB life,***63,** 1061-1067.

Rosales-reyes, R., Gayosso-vázquez, C., Fernández-vázquez, J. L., Jarillo-quijada M D, Rivera-BenítezC, Santos-PreciadoJ I. and Alcántar-Curiel M D. 2017. Virulence profiles and innate immune responses against highly lethal, multidrug-resistant nosocomial isolates of *Acinetobacter baumannii* from a tertiary care hospital in Mexico. *PLoS One,***12,** e0182899.

Saffari F, Monsen T, KarmostajiA, Azimabad F B. and Widerström M. 2017. Significant spread of extensively drug-resistant *Acinetobacter baumannii* genotypes of clonal complex 92 among intensive care unit patients in a university hospital in southern Iran. *JMed Microbiol,***66,** 1656-1662.

Salman J AS. and Kareem A J. 2021. Antibacterial and Anti virulence factors of Purified Dextran from *Lactobacillus gasseri* against *Pseudomonas aeruginosa. Biological,***2307,** 1191.

Sanchez-Larrayoz A F, Elhosseiny N M, Chevrette M G, Fu Y, Giunta P, Spallanzani RG, Ravi K, Pier G B, Lory Sand Maira-Litrán T. 2017. Complexity of complement resistance factors expressed by *Acinetobacter baumannii* needed for survival in human serum. *The JImmunol,***199,** 2803-2814.

Skerniškytė J, Krasauskas R, Péchoux C, KulakauskasS, Armalytė J and Sužiedėlienė E. 2019. Surface-related features and virulence among *Acinetobacter baumannii* clinical isolates belonging to international clones I and II. *Front microbiol,***9,** 3116.

SungJ Y. 2018. Molecular characterization and antimicrobial susceptibility of biofilm-forming *Acinetobacter baumannii* clinical isolates from Daejeon, Korea. *Korean J Clin Lab Sci,***50,** 100-109.

Tand J, ChenY, Wang X, Ding Y, Sun X. and Ni Z. 2020. Contribution of the AbaI/AbaR quorum sensing system to resistance and virulence of *Acinetobacter baumannii* clinical strains. *Infect Drug Resist,***13,** 4273.

ThummeepakR, KongthaiP, LeungtongkamU and Sitthisak S. 2016. Distribution of virulence genes involved in biofilm formation in multi-drug resistant *Acinetobacter baumannii* clinical isolates. *Int Microbiol,***19,** 121-9.

VahdaniP, Yaghoubi T and Aminzadeh Z. 2011. Hospital acquired antibiotic-resistant *Acinetobacter baumannii* infections in a 400-bed hospital in Tehran, Iran. *Inter J preventive med,***2,** 127.

Zeighami H, ValadkhaniF, Shapouri R, SamadiE and HaghiF. 2019. Virulence characteristics of multidrug resistant biofilm forming *Acinetobacter baumannii* isolated from intensive care unit patients. *BMC infect dis,***19,** 1-9.

Zhang Y, Xu S, Yang Y, Chou S H. and He J. 2022. A 'time bomb'in the human intestine—the multiple emergence and spread of antibiotic-resistant bacteria. *EnvironMicrobiol,***24,** 1231-1246.

Assesing the Impact of Air Pollution on Lichen (*Dirinaria picta* (sw.) Schaer: Morphological Characteristics, Magnetic Grain Analysis, and Elemental Composition

Taufik Taufikurahman[*], Rina Ratnasih Irwanto, and Dora Erawati Saragih

School of Life Sciences and Technology, Institut Teknologi Bandung, 40132 Bandung, Indonesia

Abstract

Dirinaria picta is a lichen species known for its tolerance to air pollution and its ability to accumulate pollutants in its thallus, making it a suitable bioindicator in urban areas. This study aims to assess the response of lichens to air pollution by examining their morphological characteristics, analyzing the presence of magnetic grains, and identifying the origin of elements in their tissues. Samples were collected from three locations in Bandung area which represent polluted areas, namely Juanda Street (JD) and Kebon Kawung (KK), and Padalarang Street (PD) and one location which represent as a control area with low pollution levels, namely Curug Cimahi (CC). Lichen microstructure scanning was performed using a Scanning Electron Microscope (SEM), and the presence of elements was detected through Energy Dispersive X-ray Spectroscopy (EDS). The SEM analysis revealed that samples from areas with higher air pollution levels exhibited obvious damage to their thallus, characterized by a more porous structure and the presence of cuboidal particles. Conversely, samples from control area showed a more compact structure. The EDS observations identified 14 elements present in the lichen tissues, ranked in descending order of abundance: C>Ca>O>Pb>Cu>Mn>Zn>Fe>Cr>Al>Cl>Se>Cd>K. The composition and quantity of these elements in lichen tissues were influenced by the level of air pollution generated by the number of vehicles passing through the area. The more vehicles, the higher the level of air pollution, resulting in greater stress for the D. picta population.

Keywords: Bioindicator, lichen, *Dirinaria picta,* elements, microstructure, Bandung

1. Introduction

Lichens are often used as bioindicators organisms due to their sensitivity to air pollution. They are composite organisms consisting of a symbiotic association between fungi and algae or cyanobacteria. Lichens have sensitivity due to the changes in the environment such as water, temperature, and nutrient (Weber *et al.,* 2016). When exposed to air pollution, lichens can exhibit visible changes in their growth, color, or morphology. By studying these changes, the level and types of pollutants present in the environment can be assessed. Lichen biomonitoring programs involve collecting lichen samples from different locations and analyzing them to determine the extent of air pollution (Sett and Kundu, 2016).

Using lichen as bioindicator and biomonitor has several advantages. Lichens are widespread and can be found in various habitats, including urban, rural, and remote areas. The ability of lichen to accumulate pollutants over time makes it able to provide a historical record of pollution levels in the area. Additionally, using lichens as bioindicator or biomonitor is cost-effective and non-destructive survey, making them suitable for long-term monitoring studies (Giordani, 2007; Sett and Kundu 2016; Kondo *et al.,* 2017; and Benitez *et al.,* 2018).

Air quality can have a significant impact on plant diversity in an ecosystem, particularly in areas near industrial zones or heavily urbanized regions. Air pollution, especially from industrial activities and vehicle emissions, introduces various harmful substances into the atmosphere (Omar and AlKhalil, 2019, Aldgini *et al.,* 2019)**.** Studies conducted in cities across Indonesia, including Jakarta, Semarang, Pekan Baru, Kendari, and Medan, have provided valuable insights into the relationship between lichens and air pollution (Kondo *et al.,* 2017).

The production of chemical elements, including heavy metals, is often associated with the burning of fossil fuels, primarily from vehicles and industrial activities (Nobel *et al.,* 2003). The combustion of fossil fuels releases pollutants into the atmosphere, which can then be deposited onto lichens and other surfaces. Lichens, due to their ability to absorb and accumulate substances from the environment, can serve as indicators of the presence and levels of these harmful elements in the surrounding area (Kim et al., 2007; Aslan et al., 2010; Pirintsos et al., 2011; Polienik *et al.,* 2008). By analyzing the elemental composition of lichens and identifying heavy metal elements like Cd, Cu, Pb, the extent of pollution and the potential risks they pose to both the environment and human health can be predicted (Bold *et al.,* 1987; Al-

---

[*] Corresponding author. e-mail: taufik@itb.ac.id.

Weher, 2008; Omar and AlKhalil, 2019; Alsholaili and Bani-Hasan, 2018)**.** This information can be valuable for monitoring and mitigating the impacts of anthropogenic activities on ecosystems. Analyzing the presence and distribution of these non-metallic elements, including carbon, oxygen, and selenium, can provide insights into the sources and transport mechanisms of pollutants in the environment (Al-Weher, 2008; Omar and AlKhalil, 2019).

Dirinaria picta has been known as lichen species that can tolerate pollution areas of the city (Lawal *et al.,* 2023). *D. picta* is a species that may develop and grow rapidly in urban areas; therefore, *D. picta* can be regarded as inhabitant of urban areas (Abas *et al.,* 2022). A previous study in Greater Bandung showed that *D. picta* species could live in all observed locations based on the value of atmospheric purity, both in the highest and the lowest air polluted areas (*Rahmatia, 2003*; Saragih, 2022).

Based on The Central Board of the Central Bureau of Statistics for the City of Bandung for the 2020 period, Greater Bandung area is one of the 5th most populous areas in Indonesia with the number of vehicles in 2018 reaching 1,811,498 with an average increase of vehicles 5% per year. The ratio of the number of vehicles to the population is 3:4 with 72% of all registered vehicles being motorbikes (The Central Bureau of Statistics for the City of Bandung, 2020).

The emissions from vehicles can include various pollutants such as particulate matter (specifically PM10, referring to particles with a diameter of 10 micrometers or less), lead, carbon monoxide (CO), hydrocarbons (HC), and nitrogen oxides (NOx) (Kim *et al.,* 2007). Monitoring the health and presence of lichens can provide insights into the extent and impacts of heavy metal pollution in ecosystems and help assess the overall health of the environment ecosystems (Urpreti *et al.,*,2015; WHO, 2016; Vannini *et al*., 2021).

This study aims to assess the response of lichens to air pollution by examining their morphological characteristics, analyzing the presence of magnetic grains, and identifying the origin of elements in their tissues. This research is focused on identifying mineral types, microstructure, and mineral content of *D. picta* samples found in Greater Bandung area.

In the investigation of lichens as bioindicators for assessing air pollution, beyond furnishing detail on the diversity and abundance of lichens in regions with differing pollution levels, it is imperative to include supplementary information pertaining to the anatomical status of lichen resulting from exposure to diverse pollutant. This additional data is crucial because alterations in anatomical structure have the potential to lead to the mortality of lichens. Studying the microstructure conditions of lichens, including their mineral and metal contents, is a valuable tool for monitoring and managing environmental pollution. It provides crucial information for understanding the impact of human activities on ecosystems and guides efforts to protect and restore the environment.

2. Material and Methods

Sampling was carried out at three locations in Bandung area heavy traffic sites, namely Juanda street (JD)

(6°52'22"S;107°36'59"E), Kebon Kawung street (KK) (6°54'45"S;107°36'05"E), and Padalarang street (PD) (6°50'38"S;107°29'11"E), and one site with low traffic activity, i.e. Curug Cimahi as a control area (CC) (6°47'55"S;107°34'32"E) (Figure 1). The amount of sample taken was 10 g for each area.

Figure 1. Research Study Area in Bandung City

The four locations show differences in terms of vehicle emissions caused by differences in traffic volume and air environmental conditions. According to the categorization of air quality levels based on IAP values (Kommision Reinhaltung der Luft im VDI und DIN, 1995), the observation station with the highest to the lowest level of air pollution is KK, PD, JD, while CC showed the lowest. IAP was calculated on the preliminary study in four locations (JD, PD, KK, and CC). The results are presented in Table 1.

Table 1. IAP (Index of Atmospheric Purity) measurement results

Location	IAP	Pollution Levels	Information
Juanda Street (JD)	24.85	Level B	Highly polluted
Kebon Kawung Street (KK)	10.21	Level A	Very highly polluted
Raya Padalarang (PD)	17.70	Level B	Highly polluted
Curug Cimahi (CC)	46.65	Level E	Very low polluted

Characterization test of lichen samples from each study location using Scanning Electron Microscopy (SEM) accompanied by Electron Dispersive Spectroscopy (EDS) was carried out to observe how the shape of the topographic structure or lichen surface, structural defects, shape, and size of material granules, as well as an elemental composition and impurities in the lichen sample. The analysis of the structure and composition of the lichen was carried out in the laboratory of the Geological Survey Center Laboratory, Bandung. The sample was fixed using formalin then dehydrated and embedded in paraffin. The sample was then sliced using a microtome with a final sample thickness of 3μm, then the incision was placed on an object glass. Furthermore, the incision was deparaffinized by washing it with xylene at 37°C for 2 hours. After that, the samples were washed using 100% ethanol at room temperature for 1 hour. The samples were then left overnight at room temperature to dry (Saragih, 2022).

Before being observed by SEM, the sample was glued to carbon tape that had been placed in a cuvette and then coated with a conductive layer, namely aluminum using an ion sputtering machine for 1 minute. The cuvettes were then placed in the specimen holder and inserted into the scan tool. Observations to scan the topography and morphology of the sample were carried out with an accelerating voltage of 20 kV with a magnification of 2000x (determination of the elemental composition of individual particles), 1000x and 5000x magnification (lichen surface), and 1000x magnification (lichen cross-section) (Conti *et al.,* 2001).

3. Results and Discussion

3.1. Micrograph Cross-Sectional

A comparison of the results of cross-sectional micrograph analysis of the *D. picta* samples that were obtained from KK (very highly polluted) and CC (very low polluted) are shown in figure 2 (A and B). Sample of *D. picta* that was collected from KK location had cubes resembling particles with uneven and irregular sizes, while sample of *D. picta* that was collected from CC location showed less number of those particles. Lichen that live on high levels of pollution absorb more particles than lichen that live on low level of pollution, and this particle was shown uneven and irregular sizes, which could disrupt metabolic processes in lichen tissue and lead to the death of the tissue (Taufikurahman *et al.,* 2010).

(A)   (B)
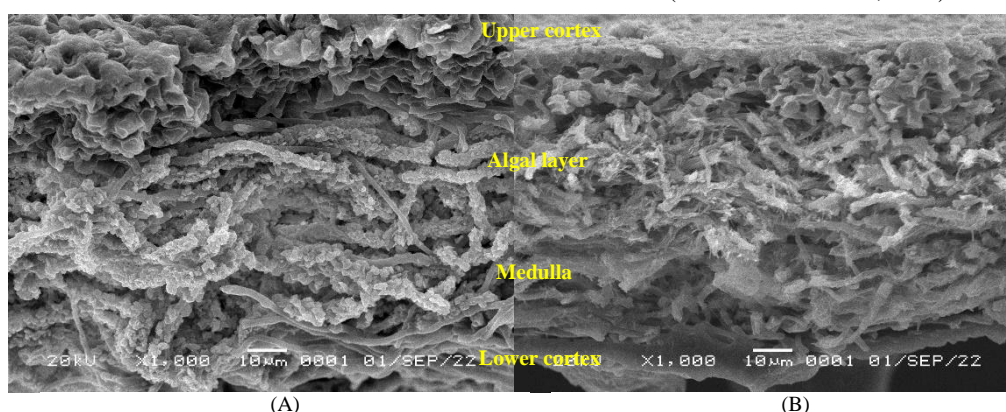
Figure 2. Micrograph cross-sectional SEM images of *D. picta* (1000x magnification) from: (A) KK location (very high polluted area); (B) CC location (very low polluted area).

The tissue in figure 2A (on area with high pollution) appears more sparse compared to figure 2B (area with low pollution). The presence of pollutants causes gaps in the algal tissue and medulla. The damage, porous structure, and accumulation of particles seen in lichens from polluted areas are a consequence of the pollutants emitted by vehicles, industries/factories, and other human activities, while lichens from unpolluted areas maintain a healthier and more intact surface structure (Kim *et al.,* 2007; Wintermans *et al.,* 1965).

3.2. Optical Micrography

Optical micrography results of an examination of the surface microstructure of the *D. picta* thallus at 1000x magnification with a resolution of 10µm and a voltage of 20 kV can be seen in Figure 3 (A-D). It can be observed that lichens from areas with higher levels of air pollution exhibit visible damage to their thallus. Air pollutants can lead to a porous structure in the lichen and an accumulation of particles that form cubes on the surface of the thallus. In contrast, lichen samples from very low polluted area typically have a more compact and denser structure due to the lower levels of air pollution, and there is no significant accumulation of particles observed on the surface of the lichen's thallus (Taufikurahman *et al.,* 2010). The accumulation of pollutants, especially heavy metals, in the lichen thallus can lead to a range of physiological and structural changes in these organisms (Tripp *et al.,* 2016). This disparity in surface structure between lichens from polluted and unpolluted areas serves as a notable indicator of the impact of air pollution on lichens.

(A)   (B)

(C)   (D)
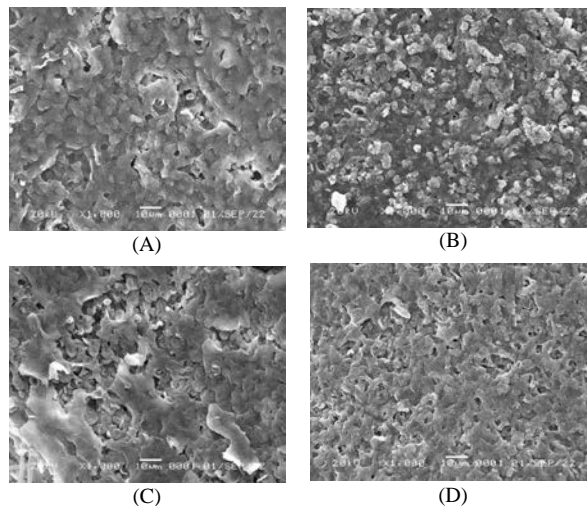
Figure 3. SEM image micrograph surface of the *D. picta* sample (1000x magnification). Sample were obtained from: (B) JD (Highly polluted area); (A) KK (highest polluted area); (C) PD (Highly polluted area); (D) CC (lowest polluted area)

3.3. Topographical Structure

The differences in the topographical structure and defects in the surface structure of the lichen samples from each study location can be seen in SEM-EDS with a magnification of 5000x with a resolution of 5µm and a voltage of 20 kV (Figure 4). The results of surface and elemental composition observations showed that lichens in highly polluted areas appear to have many cube-shaped particles which is magnetic grains, whereas at lower

pollution levels, the number of cube-shaped particles is less. Meanwhile, in areas with very low pollution, no cubic particles were seen.

(A) (B)
(C) (D)
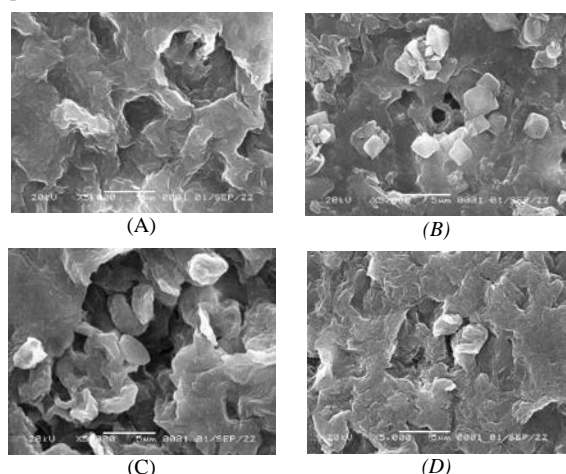
Figure 4. SEM image micrograph of the surface and elemental composition of the talus of the *D. picta* sample (5000x magnification) from: (A) JD (Highly polluted area); (B) KK (Very highly polluted area); (C) PD (Highly polluted area); (D) CC (Very low polluted area)

Magnetic grains in the sample which have been suggested to come from two different sources, namely pedogenic and anthropogenic. In the samples obtained from KK (very highly polluted) and PD (highly polluted area), there are a few magnetic grains that have an octahedral or angular shape. These grains show signs of damage at the corners, indicating that they might originate from pedogenic sources, such as natural magnetic minerals found in the environment (Olomukoro and Azubuike, 2009). On the other hand, the dominant spherical grains are believed to come from anthropogenic sources from polluted area. These grains are typically associated with ash or dust found on the sides of roads, as well as pollutants emitted from the burning of fossil fuels by vehicles (Ribeiro *et al.,* 2016; Richardson, 1993).

3.4. Elemental Composition

The results of the analysis of elemental composition in the lichen samples indicated the presence of several elements present in the thallus. Several metallic and non-metallic elements were detected in all samples including C, Ca, O, Pb, Cu, Mn, Zn, Fe, Cr, Al, Cl, Se, Cd, and K (Table 2). The average EDS spectrum of *D. picta* shows the percentage by weight of elements (%) found in the lichen thallus from highest to lowest to be C>Ca>O>Pb>Cu>Mn>Zn>Fe>Cr> Al>Cl>Se>Cd>K (Figure 5).

The number of elements found in highly polluted areas (KK) was 12 elements, while in less polluted areas (PD and JD) 11 elements. In contrast, area with very low pollution (CC), only 8 elements were found. C levels at all locations were the highest in lichen tissue compared to other elements (more than ten times), with the lowest C value (54.57%) found in highly polluted areas and the highest C value (63.82%) in areas with lower pollution. Compared to polluted area, percentage of Pb levels in low polluted area was very low (2.07%), while oxygen (13.26%) and Ca levels (12.56%) showed the highest level. In polluted areas, the accumulation of polluting elements causes oxygen and Ca levels in lichen tissue to decrease.

Carbon and oxygen are non-metallic elements that can be found in both solid and gaseous forms. In the air, oxygen constitutes approximately 20.95% of the composition of dry air. Carbon can be present in the form of aerosols or small solid objects that are suspended in the air. Carbon aerosols can originate from various sources, including combustion processes, industrial emissions, vehicle exhaust, and natural sources such as wildfires. These aerosols can contain carbonaceous particles, which contribute to air pollution and can be deposited on surfaces such as lichen thalli (WHO 2016).

Table 2. Elemental composition in *D. picta* samples obtain from EDS analysis

Element	Mass (%)			
	KK (Very highly polluted area)	PD (Highly polluted area)	JD (Highly polluted area)	CC (Very low polluted area)
C	54.57	59.29	63.82	61.43
O	3.85	7.23	4.48	13.26
Al	1.52	0.57	3.02	0.42
Cl	1.92	-	0.41	-
K	1.05	-	1.21	-
Ca	8.05	7.47	6.93	12.56
Cr	7.02	-	-	-
Mn	4.17	5.14	4.36	-
Fe	2.38	2.19	1.3	3.41
Cu	6.16	5.97	6.18	3.61
Zn	2.09	4.05	2.77	3.24
Pb	8.27	7.5	6.73	2.07
Se	-	0.35	-	-
Cd	-	0.24	-	-
Total	100	100	100	100

The analysis of elemental composition in lichens could provide information on sources and types of contamination in the research area. The elemental composition and mass percentages found in lichens are influenced by both biological processes carried out by the lichens themselves and anthropogenic inputs from human activities (WHO, 2016). Road traffic activity, in particular, can contribute to the contamination of lichens by increasing the emission of soil particles that are absorbed into the lichen thallus. These particles can contain various elements, including heavy metals such as Cd, Cu, and Pb (Cite). These heavy metal elements are known to be harmful to human health (Urpeti *et al.,* 2015; Kim *et al.,* 2007**;** Ezemonye and Tongo, 2009).

In addition, the non-metallic element found in the samples is selenium (Se). Se element can be naturally present in soil and rocks, and it can become airborne through processes such as wind erosion or human activities like mining and agricultural practices (Omar and AlKhalil, 2019; Ezemonye and Tongo, 2009)**.** The presence of Se in lichen samples suggests that it may have originated from the deposition of soil particles onto the lichen thallus (Aslan *et al.,* 2010; Vannini *et al.,* 2021).
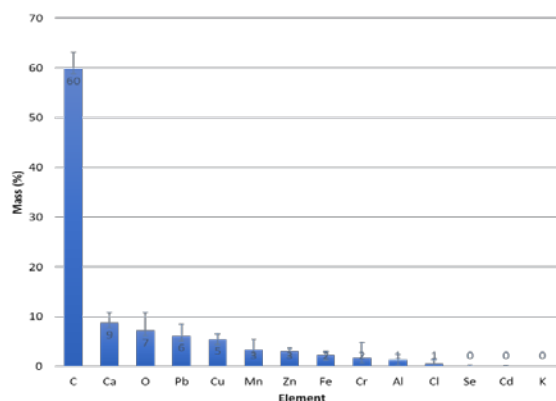
Figure 5. Element composition and the average elemental mass in samples of lichen D.*picta*;Bar showed standar deviation

The accumulation of particles in the algal layer and medulla of *D. picta* is influenced by pollution from vehicles and daily weather conditions. When the lichen is hydrated, it can absorb nutrients and contaminants directly from the air through its surface (Varela *et al.,* 2018; Tripp *et al.,* 2016; Urpeti *et al.,* 2015). These substances are then concentrated and transformed into a slow-release form within the lichen's structure. This process allows the lichen to efficiently extract and store nutrients while also retaining pollutants present in the surrounding environment (Pirintsos *et al.,* 2011; Vannini *et al.,* 2021).

The particles that accumulate in the algal layer will interfere with the photosynthesis process in the lichen because the chlorophyll in the algal layer cannot function optimally to absorb sunlight in the form of electrons, so the photosynthesis process will be disrupted due to being covered by ever-increasing particles (Aslan *et al.,* 2010; Kim *et al.,* 2007).

The specific types of contaminants and their sources may vary depending on the location and environmental conditions (Aldgini *et al.,* 2019; Al-Weher, 2008; Kim *et al.,* 2007). Vehicle emissions, which often contain pollutants such as particulate matter, nitrogen oxides, and sulfur compounds, can contribute to the accumulation of particles in lichens. Additionally, weather conditions, such as wind patterns or atmospheric deposition, can also influence the level of particle deposition on lichens (Kim *et al.,* 2007; Tripp *et al.,* 2016).

The presence of Zn is often associated with urban and industrial areas. Industrial processes, emissions from factories, and urban pollution, including vehicle exhaust, can release zinc-containing particles into the air (Omar and AlKhalil, 2019). Element Mn on the other hand, is generally linked to agricultural activities. Agricultural practices, such as the use of fertilizers or the application of pesticides, can introduce manganese into the environment (Ezemonye and Tongo, 2009). It can then be transported through air or water and subsequently deposited onto lichen thallus.

Element Fe in lichen thallus are often associated with the contribution of small soil and airborne particles, including dust, smoke, and vapor, with a diameter of fewer than 100 micrometers. These particles can be derived from various sources, including natural processes (e.g., wind erosion, volcanic emissions) and human activities (e.g., combustion of fossil fuels, industrial emissions) (Nobel *et al.,* 2003; Omar and AlKhalil, 2019). The deposition of these particles onto lichen surfaces can lead to the accumulation of Fe in lichen thalli (Aslan *et al.,* 2010; Vannini *et al.,* 2021). The accumulation of heavy metal elements such as Pb, Cu, Cd, Al, Zn, and Cr in lichens can have detrimental effects on their health and survival.

When lichens are exposed to high levels of these heavy metals, they can exhibit various symptoms of damage and stress such as chlorosis and necrosis. This discoloration occurs due to the disruption of chlorophyll production and photosynthetic processes (Cevik *et al.,* 2008; Kondo *et al.,* 2017). The accumulation of heavy metals can disrupt cellular functions and lead to the death of lichen tissues, resulting in the browning or blackening of affected areas (Benitez *et al.,* 2018; Kaffer *et al.,* 2011). The toxic effects of heavy metals can impair the lichen's metabolic processes (Muthu *et al.,* 2020), including nutrient absorption, respiration, and reproduction, leading to their decline and eventual death.

Heavy metal elements such as Pb, Cu, and Cd are harmful to human health (Giordani 2007; Rundel 1978; Robiansyah 2006). The amount of these elements in the air is affected by the volume or density of traffic, distance from highways and industrial areas, and wind direction. Other elements such as Ca and K (alkaline earth metals) are thought to accumulate in lichen due to particles in the form of dust carried by the wind, while Cl elements (halogen gases) are elements with a low pH and are acidic (Aslan *et al.,* 2010; Vannini *et al.,* 2021). The presence of Cl in a lichen is thought to occur due to the accumulation of rainwater flow and the absorption mechanism of lichen from its substrate.

The biodiversity of organisms like lichen, fungi, and those attached to plant parts like fruits and leaves refers to the physiochemical properties of the environment such as PH of the soil, temperature, and humidity (Alsohaili and Bani-Hasan, 2018). Different environmental conditions create distinct habitats, which, in turn, affect the types of organisms that can thrive in those environments (Sett & Kundu 2016)**.**

4. Conclusion

Lichens from areas with higher levels of air pollution showed obvious damage to the thallus, resulting in a more porous structure and the accumulation of cube-like particles on the surface. Lichens exposed to high levels of pollution absorbed more particles than those in areas with low pollution levels. These particles were uneven and irregular in size, which could disrupt metabolic processes in lichen tissue and potentially lead to tissue death. Meanwhile, lichen samples from very low polluted areas had a smoother and compact surface structure and showed no piles of particles. The number of elements found in highly polluted areas was higher than in less polluted areas.

Acknowledgment

References

Abas, A., Asnawi, N. H., Aiyub, K., Awang, A., & Abdullah, S. R. 2022. Lichen Biodiversity Index (LBI) for the Assessment of Air Quality in an Industrial City in Pahang, Malaysia. *Atmos.*, *13*(**11**), 1905.

Aldgini, H. M., Al-Abbadi, A. A., Abu-Nameh, E. S., & Alghazeer, R. O. 2019. Determination of metals as bio indicators in some selected bee pollen samples. *Jordan J. Biol. Sci.* **26**(**7**): 1418-1422.

Alsohaili, S. A., & Bani-Hasan, B. M. 2018. Morphological and molecular identification of fungi isolated from different environmental sources in the Northern Eastern desert of Jordan. *Jordan J. Biol. Sci.*, 11(3).

Al-Weher, S. M. 2008. Levels of heavy metal Cd, Cu and Zn in three fish species collected from the Northern Jordan Valley, Jordan. *Jordan J. Biol. Sci.*, *1*(**1**): 41-46.

Aslan, A., Apaydın, G., Yazıcı, K., Cengiz, E., Aylıkcı, V., and Tırasoglu, E. 2010. Analysis of Trace Element Concentrations of Some Lichens of Turkey. *Asian J. Chem.*, **22**(**1**): 389-400.

Benítez, A., Aragón, G., González, Y., and Prieto, M. 2018. Functional traits of epiphytic lichens in response to forest disturbance and as predictors of total richness and diversity. *Ecol. Indic.*, **86**.18–26.

Bold, H. C., Alexopoulus, C.J., and Delevoryas, T. 1987. *Morphology of Plants and Fungi,* Fifth edition. Harper and Row Publishers, New York.

Cevik, U., Damla, N., Kobya, A.I., Bulut, V.N., Duran, C., Dalgic, G., and Bozaci, R. 2008. Assesment of metal element concentrations in mussel (M. galloprovincialis) in Eastern Black Sea, Turkey. *J. Hazard. Mater.*, **160**: 396–401.

Conti, M. E., and Cecchetti, G. 2001. Biological monitoring. Lichens as bioindicators of air pollution assessment. A review *Environ. Pollut.*, **114**(**3**): 471-492.

Ezemonye, L. I. N., and Tongo, I. 2009. Lethal and sublethal effects of atrazine to amphibian larvae. *Jordan J. Biol. Sci.*, 2(1): 29-36.

Giordani, P. 2007. Is the Diversity of Epiphytic Lichens a Reliable Indicator of Air Pollution? A Case Study from Italy. *Environ. Pollut.*, **146**: 317-323.

Kaffer, M.I., Martins, S.M.D.A., Alves, C., Pereira, V.C., Fachel, J., and Vargas, V.M.F. 2011. Corticolous Likens as Environmental Indikators in Urban Areas in Southern Brazil. *Ecol. Indic.*, **11**: 1319–1332.

Kim, W.S.J., Doh, Y.H., and Park, Y.S.T. 2007. Two-year magnetic monitoring in conjunction with geochemical and electron microscopic data of roadside dust in Seoul, Korea. *Atmos. Environ.*, **41**: 7627–7641.

Kommision Reinhaltung der Luft im VDI und DIN, 1995. Messen von Immissions wirkungen. *Measurement of Immission Effects*, Dusseldorf.

Kondo, A., Hamonangan, S., Soda, A., Kaga, Y., Inoue, Y., Eguchi, M., and Yasaka, Y. (2017). Impacts of converting from leaded to unleaded gasoline on ambient lead concentration in Jakarta metropolitan area. *J. Environ. Sci.*, **23**: 709-713.

Lawal, O., Ogugbue, C. J., & Imam, T. S. 2023. Mining association rules between lichens and air quality to support urban air quality monitoring in Nigeria. *Heliyon*, 9(1).

Muthu, S., Murugan, M., Rajendran, K., & Ponnusamy, P. 2021. An Assessment of Proximate Composition, Antioxidant Activities and LC/MS Based Phytochemical Profiling of Some Lichen Species Collected From Western Ghats of Southern Part of India. *Jordan J. Biol. Sci.*, *14*(4).

Nobel, W., Kost-Rick, R., Honnen, W., and Blum, T. 2003. *Metal Biomonitoring Near A Heavily-Trafficked High Way Using Standardized Methods.* Departement of Apllied Chemistry, University of Applied Sciences.

Olomukoro, J. O., & Azubuike, C. N. 2009. Heavy metals and macroinvertebrate communities in bottom sediment of Ekpan Creek, Warri, Nigeria. *Jordan J. Biol. Sci.*, *2*(**1**): 1-8.

Omar, G. I., and AlKhalil, S. I. 2019. A Study of the Environmental Impacts of the Gishori Industrial Complex on Plant Diversity in Tulkarm, Palestine. *Jordan J. Biol. Sci.*, *12*(4).

Pirintsos, S.A., Paoli, L., Loppi, S., and Kotzabasis, K. 2011. Photosynthetic performance of lichen transplants as early indicator of climatic stress along an altitudinal gradient in the arid Mediterranean area. *Clim. Change.*, **3**: 305–328.

Polienik, H., Simoncic, F., and Batic, F. 2008. Monitoring Air Quality with Lichenes. A Comparison between Mapping in Forest Sites and in Open Areas. *Environ. Pollut.*, **151**: 395-400.

Rahmatia, D. 2003. *Hubungan Mikroklimat dan pH Substrat di Hutan Pinus, Transisi, dan Campuran Gunung Tangkuban Perahu Terhadap Kadar Asam Usnat Liken Kerak Usnea sp.* Undergraduate Thesis in Biology, School and Life Technology ITB., 66-68

Ribeiro, M.C., Pinho, P., Branquinho, C., Llop, E., and Pereira, M.J. 2016. Geostatistical uncertainty to assess air quality using high spatial resolution lichen data. a health study in the urban area of Sines. *Portugal Sci. Total Environ.*, **562**: 740–750.

Richardson, D. H. S. 1993. *The physiology of drying and rewetting in lichens*. pp. 275-296 in *Stress Tolerance of Fungi* (Ed. DH Jennings). Academic Press, London.

Robiansyah, I. 2006. Lepraria sp. Sebagai Indikator Pencemaran Timbal (Pb) di Udara Pada Tiga Lokasi di Kota Bandung. *Skripsi Sarjana Biologi*. Undergraduate Thesis in Biology, School and Life Technology ITB.

Rundel, P.W. 1978. The ecological role of secondary lichen substances. *Biochem. Syst. Ecol.*, **6**: 157–170.

Sett, R., and Kundu, M. 2016. Epiphytic Lichens - Their Usefulness as Bioindicators of Air Pollution. *DJRES.*, **3**. 17-24.

Saragih, D. E. 2022. *Biomonitoring of Environmental Quality and Characterization of Lichene Microstructure as Bioindicators of Pollution Levels in Greater Bandung area*, Master's Thesis, Institut Teknologi Bandung.

Taufikurahman., Fernando, M., and Sari, R. M., 2010. Using Lichen As Bioindicator For Detecting Level Of Environmental Pollution. *Proceedings of the Third International Conference on Mathematics and Natural Sciences (ICMNS 2010)*. pp 388-394

The Central Bureau of Statistics for the City of Bandung. 2020https://bandungkota.bps.go.id/subject/17/transportasi.html. Downloaded on February 2, 2023

Tripp, E.A., Lendemer, J.C., Barberán, A., Dunn, R.R., and Fierer, N. 2016. Biodiversity gradients in obligate symbiotic organisms. exploring the diversity and traits of lichen propagules across the United States. *J. Biogeogr.*, **43**: 1667–1678.

Upreti, D.K., Bajpai, R., Nayaka, S. 2015. Lichenology. Current Research in India *in* Bahadur, B., Venkat Rajam, M., Sahijram, L., Krishnamurthy, K. (eds) *Plant Biology and Biotechnology*. Springer, New Delhi.

Vannini, A., Tedesco, R., Loppi, S., Di Cecco, V., Di Martino, L., Nascimbene, J., Dallo, F., Barbante, C. 2021. Lichens as monitors of the deposition of potentially toxic elements in high elevation Mediterranean ecosistems. *Sci. Total Environ.*, **798**: 149-169.

Varela, Z., López-Sánchez, G., Yáñez, M., Pérez, C., Fernandéz, J.A., Matos, P., Branquinho, C., and Aboal, J.R. 2018. Changes in epiphytic lichen diversity are associated with air particulate matter levels. the case study of urban areas in Chile. *Ecol. Indic.,* **91**: 307–314.

Wintermans, D. M. 1965. Spectrophotometric Characteristics of Chlorophylls *a* and *b* and Their Phenophytins in Ethanol. *Biochim. Biophys. Acta.,* **2**: 448-453.

Weber B, Büdel B, Belnap J. 2016. *Biological soil crusts as an organizing principle in drylands*. Cham, Switzerland: Springer.

WHO. 2016. WHO Releases Country Estimates on Air Pollution Exposure and Health Impact, https://apps.who.int/mediacentre/news/releases/2016/airpollutionestimates/en\/index.html. Downloaded on February 2, 2023.

Evaluation of Bis-biphenyl Salicylaldehyde Schiff Base Derivatives for Alpha-Glucosidase Inhibition: Anticancerous Activity and Molecular Modelling Studies

Taher S. Ababneh[1,*], Taghreed M. Jazzazi[1], Mazhar Al Zoubi[2], Tareq. M. Alshboul[3], Walhan Alshaer[4], Abd Al-Aziz A. Abu-Saleh[5], Mansour H. Almatarneh[6], Mohammed-Jamal A. Shammout[7], Iyad Y. Natsheh[8], Majd M. Alsaleh[8]

[1]*Department of Chemistry, Yarmouk University, Irbid 21163, Jordan, email: tababneh@yu.edu.jo;* [2]*Department of Basic Medical Sciences, Faculty of Medicine, Yarmouk University, Irbid 21163, Jordan;* [3]*Department Of Scientific Service Courses, Faculty of Science,Yarmouk University, Irbid 21163, Jordan;* [4]*Cell Therapy Center, The University of Jordan, Amman 11942, Jordan;* [5]*Department of Chemistry and Biochemistry, University of Windsor, ON, N9B 3P4, Canada;* [6]*Department of Chemistry, The University of Jordan, Amman 11942, Jordan;* [7]*Chemistry Department, Faculty of Science, Applied Science Private University, P.O. Box 166, Amman 11931, Jordan;* [8]*Department of Medical Applied Sciences, Zarqa University College, Al-Balqa Applied University, Salt, Jordan*

Abstract

In this study, we have successfully synthesized four symmetrical Schiff base ligands (L1, L2, L3 and L4), through the condensation reaction of 2,2'-diamino-4,4'-dimethyl-1,1'-biphenyl with 2-hydroxy-3-methoxy-5-nitrobenzaldehyde, 3-bromo-5-chloro-2-hydroxybenzaldehyde, 2-hydroxy-5-methoxy-3-nitrobenzaldehyde and 3-bromo-2-hydroxy-5-nitrobenzaldehyde, respectively. Characterization of the ligands was accomplished using elemental analysis, and infrared spectroscopy. To elucidate their potential biological activity, the binding affinities of the synthesized compounds towards alpha-glucosidase inhibition were assessed employing induced-fit molecular docking calculations. The docking analysis revealed diverse interactions, such as salt-bridge, hydrogen bonding, π-stacking, and hydrophobic interactions, facilitating a proper fit of these compounds into the binding pocket of α-glucosidase. Additionally, the prepared ligands' anti-cancer potential was evaluated against various cell lines. In the initial investigation, the IC_{50} of the synthesized compounds against three cancer cell lines (MDA-MB-231, MCF-7, and A549) and a normal fibroblast cell line (HDF) as a control was determined using the MTT assay. The results demonstrated a decreasing selective cytotoxic effect of compounds L1, L3, and L2 against the MDA-MB-231 breast cancer cell line. Additionally, compound L1 exhibited the lowest IC_{50} value against the A549 lung cancer cell line. Subsequently, the cytotoxic impact of the bis-biphenyl salicylaldehyde Schiff base derivatives were further explored on the MDA-MB-231 breast cancer cell line using the MTT assay. The results revealed that the derivatives demonstrated noteworthy cytotoxic activity against the cancer cell line, with compound (L3) exhibiting the highest toxic effect at a concentration of 25 µg/ml, resulting in a reduction of cell viability by 34.23% compared to the control group. These findings highlight the promising anti-cancer properties of the synthesized ligands and warrant further exploration of their potential applications.

Keywords: Schiff bases, molecular docking, α-glucosidase, anti-cancer

1. Introduction

Diamine Schiff bases are a type of organic compound consisting of a Schiff base linkage (-N=CH-) formed from the reaction of a diamine and an aldehyde or ketone. The diamine portion of the molecule consists of two amino groups ($-NH_2$) attached to a biphenyl or naphthalene core, while the aldehyde or ketone component is usually an aromatic or heteroaromatic derivative such as salicylaldehyde or pyridine-2-carboxaldehyde (Dalia *et al.*, 2018). Schiff bases have received significant attention in recent years due to their wide array of pharmacological properties including but not confined to antimicrobial (Chambhare *et al.*, 2003), antifungal (Chohan *et al.*, 2010), anticancer (Gupta*et al.*, 2023), and anti-inflammatory (Przybylski *et al.*, 2009) activities.

Recently, we have reported the synthesis, catalytic applications and antiproliferative effects of Schiff base derivatives of 2,2'-diamino-1,1'-biphenyl-salicylaldehyde (Ababneh *et al.*, 2021; Jazzazi, *et al.*, 2019; Al-Shboul *et al.*, 2018). Herein, we present the preparation and characterization of four novel symmetrical Schiff base ligands (L1, L2, L3 and L4) via the condensation reaction of 2,2'-diamino-4,4'-dimethyl-1,1'-biphenyl with salicylaldehyde derivatives, as demonstrated in **Scheme 1**.

The analysis of bis-biphenyl salicylaldehyde Schiff base derivatives as possible inhibitors of alpha-glucosidase by the incorporation of molecular dynamics (MD) simulations, represents a significant step in the search for

---

* Corresponding author. e-mail: tababneh@yu.edu.jo.

effective anti-diabetic medications. These Schiff base compounds have demonstrated significant promise for inhibiting alpha-glucosidase, a key enzyme in the breakdown of carbohydrates (Daoud, *et al.*, 2021). In this work, we have performed a molecular docking analysis on the human α-glucosidase enzyme to gain insights into the interactions between the ligands and the enzyme and to attain an understanding of the stability and conformational dynamics exhibited by ligand-enzyme complexes.
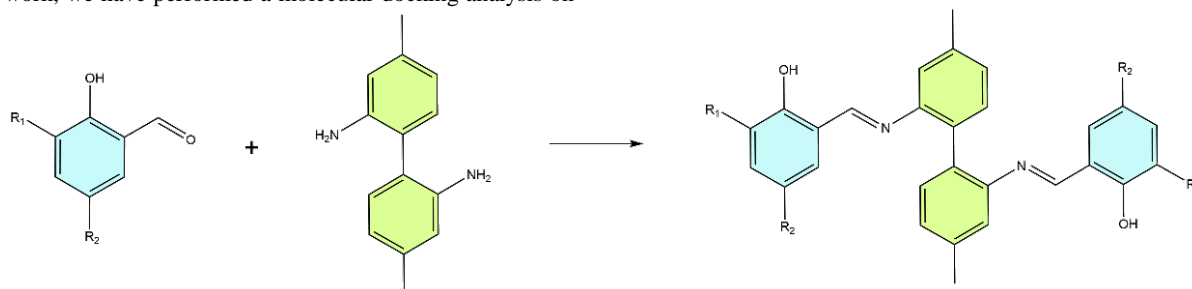
Scheme 1. Synthesis of L1 (R_1=OCH$_3$, R_2=NO$_2$), L2 (R_1=Br, R_2=Cl), L3 (R_1= NO$_2$, R_2= OCH$_3$) and L4 (R_1=Br, R_2=NO$_2$) Schiff base ligands via the reaction of 2,2'-diamino-4,4'-dimethyl-1,1'-biphenyl with 2-hydroxy-3-methoxy-5-nitrobenzaldehyde,3-bromo-5-chloro-2-hydroxybenzaldehyde, 2-hydroxy-5-methoxy-3-nitrobenzaldehyde and 3-bromo-2-hydroxy-5-nitrobenzaldehyde in a 1:2 molar ratio, respectively.

Building upon our analysis of the interaction dynamics between Schiff base compounds and alpha-glucosidase through molecular docking, our investigation extends to evaluate the cytotoxic impact of the newly synthesized bis-biphenyl-salicylaldehyde Schiff base derivatives (L1, L2, L3, and L4) against three cancer cell lines (MDA-MB-231, MCF-7, and A549) along with a normal fibroblast cell line (HDF) serving as a control. Triple-negative breast cancer (TNBC) has a greater morbidity than other breast cancer (BC) types because of its high molecular heterogeneity, propensity for metastatic spread, and poor prognosis. Because TNBC lacks the ER, PR, and HER2 receptors for estrogen, progesterone, and human epidermal growth factor, there are currently no viable treatments for TNBC (Chang-Qing*et al.*, 2020). TNBC is not susceptible to endocrine treatment or molecular targeted therapy because of its unique molecular profile. As a result, chemotherapy is the primary systemic treatment, although postoperative adjuvant chemoradiotherapy is ineffective. Tumor recurrence will eventually result from the remaining metastatic lesions. In certain nations, bevacizumab has been used in conjunction with chemotherapeutic medications to treat TNBC; however, this has not appreciably increased patient survival time (Yin *et al.*, 2020; Shawish *et al.*, 2023). Therefore, the creation of novel treatment plans and objectives is essential.

2. Materials and Methods

2.1. Synthesis and Characterization of Schiff Bases

The elemental analyses (C, H and N) were carried out on a Perkin Elmer 240 elemental analyzer. ^{1}H-NMR spectra were recorded on a Bruker AC 400 spectrometer in CDCl$_3$. Infrared spectra were recorded using KBr on Bruker FT-IR-4100 spectrometer over the range 4000–400 cm^{-1}. All commercially available substrates were used without further purification. The target amine reactant, 2,2'-diamino-4,4'-dimethyl-1,1'-biphenyl, was synthesized as a yellow solid with a yield of 89% following a procedure described in a previously published work (Al-Shboul *et al.*, 2018).

The synthetic protocol for Schiff bases (L1, L2, L3 and L4) involved the combination of 0.471 mmol of 2,2'-diamino-4,4'-dimethyl-1,1'-biphenyl with 0.942 mmol of a salicylaldehyde derivative in 20 ml of absolute methanol. The resulting mixture was refluxed overnight, during which time the corresponding Schiff base precipitated as a colored solid. The solid was subsequently collected through filtration, washed with cold methanol, and dried to yield the desired product, as depicted in **Scheme 1**.

Infrared spectra of the prepared ligands exhibit a characteristic peak at (1620-1637) cm^{-1} attributed to the imine (C=N) moiety, where the broad bands observed at (3048-3070) cm^{-1} are due to the presence of OH groups.

The results of the elemental analysis, which align with the calculated values and physical properties of the obtained ligands (L1, L2, L3 and L4) are reported in **Table 1**.

Table 1. Elemental analysis results and other physical properties of the isolated ligands

Ligand	Formula	F.Wt (g/mol)	Color	Yield (%)	Elemental Analyses Calculated (Found) (%) C H N
L1	$C_{30}H_{26}N_4O_8$	570.55	Red	49.2	63.15, 4.59, 9.82 (63.08), (4.45), (9.81)
L2	$C_{28}H_{20}Br_2Cl_2N_2O_2$	647.18	yellow	54.32	51.96, 3.12, 4.33 (51.89), (3.10), (4.31)
L3	$C_{30}H_{26}N_4O_8$	570.55	Red	60.58	63.15, 4.59, 9.82 (63.12), (4.52), (9.79)
L4	$C_{28}H_{20}Br_2N_4O_6$	668.29	orange	53.06	50.32, 3.02, 8.38 (50.29), (2.99), (8.35)

The spectral data obtained from the ^{1}H NMR analysis of the isolated Schiff bases have been selectively presented in **Table 2**.

Table 2. Selected ^{1}H-NMR parameters of the Schiff bases

	L1	L2	L3	L4
^{1}H NMR				
δ(OH)	14.08	13.29	13.52	15.06
δ(N=CH)	8.38	8.15	8.36	8.46
δ(CH$_3$)	2.41	2.39	2.39	2.43
δ(OCH$_3$)	3.88	-	3.71	-

2.2. Alpha-glucosidase docking study methodology

The initial coordinates of the human lysosomal acid α-glucosidase protein were retrieved from the RCSB [PDB entry 5NN8] determined at 2.45 Å resolution (Roig-Zamboni*et al*., 2017). We prepared the protein using the Protein Preparation Wizard (Sastry *et al*., 2013) of Schrodinger software to resolve clashes and missing atoms. This procedure addresses steric hindrance and unfavorable interactions among atoms, enhancing the accuracy of the protein structure by optimizing side-chain conformations and resolving clashes resulting from overlapping atoms. Protonation states of titratable residues were assigned using PROPKA (Bas *et al*., 2008). To conduct the molecular docking, we removed the co-crystalized ligand (acarbose) and waters from the binding pocket. The grid cell is located at the active site of the protein and centroid to the co-crystallized ligand. LigPrep tool of Schrodinger software (Schrödinger, LLC, New York, NY, 2021) was used to generate and minimize conformations (i.e., ring conformations and stereoisomers) of the compounds. Epik software (Shelley *et al*., 2007) was used for proper treatment of compound protonation states at a pH of 7.4 (±1). Finally, the prepared compounds were docked into the binding pocket of the preprocessed protein pocket by utilizing the induced fit docking (IFD) protocol (Sherman *et al*., 2006). IFD accounts for both ligand and protein flexibility, which results in an optimal protein-ligand binding mode. The glide extra precision (XP) docking score was chosen as the measure of the binding affinity of the compounds with the best-docked poses. To validate our docking experiment, we compared the docked poses generated by the induced-fit docking with the crystallographic pose of acarbose complexed within the α-glucosidase enzyme. The RMSD value of 1.48 Å (**Figure 1**) indicated that the docking method successfully reproduced the crystallographic pose of acarbose compound.
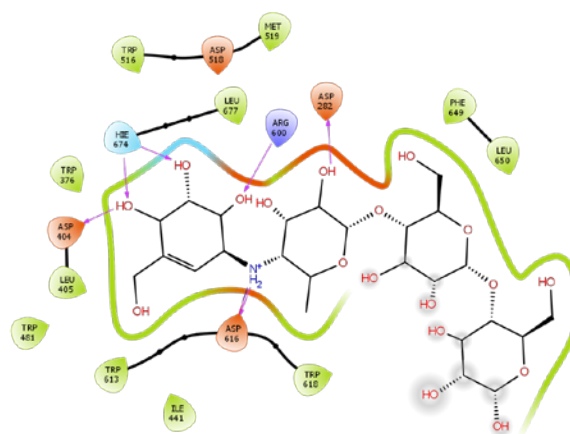
Figure 1. The 2D interaction map of acarbose with the binding site residues of the α-glucosidase enzyme. Only protein residues that are within 3 Å of the bound compound are shown. The docking method successfully reproduced the crystallographic pose of acarbose compound with an RMSD value of 1.48 Å.

2.3. Preliminary research

2.3.1. Cell culture

The MCF7, A549, and MDA-231 were obtained from (ATCC), and the human dermal fibroblast cell line (HDF) was isolated in the (Cell Therapy Center/University of Jordan/Amman-Jordan). MCF7 and A549 were cultured in RPMI 1640 Medium, while MDA-MB-231 and HDF were cultured in EMEM (Eagle's Minimum Essential Medium) and DMEM (Dulbecco's Modified Eagle Medium), respectively. A 5% penicillin-streptomycin (100 IU/mL–100 g/mL) and a 10% fetal bovine serum were added to all media, along with 1% L-glutamine for RPMI and EMEM and 2% L-glutamine for DMEM. We incubated all cell lines at 37 °C with 5% CO$_2$. Cells were subcultured every 3-5 days with 0.05% trypsin-EDTA, depending on their confluency.

2.3.2. Cell viability (MTT)

For calculating the IC$_{50}$ of our compounds, MCF7, A549, MDA-231, and HDF were cultured in 96 well plates with 9000 cells/well, except for A549, we seeded 6500 cells/well, for 24 hours to allow attachment of the cells. Then, cells were treated with different concentrations of L1, L2, L3 and L4 (0 to 500 µM) dissolved in DMSO for 72 hours. 15 µl of MTT salt (3-(4,5-dimethylthiazol-2-yl)-2,5-diphenyltetrazolium bromide) was added per well with 100 µl of new media, for 3 hours. To stop the reaction and dissolve the formazan, 50 µl of DMSO was added to each well. The Glomax microplate reader (Promega, Madison, WI, USA) was used to measure absorbance at 560 nm.

2.4. 2.4 Main research process optimization

For experiment optimization, normal fibroblast cell lines were used to evaluate the safety profile, while triple negative breast cancer cell line (MDA-MB-231) was used for anticancer activity. In this study, different concentrations of the chemical compounds (50, 25, 12.5 µg/ml) were used for safety profile evaluation. However, only the concentration of 25 µg/ml was chosen to evaluate cytotoxic effect against cancer cell lines due to its high safety compared to 50 µg/ml concentration and its high anticancer activity compared to 12.5 µg/ml concentration.

2.4.1. MTT assay

An MTT colorimetric test (3-[4, 5-dimethylthiazol-2-yl]-2,5 diphenyl tetrazolium bromide assay) was used to assess cell viability in both normal and cancer cell lines following the described procedure (Juengel *et al*., 2019). In brief, cells (50 μL, 1X 10^5 cells/mL) were planted onto 96-well plates. After 24, 48, and 72 hours, MTT reagent was added for 4 hours. The plates were incubated overnight at 37 °C and 5% CO_2. Each well's absorbance at 550 nm was measured with a microplate enzyme-linked immunosorbent assay (ELISA) reader. The data were presented as mean cell numbers after eliminating background absorbance.

3. Results and Discussion

3.1. Alpha-glucosidase docking study

The outcomes of the induced fit docking computations are presented below. While the co-crystallized ligand produced a docking score of -14.9, the proposed compounds exhibited moderate docking scores of -5.7, -5.8, -6.2, and -7.6 for L1, L2, L3, and L4, respectively. This difference in the docking score is due to the fact that the anchoring mechanism of acrabose compound relies heavily on interactions involving hydrogen bonds. In contrast, the synthesized compounds consist of aromatic rings and hydrophobic substituents, which are primarily involved in hydrophobic interactions (**Figure 2**). These compounds tend to have a lower dehydration enthalpic cost (desolvation effects) than hydrophilic molecules such as acarbose (Bodnarchuk, 2016). Therefore, although these compounds have lower docking scores compared to acarbose, their total binding affinities could potentially be increased due to their low dehydration enthalpic costs and low conformational entropies, since they have a small number of rotatable bonds (Klebe, 2015). Furthermore. the synthesized compounds may have their binding affinities increased by carefully adding certain functional groups, especially OH- groups, which are known to improve hydrogen bond interactions. This strategy offers encouraging directions for future study in this area.
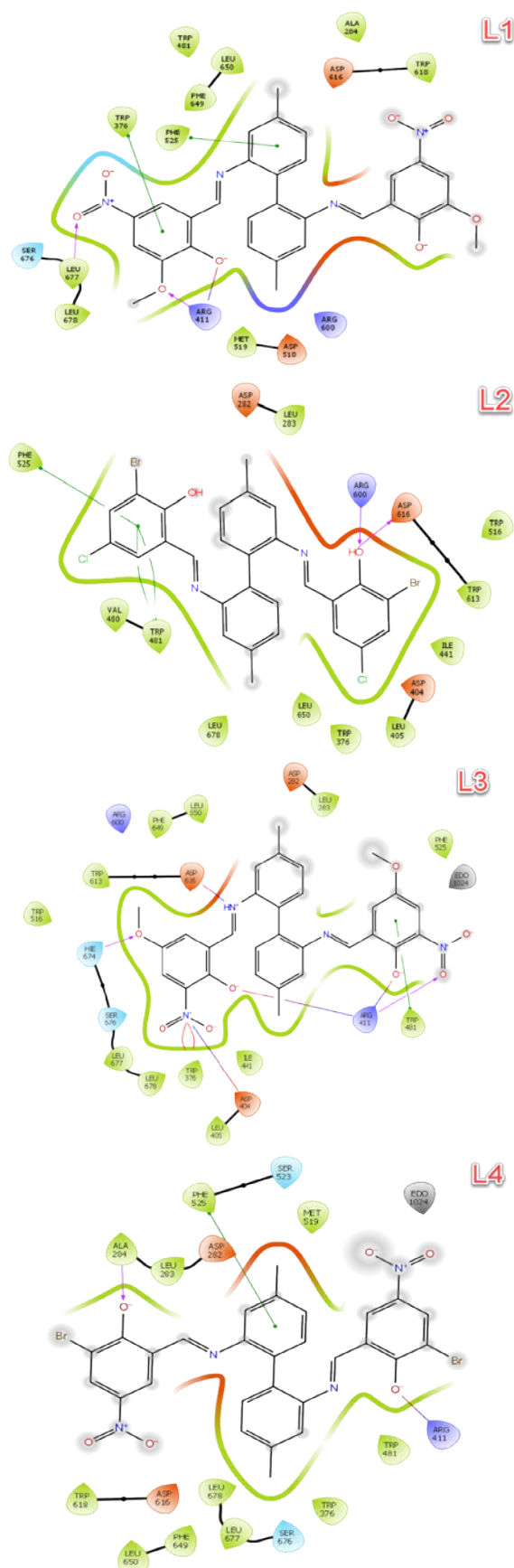
Figure 2. The 2D interaction map of the compounds (L1, L2, L3 and L4, respectively) with the binding site residues of the α-glucosidase enzyme. Only protein residues that are within 3 Å of the bound compounds are shown.

3.2. Preliminary research

The tested compounds showed cytotoxic activity against MDA-MB-231, MVF-7, and A549 cancer cell lines with variable IC_{50}. Compounds L4 and L1 showed the lowest IC_{50} against the MDA-MB-231 breast cancer cell line, 20.7 µM, and 37.9 µM, respectively. In addition, L1 showed the lowest IC_{50} against the A549 lung cancer cell line (36.4 µM). Generally, all tested compounds showed a selective cytotoxic effect against the MDA-MB-231 cancer cell line compared to the other cell lines; however, L4 showed low IC_{50} against all cell line types including the normal fibroblasts (**Table 3**). In summary, the results suggest that the tested compounds (L1, L2, and L3) are selective against MDA-MB-231 compared to other cancer cell lines and normal fibroblasts. However, the L4 compound showed the lowest IC_{50} against all tested cell lines, especially the MDA-MB-231 breast cancer cell line (**Figure 3**).

Table 3. Cytotoxic activity results against MDA-MB-231, MVF-7, and A549 cancer cell lines with variable IC_{50}

Compound	$IC_{50} \pm SD$ (µM)			
	MDA-MB-231	MCF-7	A549	Fibroblast
L1	37.9±1.8	123.1±8.4	36.4±2.8	65.4±12.1
L2	66.3±4.9	146.8±22.7	135.5±7.8	102.3±10.5
L3	54.5±4.8	64.7±13.9	91.6±4.9	64.9±8.8
L4	20.7±6.3	34.4±5.0	41.6±4.5	34.8±7.8
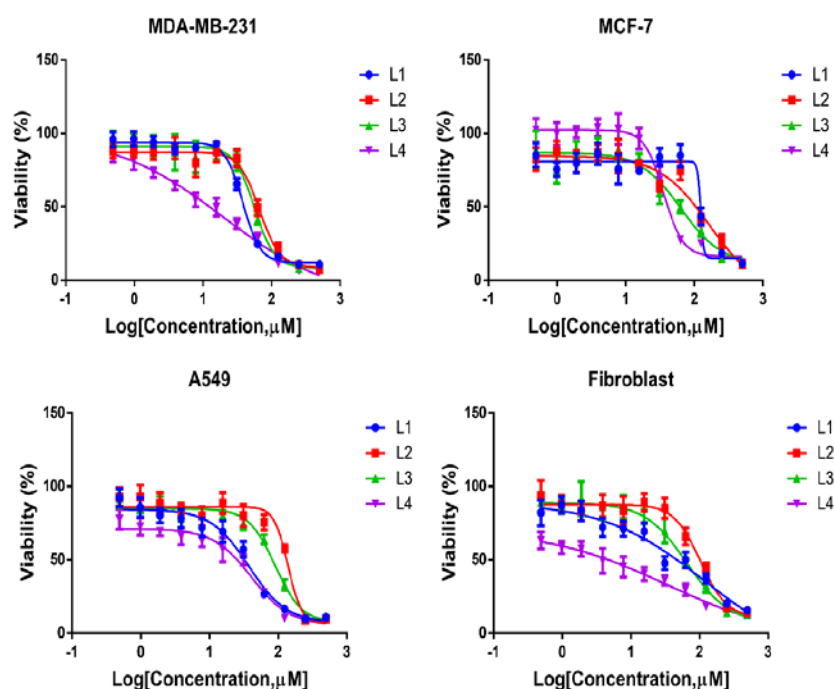
Figure 3. Graphical views of the Cytotoxic activity results against MDA-MB-231, MVF-7, and A549 cancer cell lines

3.3. Main research process optimization

3.3.1. Safety Profile

The Results revealed that (25 µg/ml) concentration of bis-biphenyl salicylaldehyde Schiff base derivatives against the normal cell lines showed (83.06, 80.4, 71.22, 72.85 % cells survival) for (L1, L2, L3, L4), respectively, as shown in **Figure 4**. These findings suggest that these compounds are considered relatively safe, given their cell survival rates exceeding 50% against normal cells. Moreover, the stability of these compounds was evaluated by measuring the survival rate unit within 72 hr and the results revealed that the survival rate remained constant with 72.04 % survival rate compared to their control.
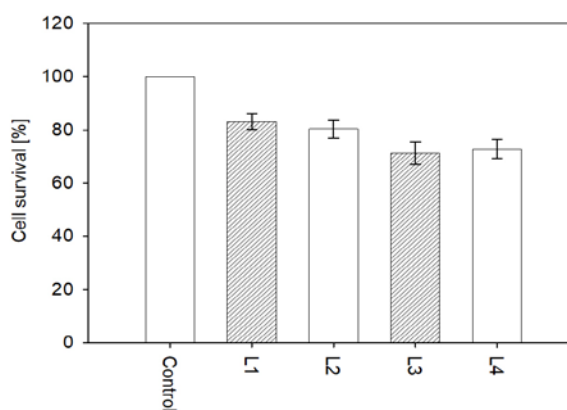
Figure 4. Survival rate of fibroblast normal cells at 25 µg/ml of bis-biphenyl salicylaldehyde Schiff base derivatives

3.3.2. Cytotoxic activity

Bis-biphenyl salicylaldehyde Schiff base derivatives showed selective cancer cell line cytotoxicity against (MDA-MB-231) breast cancer cell line, with inhibition rates of (25.97, 24.43, 34.23, 33.08 %) for (L1, L2, L3, L4), respectively compared to their controls at 25 μg/ml concentration as shown in **Figure 5**. Even though we choose this concentration as the ideal concentration for cancer inhibition after weighing the safety and activity of each concentration, our results revealed the stable effect of these derivative upon time intervals and their dose dependent relation as shown in **Figures 5** and **6**.

Our results revealed that the effect of these derivatives is stable with time, which means that the cells showed mild growth after the application of these chemicals particularly in L1 and L4 and showed no growth within 48

hr and mild elevation in growth in sample L2 after 72 hr; however, the most inhibition stability was revealed by L3 sample as illustrate in **Figure 5**. As detailed in a research report, certain 1,3,4-thiadiazole derivatives bearing Schiff base moiety demonstrated antitumor activity against the MCF-7 breast cancer cell line, showcasing IC_{50} values of 4.56 mM and 4.25 mM. which were associated with the presence of functional groups R=4-OCH$_3$ and R=4-NO$_2$ (Zhang *et al*., 2014). In another study, the highest inhibitory activity against cancer cells was detected for a Schiff base derived from 1,3,4-thiadiazole compound bearing three O-CH$_3$ groups (Gür *et al*., 2020). These outcomes can be ascribed to the presence of distinct functional groups, specifically for L3 (R$_1$= NO$_2$, R$_2$= OCH$_3$) underscoring the significance of the structure-activity relationship.
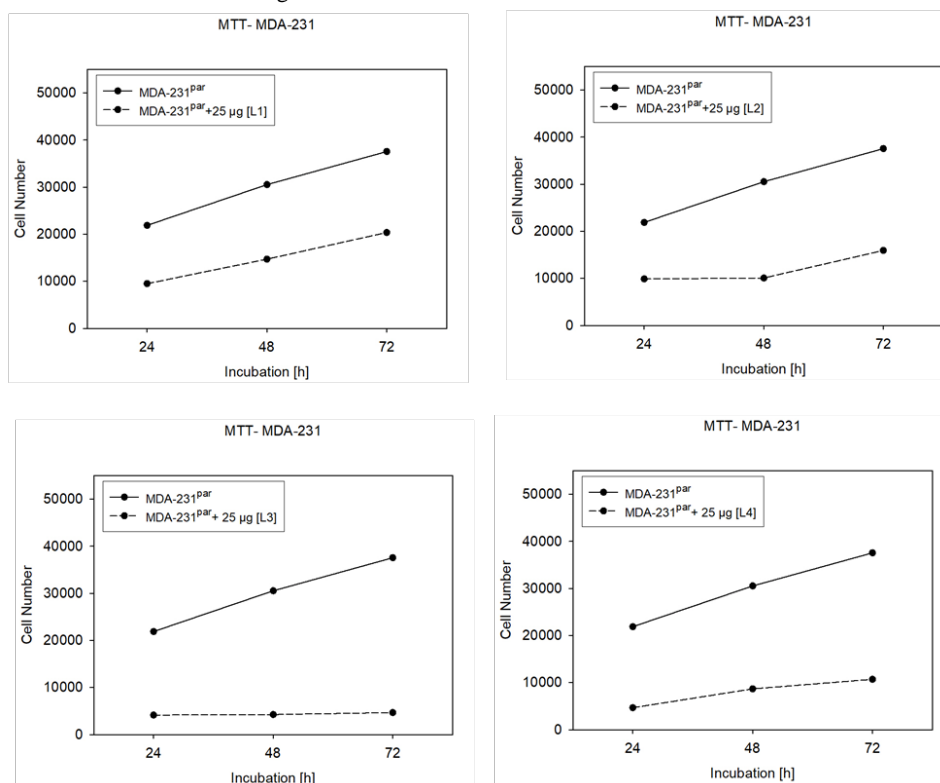
Figure 5. Cytotoxic activity of bis-biphenyl salicylaldehyde Schiff base derivatives against (MDA-MB-231) breast cancer cell line.

Our results demonstrated that there is a direct relationship between dose and activity, as **Figure 6** illustrates; however, when applying these chemicals *in vivo* or in proceeding clinical trials, the safety for each dose should be weighted with its activity before its usage. Hence, these findings provide groundwork for enhancing both the effectiveness and the specificity of this series of

compounds. In summary, the tested bis-biphenyl salicylaldehyde Schiff base derivatives displayed significant cytotoxicity against the MDA-MB-231 breast cancer cell line, with ligand L3 exhibiting the highest toxicity at 25 μg/ml, reducing cell viability by 34.23% compared to the control group.
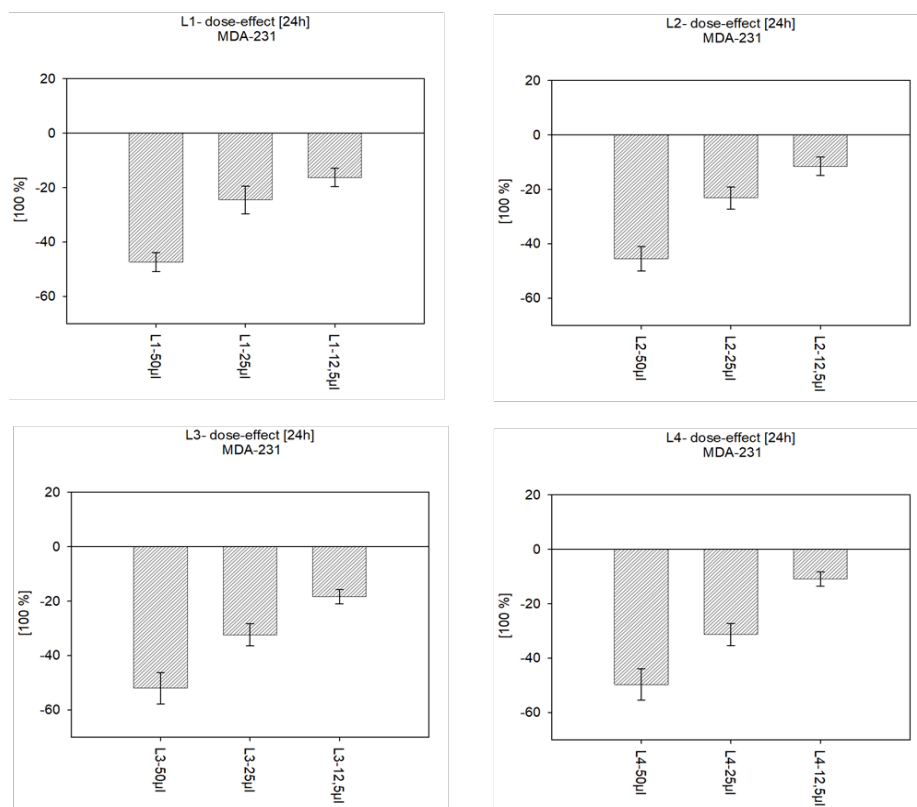
Figure 6. The relationship between dose and cytotoxicity of bis-biphenyl salicylaldehyde Schiff base derivatives against (MDA-MB-231) breast cancer cell line.

4. Conclusion

Four new symmetrical Schiff base ligands have been prepared and characterized by different spectroscopic techniques and elemental analysis. The induced-fit docking computations showed that the proposed compounds had moderate docking scores compared to the co-crystallized ligand acarbose, while the docking scores suggest that the proposed compounds may not be as effective as acarbose in binding to the target site; their unique physiochemical properties (*i.e.*, hydrophobicity and rigidity) could still make them viable candidates for further study and optimization. Compounds L4, L1, and L3 showed selective anticancer activity against the MDA-MB-231 breast cancer cell line and L1 showed a potential selectivity against the A549 lung cancer cell line, while L4 showed a pan-cytotoxic effect against all types of cells. The viability percentages of the normal fibroblast cell-line were calculated at (83.06, 80.4, 71.22, 72.85 %) for (L1, L2, L3, L4), respectively, at the concentration 25.0 µg/ml. Results revealed that normal fiber cell lines are not affected by the derivatives, indicating their potential selectivity towards cancer cells. These findings suggest that the derivatives have promising anti-cancer properties and warrant further investigation to determine the mechanism of action and in vivo efficacy of these compounds.

Acknowledgments

References

Ababneh TS, El-Khateeb M, Tanash AK, Al-Shboul TMA, Shammout MJA, Jazzazi TMA, Alomari M, Daoud S and Talib WH. 2021. Synthesis, computational, anticancerous and antiproliferative effects of some copper, manganese and zinc complexes with ligands derived from symmetrical 2,2'-diamino-4,4'-dimethyl-1,1'-biphenyl-salicylaldehyde. *Pol J Chem Tech.*, **23:**7-15.

Al-Shboul TMA, Ziemann S, Görls H, Jazzazi TMA, Krieck S and Westerhausen M. 2018. Synthesis of dipotassium 2,2'-bis(2-oxidobenzylideneamino)-4,4'-dimethyl-1,1'-biphenyl derivatives and use as ligand transfer reagent. *Eur J Inorg Chem.*, **2018**:1563-1570.

Bas DC, Rogers DM and Jensen JH. 2008. Very fast prediction and rationalization of pKa values for protein–ligand complexes. *Proteins*, **73**: 765-783.

Bodnarchuk MS. 2016.Water, water, everywhere… It's time to stop and think. *Drug Discov Today*, **21**: 1139-1146.

Chambhare RV, Khadse BG, Bobde AS and Bahekar RH. 2003. Synthesis and preliminary evaluation of some N-[5-(2-furanyl)-2-methyl-4-oxo-4H-thieno[2,3-d]pyrimidin-3-yl]-carboxamide and 3-substituted-5-(2-furanyl)-2-methyl-3H-thieno[2,3-d]pyrimidin-4-ones as antimicrobial agents. *Eur J Med Chem.*, **38**: 89-100.

Chang-Qing Y, Jie L, Shi-Qi Z, Kun Z, Zi-Qian G, Ran X, Hui-Meng L, Ren-Bin Z, Gang Z, Dachuan Y and Chen-Yan Z. 2020. Recent treatment progress of triple negative breast cancer. *Prog Biophys Mol Biol.*, **151**:40-53.

Chohan ZH, Sumrra SH, Youssoufi MH and Hadda TB. 2010. Metal based biologically active compounds: Design, synthesis, and antibacterial/antifungal/cytotoxic properties of triazole-derived Schiff bases and their oxovanadium(IV) complexes. *Eur J Med Chem.*, **45**: 2739-2747.

Dalia SF, Afsan F, Hossain MS, Khan MN, Zakaria C, Kudrat-E-Zahan M and Ali MH. 2018. A short review on chemistry of Schiff base metal complexes and their catalytic application. *Int J Chem Stud.*, **6**: 2859–2866.

Gupta S, Pandey SK, Kumar S, Gautam RN, Patel AK, Bharty MK, Kushwaha D, Acharya A and Butcher RJ. 2023. Experimental, spectroscopic, and theoretical investigation on structural and anticancer activities of Schiff bases derived from isonicotinohydrazide. *J Mol Struct.*, **1293**: 136212.

Gür M, Yerlikaya S, Şener N, Özkınalı S, Baloglu MC, Gökçe H, Altunoglu YC, Demir S andŞener İ. 2020. Antiproliferative-antimicrobial properties and structural analysis of newly synthesized Schiff bases derived from some 1,3,4-thiadiazole compounds. *J Mol Struct.*, **1219**: 128570.

Jazzazi TMA, Ababneh TS and Abboushi EK. 2019. Zinc(II) complexes of symmetrical tetradentate Schiff base ligands derived from 2,2'-diamino-6,6'-dibromo-4,4'-dimethyl- 1,1'-biphenyl-salicylaldehyde: synthesis, characterization and computational study. *Jordan J Chem.*, **14:** 81–87.

Juengel E, Natsheh I, Najafi R, Rutz J, Tsaur I, Haferkamp A, Chun FKH and Blaheta RA. 2019. Mechanisms behind temsirolimus resistance causing reactivated growth and invasive behavior of bladder cancer cells in vitro.*Cancers,* **11**:777.

Klebe G. 2015. Applying thermodynamic profiling in lead finding and optimization.2015. *Nat Rev Drug Discov*., **14**: 95–110.

Przybylski P, Huczyński A, Pyta K, Brzezinski B and Bartl F. 2009. Biological properties of Schiff bases and azo derivatives of phenols. *Curr Org Chem.*, **13**:124-148.

Roig-Zamboni V, Cobucci-Ponzano B, Iacono R,Ferrara MC, Germany S, Bourne Y, Parenti G, Moracci M and Sulzenbacher G.2017. Structure of human lysosomal acid α-glucosidase–a guide for the treatment of Pompe disease. *Nat Commun.*, **8**: 1111.

Sastry GM, Adzhigirey M, Day T, Annabhimoju R and Sherman W. 2013. Protein and ligand preparation: parameters, protocols, and influence on virtual screening enrichments. *J Comput Aided Mol Des.*, **27**: 221–234.

Schrödinger Release 2022-3: LigPrep, Schrödinger, LLC, New York, NY, 2021.

Shawish I, Barakat A, Aldalbahi A, Alshaer W, Daoud F, Alqudah DA, Al Zoubi M, Hatmal MM, Nafie MS, Haukka M, Sharma A, de la Torre BG, Albericio F and El-Faham A. 2022. Acetic acid mediated for one-pot synthesis of novel pyrazolyl *s*-triazine derivatives for the targeted therapy of triple-negative breast tumor cells (MDA-MB-231) *via* EGFR/PI3K/AKT/mTOR signaling cascades. *Pharmaceutics,* **14**: 1558.

Shelley JC, Cholleti A, Frye LL,Greenwood JR, Timlin MR and Uchimaya M. 2007. Epik: a software program for pK a prediction and protonation state generation for drug-like molecules. *J Comput Aided Mol Des.*, **21**: 681–691.

Sherman W, Day T, Jacobson MP, Friesner RA and Farid R. 2006. Novel procedure for modeling ligand/receptor induced fit effects. *J Med Chem.*, **49**: 534-553.

Yin L, Duan JJ, Bian XW and Yu SC. 2020. Triple-negative breast cancer molecular subtyping and treatment progress. *Breast Cancer Res.*, **22**: 61.

Zhang K, Wang P, Xuan LN, Fu XY, Jing F, Li S, Liu YM and Chen BQ. 2014. Synthesis and antitumor activities of novel hybrid molecules containing 1, 3, 4-oxadiazole and 1, 3, 4-thiadiazole bearing Schiff base moiety.*Bioorg Med Chem Lett.*, **24**: 5154-5156.

Community Structure of the Family (Scorpaenidae: Scorpionfishes) in Relation to Habitat and Depth Along the Jordanian Coast of the Gulf of Aqaba, Red Sea

Maroof Khalaf [1,*], Thaqef Al-Khasawneh[1], Mohammad Wahsha[2], Wissam Hayek[3], Mohammad Al-Zibdah[1], and Tariq Al-Najjar[1]

[1] Faculty of Basic and Marine Sciences, The University of Jordan, Aqaba Branch, Jordan; [2] Marine Science Station, The University of Jordan, Aqaba Branch, Jordan; [3] Department of Geography, The University of Jordan, Amman, Jordan

Abstract

The community structure of the fish family Scorpaenidae was investigated at nine sites along the Jordanian coast, examining various sites, depths, and habitats. The study employed a visual census technique with SCUBA diving for data collection. To present the findings, GIS maps were generated using ArcMap 10.8.1, showcasing the projected benthic cover, frequency of appearance, and relative abundance of the species. The community indices were computed using PRIMER-5 software (Primer-E 2000). The survey recorded a total of 417 scorpionfish individuals, representing seven different species, across 87 belt transects located at nine coastal sites. The average number of scorpionfish individuals per transect was approximately 4.8. Notably, three out of the seven species accounted for a significant 79.8% of all observed individuals. These dominant species were *Pterois miles*, which exhibited the highest relative abundance at 37.9%, followed by *Synanceia verrucosa* at 21.3%, and *Pterois radiata* at 5.4%. Further analysis of the data revealed that *P. miles* was most prevalent in both coral reef habitats (RA=55.6%) and sandy habitats (RA=47.0%). On the other hand, *S. verrucosa* showed the highest abundance in the seagrass habitat with a relative abundance of 53.4%. Additionally, *P. miles* was the most abundant fish species at a depth of 9 m, accounting for 46.9% of the population, while both *S. verrucosa* and *Scorpaenopsis diabolus* shared the highest relative abundance at reef flats with 44.4% each. Moreover, *P. miles* was the most commonly observed species across all sites, with a frequency of appearance (FA) of 70.1%. In the seagrass habitat, *S. verrucosa* dominated, with an FA of 88.9%. Furthermore, *P. miles* was frequently encountered at the sandy bottom and coral reef habitats, with FAs of 82.5% and 58.3% respectively. Reef flats showed an equal prevalence of both *S. verrucosa* and *P. miles*, each accounting for 50.0% of the observed scorpionfish. Cluster analysis revealed the presence of two main groups: the northern natural sites GH, HA, and PLB formed the first group, while the remaining sites constituted the second group. The species richness was found to be highest at a depth of 6 m, whereas the lowest richness was observed at reef flats. The sandy habitat exhibited the highest diversity index, while the coral reef habitats displayed the lowest diversity. This comprehensive survey provides valuable insights for decision-makers and managers, aiding them in making informed decisions to ensure the safety of beach users and visitors to Aqaba. Additionally, it contributes to public awareness regarding the potential risks posed by these fishes, thereby reducing the likelihood of injuries caused by encounters with them.

Keywords: Scorpionfish; Gulf of Aqaba; Fish mapping; Scorpaenidae

1. Introduction

The Red Sea, renowned for its unique ecological and biological characteristics, stands as a hub of marine biodiversity, harbouring a remarkable diversity of over 1,200 fish species (Golani and Bogorodsky 2010). From diminutive reef fish to sizable predatory species, these fish showcase a stunning array of colours and behaviours. Notably, Khalaf (2004) meticulously documented 507 fish species inhabiting the Jordanian coast of the Gulf of Aqaba, including 18 species from the Chondrichthyes group and 489 species from the Ostichthyes group. Numerous studies have been conducted to explore different facets of this marine biodiversity, including research on the community structure, biogeography, and assemblage composition of fish species, as well as their roles as indicators of benthic habitats (Khalaf and Kochzius 2002a, 2002b; Khalaf and Crosby 2005). Furthermore, Brokovich et al. (2006) examined the influence of various substrate variables, particularly physical complexity and live coral cover, on the richness and abundance of coral reef fish communities. The research highlighted that substrate attributes play a direct role in shaping fish community parameters, such as the species composition and food availability. Consequently, these factors significantly impact community intricacy, diversity, and richness (Roberts and Ormond 1987).

Notably, about two-thirds of venomous vertebrates in the world are venomous marine fish, including stingrays,

---

* Corresponding author. e-mail: m.khalaf@ju.edu.jo.

scorpion, zebra, and stone fishes, as well as certain types of sharks, catfish, and blennies (Church and Hodgson 2002; Sivan 2009). Among them, the Reef Stonefish (*Synanceia verrucosa*) is frequently encountered by humans and poses a venomous threat. While the Gulf of Aqaba is home to various harmful marine organisms that can be fatal or cause severe injuries (Wahsha et al. 2021), the severity of injury typically depends on factors such as the amount of venom, individual responses, and the nature and location of the injury (Smith et al. 2016). Despite the lack of previous research on the distribution patterns of hazardous fish along the Jordanian coast, national reports indicate that numerous people visit Aqaba beaches during the summer holidays. Notably, 72% of injuries were incurred by visitors rather than locals (Mutair et al. 2006).

The primary objective of this research is to delve into the community structure and spatial distribution of scorpion fishes across various locations, depths, and habitats along the Jordanian coast of the Gulf of Aqaba.

2. Materials and Methods

2.1. Study Area:

The Gulf of Aqaba, measuring 180 km in length and up to 20 km in width, is a semi-enclosed sea distinguished by its numerous distinctive natural and physical characteristics. This geographic isolation is primarily attributed to the narrow Straits of Tiran, which have a considerable depth of approximately 260 m. While a substantial portion of the Gulf boasts significant depths exceeding 1800 m, the northern sector features a relatively shallow shelf that runs alongside major human population centers. The Jordanian coast, extending for 27 km, is bordered by a series of reefs along approximately 13 km of its shoreline. These reefs are separated by sandy bottoms, frequently adorned with lush seagrass meadows (UNEP/IUCN 1988). The Gulf's waters are renowned for their tranquil nature and exceptional clarity, allowing for high visibility. The tides in the region display minimal fluctuations, with semidiurnal and diurnal variations measuring less than one meter (Manasrah 2002).

2.2. Stud sites

The underwater habitats in various areas of Aqaba can be described as follows: The Hotel Area (HA) features a bottom with a seagrass habitat. The Al-Gandoor Area (GH) is primarily characterized by seagrass habitat. The Phosphate Loading Berth (PLB) is distinguished by a combination of seagrass and sandy habitat. The Marine Science Station (MSS) is characterized by hard coral. Barracuda Beach (BB) has a sandy bottom with corals. The Marine Park (MB) features a sandy bottom, while Sodasyat (SOD), Tala Bay Radisson (TBR), and Tala Bay Movenpick (TBM) are all characterized by a sandy bottom.

To gain deeper insights into the coastal areas, an investigation was conducted between April 2018 and May 2019. The study covered nine distinct sites along the Jordanian coast (Figure 1), each denoted by an abbreviation and the number of transects surveyed in parentheses: Hotel Area (HA: 9); Ghandoor Beach (HB: 9); Phosphate Loading Berth (PLB: 9); Marine Science Station (MSS: 12); Marine Park (MP: 9); Barracuda Beach

(BB: 12); Sodasyat (SOD: 9); Tala Bay Radisson (TBR: 9); Tala Bay Movenpick (TBM: 9).
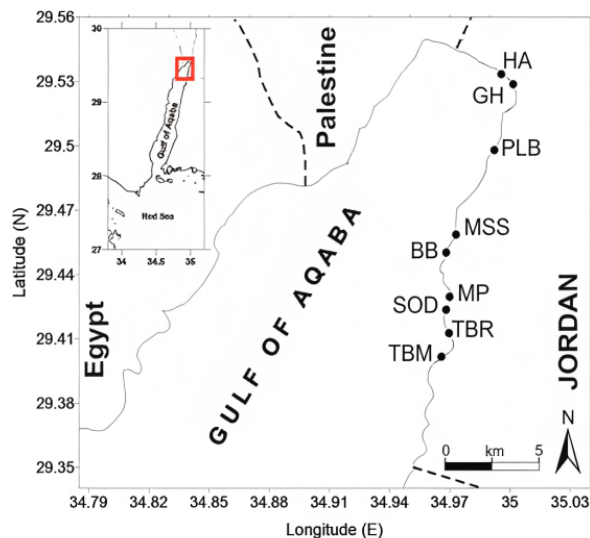
Figure 1. Locations of the study sites, which include the Hotel Area (HA), Ghandor (GH), Phosphate Loading Berth (PLB), Marine Science Station (MSS), Marine Park (MP), Barracuda Beach (BB), Sodasyat (SOD), Tala Bay Radisson (TBR), and Tala Bay Movenpick (TBM).

2.3. Visual census

Scorpion fish surveys were conducted using the visual census technique with SCUBA diving, following the protocol outlined by English et al. (1994). The survey includes three sets of replicated transects, each spanning a distance of 50 meters. These replicates were established at each of the three specific shallow depths: 3, 6, and 9 m``. The replicate transects were carefully placed in sequence, with a distance of 10–20 m between each one. In addition to the aforementioned transects, another set of three fish transects was carried out on the reef flat, at depths of less than 2 m, focusing on sites with coral reef habitats (i.e. the MSS). During the surveys, a waiting period of approximately 10 minutes was observed to allow the fish to return to their normal behavior before counting commenced. Once the waiting period was over, the observer swam along the transects and meticulously recorded all Scorpion fish sightings within a 1.5-m radius on each side of the line and 3 m above the transect. Each transect took about 20-25 minutes to complete. To assess the benthic community, the point intercept method, as modified after the work of English et al. (1994), was employed. This method involved recording the percentage of live hard and soft coral cover, seagrass, dead coral/rock, and sediment (sand). To ensure the identification of dangerous marine organisms, the guidelines established by Randall (2010), Myers (1991), and Khalaf and Disi (1997) were adhered to. By employing these rigorous methodologies and adhering to established protocols and guidelines, the scorpion fish populations and benthic communities were thoroughly and accurately studied, contributing valuable insights to marine research.

2.4. Statistical analysis and diversity calculations

The statistical analysis employed in this study follows the methods outlined by Sokal and Rohlf (1981), which were implemented using the StatView computer software.

Additionally, community indices such as the number of species (S), fish abundance (N), species richness (d), and species diversity (H´) were computed using the PRIMER-5 software developed by Primer-E (2000).

The abundance of fish species was described by two metrics: relative abundance (RA) and frequency of appearance (FA). The calculations for these metrics are as follows:

$$RA = \frac{Xi}{Ya} \times 100$$

where Xi represents the pooled average abundance of species i from each depth and site, and Ya represents the pooled average abundance of all species from each depth and site.

$$FA = \frac{Ni}{Nt} \times 100$$

where Ni denotes the number of transects in which species I was present, and Nt represents the total number of all transects.

Species diversity was evaluated using the Shannon-Weaver Diversity Index (Ludwig and Reynolds 1988):

$$H' = - \sum (pi \ln pi)$$

where pi is the proportion of all individuals counted that belonged to species i.

Species richness (d) was determined using the following formula:

$$d = S / N$$

where S is the total number of species observed, and N is the total number of individuals counted.

Cluster analysis and ANOSIM (analysis of similarities), were conducted using the PRIMER-5 software (Primer-E 2000). To examine the significant differences (p≤0.05) between (sites, depth, and habitat) concerning the number of species, species richness, and Shannon-Wiener diversity index, the group variations were measured using a One-Way Analysis of Variance (ANOVA). For presenting GIS maps related to the projected benthic cover, frequency of appearance, and relative abundance, ArcMap 10.8.1 software was utilized.

3. Results

3.1. Benthic coverage

The distribution of benthic coverage in the study area was thoroughly examined and presented in Figure 2. Among the surveyed sites, the MSS exhibited the highest proportion of live hard coral cover, accounting for an impressive 48.3%. In comparison, TBR came in second with a cover of 12.0%, while GH had the least hard coral cover, with a mere 0.4%. Hence, the MSS site stands out as a remarkable coral reef habitat. As for soft coral cover, GH led with 12.7%, closely followed by TBR with 9.8%. In terms of seagrass cover, HA, PLB, and GH were the highest, with percentages of 61.8%, 54.0%, and 45.6%, respectively. These three sites were identified as significant seagrass habitats, contributing substantially to the overall ecosystem. The sandy habitats were prominently represented in five sites, with BB having the highest sand cover at 72.7%, followed by TBR (54.9%), MP (54.5%), TBM (45.1%), and SOD (43.1%). Notably, the sand cover percentages varied across different depths, with 46.5% at 3 m depth, 45.3% at 6 m, and 44.2% at 9 m. Additionally, the distribution of hard coral cover was found to be predominantly concentrated in the reef flat, accounting for 44.7% of the coverage, followed by rocky habitats at 30.7%.
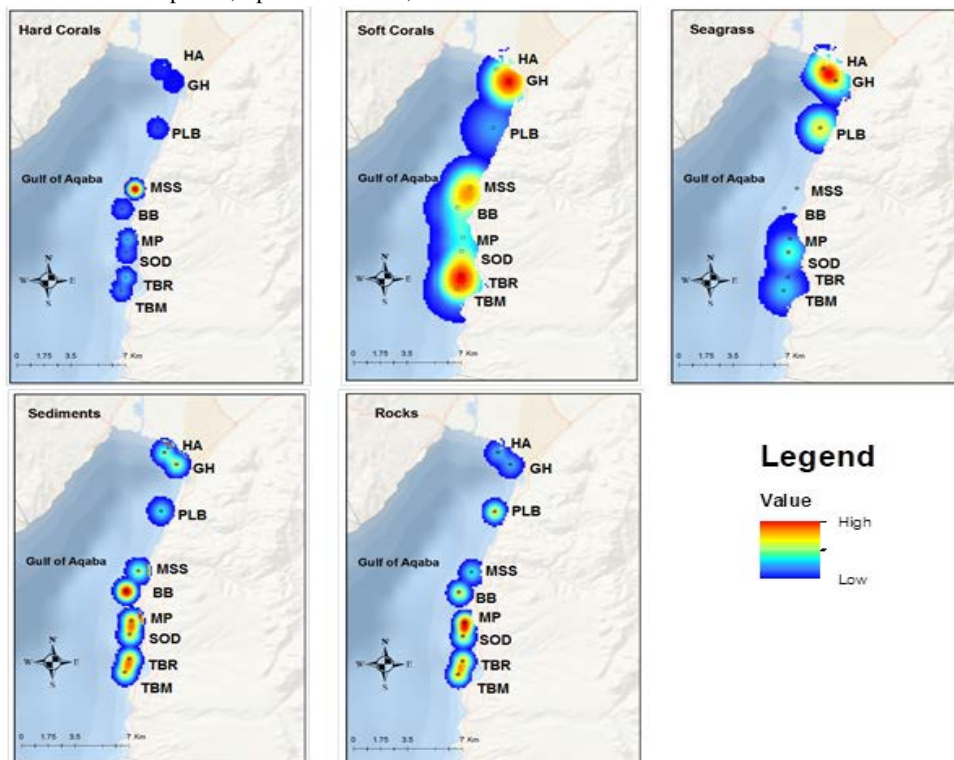
Figure 2. Distribution of Benthic Habitats; Hard Corals, Soft Corals, Seagrass, dead coral/rock and sediment at the nine sites along Gulf of Aqaba, Jordan.

3.2. Scorpion fish assemblages

A total of 417 scorpion fishes from 7 distinct species were meticulously recorded. The investigation involved the examination of 87 belt transects, which were strategically positioned at 9 diverse coastal sites spanning from the northern to the southern borders of the region. The findings revealed an average of approximately 4.8 scorpion fish individuals per transect.

3.3. Dominant Scorpion fish species at various sites

Based on the relative abundance (RA) calculations, three species were found to be the most abundant in this study. *Pterois miles* ranked first with a relative abundance of 37.9%, followed by *Synaneia verrucosa* at 21.3%, and *Pterois radiata* at 20.6%, collectively representing 79.8% of the total counted individuals. Among the nine sites studied, *P. miles* dominated at seven locations, with its RA varying from 8.6% at PLB to 60.7% at MP. *S. verrucosa* had the highest abundance at two sites, with RA ranging from 5.0% at SOD to 71.4% at PLB. Interestingly, *S. verrucosa* was not observed at the TBR and TBM sites (Figure 3).
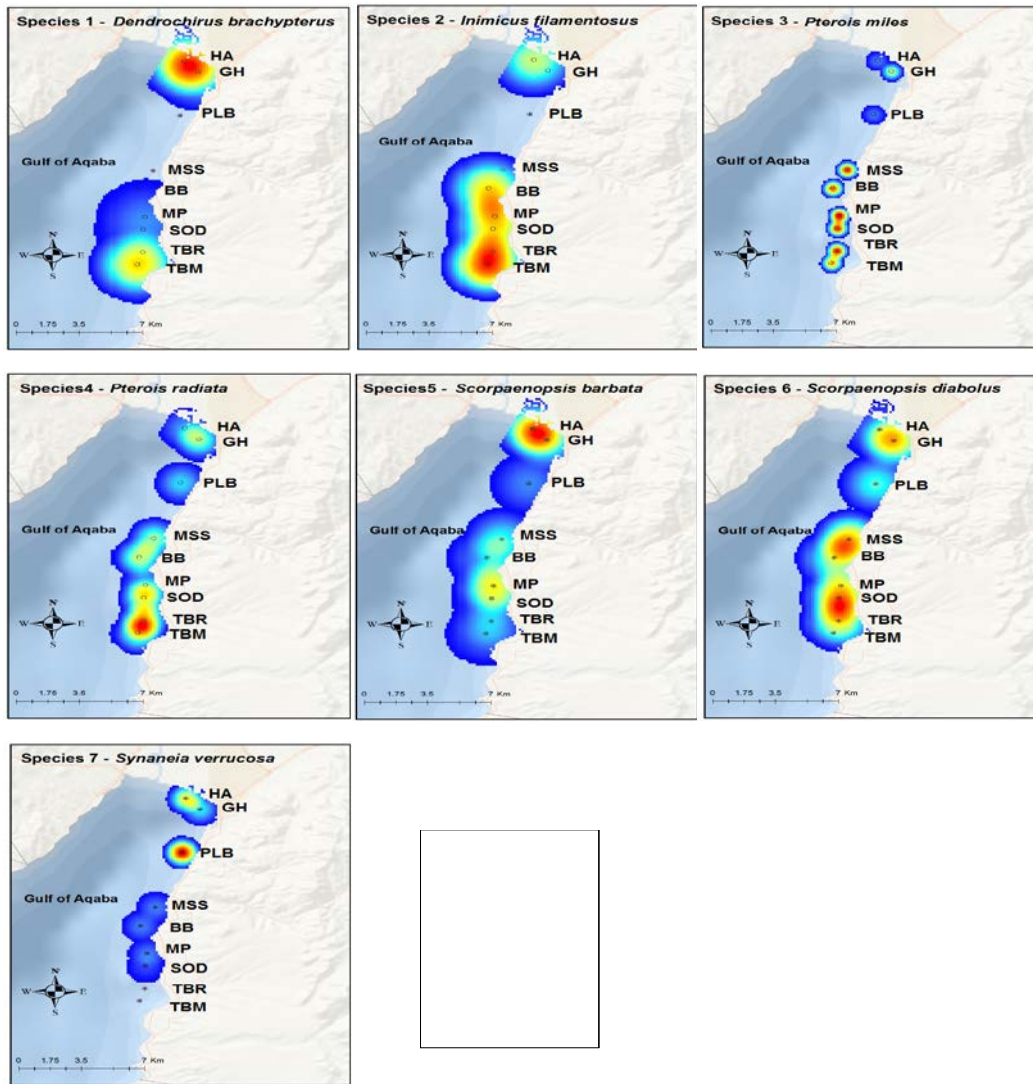
Figure 3. Projected relative abundance of seven species currently under investigation at the nine sites along Jordanian Gulf of Aqaba

3.4. Frequency of Appearance (FA)

The scorpionfish species observed on the Jordanian coast of the Gulf of Aqaba were well-documented in a study (Figure 4). Among the prevalent species, *P. miles* had the highest occurrence with a frequency of 70.1%, followed by *P. radiate* at 54.0%, and *S. verrucosa* at 41.4%. The distribution of these species varied across different locations, as indicated in Figure 3. At GH, five fish species were found to be most frequent, while three fish species were most commonly observed at HA. Additionally, two fish species were predominant at TBR, and one particular species stood out as the most common at TBM sites.
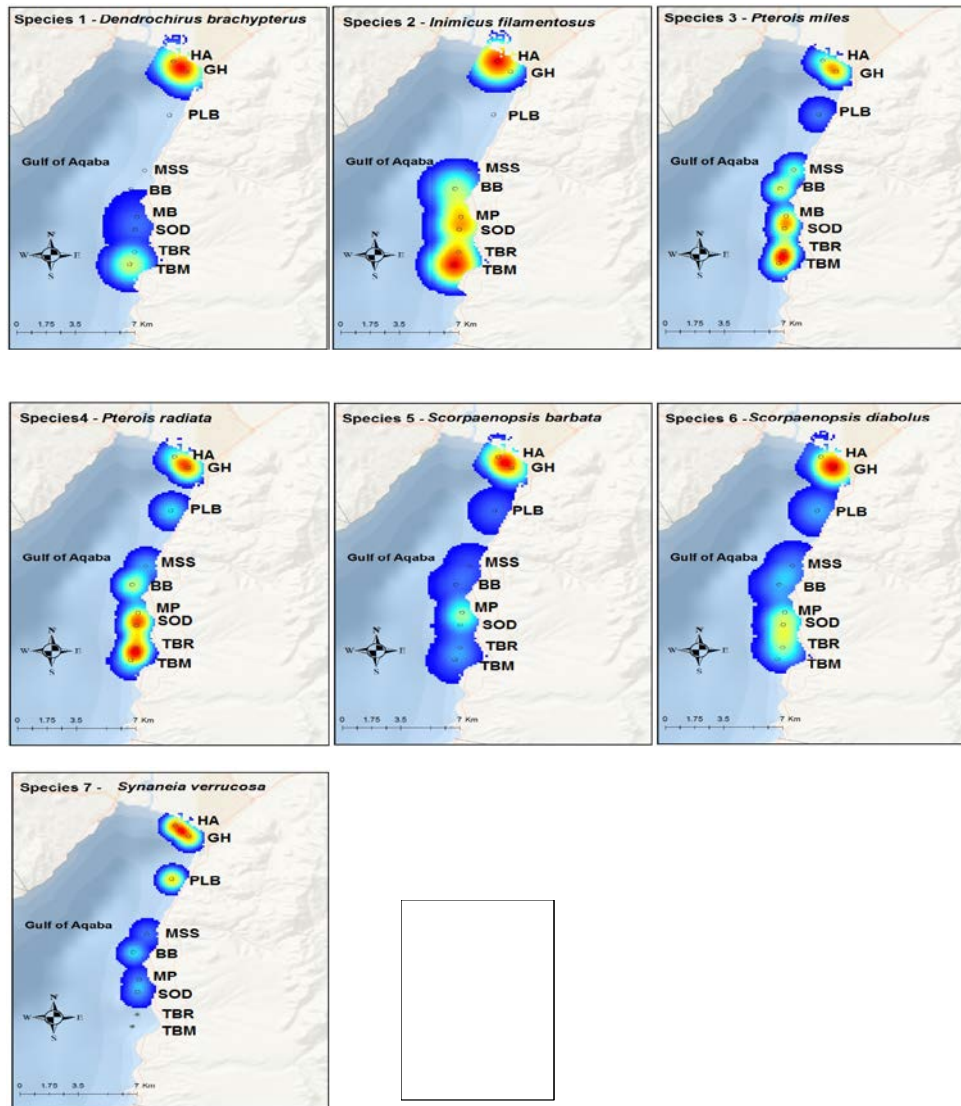
Figure 4. Projected Frequency of Appearance for the seven species under investigation at the nine sites along Jordanian Gulf of Aqaba.

3.5. Diversity Parameters

The data presented in Figure 5 displays the average values for various biodiversity measures across each site. The median number of species (S) ranged from 1.33 at the MSS site to 4.56 at the GH site. Similarly, the median number of individuals (N) varied from 1.78 at the MSS site to 10.44 at the GH site. Median species richness (d) showed a range from 0.36 at the MSS site to 1.53 at the GH site. Lastly, the Shannon-Wiener diversity index (H') exhibited a range from 0.22 at the MSS site to 1.38 at the GH site.
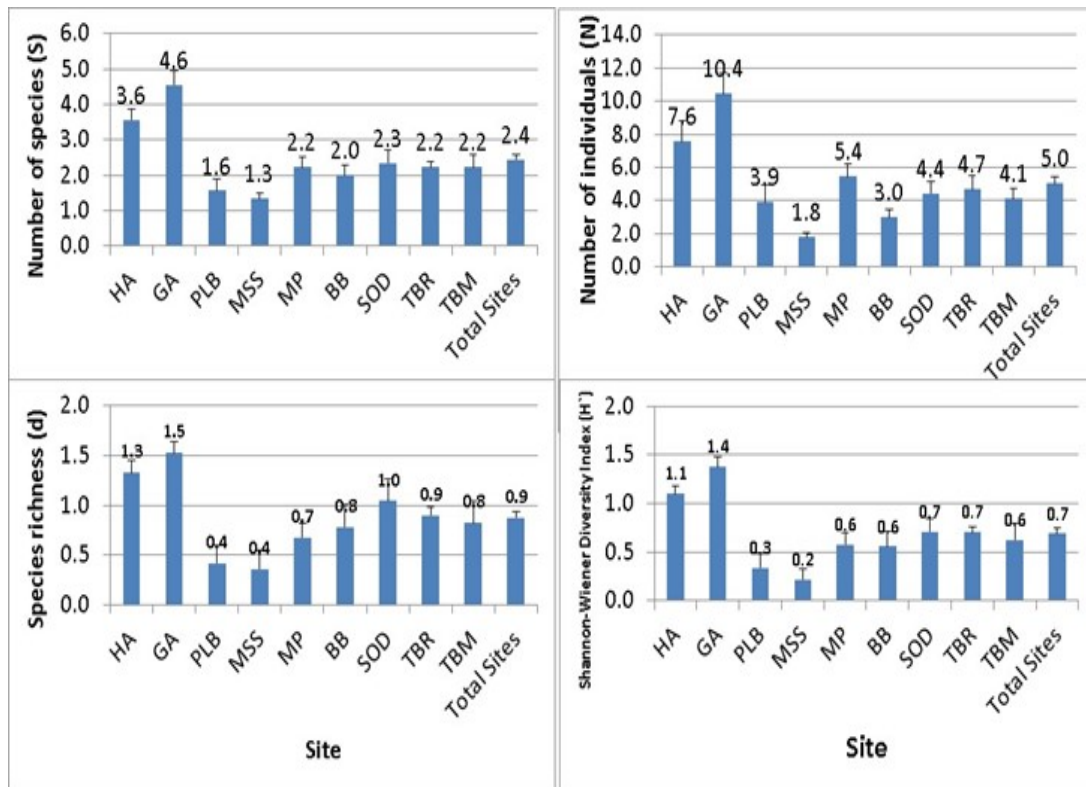
Figure 5. Average number of species (S), average number of individuals (N), average species richness (d), and average Shannon-Wiener Diversity Index (H') per 250 m² at different study sites situated along the Jordanian coastal waters. The study sites are identified as follows: Hotel Area (HA), Ghandor (GH), Phosphate loading berth (PLB), Marine Science Station (MSS), Marine Park (MP), Barracuda Beach (BB), Sodasyat (SOD), Tala Bay Radisson (TBR), and Tala Bay Movenpick (TBM).

3.6. Dominant Scorpionfish species by habitat

Table 1 presents the dominant scorpionfish species observed in different habitats. The data indicates that *P. miles* exhibited the highest abundance in both coral reef habitats (RA of 55.6%) and sandy habitats (RA=47.0%). On the other hand, *S. verrucosa* was found to be the most abundant scorpionfish species in seagrass habitats, with a relative abundance of 53.4%.

Table 1. Relative fish abundance (RA) data for three distinct habitat types along the Jordanian coast: seagrass (SG), coral reef, and sandy (SD) habitat. The calculation was performed per 250 m² transect. The number of individuals (N) in each habitat type was taken into consideration during the analysis.

Fish Species	SG	CR	Sand
D. brachypterus	13.6	0.0	7.8
I. filamentosus	1.9	0.0	1.7
P. miles	8.7	55.6	47.0
P. radiate	11.7	22.2	23.6
S. barbata	8.7	5.6	5.4
S. diabolus	1.9	5.6	3.7
S. verrucosa	53.4	11.1	10.8

3.7. Frequency of Appearance (FA)

The most common dangerous fish species found in seagrass habitats was *S. verrucosa*, constituting 88.9% of the occurrences, with *P. miles* and *P. radiata* following at 38.9% each. In contrast, the prevalent fish species in sandy habitats was *P. miles* (82.5%), while *P. radiata* followed closely at 64.9% for each species. Moreover, in coral reef environments, the dominant fish species was *P. miles*, accounting for 58.3% of the occurrences, while *P. radiata* accounted for 25.0% (Table 2)

Table 2. Frequency of appearance (FA) calculated for Seagrass (SG), Coral reef (CR) and Sandy (SD) habitats along the Jordanian coast.

Fish species	SG	CR	SD
D. brachypterus	33.3	0.0	26.3
I. filamentosus	11.1	0.0	8.8
P. miles	38.9	58.3	82.5
P. radiata	38.9	25.0	64.9
S. barbata	33.3	8.3	22.8
S. diabolus	11.1	8.3	17.5
S. verrucosa	88.9	16.7	31.6

3.8. Diversity Parameters

The seagrass habitat exhibited the highest average number of species (S=2.7), with sandy bottoms following closely behind (S=2.5), and the coral reef had the lowest number of species (S=1.2). Regarding the number of individuals, seagrass hosted the most significant population (N=5.7), while the coral reef had the lowest number of individuals (N=1.5). The species richness was at its highest in the seagrass habitat (d=1.1) and reached its lowest in the coral reef (d=0.7). Analyzing the Shannon

Diversity Index, both sandy and seagrass habitats showed the highest value (H`=0.7 each) (Figure 6).
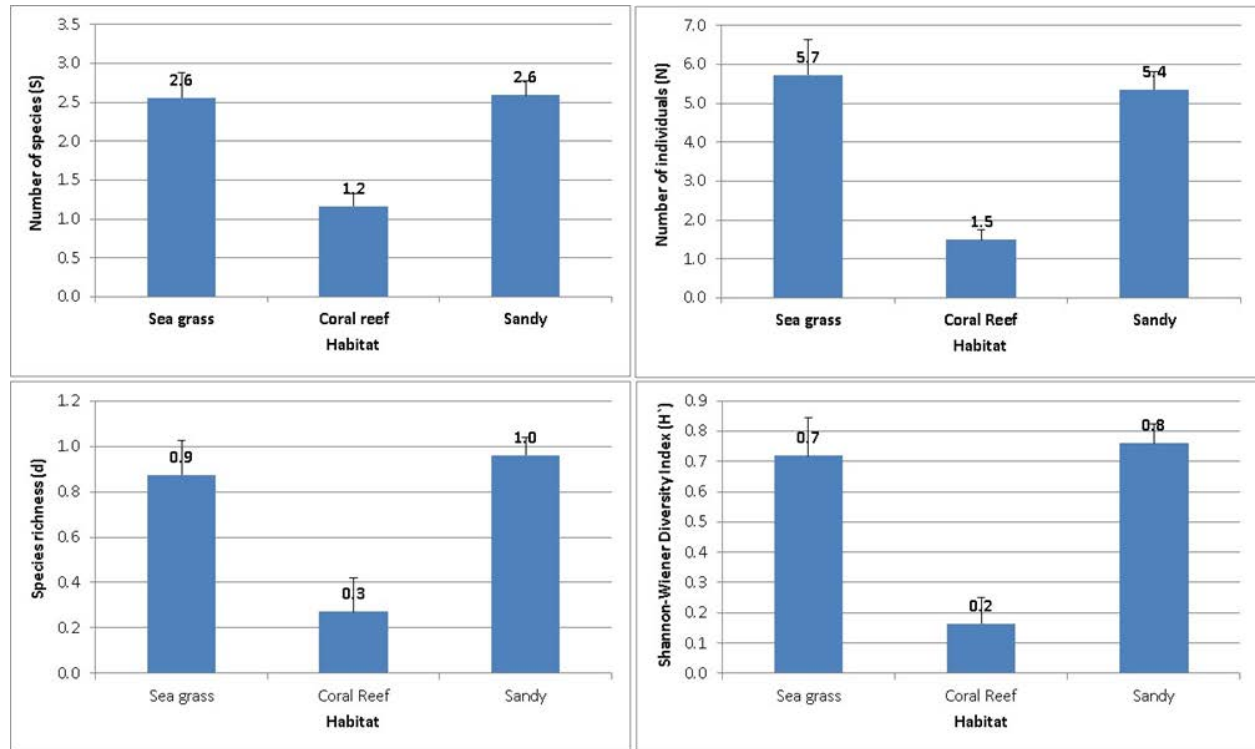
Figure 6. Average number of species (S), average number of individuals (N), average species richness (d), and average Shannon-Wiener Diversity Index (H') per 250 m² across different habitats along the Jordanian coast in the Gulf of Aqaba.

3.9. Dominant Scorpionfish species by depth

Table 3 displays the predominant fish species found at different depths. The distribution patterns of the fish species varied depending on the depth. Among these, *S. verrucosa* and *Scorpaenopsis diabolus* were the most abundant scorpionfish at RF, with each species accounting for 44.4% of the relative abundance (RA). On the other hand, *P. miles* dominated at 3 m, 6 m, and 9 m depths, with RAs of 36.1%, 34%, and 46.9% respectively.

Table 3. Relative fish abundance (RA) calculated at different depths along the Jordanian coast. The data incorporates the reef flat (RF), as well as depths of 3m, 6m, and 9m, which were combined in 250 m² transects.

Fish species	RF depth	3 m	6 m	9 m
D. brachypterus	0.0	12.3	8.3	6.9
I. filamentosus	0.0	0.0	3.2	1.5
P. miles	0.0	36.1	34.0	46.9
P. radiate	0.0	22.1	17.9	23.8
S. barbata	44.4	5.7	5.8	4.6
S. diabolus	11.1	2.5	3.8	3.1
S. verrucosa	44.4	21.3	26.9	13.1

3.10. Frequency of Appearance (FA)

Among the various scorpionfish species found at the reef flat, *S. Verrucosa* and *Scorpaenopsis diabolus* were the two most prevalent ones, each accounting for 50.0% of the observed occurrences. Notably, *P. miles* emerged as the dominant fish species at depths of 3 and 9 m, with a frequency of occurrence (FA) value of 74.1%. At a depth of 6 m, its FA increased further to 77.8% (Table 4).

Table 4. Frequency of appearance (FA) values computed for different depths on the reef flat (RF) of the Jordanian coast. The depths considered are 3m, 6m, and 9m.

Fish species	RF depth	3 m	6 m	9 m
D. brachypterus	0.0	29.6	25.9	22.2
I. filamentosus	0.0	0.0	18.5	7.4
P. miles	0.0	74.1	77.8	74.1
P. radiata	0.0	51.9	55.6	66.7
S. barbata	50.0	22.2	22.2	18.5
S. diabolus	16.7	11.1	22.2	11.1
S. verrucosa	50.0	48.1	48.1	25.9

3.11. Diversity parameters

When analyzing depth-related factors, it becomes evident that the fish species distribution varies significantly across different transects (Figure 7). Among the transects studied, those at a depth of 6 m stand out with the highest number of fish species per transect (S=2.70). Following this, the 3-m deep transects also exhibit considerable species richness (S=2.37), while the 9-m deep transects have a slightly lower number of species (S=2.26). On the other hand, the reef flat (RF) transects show the lowest species count (S=1.16).
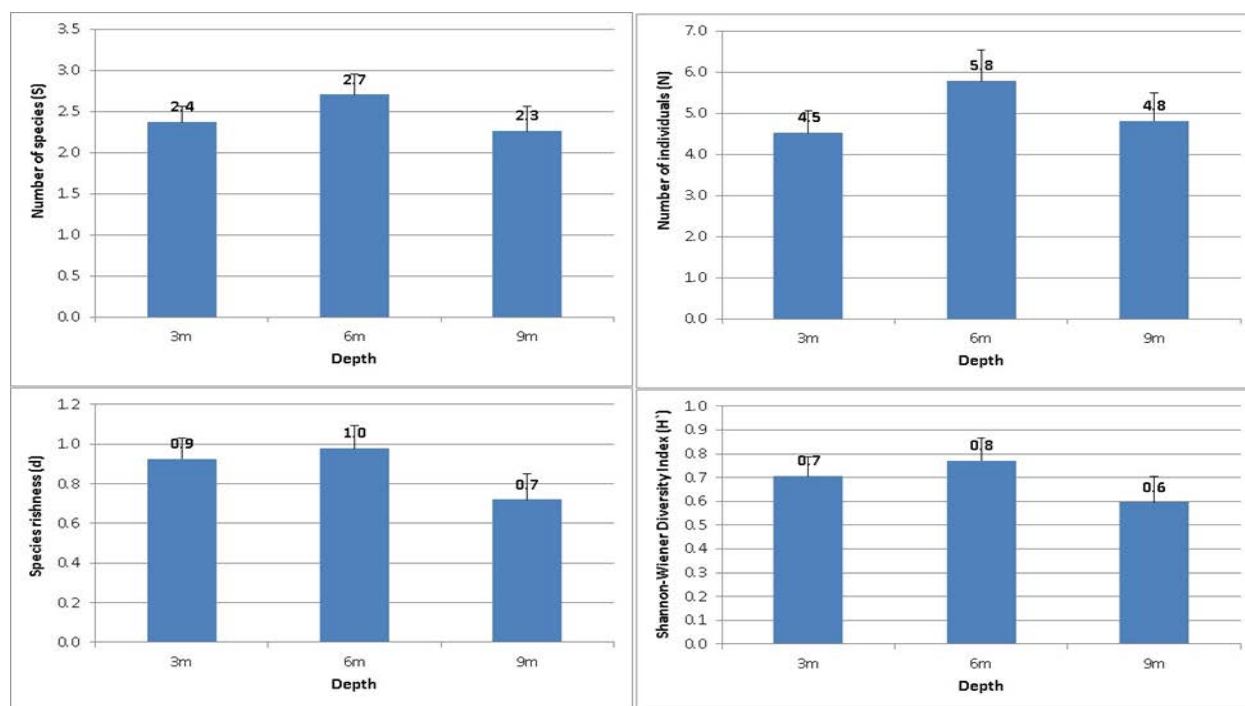
Figure 7. Average values of different ecological parameters measured per 250 m^2 at varying depths (3m, 6m, and 12m) along the Jordanian coast. These parameters include the mean number of species (S), the mean number of individuals (N), the mean species richness (d), and the mean Shannon-Wiener Diversity Index (H').

Regarding the abundance of individuals, the 6-m deep transects again come out on top, hosting the highest number of fish per transect (N=5.78). The 9-m deep transects show a substantial presence of fish (N=4.81), and the 3-m deep transects have a somewhat lower number of individuals (N=4.52). In contrast, the reef flat (RF) transects exhibit the lowest number of individuals (N=1.50).

To assess species richness, we calculated the dominance index (d) for each transect. The 6-m deep transects demonstrate the highest species richness (d=1.10), followed closely by the 3-m deep transects (d=1.04). Comparatively, the reef flat depth records the lowest species richness (d=0.91).

The Shannon-Diversity Index provides insight into the overall diversity within each transect. The 6-m deep transects display the highest diversity (H`=0.8), indicating a more balanced distribution of species. In comparison, the 3-m deep transects show slightly lower diversity (H`=0.7). The reef flat (H`=0.2), however, exhibits the lowest diversity, suggesting a less even distribution of species in this area.

Table 5 presents the statistical significance analysis for the variables S, N, d, and H` with respect to sites, depths, and habitat. The findings indicated a notable distinction between sites and habitat (p<0.05). However, no significant differences were observed among various depths for the variables S, N, d, and H.

Table 5. One-way ANOVA comparison test for mean number of species (S), mean fish abundance (N), species richness (d) and Shannon-Wiener Index (H`) at sites (7 sites), depths (RF, 3 m, 6 m, and 9m), and habitat (coral reef, sandy and seagrass) along the Jordanian coast.

Significance	S	N	D	H`
Between sites	< 0.0001	< 0.0001	< 0.0001	< 0.0001
Between depths	0.4274	0.3853	0.2543	0.4090
Between habitat	0.0019	0.0009	0.0019	0.0004

3.12. Site similarities

The analysis of the clusters has unveiled distinct patterns across the various sites, as depicted in Figure 8. Group A includes sites such as the Marine Science Station (MSS), Marine Park (MP), Barracuda Beach (BB), Sodasyat (SOD), Tala Bay Radisson (TBR), and Tala Bay Movenpick (TBM). These sites collectively represent the middle and southern regions of the Jordanian coastline along the Gulf of Aqaba. Conversely, Group B comprises the northern locations, including the Hotel Area (HA), Ghandor (GH), and Phosphate Loading Berth (PLB).
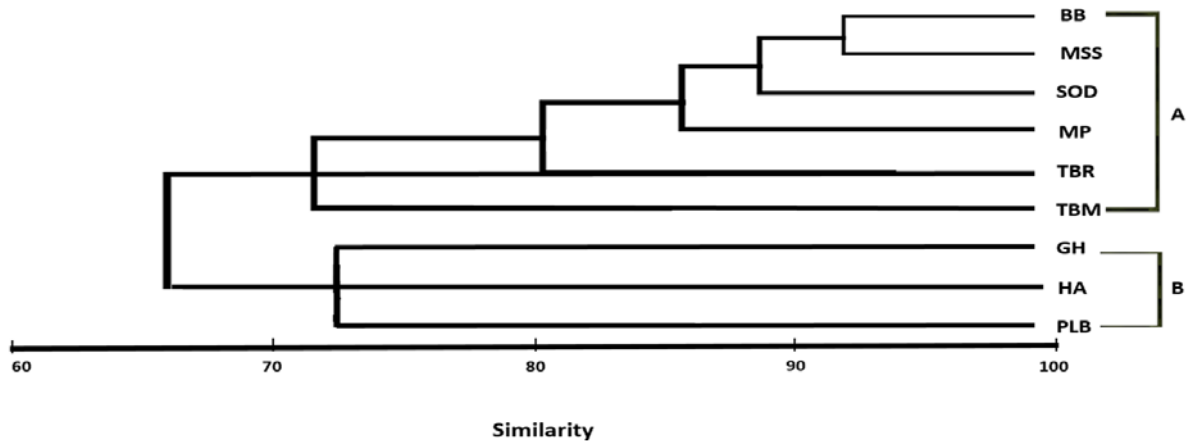
Figure 8. Dendrogram plot illustrating the comparative similarity among various sites including Hotel Area (HA), Ghandor (GH), Phosphate Loading Berth (PLB), Marine Science Station (MSS), Marine Park (MP), Barracuda Beach (BB), Sodasyat (SOD), Tala Bay Radisson (TBR), and Tala Bay Movenpick (TBM). The labels 'A' and 'B' denote distinct group clusters.

4. Discussion

Historically, research along the Jordanian coastline has predominantly been dedicated to commercial and coral reef fish, focusing on biological, ecological, and taxonomical aspects (Wahbeh and Ajiad 1987; Wahbeh 1992; Khalaf and Disi 1997; Al-Rousan et al. 2005; Khalaf and Crosby 2005; Khalaf and Krupp 2008; Krupp et al.,2009). However, there is a conspicuous absence of studies on hazardous marine creatures in this region. As beach traffic escalates due to local and international tourism, it is vital to gather precise information about these potentially dangerous animals. Moreover, the Jordanian coastline is grappling with considerable strain from rapid development and excessive exploitation of marine resources. Scorpion fishes, although not innately aggressive toward humans, can inflict harm due to human ignorance (Khalaf and Disi 1997). Thus, enhancing awareness and exercising caution in shallow waters are recommended preventative steps. Touching underwater objects while swimming or diving is strongly discouraged. The information, maps, and data derived from this research can assist policymakers in making informed decisions about beach safety and raise public awareness about the potential risks associated with dangerous Scorpion fishes. This knowledge can guide actions to lower injury risks and increase overall safety for beachgoers.

Of the globally recognized 219 scorpion fish species (Eschmeyer and Fong 2013), 19 are found in the Red Sea (Golani and Bogorodskey 2010), and 26 in the Arabian Sea. The Jordanian side of the Gulf of Aqaba hosts 14 identified species (Khalaf and Kochzius 2002a). This study adds seven species found at shallow depths across nine coastal sites to the existing knowledge of scorpion fish distribution, providing a basis for future research and conservation endeavors. The fish community distribution and abundance are largely dictated by depth and benthic habitat. The studies of Khalaf and Kochzius (2002a) have demonstrated that fish species richness is associated with substrate cover, habitat diversity, and live hard coral cover.

The statistical analysis showed distinctive differences among the sites for certain species, such as *Dendrohairus brachypterus, Pterois miles, P. radiata, S. barbatus*, and *S. verrucosa,* with *P. miles* being particularly abundant along the Jordanian coast, followed by *S. verrucosa*. This pattern may be attributed to the high prevalence of *P. miles* at seven sites and *S. verrucosa* at two sites. The habitats preferred by *P. miles* are coral reefs and sandy areas with sporadic corals, with their abundance possibly being influenced by food availability. Small fish species like *Neopomacentrus miryae, Chromis viridis,* and *Pseudanthias squamipinnis* inhabit patchy coral heads in the region. Conversely, species such as *Diplodus noct, Gerris oyena*, and *Scalopsis ghonam*, known to reside in sandy bottoms, may serve as a food source for *S. verrucosa*, which is mainly abundant at the PLB and HA sites. These sites feature sandy bottoms where *S. verrucosa* can bury itself, as noted by Khalaf and Disi (1997).

There were considerable differences in fish community structure and spatial distribution among coral reefs and seagrass beds. Coral reefs and seagrass beds surrounding Marsa Abu Dabab had fish communities typical of other inshore areas of the northern Red Sea. While some species were confined to either seagrass or coral reefs, others were widely distributed along the gradient. The settlement of larval and juvenile fish is also pivotal in determining the structure and stability of reef fish communities, with substrate type selection playing a role (Williams and Sale 1981). Many reef fish species prefer settling on live corals (Booth and Beretta 2002).

The GH site exhibited the greatest number of species, fish abundance, species richness, and species diversity, closely followed by the Hotel Area (HA). These sites were remarkably similar, sharing adjacent positions and similar habitat characteristics. Both contained small coral patches and rocks, creating ideal conditions for the species studied, as they use these features for camouflage and prey capture (Khalaf and Disi 1997). Habitat complexity accounted for 71% of the variation in species richness and 22% of total fish abundance variation, according to Gratwicke and Speight (2005).

Based on standardized and square root analysis, this study detected significant variations in the distribution patterns of scorpionfishes across different sites along the Jordanian coast of the Gulf of Aqaba. The dendrogram suggests the existence of two main clusters. The structure of dangerous marine organisms in GH and HA showed notable differences from other sites. The habitat in the northern part of the coast seemed to affect the presence of

scorpionfishes. Brokovich et al. (2006) reported a strong correlation between fish assemblages and different habitat types at the northern tip of the Gulf of Aqaba, a finding echoed by Khalaf and Kochzius (2002a). While Brokovich et al. (2006) stressed the importance of depth as a critical factor impacting fish community distribution and abundance, the results from this study contradicted their findings from the western side of the Gulf of Aqaba. This discrepancy might be attributed to the lower depths surveyed in this study, ranging from the reef flat to only 9 m deep.

This study found that the highest fish abundance occurred at 3 m deep transects, whereas the lowest number of fish species and individuals were observed in the reef flat area. This could be due to the unique conditions of this habitat. The reef's flat area is exposed to various physical factors, such as wind, waves, and sunlight, which result in a complex environment. In addition to rocks, sand, or mud, these physical factors pose different challenges to the organisms inhabiting this area. Species living in such environments need to be capable of tolerating significant fluctuations in salinity and moisture and withstand the potential impact of powerful waves to survive. *P. miles* was the most abundant fish species at 3, 6, and 9 m deep transects. This fish typically inhabits coral reef areas hosting schools of small fish, which are their primary food source. However, this species is considered one of the most common fish species in the *Pterois* genus (Khalaf and Disi 1997; Khalaf and Kochzius 2002a). Significant differences were observed in fish abundance, species richness, and diversity between sites and habitats. Statistical significance for fish assemblage showed a significant difference between habitats and sites. Fishes were most abundant in the GH and HA sites, which are dominated by seagrass, with some sandy and small coral patches. On the other hand, seagrass habitats had the highest diversity of fishes, whereas sand and coral reefs had lower diversity and fish abundance. These findings were also reported by Aguilar-Perera and Appeldoorn (2008), who observed that fish assemblages in seagrass beds were more diverse than in sandy and coral reef habitats. Aguilar-Perera and Appeldoorn (2008) concluded that seagrass beds are an important habitat for a number of fish species due to the diversity of food resources and availability of hiding places.

5. Conclusions

In conclusion, this study has elucidated the community structure and distribution patterns of scorpion fishes along the Jordanian shoreline of the Gulf of Aqaba. The investigation pinpointed seven unique species of scorpion fish inhabiting various coastal locations and depths, with *Pterois miles* and *Synaneia verrucosa* standing out as the most prevalent species. Moreover, the research underscores the significant impact of specific locations and habitats on the abundance, species richness, and diversity of these fishes. Coral reef habitats were characterized by the greatest fish abundance and diversity, while seagrass habitats demonstrated superior species richness. The study has also revealed striking disparities in the community structure and spatial distribution of fish across northern locales compared to middle and southern areas. These findings offer invaluable insights for policymakers and beachgoers alike, promoting enhanced safety measures and fostering awareness regarding the potential hazards posed by these dangerous marine creatures. On the whole, this research augments the existing body of knowledge regarding scorpion fish distribution and could act as a cornerstone for future conservation endeavors in the region.

6. Acknowledgements

7. References

Aguilar-Perera, A., and R.S. Appeldoorn. 2008. Spatial distribution of marine fishes along a cross-shelf gradient containing a continuum of mangrove seagrass-coral reefs off southwestern Puerto Rico. *Estuarine Coast Shelf Sci* 76: 378-394.

Al-Rousan, S., Rasheed, M., Khalaf, M.A., and M. Badran. 2005. Ecological and geochemical characteristics of bottom habitats at the northern Jordanian coast of the Gulf of Aqaba. *Chem Ecol* 21(4): 227-239.

Booth, D.J., and G.A. Beretta. 2002. Changes in a fish assemblage after a coral bleaching event. *Mar Ecol Prog Ser* 245: 205-212.

Brokovich, E., Baranes, A., and M. Goren. 2006. Habitat structure determines coral reef fish assemblages at the northern tip of the Red Sea. *Ecological Indictors* 6: 494−507.

doi:10.1016/j. ecolind.2005.07.002

Church, J.E., and W.C. Hodgson. 2002. The pharmacological activity of fish venoms. *Toxicon* 40(8): 1083-1093. doi:10.1016/s0041-0101(02)00126-5

English, C., Wilkinson, C., and V. Baker. 1994. *Survey manual for tropical marine resources*. Australian Institute of Marine Science, Townsville.

Eschemeyer, W.N., and J.D. Fong. 2013. *Species of fishes by family/subfamily*. Available at: http://research.calacademy.org/research/ichthyology/catalog/SpeciesByFamily.asp (accessed 16 July 2013).

Golani, D., and S.V. Bogorodsky. 2010. The fishes of the Red Sea - reappraisal and updated checklist. *Zootaxa* 2463: 1-135.

Gratwicke, B., and M.R. Speight. 2005. The relationship between fish species richness, abundance and habitat complexity in a range of shallow tropical marine habitats. *J Fish Biol* 66 (3): 650-667.

Khalaf, M.A. 2004. Fish fauna along the Jordanian Coast - Gulf of Aqaba. *J Faculty Marine Sci* 15: 23-50.

Khalaf, M.A., and A.M. Disi. 1997. *Fishes of the Gulf of Aqaba*. Marine Science Station, Aqaba, Publication no. 8M.

Khalaf, M.A., and M. Kochzius. 2002a. Community structure and biogeography of shore fishes in the Gulf of Aqaba, Red Sea. *Helgol Mar Res* 55: 252-284.

Khalaf, M.A., and M. Kochzius. 2002b. Changes in trophic community structure of the shore fishes at an industrial site in the Gulf of Aqaba, Red Sea. *Mar Ecol Prog Ser* 239: 287-299.

Khalaf, M.A., and M. Crosby. 2005. Assemblage structure of butterflyfish and their use as indicators of Gulf of Aqaba benthic habitat in Jordan. *Aquatic Conserv* 15: S27-S43.

Khalaf, M.A., and F. Krupp. 2008. A new species of *Symphysanodon* (Perciformes: Symphysanodontidae) from the Gulf of Aqaba, Red Sea. *Aqua* 4: 2-14.

Krupp, F., Zanjonz, U., and M. Khalaf. 2009. A new species of the deepwater cardinal fish genus Epigonus (Perciformes: Epigonidae) from the Gulf of Aqaba, Red Sea. *Aqua* 15: 4-15.

Manasrah, R. 2002. The general circulation and water masses characteristics in the Gulf of Aqaba and northern Red Sea. Ph.D. thesis, Meereswissenschaftliche Berichte Institut für Ostsee Forschung Warnemünde, Universität Rostock.

Mutair, R.M.D., Amayreh, W., Salayta, G., and I. Khashashneh. 2006. Marine animal injuries to children in the south of Jordan. *Middle East J Family Medicine* 4(5).

Myers, R.F. 1991. *Micronesian reef fishes: A practical guide to the identification of the inshore marine fishes of the tropical Central and Western Pacific*. Coral Graphica, USA, 298 p.

Primer-E. 2000. PRIMER 5 (Plymouth Routines in Multivariate Ecological Research). PRIMER-e, Plymouth Marine Laboratory, UK.

Randall, J.E. 2010. *Shore Fishes of Hawaii: Revised Edition*. University of Hawaii Press.

Roberts, C.M., and R.F.G. Ormond. 1987. Habitat complexity and coral reef fish diversity and abundance on Red Sea fringing reefs. *Marine Ecol Progr Series* **41**: 1–8.

doi:10.3354/ meps041001

Sivan, G. 2009. Fish venom: pharmacological features and biological significance. *Fish Fisheries* 10(2): 159-172.

Smith, L., Stern, J.H., Girard, M.G., and M.P. Davis. 2016. Evolution of venomous cartilaginous and ray-finned fishes. *Integr Comp Biol* 56: 950-961.

Sokal, R.R., and J.F. Rohlf. 1981. *Biometry, the principles and practice of statistics in biological research*. San Francisco: W.H. Freeman, 859 p.

UNEP/IUCN. 1988. *Coral reefs of the world*. UNEP Regional Sea Directories and Bibliographies. IUCN, Gland, Switzerland and Cambridge; UK/UNEP, Nairobi, Kenya.

Wahbeh, M.I. 1992. Some aspects of reproduction and growth of three species of fusilier (Pisces: Caesionidae) from Aqaba, Red Sea, Jordan, *Dirasat* 19(B): 157-172.

Wahbeh, M.I., and A. Ajiad. 1987. Some fishes from the Jordanian coast of the Gulf of Aqaba. *Dirasat* 1: 137-154.

Wahsha, M., Al-Tarawneh, H., Khalaf, M., Hayek, W., Sbaihat, M., and T. Al-Najjar. 2021. Cardiovascular responses to Stonefish Synanceia verrucosa venom in balb/c mice. *Fresenius Environ Bull* 30(2): 891-898.

Williams, McB., and P.F. Sale. 1981. Spatial and temporal patterns of recruitment of juvenile coral reef fishes to coral habitats within One Tree Lagoon, Great Barrier Reef. *Mar Biol* **65**: 245-253.

Diversity of Bioactive Metabolites Produced by Thermophilic *Bacillus* Strains Isolated from Jordanian Hot Springs

Khalid Fandi[1,*], Muhanad Massadeh[2] and Abdelrahman Tawaha[1]

[1]*Department of Biological Sciences, Al-Hussein Bin Talal University, Ma'an, Jordan;* [2] *Department of Biology and Biotechnology, Faculty of Sience, The Hashemite University, Al-Zarqa, Jordan*

Abstract

This study explores the metabolic diversity of thermophilic *Bacillus* species isolated from Jordanian hot springs. Sixteen strains from Ma'en thermal springs, exhibiting robust growth at elevated temperatures (45-55°C), were investigated for their potential in producing valuable bioactive compounds. Crude extracts, obtained through organic solvent extraction, underwent HPLC-MS analysis to reveal secondary metabolite spectra under various growth conditions. Strains M5a, M13a, and M1c displayed potential in producing biologically active metabolites. The purification process of the M5a strain extracts involved sequential techniques including silica gel, Sephadex LH-20, RP18 column chromatography, and preparative TLC. This process resulted in the isolation of diverse compounds, including indole derivatives (1-acetyl-β-carboline, indole-3-carboxylic acid, tryptophol), adenosine, tyrosol, p-hydroxy-benzaldehyde, ferulic acid, uracil, 3-methyl uracil, and the identification of four diketopiperazine derivatives (cyclo (Phe, Pro), cyclo (Pro, Ile), cyclo (Leu, Pro), and cyclo (Pro, Tyr)). Structural validation of these compounds was achieved through AntiBase, utilizing 1H NMR and MS data and literature comparisons. Despite similar metabolic profiles, strains exhibited varying activities, including antimicrobial potential. This study marks the first report on purified biochemical compounds from thermophilic bacteria, emphasizing untapped microbial diversity in thermal springs. Intriguing activities and distinct UV-absorbing bands on TLC suggest promising prospects for isolating novel, active metabolites. This research enhances our understanding of the biotechnological potential of thermophilic *Bacillus* strains, emphasizing the importance of exploring their chemodiversity for industrial applications and functional genomics.

Keywords: LC-MS/MS, Thermophilic bacteria, Metabolites diversity, Bacillus, hot springs

1. Introduction:

Extremophiles, a fascinating group of microorganisms, thrive and reproduce under extreme environmental conditions, such as high temperatures, extreme pH levels, elevated ion concentrations, and radioactivity. This unique adaptation involves the evolution of specialized biological components and metabolic pathways that enable survival and growth in challenging environments (Krishnaraj and Sani, 2017; Singh *et al*., 2019). In recent years, the significant interest in extremophiles has been driven by their ability to catalyze chemical reactions under severe conditions, offering potential applications across various industries (Dumorne and Cordova, 2017; Geng *et al*., 2018; van den Burg, 2003).

Among extremophiles, thermophilic microorganisms, flourishing in warm environments, play a pivotal role in the synthesis of fuels and chemicals. Their proficiency in operating under high-temperature conditions enhances product yields and mitigates contamination risks, making them particularly attractive for industrial applications. Additionally, thermophiles serve as rich sources of thermostable enzymes crucial for industrial processes (Böhme *et al*., 2020; Rigoldi *et al*., 2018). The temperature spectrum for thermophilic microorganisms categorizes them into moderate thermophiles thriving at 50–60 °C, extreme thermophiles at 60–80 °C, and hyperthermophiles at 80–110 °C (Baker *et al*., 2001). Extreme thermophiles, with their exceptional thermal stability and ability to grow at temperatures exceeding 80°C, present promising candidates for applications such as high-temperature fermentation, waste treatment, and mineral leaching (Brock, 1986; Kelly and Brown, 1993; Kelly *et al*., 1994). Researchers find significant value in thermophiles due to their unique characteristics and potential applications in biotechnology.

In this context, the study of gene function on a genome-wide scale, known as functional genomics, has been instrumental in unraveling the molecular mechanisms underpinning the adaptation of thermophiles to extreme conditions. A significant outcome of functional genomics research on thermophilic microorganisms is the identification of heat shock proteins (HSPs) (Hartl *et al*., 2011; Lindquist and Craig, 1988; Morimoto, 1998; Parsell and Lindquist 1993). These proteins play a critical role in preventing protein denaturation and aggregation, thereby shielding cells from the adverse effects of high temperatures (Kuczynska-Wisnik *et al*., 2002).

---

* Corresponding author. e-mail: fandikh@ahu.edu.jo , fandikh@yahoo.com .

Delving into the realm of cellular stress responses in *Escherichia coli* (*E. coli*), Kuczynska-Wisnik *et al.* (2002) explored the protective function of the diminutive heat-shock proteins IbpA and IbpB, shedding light on how these proteins prevent the aggregation of endogenous proteins denatured in vivo during severe heat shock. This work significantly contributes to understanding the cellular response to extreme heat shock in *E. coli*, underscoring the crucial role of IbpA and IbpB as guardians against protein aggregation. In response to heat stress, additional genes implicated in protein folding, modification, and degradation have been found to be upregulated, marking another avenue of interest in functional genomics research on thermophiles. A crucial aspect of this research involves the exploration of the metabolic pathways enabling thermophilic microorganisms to thrive in high-temperature environments. The identification of genes involved in the production of compatible solutes, such as trehalose and proline, has provided insights into how thermophiles maintain cellular integrity and prevent protein denaturation under extreme conditions.

Continued progress in understanding the molecular mechanisms behind the adaptation of thermophilic microorganisms to high-temperature environments is facilitated by functional genomics. This ongoing exploration offers valuable insights into the potential applications of these unique organisms across disciplines like biotechnology and environmental science by identifying key genes and pathways involved in these processes.

Noteworthy among the rich sources of thermophilic bacteria are Jordan's hot springs, recognized for their capacity to produce thermostable enzymes and bioactive substances (Al-Daghistani *et al.*, 2021; Obeidat and Al-Shomali, 2023), which constitute a valuable reservoir of thermophilic bacteria. This study is dedicated to addressing the existing knowledge gaps concerning aerobic thermophilic bacteria derived from Jordan's hot springs. Despite their diverse metabolic processes, these bacteria remain relatively unexplored. Our investigation aims to elucidate the production of biochemical compounds by these bacteria when cultured using various media as the exclusive source of carbon. Through a comprehensive exploration of their metabolic capabilities, our study seeks to unveil the untapped biotechnological potential of thermophilic *Bacillus* strains and contribute to a broader comprehension of the roles of extremophiles in natural product discovery. Significantly, this work marks the inaugural report on the purified biochemical compounds profiled from thermophilic bacteria, emphasizing its novelty and potential impact on biotechnology.

2. Materials and Methods

2.1. Sampling of Thermal Springs Water:

Water samples were carefully gathered from diverse points within Ma'en's primary thermal springs in Jordan, utilizing sterile thermal glass tubes (50 ml). The collection points were strategically selected away from the peripheries, and samples were obtained from a depth of 15 cm below the spring's surface. Subsequently, the samples were promptly transported to the laboratory for immediate culturing. The collected thermal water exhibited temperatures ranging from 45°C to 60°C and a pH between 7.2 to 7.8. This approach was implemented to ensure a representative sample of thermophilic aerobic bacteria.

2.2. Isolation and cultivation of thermal bacterial strains

The culturing of water samples from each tube was carried out in a nutrient broth (NB) medium. Specifically, 5 ml from each sample was introduced into 50 ml of nutrient broth containing 1.5% peptone, 0.5% NaCl, 0.5% meat extract, 0.03% K_2HPO_4, and adjusted to a pH of 7.2. The mixture was then incubated at 50°C for 48 hours with agitation at 180 rpm in a laboratory shaker. Subsequently, a loopful from each culture was streaked onto nutrient agar plate and subjected to the same incubation conditions. Pure cultures were established through successive transfers on new nutrient agar plates, resulting in sixteen isolates designated as M1a, M2a, M3a, M4a, M5a, M1b1, M13a, M1c, M2c, M3c, M3c1, M4d22a, M4c, M5a2, M5b1, and M5b2.

2.3. Cultivation and crude extract preparation for pre-screening

The sixteen selected isolates were cultured as subcultures on agar plates for 24 hours at 50°C. This was achieved using 1.5% nutrient agar, composed of beef extract (3 g/l), peptone (5 g/l), NaCl (8 g/l), and agar (15 g/l). Subsequently, the resulting subcultures were utilized to inoculate Erlenmeyer flasks (1000 mL) with a half loop of growth obtained from the colonies on agar plates. Each flask contained 250 mL of NB medium, with the pH adjusted to 7.8 prior to sterilization. These flasks were then incubated at 50°C on a linear shaker set to 180 rpm for 24 hours.

For the large-scale preparation of crude extracts for each strain, cultivation was carried out using 5 ml of culture obtained from the previous step. This culture was inoculated into four separate 250 mL Erlenmeyer flasks (a total volume of 1L) containing NB medium. Additionally, L-Valine and L-Lucine amino acids were added to the culture medium at concentrations of 0.3% and 0.01%, respectively. The incubation continued for 2 days on a linear shaker under the same aforementioned conditions. Following the harvesting of the dark brown culture, the broth underwent filtration over a celite bed using vacuum filtration with a Buchner funnel to separate the biomass from the liquid phase. After filtration, the biomass scraped from the top of the filter underwent ethyl acetate extraction three times (3 ×). Each extraction cycle occurred under ultrasonic irradiation (Ultraturrax: Janke & Munkel KG) for 10 min per cycle. Simultaneously, the liquid phase was extracted twice with ethyl acetate. Subsequently, the organic phases from all these extractions were combined and then concentrated by evaporation using a rotary evaporator (Rotavapor R152) to obtain the crude extracts. For quantification, the crude extract was suspended in 10% CH_2Cl_2, dried with air, and stored in a refrigerator at 4°C. These extracts underwent a comprehensive analysis, including chemical and biological screening, as well as HPLC-MS analysis.

2.4. Media optimization and production

Five distinct media, which were modified in Laatsch's laboratory, were employed to determine the most efficient

medium for the large-scale cultivation of thermophiles. These five different media, labeled as A, B, C, D, and E, consisted of the following component: **A**: yeast extract 4 g, malt extract 10 g, , and glucose 4 g in 1 L of dH_2O, **B**: mannitol 20 g, soya been fat 20 g, and in 1 L of dH_2O, **C**: peptone 2 g, glucose anhydrous 10 g, , yeast extract 1 g, and meat extract 1 g in 1 L of dH_2O, **D**: yeast extract 40 g, $CaCl_2$ 45 g, glucose 5 g, and in 1 L of dH_2O, **E**: yeast extract 5 g, trypton 10 g, , NaCl 10 g, and glucose 5 g in 1 L of dH_2O,). The pH of each medium was adjusted to 7.8 before undergoing autoclaving at 121°C for 15 minutes. Before autoclaving at 121°C for 15 minutes, the pH of each medium was adjusted to 7.8. The bacterium was then cultivated in an incubator shaker at 55°C, with agitation at 180 rpm, for a period of 3-5 days.

2.5. Chemical screening

For the chemical screening process, a combination of TLC with spraying reagents and HPLC-MS methods was employed.

2.5.1. Thin layer chromatography (TLC)

The crude extracts obtained from the selected strains underwent Thin-Layer Chromatography (TLC) analysis to examine the nature of secondary metabolites produced by them. In this procedure, a small sample drop was accurately deposited onto the TLC plate using a capillary and allowed to dry. Each extract was applied to two TLC plates. To ensure an appropriate sample quantity (ranging from 2 to 5 micrograms) on the plate, this spotting process was repeated by overlaying additional drops onto the initial spot. Subsequently, the TLC plates were developed using a solvent system comprising CH_2Cl_2 and 5% MeOH. After development, the zones on the plates were observed under ultraviolet (UV) light at both 254 nm and 366 nm wavelengths. Components exhibiting UV absorption or fluorescence were identified and marked accordingly. Following UV visualization, one plate underwent staining with an anisaldehyde/H_2SO_4 spraying reagent (anisaldehyde, methanol, H_2SO_4, acetic acid), while the second plate was sprayed with Ehrlich's reagent (HCl 37%, 4-dimethylamino benzaldehyde, MeOH) to detect different colored bands of compounds in the extracts, specifically designed for the detection of indoles. This treatment served to further pinpoint areas of interest. The resulting colored bands, resembling a metabolic fingerprint, resulted from reactions between the spray reagent and the metabolites. These bands were carefully marked and systematically documented through scanning procedures.

2.5.2. 2.5.2 High-Performance Liquid Chromatography-Mass Spectrometry (HPLC-MS)

The preparation of samples holds paramount importance when employing a High-Performance Liquid Chromatography-Mass Spectrometry (HPLC-MS) method for the analysis of biological samples. It necessitates the establishment of fundamental principles encompassing robustness and uniformity, which are prerequisites for any analytical assay. Typically, a concentration range spanning from 1 to 5,000 ng/ml is requisite for this purpose. Methanol/water was chosen as the solvent for this procedure, with methanol (LiChrosolv hypergrade for liquid chromatography) procured from Merck.

2.6. Extraction and purification of the active compounds

Selected strains were expanded through fermentation on a scale of 15-30 liters, and crude extracts were processed through chromatography and preparative thin-layer chromatography (PTLC) for additional purification steps.

2.6.1. Large-Scale Fermentation and crude extraction

A 30-liter fermentation of thermophilic *Bacillus* strain Ma5 was conducted by employing two sets of 60 Erlenmeyer flasks (1 L each), with each flask containing 250 mL of medium D. This fermentation was carried out at pH 7.8, using a linear incubator shaker set at 180 rpm and 55°C for a duration of 5 days. After harvesting the culture, the broth was filtered over celite using a filter press (Schenk Niro 212 B40) to separate the biomass from the liquid phase. The water phase was extracted by adsorption on Amberlite XAD-16 resin (obtained from Rohm and Haas, Frankfurt, Germany) in a large-size glass column (1.2 m x 10 cm). After washing with distilled water (2 L) to remove salts and sugars, the column was eluted with methanol. The methanol extract was concentrated in vacuo at 40°C to the aqueous residue. The remainder was re-extracted by ethyl acetate (3-4 times). Meanwhile, biomass was extracted using ethyl acetate (3 ×) followed by acetone (2 ×) under ultrasonic irradiation and mixed for 15 min each time. The acetone extract was concentrated in vacuo and the obtained aqueous residue was again extracted with ethyl acetate (2 ×). The ethyl acetate extracts obtained from both the filtrate and biomass, which contained bioactive metabolites, were combined and dried using a rotary evaporator (Rotavapor R152). This process yielded 6.94 grams of crude extracts in the form of dark brown residues.

2.6.2. Purification of the active compounds and structural elucidation

The crude extract (6.94 g) underwent fractionation through flash chromatography on silica gel column (1.5 × 50 cm) packed with 30 g of silica gel (Kieselgel 60, 230 ~ 400 mesh, Merck, Germany). Fractionation occurred by elution with a CH_2Cl_2: MeOH solvent mixture using a gradient of concentrations (1, 3, 5, 10, 20, 40, and 50%, vol/vol). The resulting fractions were monitored by TLC (CH_2Cl_2/MeOH 19:1, spraying with an anisaldehyde/H_2SO_4 acid reagent and warming). Fractions with similar profiles in analytical high-performance liquid chromatography (HPLC) and TLC were combined, yielding four primary fractions labeled as I, II, III, and IV. The first fraction I underwent re-fractionated on silica gel column chromatography (1.2 × 30 cm, packed with 15 g of silica gel, CH_2Cl_2–MeOH), followed by purification on Sephadex LH-20 (column 5 × 40 cm, CH_2Cl_2 -40% MeOH). Fraction III underwent further purification through silica gel column chromatography, Sephadex LH-20 in a column (86 × 2.0 cm) eluted with CH_2Cl_2: 40% MeOH, and Preparative TLC (PTLC). The section of the PTLC plate containing a fraction was scraped, dissolved in methanol. The mixture was then centrifuged to separate from silica, and the obtained supernatant was further subjected to filtration. Following filtration, the solvent evaporated. The resulting precipitate was dried and then washed with a mixture of cyclohexane /CH_2Cl_2. Subsequently, it was dissolved in CH_2Cl_2 with 10%

MeOH to obtain the purified fraction. Fraction II was re-chromatographed on a Sephadex LH-20 column (5 × 40 cm) using H_2O-MeOH mixtures for elution, resulting in three major sub-fractions. Sub-Fraction 1 was identified as fat using TLC and spraying reagents. Major Sub-fraction 2 (1 g) underwent re-chromatography on a Sephadex LH-20 column (2 × 20 cm), eluted with H_2O-MeOH mixtures, and further purified on an RP-18 column (2 × 20 cm) with elution using 10 to 50% MeOH, resulting in a white precipitate. Fraction IV was also purified on Sephadex LH-20 (MeOH), followed by RP-18 silica gel (MeOH/H_2O gradient 10 to 50% MeOH). The isolated pure compounds derived from distinct chromatographic fractions of the filtrate extract were characterized by PTLC and size exclusion chromatography. Their structures were elucidated through the analysis of 1 and 2D high field NMR spectroscopy (up to 600 MHz), MS, UV, and IR data, and were further validated by comparing them with information from the AntiBase database (Laatsch, 2009).

3. Results and Discussion

3.1. TLC Analysis and Optimization of Growth Medium

The investigation focused on analyzing extracts derived from the crude extract of three thermophilic *Bacillus* strains, meticulously chosen from a pool of sixteen isolates obtained from Jordan hot springs. These strains, cultivated under diverse growth conditions, revealed substantial differences in the profiles of biochemical compounds, as indicated by TLC plates. The TLC chromatogram profiles exhibited notable variations in metabolite production among the selected strains (Fig. 1 and Fig. 2). Remarkably, $CaCl_2$ medium (D) emerged as the most favorable for metabolite production, demonstrating superior results compared to the other four growth media tested (Fig. 1). The observed variations in TLC profiles suggest a dependency of metabolite production on the growth conditions and media composition. $CaCl_2$ medium (D)

was identified as a superior medium for metabolite production, aligning with the findings from the TLC results. Significantly, three out of the sixteen screened strains, namely M5a, M13a, and M1c, demonstrated substantial potential for production biologically active metabolites (Fig. 2). Notably, these three strains exhibited noteworthy antimicrobial activity, particularly against gram-positive bacteria, aligning with previous findings highlighting the heightened antagonistic activity of *Bacillus* species against this bacterial group (Gomez-Escribano and Bibb, 2011). This specificity against gram-positive bacteria is consistent with reports indicating superior antagonistic activity of *Bacillus* sp. against this bacterial group (Jia *et al*., 2020; Yilmaz *et al*., 2006). While *Bacillus* species are widely recognized as rich sources of antimicrobial compounds, with numerous reports documenting their antimicrobial potential (Nagai *et al*., 2003), this study underscores that thermophilic *Bacillus* strains, especially those obtained from Jordan hot springs, remain relatively unexplored for the discovery of novel and stable antimicrobial compounds (Gebhardt *et al*., 2002). The untapped potential was further highlighted as recent studies continue to unveil the isolation of novel antimicrobial agents from the *Bacillus* genus (Davies, 2013; Nielsen *et al*., 2017). Nevertheless, our investigation positions thermophilic *Bacillus* strains, particularly those obtained from Jordan hot springs, as promising resources for the discovery of novel and stable antimicrobial compounds, showcasing their potential for diverse biotechnological applications (Xiao *et al*., 2021). Consequently, these strains were scaled up and subjected to further characterization and purification of the biologically active compounds, paving the way for future exploration and potential applications in various fields. The intriguing activities and clearly identifiable UV-absorbing bands on TLC indicate promising avenues for future efforts in isolating novel and active metabolites from these strains.
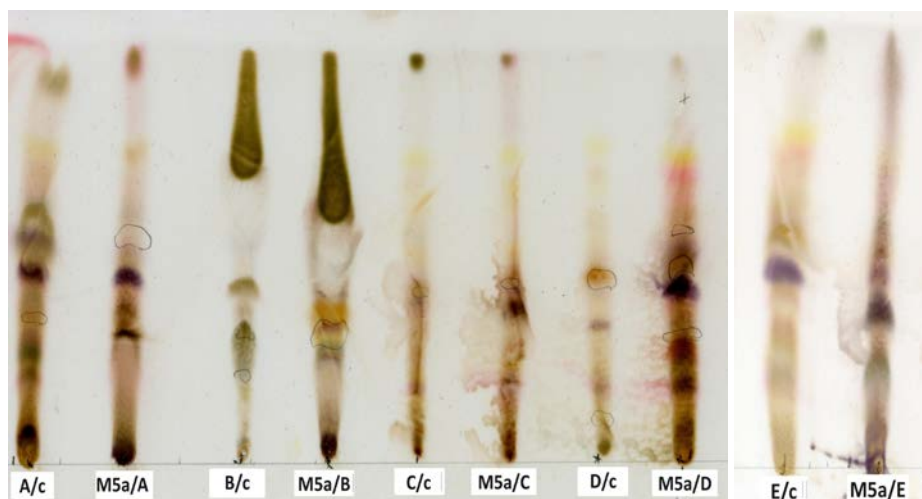
Figure 1. TLC chromatogram profile depicting the production of metabolites from the thermophilic bacillus strain (M5a) in various growth media (A, B, C, D and E). The control samples for each corresponding medium are indicated as A/c, B/c, C/c, D/c, and E/c.
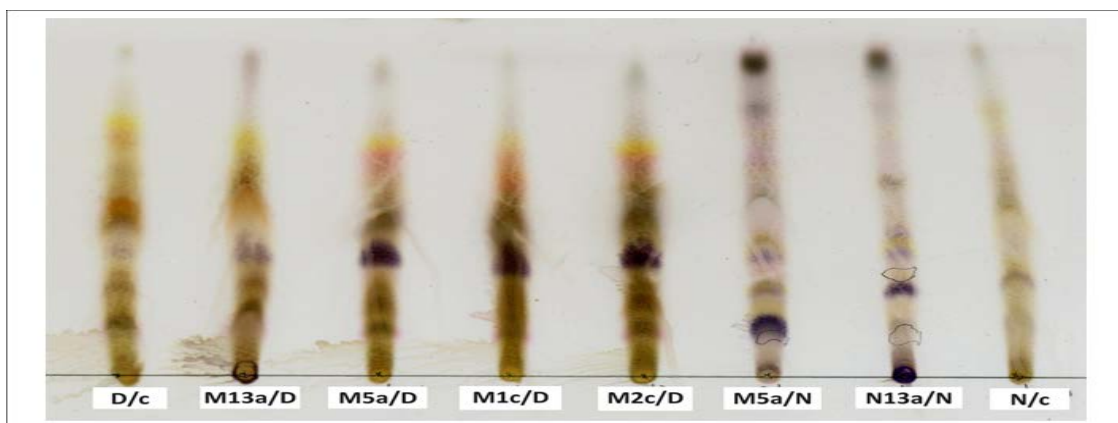
Figure 2. A comparison of the TLC chromatogram profiles illustrating the production of metabolites from various thermophilic Bacillus strains (M5a, M13a, M1c, and M2c). The strains and their corresponding media are provided, along with controls (D/c for CaCl2 medium and N/c for nutrient broth).

3.2. LC-MS/MS Analysis: Revealing the Complexity and Diversity of Metabolites in Thermophilic Bacillus Strains

Expanding upon the insights garnered from TLC analysis and the optimization of growth media, LC-MS/MS analysis was employed to provide a more comprehensive exploration of the metabolites produced by thermophilic *Bacillus* strains. This in-depth analysis included the fermentation extracts of selected strains (M5a, M13a, and M1c) as well as additional strains that exhibited variation in metabolite production. This advanced analytical approach provided a deeper understanding of the metabolites produced under varying growth conditions, revealing a rich tapestry of secondary metabolites with distinct profiles (Fig. 3). The LC-MS/MS analysis unveiled diverse profiles of secondary metabolites across the selected strains, shedding light on the intricacies of their metabolic pathways under varying growth conditions (Fig. 3). The results unveiled a diverse array of secondary metabolite profiles influenced by varying growth conditions. Notably, $CaCl_2$ medium (D) emerged as the most favorable for metabolite production, showcasing the highest yields when compared to the other four tested growth media. This is exemplified by the distinct profile spectrum of the selected strain M5a under different growth conditions (Fig. 4). The LC-MS/MS analysis played a pivotal role in this exploration, providing a deeper understanding of the metabolites (Xiao *et. al*., 2012). The meticulous sample preparation, utilizing methanol/water as the solvent, ensured robust and uniform results. The chosen concentration range of 1 to 5,000 ng/ml optimized sensitivity and allowed for the detection of a broad range of metabolites (Chhonker *et al*., 2023). The utilization of HPLC-MS unraveled a plethora of metabolites, accentuating the complexity and diversity of secondary metabolite production within thermophilic bacteria. The observed diversity in LC-MS/MS profiles among the selected strains further underscores the vast potential of thermophilic bacteria to produce a wide array of biologically active secondary metabolites. These variations in metabolite profiles serve as a testament to the significance of optimizing growth conditions for the enhanced production of specific metabolites, adding a layer of intricacy to the metabolic capabilities of thermophilic strains. Such endeavors will unravel the potential applications of these compounds in pharmaceuticals and other industries. The comprehensive analytical foundation laid by TLC and LC-MS/MS serves as a cornerstone for understanding the metabolic intricacies of these thermophilic strains, propelling us forward into further exploration within the realm of bioactive compound discovery.
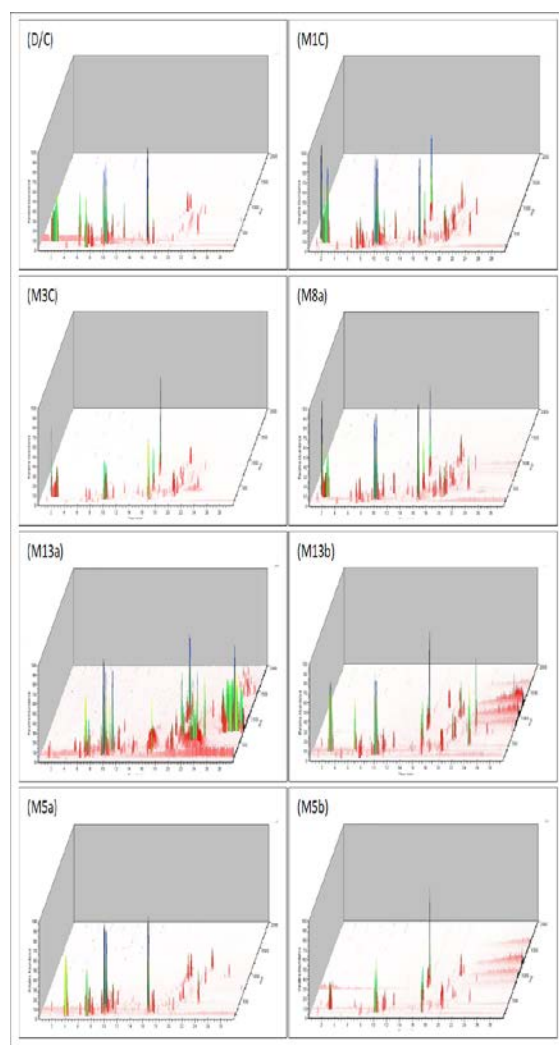
Figure 3. LC-MS/MS screening profile of metabolite production by different strains of thermophilic bacteria under growth media D, as derived from crude extracts. Strains are labeled with the number, and D/C refers to the control group.
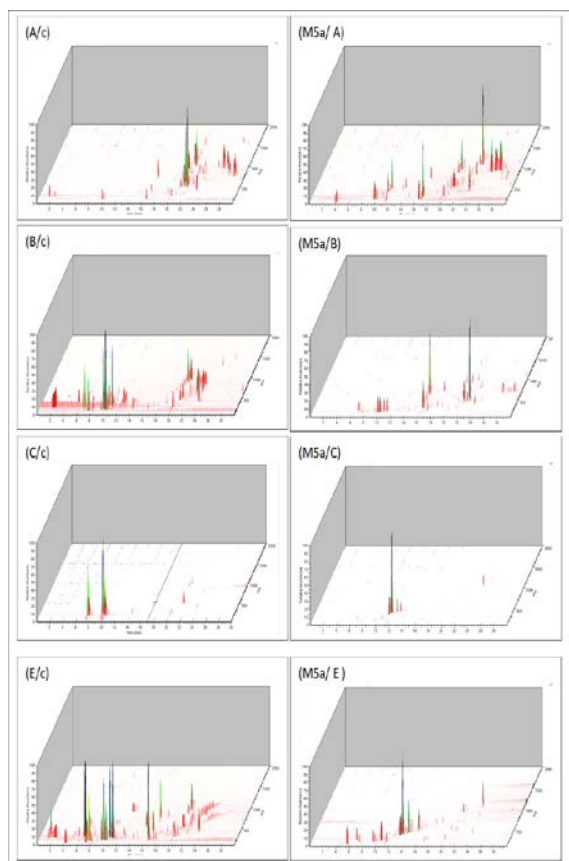
Figure 4. LC-MS/MS screening profile of metabolite production by the thermophilic *Bacillus* strain M5a under various growth media conditions (A, B, C, and E). The strain is denoted along with the respective media, and controls (C) are also specified with their corresponding media.

3.3. Purification and structure elucidation of the active compounds

Bulk fermentation, crucial for large-scale production, was conducted utilizing $CaCl_2$ medium (D), previously identified as the optimal medium for metabolite production. Following the fermentation process, cell separation and extraction were meticulously carried out using three distinct solvents: methanol, ethyl acetate, and acetone as illustrated in Fig. 5. The distinct TLC chromatogram profiles facilitated a clear differentiation of metabolites extracted using these solvents, revealing their efficiency in extracting diverse components from the M5a strain (Fig. 5). The amalgamation of these extracts yielded a total of 6.94 g of crude extract obtained from both the cell mass and the liquid phase. Subsequently, the components of the crude extract underwent purification through Flash chromatography on a silica gel column. TLC profiles were instrumental in guiding the purification process, leading to the isolation of four primary fractions (Fig. 6). Each of the distinct fractions (Fraction I, Fraction II, Fraction III, and Fraction IV) encompassed unique components with potential bioactive properties. The subsequent TLC chromatogram, generated from the four primary fractions obtained through flash chromatography on a silica gel column (Fig. 6), unequivocally illustrated the efficacy of the purification process. Each fraction underwent meticulous collection and further analysis. Fraction II underwent re-chromatography on a Sephadex LH-20 column, resulting in the generation of three major

sub-fractions. These sub-fractions were subsequently subjected to further purification on an RP-18 column, leading to the isolation and identification of various indole and indole derivative compounds, including 1-acetyl-β-carboline (1), indole-3-carboxylic acid (2) tryptophol (3), adenosine (4), and tyrosol (5). Fraction IV underwent purification on Sephadex LH-20, followed by RP-18 silica gel, yielding p-hydroxy-benzaldehyde (6) and ferulic acid (7) (refer to Table 1). The subsequent purification steps for Fraction I involved re-fractionation and purification on Sephadex LH-20, employing additional chromatographic techniques. Fractions underwent re-fractionation on a silica gel column, preparative TLC, and purification on a Sephadex LH-20 column, resulting in the isolation of uracil (8) and 3-methyl uracil (9) (refer to Table 1). Fraction III underwent a rigorous purification process, including silica gel column chromatography, Sephadex LH-20, and preparative TLC. This comprehensive methodology highlights the meticulous approach utilized in the isolation and purification of active compounds, resulting in the identification of four diketopiperazine derivatives: cyclo (Phe, Pro) (10), cyclo (Leu, Pro) (11), cyclo (Pro, Ile) (12), and cyclo (Pro, Tyr) (13). The chemical structures of the isolated compounds were rigorously validated through comparisons with the AntiBase database (Laatsch, 2009), confirming their identities. The determination of these structures involved comprehensive spectroscopic analyses, including 1H NMR, HR-ESI-MS, and mass spectrometry, aligning with literature data (Table 1). The isolation of various bioactive compounds from thermophilic *Bacillus* strains, particularly those from Jordanian thermal springs, signifies a significant discovery. These compounds, encompassing indoles, their derivatives, and diketopiperazines, present diverse biological activities with potential applications (Table 1). The identification of indole and indole derivative compounds, such as 1-acetyl-β-carboline, tryptophol, and indole-3-carboxylic acid, is noteworthy. Indole derivatives have garnered significant attention due to their wide-ranging biological activities and anticancer (Kaushik *et al*., 2013; Kumar & Ritika, 2020; Salerno *et al*., 2023). For instance, 1-acetyl-β-carboline (compound 1) has been reported to exhibit antitumor activity antioxidant, and neuroprotective properties (Ayipo *et al*., 2021; Moura *et al*., 2007; Venkataramana *et al*., 2018), suggesting potential implications for cancer research and therapy. Additionally, the isolation of indole-3-carboxylic acid (2) and tryptophol (3) highlights the potential involvement of these strains in neurotransmission, sleep regulation, and plant growth regulation, as indole derivatives are known to play critical roles in these processes (Chen *et al*., 2020; Fernstrom, 2013). Moreover, adenosine (4) is of interest due to its involvement in various physiological processes, such as neurotransmission and vasodilation, with pharmaceutical applications in cardiovascular medicine (Fredholm *et al*., 2001). Tyrosol (5) with antioxidant, anti-inflammatory, and cardioprotective properties, may contribute to the health benefits associated with the Mediterranean diet (Visioli *et al*., 2002). Other indole derivatives like p-hydroxy-benzaldehyde (6) have exhibited antibacterial and antifungal properties (Cushnie and lamb, 2011; Erdogan *et al*., 2000; ~~Santos *et al*., 2018~~; Valentina *et al*., 2009). This suggests that these thermophilic *Bacillus* strains may

produce compounds with potential antimicrobial applications, which is highly relevant in the context of antibiotic resistance. Compound 7, ferulic acid exhibits antioxidant, anti-inflammatory properties and is known for its strong cholesterol-lowering effects (Bumrungpert *et al.*, 2018; Srinivasan *et al.*, 2007; Thapliyal *et al.*, 2021), aligning with the interest in natural compounds for managing hypercholesterolemia and related health concerns (Ghaisas *et al.*, 2014; Luo *et al.*, 2022; Kwon *et al.*, 2009). The identification of uracil, and 3-methyl uracil further enriches the repertoire of isolated compounds, plying fundamental roles in genetics DNA replication, and their analogs offering potential applications in chemotherapy and antiviral drugs (Jordheim *et al.*, 2013; Ladner 2001; Seley-Radtke and Yates 2018). Moreover, the isolation of diketopiperazine derivatives, including cyclo (Phe, Pro), cyclo (Pro, Ile), cyclo (Leu, Pro), and cyclo (Pro, Tyr), highlights the structural diversity of these thermophilic *Bacillus* strains. The antibacterial, antiviral, and antifungal properties of diketopiperazine derivatives have been well-documented (Kumar *et al.*, 2012; Ren *et al.*, 2022; and Song *et al.*, 2021). Our study is consistent with these reports, as the bacterial strains that produced these compounds demonstrated promising antimicrobial activity, particularly against gram-positive bacteria. This is in line with previous findings that suggest *Bacillus* species, including thermophilic strains, often exhibit strong antagonistic activity against gram-positive bacteria (Nishanth *et al.*, 2012). Certain diketopiperazine derivatives have been investigated for their cytotoxic effects on cancer cells, indicating potential antitumor activity. While our study did not directly assess the antitumor properties of these compounds, it is noteworthy that cyclo (Pro, Tyr) (13) was among the derivatives we isolated. This compound has been previously studied for its antitumor potential (Ding *et al.*, 2020; Karanam and Arumugam, 2020). Additionally, the antioxidative properties of diketopiperazines align with our findings, as these compounds may help protect cells from oxidative damage. Oxidative stress is implicated in various diseases, and the antioxidant activity of diketopiperazine derivatives could have potential health benefits. Our research adds to the expanding body of evidence supporting the biological activities of diketopiperazine derivatives. While further research and specific assays are needed to fully harness their therapeutic potential, our findings underscore the biotechnological and pharmaceutical promise of thermophilic *Bacillus* strains as sources of diverse and bioactive metabolites. This study highlights the rich potential of thermophilic *Bacillus* strains as sources of diverse biologically active compounds. The identification of known bioactive compounds, coupled with the discovery of structurally unique molecules, opens avenues for further research and development in biotechnology and pharmaceuticals. Future explorations could strategically focus on delving deeper into the specific applications of these compounds, optimizing growth conditions for enhanced metabolite production, and exploring potential

synergies among different compounds. Consequently, our study positions thermophilic *Bacillus* strains as invaluable resources for ongoing investigations in the realm of natural product discovery. The untapped potential of thermophilic *Bacillus* strains emphasizes the importance of further exploration to harness novel compounds for various industrial and medical purposes, contributing to our growing understanding of extremophiles roles in producing bioactive molecules with diverse functions in different ecosystems and industries.
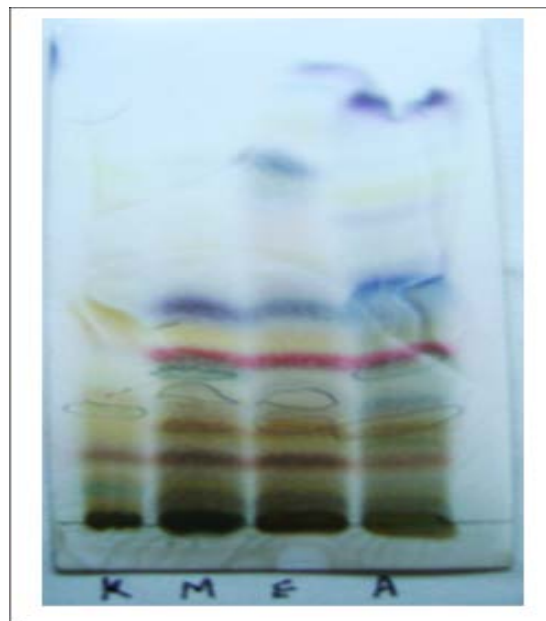
Figure 5. TLC chromatogram of metabolites from the M5a strain extracted using different solvents (K: control, M: methanol, E: ethyl acetate, A: acetone)
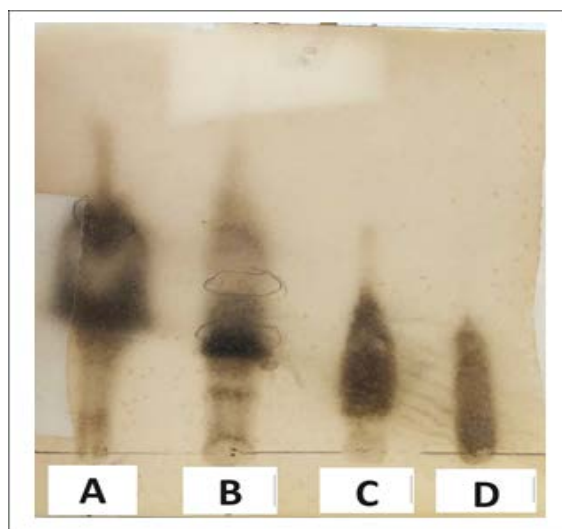
Figure 6: TLC chromatogram of the four primary fractions derived from the M5a strain through flash chromatography on a silica gel column (A: Fraction I, B: Fraction II, C: Fraction III, D: Fraction IV).

Table 1: Chemical structures composition of various metabolic

Metabolite	Compound	Chemical structure	Biological activity
Indole	1-acetyl-β-carboline (1)		Exhibited antitumor & antioxidant activity,
	Indole-3-carboxylic acid (2)		Plant growth regulation
	Tryptophol (3)		Play critical roles in neurotransmission and mood regulation
Indole derivatives	Adenosine (4)		Associated with antibacterial and antifungal activities
	Tyrosol (5)		Possess antibacterial and antifungal activities
	p-hydroxy-benzaldehyde (6)		Boost antioxidant activity and wound healing possess strong cholesterol-lowering effects
	Ferulic acid (7)		Strong agent in prevention of Hypercholesterolemia exhibits antioxidant, anti-inflammatory, and potential anticancer properties
	Uracil (8)		Uracil analogs are used in chemotherapy
	3-methyl uracil (Thymine) (9)		Thymine analogs are used in chemotherapy and antiviral drugs
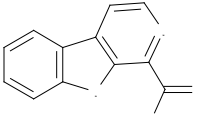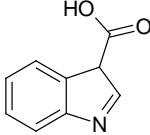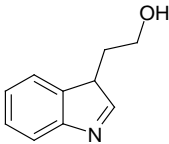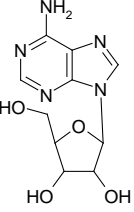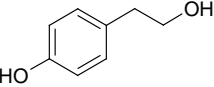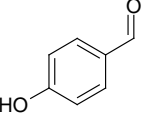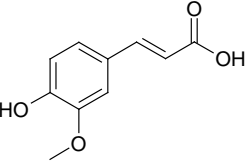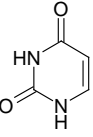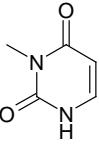
compounds extracted from the Thermophilic *Bacillus* species of
M5a strain.

Diketopiperazine derivatives

Cyclo (Phe, Pro) (10)
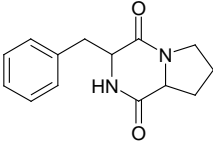
Cyclo (Leu, Pro) (11)

antimicrobial activity antibacterial and antifungal activity

Cyclo (Pro, Ile) (12)
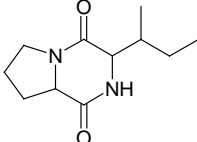
Cyclo (Pro, Tyr) (13)
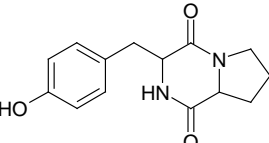
antitumor activity

4. Conclusions

This study delved into the bioactive potential of thermophilic *Bacillus* strains isolated from Jordanian hot springs, employing a holistic approach to metabolite analysis. TLC analysis and optimization of growth media revealed substantial variations in biochemical profiles, with $CaCl_2$ medium (D) identified as optimal for metabolite production. LC-MS/MS analysis provided a comprehensive exploration of secondary metabolites, showcasing the complexity and diversity influenced by varying growth conditions. The subsequent purification process yielded bioactive compounds with diverse properties, including antitumor, antioxidant, antimicrobial, and cholesterol-lowering effects. This research emphasizes the untapped potential of thermophilic *Bacillus* strains as prolific sources of diverse and bioactive metabolites. The identification of known compounds, coupled with the discovery of unique molecules, adds depth to our understanding of these strains' capabilities. Future research directions may focus on exploring specific applications, optimizing growth conditions, and investigating potential synergies between different compounds. In summary, this study positions thermophilic *Bacillus* strains as valuable resources for continued exploration in the realm of natural product discovery, contributing to our understanding of their untapped biotechnological and pharmaceutical potential.

Acknowledgements

References

Al-Daghistani HI, Mohammad BT, Kurniawan TA, Singh D, Rabadi AD, Xue W, Avtar R, Othman MHD and Shirazian S. 2021. Characterization and applications of Thermomonas hydrothermalis isolated from Jordan's hot springs for biotechnological and medical purposes. *Process Biochem.*, **104**: 171-181.

Ayipo YO, Mordi MN, Mustapha M and Damodaran T. 2021. Neuropharmacological potentials of β-carboline alkaloids for neuropsychiatric disorders. *Eur J Pharmacol.,* **15(893):** 173837. doi: 10.1016/j.ejphar.2020.173837.

Bumrungpert A, Lilitchan S, Tuntipopipat S, Tirawanchai N & Komindr S. 2018. Ferulic acid supplementation improves lipid profiles, oxidative stress, and inflammatory status in hyperlipidemic subjects: A randomized, double-blind, placebo-controlled clinical trial. *Nutrients,* **10(6):** 713. https://doi.org/10.3390/nu10060713

Baker G, Gaffar S, Cowan DA and Suharto ARI. 2001. Bacterial Community Analysis of Indonesian Hotsprings. *FEMS Microbiol Lett.*, **200 (1)**: 103-109.

Böhme B, Moritz B, Wendler J, Hertel TC, Ihling C, Brandt W, et al. 2020. Enzymatic activity and thermoresistance of improved microbial transglutaminase variants. *Amino Acids.*, **52**: 313–316.

Brock TD. 1986. **The Thermophiles, General, molecular, and applied microbiology**, John Wiley & Sons, New York.

Chen C, Qi F, Xu Z, Li X and Luo H. 2020. Antitumor activity of 1-acetyl-β-carboline from Streptomyces sp. CB03234. *Front Microbiol.*, **11:** 1275.

Chhonker YS, Aldhafiri WN, Soni D, Trivedi N, Steinbronn C, Johnson C, et al. 2023. Simultaneous LC-MS/MS method for the quantitation of Azithromycin, Hydroxychloroquine, and its metabolites in SARS-CoV-2(-/+) populations using dried blood spots. *Sci Rep.* **13(1)**: 16428. doi: 10.1038/s41598-023-43185-9. PMID: 37777555; PMCID: PMC10542348.

Cushnie TPT and Lamb AJ. 2011. Recent Advances in Understanding the Antibacterial Properties of Flavonoids. *Int J Antimicrob Agents*, **38:** 99-107. https://doi.org/10.1016/j.ijantimicag.2011.02.014.

Davies J. 2013. Specialized microbial metabolites: functions and origins. *J Antibiot.*, **66**(7): 361-364. doi: 10.1038/ja.2013.61. PMID: 23756686.

Ding Z, Li F, Zhong C, Li F, Liu Y, Wang S, Zhao J and Li W. 2020. Structure-based design and synthesis of novel furan-diketopiperazine-type derivatives as potent microtubule inhibitors for treating cancer. *Bioorg Med Chem.*, **8**(10): 115435. doi: 10.1016/j.bmc.2020.115435. PMID: 32278711.

Dumorne K and Cordova DC. 2017. Astorga-Elo M, Renganathan P. Extremozymes: a potential source for industrial applications. *J Microbiol Biotechnol.*, **27**: 649–59.

Erdogan I, Sener B and Hega T. 2000. Tryptophol, a plant auxin isolated from marine sponge *Ircinia spinulosa. Biochem Syst Ecol.*, **28**: 793-794.

Fernstrom JD. 2013. Large neutral amino acids: dietary effects on brain neurochemistry and function. *Amino Acids,* **45**: 419–430. https://doi.org/10.1007/s00726-012-1330-y

Fredholm BB, IJzerman AP, Jacobson KA, Klotz KN and Linden J. 2001. International Union of Pharmacology. XXV. Nomenclature and classification of adenosine receptors. *Pharmacol Rev.*, **53**(4): 527-52. PMID: 11734617; PMCID: PMC9389454.

Gebhardt K, Schimana J, Muller J, Fielder HP, and Kallenborn HG. 2002. Screening for biologically active metabolites with endosymbiotic bacilli isolated from arthropods. *FEMS Microbiol Lett.*, **217**: 199-205.

Geng A, Cheng Y, Wang Y, Zhu D, Le Y, Wu J, et al. 2018. Transcriptome analysis of the digestive system of a wood-feeding termite (*Coptotermes formosanus*) revealed a unique mechanism for effective biomass degradation. *Biotechnol Biofuels*, **11**: 24.

Ghaisas MM, Kshirsagar SB and Sahane RS. 2014. Evaluation of Wound Healing Activity of Ferulic Acid in Diabetic Rats. *Int Wound J.,* **11**: 523–532.

Gomez-Escribano JP and Bibb MJ. 2011. Engineering Streptomyces coelicolor for heterologous expression of secondary metabolite gene clusters. *Microbial Biotech.*, **4**(2): 207-215.

Hartl FU, Bracher A, Hayer-Hartl M. 2011. Molecular chaperones in protein folding and proteostasis. *Nature*, **475**(7356): 324-332. doi:10.1038/nature10317

Jia L, Kosgey JC, Wang J, Yang J, Nyamao RM, Zhao Y, et al. 2020. Antimicrobial and mechanism of antagonistic activity of *Bacillus* sp. A2 against pathogenic fungus and bacteria: The implication on honey's regulatory mechanism on host's microbiota. *Food Sci Nutr.*, **8**(9): 4857-4867. doi: 10.1002/fsn3.1770. PMID: 32994947; PMCID: PMC7500754.

Jordheim LP., Durantel D, Zoulim F and Dumontet C. 2013. Advances in the development of nucleoside and nucleotide analogues for cancer and viral diseases. *Nat Rev Drug Discov.*, **12**: 447–464.

Karanam G and Arumugam MK. 2020. Reactive oxygen species generation and mitochondrial dysfunction for the initiation of apoptotic cell death in human hepatocellular carcinoma HepG2 cells by a cyclic dipeptide Cyclo(-Pro-Tyr). *Mol Biol Rep.*, **47**(5): 3347-3359. doi: 10.1007/s11033-020-05407-5. PMID: 32248385.

Kaushik NK, Kaushik N, Attri P, Kumar N, Kim CH, Verma AK and Choi EH. 2013. Biomedical Importance of Indoles. *Molecules*, **18**(6): 6620-6662. https://doi.org/10.3390/molecules18066620

Kelly RM and Brown SH. 1993. Enzymes from high temperature microorganisms. *Curr Opin Biotech.,* **4**: 188-193.

Kelly RM, Peeples TL, Halio SB, Rinker KR and Duffaud GD. 1994. Extremely thermophilic microorganisms: metabolic strategies, genetic characteristics and biotechnological potential. *An New York Ac Sci.,* **745**: 409-425.

Krishnaraj RN and Sani RK. 2017. Introduction to extremozymes. In: Sani RK and Krishnaraj RN (Eds.), **Extremophilic enzymatic processing of lignocellulosic feedstocks to bioenergy**. Cham: Springer International Publishing, pp. 1–4.

Kuczynska-Wisnik D, Kędzierska S, Matuszewska E, Lund P, Taylor A, Lipinska B and Laskowska E. 2002. The Escherichia coli small heat-shock proteins IbpA and IbpB prevent the aggregation of endogenous proteins denatured in vivo during extreme heat shock. *Microbiol.,* **148**(6): 1757-1765.

Kumar S, Ritika. 2020. A brief review of the biological potential of indole derivatives. *Futur J Pharm Sci.,* **6**: 121. https://doi.org/10.1186/s43094-020-00141-y

Kumar SN, Siji JV, Nambisan B and Mohandas C. 2012. Activity and synergistic antimicrobial activity between diketopiperazines against bacteria in vitro. *Appl Biochem Biotechnol.*, **168**(8): 2285-96.

Kwon EY, Cho YY, Do GM, Kim HJ, Jeon SM, et al. 2009. Actions of ferulic acid and vitamin E on prevention of hypercholesterolemia and atherogenic lesion formation in apolipoprotein E-deficient mice. *J Med Food,* **12**(5): 996-1003. doi: 10.1089/jmf.2009.0105. PMID: 19857062

Laatsch H. 2009. AntiBase; A Natural Product Database for Rapid Structure Determination, Wiley VCH, Weinheim,

Ladner RD. 2001. The role of dUTPase and uracil-DNA repair in cancer chemotherapy. *Curr Protein Pept Sci.*, **2**(4): 361-370. doi:10.2174/138920301338099

Lindquist S and Craig EA. 1988. The heat-shock proteins. *Annu Rev Genet.*, **22**: 631-677.

Luo Z, Li M, Yang J, Li J, Zhang Y, Liu F, El-Omar E, Han L, Bian J, Gong L and Wang M. 2022. Ferulic acid attenuates high-fat diet-induced hypercholesterolemia by activating classic bile acid synthesis pathway. *Front Nutr.,* **21**: 9:976638. doi: 10.3389/fnut.2022.976638. PMID: 36211528; PMCID: PMC9536491.

Morimoto RI. 1998. Regulation of the heat shock transcriptional response: cross talk between a family of heat shock factors, molecular chaperones, and negative regulators. *Genes Dev.*, **12**(24): 3788-3796.

Moura DJ, Richter MF, Boeira JM, Pêgas Henriques JA and Saffi J. 2007. Antioxidant properties of beta-carboline alkaloids are related to their antimutagenic and antigenotoxic activities. *Mutagenesis*, **22**(4): 293-302.

Nagai K, Kamigiri N, Arao K, Suzumura Y, Kawano M and Yamaoka H. 2003. YM-266183 and YM-266184, novel thiopeptide antibiotics produced by *Bacillus cereus* isolated from marine sponge. *J Antibiot.*, **56**: 123-128.

Nielsen TH, Christophersen C and Anthoni U. 2017. Siderophore production by *Pseudomonas* sp. F113 during growth on coexisting pyoverdine-producing and pyoverdine-non-producing bacteria on barley roots. *FEMS Microbio Ecol.*, **92**(8): fix103.

Nishanth KS, Mohandas C, Siji JV, Rajasekharan KN and Nambisan B. 2012. Identification of antimicrobial compound, diketopiperazines, from a Bacillus sp. N strain associated with a rhabditid entomopathogenic nematode against major plant pathogenic fungi. *J Appl Microbiol.,* **113**(4): 914-24.

Obeidat M, and Al-Shomali B. 2023. Moderately Thermophilic Bacteria from Jordanian Hot Springs as Possible Sources of Thermostable Enzymes and Leukemia Cytotoxic Agents. *Jordan J Biol Sci.*, **16**(3): 413-424.

Parsell DA and Lindquist S. 1993. The function of heat-shock proteins in stress tolerance: degradation and reactivation of damaged proteins. *Annu Rev Genet.*, **27**: 437-496.

Ren Z, Xie L, Okyere SK, Wen J, Ran Y, Nong X and Hu Y. 2022. Antibacterial Activity of Two Metabolites Isolated from

Endophytic Bacteria *Bacillus velezensis* Ea73 in *Ageratina adenophora. Front Microbiol.*, **13**: 860009. doi: 10.3389/fmicb.2022.860009. PMID: 35602058; PMCID: PMC9121010.

Rigoldi F, Donini S, Redaelli A, Parisini E and Gautieri A. 2018. Review: engineering of thermostable enzymes for industrial applications. *APL Bioeng.*, **2:** 011501.

Salerno S, Barresi E, Baglini E, Poggetti V, Da Settimo F and Taliani S. 2023. Target-Based Anticancer Indole Derivatives for the Development of Anti-Glioblastoma Agents. *Molecules*, **28:** 2587. doi: 10.3390/molecules28062587

Seley-Radtke KL and Yates MK. 2018. The evolution of nucleoside analogue antivirals: A review for chemists and non-chemists. Part 1: Early structural modifications to the nucleoside scaffold. *Antiviral Res.*, **154:** 66–86. https://doi.org/10.1016/j.antiviral.2018.04.004

Singh P, Jain K, Desai C, Tiwari O and Madamwar D. 2019. Microbial community dynamics of extremophiles/extreme environment. In: Das S, Dash HR (Eds.), **Microbial diversity in the genomic era**. Academic Press, pp. 323–32.

Song Z, Hou Y, Yang Q, Li X and Wu S. 2021. Structures and Biological Activities of Diketopiperazines from Marine Organisms: *A Review Mar Drugs*, **19(8)**: 403. doi: 10.3390/md19080403. PMID: 34436242; PMCID: PMC8398661

Srinivasan M, Sudheer AR and Menon VP. 2007. Ferulic Acid: therapeutic potential through its antioxidant property. *J Clin Biochem Nutr.*, **40(2):** 92-100. doi: 10.3164/jcbn.40.92. PMID: 18188410; PMCID: PMC2127228.

Thapliyal S, Singh T, Handu S, Bisht M, Kumari P, Arya P, Srivastava P and Gandham R. 2021. A Review on Potential Footprints of Ferulic Acid for Treatment of Neurological Disorders. *Neurochem Res.*, **46(5):** 1043–1057. https://doi.org/10.1007/s11064-021-03257-6

Valentina P, Ilango K, Yamuna K, Purushothaman D, Rani and Samyuktha A. 2009. QSAR analysis on β- Carboline as antitumor agent. *J Young Pharmacists,* **1(1):** 77-81.

van den Burg B. 2003. Extremophiles as a source for novel enzymes. *Curr Opin Microbiol.*, **6:** 213–8.

Venkataramana Reddy PO, Hridhay M, Nikhil K, Khan S, Jha PN, Shah K and Kumar D. 2018. Synthesis and investigations into the anticancer and antibacterial activity studies of β-carboline chalcones and their bromide salts. *Bioorg Med Chem Lett.,* **28(8):** 1278-1282. doi: 10.1016/j.bmcl.2018.03.033. PMID: 29573910; PMCID: PMC6423518.

Visioli F, Poli A, and Galli C. 2002. Antioxidant and other biological activities of phenols from olives and olive oil. *Med Res Rev.*, **22(1):** 65-75. doi:10.1002/med.1028

Xiao D, Liu J, Zhu F, Wei X, and Fan L. 2021. Metabolomic analysis of the antimicrobial activity of Bacillus velezensis BAC03 against the rice bacterial leaf blight pathogen Xanthomonas oryzae pv. oryzae. *Front Microbiol.*, **12**: 764196.

Xiao JF, Zhou B and Ressom HW. 2012. Metabolite identification and quantitation in LC-MS/MS-based metabolomics. *Trends Analyt Chem.*, **1(32):** 1-14.

Yilmaz M, Soran H and Beyatli Y. 2006. Antimicrobial activities of some *Bacillus* sp. Strains isolated from the soil. *Microbiol Res.,* **161:** 127-131.

Coccolithophore Assemblages from Gulf of Aqaba Sediments and their Response to Climate Change

Mohammad Alqudah[1,*], Saber Al-Rousan[2], Albeshr Hussein[1], Wesam Al khateeb[3]

[1] Department of Earth and Environmental Sciences, Faculty of Science, Yarmouk University, Shafeeq Irsheidat Street, 21163 Irbid, Jordan;
[2] Department of Geology, School of Science, The University of Jordan, 11942 Amman, Jordan; [3] Department of Biological Sciences,
Faculty of Science, Yarmouk University, Shafeeq Irsheidat Street, 21163 Irbid, Jordan

Abstract

The Gulf of Aqaba exhibits a nearly closed marine ecosystem, characterized by oligotrophic conditions, which give it the potential for phytoplankton to flourish. Coccolithophore samples were taken from two different sediment cores that were collected from the northern Gulf of Aqaba during the OceanX expedition. This study aims to construct the sea surface temperature over the past few hundred years by counting fossil coccolithophore communities in the northern Gulf of Aqaba through time.

The forty-eight smear slides were prepared for coccolithophore identification and paleo-ecological investigation, and then studied under a polarized microscope with 1500x magnification. Taxonomic identification of coccolithophores is based on the outer scale found in the slides. A total of 300 specimens were counted in each slide. To assess the temperature, diversity and the relationship between species abundances, statistical indices were applied on the counted specimens. Coccolithophore assemblages are extremely abundant in well-preserved conditions, allowing for clear identification and an exact assessment of climatic change based on paleo-ecological studies. The *Gephyrocapsa* group, *Emiliana* group, *Helicosphaera* spp, *Reticulofenestra* spp, *Coccolithus* spp, *Pontosphaera* spp, *Braarudosphaera* spp and *Umbilicosphaera* spp were found in high numbers throughout all the cores. The *Emiliana* Group was the most abundant genus throughout all the cores, indicating long-term warming. Throughout core 3, the results showed a strong relation between *Gephyrocapsa* spp and the other coccolithophores, such as *Coccolithus* spp, *Helicosphaera* spp, and *Braarudosphaera* spp, as all of these species prefer cold water. The fluctuations in the numbers of the cold-preference (*Gephyrocapsa*) group versus warm-preference coccolithophores (*Emiliana* Group) led to tracking periodic changes in climate. The significant increase in numbers of *Gephyrocapsa oceanica*, *Gephyrocapsa muellerae*, *Gephyrocapsa ericsonii*, and *Calcidiscus leptoporus* in some samples, relative to the *Emiliana* Group, reveals that a cold environmental period dominated the Gulf during the Holocene.

Keywords: Coccolithophores, Gulf of Aqaba, Paleoclimate, warm-preference coccolithophores, cold-preference coccolithophores

1. Introduction

The Gulf of Aqaba represents the northern extension of the Red Sea. The restriction of the Red Sea Basin imposes harsh and extreme conditions. It is characterized with low productivity, low oxygen content, and negligible drainage system (Winter *et al.* 1979; Winter 1982; Legge *et al.* 2006). The nannoplankton community in the Red Sea and Gulf of Aqaba displays a fragile pattern due to climate change. Coccolithophores, in particular, are tiny organisms that live in the photic zone and thrive in oligotrophic conditions. Nannoplankton species, therefore, can be used as paleoclimatic proxies in such environments. As an example, *Gephyrocapsa oceanica* is a cosmopolitan bloom-forming coccolithophore species (Bendif and Young 2014), but it dominated the neritic environment (Okada and Honjo 1975). *Emiliania huxleyi* is usually common in open oceans, but it is scarce in various neritic environments (Okada and Honjo 1975).

Sea surface temperature can be estimated based on the relative abundance of *Gephyrocapsa* because it has morphotypes, including a mean bridge angle of less than 27° and a length longer than 2.4 µm (Bollmann 1997; Bollmann *et al*. 2002). Moreover, good correspondence has been found between *Gephyrocapsa* and alkenone, in defining paleotemperature (Henderiks and Bollmann 2004). It has also been found that *G. oceanica* and *H. carteri* are valuable nutrient-indicator species in the Red Sea, while *U. sibogae, R. claviger* and *F. profunda* are oligotrophic indicators (Aljahdali 2021).

The present study investigates the coccolithophore community and its diversity in the northern Gulf of Aqaba. The investigation of changes in the abundance of calcareous nannofossil associations is fundamental for palaeoclimatic and palaeo-oceanographic reconstructions (Buccianti and Esposito 2004). This study aims to construct the sea surface temperature over the past few hundred years. It describes the seasonal dynamics of different species and assesses their relationship with different climatic conditions. This research interprets the

distribution patterns and infers the paleoecology of fossil coccolithophore communities in the northern Gulf of Aqaba.

2. Materials and Methods

Two sediment cores (Sites 1 and 3), among seven different cores were collected from the northern Gulf of Aqaba during the OceanX expedition in July 2022 (Figure 1). A total of 48 samples were examined: eight samples from site 1 and 40 samples from site 3. Smear slides were prepared from each sample, following the standard procedure of Roth (1984). Table 1 shows the longitude, latitude and depth for each core.

Table 1. Coordinates and depth information of the studied cores.

Core number	Longitude	Latitude	Altitude (m)	Thickness (cm)
Core 1	29.494706	34.982516	-350	8
Core 3	29.417155	34.944383	-698	40
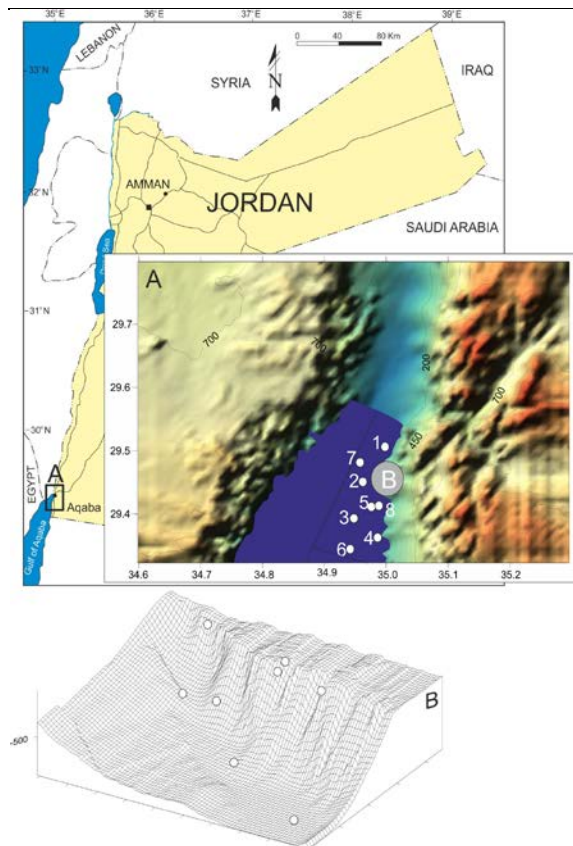
Figure 1. Map of the northern Gulf of Aqaba showing the locations of the collected sediment cores. A) Location of the eight sites within the Aqaba Economic Zone; B) Depth image illustrates the position of the eight drilled cores. Bathymetric data obtained from the OceanX expedition.

Taxonomic identifications of the coccolithophores are based on their calcitic plate (calcareous nannofossils). This was performed using a transmitted light microscope, a Nikon Type with a magnification of 1500x, located at the Department of Earth and Environmental Sciences in Yarmouk University. Due to the high abundance of the calcareous nannofossil specimens in the studied samples, relative abundances of species were measured from counting 300 calcareous nannofossil specimens per 30 fields of view in each smear slide. The Temperature Index, which is an estimation of sea surface temperature, was then calculated, in order to provide information on the paleo-environment of the Gulf. In this study, *Gephyrocapsa, Calcidiscus,* and *Coccolithus* were considered to be cold water species, based on the description by Bollmann (1997) and supported by Buccianti and Esposito (2004).

The diversity of the coccolithophores is expressed by two indices: the Heterogeneity Index (or Shannon Index) (H) and Dominance (D). High values of the Shannon index indicate highly diverse assemblages (Linnert *et al*. 2011). The Shannon Index equation used in this study was applied following Giraldo Gomez *et al*. (2018).

Furthermore, in order to assess the relationship between the abundance of the different species, a linear Pearson correlation and de-trended correspondence analysis (DCA) were performed. The Shannon Diversity (H), Dominance (D), and Detrended Correspondence Analysis (DCA) were performed based on the counts using the PAST software (Hammer *et al*. 2001).

3. Results and Discussion

3.1. Coccolithophore assemblages

Coccolithophores were abundant in both sediment cores and *Gephyrocapsa oceanica* (Figures 2a and b) and *Emiliania huxleyi* (Figures 2c and d) were the most common species in the samples. However, the numbers of these species fluctuated throughout the samples. Figures 3 and 4 represent numbers of the coccolithophores species counted in the sediment cores from sites 1 and 3, respectively. Numbers of *Emiliania huxleyi* species*,* on the one hand, exceeds 300 specimens in samples 6, 25-28, and 39 cm (site 3) and at the top 5 samples in site 1. The count of *Emiliania huxleyi* declines at the bottom of site 1 and in samples 10-17 from site 3, where 2-72 specimens were counted in those samples (Figures 3 and 4).

The number of *Gephyrocapsa oceanica* was relatively high at the base of the core samples of site 1 and site 3 and fluctuated throughout site 3. Almost 300 specimens of *Gephyrocapsa* were counted at base of site 3 (Figures 3). However, numbers of individuals dropped down to 36 specimens in sample 26. High numbers of *Gephyrocapsa oceanica* were observed to be associated with an increase in the numbers of *Helicosphaera* spp (Figures 2f and 2g), *Coccolithus* spp (Figure 2h) and *Calcidiscus* spp (Figure 2 k). Less common species, such as *Umbilicosphaera* spp (Figure 2i), *Scyphosphaera* spp (Figure 2j) and *Braarudosphaera* (Figure 2l), were also observed in the samples.
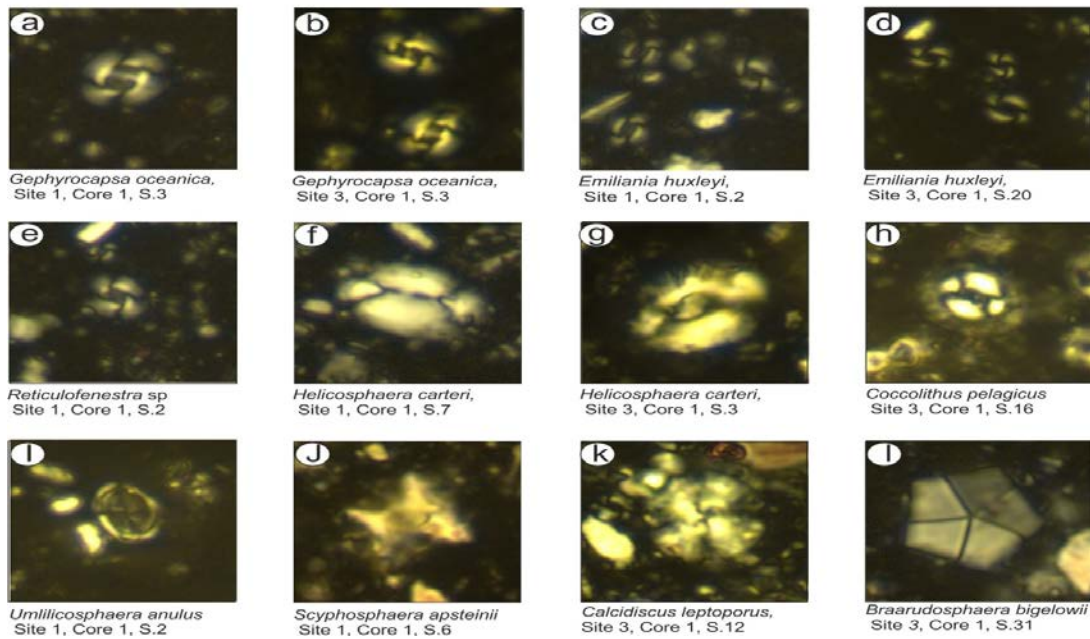
Figure 2. Nannofossil species found in sediment cores from sites 1 and 3.
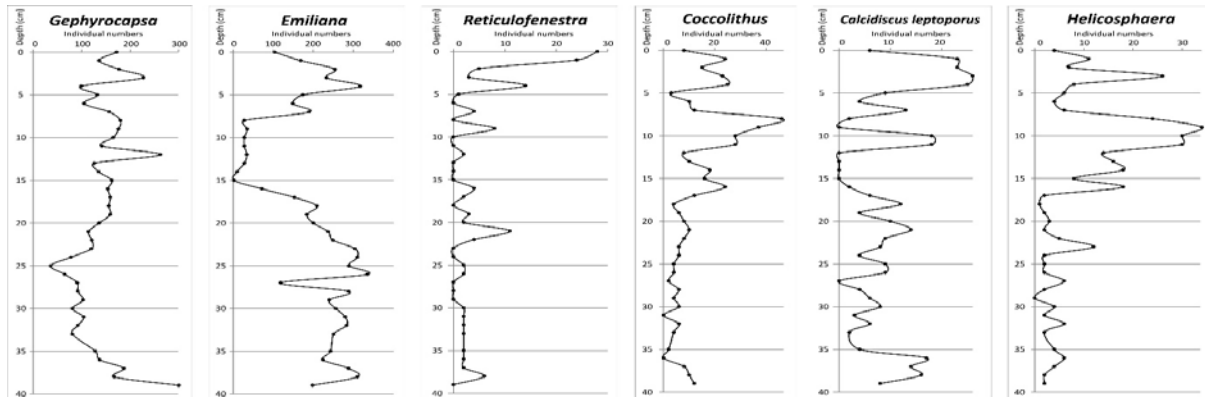
Figure 3. Relative abundances of the most common coccolithophore species from site 3, core 1. Depths in cm.
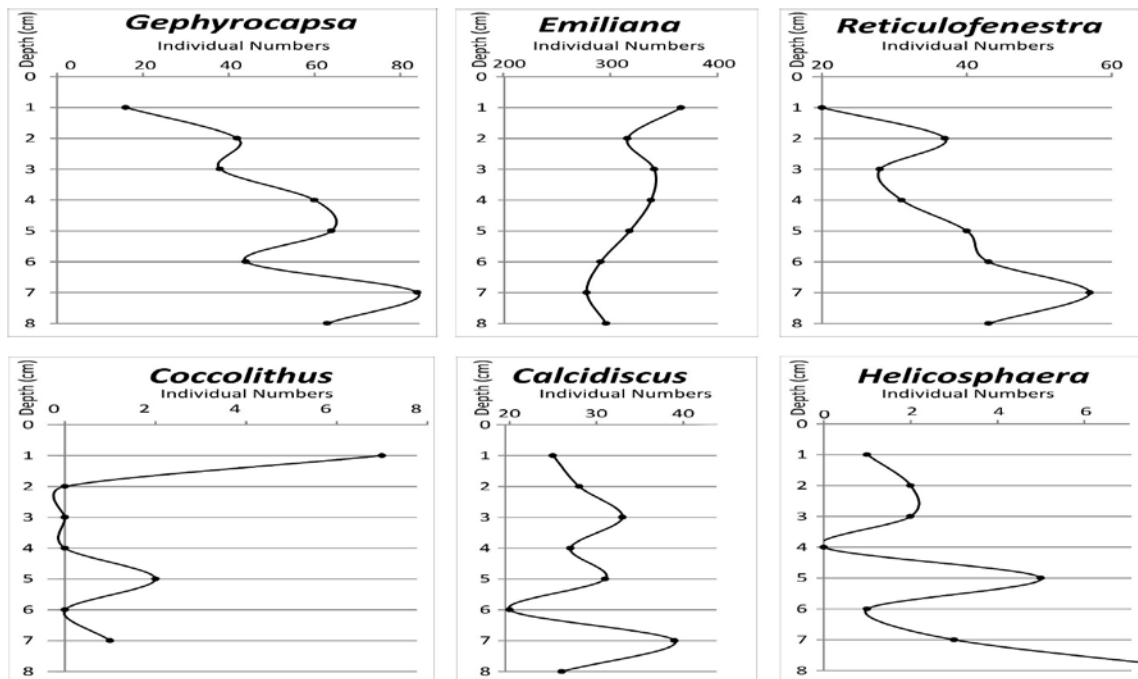
Figure 4. Relative abundances of the most common coccolithophores species from site 1, core 1.

3.2. Relative abundance

At site 3, the percentage of *Gephyrocapsa* spp ranged between 10-79%, reaching its maximum in sample 13 and its minimum in sample 26 (Figure 5). *Emilliana* spp was dominant in the samples as well, ranging between 1% in sample 16 and reaching its maximum of 84% in sample 26. There was a clear negative trend, as shown in figure 5, in *Emilliana* relative abundance, particularly in samples 10-17, compared to a relatively increase in *Gephyrocapsa* relative abundance values. *Reticulofenestra* spp had a maximum of 8% at the surface, and its percentage decreased downwards, through the core. *Coccolithus* spp reached its maximum of 15% in sample 9, *Helicosphaera* spp was 11% in sample 12, and the percentage of other species was negligible.
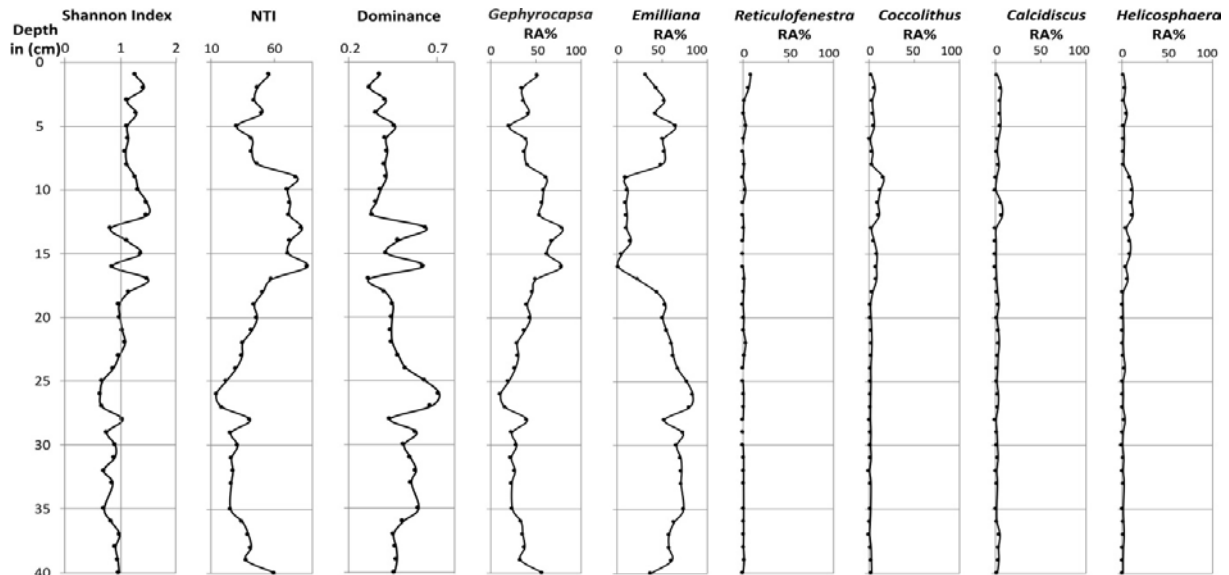
Figure 5. Diversity indices, NTI, and relative abundance of counted calcareous nannofossils from site 3.

Three groups were recognized in sample 1 (site 3, surface of sediments): *Gephyrocapsa, Emilliana,* and *Reticulofenestra*. The rest of the species were almost absent. The surface sample displayed a high percentage of *Gephyrocapsa* spp relative to *Emilliana*. In fact, the percentage of both *Gephyrocapsa* spp and *Emilliana* spp fluctuated in the site (Figure 5). Samples 2-9 showed a high percentage of *Emilliana* spp and a low percentage of *Gephyrocapsa* spp. This trend changed, as *Gephyrocapsa* spp appeared in high percentages in samples 10 to 17, in association with *Coccolithus* spp and *Helicosphaera* spp. Then, the trend was steady, with a high percentage of *Emilliana* spp, and this continued to the bottom of the core.

3.3. Diversity Indices

Two main indices were determined from the samples: the Heterogeneity Index (H) and Dominance (D). Based on the Heterogeneity Index, a diverse system was observed in four different areas, in terms of an increasing Heterogeneity Index (Figure 5); samples 2 and 4 (close to the surface), samples 9, 10, 11, and 12, a few lower samples (15 and 17), and sample 28 in the middle of the core. Three areas of Heterogeneity Index, showing a lower Shannon Index value, were observed throughout the core. The surface represents the first area and includes samples 3, 5, 6, 7 and 8. Samples 13, 14 and 16 represent another period of low diversity, and samples from 19 to 40 also showed a low diversity pattern.

The Dominance Index showed a fixed value of around 0.3 in most of the samples from site 3 (Figure 5). However, there was an observed relation between increasing Dominance Index associated with low Shannon Index values. This was clearly observed in samples 13, 16, 25, 26, and 27. The coccolithophore assemblages in these samples were dominated by one species. In another way, samples showed a drop in the Dominance Index value, which also matched an increase in the Shannon Index values, such as in samples 12, 14, 25 and 27. In these samples, coccolithophore assemblages were diverse, and many species flourished.

3.4. Nannofossil Temperature Index

Based on the Nannofossil Temperature Index (NTI) curve (Figure 5), three periods of distinctive variation in NTI values were recognised at site 3. Low values of the NTI in samples 1-8 of core 1 suggest that the sea surface temperature was high in the top 8 cm of the sediments. NTI values increased significantly and were associated with a dramatic decrease in the numbers of upper photic zone species, suggesting a lower sea surface temperature in sediment samples from 9-16 cm. The NTI values were at a minimum in the samples from 18 cm to the bottom. Coccolithophores can be divided into two groups, based on their climatic preferences: upper photic zone species, like *Emiliania huxleyi,* and lower photic zone species, such as *Gephyrocapsa* spp, *Helicosphaera* spp, and *Coccolithus* spp. The latter group showed fluctuations in their abundance. Therefore, three climatic periods can be interpreted. The first period, at the top, is characterised by a decline in cold water taxa (lower photic zone species), and is correlated with the first eight samples from the surface. The second period, where the NTI is higher than the periods above and below, is considered to be colder. In this period, cold water taxa were higher in numbers. The last period, which extends to the bottom of the core, is

characterised by the dominance of warm water taxa (upper photic zone species). This implies that two warm periods were interrupted by short cooling periods in the last few hundred years (the ages and sedimentation rate have been estimated from ^{14}C dating conducted on deep sediments in the Gulf of Aqaba, by Al-Rousan *et al*. (2004)).

3.5. Correlations

The results of a Detrended Correspondence Analysis (DCA) and Pearson Linear Correlation applied to samples from site 3 are shown in Figures 6 and 7. Coccolithophore species were grouped differently along axis 1 and 2 in Figure 6. Two groups can be distinguished, and both are

circled in Figure 6. *Emiliania*, *Calcidiscus* spp., *Umbilicosphaera* spp, and *Scyphoshaera* spp. are correlated in samples 3, 5, 19, 22, 23, 24, 30, 35, 37, and 38. All of these samples showed a low NTI, which correlates the abundance of these species with the warm water taxa. On the other hand, *Gephyrocapsa* spp, *Helicosphaera* spp, and *coccolithus* spp are associated with each other and with samples 2, 4, 7, 8, 18, 20, and 39, whilst samples 9, 10, 11, 12, 13, 14, 15, 16, and 17 showed extreme values where cold-water taxa were dominant, and there was a decline in warm water taxa.
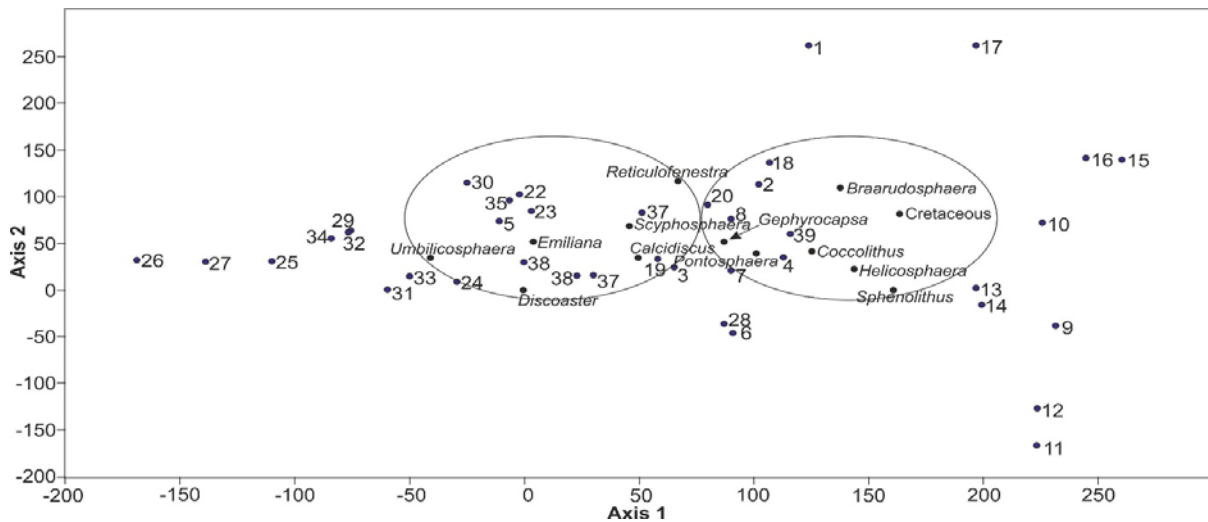
Figure 6. Detrended Correspondence Analysis (DCA) representing the abundance of certain coccolithophore species in the samples. Low NTI species grouped together within the two circles.
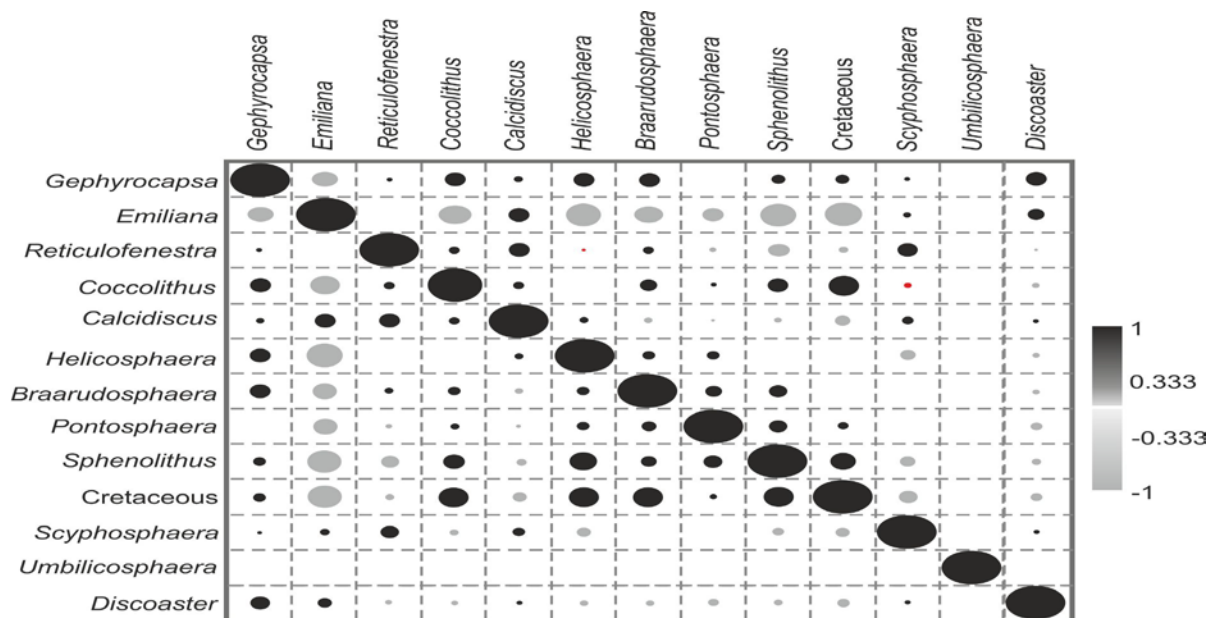
Figure 7. Linear correlation between different coccolithophore species. Black color represents the positive, and gray is for the negative correlation.

The relationship observed when Linear Correlation was applied to the results is shown in Figure 7. Black represents a positive relationship, while grey represents a negative correlation. The results showed a strong relation between *Gephyrocapsa* spp and other coccolithophores spp. such as *Coccolithus* spp, *Helicosphaera* spp, and *Braarudosphaera* spp, as all of these species are of cold-

water preference. However, *Gephyrocapsa* spp was correlated negatively with *Emiliania* spp, which has a clearly negative correlation with *Helicosphaera* spp, *Sphenolithus* spp, and *Coccolithus* spp, and a weak positive correlation with *Calcidiscus* spp. Therefore, two groups can be subdivided, based on the Linear Correlation:

the *Gephyrocapsa* group and its associations, and the *Emiliania* group and its associations.

3.6. Coccolithophores in response to climatic events

The Red Sea is characterised by an elongated basin that was formed by extensional forces in the Miocene (Sharland *et al*. 2001). It has an arid environment with insignificant precipitation (22 mm/year) and runoff (Al-Rousan *et al*. 2006). Nutrients are brought into the basin through flash floods, that transfer terrestrial material into the Gulf (Manasrah *et al*. 2004), and in the Gulf there is a seasonal current flowing along the west coast, mixing up the terrestrial material into all parts of the Gulf (Genin and Paldor 1998; Berman *et al*. 2000; Manasrah *et al*. 2004, 2006). However, the absence of rivers or major streams flowing into the Gulf of Aqaba leads to a poor supply of nutrients, such as nitrogen or phosphorus compounds, to the water, keeping the planktonic primary production very low (Al-Rousan *et al*. 2006).

Calcareous nannofossils were abundant in such environment. However, diversity and abundances of nannoplanktons were dependent mostly on climate, and this decreased several times during the warming periods (Winter, 1994; Guerreiro *et al*., 2023) (Figure 8). Guerreiro *et al*., 2023 reported the relationship between diversity and abundances of coccolithophores community and stratified oligotrophic and warm conditions. However, extreme warming conditions were reflected by a significant reduction in coccolithophore numbers and, therefore, the establishment of a mono-species pattern. Species that were not adapted to cooling in the water column were reflected in fluctuations in the Heterogeneity Index (H). More specifically, despite the reduction in species numbers during extreme conditions at the sea surface, the *Gephyrocapsa* group, *Coccolithus* spp, and *Helicosphaera* spp continued, and even dispersed during the cooling of the sea surface. Guerreiro et al., 2013 related the abundances of *Gephyrocapsa* in temperate to cooling in water column. The *Emiliania* group and *Calciduscus* spp thrived in the mild or warm conditions correlated with different cases in Atlantic and Miditerranian Sea (Dimiza *et al*., 2008; Guerreiro *et al*., 2023).
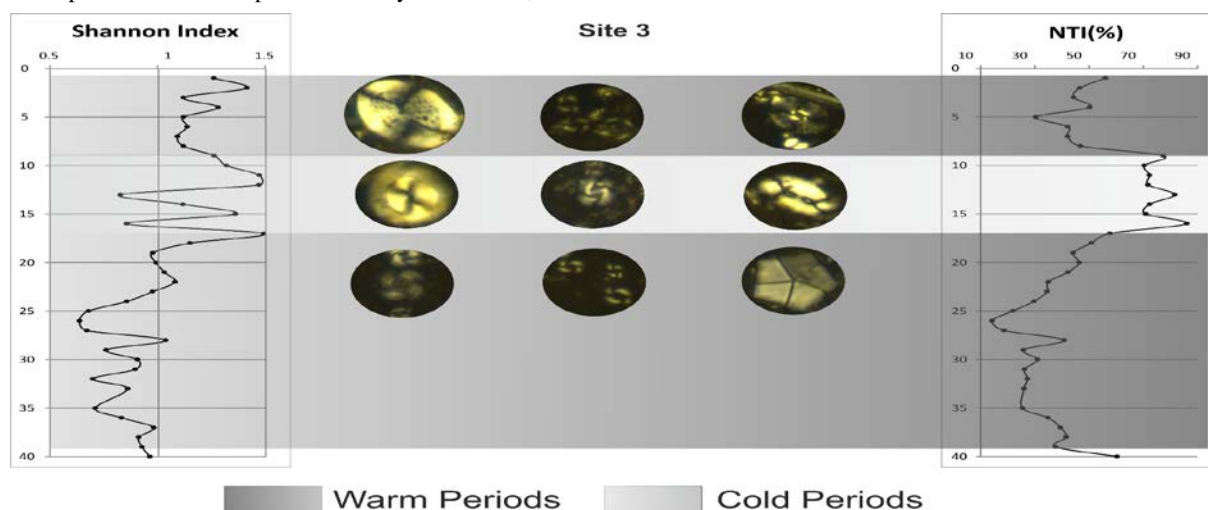
Figure 8. The three climatic periods detected throughout the sediment core based on the calcareous nannofossil study.

During the cold period, the depth of the Strait of Bab el Mandeb was reduced to 17 m, leading to an increase in salinity due to the high evaporation rate. The hypersaline conditions reached the tolerance limit for various planktonic organisms (Winter 1982; Winter *et al*. 1994), causing an absence of planktonic foraminifera and calcareous nannofossils, and the occurrence of mono-species patterns in the north of the Red Sea (Winter 1982; Winter *et al*. 1994). Legge *et al*. (2006) confirmed that extreme conditions with enhanced salinities during the cold period are characterised by high values of *Gephyrocapsa* spp. Based on the correlation analysis and the NTI values, coccolithophores can be divided into two groups, in response to climate: upper photic zone species, such as *Emiliania huxleyi*, and lower photic zone species, such as *Gephyrocapsa* spp, *Helicosphaera* spp, and *coccolithus* spp. Each group was dominant and flourished in their preferred environment.

4. Conclusion

Highly abundant and diverse nannoplankton were found in both shallow and deep sediment cores from the northern Gulf of Aqaba. *Emilliana* spp and *Gephyrocapsa* spp are the dominant species in the sediments, with low abundances of *Helicosphaera* spp, *Reticulofenestra* spp, *coccolithus* spp and *Calcidiscus* spp. Coccolithophore groups, like *Gephyrocapsa, Helicosphaera* and *coccolithus,* showed fluctuation in their abundance, reflecting changes in their preferred climatic conditions. By applying NTI on the studied samples, three climatic periods were recognized. Two warm periods were interrupted by short cooling periods over the last few hundred years. Biodiversity varied through time, where coccolithophores were not tolerant to both extreme cooling and warming conditions. Although the top intervals of both sediment cores represent stressed environments, the primary production system is functioning well.

5. Taxonomic list

Braarudosphaera Deflandre (1947)
  B. bigelowii (Gran and Braarud, 1935) Deflandre (1947)
Calcidiscus Kamptner (1950)
  C. leptoporus (Murray and Blackman, 1898)
Coccolithus Shwarz (1894)

C. pelagicus (Wallich, 1877) Schiller (1930)

Emilliana Hay and Mohler in Hey et al. (1967)

E. huxleyi (Lohmann, 1902) Hay and Mohler in Hey et al. (1967)

Florisphaera Okada and Honjo (1973)

F. profunda Okada and Honjo (1973)

Gephyrocapsa Kamptner (1943)

G. oceanica Kamptner (1943)

Helicosphaera Kamptner (1954)

H. carteri (Wallich, 1877) Kamptner (1954)

Pontosphaera Lohmann, 1902

Rhabdosphaera Haeckel (1894)

R. claviger Murray and Blackman, 1898

Reticulofenestra Hay, Mohler and Wade (1966)

Scyphosphaera Lohmann, 1902

S. apsteinii Lohmann, 1902

Sphenolithus Deflandre in Grasse (1952)

Umbilicosphaera Lohmann, 1902

U. anulus Young et al., (2003)

U. sibogae (Weber-van Bosse, 1901) Gaarder (1970)

Acknowledgment

References

Aljahdali, M.H. 2021. Distribution and diversity of Coccolithophores in surface sediments of the northern Red Sea: Coccolith accumulation in brine pools and observation of productivity. *Arabian J Sci Eng* 46: 601-615.

Al-Rousan, S., Pätzold, J., Al-Moghrabi, S., and G. Wefer. 2004. Invasion of anthropogenic CO2 recorded in planktonic foraminifera from the northern Gulf of Aqaba. *Int J Earth Sci (Geol Rundsch)* 93: 1066–1076. doi:10.1007/s00531-004-0433-4.

Al-Rousan, S., Rasheed, M., Al-Horani, F., and R. Manasreh. 2006. Geochemical and textural properties of carbonate and terrigenous sediments along the Jordanian coast of the Gulf of Aqaba. *J Oceanog* 62: 839–849.

Berman, T., Paldor, N., and S. Brenner. 2000. Simulation of wind-driven circulation in the Gulf of Elat (Aqaba). *J Mar Sys* 26: 349–365.

Bendif, E., and G. Young. 2014. On the ultrastructure of Gephyrocapsa oceanica (Haptophyta) life stages. *Algologie* 35(4): 379-388.

Bollmann, J., Henderiks, J., and B. Bernhard. 2002. Global calibration of Gephyrocapsa coccolith abundance in Holocene sediments for paleotemperature assessment. *Paleoceanog* 17(3): 1035. doi:10.1029/2001PA000742.

Bollmann, J. 1997. Morphology and biogeography of Gephyrocapsa coccoliths in Holocene sediments. *Marine Micropaleontol* 29: 319-350.

Buccianti, A., and P. Esposito. 2004. Insights into Late Quaternary calcareous nannoplankton assemblages under the theory of statistical analysis for compositional data. *Palaeogeog Palaeoclimatol Palaeoecol* 202: 209-227.

Dimiza M. D., Triantaphyllou M. V., Dermitzakis M. D. 2008. Seasonality and ecology of living coccolithophores in e. Mediterranean coastal environments (Andros island, middle Aegean Sea). *Micropaleontology* 54 (1), 59–75.

Genin, A., and N. Paldor. 1998. Changes in the circulation and current spectrum near the tip of the narrow, seasonally mixed Gulf of Elat (Aqaba). *Isr J Earth Sci* 47: 87–92.

Giraldo Gomez, V., Mutterlose, J., Podlaha, O., Speijer, R., and P. Stassen. 2018. Benthic foraminifera and geochemistry across the Paleocene–Eocene Thermal Maximum interval in Jordan. *J Foraminiferal Res* 48(2): 100–120.

Guerreiro C., Oliveira A., Cachão M., de Stigter H., Sá C., Borges C., et al. (2013). Late winter coccolithophore bloom off central Portugal in response to river discharge and upwelling. Cont. *Shelf Res*. 59, 65–83. doi: 10.1016/j.csr.2013.04.016

Guerreiro C.V., Ferreira A., Cros L., Stuut .-B., Baker A., Tracana A., Pinto C., Veloso V., Rees A.P., Cachão M.A. P., Nunes T., Brotas V., 2023. Response of coccolithophore communities to oceanographic and atmospheric processes across the North- and Equatorial Atlantic. *Frontiers in Marine Science* 10.

Hammer, O., Harper, D.A.T., and P.D. Ryan. 2001. PAST: paleontological statistics software package for education and data analysis. *Palaeontologia Electronica* 4: 1–9.

Henderiks, J., and J. Bollmann. 2004. The Gephyrocapsa sea surface palaeothermometer put to the test: comparison with alkenone and foraminifera proxies off NW Africa. *Marine Micropaleontol* 50: 161-184.

Okada, H., and S. Honjo. 1975. Distribution of coccolithophores in marginal seas along the western Pacific Ocean and in the Red Sea. *Marine Biol* 31: 271–285.

Legge, H.L., Mutterlose, J., and H.W. Arz. 2006. Climatic changes in the northern Red Sea during the last 22,000 years as recorded by calcareous nannofossils. *Paleoceanog* 21: PA1003. doi:10.1029/2005PA001142.

Linnert, C., Mutterlose, J., and J.O. Herrle. 2011. Late Cretaceous (Cenomanian Maastrichtian) calcareous nannofossils from Goban Spur (DSDP Sites 549, 551): Implications for the palaeoceanography of the proto North Atlantic. *Palaeogeogr Palaeoclimatol Palaeoecol* 299: 507–528.

Manasrah, R., Badran, M., Lass, H.U., and W. Fennel. 2004. Circulation and winter deep-water formation in the northern Red Sea. *Oceanologia* 46(1): 5–23.

Manasrah, R., Rasheed, M., and M. Badran. 2006. Relationships between water temperature, nutrients and dissolved oxygen in the northern Gulf of Aqaba, Red Sea. *Oceanologia* 48(2): 237–253.

Sharland, P.R., Archer, R., Casey, D.M., Davies, R.B., Hall, S.H., Heward, A.P., Horbury, A.D., and M.D. Simmons. 2001. Arabian Plate Sequence Stratigraphy, 2. GeoArabia Spec Publ, Gulf PetroLink, Bahrain, 371 p.

Winter, A., Reiss, Z., and B. Luz. 1979. Distribution of living coccolithophore assemblages in the Gulf of Elat (ʾAqaba). *Marine Micropaleontol* 4: 197–223.

Winter, A. 1982. Paleoenvironmental interpretation of Quaternary coccolith assemblages from the Gulf of Aqaba (Elat), Red Sea. *Rev Esp Micropaleontol* 14: 291–314.

Winter, A., Jordan, R.W., and P.H. Roth. 1994. Biogeography of living coccolithophores in ocean waters. In: *Coccolithophores*. Eds: A. Winter, and W.G. Siesser, 161-177. New York: Cambridge Univ Press.

Carbapenem-resistant *Acinetobacter baumannii* from Jordan: Complicated Carbapenemase Combinations

Esra'a M. AlFaris[1], Nehaya Al-Karablieh[2,3,*], Nidal A. Odat[4], Rayane Rafei[5]

[1] *Department of Biotechnology, Faculty of Agricultural Technology, Al-Balqa Applied University, Salt, Jordan;* [2] *Department of Plant Protection, School of Agriculture, The University of Jordan, Amman, Jordan;* [3] *Hamdi Mango Center for Scientific Research, The University of Jordan, Amman, Jordan;* [4] *Department of Medical Laboratories, Faculty of Science, Al-Balqa Applied University, Salt, Jordan;* [5] *Laboratoire Microbiologie Santé et Environnement (LMSE), Doctoral School for Science and Technology, Faculty of Public Health, Lebanese University, Tripoli, Lebanon*

Abstract

Acinetobacter baumannii is an opportunistic Gram-negative bacterium that has recently emerged as a clinically important pathogen. It is the most common *Acinetobacter* species associated with hospital-acquired infections worldwide. This study aimed to investigate the resistance characteristics of clinical carbapenem-resistant *A. baumannii* isolates from Jordanian hospitals. Between May 2018 and May 2019, a total of 190 isolates of *Acinetobacter* were collected from patients diagnosed with upper respiratory tract infection (47.5%), sepsis (15.4%), skin infection (14.2%), bronchitis (8.6%), urinary tract infection (4.3%), meningitis (3.7%), diabetes (2.5%), necrotizing fasciitis (1.9%), and cancer, peritonitis, and pneumonia (0.6% each) from seven Jordanian hospitals. Vitek GN ID Cards were employed to identify them, and the identification was validated by the detection of *Acinetobacter* spp. *recA* gene (100%), *A. baumannii* intergenic spacer region (85.3%), and the *A. baumannii rpoB* gene (85.3%). The Vitek AST-N222 and AST-XN05 cards were utilized to determine the minimum inhibitor concentration for a variety of antibiotics including Gentamicin, Tobramycin, Piperacillin-tazobactam, Ticarcillin-clavulanic acid, Ticarcillin, Imipenem, Meropenem, Cefepime, Ceftazidime, Ceftriaxone, Ciprofloxacin, Levofloxacin, Trimethoprim-sulfamethoxazole, Piperacillin, Minocycline, and Tetracycline. The E-test was performed to evaluate the effectiveness of Colistin against all *A. baumannii* isolates. According to the resistance profiles, the isolates had a multidrug resistance profile, with the largest resistance percentage being 98.8% for Tetracycline and the lowest being 23.5% for Minocycline. The Carbapenem-resistant isolates exhibited rates of 98.1% and 87.7% resistance to Meropenem and Imipenem, respectively. On the contrary, the isolates were 98.7% sensitive to Colistin. The most prevalent carbapenem resistance genes among the Jordanian *A. baumannii* isolates were $bla_{OXA-23-like}$, $bla_{OXA-51-like}$, bla_{OXA-69}, and $ISAba1$, which were detected in all *A. baumannii* isolates (100%) in this study. Despite the high prevalence of multidrug resistance in the Jordanian isolates, Colistin may be a viable treatment for *A. baumannii* infection.

Keywords: Acinetobacter baumannii, Carbapenemase, Colistin, $bla_{OXA-23-like}$, $bla_{OXA-51-like}$, bla_{OXA-69}, ISA_{ba1}, Jordan

1. Introduction

Acinetobacter baumannii is an opportunistic Gram-negative bacterium that has recently emerged as a clinically important pathogen due to its association with hospital-acquired infections worldwide. Examples on these infections include wide range of nosocomial infections such as, bloodstream infections, urinary tract infections, wound infections, pneumonia and meningitis, primarily those acquired in the community or from war and natural disasters (Ababneh et al., 2021; El-Khatib et al., 2021; Al-Tamimi et al., 2022). This bacterium lives in the human body and is usually detected in moist environments and on contaminated tools and materials used by patients in hospitals (Shatnawi et al., 2021). Consequently, *A. baumannii* frequently colonize hospitalized patients, resulting in invasive sporadic infection and hospital outbreaks, particularly among critically sick patients and intensive care unit (ICU) patients (Ghaith et al., 2017).

Imipenem, a Carbapenem, is the medication of choice for severe infections caused by *A. baumannii*. In recent years, this pathogen has become a major source of concern due to the extensive use of Carbapenems. The emergence of Carbapenem-resistant *A. baumannii* has drastically reduced the number of antibiotics available to individuals infected with multidrug-resistant (MDR) *A. baumannii* (Nguyen and Joshi, 2021). Colistin is another medication that is often used as a first-line therapy for *A. baumannii* infections in Jordan (Samrah et al., 2016). In Jordan, as in many other countries, MDR *A. baumannii* poses a major threat to patients and places an economic burden on healthcare systems from increased healthcare costs, prolonged hospitalization, ICU admissions, higher mortality rates, resource utilization for infection control, challenges in antibiotic development, and the broader impact on public health. Efforts to address antimicrobial resistance and enhance infection control practices are crucial to mitigating these economic challenges.

---

[*] Corresponding author. e-mail: n.alkarablieh@ju.edu.jo.

Carbapenem resistance in *A. baumannii* is often associated with the production of carbapenemases, enzymes that hydrolyze carbapenem antibiotics. The carbapenemases found in *A. baumannii* belong to different classes. Here are some of the carbapenemases commonly associated with carbapenem-resistant *A. baumannii*: The oxacillinase group, OXA-type carbapenemases, which belong to Class D β-lactamases, such as OXA-23, OXA-24, OXA-58 that are encoded by $bla_{OXA-23-like}$, $bla_{OXA-24-like}$, and $bla_{OXA-58-like}$ genes respectively; OXA-23 is one of the most prevalent carbapenemases in *A. baumannii* and is associated with resistance to carbapenems (Mentasti et al., 2020). Metallo-β-lactamases (MBLs), which belong to Class B β-lactamases, are zinc-dependent enzymes that hydrolyze carbapenems and are resistant to β-lactamase inhibitors such as IMP, and VIM. While MBLs are more commonly associated with other Gram-negative bacteria, they have been found in *A. baumannii* isolates as well (Tooke et al., 2019). New Delhi metallo-β-lactamase (NDM) is a type of MBLs that has been reported in *A. baumannii* strains. The New Delhi metallo-β-lactamase 1 gene (*NDM-1*) carbapenemase has been described in *A. baumannii* worldwide, the highest prevalence was reported in the Indian subcontinent, Middle East, Algeria, Brazil, Pakistan, Balkans, and the United Kingdom (Wu et al., 2019). *Klebsiella pneumoniae* carbapenemase (KPC) has been reported in some *A. baumannii* isolates such as KPC-3 (Caneiras et al., 2018). Furthermore, resistance to carbapenems in *A. baumannii* has been associated with the presence of the *ISAba1* gene, which acts as a promoter for the $bla_{OXA-51-like}$ and, most likely, $bla_{OXA-23-like}$ carbapenemase genes (Vahhabi et al., 2021).

The current study aimed to identify the carbapenem-resistant genes in Jordanian clinical *A. baumannii* isolates, with a focus on genes encoding carbapenemases class D, oxacillinase *OXA*s, and class B, *NDM-1*.

2. Materials and Methods

2.1. Collection of A. baumannii isolates

From May 2018 to May 2019, a total of 190 bacterial isolates were randomly collected from seven Jordanian hospitals: Al Basheer Hospital, Al Khalidi Medical Center, Islamic Hospital, Jordan University Hospital, Prince Hamza Hospital, Royal Medical Services, and The Specialty Hospital. Information about the patients, including nationality, age, gender, and sample source such as abdominal and pleural fluids, blood culture, bronchoalveolar lavage, cancer tissue, cerebrospinal fluid, pus, specimen collection trap, sputum, swabs, and urine, was collected for each isolate. The isolates were sub-cultured on MacConkey agar (Mast Group, UK) and incubated for 20–24h at 35°C ± 2°C. The pure culture of each isolate was stored at -80°C in 20% glycerol (Cryobank, Mast Group, UK) for further use (Al-Karablieh et al., 2017).

2.2. Identification of the collected isolates

Fresh pure culture of the collected isolates, 1mm in diameter, and the transparent colonies on MacConkey agar were tested for oxidase. The isolates exhibiting negative results in the oxidase test were chosen for further identification by an automated Vitek®2 compact system using GN ID Cards (BioMérieux, Marcy-l'Etoile, France). Furthermore, the genomic DNA was extracted with the Quick–DNA miniprep plus kit (Zymo Research, USA) following the recommendations of the manufacturer. The purity and concentration of DNA were quantified using a NanoDrop™ spectrophotometer (Thermo Fisher Scientific, USA). The concentration of the extracted DNA was adjusted to 100ng/µl. Duplex polymerase chain reaction (PCR) was conducted with a programmable thermocycler (S1000 thermal cycler Bio-Rad, USA) targeting the *recA* gene of *Acinetobacter* spp., and an internal 208bp region on the ITS region in *A. baumannii* (Chen et al., 2007). For further validation of the identification, conventional PCR was employed to detect the DNA-directed RNA polymerase subunit beta encoding gene, *rpoB*, in *A. baumannii* (Schleicher et al., 2013). Table 1 lists the all primers used in the present study.

Table 1. List of all primers used in the current study for identification of the collected isolates and detection of carbapenemase-encoding genes.

Primer	Target gene	Sequence (5' - 3')	Size (bp)	Reference
Identification				
P-Ab-ITSF	ITS	AGAGCACTGTGCACTTAAG	208	(Chen et al., 2007)
P-Ab-ITSR		CATTATCACGGTAATTAGTG		
P-rA1-F	*recA*	CCTGAATCTTCTGGTAAAAC	425	(Chen et al., 2007)
P-rA2-R		GTTTCTGGGCTGCCAAACATTAC		
Ac696F	*rpoB*	TAYCGYAAAGAYTTGAAAGAAG	350	(Schleicher et al., 2013)
Ac1093R		CMACACCYTTGTTMCCRTGA		
Carbapenemase-encoding genes				
ISAba1	*ISAba1*	CATTGGCATTAAACTGAGGAGAAA	451	(Ruiz et al., 2007)
ISAba2		TTGGAAATGGGGAAAACGAA		
NDM-F	*blaNDM-1*	GGTGCATGCCCGGTGAAATC	660	(Bonnin et al., 2012)
NDM-R		ATGCTGGCCTTGGGGAACG		
OXA23-F1	*bla$_{OXA-23-\text{like}}$*	TGCTCTAAGCCGCGCAAATA	130	(Mesli et al., 2013)
OXA23-R1		TGACCTTTTCTCGCCCTTCC		
OXA24-F	*bla$_{OXA-24-\text{like}}$*	CAAATGAGATTTTCAAATGGGATGG	123	(Mesli et al., 2013)
OXA24-R		TCCGTCTTGCAAGCTCTTGAT		
OXA51like-F	*bla$_{OXA-51-\text{like}}$*	AACATTAAAGCACTCTTACTTATAAC	171	(Adams-Haduch et al., 2011)
OXA51like-R		TTGTTGGATAACTAAAACACCCGT		
OXA58-F	*bla$_{OXA-58-\text{like}}$*	CGCAGAGGGGAGAATCGTCT	102	(Mesli et al., 2013)
OXA58-R		TTGCCCATCTGCCTTTTCAA		
OXA-69A	*bla$_{OXA-69}$*	CTAATAATTGATCTACTCAAG	975	(Hamouda et al., 2010)
OXA-69B		CCAGTGGATGGATGGATAGATTATC		

2.3. Antimicrobial susceptibility test of A. baumannii isolates

The minimal inhibition concentration (MIC) was checked for different antibiotics by the Vitek®2 compact instrument, using AST-N222 and AST-XN05 cards to target specific antibiotics (BioMérieux, Marcy-l'Etoile, France) according to the Clinical Laboratory Standards Institute (CLSI, 2019), following the guidelines for antibiotics breakpoints. Twelve antibiotics from eight antibiotics group and three antibiotic combinations were evaluated against the 162 *A. baumannii* isolates, namely, Aminoglycosides (Gentamicin [4–16 µg mL^{-1}], and Tobramycin [4–16 µg mL^{-1}]), β-lactam combination agents (Piperacillin-tazobactam [16/4–128/4 µg mL^{-1}], Ticarcillin-clavulanic acid [16/2–128/2 µg mL^{-1}], and Ticarcillin [16–128 µg mL^{-1}]), Carbapenem (Imipenem [2–8 µg mL^{-1}], and Meropenem [2–8 µg mL^{-1}]), Cephems (Cefepime [8–32 µg mL^{-1}], Ceftazidime [8–32 µg mL^{-1}], and Ceftriaxone [8–64 µg mL^{-1}]), Fluoroquinolones (Ciprofloxacin [1–4 µg mL^{-1}], and Levofloxacin [2–8 µg mL^{-1}]), Folate pathway antagonists (Trimethoprim-sulfamethoxazole [2/38–4/76 µg mL^{-1}]), Penicillins (Piperacillin [16–128 µg mL^{-1}]), Tetracyclines (Minocycline [4–16 µg mL-1], and Tetracycline [4–16 µg mL^{-1}]). Furthermore, the E-test (BioMérieux, Marcy-l'Etoile, France) was conducted to assess the efficacy of Colistin against all *A. baumannii* isolates.

2.4. Molecular detection of carbapenemase-encoding genes

Conventional PCRs were conducted for the detection of intrinsic carbapenemases genes encoding *bla$_{OXA-23-\text{like}}$*, *bla$_{OXA-24-\text{like}}$*, *bla$_{OXA-51-\text{like}}$*, *bla$_{OXA-58-\text{like}}$*, *bla$_{OXA-69}$*, bla$_{NDM-1}$, and ISA$_{ba1}$. The PCR cycles and conditions were performed following the protocol described by the authors of the primers. *A. baumannii* NCTC 13301 was utilized as a positive control for $_{OXA}$ carbapenemases genes and *Klebsiella pneumonia* NCTC 13443 as a positive control for Metallo-β-lactamase (bla$_{NDM-1}$).

2.5. Statistical Analysis

Statistical analysis was performed using SPSS software, version 21, and analysis of variance (ANOVA) was conducted to determine mean separation at the 0.05 probability level based on the least significant difference.

3. Results

3.1. Identification of the collected isolates

The Vitek®2 GN ID Cards and the detection of the *recA* gene of *Acinetobacter* spp. revealed the presence of *Acinetobacter* spp. in 182 bacterial isolates. The detection of the ITS region of *A. baumannii*, and *rpoB* in 162 bacterial isolates revealed the presence of *Acinetobacter baumannii*. These, 162 isolates, were chosen for further testing as representatives for clinical Jordanian isolates of *A. baumannii*. It is noteworthy that more than half of the *A. baumannii* isolates (51.8%) in this study were collected from military hospitals, in particular Prince Hamza Hospital and Royal Medical Services, followed by public hospitals (29%), particularly Al Basheer Hospital and Jordan University Hospital, and the lowest percentage (19.1%) were collected from private hospitals, particularly Al Khalidi Medical Center, Islamic Hospital, and The Specialty Hospital. (Table 2).

Table 2. The distribution of A. baumannii isolates depends on sampling hospitals.

Hospital	No. of samples	%
AL Basheer Hospital	20	12.3
Al Khalidi Medical Center	12	7.4
Islamic Hospital	14	8.6
Jordan University Hospital	27	16.7
Prince Hamza Hospital	24	14.8
Royal Medical Services	60	37
Specialty Hospital	5	3.1
Total	162	100

3.2. The infections associated with A. baumannii

The distribution of *A. baumannii* isolates was varied according to the origin of the place of the collection, with sputum being the major source of the pathogen (in 47.5% of the samples), followed by blood culture (15.4%), pus (14.2%), specimen collection trap (7.4%), urine (4.3%), swabs (4.3%), cerebrospinal fluid (3.7%), bronchoalveolar lavage (1.2%), abdominal and pleural fluids (0.6%), and cancer (0.6%). The samples were mainly collected from patients diagnosed with upper respiratory tract infection (47.5%), followed by those diagnosed with sepsis (15.4%); skin infection (14.2%); bronchitis (8.6%); urinary tract infection (4.3%); meningitis (3.7%); diabetes (2.5%); necrotizing fasciitis (1.9%); and cancer, peritonitis, and pneumonia (0.6% each) (Table 3).

Table 3. The distribution of *A. baumannii* isolates depends on the infection type.

Infection type	No. of samples	%
Bronchitis	14	8.6
Cancer	1	0.6
Diabetes	4	2.5
Meningitis	6	3.7
Necrotizing fasciitis	3	1.9
Peritonitis	1	0.6
Pneumonia	1	0.6
Sepsis	25	15.4
Skin infection	23	14.2
Upper respiratory tract infection	77	47.5
Urinary tract infection	7	4.3
Total	162	100

A variation was found in the infection with *A. baumannii* isolates according to patient ages, which ranged from 3 to 80 years old. The majority of the infected patients were males (68%). Nearly all patients had Jordanian nationality (97.5%), with few having Iraqi (1.3%) and Libyan (1.2%) nationalities.

3.3. Antimicrobial susceptibility of A. baumannii isolates

The results of the antimicrobial susceptibility test by Vitek AST cards revealed that 98.8% of *A. baumannii* isolates were resistant to Tetracycline; 98.1% were resistant to Ceftazidime, Ceftriaxone, Ciprofloxacin, Meropenem, Piperacillin, Piperacillin-tazobactam, Ticarcillin, and Ticarcillin-clavulanic acid; 97.5% to Cefepime; 95% to Levofloxacin; 87.7% to Imipenem; 73.5% to Gentamicin; 68.5% to Tobramycin; 67.9% to Trimethoprim-sulfamethoxazole; and 23.5% to Minocycline according to (CLSI, 2019) (Table 3).

The results of the E-test of Colistin against *A. baumannii* isolates indicated that 98.7% of *A. baumannii* isolates were sensitive to Colistin (MIC ≤ 0.5), and only 1.3% (two isolates) were resistant to Colistin (Fig. 1).

Figure 1. Antimicrobial susceptibility of *A. baumannii* isolates to Colistin by E-test.

All the tested *A. baumannii* isolates (162) resulted in expected amplicon size of the following genes: $bla_{OXA-23-like}$, $bla_{OXA-51-like}$, bla_{OXA-69}, and *ISAba1*. While 95% of the *A. baumannii* isolates formed the expected amplicon size of the $bla_{OXA-24-like}$ gene, 80% formed the expected amplicon size of the *blaNDM-1* gene, and 40% of the isolates formed the expected amplicon size of the $bla_{OXA-58-like}$ gene.
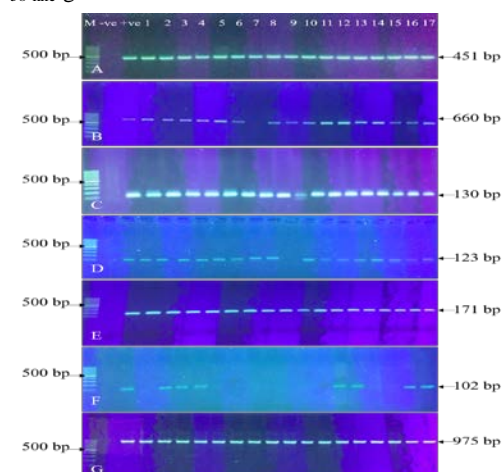
Figure 2. Examples of agarose gel electrophoresis of PCR products: **A**, ISAba1/ISAba2 primers for *ISAba1*, **B**, NDM-F/ NDM-R primers for *blaNDM-1*, **C**, OXA23-F1/ OXA23-R1 primers for $bla_{OXA-23-like}$, **D**, OXA24-F/ OXA24-R primers for $bla_{OXA-24-like}$, **E**, OXA51like-F/OXA51like-R primers for $bla_{OXA-51-like}$, **F**, OXA58-F/ OXA58-R primers for $bla_{OXA-58-like}$, **G**, and OXA-69A/ OXA-69B primers for bla_{OXA-69}. The DNA ladder was 1000 bp (M), deionized sterile water was used as negative control (-ve), gDNA of *A. baumannii* NCTC 13301 was used as a positive control for $_{OXA}$ carbapenemases genes and gDNA *Klebsiella pneumonia* NCTC 13443 as a positive control for Metallo-β-lactamase (bla_{NDM-1}) (+ve). Lane 1-17: representative samples of gDNA of Jordanian *A. baumannii* isolates.

4. Discussion

As carbapenems are usually the most practical therapy for many multi-resistant bacterial strains, the emergence of carbapenem-resistant *A. baumannii* has become a global concern (Ababneh et al., 2021; Al-Tamimi et al., 2022). The most common resistance mechanism in *A. baumannii* is the expression of Class D β-lactamases, such as OXA-23, OXA-24, OXA-58 enzymes. These enzymes were initially distinguished by their ability to efficiently

hydrolyze isoxazolyl-type β-lactams such as oxacillin. Due to this substrate preference, these enzymes are also known as oxacillinases or (OXAs) (June et al., 2014). Furthermore, MBLs, which are Class B β-lactamases, can be particularly harmful if found in *A. baumannii*-infected individuals due to their broad spectrum of powerful carbapenemase activity and resistance to β-lactamase inhibitors (Vahhabi et al., 2021). Mobile genetic elements, integrons, and plasmids can help disseminate MBLs across *A. baumannii* (Partridge et al., 2018).

Recent Middle Eastern wars, which have resulted in a significant number of immigrants and refugees, as well as a lack of access to competent medical treatment, are likely contributing factors to multi-drug-resistant organisms, increased resistance patterns, and expanding incidence rates (Nawfal Dagher et al., 2020; Helou et al., 2022). Hence, ongoing monitoring and surveillance are essential for forecasting and mandating suitable steps when necessary (Bessong and Guerrant, 2017). Therefore, Jordanian hospitals must further the invention and adoption of rapid and accurate diagnostic procedures. Collaboration with academic institutions, research centers, and private companies to support innovative projects focused on rapid and accurate diagnostics. Training programs should be provided for healthcare professionals to ensure they are proficient in using new diagnostic technologies. Other strategies include implementing financial incentives for hospitals to adopt and integrate rapid and accurate diagnostic procedures, conducting pilot programs to assess the feasibility and effectiveness of new diagnostic procedures in real-world hospital settings, collaboration with international organizations, research institutions, and healthcare providers to share knowledge and experiences related to the adoption of advanced diagnostics, and educating the public about the benefits of rapid and accurate diagnostics in improving healthcare outcomes. By implementing these strategies, Jordanian hospitals can contribute to the advancement and adoption of rapid and accurate diagnostic procedures, ultimately improving patient care and outcomes.

Using data from the Vitek 2 compact system, 162 *Acinetobacter* isolates were reported with a 99% high accuracy rate in this investigation. Several investigations have indicated that the automated Vitek 2 system is useful, accurate, and rapid in bacterial identification (Al-Karablieh et al., 2022). However, as previously reported, the identification was furthered using the molecular detection of *recA Acinetobacter* spp. at the genus level by 425 bp amplicon detection, and detection of *A. baumannii* ITS and *ropB* genes at the species level by 208 bp and 350 bp amplicons detection, respectively (Chen et al., 2007; Schleicher et al., 2013).

The sensitivity of the *A. baumannii* isolates to Imipenem and Meropenem in the disc diffusion test was lower than that in the test using Vitek AST cards, revealing the accuracy of the Vitek AST cards due to determination of the MIC values. However, the findings regarding the resistance of *A. baumannii* isolates to Imipenem and Meropenem measured by Vitek AST cards were similar to that observed in a previous Jordanian study, 94%, and 88% for Imipenem and Meropenem, respectively (El-Khatib et al., 2021). Moreover, the percentage of MDR *A. baumannii* isolates in this study,

98.8%, was higher than the percentage reported in a previous Jordanian study, 76.8% (Al-Tamimi et al., 2022).

The majority of the isolates in this study were sensitive to Colistin and Minocycline, which is consistent with a previous Jordanian study that found Colistin and Tigecycline to have the lowest resistance rate (Al-Tamimi et al., 2022). A study from the Holy Cities of Makkah and Al-Madinah of Saudi Arabia revealed that all *A. baumannii* isolates were susceptible to Colistin, while 95% of isolates were susceptible to Tigecycline (Al-Sultan, 2021). Another study from Riyadh, Saudi Arabia revealed that 30% of *A. baumannii* isolates were resistant to Colistin, and 56% were resistant to Tigecycline (Al-Agamy et al., 2017).

The tolerance to these antibiotics is crucial due to the global tendency of utilizing Colistin in dealing with of MDR *A. baumannii* infections (Chen et al., 2015). Colistin resistance in *A. baumannii* has previously been reported in Spain (Khoshbakht et al., 2023) and Kingdom of Bahrain (Al-Rashed et al., 2023), and a study from China reported a lower resistance rate to minocycline and tigecycline (Zhu et al., 2022). However, in this study, two Colistin-resistant *A. baumannii* isolates were identified and considered pan-drug resistant bacteria.

According to the findings of this study, Jordan has a higher percentage of carbapenem-resistant *A. baumannii* than surrounding countries, including Lebanon (60%) (Rafei et al., 2015), Turkey (79%) (Kulah et al., 2010), Egypt (70%) (Al-Agamy et al., 2014), Saudi Arabia (85.7%) (Elabd et al., 2015), and Iraq (85%) (Hussein et al., 2013), and this percentage is extremely close to Italy's reported percentage of 90.8% (Mezzatesta et al., 2012). The prevalence of carbapenem-resistant *A. baumannii* is growing in Jordan, with the proportion of carbapenem-resistant *A. baumannii* estimated to be 60% in 2014 (Obeidat et al., 2014). In the current study, carbapenem-resistant *A. baumannii* was found in 98.1% of the tested isolates, which is similar to the previously reported prevalence rates of carbapenem-resistant *A. baumannii* in Jordan of 90.6% and 99.2% (Ababneh et al., 2021; Al-Tamimi et al., 2022), respectively. The reasons for the high prevalence of carbapenem resistance *A. baumannii* might be the result of antibiotic abuse and misuse in healthcare settings, insufficient infection control measures in healthcare facilities, and the movement of individuals across borders, which can contribute to the worldwide spread of antibiotic-resistant strains.

The majority of the carbapenem-resistant *A. baumannii* came from Military hospitals followed by public hospitals, which might be related to challenges facing these hospitals in maintaining optimal hygiene and infection control practices due to the high numbers of patients in these hospitals, which contribute to the persistence of the *A. baumannii* in the environment. The majority of the carbapenem-resistant *A. baumannii* came from Jordanian men, consistent with previous Jordanian studies that found an elevated frequency of *A. baumannii* infections in Jordanian adult males (Ababneh et al., 2021; El-Khatib et al., 2021; Al-Tamimi et al., 2022). Military personnel may sustain injuries during combat, leading to open wounds and increased susceptibility to infections. *A. baumannii*, known for its ability to cause wound infections, can thrive in the environment and infect individuals with compromised immune systems. In conflict zones like

Jordan, injured soldiers may be rapidly evacuated to military hospitals for treatment. The transfer of individuals with infections, including *A. baumannii*, from different locations can contribute to the spread of the bacterium within military healthcare facilities. The use of broad-spectrum antibiotics is common in military settings to treat infections. Prolonged and widespread use of antibiotics can contribute to the development of multidrug-resistant strains of bacteria, including *A. baumannii*.

Similar to a previous Jordanian study (El-Khatib et al., 2021), over half of the carbapenem-resistant *A. baumannii* isolates tested in this study were collected from sputum; however, another Jordanian investigation found that the majority of *A. baumannii* isolates were obtained from wounds (Al-Tamimi et al., 2022).

In dedpth genetic analysis of the studied samples can help in elucidation of many mechanisms that result in *A. baumannii* being both highly infectious and extremely resistant. This study found that the dominant resistant genes among carbapenem-resistant Jordanian *A. baumannii* isolates are $bla_{OXA-23\text{-like}}$, $bla_{OXA-51\text{-like}}$, bla_{OXA-69}, ISA_{ba1}, which were found in all tested, 100%, carbapenem-resistant Jordanian *A. baumannii* isolates, followed by 95% for $bla_{OXA-24\text{-like}}$, 80% for of $blaNDM-1$ and 40% for $bla_{OXA-58\text{-like}}$. The most prevalent encoding genes of MBLs and OXAs in Mediterranean Arab countries are bla_{IMP}, bla_{KPC}, bla_{NDM-1}, $bla_{OXA-23\text{-like}}$, $bla_{OXA-24\text{-like}}$, $bla_{OXA-51\text{-like}}$, $bla_{OXA-58\text{-like}}$, and bla_{OXA-69} and bla_{VIM} (Salih and Shafeek, 2019; Shayea and Ali, 2022). The current study is the first in Jordan to show an elevated prevalence of bla_{NDM-1} of 80% among carbapenem-resistant *A. baumannii* isolates compared to the 10.4% previously reported (Ababneh et al., 2021), indicating the fast expansion of bla_{NDM-1} in Jordan. Recent investigations from the Arab area have yet to discover bla_{NDM} or bla_{NDM-1} genes in carbapenem-resistant *A. baumannii*. However, bla_{NDM} was discovered in a few carbapenem-resistant *A. baumannii* isolates collected from Syrian hospitalized patients in Lebanon (Rafei et al., 2014).

5. Conclusion

This study found that *A. baumannii* is widespread in Jordan and can cause major hospital infections. A high frequency of carbapenem resistance was reported among Jordanian *A. baumannii* isolates. The major resistance genes among Jordanian *A. baumannii* isolates were $bla_{OXA-23\text{-like}}$, $bla_{OXA-51\text{-like}}$, bla_{OXA-69}, and ISA_{ba1}. This significant resistance will impair the effectiveness of valuable medications that treat *A. baumannii* invasive infections. Despite the high prevalence of multidrug resistance in Jordanian *A. baumannii* isolates, Colistin and Tigecycline may be viable treatment for *A. baumannii* infection. Combining different classes of antibiotics can enhance effectiveness and reduce the risk of resistance development.

Therefore, further studies are warranted to determine the efficiency of combining Colistin and Tigecycline with Jordanian medicinal plants to control *A. baumannii* infection.

6. Ethical approval

The authors have complete confidence that publishing this manuscript will not cause any ethical concerns.

Conflict of interests

The authors declare that they have no conflicts of interest.

References

Ababneh Q, Aldaken NA, Jaradat Z, Al Sbei S, Alawneh DA, Al-zoubi EA, Alhomsi T and Saadoun I. 2021. Molecular epidemiology of carbapenem-resistant *Acinetobacter baumannii* isolated from three major hospitals in Jordan. *Int J Clin Pract.*, **75(12)**: e14998.

Adams-Haduch JM, Onuoha EO, Bogdanovich T, Tian GB, Marschall J, Urban CM, Spellberg BJ, Rhee D, Halstead DC, Pasculle AW and Doi Y. 2011. Molecular epidemiology of carbapenem-nonsusceptible *Acinetobacter baumannii* in the United States. *J Clin Microbiol.*, **49(11)**: 3849-3854.

Al-Agamy MH, Jeannot K, El-Mahdy TS, Shibl AM, Kattan W, Plésiat P and Courvalin P. 2017. First detection of GES-5 carbapenemase-producing *Acinetobacter baumannii* isolate. *Microb Drug Resist.*, **23(5)**: 556-62.

Al-Agamy MH, Khalaf NG, Tawfick MM, Shibl AM and El Kholy A. 2014. Molecular characterization of carbapenem-insensitive *Acinetobacter baumannii* in Egypt. *Int J Infect Dis.*, **22**: 49-54.

Al-Karablieh N, Al-Horani FA, Alnaimat S and Abu Zarga MH. 2022. Prevalence of *Vibrio coralliilyticus* in stony coral Porites sp. in the Gulf of Aqaba, Jordan. *Lett Appl Microbiol.*, **75(2)**: 460-469.

Al-Karablieh N, Mutlak I and Al-Dokh A. 2017. Isolation and identification of *Pseudomonas viridiflava*, the causal agent of fruit rotting of *Cucumis sativus*. *Jordan J Agri Sci.*, **13(1)**: 79-91.

Al-Rashed N, Bindayna KM, Shahid M, Saeed NK, Darwish A, Joji RM and Al-Mahmeed A. 2023. Prevalence of carbapenemases in carbapenem-resistant *Acinetobacter Baumannii* isolates from the Kingdom of Bahrain. *Antibiotics*, **12(7)**:1198.

Al-Sultan AA. 2021. Prevalence of High-Risk Antibiotic Resistant *Acinetobacter baumannii* in the Holy Cities of Makkah and Al-Madinah. *Open Microbiol J.*, **15**: 145-151.

Al-Tamimi M, Albalawi H, Alkhawaldeh M, Alazzam A, Ramadan H, Altalalwah M, Alma'aitah A, Al Balawi D, Shalabi S, Abu-Raideh J, Khasawneh A I, Alhaj F and Hijawi K. 2022. Multidrug-Resistant *Acinetobacter baumannii* in Jordan. *Microorganisms,* **10(5)**: 849.

Bessong PO and Guerrant RL. 2017. Improving our understanding of antibiotic resistance: The relevance of surveillance at the population level. *S Afr Med J.,* **107(3)**: 167-167.

Bonnin RA, Naas T, Poirel L and Nordmann P. 2012. Phenotypic, biochemical, and molecular techniques for detection of metallo-β-lactamase NDM in *Acinetobacter baumannii*. *J Clin Microbiol.*, **50(4)**:1419-1421.

Caneiras C, Calisto F, Jorge da Silva G, Lito L, Melo-Cristino J and Duarte A. 2018. First description of colistin and tigecycline-resistant *Acinetobacter baumannii* producing KPC-3 carbapenemase in Portugal. *Antibiotics.***7(4)**:96.

Chen TL, Siu LK, Wu RC, Shaio MF, Huang LY, Fung CP, Lee CM and Cho WL. 2007. Comparison of one-tube multiplex PCR, automated ribotyping and intergenic spacer (ITS) sequencing for rapid identification of *Acinetobacter baumannii*. *Clin Microbiol Infect*., **13(8)**: 801-806.

Chen YP, Lu PL and Kuo CM. 2015. An increasing trend of Carbapenems resistance *Acinetobacter baumannii* (CRAB) and CRAB's co-resistance to ceftazidime, gentamicin, cefepime, levofloxacin and amikacin in a Taiwan regional hospital. *J Microbiol Immunol Infect*., **48(2)**: 126-127.

CLSI, 2019. Performance standards for antimicrobial susceptibility testing. 29th edition, CLSI supplement M100. Clinical and Laboratory Standards Institute, Wayne, PA.

Elabd FM, Al-Ayed MS, Asaad AM, Alsareii SA, Qureshi MA and Musa H A. (2015). Molecular characterization of oxacillinases among carbapenem-resistant *Acinetobacter baumannii* nosocomial isolates in a Saudi hospital. *J Infec. Public Health*., **8(3)**: 242-247.

El-Khatib L, Al-Dalain S, Al-Matarneh R, Al-Bustanji S, Al-Dmour M, Al-Amarin Y and Gaber Y. 2021. Prevalence of multi-drug resistant *Acinetobacter baumannii* (MDRAB) in Amman Jordan during 2018. *Infect Disord Drug Targets*., **21(1)**: 105-111.

Ghaith DM, Zafer MM, Al-Agamy MH, Alyamani EJ, Booq RY and Almoazzamy O. 2017. The emergence of a novel sequence type of MDR *Acinetobacter baumannii* from the intensive care unit of an Egyptian tertiary care hospital. *Ann Clin Microbiol Antimicrob*., **16(1)**: 1-8.

Hamouda A, Evans BA, Towner KJ and Amyes SG. 2010. Characterization of epidemiologically unrelated *Acinetobacter baumannii* isolates from four continents by use of multilocus sequence typing, pulsed-field gel electrophoresis, and sequence-based typing of bla(OXA-51-like) genes. *J Clin Microbiol*., **48(7)**: 2476-2483.

Helou M, Van Berlaer G and Yammine K. 2022. Factors influencing the occurrence of infectious disease outbreaks in Lebanon since the Syrian crisis. *Pathog Glob Health*., **116(1)**: 13-21.

Howard A, O'Donoghue M, Feeney A and Sleator RD. 2012. *Acinetobacter baumannii*: an emerging opportunistic pathogen. *Virulence* **3(3)**: 243-250.

Hussein H, Al-Mathkhury HJF and Sabbah A. 2013. Imipenem-Resistant *Acinetobacter baumannii* isolated from patients and hospitals environment in Baghdad. *Iraqi J Sci*., **54(4)**: 803-812.

June CM, Vallier BC, Bonomo RA, Leonard DA and Powers RA. 2014. Structural origins of oxacillinase specificity in class D β-lactamases. *Antimicrob Agents Chemother*., **58(1)**: 333-341.

Khoshbakht R, Panahi S, Neshani A, Ghavidel M and Ghazvini K. 2023. Novel approaches to overcome Colistin resistance in *Acinetobacter baumannii*: Exploring quorum quenching as a potential solution. *Microb Pathogen*., **182**: 106264.

Kulah C, Mooij MJ, Comert F, Aktas E, Celebi G, Ozlu N, Rijnsburger MC and Savelkoul PH. 2010. Characterisation of carbapenem-resistant *Acinetobacter baumannii* outbreak strains producing OXA-58 in Turkey. *Int J Antimicrob Agents*., **36(2)**: 114-118.

Mentasti M, Prime K, Sands K, Khan S and Wootton M. 2020. Rapid detection of OXA-23-like, OXA-24-like, and OXA-58-like carbapenemases from *Acinetobacter* species by real-time PCR. *J Hosp Infect*., **105(4)**: 741-746.

Mesli E, Berrazeg M, Drissi M, Bekkhoucha SN and Rolain JM. 2013. Prevalence of carbapenemase-encoding genes including New Delhi metallo-β-lactamase in *Acinetobacter* species, Algeria. *Int J Infect Dis*., **17(9)**: e739-743.

Mezzatesta ML, D'Andrea MM, Migliavacca R, Giani T, Gona F, Nucleo E, Fugazza G, Pagani L, Rossolini GM and Stefani S. 2012. Epidemiological characterization and distribution of carbapenem-resistant *Acinetobacter baumannii* clinical isolates in Italy. *Clin Microbiol Infect*., **18(2)**: 160-166.

Nawfal DT, Al-Bayssari C, Diene SM, Azar E and Rolain JM. 2020. Bacterial infection during wars, conflicts and post-natural disasters in Asia and the Middle East: a narrative review. *Expert Rev Anti Infect Ther*., **18(6)**: 511-529.

Nguyen M and Joshi SG. 2021. Carbapenem resistance in *Acinetobacter baumannii*, and their importance in hospital-acquired infections: a scientific review. *J Appl Microbiol*., **131(6)**: 2715-38.

Obeidat N, Jawdat F, Al-Bakri AG and Shehabi AA. 2014. Major biologic characteristics of *Acinetobacter baumannii* isolates from hospital environmental and patients' respiratory tract sources. *Am J Infect Control*., **42(4)**: 401-404.

Partridge SR, Kwong SM, Firth N and Jensen SO. 2018. Mobile genetic elements associated with antimicrobial resistance. *Clin Microbiol Rev*., **31(4)**:10-128.

Rafei R, Dabboussi F, Hamze M, Eveillard M, Lemarié C, Mallat H, Rolain JM, Joly-Guillou ML and Kempf M. 2014. First report of blaNDM-1-producing *Acinetobacter baumannii* isolated in Lebanon from civilians wounded during the Syrian war. *Int J Infect Dis*., **21**: 21-23.

Rafei R, Pailhoriès H, Hamze M, Eveillard M, Mallat H, Dabboussi F, Joly-Guillou ML and Kempf M. 2015. Molecular epidemiology of *Acinetobacter baumannii* in different hospitals in Tripoli, Lebanon using bla(OXA-51-like) sequence based typing. *BMC Microbiol*., **15(1)**: 1-7.

Ruiz M, Marti S, Fernandez-Cuenca F, Pascual A and Vila J. 2007. Prevalence of IS(Aba1) in epidemiologically unrelated *Acinetobacter baumannii* clinical isolates. *FEMS Microbiol Lett*., **274(1)**: 63-66.

Salih TS and Shafeek RR. 2019. *In silico* detection of acquired antimicrobial resistance genes in 110 complete genome sequences of *Acinetobacter baumannii*. *Jordan J Biol Sci*., **12(5)**: 589-594.

Samrah S, Bashtawi Y, Hayajneh W, Almomani B, Momany S and Khader Y. 2016. Impact of colistin-initiation delay on mortality of ventilator-associated pneumonia caused by *A. baumannii*. *J Infect Dev Ctries*., **10(10)**: 1129-1134.

Schleicher X, Higgins PG, Wisplinghoff H, Körber-Irrgang B, Kresken M and Seifert H. 2013). Molecular epidemiology of *Acinetobacter baumannii* and *Acinetobacter nosocomialis* in Germany over a 5-year period (2005-2009). *Clin Microbiol Infect*., **19(8)**: 737-742.

Shatnawi M, Abubaker S, Odat N and Majdalawi M. 2021. Antimicrobial activity and micropropagation of some reare and endangered plants of Jordan. *J Ecol Eng*., **22(4)**: 151-158.

Shayea R H, Ali M R, (2022). ERIC-PCR genotyping and clonal genetic linkage between Carbapenem-Resistant *Acinetobacter baumannii* isolates. *Jordan J Biol Sci*., **15(4)**: 689-696.

Tooke CL, Hinchliffe P, Bragginton EC, Colenso CK, Hirvonen VHA, Takebayashi Y and Spencer J. 2019. β-Lactamases and β-Lactamase inhibitors in the 21st Century. *J Mol Biol*., **431(18)**: 3472-3500.

Vahhabi A, Hasani A, Rezaee MA, Baradaran B, Hasani A, Kafil HS and Soltani E. 2021. Carbapenem resistance in *Acinetobacter baumannii* clinical isolates from northwest Iran: high prevalence of OXA genes in sync. *Iran J Microbiol*., **13(3)**: 282-293.

Wu W, Feng Y, Tang G, Qiao F, McNally A and Zong Z. 2019. NDM metallo-β-lactamases and their bacterial producers in health care settings. *Clin Microbiol Rev*., **32(2)**:10-128.

Zhu Y, Zhang X, Wang Y, Tao Y, Shao X, Li Y and Li W. 2022. Insight into carbapenem resistance and virulence of *Acinetobacter baumannii* from a children's medical centre in eastern China. *Ann Clin Microbiol Antimicrob*., **21(1)**: 47.

Gymnascella thermotolerans-GTE-21, an Endophytic Fungus in *Euphorbia geniculata* as a Versatile Producer of Bioactive Metabolites

Soad A. El-Zayat[1,2], Noha M. Kamel[1,2], Fatma F. Abdel-Motaal[1,2,*], Magdi A. El-Sayed[1,3], Mostafa Abdelrahman[1,4], Mohamed Abou-Ellail[5], Abou El-Hamd H. Mohamed[6], Doaa B. Darwish[7]

[1]Botany Department, Faculty of Science, Aswan University, Aswan 81528, Egypt; [2]Unit of Environmental Studies and Development, Aswan University, Aswan 81528, Egypt; [3]Molecular Biotechnology Program, Biological Sciences Department, Faculty of Science, Galala University, New Galala City, Egypt;[4]Institute of Genomics for Crop Abiotic Stress Tolerance, Texas Tech University, Lubbock 79415, Texas, USA; [5]Department of Genetics, Faculty of Agriculture and Natural Resources, Aswan University, Aswan 81528, Egypt; [6]Chemistry Department, Faculty of Science, Aswan University, Aswan 81528, Egypt; [7]Botany Department, Faculty of Science, Mansoura University, Mansoura 35511, Egypt

Abstract

The thermophilic fungus *Gymnascella thermotolerans* GTE-21 produces a significant amount of both volatile and non-volatile compounds with potent antifungal and anticancer properties. Gas chromatography-mass spectrometry (GC-MS) was utilized to identify 14 volatile organic compounds (VOCs) released by *G. thermotolerans*. The most predominant compound identified was diisooctyl phthalate, constituting 71.99% of the total VOCs, followed by phenol, 2-methoxy-4-(2-propenyl) at 7.12%. The GTE-21's VOCs demonstrated significant antifungal growth inhibition activity of 42.5% against *Fusarium solani* and 39.03% against *Alternaria alternata*. Additionally, GTE-21's crude extract exhibited substantial antibacterial effects, evidenced by inhibition zones of 1.5 cm against *S. epidermidis*, 1.4 cm against *C. ciferrii*, and 1.3 cm against *S. aureus*. The CH_2Cl_2:MeOH (1:1) fraction was more effective against human pathogens, producing the largest zones of inhibition of 1.1 and 1.03 cm against *S. epidermidis* and *C. ciferrii*, respectively. The evaluation of GTE-21's antifungal activity using the Evans blue assay showed that fungal spores treated with GTE-21's crude extract exhibited 96.2% inhibition at a concentration of 25 mg/ml. Similarly, the fractions CH2Cl2:MeOH (1:1) and CH2Cl2:MeOH (9:1) demonstrated spore inhibition rates of 96.3% and 94.3%, respectively. The EtOAc crude extract demonstrated pronounced cytotoxic effects against the SKOV-3 and MDA-MB-231 cancer cell lines. For SKOV-3, cell viability decreased to 3.40% and 0.47% at concentrations of 50 and 100 µL, respectively. In the case of MDA-MB-231, cell viability was reduced to 0.19% at both 50 and 100 µL concentrations.

Keywords: Antimicrobial Activity, Anticancer, *Gymnascella thermotolerans*, Volatile Organic Compounds

1. Introduction

Euphorbia geniculata, a member of the *Euphorbiaceae* family, is characterized by its production of a white milky latex. This latex has traditionally been used as a purgative and lactogenic agent and for treating gonorrhea, migraines, and warts. Additionally, it is used in the manufacturing of fish poison, pesticides and toxins (Kumar *et al.*, 2010).

Endophytes, a beneficial class of microorganisms, are known for colonizing various plants while maintaining a symbiotic relationship that does not harm their hosts (Rodriguez *et al.*, 2009). Endophytes are considered invaluable in the realm of drug discovery due to their production of volatile and non-volatile bioactive metabolites with crucial biological functions (Priti *et al.*, 2009). These compounds are leveraged in biofuel production and exhibit a range of biological properties, such as cytotoxic, anticancer, antimicrobial, antidiabetic, antioxidant and antiproliferative activities (Fernandes *et al.*, 2015).

Endophytic fungi can generate complex combinations of volatile organic compounds (VOCs), which may protect their host plants from phytopathogens either directly or indirectly by enhancing plant resistance (Tahir *et al.*, 2017). These VOCs span various chemical classes, including esters, alkynes, alkenes, alkanes, alcohols, terpenoids, aldehydes, ketones, and sulfur-containing compounds (Mitchell et al., 2010). Notably, compounds such as 2-undecanone, nonanal, dimethyl trisulfide, n-decanal cyclohexanol, and benzothiazole have shown biocontrol activity (Xie *et al.*, 2018).

Currently, cancer ranks as the leading cause of death worldwide, with the World Health Organization (WHO) identifying it as a primary cause of morbidity and mortality. It has been determined that endophytic fungi

---

* Corresponding author. e-mail: fatma.fakhry@aswu.edu.eg.

provide a consistent and abundant source of anticancer agents. Early investigations have revealed that the bioactive compounds naturally produced by endophytes may offer a new foundation for the development of innovative anticancer medications (Xie and Zhou, 2017).

Thermophilic fungi are extremophiles that are able to reproduce and develop within a temperature range of 45 °C and 61 °C (De Oliveira *et al.*, 2015). Therefore, temperature is considered as the key factor influencing the structural and functional properties of endophytic biomolecules, as well as maintaining the integrity of their cellular components. These unique biomolecules have garnered the interest of chemists and biotechnologists working in the field of natural products, and numerous applications of thermophiles-derived compounds have been seen in current biotechnology (Atalla, *et al.*, 2019, 2020[a, b]; Elsehemy, *et al.*, 2020).

The increasing problem of drug-resistant bacteria necessitates the urgent need for the development of more effective and powerful antimicrobial drugs. Recent theoretical developments have shown that numerous endophytic fungi have the potential to produce antimicrobial compounds, facilitating the creation of novel pharmaceutical medications. Fungi also produce a wide range of antioxidants, including flavonoids, alkaloids, steroids and phenols, and these compounds can scavenge the excess reactive oxygen species (ROS) that accumulate in our body (Hamed, *et al.*, 2015, Gauchan *et al.*, 2020).

In our study, we focused on thermotolerant endophytes that can produce bioactive secondary metabolites with cytotoxic, antibacterial and antioxidant effects. This study aims to demonstrate that endophytic fungi are valuable natural sources for the discovery of novel drugs, offering potential benefits to the food, pharmaceutical, and agricultural industries.

2. Materials and methods

2.1. Isolation and Identification of fungi

Euphorbia geniculata plant samples were collected from the field station at Aswan University, Egypt. The surface of the whole plant was sterilized using 70% ethanol for one minute followed by five minutes in a 5% sodium hypochlorite solution. Following sterilization, the plant was rinsed twice in sterile distilled water. The plant leaves, stems and roots were sliced longitudinally into small segments of 0.5-1.0 cm and placed on sterile Petri dishes containing Potato Dextrose Agar (PDA) medium (Sigma-aldrich, India). Three replicates of the Petri plates were incubated at a temperature of 45°C for two weeks. The emerging fungi were then transferred to fresh PDA plates for purification and stored on PDA agar slants at 4°C for further use. The morphological characteristics of the isolated fungus were utilized for its identification, primarily through an assessment of its colony visual appearance, mycelium color, structure and ascomata according to Zhou *et al.* (2016). Subsequently, we validated the identification through molecular means by sequencing the rDNA gene, using outsource service at Solgent Company located in Daejeon, South Korea. Fresh fungal cultures were incubated on PDA medium at 28° C for 7 days. Fungal DNA was extracted by CTAB method (Suarez *et al.*, 2005, Gontia-Mishra *et al.*, 2014). Prior to

sequencing, amplification of the ribosomal rRNA gene (rDNA) was conducted by employing the polymerase chain reaction (PCR) technique. Two Universal primers, internal transcript scarcer 1 and 2 (ITS1 and ITS4, forward and reverse, respectively) were used in the reaction mixture. ITS1 (5' - TCC GTA GGT GAA CCT GCG G - 3'), and ITS4 (5'- TCC TCC GCT TAT TGA TAT GC - 33') primers were obtained from Sigma Korea. Finally, the specified PCR amplicon underwent verification using 1% electrophoresis agarose gel. To identify the sequence homology, the BLAST tool available on the NCBI website was utilized. Furthermore, the MEGA6 program was employed to construct the phylogenetic tree according to Tamura *et al.* (2013)*.*

2.2. Extraction and fractionation

Fresh mycelium of *G. thermotolerans* grown on PDA medium for 6 days was inoculated into potato dextrose broth (PDB) medium and placed on a shaker at 180 rpm for 20 days at 45°C. The fungal culture was treated with 200 mL of ethyl acetate (EtOAc) (Sigma-aldrich, India) and allowed to stand overnight. Subsequently, the mixture underwent ultrasonication for 10 minutes and was filtered using a Büchner funnel under vacuum. Medium (water phase) and the filtrate containing EtOAc phase were collected for further work up, and the isolated mycelia (cell debris) were discarded. The water phase (medium) and EtOAc phase were then separated using a separator funnel. A rotary evaporator was then employed to concentrate and evaporate the EtOAc phase under vacuum conditions (Xu, 2010).

2.3. Flash Chromatography

Before loading the EtOAc fungal crude extract, the column was packed with dried Silica Gel and saturated with mobile solvents. The mobile phase was pumped through the column using air pressure. The solvents used in sequential order for the mobile phase were: Hexane, Methylene chloride (CH_2Cl_2), CH_2Cl_2: MeOH (1:1), CH_2Cl_2: MeOH (9:1) and MeOH. The fractions collected from each solvent system were then dried, following the method outlined by Gatto *et al.* (2013), with some modifications.

The GC-MS analyses were carried out by Nawah Scientific Inc., using a Thermo Scientific TRACE GC Ultra integrated with a Thermo Scientific ISQ quadrupole MS (Thermo Scientific, USA). The AMDIS software served as the de-convolution tool for the identification of compounds, by matching the obtained MS with those in the Wiley and NSIT library databases. Next, the relative abundance of each compound was determined by calculating its percentage of the total peak area in the chromatogram (Gomathi *et al.*, 2015).

2.4. Screening of Bioactive properties of G. thermotolerans-GTE-21 metabolites

2.4.1. Antimicrobial assay of fungal endophyte-GTE-21

The antimicrobial activity of crude extracts derived from fungal endophyte GTE-21 and its fractions was assessed using multiple methods, including the disc diffusion method, antifungal activity of VOCs, the agar plate diffusion assay, and Evans blue method, as described by Balouiri *et al.* (2016).

2.4.2. Test organisms

Human pathogens, including *Escherichia coli* Ec31, *Klebsiella pneumoniae* Kp11, *Staphylococcus aureus* Sa9, *Staphylococcus epidermidis* Se 23, *Candida ciferrii* Cc 501 and *Candida albicans* Ca 20, along with plant pathogens such as *A. alternata*, *C. specifier* CSN-20 and *F. solani* FSN-20 were obtained from the Mycology Laboratory, Botany Department, Aswan University.

2.4.3. Disc diffusion method of crude extracts and fractions of GTE-21

The experiment involved inoculating Petri dishes filled with nutrient agar medium (Signa-Aldrich, India) with the test organisms, including human pathogens. Sterilized paper disks soaked in fungal crude extracts and fractions dissolved in a CH2Cl2 and MeOH (1:1) solution were then placed on a bacterial lawn spread on the agar medium surface.

The negative control consisted of a disk without any endophytic fungal extracts. We evaluated the presence or absence of an inhibition zone surrounding the discs by incubating the plate overnight at 37°C, as described by Schulz *et al*. (1995).

2.4.4. Antifungal activity of VOCs of GTE-21

Following the method established by Strobel *et al*. (2001), the antifungal activity of GTE-21's VOCs was assessed against plant pathogenic fungi *A. alternata*, *C. specifier*, and *F. solani*. For each assay, two 6.0 cm diameter Petri dishes were placed inside larger 12 cm diameter Petri dishes. In the first plate, GTE-21 was inoculated at the center of the PDA media and allowed to grow for four days at 28°C to enhance VOC production. Subsequently, the targeted fungal species was inoculated onto the second Petri dish. Both plates were securely sealed using Parafilm and subjected to an additional three-day incubation period. After incubation, the extent of fungal growth was measured, enabling the calculation of the inhibition percentage as shown in the following formula:

$$\% \text{ Inhibition} = \frac{Dc - Ds}{Dc} \times 100$$

Where: Dc = average diameter of colony growth in the control group and, Ds = average diameter of mycelial growth in treatment group (Singh and Tripathi, 1999).

2.4.5. Agar plate diffusion assay

Fungal EtOAc crude extracts and fractions, as previously mentioned, were added to PDA media at a concentration of 2.0 mg/mL and thoroughly mixed. The antifungal effect against microorganisms was evaluated using the poisoned food method. A mycelial disc of the pathogen (*A. alternata*, *C. specifier*, and *F. solani*) was placed at the center of a 6.0 cm plate (Balouiri *et al*., 2016). After 7 days of incubation at 28°C, the diameters of fungal growth on both control and treatment plates were measured. The percentage of growth inhibition was then calculated following the method described by Singh and Tripathi, (1999).

2.4.6. Evans blue method

Antifungal activity was also assessed by Evans blue staining method on *F. solani*, which exhibited clear results compared to *A. alternata* and *C. specifier*. Briefly, *F.*

solani spores were cultured in Potato Dextrose Broth (PDB) at 28±2°C for five days. Next, the mycelia were separated through filtration, and the conidial cells were isolated using centrifugation at 5000 rpm for 10 min. The EtOAc crude extracts and fractions at concentrations of 10 and 25 mg/mL were added to the tubes containing the spores. Additionally, a control set containing only the inoculum was prepared. All the tubes were incubated at 28±2°C for intervals of 1h, 3h, and 24h. After each period, the tubes were centrifuged and 0.05% Evans blue was applied to 10 µl of the residual culture. Excess dye was then washed from the hyphae using sterile distilled water. The difference between dead and live cells was observed under a light microscope (Semighini and Harris, 2010)**.**

2.5. 2.6. Cytotoxic activity

2.5.1. Cell culture

The breast and ovarian cancer cell lines were obtained from Nawah Scientific Inc, Egypt. Breast and ovarian cell lines were cultured in Dulbecco's Modified Eagle Medium (DMEM) and Roswell Park Memorial Institute Medium (RPMI), respectively, both supplemented with 100 units/mL of penicillin, streptomycin and 10% heat-inactivated fetal bovine serum. The cancer cell lines were maintained at 37 °C in a humidified environment with 5% CO_2 (Allam *et al*., 2018).

2.5.2. In vitro Cytotoxicity assay

The cytotoxic effect of endophytic fungal extracts (GTE-21) was evaluated using Sulforhodamine B (SRB) assay against human breast and ovarian cell lines at different concentrations of 0.01, 0.1, 1, 10, 50 and 100 ug/mL. The surviving fraction and cell viability were determined (Allam *et al*., 2018).

2.6. Antioxidant activity assays:

To evaluate the antioxidant activity of endophytic fungal crude extracts and fractions, analytical assays were performed on all tested fractions using two different experimental techniques.

2.6.1. DPPH free radical scavenging activity method

To evaluate the antioxidant activity in the investigated samples, changes in the absorbance of DPPH radicals were determined. The endophytic fungal extracts and fractions at a final concentration of 1 mg/mL were prepared. A 0.5 mmol/L DPPH solution was prepared in 95% MeOH. Then, 0.1 mL of fungal extract/fraction was diluted with 95% MeOH, followed by the addition of 2 mL of the DPPH solution. The mixture was incubated at room temperature under dark conditions for 30 minutes. Following the incubation period, the absorbance was measured at 517 nm, as described by Brand-Williams *et al*. (1995).

2.6.2. Total antioxidant capacity method

The assay was conducted following the method outlined by Prieto *et al*. (1999). A 50 µl of each extract was combined with 1 mL of the reaction solution, consisting of 4 mM ammonium molybdate $(NH_4)_2MoO_4$, 0.6 M H_2So_4 and 28 mM Na_2PO_4. The capped tubes were then incubated in a thermal block at 95°C for 90 minutes. After cooling, the absorbance was measured at 695 nm for each sample, using a blank as a reference. The blank solution comprised 1 ml of the reagent solution and an

appropriate volume of the same solvent utilized for the sample, and it was incubated under the same conditions as the remaining samples. The antioxidant capacity was expressed in terms of ascorbic acid equivalent.

2.7. Statistical analysis

Data were collected and subjected to one-way analysis of variance (ANOVA). The significant difference at $P < 0.05$ between the treatment groups and the control was determined using Minitab's Student's t-test. Values represent mean ± standard errors (SEs) of four biological replicates. Correlation analysis was conducted using the Corrplot package in R v4.3.2.

3. Result

3.1. Morphological and Molecular identification

The colony of *G. thermotolerans* exhibits a white color on the obverse and a yellow color on the reverse, with a flat edge. Colonies are flat to low convex, with an irregular or regular and nearly transparent border. The hypha appears hyaline and light yellowish in color, with ascomata become visible at maturity after 15 days of cultivation. Subsequent molecular analysis confirmed that our *G. thermotolerans*-GTE-21 (Basionym: *Gymnoascus thermotolerans*), exhibited 99% similarity to the NCBI accession number MW590717 (Fig. 1).
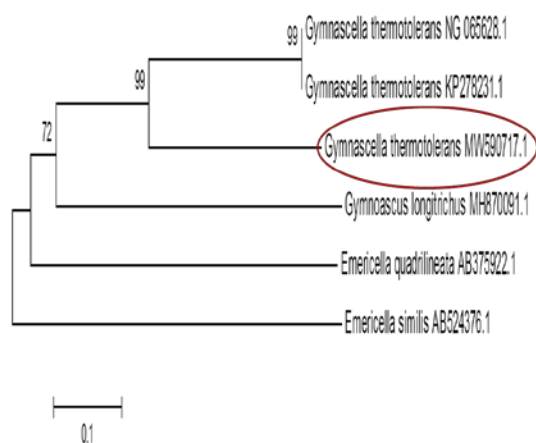
Figure 1. Phylogenetic analysis of the isolated *G. thermotolerans* endophyte and other closely related fungi obtained from the NCBI database. The phylogenetic relationships were determined based on the homology of their nuclear ribosomal internal transcribed spacer sequences. The scale bar represents the tree evolutionary distance.

3.2. GC-MS analysis of EtOAc crude

GC-MS analysis was conducted to determine the chemical compositions of the EtOAc extract of dried GTE-21 (Table 1). A total of 14 volatile organic compounds (VOCs) were identified, indicating the presence of various bioactive substances at different retention times (RT).The mass spectra were used to determine the peaks of each component (Fig. 2). These compounds were recognized by their chemical formulae, RT, molecular weight and percentage of peak area (Table 1). Among the identified VOCs, diisooctyl phthalate (71.99%), phenol, 2-methoxy-4-(2-propenyl) (7.12%), and 1,6-octadien-3-ol, 3,7-dimethyl emerged as the predominant compounds, based on their RT and peak area percentages.
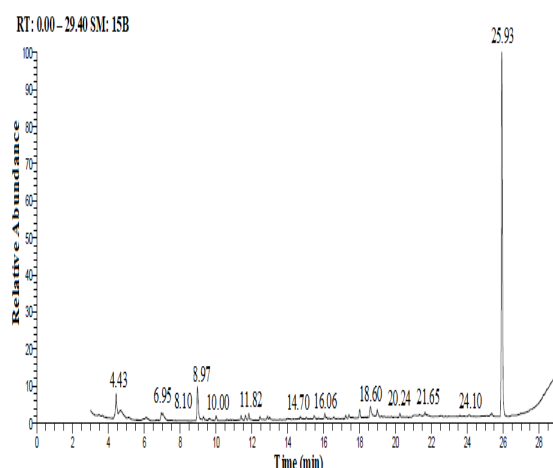
Figure 2: Chromatogram of GC-MS spectra of GTE-21 ethyl acetate crude extract.

Table (1): Volatile organic compounds of *G. thermotolerans* (GTE-21)

Chemical Compounds	Structure	Formula	RT (min)	M.W	Area %	Pharmacological actions
3,7-Dimethyl-1,6-Octadien-3-Ol (Linalool) (Monoterpenoid)		$C_{10}H_{18}O$	4.43	154	4.99	Anti-inflammatory, antioxidant, anticancer and antimicrobial Cherbal *et al.*, 2023
1,5-Dimethyl-1-vinyl-4-hexenyl-2- aminobenzoate (Linalyl aminobenzoate) or Linalyl ester		$C_{17}H_{23}NO_2$	7.02	273	2.09	Antioxidant and antibacterial Ouedrhiri *et al.*, 2015
Phenol,2- methoxy-4- (2-propenyl)- (Aromatic Compound)		$C_{10}H_{12}O_2$	8.97	164	7.12	Antioxidant and anticancer Satoh *et al.,* 1998
β-Caryophyllene (Bicyclic Sesquiterpene)		$C_{15}H_{24}$	9.99	204	1.01	Antioxidant, anticancer and antimicrobial (Dahham *et al.*, 2015)
1-Cyclohexyl-N-methyl-propan-2-amine (Aliphatic Secondary Amine)		$C_{10}H_{21}N$	11.39	155	0.86	Heart block treatment (Day and Viar, 1951)
2,4-Di-tert-butylphenol (Aromatic Compound)		$C_{14}H_{22}O$	11.64	206	0.91	Antioxidant anti-Inflammatory cytotoxicity insecticidal and nematocidal antimicrobial and antiviral activity (Zhao *et al.,* 2020)
4-Allyl-2-methoxy phenylacetate (Aromatic Compound)		$C_{12}H_{14}O_3$	11.82	206	1.18	Antioxidant Hidalgo *et al.*, 2009
3,7,11-Trimethyl-1,6,10-Dodecatrien-3-Ol (Sesquiterpene Alcohol)		$C_{15}H_{26}O$	12.45	222	0.67	Antimicrobial Madhumathi *et al.*, 2014
7,9-Di-tert-butyl-1-oxaspiro (4,5)deca-6,9-diene-2,8-dione (Spiro compound)		$C_{17}H_{24}O_3$	18.00	276	1.60	Antioxidant Singh *et al.*, 2018
Phthalic acid, butyl undecyl ester (Phthalic acid Ester)		$C_{23}H_{36}O_4$	18.59	376	2.45	Antioxidant and antimicrobial Nsofor et al., 2023
1-Nonadecene (Aliphatic Hydrocarbon)		$C_{19}H_{38}$	18.98	266	1.41	Antibacterial, antidiabetic and antitumor Amudha *et al.*, 2018
Oleic Acid (Unsaturated Fatty Acid)		$C_{18}H_{34}O_2$	20.24	282	0.76	Anti-inflammatory, antioxidant, anticancer and antimicrobial Cherbal *et al.* 2023
Trans-13-Octadecenoic acid (Unsaturated Fatty Acid)		$C_{18}H_{34}O_2$	21.64	282	0.74	Anti-inflammatory Khan *et al.*, 2022
Diisooctyl phthalate (Phthalic acid Ester)		$C_{24}H_{38}O_4$	25.93	390	71.99	Anti-inflammatory, antioxidant, anticancer, and antimicrobial Saeed *et al.*, 2020
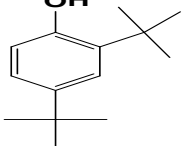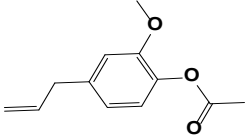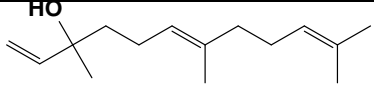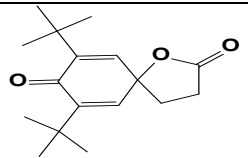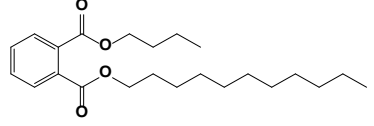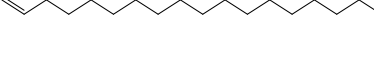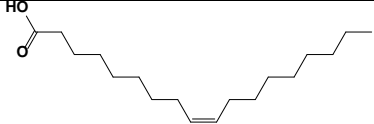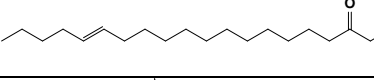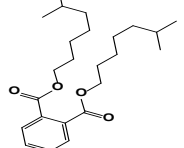
3.3. Disc diffusion method of crude and fractions of GTE-21

Antimicrobial compounds from fungi represent a highly promising source for the development of new antibiotics with novel mechanisms of action, aimed at overcoming bacterial drug resistance (Bhatnagar and Kim, 2010). Our results showed that the crude extract of GTE-21 exhibited the highest antimicrobial activity with inhibition diameter of 1.5, 1.4 and 1.3 cm against *S. epidermidis*, *C. ciferrii* and *S. aureus* respectively. The CH2Cl2:MeOH (1:1) fraction showed superior efficacy against human pathogens, producing the largest inhibition zones of 1.1 cm against *S. epidermidis* and 1.03 cm against *C. ciferrii*. In comparison, the MeOH fraction resulted in a 1.2 cm inhibition zone against *S. epidermidis*, but showed no activity against *C. ciferrii* and *S. aureus* (Fig. 3).

Our results indicate that the crude extract successfully inhibited *C. ciferrii*, producing an inhibition zone of 1.4 cm. Furthermore, the CH_2Cl_2:MeOH (1:1) fraction and hexane were more effective against *C. ciferrii* pathogen, yielding inhibition zones of 0.9 and 1.03 cm, respectively. In contrast, the CH_2Cl_2:MeOH (9:1) and MeOH fractions did not exhibit any inhibitory effect on *C. ciferrii*. The pathogen *S. aureus* was susceptible to the crude extract and the CH_2Cl_2 fraction, with inhibition zones of 1.3 cm and 0.6 cm, respectively, whereas the MeOH fraction showed no inhibitory activity. Additionally, the crude extract and the CH_2Cl_2:MeOH (1:1) and MeOH fractions inhibited *S. epidermidis*, resulting in inhibition zones of 1.5, 1.1 and 1.2 cm, respectively. In contrast, *C. albicans*, *E. coli* and *K. pneumonia* exhibited resistance against all tested fractions and the crude extract.
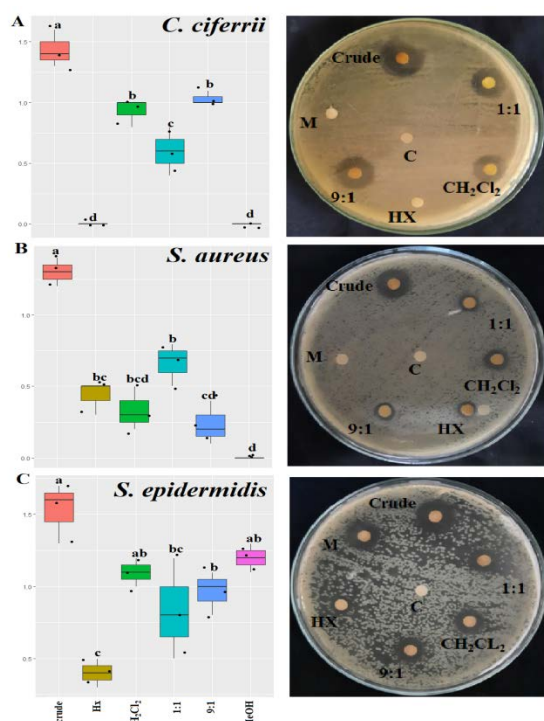
Figure 3: Effects of crude extracts and fractions on human pathogens, including *C. ciferrii* **(A)**, *S. aureus* **(B)** and *S. epidermidis* **(C)** using *in vitro* agar disc diffusion assay. Box plot diagram showing inhibition zones. Different alphabetical letters show significant differences at $P < 0.05$ using Tukey's HSD test.

3.4. Antifungal activity of VOCs of GTE-21

The antifungal activity of GTE-21's VOCs was evaluated against phytopathogenic fungi, including *A. alternata*, *C. specifier*, and *F. solani*. Among all tested pathogens, *F. solani* exhibited the highest inhibition at 42.5%, followed by *A. alternata* with 39.03%, while *C. specifier* showed no inhibition (Fig. 4).
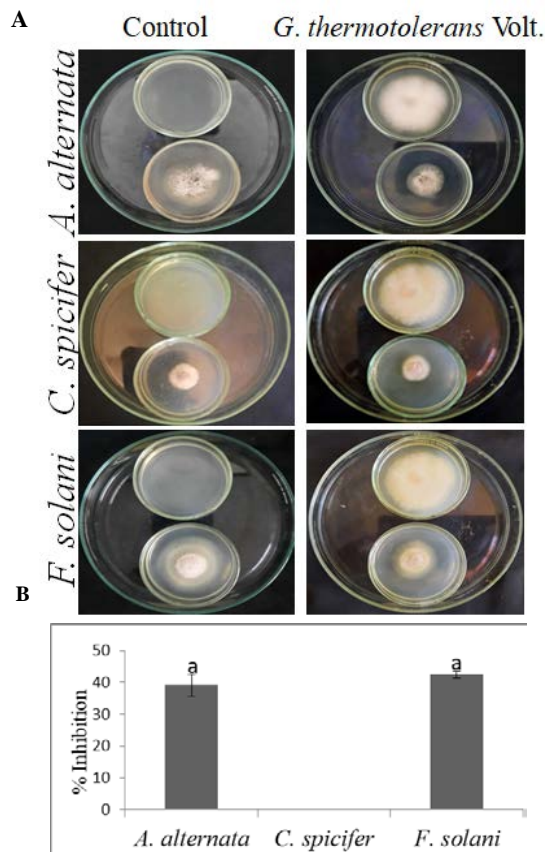
Figure 4. Antifungal efficacy of GTE-21's volatile organic compounds (VOCs) against different phytopathogens, illustrated through (A) Petri plate assay and (B) inhibition percentages. Different alphabetical letters indicate significant differences at $p < 0.05$ using Tukey's HSD test.

3.5. Agar diffusion method

The diameter of the inhibition zones can be used to calculate the percentage of growth inhibition of the chosen phytopathogenic fungus (*A. alternata*, *F. solani*, and *C. specifier*) at a concentration of 2.0 mg/ml of GTE-21 crude, and fractions were calculated (Balouiri *et al*., 2016).

Our research revealed that the crude extract of GTE-21, as well as the CH2Cl2:MeOH (1:1) and CH2Cl2:MeOH (9:1) fractions, demonstrated the highest inhibition rates against A. alternata, with percentages of 72.2%, 71.2%, and 70.3%, respectively, compared to the control. Conversely, the hexane, CH2Cl2, and MeOH fractions exhibited the lowest inhibition rates at 23.1%, 25.9%, and 12.03%, respectively.

"In addition, the crude extract inhibited fungal mycelial growth of C. specifier with a high inhibition percentage of 93.05%. The CH2Cl2:MeOH (1:1) fraction inhibited it by 68.05%, the CH2Cl2:MeOH (9:1) fraction reduced the growth by 58.3%, and both the CH2Cl2 and Hexane fractions reduced the pathogen growth by 30.5% and 25%

respectively." By contrast, the MeOH fraction inhibited the pathogen with low percentage 5.5%.

Also, the CH2Cl2: MeOH (9:1) and CH2Cl2: MeOH (1:1) fractions inhibited the growth of F. solani by 54.7%, 43.5%, and 38.4% respectively. CH2Cl2, Hexane, and MeOH inhibited by 33.3%, 28.2%, and 27.3%. (Fig. 5).
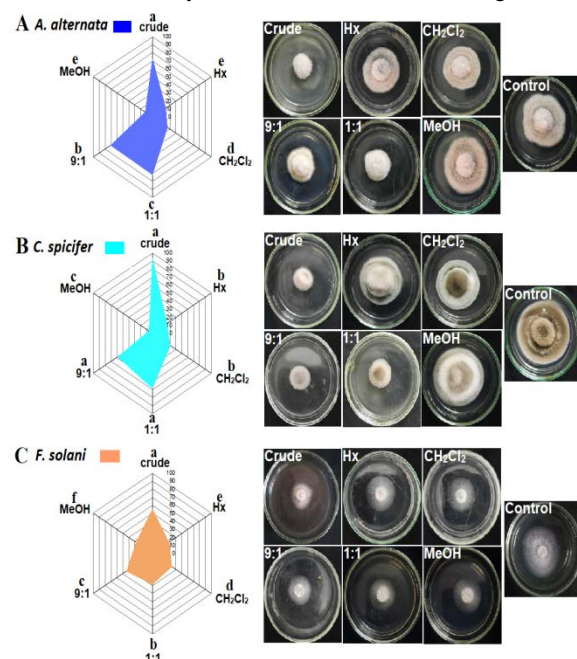
Figure 5. Effect of EtOAc crude extracts and fractions on phytopathogenic fungi using agar diffusion method. Radar plot indicate percentage of inhibition against **(A)** *A. alternata*, **(B)** *C. specifier* and **(C)** *F. solani*. Different alphabetical letters on rader plot indicate significant differences at $p < 0.05$ using Tukey's HSD test.

3.6. Evans blue method

Antifungal activity of the extract and crude was assessed by Evans Blue Staining method on *F. solani*. The fungal spores treated with crude, CH_2Cl_2: MeOH (1:1) and CH_2Cl_2 at concentration 10 mg/ml were more affected than Hexane, CH_2Cl_2: MeOH (9:1) and MeOH. Whereas the fungal spores treated with a concentration of 25 mg/ml were strongly affected by the crude, CH_2Cl_2: MeOH (1:1), CH_2Cl_2: MeOH (9:1), and MeOH, the spores showed little effect when treated with Hexane and MeOH. A relatively high suppression of spore germination (<80%) was detected at 25μg/ml. The untreated control conidia maintained their natural coloration. The crude extract showed 41.07% effect at a concentration of 10 mg/ml, while the CH2Cl2: MeOH (1:1) fraction showed 32.7% effect. Conidia treated with the crude extract showed 96.2% effect at a concentration of 25 mg/ml. The CH2Cl2: MeOH (1:1) and CH2Cl2: MeOH (9:1) fractions were affected by 96.3% and 94.3% respectively. But the spores of *Fusarium* were little affected by Evan's blue when treated with CH_2Cl_2 fraction at concentration 10 and 25 mg/ml (Fig. 6).
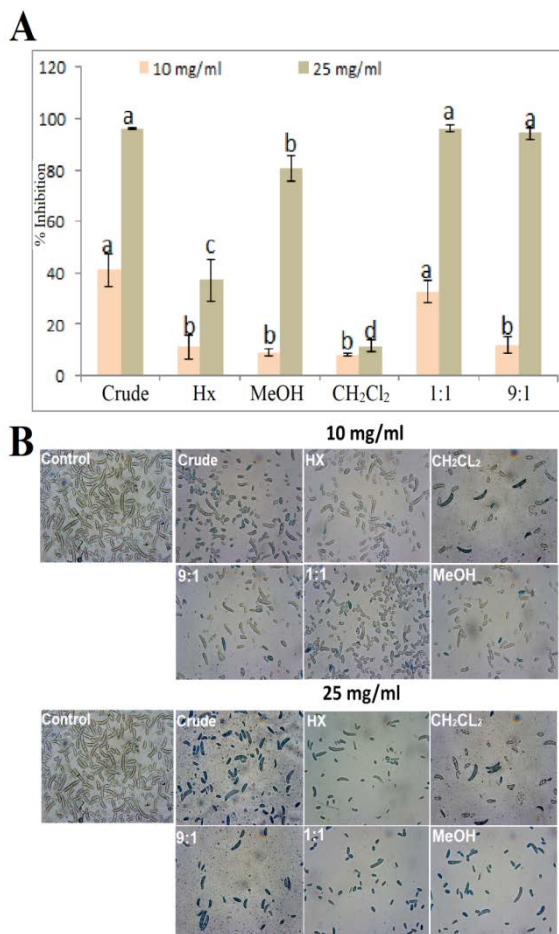
Figure 6. Effect of the crude and fractions on the viability of *F. solani* conidia by Evan blue method. Letters (a, b, c and d) indicate significant differences (p < 0.05) (ANOVA after Tukeys test analysis).

3.7. Screening of cytotoxic activity

Our findings on crude and fractions of GTE-21 showed highly cytotoxicity effects on the two cell lines (SKOV-3 and MDA-MB-231) with variable extent causing damaging (Figs. 7, 8, 9).

The EtOAc Crude displayed the highest significant cytotoxicity against SKOV-3 and MDA-MB-231 cell line with viability 3.4 and 0.47 % for concentration 50 and 100 μl respectively for SKOV-3 and 0.193 and 0.194% for concentration 50 and 100 ul respectively on MDA-MB-231.

The viability of SKOV-3 and MDA-MB-231 cells was strongly affected by the fraction CH2Cl2: MeOH (9:1) at 50 and 100 µl, resulting in viability values of 70.3% and 24.3% for SKOV-3 and 41.83% and 6.56% for MDA-MB-231, respectively (Fig. 8).

The concentration of 100 µl of the fractions MeOH, CH_2Cl_2: MeOH (1:1) and CH_2Cl_2 exhibited strong viability percentage 38.16, 37.02 and 26.75% respectively on breast cancer; on ovarian cancer they exhibited 44.56667, 49.45333 and 84.01667% respectively, yet, the Hexane fraction exhibited the least cytotoxicity on SKOV-3 and MDA-MB-231, with viabilities of 93.9933% and 68.9144% respectively (Fig. 9).
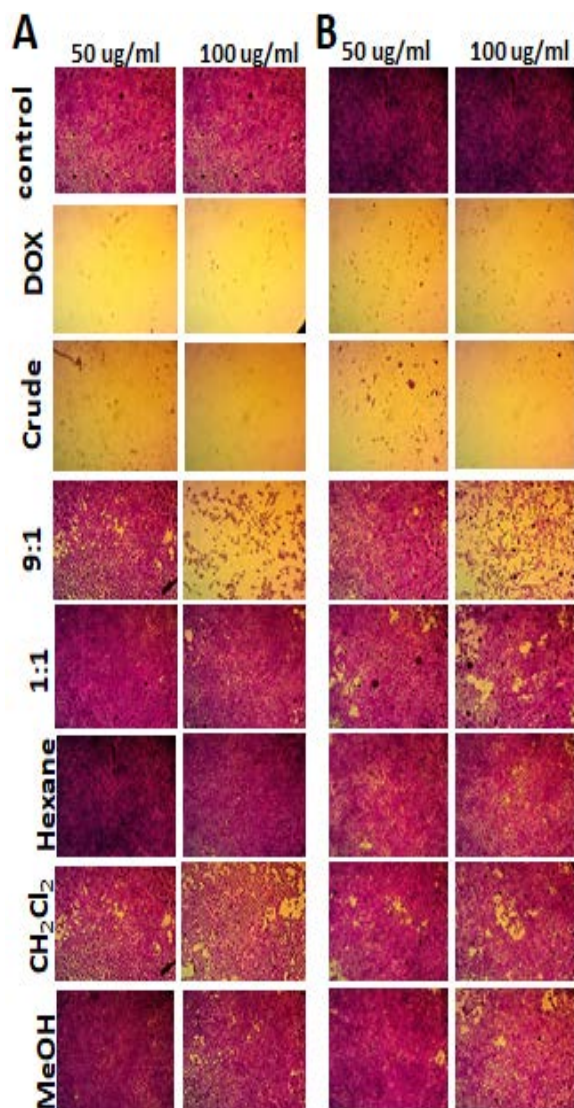
Figure 7. Crude and fractions effect on the cancer cells (A) MDA-MB-231 and (B) SKOV-3 at concentration 50 and 100 µg/ml.
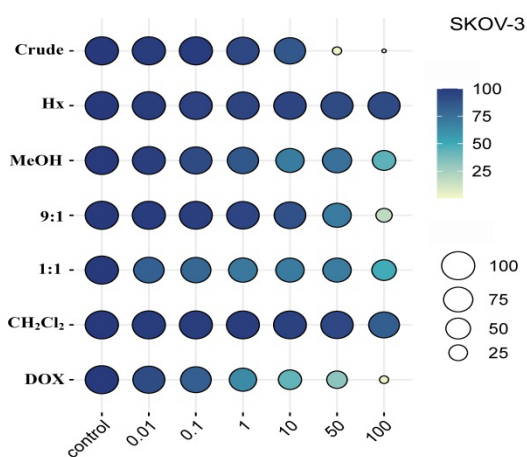
Figure 8. Dot plot illustrating viability percentage in SKOV-3 cells at various concentrations using a cytotoxicity Assay.
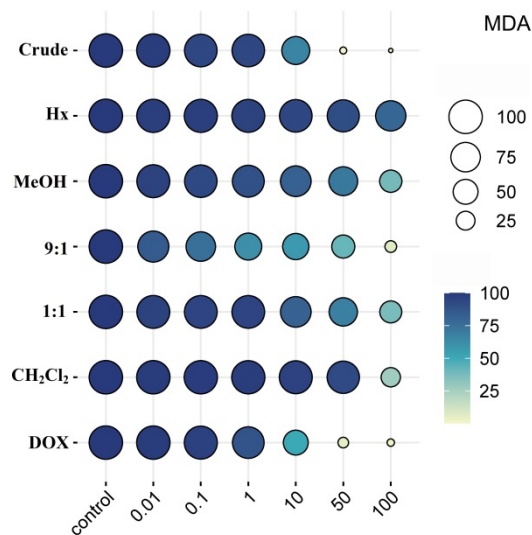
Figure 9. Dot plot illustrating viability percentage in MDA-MB-231 cells at various concentrations using a cytotoxicity Assay.

3.8. Antioxidant activity assays

3.8.1. DPPH free radical scavenging activity

The crude extract of EtOAc and the CH2Cl2: MeOH (1:1) fraction showed high scavenging activities of 63.1% and 58.06%, respectively. The methanolic fraction, CH2Cl2: MeOH (9:1), and the CH2Cl2 extract showed scavenging activities of 47.12%, 54.6%, and 52.56%, respectively. In contrast, the hexane fraction exhibited the least antioxidant activity at 11.4% (Fig. 10).

3.8.2. Determination of total antioxidant capacity (TAC)

Crude and CH_2Cl_2: MeOH (1:1) fraction showed high TAC (0.32±0.012 and 0.38±0.014) mg/ml followed by CH_2Cl_2: MeOH (9:1) and CH_2Cl_2 (0.29±0.01 and 0.24±0.03) mg/ml respectively. Hexane and MeOH fractions showed the lowest TAC (0.16±0.009 and 0.11±0.02 mg/ml respectively) (Fig. 10).
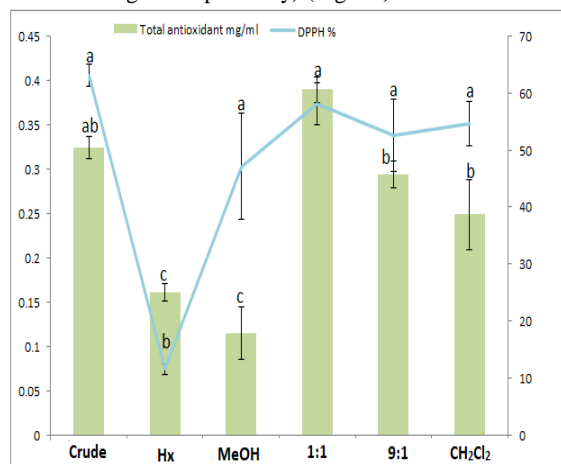
Figure 10. Antioxidant activity of the crude extracts and fractions of *G. thermotolerans*.

The correlation between all activities of *G. thermotolerans* crude and fractions extractions was clarified in figure 11. We did this correlation by metaboanalyst (https://genap.metaboanalyst.ca/ModuleView.xhtml)
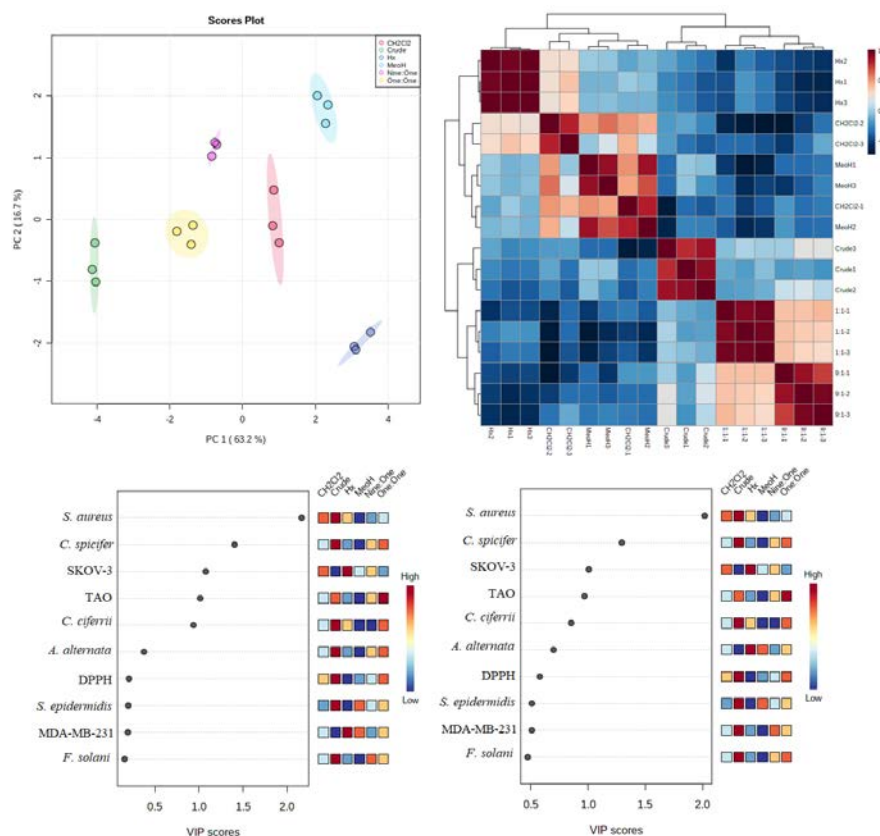
Figure 11. Principal component analysis (PCA), correlation heatmap, and variable importance in projection (VIP) scores for all examined parameters using crude extracts and fractions of *G. thermotoleran.*

4. Discussion

Several endophytic fungal strains have been discovered, and it has been claimed that they produce novel bioactive compounds in anticancer tests (Stierle and Stierle, 2015). Our results showed that the endophyte fungi *G. thermotolerans* produced VOCs and non-VOCs with antimicrobial, antioxidant and anticancer activities. Diisooctyl phthalate, Phthalic acid, 7, 9-Di-tert-butyl-1-oxaspiro (4, 5) deca-6, 9-diene-2, 8-dione and 1-Nonadecene were the most active VOCs. These compounds are active due to their action in disrupting the membrane properties of pathogenic fungi and bacteria (Casillas *et al.*, 2021). Moreover, as highlighted by Li *et al.*, (2021), certain active constituents such as fengycin induce alterations in the mycelial morphology of the cell membrane and cell wall in rice blast fungus. This process concurrently reduces the mitochondrial membrane potential, leading to the accumulation of reactive oxygen species (ROS) and consequent cytotoxic effects.

The anticancer medications derived from plants, such as taxol, etoposide, vincristine and irinotecan are currently used in clinical settings to treat a variety of human cancers (Balunas and Kinghorn, 2005). This work explores how some of these compounds were extracted from endophytes and reports on their cytotoxic effects on different cell lines. Endophytic fungi isolated from some medicinal plant like *Litsea cubeba* (Deka and Jha, 2018), *Pelargonium graveolens* (Yasser *et al.,* 2020) and *Solenostemma arghel* (Abdel-Motaal *et al.*, 2021) showed promising antimicrobial activity against selected pathogenic microbes.

Our result demonstrated that the Chemical composition of GTE-21 crude by GC-MS analyses was 14 VOCs compounds, and the predominant compounds were diisooctyl phthalate (71.99 %). This agrees with Weikl *et al.* (2016) who proved that fungi emitted more VOCs like *Alternaria* that produced VOCs like 3-octanone. Also, Plaszkó *et al.* (2020), reported *Macrophomina*, *Penicillium*, *Aspergillus* and *Fusarium* emitted numerous VOCs such as styrene and benzaldehyde.

In line with our observations, the crude extract of GTE-21 demonstrated the most significant antimicrobial activity, exhibiting inhibition diameters of 1.5 cm, 1.4 cm, and 1.3 cm against *S. epidermidis, C. ciferrii,* and *S. aureus*, respectively. This enhanced antimicrobial effect can be attributed to the presence of active compounds, including VOCs such as diisooctyl phthalate, oleic acid, butyl undecyl ester, and β-Caryophyllene, as well as non-VOCs like diisooctyl phthalate and dibutyl phthalate (unpublished data). Previous studies have indicated that these compounds possess antimicrobial properties (Stierle and Stierle, 2015). Despite the lack of a clear understanding regarding the mechanisms responsible for the antimicrobial activity of these VOCs and non-VOCs, several hypotheses propose that their action may involve disrupting membrane properties and inducing reactive oxygen species within the bacterial cells, potentially contributing to the observed biological effects activity (Casillas *et al.*, 2021).

Handayani and Aminah, (2017) proved that the agar diffusion method was used to test the bioactivity of symbiotic fungi's EtOAc extract against four bacterial pathogens *Basillus subtilis* 1.4 cm, *Staphylococcus*

epidermidis 1.15 cm, *Salmonella typosa* 1.025 cm and *Escherichia coli* 1.47 cm.

The marine sponge-associated fungus *Acanthostrongylophora ingens* exhibits considerable promise as a prospective reservoir of bioactive compounds with potential applications in the pharmaceutical and medical domains, particularly in the context of generating antibacterial and anticancer agents (Handayani and Aminah, 2017). VOCs from GTE-21 were investigated for their antifungal properties against plant pathogenic fungus. The inhibition percentage was highly against *F. solani* at 42.5 %, and *A. alternata* at 39.03 %. This result is attributed to the presence of a phthalate compound with large percentage in EtOAc extract which, according to Habib and Karim (2009), possess antifungal and anticancer activities. Similarly, VOCs produced by *T. spirale* indicated numerous compounds with antifungal action, especially ethanol and phenyl ethyl alcohol. VOCs of *T. asperellum* increased resistance to leaf spot pathogens on lettuce (Baiyee *et al.*, 2019, Wonglom *et al.*, 2020).

The antifungal activity of GTE-21 was assessed using the Evans blue method. The results showed that spores treated with Crude were affected by 96.2% at a concentration of 25 mg/ml. Additionally, the fractions CH2Cl2: MeOH (1:1) and CH2Cl2: MeOH (9:1) were affected by 96.3% and 94.3% respectively. In a study by Dissanayake et al. (2015), it was reported that compounds from *Acorus calamus* had an effect on the *F. oxysporum* pathogen, resulting in dead cells that were stained by Evan blue stain.

The results of our study on crude and fractions of GTE-21 showed highly cytotoxic effects on two cell lines (SKOV-3 and MDA-MB-231). These findings are consistent with those of Uzma et al. (2018), who reported that 2,14-dihydrox-7-drimen-12,11-olide isolated from *A. glaucus* from *Ipomoea batatas* leaves has anticancer properties.

The production of novel chemicals by a number of endophytic fungal strains that are helpful in anticancer assays has been discovered (Stierle and Stierle, 2015). Mclaughlin *et al.* (1998) informed that the drug's cytotoxic effect has the potential to influence and disrupt the fundamental processes involved in cell division, growth, and differentiation. One of these pathways may be responsible for this extract's cytotoxic action.

5. Conclusion

The endophytic thermophilic fungus *G. thermotolerans* GTE-21 has been found to harbor bioactive secondary metabolites, comprising both volatile (such as Diisooctyl phthalate, Phthalic acid, 7,9-Di-tert-butyl-1-oxaspiro(4,5)deca-6,9-diene-2,8-dione, 1-Nonadecene, oleic acid, butyl undecyl ester, and β-Caryophyllene) and non-VOCs (specifically diisooctyl phthalate and dibutyl phthalate). These secondary metabolites have shown potential in inhibiting the growth of key plant pathogenic fungi and human pathogenic bacteria, alongside exhibiting anticancer and antioxidant properties. The VOCs from GTE-21 notably inhibited *F. solani* by 42.5% and *A. alternata* by 39.03%. On the other hand, non-VOCs within GTE-21's crude extract showed remarkable inhibitory action against *A. alternata* at 72.2% and were exceptionally effective against *C. specifier* with an

inhibition rate of 93.05%. Thus, the thermophilic endophytic fungus *G. thermotolerans* GTE-21 is a promising source of bioactive compounds, with ongoing research in our laboratory aimed at isolating and identifying the most potent bioactive pure compounds.

Acknowledgment

References

Abdel-Motaal FF, Kamel MN, El-Sayed AM, Abou-Ellail M. 2021. Biocontrol of sweet melon fruit rot caused by *Fusarium solani* using an endophytic fungus isolated from the medicinal plant *Solenostemma arghel*. JJBS, **14(3):** 523 – 527.

Allam RM, Al-Abd AM, Khedr A, Sharaf OA, *et al.* 2018. Fingolimod interrupts the cross talk between estrogen metabolism and sphingolipid metabolism within prostate cancer cells. Toxicol Lett, **291**: 77-85.

Amudha P, Jayalakshmi M, Pushpabharathi N, Vanitha V. 2018. Identification of bioactive components in Enhalus acoroides seagrass extract by gas chromatography-mass spectrometry. AJPCR, **11(10)**:313-5.

Atalla SM, Gamal NG, Awad HM, Ali NF. 2019. Production of pectin lyase from agricultural wastes by isolated marine *Penicillium expansum* RSW_SEP1 as dye wool fiber. Heliyon. **1**; 5 (8).

Atalla, SMM, Ahmed, NE, Awad, HM, El Gamal, NG, El Shamy, AR 2020a. Statistical optimization of xylanase production, using different agricultural wastes by *Aspergillus oryzae* MN894021, as a biological control of faba bean root diseases. Egypt. J. Biol. Pest Control, **30**: 125.

Atalla, SMM, EL Gamal, NG, Awad, HM 2020b. Chitinase of Marine *Penicillium chrysogenum* MH745129: Isolation, Identification, Production and Characterization as Controller for Citrus Fruits Postharvest Pathogens. Jordan J. Biol. Sci., **13(1)**: 19-28.

Atalla SM, Gamal NG, Awad HM, Ali NF. 2019. Production of pectin lyase from agricultural wastes by isolated marine *Penicillium expansum* RSW_SEP1 as dye wool fiber. Heliyon. **1**; 5 (8).

Baiyee B, Pornsuriya C, Ito S, Sunpapao A. 2019. *Trichoderma spirale* T76-1 displays biocontrol activity against leaf spot on lettuce (*Lactuca sativa* L.) caused by *Corynespora cassiicola* or *Curvularia aeria*. Biol control, **129:** 195-200

Balouiri M, Sadiki M, Ibnsouda KS. 2016. Methods for in vitro evaluating antimicrobial activity: a review. JPA, **6 (2)**: 71-79.

Balunas MJ, Kinghorn AD. 2005. Drug discovery from medicinal plants. Life sci, **78(5)**: 431-441.

Bhatnagar I, Kim S. 2010. Immense essence of excellence: marine microbial bioactive compounds. Mar drugs, **8(10)**: 2673-2701.

Brand– Williams W, Cuvelier ME and Berset C. 1995. Use of free radical method to evaluate antioxidant activity. LWT-Food sci and Technol, **28(1)**: 25-30.

Casillas-Vargas G, Ocasio-Malavé C, Medina S, Morales-Guzmán C, Del Valle RG, Carballeira NM, Sanabria-Ríos DJ. 2021. Antibacterial fatty acids: An update of possible mechanisms of action and implications in the development of the next-generation of antibacterial agents. Prog lipid res. 82:101093.

Cherbal A, Bouabdallah M, Benhalla M, Hireche S, Desdous R. 2023. Phytochemical Screening, Phenolic Content, and Anti-Inflammatory Effect of Foeniculum vulgare Seed Extract. PNF., **28(2)**:141.

Dahham SS, Tabana YM, Iqbal MA, Ahamed MB, Ezzat MO, Majid AS, Majid AM. 2015. The anticancer, antioxidant and antimicrobial properties of the sesquiterpene β-caryophyllene from the essential oil of Aquilaria crassna. Molecules. **20(7)**:11808-29.

Day J, Viar WN 1951. A case of heart block treated with 1-cyclohexyl-2-methylaminopropane (benzedrex). AHJ, 42: 733-736.

Deka D, Jha KD. 2018. Antimicrobial activity of endophytic fungi from leaves and barks of *Litsea cubeba* Pers., a traditionally medicinal plant of north east India. JJBS, **11**: 73 – 79

De Oliveira TB, VCP, Barbosa FN, Ferro M, Meirelles LA, Sette LD, Gomes E, Rodrigues A 2016. Fungal communities in pressmud composting harbor beneficial and detrimental fungi for human welfare. Microbiology, **162**: 1147–1156.

Dissanayak ML, Ito SI, and Akakabe Y. 2015. TLC bioautography guided detection and biological activity of antifungal compounds from medicinal plant *Acorus calamus* Linn. Asian J Plant Pathol, **9**: 16-26.

Elsehemy IA, El Deen AM, Awad HM, Kalaba MH, Moghannem SA, Tolba IH, Farid MA. 2020. Structural, physical characteristics and biological activities assessment of scleroglucan from a local strain *Athelia rolfsii* TEMG. Int. J. Biol. Macromol. **163**:1196-207.

Fernandes EG, Pereira OL, da Silva CC, Bento CBP, de Queiroz MV. 2015. Diversity of endophytic fungi in *Glycine max*. Microbiol Res, **181**: 84-92.

Gatto MA, Sanzani SM, Tardia P, Linsalata V, Pieralice M, Sergio L, Di Venere D. 2013. Antifungal activity of total and fractionated phenolic extracts from two wild edible herbs. Sci. res., **5(8)**: 8

Gauchan DP, Kandel P, Tuladhar A, Acharya A, Kadel U, Baral, AGarcía-Gil MR. 2020. Evaluation of antimicrobial, antioxidant and cytotoxic properties of bioactive compounds produced from endophytic fungi of Himalayan yew (*Taxus wallichiana*) in Nepal. F1000Research, 9.

Gomathi D, Kalaiselvi M, Ravikumar G, Devaki K, Uma C. 2015. GC-MS analysis of bioactive compounds from the whole plant ethanolic extract of *Evolvulus alsinoides* (L.) L. JFST, **52(2)**: 1212-1217.

Gontia-Mishra I, Tripathi N and Tiwari SA. 2014. A Simple and rapid DNA extraction protocol for filamentous fungi efficient for molecular studies. IJBT **13**: 536-539.

Habib MR, Karim MR. 2009. Antimicrobial and cytotoxic activity of di-(2-ethylhexyl) phthalate and anhydrosophoradiol-3-acetate isolated from *Calotropis gigantea* (Linn.) flower. Mycobiology, **37(1)**: 31-36.

Hamed ER, Awad HM, Ghazi EA, El-Gamal NG, Shehata HS. 2015. *Trichoderma asperellum* isolated from salinity soil using rice straw waste as biocontrol agent for cowpea plant pathogens. J. Appl. Pharm. Sci. 5 (2):091-98.

Handayani D and Aminah I. 2017. Antibacterial and cytotoxic activities of ethyl acetate extract of symbiotic fungi from West Sumatra marine sponge *Acanthrongylophora ingens*. J. Appl. Pharm. Sci., **7(2)**: 237-240.

Hidalgo ME, De la Rosa C, Carrasco H, Cardona W, Gallardo C, Espinoza L. 2009. Antioxidant capacity of eugenol derivatives. Quimica Nova. **32**:1467-70.

Khan MS, Uzair M, Hanif M, Jabeen M, Chaudhary BA. 2022. Anti-inflammatory potential of spectroscopically analyzed trans-13-octadecenoic acid of Yucca elephantipes Regel roots: in-vitro and in-vivo analysis. Pak. J. Pharm. Sci., 1;35(6).

Kumar S, Malhotra R, Kumar D. 2010. *Euphorbia hirta:* its chemistry, traditional and medicinal uses, and pharmacological activities. Phcog. Rev., **4(7)**: 58

Li X, Zhao H, Chen X. 2021. Screening of marine bioactive antimicrobial compounds for plant pathogens. Marine Drugs. 19(2):69.

Madhumathi V, Vijayakumar S. 2014. Identification of novel cyanobacterial compounds for oral disease through in vitro and insilico approach. Biomedicine & Aging Pathology. 1;4(3):223-8.

McLaughlin JL, Rogers LL, Anderson JE. 1998. The Use of Biological Assays to Evaluate Botanicals. Drug Inf J, **32(2)**: 513-524.

Mitchell AM, Strobel GA, Moore E, Robison R, and Sears J. 2010.Volatile antimicrobials from *Muscodor crispans*, a novel endophytic fungus. Microbiol., **156(1)**: 270-277.

Nsofor WN, Nwaoguikpe RN, Ujowundu FN, Keke CO, Uba MT, Edom CV. 2023. Phytochemical, GC-MS, FTIR and Amino acid profile of methanol extract of *Tetrapleura tetraptera* fruit. JDDT. **13(2)**:61-9.

Ouedrhiri W, Bouhdid S, Balouiri M, Lalami AE, Moja S, Chahdi FO, Greche H. 2015. Chemical composition of *Citrus aurantium* L. leaves and zest essential oils, their antioxidant, antibacterial single and combined effects. J. Chem. Pharm. Res **7(1)**:78-84.

Plaszkó T, Szűcs Z, Kállai Z, Csoma H, Vasas G, Gonda S. 2020. Volatile organic compounds (VOCs) of endophytic fungi growing on extracts of the host, horseradish (Armoracia rusticana). Metabolites, **10(11)**: 451.

Prieto P, Pineda M and Aguilar M. 1999. Spectrophotometric quantitation of antioxidant capacity through the formation of a phosphomolybdenum complex: specific application to the determination of vitamin E. Anal. Biochem., **269(2)**: 337-341.

Priti V, Ramesha BT, Singh S. 2009. How promising are endophytic fungi as alternative sources of plant secondary metabolites. Cur. Sci., **97(4)**: 477-478.

Rodriguez R, White J Jr, Arnold A, Redman RA. 2009. Fungal endophytes: diversity and functional roles. New phytol., **182(2)**: 314-330.

Saeed A, Abotaleb S, Alam N, ELMehalawy A, Gheda S. 2020. In vitro assessment of antimicrobial, antioxidant and anticancer activities of some marine macroalgae. EJOB., **60(1)**:81-96.

Satoh K, Ida Y, Sakagami H, Tanaka T, Fujisawa S. 1998. Effect of antioxidants on radical intensity and cytotoxic activity of eugenol. Anticancer res., **18(3A)**:1549-52.

Schulz B, Sucker J, Aust H. 1995. Biologically active secondary metabolites of endophytic *Pezicula* species. Mycol. Res., **99(8)**: 1007-1015.

Semighini CP and Harris SD. 2010. Methods to detect apoptotic-like cell death in filamentous fungi. In Molecular and Cell Biology Methods for Fungi (pp. 269-279) Humana Press.

Singh G, Gollapalli R, Blinder A, Patel M. 2018. Identification of leachable impurities in an ophthalmic drug product originating from a polymer additive Irganox 1010 using mass spectroscopy. J. Pharma. Biomed. Anal. 152:197-203.

Singh J, Tripathi NN. 1999. Inhibition of storage fungi of blackgram *Vigna mu*ngo by some essential oils. Flavour Fragr. J, **14(1)**: 1-4.

Stierle AA, and Stierle DB 2015. Bioactive secondary metabolites produced by the fungal endophytes of conifers. Nat. prod. Commun.,**10**: 1671–1682.

Strobel GA, Dirkse E, Sears J, Markworth C. 2001. Volatile antimicrobials from Muscodor albus, a novel endophytic fungus. Microbiol, **147(11)**: 2943–2950.

Suarez MB, Walsh K and Boonham N. 2005. Development of realtime PCR (Taq-Man) assays for the detection and quantification of *Botrytis cinerea* in planta. Plant Physiol Biochem, **43(9)**: 890-899.

Tahir HAS, Qin G, Wu H, Niu Y, Rong H, and Gao X. 2017. *Bacillus* volatiles adversely affect the physiology and ultrastructure of *Ralstonia solanacearum* and induce systemic resistance in tobacco against *Bacillus* wilt. Sci. Rep. **7**: 40481.

Tamura K, Stecher G, Peterson D, Filipski A, Kumar S. 2013. MEGA6: molecular evolutionary genetics analysis version 6.0. Mol. Biol. Evol. **30:** 2725–2729.

Uzma F, Mohan CD, Hashem A, Konappa NM, Rangappa S, Kamath PVand Abdallah EF. 2018. Endophytic fungi alternative sources of cytotoxic compounds: a review. Front Pharmacol, **9**: 309.

Weikl F, Ghirardo A, Schnitzler JP and Pritsch K. 2016. Sesquiterpene emissions from *Alternaria alternata* and *Fusarium oxysporum*: Effects of age, nutrient availability and co-cultivation. Sci Rep, **6(1)**: 1-12.

Wonglom P, Ito SI, Sunpapao A. 2020. Volatile organic compounds emitted from endophytic fungus *Trichoderma asperellum* T1 mediate antifungal activity, defense response and promote plant growth in lettuce (*Lactuca sativa*). Fungal Ecol, **43**: 100867.

Xie S, and Zhou J. 2017. Harnessing plant biodiversity for the discovery of novel anticancer drugs targeting microtubules. Front Plant Sci **8**: 720.

Xie S, Zang H, Wu H, Uddin RF, and Gao X. 2018. Antibacterial effects of volatiles produced by *Bacillus strain* D13 against *Xanthomonas oryzae* pv. *oryzae*. Mol. Plant Pathol **19**: 49-58.

Xu J. 2010. Secondary metabolites from the endophytic fungus *Pestalotiopsis sp.* JCM2A4 and its microbe-host relationship with the mangrove plant *Rhizophora Mucronata* (Doctoral dissertation Düsseldorf, Univ., Diss.

Yasser MM, Marzouk AM, El-Shafey MN, Shaban AS. 2020. Diversity and antimicrobial activity of endophytic fungi from the medicinal plant *pelargonium graveolens* (geranium) in middle Egypt. JJBS, **13 (2):** 197 – 205.

Zhou N, Zhang Y, Liu F, Cai L. 2016. Halophilic and thermotolerant *Gymnoascus* species from several special environments, China. Mycologia, **108(1)**: 179-191.

Zhao F, Wang P, Lucardi RD, Su Z, Li S. 2020. Natural sources and bioactivities of 2, 4-di-tert-butylphenol and its analogs. Toxins. **12(1)**:35.

Valuation and Mapping of Marine Ecosystem Services in the Jordanian Gulf of Aqaba, Red Sea

Wissam Y Hayek[1,*], Tariq H Al-Najjar[2], Riyad S Manasrah[3], Fuad A Al-Horani[2] and Mohammad A Wahsha[4]

[1] *Department of Geography, School of Arts, The University of Jordan, Amman, Jordan;* [2]*School of Basic and Marine Sciences, The University of Jordan, Aqaba Branch, Jordan;* [3] *Department of Physics, School of Science, The University of Jordan, Amman, Jordan;* [4] *Marine Science Station, The University of Jordan, Aqaba Branch, Jordan*

Abstract

Marine ecosystems play a vital role in supporting human well-being and coastal communities, offering essential ecosystem services (ES). This study focuses on the Gulf of Aqaba in Jordan, aiming to assess and map marine ecosystem services by leveraging stakeholder perceptions. To achieve this objective, a comprehensive survey was conducted with 64 participants representing diverse demographics. The survey, coupled with Participatory Geographic Information System (PGIS) exercises, gathered data on the awareness and valuation of ecosystem services. The integration of PGIS, a participatory mapping methodology, facilitated stakeholder involvement in spatial mapping exercises. This approach not only captured local knowledge but also enhanced the mapping process, providing a more nuanced and comprehensive understanding of stakeholder perspectives on marine ecosystem services in the Gulf of Aqaba. The results contribute to evidence-based decision-making, sustainable resource management, and the implementation of international agreements and policies for marine conservation and development in this ecologically important region.

Keywords: Marine Ecosystem Services, Mapping, PGIS, Aqaba

1. Introduction

Marine ecosystems are integral to global well-being, offering essential ecosystem services (ES) vital for human welfare and coastal communities (Ma et al., 2023; Costanza et al., 2014; Barbier et al., 2011). Recognized for provisioning, regulating, cultural, and supporting services, these ecosystems play a multifaceted role in sustaining life (Asante et al., 2023; Burkhard et al., 2012, 2014; Van de Pol et al., 2023). The ecosystem-based approach (EBA) has emerged as a key framework for incorporating ES into decision-making, providing a holistic perspective crucial for long-term societal sustainability (Ruskule et al., 2023; Costanza et al., 2014).

This study focuses on the Gulf of Aqaba in Jordan, employing EBA to map and understand marine ES for effective decision-making, resource management, and alignment with international conservation and development policies (Cordero-Penín et al., 2023; Béné et al., 2016). Drawing inspiration from relevant studies, particularly those employing Participatory Geographic Information Systems (PGIS) methodologies, this research adopts a stakeholder perception approach (Brown et al., 2014). Notably, Brown et al. (2014) demonstrate the efficacy of PGIS in assessing social and cultural values associated with public lands, revealing significant associations between values, land types, and potential management conflicts. In their studies conducted in 2015 and 2016, Brown and colleagues, as well as the work by Munro and colleagues in 2017, redirect attention towards marine ecosystems. They emphasize the significance of stakeholder engagement and participatory approaches, delving into a nuanced examination of stakeholder perspectives and their impact on mapping outcomes.

Expanding beyond specific regions, Burdon et al. (2019) emphasize a stakeholder-driven approach to understanding marine natural capital and societal benefits, showcasing its global significance. Hermes et al. (2018) provide an editorial overview, stressing the diverse methods for assessing recreational ecosystem services (RES) and the necessity of integrating RES information into decision-making. Karimi et al. (2015) contribute insights into social-ecological hotspots, demonstrating the need for integrating social and ecological data. Wangai et al. (2016) extend the scope to Africa, advocating for localized assessments and addressing trade-offs and synergies. This collective body of literature establishes a foundation for understanding and mapping marine ecosystem services, with a focus on stakeholder engagement, participatory GIS methodologies, and the integration of diverse perspectives as crucial elements for comprehensive marine management.

---

[*] Corresponding author. e-mail: w.hayek@ju.edu.jo.

2. Materials and Methods

2.1. Study Area

Aqaba, a coastal city located in the southern part of Jordan along the northeastern coast of the Red Sea, was chosen as the study site. Positioned strategically at the northern tip of the Gulf of Aqaba, which is an extension of the Red Sea, Aqaba offers a remarkable environment for the investigation. The region is renowned for its rich marine biodiversity and unique coral reef ecosystems, making it a significant hotspot for marine ecosystem services. With geographical coordinates ranging from approximately 29°27'N to 29°36'N latitude and 34°57'E to 35°03'E longitude, Aqaba boasts a coastline stretching over 27 kilometres, encompassing diverse marine habitats such as coral reefs, seagrass meadows, and rocky shores, each providing distinct ecosystem services (Al-Najjar et al. 2019). The Gulf of Aqaba, a semi-enclosed water body, represents the northernmost extension of the Red Sea and is connected to its main body via the Strait of Tiran (Al-Najjar et al. 2019). Stretching approximately 180 km in length, with a width of 14-24 km, and reaching a maximum depth of 1825 m, the study area is bordered by arid deserts (Khalaf et al. 2019). The Jordanian coastline extends for 27 km, and the width of the Gulf bordered by Jordan ranges from 5 km at the northern border to 17 km at the southern border (Al-Najjar et al. 2018) (Figure 1). Along most of the coastline throughout the Gulf, fringing reefs can be found, adding to the region's ecological significance.
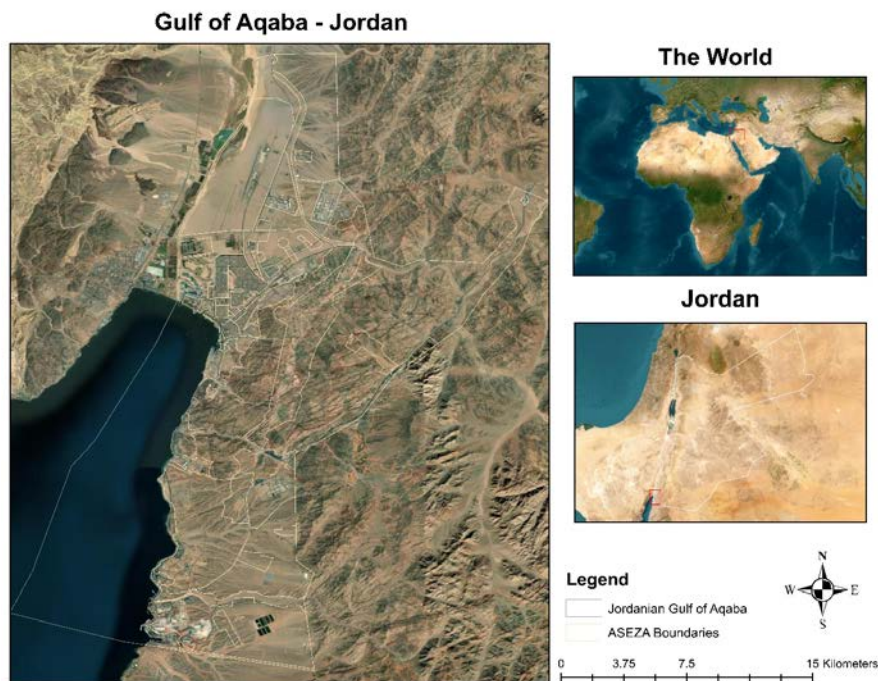
Figure 1. Study area - Aqaba coastline – Jordan.

Table 1, which presents the demographic information of the participants, shows a diverse range of ages, occupations, and educational backgrounds. This diversity is crucial for understanding the varied perspectives on ecosystem services. The table highlights a significant representation of young adults, which aligns with the emerging environmental consciousness observed in the survey responses.

Figure 2, depicting the GIS map of ecosystem service distribution, illustrates significant spatial variations. The coastal regions near urban centers show a higher dependence on ecosystem services, as indicated by the denser color gradients. This pattern underscores the intricate relationship between urban development and marine ecosystems.
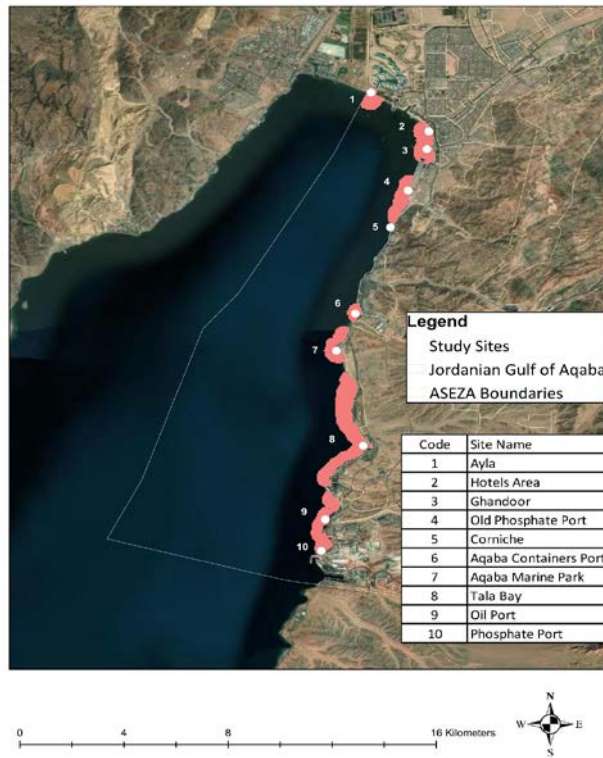
Figure 2. Corals-seagrass interaction areas as a result of the snorkeling and GIS analysis.

2.2. Data Collection

The flow of data collection is depicted in Figure 3 Snorkeling surveys were conducted along the 27 km shoreline of the Gulf of Aqaba, resulting in a total of 8,278 data points collected from 45 sites. For each point, the prevalent habitat (corals, seagrass, rocks, and sand) was recorded. After that, a GIS map reflecting the 10 most dominant corals–seagrass interaction sites along the entire coastline was prepared. To assess marine ecosystem services along the 10 sites, we used a stakeholder perception approach, incorporating the perspectives of coastal users through a questionnaire survey (Appendix 1).
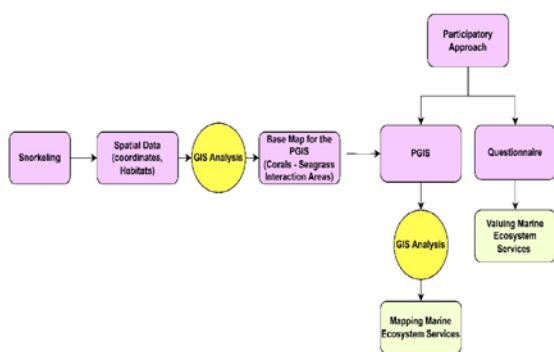
Figure 3. Adopted methodology for data collection and analysis.

The questionnaire captured information on stakeholders' awareness, utilization, preferences, and perceived importance of marine ecosystem services. It included sets of questions to gather demographic information, assess awareness of ecosystem services, evaluate the importance of services, and identify their locations on a map. Respondents were given the flexibility to specify additional services and provide qualitative

insights on sustainable management and conservation actions in Aqaba.

To incorporate spatial local knowledge about the locations of marine ecosystem services, we employed the Participatory Geographic Information Systems (PGIS) approach within the identified corals-seagrass interaction areas in the questionnaire. Utilizing GIS, the acquired spatial data were used to develop maps representing the distribution of ecosystem services based on marine resource users' perceptions.

2.3. Data analysis

The collected data from the questionnaire survey underwent statistical analysis to determine the relative importance of each identified marine ecosystem service. Descriptive statistics, including means and percentages, were calculated to summarize the rankings provided by the respondents, offering an initial indication of the perceived importance of different services and enabling comparisons among them. A higher ranking assigned to a service indicated a greater perceived value or importance.

To map the corals-seagrass interaction areas and marine ecosystem services, GIS technology was employed to enable spatial representation and visualization across the study area. The process involved several key steps:

1. Data Preparation: The initial step involved integrating the percentages of responses from the participants who identified marine ecosystem services along the 10 sites into the attribute table of the GIS data layer representing these locations. This data integration ensured that it was ready for further spatial analysis.

2. Spatial Interpolation: Spatial analysis was conducted using the Inverse Distance Weighting (IDW) interpolation method. This process aimed to estimate values for the remaining points that lacked responses, creating a continuous surface representing the

distribution of marine ecosystem services across the entire study area. The interpolation provided valuable insights into the spatial distribution of identified ecosystem services, enabling a comprehensive visualization of the phenomena.

3. Define Study Area: To focus the representation within the borders of the Gulf of Aqaba, the raster data resulting from the spatial interpolation was clipped. This step ensured that the visualization was limited to the specific area of interest, making the map's context clear and relevant to the study's objectives.

Visualization: The final step involved visually representing the results using a gradient colour scheme. Distinct colours were assigned to different values or ranges of percentages of marine ecosystem services identified. For instance, areas with lower percentages of marine ecosystem services were depicted using green, while areas with higher percentages were represented using red. The gradient between green and red effectively showcased the varying levels of presence and absence of marine ecosystem services across the study area, providing an easily interpretable map for the stakeholders and decision-makers.

2.4. Demographics of Study Participants

Figure 4 details the demographics of our 64 study participants. The gender breakdown shows 61% male and 39% female participants. Age distribution was varied, with 16% under 18 years, 19% between 18 and 24, 25% between 25 and 34, 16% between 35 and 44, and 24% over 45 years old. Occupationally, participants included 9% coastal community members, 45% tourists or visitors, and 41% local business owners or employees. No participants were from environmental, governmental, or policy sectors, with 5% categorizing their occupation as "Other." Educationally, 28% completed primary or secondary education, 36% held bachelor's degrees, 27% had master's degrees, and 9% possessed Ph.Ds or equivalent, with no "Other" educational backgrounds reported.
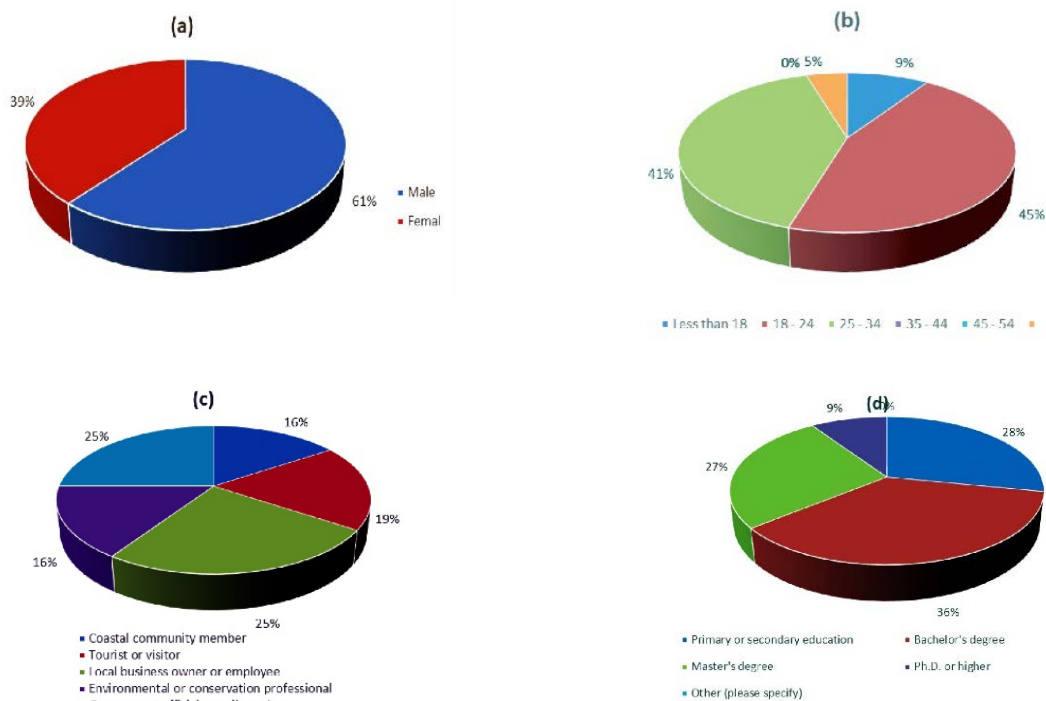
Figure 4. Demographic information about the study participants: (a) Gender, (b) Age, (C) Occupation, (d) Education Level.

2.5. Awareness of Ecosystem Services

Survey findings (Figure 5a) show varied understanding of marine ecosystem services among participants. Sixteen percent were very familiar, 41% moderately familiar, 28% slightly familiar, and 16% unfamiliar. This underscores the need for enhanced public education on marine ecosystems' ecological importance in Aqaba.

Regarding threats to these services (Figure 5b), 22% were very aware, 44% moderately aware, and 34% slightly aware, with no participants completely unaware. This highlights the success of existing public awareness campaigns and the importance of their continuation for marine ecosystem conservation in Aqaba.
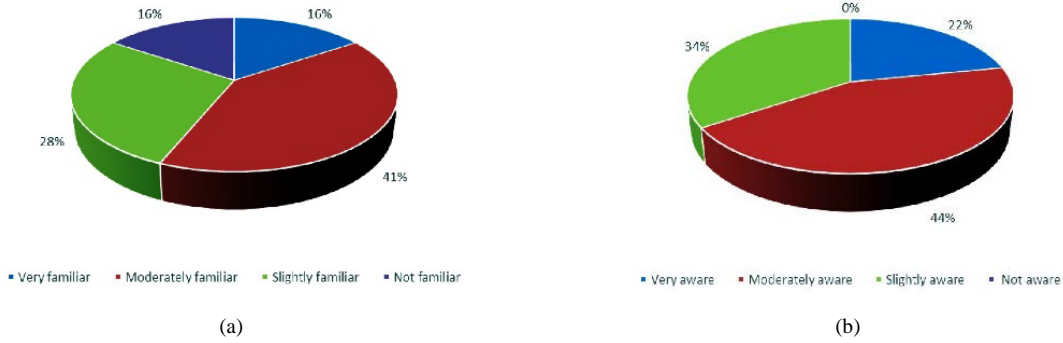
Figure 5. Results of the questionnaire: (a) familiarity with the concept of marine ecosystem services, (b) awareness of potential threats facing marine ecosystem services in Aqaba.

2.6. Prioritization of Marine Ecosystem Services

Participants' ranking of marine ecosystem services (Figure 6) reveals diverse valuations. Provisioning services were ranked first by 22% and second by 28%, showing appreciation for tangible benefits. Regulating services were top priority for 47% and second for 28%, indicating an understanding of ecological balance importance. Cultural services ranked third by 39%, reflecting a balance of priorities. Supporting services were first for 13% but third for 39%, showing varied significance.
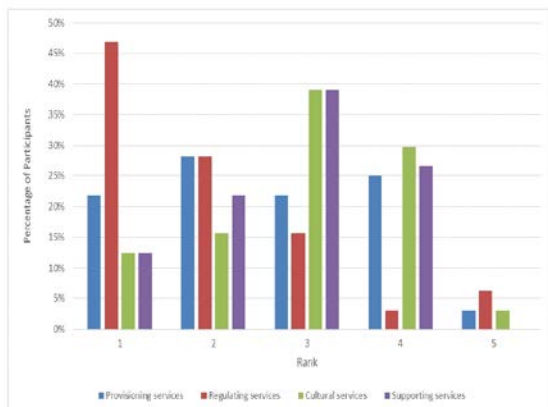
Figure 6. Identifying and valuing marine ecosystem services.

In Figure 7, all participants acknowledged awareness of threats to these services. Provisioning services ranked as top priority for 3%, second for 30%, but third for 48%. Regulating services were top for 3%, third for 31%, but fifth for 25%. Cultural services were most important for 6%, but fifth for 31%. Supporting services ranked first by 20%, second by 19%, but fifth by 14%.
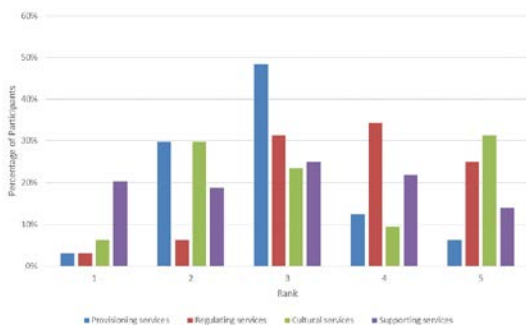
Figure 7. Awareness of potential threats to marine ecosystem services in Aqaba.

2.7. Locations of Marine Ecosystem Services

PGIS findings (Figure 8) indicate participant perceptions of marine ecosystem services across ten Aqaba coastline sites. Aqaba Marine Park was highlighted by 39% for significant ecological benefits. Tala Bay followed with 31%. Lower perceived ecosystem services were noted in Ghandoor, Old Phosphate Port, and Phosphate Port (9% each). The Hotels Area and Aqaba Containers Port were recognized by 22% and 9%, respectively. The Corniche and Oil Port each received 9% acknowledgments for their ecological contributions.
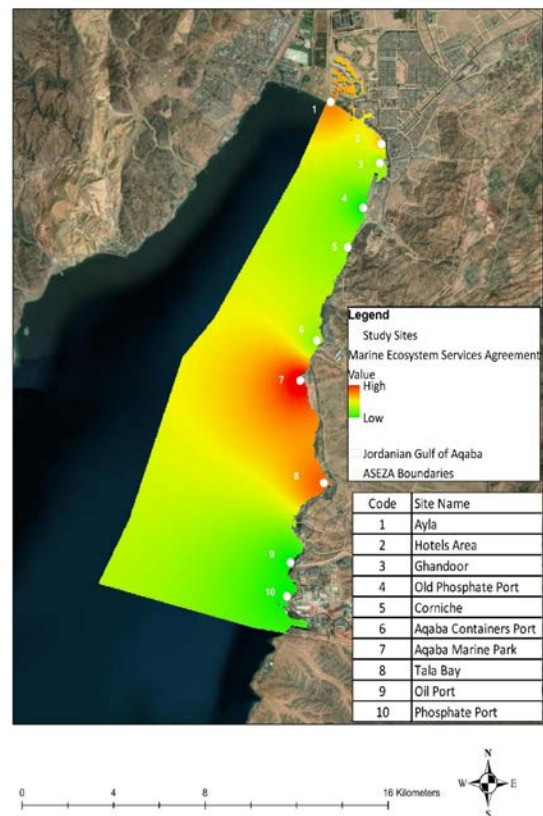
Figure 8. Level of agreement on the locations of marine ecosystem services as a result of the PGIS.

3. Discussion

The collection of demographic data from participants in our study was crucial for understanding the varied perspectives that influence the identification of ecosystem services in the Gulf of Aqaba, Jordan. We engaged a demographically diverse group, including individuals from

different generations, with equal representation of genders and a wide age range. This diversity enriched our assessment of ecosystem service preferences and highlighted the importance of including varying viewpoints in such studies (Milfont & Sibley, 2012). We focused on stakeholders like coastal community members, tourists, and local business affiliates, emphasizing their critical role in ecosystem services management (Christie et al., 2017). However, the exclusion of environmental experts and government officials from our study participants indicates an area for improvement in future research, emphasizing the need to incorporate their specialized knowledge into ecosystem services mapping (Daw et al., 2011).

Our findings also showed that educational backgrounds significantly influence perceptions of ecosystem services. We observed a wide range of educational levels among participants, from those with primary or secondary education to a smaller cohort with doctoral or higher qualifications (Chan et al., 2016; Liquete et al., 2013). The presence of a substantial number of participants with bachelor's and master's degrees suggests a heightened level of environmental awareness, beneficial for informed decision-making in ecosystem services management. This robust demographic data collection aids in understanding how sociodemographic factors impact ecosystem service preferences, reinforcing the importance of involving a diverse range of stakeholders in the development of sustainable ecosystem management policies (Plieninger et al., 2013).

Awareness of marine ecosystem services is vital for stakeholder engagement and fostering environmental consciousness in the region (Tamire et al., 2023; Gifford, 2011). Our study revealed varied levels of familiarity with marine ecosystem services among participants, with a considerable number only moderately knowledgeable. This finding points to the need for targeted initiatives to enhance understanding of the role of marine ecosystems in providing essential services in Aqaba.

Our survey also indicated a promising level of awareness among participants about potential threats to marine ecosystem services in Aqaba. Most participants exhibited at least a moderate awareness, with many highly informed about these threats. This awareness is a valuable asset for conservation efforts and informed decision-making aimed at protecting the region's marine biodiversity and ecosystem services. However, maintaining this awareness requires continuous educational and communication initiatives to keep stakeholders engaged and proactive in addressing challenges to marine ecosystem services in Aqaba.

The valuation of marine ecosystem services was revealed as a complex process, reflecting varied priorities among participants (Saarikoski et al., 2022; Chan et al., 2016). Provisioning services, like fishery resources, were highly valued for their direct benefits. However, the limited focus on other provisioning benefits like raw materials or medicinal resources suggests a gap in understanding their broader ecological contributions.

Participants also expressed diverse views on regulating services, crucial for maintaining environmental balance. This diversity in perspectives necessitates tailored communication strategies to convey the importance of regulating services and their interconnectivity with other ecosystem functions.

Cultural services, offering non-material benefits, were valued differently by participants, underlining the need to accommodate diverse cultural perspectives in ecosystem management strategies.

The study also highlighted the importance of supporting services, foundational for other ecosystem services. These services were viewed as significant by participants, even if not always ranked as the top priority.

Our study highlights the critical need for an inclusive approach to ecosystem management in the Gulf of Aqaba. Recognizing and valuing the diverse perspectives and priorities of various stakeholders is key to fostering sustainable practices and preserving the marine ecosystems in the region (Díaz-Siefer et al., 2023).

The study's results show a positive trend in participants' awareness of potential threats to marine ecosystem services in Aqaba, indicating that environmental education efforts have had a certain impact. However, to maintain and enhance this level of awareness, ongoing educational initiatives are vital to ensure the community remains actively informed and engaged in conservation efforts.

Furthermore, the analysis of ecosystem services rankings reflects the different levels of importance assigned by participants, underscoring the necessity for tailored communication strategies and inclusive approaches in ecosystem management. The application of Participatory Geographic Information Systems (PGIS) in our research provided critical insights into local community perceptions of marine ecosystem services along the Aqaba coastline. This approach highlighted the ecological significance of specific areas and pinpointed locations where increased awareness and education could be beneficial (Carriea et al., 2022).

Collectively, the integration of demographic data, awareness levels, and PGIS findings offers a comprehensive framework for decision-makers, policymakers, and environmental managers. This integrated approach supports the development of informed, inclusive, and participatory strategies for effective marine ecosystem management in the Gulf of Aqaba.

4. Conclusions

This study emphasizes the critical role of incorporating stakeholder perceptions and values in the identification and mapping of marine ecosystem services in Aqaba, Jordan. It underscores the vital importance of stakeholder engagement and the integration of diverse perspectives in marine ecosystem management. Key highlights of this study include:

- The essential role of stakeholder engagement in providing valuable insights for effective conservation and management strategies, ensuring a comprehensive understanding of marine ecosystem services.
- The importance of inclusive decision-making processes that integrate diverse perspectives, leading to more informed and holistic approaches to marine ecosystem management. This integration prioritizes the well-being of both human communities and nature.
- The necessity of ongoing educational campaigns to maintain and enhance stakeholders' awareness of potential threats to marine ecosystem services.

- The use of Participatory Geographic Information Systems (PGIS) as a community-centered approach, which incorporates local knowledge and makes conservation efforts more meaningful and relevant.
- The empowerment of decision-makers through the GIS map to effectively prioritize conservation actions and sustainable development efforts.
- The contribution of understanding marine ecosystem services to the development of evidence-based policies and practices that promote human well-being and ecological preservation.
- The development of holistic conservation strategies by incorporating stakeholder perspectives, leading to more inclusive and effective strategies for safeguarding the marine environment's health and resilience.
- The emphasis on continuous efforts to engage stakeholders and integrate diverse perspectives for the long-term sustainability of marine ecosystem services in the Gulf of Aqaba.

In essence, the findings of this study offer a valuable resource for coastal management and marine conservation efforts. By acknowledging and integrating the values and perceptions of local communities, the study fosters a balanced relationship between human activities and the marine environment. This approach supports the well-being of both coastal communities and nature in the Gulf of Aqaba, highlighting the synergy between human development and environmental stewardship.

5. Recommendations

Based on our findings, we urge the adoption of an inclusive approach to marine ecosystem management in Aqaba, emphasizing the need for robust stakeholder engagement and participatory decision-making processes. Key actions include launching targeted educational campaigns to raise public awareness about marine ecosystems' value and threats, and expanding the use of Participatory Geographic Information Systems (PGIS) to incorporate local knowledge in conservation strategies. We recommend fostering collaborations among government agencies, environmental groups, and the community to develop policies that balance ecological preservation with human needs. Additionally, continuous research and adaptive management practices are essential to address emerging challenges and ensure the sustainability of marine biodiversity and ecosystem services in the region.

Acknowledgments

References and Further Reading

Al-Najjar, T., Dahiyat, N., Sharari, N., Wahsha, M., and M. Khalaf. 2019. Levels of mercury in three species of tuna (*Katsuwonus pelamis*, *Auxis thazard* and *Euthynnus affinis*) collected from the Jordanian coast of the Gulf of Aqaba, Red Sea. *FEB* 28(5): 4304-4310.

Al Najjar, T., Al Tawaha, M., Wahsha, M., and A.A. Hilal. 2018. Heavy metals in the sea urchin *Diadema setosum* from the Gulf of Aqaba. *FEB* 27(6): 4149-4155.

Arkema, K.K., Verutes, G.M., Wood, S.A., Clarke-Samuels, C., Rosado, S., Canto, M., Rosenthal, A., Ruckelshaus, M., Guannel, G., Toft, J., and J. Faries. 2015. Embedding ecosystem services in coastal planning leads to better outcomes for people and nature. *Proc Nat Acad Sci* 112(24): 7390-7395.

Asante, F., Bento, M., Broszeit, S., Bandeira, S., Chitará-Nhandimo, S., Amoné-Mabuto, M. and Correia, A.M., 2023. Marine macroinvertebrate ecosystem services under changing conditions of seagrasses and mangroves. *Mar Environ Res*, p.106026.

Barbier, E.B., Hacker, S.D., Kennedy, C., Koch, E.W., Stier, A.C., and B.R. Silliman. 2011. The value of estuarine and coastal ecosystem services. *Ecol Monogr* 81(2): 169-193.

Béné, C., Arthur, R., Norbury, H., Allison, E.H., Beveridge, M., Bush, S., Campling, L., Leschen, W., Little, D., Squires, D. and Thilsted, S.H., 2016. Contribution of fisheries and aquaculture to food security and poverty reduction: assessing the current evidence. *World Dev*, 79, pp.177-196.

Brown, G., Strickland-Munro, J., Kobryn, H. and Moore, S.A., 2016. Stakeholder analysis for marine conservation planning using public participation GIS. *Appl Geogr* , 67, pp.77-93.

Brown, G., Hausner, V.H. and Lægreid, E., 2015. Physical landscape associations with mapped ecosystem values with implications for spatial value transfer: An empirical study from Norway. *Ecosyst Serv* , 15, pp.19-34.

Brown, G., Weber, D. and De Bie, K., 2014. Assessing the value of public lands using public participation GIS (PPGIS) and social landscape metrics. . *Appl Geogr* , 53, pp.77-89.

Burdon, D., Potts, T., McKinley, E., Lew, S., Shilland, R., Gormley, K., Thomson, S. and Forster, R., 2019. Expanding the role of participatory mapping to assess ecosystem service provision in local coastal environments. *Ecosyst Serv*, 39, p.101009.

Burkhard, B., Kandziora, M., Hou, Y., and F. Müller. 2014. Ecosystem service potentials, flows and demands-concepts for spatial localisation, indication and quantification. *Landsc Online*34. doi:10.3097/LO.201434

Burkhard, B., de Groot, R., Costanza, R., Seppelt, R., Jorgensen, S.E., and M. Potschin. 2012. Solutions for sustaining natural capital and ecosystem services. ***Ecological Indicators*** 21: 1-6.

Carrie, R.H., Stringer, L.C., Le, T.V.H., Quang, N.H., Hackney, C.R., Pham, T.T.N. and Quinn, C.H., 2022. Recommendations to guide sampling effort for polygon-based participatory mapping used to identify perceived ecosystem services hotspots. MethodsX, 9, p.101921

Casal, G. and McCarthy, T., Marine Coastal Ecosystems in Ireland in a Three-Dimensional Context: Scientific, Legislative, and News Media. Legislative, and News Media.

Chan, K.M.A., Balvanera, P., Benessaiah, K., Chapman, M., Díaz, S., Gómez-Baggethun, E., Gould, R., et al. 2016. Opinion: Why protect nature? Rethinking values and the environment. *Proc Natl Acad Sci* 113: 1462–1465.

Christie, P., Fluharty, D., White, A.T., Eisma-Osorio, R.L., Deguit, E.T., Nohara, S., and R.S. Pomeroy. 2017. From reef to table: social and ecological factors affecting coral reef fisheries, artisanal seafood supply chains, and seafood security. *Reg Stud Mar Sci* 13: 53–68.

Cordero-Penín, V., Abramic, A., García-Mendoza, A., Otero-Ferrer, F., and R. Haroun. 2023. Mapping marine ecosystem services potential across an oceanic archipelago: Applicability and limitations for decision-making. *Ecosyst Serv* 60: 101517.

Costanza, R., de Groot, R., Sutton, P., van der Ploeg, S., Anderson, S. J., Kubiszewski, I., et al. 2014. Changes in the global value of ecosystem services. *Glob Environ Change* 26: 152-158.

Custodio, M., Moulaert, I., Asselman, J., Van der Biest, K., van de Pol, L., Drouillon, M., Lucas, S.H., Taelman, S.E. and Everaert, G., 2022. Prioritizing ecosystem services for marine management through stakeholder engagement. *Ocean Coast Manag* , 225, p.106228.

Daily, G.C., Polasky, S., Goldstein, J., Kareiva, P.M., Mooney, H.A., Pejchar, L., Ricketts, T.H., Salzman, J. and Shallenberger, R., 2009. Ecosystem services in decision making: time to deliver. *Front Ecol Environ* , 7(1), pp.21-28.

Daily, G.C., Söderqvist, T., Aniyar, S., Arrow, K., Dasgupta, P., Ehrlich, P. R., et al. 2000. The value of nature and the nature of value. *Science* 289(5478): 395-396.

Dallimer, M., Irvine, K.N., Skinner, A.M., Davies, Z.G., Rouquette, J.R., Maltby, L.L., et al. 2012. Biodiversity and the feel-good factor: Understanding associations between self-reported human well-being and species richness. *BioScience* 62(1): 47-55.

Daw, T., Adger, W.N., Brown, K., and M.-C. Badjeck. 2011. Climate change and capture fisheries: potential impacts, adaptation, and mitigation. *Curr Opin Environ Sustain* 3: 58–66.

de Groot, R.S., Wilson, M.A., and R.M. Boumans. 2002. A typology for the classification, description and valuation of ecosystem functions, goods and services. *Ecol Econ.* 41(3): 393-408.

Díaz-Siefer, P., Weishaupt, P., Pozo, R.A., Huenchuleo, C., Guerrero-Rojas, R., Gelcich, S. and Celis-Diez, J.L., 2023. Residents' valuation of ecosystem services in a Mediterranean coastal dune ecosystem: The case of the Ritoque dunes in central Chile. *J. Nat. Conserv.* , 74, p.126446.

Fisher, B., Turner, R.K., and P. Morling. 2009. Defining and classifying ecosystem services for decision making. *Ecol Econ.* 68(3): 643-653.

Fortune, J., Butler, E.C. and Gibb, K., 2023. Estuarine benthic habitats provide an important ecosystem service regulating the nitrogen cycle. *Mar. Environ. Res* ., p.106121.

Gifford, R. 2011. The dragons of inaction: Psychological barriers that limit climate change mitigation and adaptation. *Am Psychol* 66: 290–302.

Hermes, J., Van Berkel, D., Burkhard, B., Plieninger, T., Fagerholm, N., von Haaren, C. and Albert, C., 2018. Assessment and valuation of recreational ecosystem services of landscapes. *Ecosyst Serv* , 31, pp.289-295.

Inácio, M., Karnauskaitė, D., Gomes, E., Barceló, D., and P. Pereira. 2022. Mapping and assessment of future changes in the coastal and marine ecosystem services supply in Lithuania. *Sci Total Environ,* 812: 152586.

Karimi, A., Yazdandad, H. and Fagerholm, N., 2020. Evaluating social perceptions of ecosystem services, biodiversity, and land management: Trade-offs, synergies and implications for landscape planning and management. *Ecosyst Serv*, 45, p.101188.

Leslie, H.M., and K.L. McLeod. 2007. Confronting the challenges of implementing marine ecosystem-based management. *Frontiers Ecol Environ* 5(10): 540-548.

Liquete, C., Kleeschulte, S., Maes, J., Grizzetti, B., Olah, B., Zulian, G., and M.L. Paracchini. 2013. Mapping green infrastructure based on ecosystem services and ecological networks: A Pan-European case study. *Enviro Sci Policy,* 33: 98–106.

Ma, C., Stelzenmüller, V., Rehren, J., Yu, J., Zhang, Z., Zheng, H., Lin, L., Yang, H.C. and Jin, Y., 2023. A risk-based approach to cumulative effects assessment for large marine ecosystems to support transboundary marine spatial planning: A case study of the yellow sea. *J Environ Manage* , 342, p.118165

Manea, E., Di Carlo, D., Depellegrin, D., Agardy, T., and E. Gissi. 2019. Multidimensional assessment of supporting ecosystem services for marine spatial planning of the Adriatic Sea. *Ecol. Indic.* 101: 821-837.

Martín-López, B., Iniesta-Arandia, I., García-Llorente, M., Palomo, I., Casado-Arzuaga, I., Amo, D.G.D., et al. 2012. Uncovering ecosystem service bundles through social preferences. *PLoS ONE* 7(6): e38970.

Millennium Ecosystem Assessment. 2005. *Ecosystems and human well-being: wetlands and water synthesis*. World Resources Institute, Washington, DC.

Milfont, T.L., and C.G. Sibley. 2012. The big five personality traits and environmental engagement: Associations at the individual and societal level. *J. Environ. Psychol.,* 32: 187–195.

Munro, J., Pearce, J., Brown, G., Kobryn, H. and Moore, S.A., 2017. Identifying 'public values' for marine and coastal planning: Are residents and non-residents really so different?. *Ocean Coast Manage Journal*, 148, pp.9-21.

Nahuelhual, L., Vergara, X., Bozzeda, F., Campos, G., Subida, M.D., Outeiro, L., Villasante, S., and M. Fernández. 2020. Exploring gaps in mapping marine ecosystem services: a benchmark analysis. *Ocean Coast Manage Journal,* 192: 105193.

Nahuelhual, L., Vergara, X., Kusch, A., Campos, G., and D. Droguett. 2017. Mapping ecosystem services for marine spatial planning: Recreation opportunities in Sub-Antarctic Chile. *Mar Policy Journal*, 81: 211-218.

Nahuelhual, L., Laterra, P., and J. Barrena. 2016. Indicadores de servicios ecosistémicos: una revisión y análisis de su calidad. *Medio Ambiente, Gobierno de Chile.*

Pace, L.A., Saritas, O. and Deidun, A., 2023. Exploring future research and innovation directions for a sustainable blue economy. *Mar Policy Journal*, 148, p.105433.

Plieninger, T., Dijks, S., Oteros-Rozas, E., and C. Bieling. 2013. Assessing, mapping, and quantifying cultural ecosystem services at the community level. *Land Use Policy* 33: 118–129.

Rodríguez-Rodríguez, D., Castro, A.J., González-Morales, S., Iglesias-Campos, M., and F.D. Pineda. 2018. Mapping ecosystem services for environmental planning and management: A comprehensive review. *Ecosyst Serv* 31: 25-37.

Rodriguez, J.P., Beard, T.D., Bennett, E.M., Cumming, G.S., Cork, S.J., Agard, J., Dobson, A.P., and G.D. Peterson. 2006. Trade-offs across space, time, and ecosystem services. *Ecol Soc* 11(1).doi:10.5751/ES-01667-110128

Ruckelshaus, M., McKenzie, E., Tallis, H., Guerry, A., Daily, G., Kareiva, P., and S. Polasky. 2013. Notes from the field: Lessons learned from using ecosystem service approaches to inform real-world decisions. *Ecol Econ,* 115: 11-21.

Ruskule, A., Kotta, J., Saha, C.R., Arndt, P., Ustups, D., Strāķe, S. and Bergström, L., 2023. Testing the concept of green infrastructure at the Baltic Sea scale to support an ecosystem-based approach to management of marine areas. *Mar Policy*, 147, p.105374.

Saarikoski, H., Aapala, K., Artell, J., Grammatikopoulou, I., Hjerppe, T., Lehtoranta, V., Mustajoki, J., Pouta, E., Primmer, E. and Vatn, A., 2022. Multimethod valuation of peatland ecosystem services: Combining choice experiment, multicriteria decision analysis and deliberative valuation. *Ecosyst Serv*, 57, p.101471.

Spalding, M., Burke, L., Wood, S.A., Ashpole, J., Hutchison, J., and P. Zu Ermgassen. 2017. Mapping the global value and distribution of coral reef tourism. *Mar Policy* 82: 104-113.

Strand, M., Rivers, N. and Snow, B., 2023. The complexity of evaluating, categorising and quantifying marine cultural heritage. *Mar Policy*, 148, p.105449.

Tamire, C., Elias, E. and Argaw, M., 2023. A systematic review of ecosystem services assessments, trends, and challenges in Ethiopia. *WEE*, 5, pp.38-45.

Townsend, M., and A.M. Lohrer. 2019. Empirical validation of an ecosystem service map developed from ecological principles and biophysical parameters. *Front. mar. sci.* 6: 21.

Townsend, M., Thrush, S.F., Lohrer, A.M., Hewitt, J.E., Lundquist, C.J., Carbines, M., and M. Felsing. 2014. Overcoming the challenges of data scarcity in mapping marine ecosystem service potential. *Ecosyst Serv,* 8: 44-55.

Van de Pol, L., Van der Biest, K., Taelman, S.E., Peña, L.D.L., Everaert, G., Hernandez, S., Culhane, F., Borja, A., Heymans, J.J., Van Hoey, G. and Vanaverbeke, J., 2023. Impacts of human activities on the supply of marine ecosystem services: A conceptual model for offshore wind farms to aid quantitative assessments. *Heliyon*, 9(3).

Vihervaara, P., Mononen, L., Nedkov, S., Viinikka, A., et al. 2018. Biophysical mapping and assessment methods for ecosystem services. Deliverable D3.3 EU Horizon 2020 ESMERALDA Project, Grant agreement No. 642007.

Wangai, P.W., Burkhard, B. and Müller, F., 2016. A review of studies on ecosystem services in Africa. *Int. J. Sustain. Built Environ."* , 5(2), pp.225-245.

White, C., Halpern, B.S., and C.V. Kappel. 2012. Ecosystem service tradeoff analysis reveals the value of marine spatial planning for multiple ocean uses. *PNAS,* 109 (12): 4696-4701.

Wicaksono, P., Danoedoro, P., Hartono, and U. Nehren. 2016. Mangrove biomass carbon stock mapping of the Karimunjawa Islands using multispectral remote sensing. *Int. J. Remote Sens.,* 37(1): 26-52.

Yang, W., Jin, Y., Sun, T., Yang, Z., Cai, Y., and Y. Yi. 2018. Trade-offs among ecosystem services in coastal wetlands under the effects of reclamation activities. *Ecol. Indic.,* 92: 354-366.

Yose, P., Thondhlana, G. and Fraser, G., 2023. Conceptualizing the socio-cultural impacts of marine plastic pollution on human well-being–A perspective. *Mar. Pollut. Bull.* , 194, p.115285.

Appendix 1

Perception of Marine Ecosystem Services in Aqaba: Stakeholder Questionnaire

Introduction:
Thank you for participating in this survey on marine ecosystem services in Aqaba. The purpose of this questionnaire is to gather your perceptions and insights regarding the various ecosystem services provided by the marine environment in Aqaba. Your valuable input will contribute to a better understanding and appreciation of these services, ultimately aiding in their sustainable management and conservation. Please answer the following questions to the best of your knowledge and experiences.

Section One: Demographic Questions:

1. **Gender**
   a) Male   b) Female   c)——

2. **Age**
   a) Under 18   b) 18-24   c) 25-34

   d) 35-44   e) 45-54   f) 55 and above

3. **Occupation**
   a) Coastal community member   b) Tourist or visitor   c) Local business owner or employee

   d) Environmental or conservation professional   e) Government official or policymaker   f) Other (please specify)

4. **Educational Background:**
   a) Primary or secondary education   b) Bachelor's degree   c) Master's degree

   d) Ph.D. or higher   e) Other (please specify)

Section Two: Awareness about Ecosystem Services

5. **How familiar are you with the concept of marine ecosystem services?**
   a) Very familiar
   b) Moderately familiar
   c) Slightly familiar
   d) Not familiar

How aware are you of the potential threats facing marine ecosystem services in Aqaba?
   a) Very aware
   b) Moderately aware
   c) Slightly aware
   d) Not aware

Section Three: Identifying and Valuing Ecosystem Services
Please rank the following marine ecosystem services in terms of their importance to you personally (1 being the most important and 5 being the least important):
   a) Provisioning services (e.g., seafood, medicinal plants)
   b) Regulating services (e.g., climate regulation, water purification)
   c) Cultural services (e.g., recreation, spiritual significance)
   d) Supporting services (e.g., nutrient cycling, habitat formation)
   e) Other (please specify)

How would you evaluate the importance of the identified marine ecosystem services in Aqaba? (Rate each service on a scale of 1-5, with 1 being very low importance and 5 being very high importance)
   a) Provisioning services (e.g., seafood, medicinal plants)
   b) Regulating services (e.g., climate regulation, water purification)
   c) Cultural services (e.g., recreation, spiritual significance)
   d) Supporting services (e.g., nutrient cycling, habitat formation)

    e)   Other (please specify)

Section ٤: Identifying Locations of Ecosystem Services

6.   **Which specific coastal areas in Aqaba (From the attached Map) have you observed or experienced the following marine ecosystem services?** (Select all that apply)

7.   **Please indicate the relative abundance or occurrence of the following ecosystem services in each of the selected coastal areas** (Use a scale of 1-5, with 1 being very low and 5 being very high)

Coastal Area (1): [Insert Selected Coastal Area]
    a)   Provisioning services (e.g., seafood, medicinal plants)
    b)   Regulating services (e.g., climate regulation, water purification)
    c)   Cultural services (e.g., recreation, spiritual significance)
    d)   Supporting services (e.g., nutrient cycling, habitat formation)
    e)   Other (please specify)

Coastal Area (2): [Insert Selected Coastal Area]
    a)   Provisioning services (e.g., seafood, medicinal plants)
    b)   Regulating services (e.g., climate regulation, water purification)
    c)   Cultural services (e.g., recreation, spiritual significance)
    d)   Supporting services (e.g., nutrient cycling, habitat formation)
    e)   Other (please specify)

Coastal Area (3): [Insert Selected Coastal Area]
    a)   Provisioning services (e.g., seafood, medicinal plants)
    b)   Regulating services (e.g., climate regulation, water purification)
    c)   Cultural services (e.g., recreation, spiritual significance)
    d)   Supporting services (e.g., nutrient cycling, habitat formation)
    e)   Other (please specify)

Coastal Area (4): [Insert Selected Coastal Area]
    a)   Provisioning services (e.g., seafood, medicinal plants)
    b)   Regulating services (e.g., climate regulation, water purification)
    c)   Cultural services (e.g., recreation, spiritual significance)
    d)   Supporting services (e.g., nutrient cycling, habitat formation)
    e)   Other (please specify)

Coastal Area (5): [Insert Selected Coastal Area]
    a)   Provisioning services (e.g., seafood, medicinal plants)
    b)   Regulating services (e.g., climate regulation, water purification)
    c)   Cultural services (e.g., recreation, spiritual significance)
    d)   Supporting services (e.g., nutrient cycling, habitat formation)
    e)   Other (please specify)

Coastal Area (6): [Insert Selected Coastal Area]
    a)   Provisioning services (e.g., seafood, medicinal plants)
    b)   Regulating services (e.g., climate regulation, water purification)
    c)   Cultural services (e.g., recreation, spiritual significance)
    d)   Supporting services (e.g., nutrient cycling, habitat formation)
    e)   Other (please specify)

Coastal Area (7): [Insert Selected Coastal Area]
    a)   Provisioning services (e.g., seafood, medicinal plants)
    b)   Regulating services (e.g., climate regulation, water purification)
    c)   Cultural services (e.g., recreation, spiritual significance)
    d)   Supporting services (e.g., nutrient cycling, habitat formation)
    e)   Other (please specify)

Coastal Area (8): [Insert Selected Coastal Area]
    a)   Provisioning services (e.g., seafood, medicinal plants)
    b)   Regulating services (e.g., climate regulation, water purification)
    c)   Cultural services (e.g., recreation, spiritual significance)
    d)   Supporting services (e.g., nutrient cycling, habitat formation)
    e)   Other (please specify)

Coastal Area (9): [Insert Selected Coastal Area]

a) Provisioning services (e.g., seafood, medicinal plants)
b) Regulating services (e.g., climate regulation, water purification)
c) Cultural services (e.g., recreation, spiritual significance)
d) Supporting services (e.g., nutrient cycling, habitat formation)
e) Other (please specify)

Coastal Area (10): [Insert Selected Coastal Area]
a) Provisioning services (e.g., seafood, medicinal plants)
b) Regulating services (e.g., climate regulation, water purification)
c) Cultural services (e.g., recreation, spiritual significance)
d) Supporting services (e.g., nutrient cycling, habitat formation)
e) Other (please specify)

Section 4: Conclusion

8. **In your opinion, what are the key actions that should be taken to ensure the sustainable management and conservation of marine ecosystem services in Aqaba? (Open-ended question)**

Thank you for your participation in this survey! Your input is greatly appreciated and will contribute to our understanding of marine ecosystem services in Aqaba.

Name: …………………………………………………………..………………….…: الاسم

Specialty: …………………………………………………………..………………….. :التخصص

Address: …………………………………………………………..………………….. :العنوان

P.O. Box: …………………………………………………………….………. :صندوق البريد

City &Postal Code:…………………………………………..……….. :المدينة: الرمز البريدي

Country: ……………………………………………………………………….….: الدولة

Phone: …………………………………………………..…………………….……… رقم الهاتف

Fax No.: …………………………………………………………………………. :رقم الفاكس

E-mail: …………………………………..………………………………………… :البريد الإلكتروني

Method of payment: …………………………………………….……….... :طريقة الدفع

Amount Enclosed: …………………………………………………………….. :المبلغ المرفق

Signature: ……………………………………………………….……….. :التوقيع

Cheque should be paid to Deanship of Research and Graduate Studies – The Hashemite University.

I would like to subscribe to the Journal

For

- ☐   One year
- ☐   Two years
- ☐   Three years

One Year Subscription Rates		
	Inside Jordan	Outside Jordan
Individuals	JD10	$70
Students	JD5	$35
Institutions	JD 20	$90

Correspondence

Subscriptions and sales:

The Hashemite University
P.O. Box 330127-Zarqa 13115 – Jordan
Telephone: 00 962 5 3903333
Fax no. : 0096253903349
E. mail: jjbs@hu.edu.jo

المجلة الأردنية

للعلوم الحياتية

مجلة علمية عالمية محكمة

تصدر بدعم من صندوق دعم البحث العلمي و الابتكار